frontiers | Research Topics

Advanced technologies for energy saving, plant quality control and mechanization development in plant factory

Edited by
Yuxin Tong, Myung-Min Oh and Wei Fang

Published in
Frontiers in Plant Science

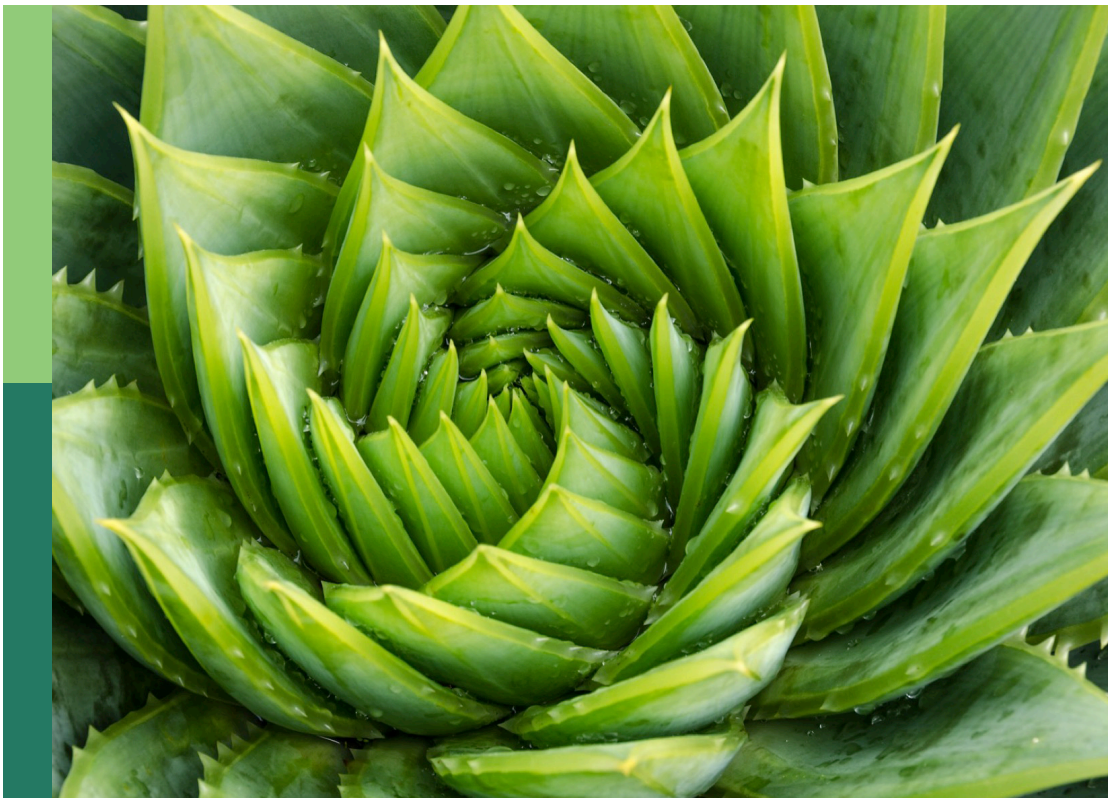

ISSN 1664-8714
ISBN 978-2-8325-2616-3
DOI 10.3389/978-2-8325-2616-3

About Frontiers

Frontiers is more than just an open access publisher of scholarly articles: it is a pioneering approach to the world of academia, radically improving the way scholarly research is managed. The grand vision of Frontiers is a world where all people have an equal opportunity to seek, share and generate knowledge. Frontiers provides immediate and permanent online open access to all its publications, but this alone is not enough to realize our grand goals.

Frontiers journal series

The Frontiers journal series is a multi-tier and interdisciplinary set of open-access, online journals, promising a paradigm shift from the current review, selection and dissemination processes in academic publishing. All Frontiers journals are driven by researchers for researchers; therefore, they constitute a service to the scholarly community. At the same time, the *Frontiers journal series* operates on a revolutionary invention, the tiered publishing system, initially addressing specific communities of scholars, and gradually climbing up to broader public understanding, thus serving the interests of the lay society, too.

Dedication to quality

Each Frontiers article is a landmark of the highest quality, thanks to genuinely collaborative interactions between authors and review editors, who include some of the world's best academicians. Research must be certified by peers before entering a stream of knowledge that may eventually reach the public - and shape society; therefore, Frontiers only applies the most rigorous and unbiased reviews. Frontiers revolutionizes research publishing by freely delivering the most outstanding research, evaluated with no bias from both the academic and social point of view. By applying the most advanced information technologies, Frontiers is catapulting scholarly publishing into a new generation.

What are Frontiers Research Topics?

Frontiers Research Topics are very popular trademarks of the *Frontiers journals series*: they are collections of at least ten articles, all centered on a particular subject. With their unique mix of varied contributions from Original Research to Review Articles, Frontiers Research Topics unify the most influential researchers, the latest key findings and historical advances in a hot research area.

Find out more on how to host your own Frontiers Research Topic or contribute to one as an author by contacting the Frontiers editorial office: frontiersin.org/about/contact

Advanced technologies for energy saving, plant quality control and mechanization development in plant factory

Topic editors

Yuxin Tong — Institute of Environment and Sustainable Development in Agriculture, Chinese Academy of Agricultural Sciences, China

Myung-Min Oh — Chungbuk National University, Republic of Korea

Wei Fang — National Taiwan University, Taiwan

Citation

Tong, Y., Oh, M.-M., Fang, W., eds. (2023). *Advanced technologies for energy saving, plant quality control and mechanization development in plant factory*. Lausanne: Frontiers Media SA. doi: 10.3389/978-2-8325-2616-3

The authors declare that the research was conducted in the absence of any commercial or financial relationships that could be construed as a potential conflict of interest

Table of contents

frontiers | Frontiers in Plant Science

TYPE Editorial
PUBLISHED 19 May 2023
DOI 10.3389/fpls.2023.1193158

OPEN ACCESS

EDITED AND REVIEWED BY
Ruslan Kalendar,
University of Helsinki, Finland

*CORRESPONDENCE
Yuxin Tong
tongyuxin@caas.cn

SPECIALTY SECTION
This article was submitted to Technical Advances in Plant Science, a section of the journal Frontiers in Plant Science

RECEIVED 24 March 2023
ACCEPTED 18 April 2023
PUBLISHED 19 May 2023

CITATION
Tong Y, Oh M-M and Fang W (2023) Editorial: Advanced technologies for energy saving, plant quality control and mechanization development in plant factory.
Front. Plant Sci. 14:1193158.
doi: 10.3389/fpls.2023.1193158

Editorial: Advanced technologies for energy saving, plant quality control and mechanization development in plant factory

Yuxin Tong[1]*, Myung-Min Oh[2] and Wei Fang[3]

[1]Institute of Environment and Sustainable Development in Agriculture, Chinese Academy of Agricultural Sciences, Beijing, China, [2]Division of Animal, Horticultural and Food Sciences, Chungbuk National University, Cheongju, Republic of Korea, [3]Department of Biomechatronics Engineering, National Taiwan University, Taiwan, China

KEYWORDS

computer vision, energy saving, plant quality control, mechanization development, plant factory

Editorial on the Research Topic
Advanced technologies for energy saving, plant quality control and mechanization development in plant factory

We are facing global problems of food shortage and/or unstable supply, resource (land, water, fossil fuel, etc.) shortages and environment degradation. To solve these problems, we need to employ plant production systems with less resource consumption and environmental degradation for high yield and quality plant production. Plant factories with artificial light (PFALs) with the benefits of 1) high input resources use efficiencies; 2) clean, safe and nutrient-rich plant production without pesticides; 3) vertical cultivation with high plant density and annual productivity; and 4) attracting young laborers due to the comfortable and labor-saving working environment, can be considered as one of the above systems. However, some major problems, such as the high initial investment and running cost, still need to be solved in PFALs. To address and update our knowledge on "*Advanced Technologies for Energy Saving, Plant Quality Control and Mechanization Development in PFAL*," we organized this Research Topic.

Plant quality control

Plant quality can be managed by environmental factors control. CO_2 concentration exerts a substrantial impact on crop yield and quality as the source of carbon, while frequent CO_2 deficiency in PFALs during the daytime limits the improvement of crop productivity. Wang et al. reviewed the current situation and research progress on CO_2 enrichment systems, including characteristics, limitations, and control strategies. Plants have different morphological and physiological responses to specific light qualities and many plant species are more sensitive to red and blue lights. Li et al. aimed to evaluate the response of leaf photosynthesis, biomass accumulation, and growth of pepper seedlings under various proportions of mixed red and blue lights. The results indicated that the red-blue ratio of 3:1 was effective in improving photomorphogenesis and photosynthesis of sweet pepper plants, achieving higher biomass accumulation and energy utilization efficiency simultaneously. Zhang et al. conducted a study to

clarify the effect of different spectral combinations on the growth, yield and nutritional quality of pea sprouts under a long photoperiod (22h light/2h dark). The red-blue ratio of 2:1 was suggested to be the suitable light quality combination for improving the growth and quality of pea sprouts under a long photoperiod. Li et al. investigated different light spectra on growth, nutritional quality and antioxidant property of winter wheat seedlings in a PFAL. The authors found that red light promoted carbohydrate accumulation in wheat seedlings, while blue light promoted the antioxidant level of wheat seedlings. The above studies can be helpful for light spectral formulating to improve plant growth, quality, and light use efficiency in PFALs. Lee and Goto explored the short-term effects of ozone exposure on the growth and accumulation of bioactive compounds in red lettuce leaves grown in a PFAL. The authors presented the efficiency and advantages of using ozone as an elicitor for bioactive compound accumulation in red leaf lettuce seedlings. Wittayathanarattana et al. presented a study to establish the short-term cooling root-zone temperature under controlled environments that could improve antioxidant capacity and bioactive compound accumulation in amaranth (*Amaranthus tricolor* L.) baby leaf without causing an abnormal appearance.

Computer vision and plant phenotype

Accurate and timely crop growth monitoring in PFALs is essential for management decision-making. Lin et al. proposed a multi-modal fusion-based deep learning model for automatically monitoring lettuce shoot fresh weight by utilizing RGB-D images. The model improved the fresh weight estimation performance by simultaneously leveraging the advantages of empirical geometric traits and deep neural features. The study suggests that the combination of multi-modal data fusion and deep neural and empirical geometric features is a promising approach for estimating fresh weight. Yoon et al. developed a model for predicting phenolic accumulation in kale (*Brassica oleracea* L. var. *acephala*) according to UV-B radiation interception and growth stage. The spatial distribution of UV-B radiation interception in plants was quantified using a ray-tracing simulation with 3D-scanned plant models. Plants adapt their photosynthetic and photoprotective pigment content to the surrounding environment, which means that changes in leaf biochemistry can be used as markers for detecting enhancements in plant nutritional quality and early warning signs of stress in PFALs, contributing to making production more efficient and precise. Cammarisano et al. proposed the use of leaf spectroscopy and mathematical modeling for non-invasive estimation of leaf pigments to monitor of plant cultivation. Ratios of pigments such as chlorophylls/carotenoids and anthocyanins/chlorophylls have demonstrated potential for indicating changes in plant stress status and nutritional quality enhancements.

Economic feasibility

Despite high expectations, the diffusion of commercial crop production in PFALs has been slowed down worldwide due to the significant initial investment and running costs. Uyeh et al. provided a decision tool that could facilitate improved decision-making in retrofitting PFALs and help efficiently facilitate mechanization and automation. The authors considered minimizing the total cost for retrofitting and maximizing the yearly net profit as two objectives and showed the usefulness of this methodology/software to compare the cost performance of different plant production systems. Zhuang et al. estimated the degree of the scale economies and found that lettuce is a well-established PFAL crop, but strawberry is not. The scale of PFALs is an important factor in determining the economic performance of PFALs' crop production. They also found that PFALs' crop production is highly sensitive, with a 30% decline in the lettuce price bring PFALs to bankruptcy, and a 20% increase in strawberries yield per unit transforming it into an economically viable PFAL crop. The results of their research can help access the economic feasibility of PFALs' crop production. Lanoue et al. discovered an innovative lighting strategy that uses 24 hours of low- intensity lighting to provide the desired amount of light for plant growth. This lighting strategy reduces capital costs for light fixtures and electricity used for air conditioning since low-intensity lighting requires fewer light fixtures and reduces heat load from lighting and plant transpiration. The strategy increased yield and nutritional contents while reducing the electricity cost per unit of product, significantly improving the sustainability of microgreen production with PFALs.

Author contributions

YT drafted the manuscript. All the authors contributed to the article and approved the submitted version.

Acknowledgments

We greatly appreciate the invaluable contributions of all the authors, reviewers, and the Chief Editor to this Research Topic.

Conflict of interest

The authors declare that the research was conducted in the absence of any commercial or financial relationships that could be construed as a potential conflict of interest.

Publisher's note

frontiers | Frontiers in Plant Science

ORIGINAL RESEARCH
published: 09 June 2022
doi: 10.3389/fpls.2022.918170

Prediction of Phenolic Contents Based on Ultraviolet-B Radiation in Three-Dimensional Structure of Kale Leaves

*Hyo In Yoon[1], Jaewoo Kim[1], Myung-Min Oh[2] and Jung Eek Son[1,3]**

[1] Department of Agriculture, Forestry and Bioresources, Seoul National University, Seoul, South Korea, [2] Division of Animal, Horticultural and Food Sciences, Chungbuk National University, Cheongju, South Korea, [3] Research Institute of Agriculture and Life Sciences, Seoul National University, Seoul, South Korea

Ultraviolet-B (UV-B, 280–315 nm) radiation has been known as an elicitor to enhance bioactive compound contents in plants. However, unpredictable yield is an obstacle to the application of UV-B radiation to controlled environments such as plant factories. A typical three-dimensional (3D) plant structure causes uneven UV-B exposure with leaf position and age-dependent sensitivity to UV-B radiation. The purpose of this study was to develop a model for predicting phenolic accumulation in kale (*Brassica oleracea* L. var. *acephala*) according to UV-B radiation interception and growth stage. The plants grown under a plant factory module were exposed to UV-B radiation from UV-B light-emitting diodes with a peak at 310 nm for 6 or 12 h at 23, 30, and 38 days after transplanting. The spatial distribution of UV-B radiation interception in the plants was quantified using ray-tracing simulation with a 3D-scanned plant model. Total phenolic content (TPC), total flavonoid content (TFC), total anthocyanin content (TAC), UV-B absorbing pigment content (UAPC), and the antioxidant capacity were significantly higher in UV-B-exposed leaves. Daily UV-B energy absorbed by leaves and developmental age was used to develop stepwise multiple linear regression models for the TPC, TFC, TAC, and UAPC at each growth stage. The newly developed models accurately predicted the TPC, TFC, TAC, and UAPC in individual leaves with $R^2 > 0.78$ and normalized root mean squared errors of approximately 30% in test data, across the three growth stages. The UV-B energy yields for TPC, TFC, and TAC were the highest in the intermediate leaves, while those for UAPC were the highest in young leaves at the last stage. To the best of our knowledge, this study proposed the first statistical models for estimating UV-B-induced phenolic contents in plant structure. These results provided the fundamental data and models required for the optimization process. This approach can save the experimental time and cost required to optimize the control of UV-B radiation.

Keywords: antioxidants, flavonoids, growth stage, light interception, plant factory

OPEN ACCESS

Edited by:
Luigi Lucini,
Catholic University of the Sacred Heart, Italy

Reviewed by:
Houcheng Liu,
South China Agricultural University, China
Ma. Cristina Vazquez Hernandez,
Tecnologico Nacional de México en Roque, Mexico
Jin Cui,
Nanjing Agricultural University, China

***Correspondence:**
Jung Eek Son
sjeenv@snu.ac.kr

Specialty section:
This article was submitted to Technical Advances in Plant Science, a section of the journal Frontiers in Plant Science

Received: *12 April 2022*
Accepted: *20 May 2022*
Published: *09 June 2022*

Citation:
Yoon HI, Kim J, Oh M-M and Son JE (2022) Prediction of Phenolic Contents Based on Ultraviolet-B Radiation in Three-Dimensional Structure of Kale Leaves. Front. Plant Sci. 13:918170. doi: 10.3389/fpls.2022.918170

INTRODUCTION

Brassica species are vegetables containing high levels of nutrients and health-promoting phytochemicals (Francisco et al., 2017). Kale (*B. oleracea* var. *acephala*) is a functional food that benefits human health, supported by much scientific evidence, and is a rich source of bioactive compounds such as polyphenols and carotenoids with antioxidant capacity (AOC;

Šamec et al., 2019). The biosynthesis of such bioactive compounds is improved through biotic and abiotic elicitation (Thakur et al., 2019). Ultraviolet (UV) radiation, especially Ultraviolet-B (UV-B; 280–315 nm), has been reported as an effective elicitor (Loconsole and Santamaria, 2021). Contrary to the long-held opinion that UV-B radiation is predominantly harmful to plants, recent studies have highlighted that a low fluence rate of UV-B radiation triggers distinct changes in the secondary metabolism, resulting in bioactive compound accumulation such as phenolics and flavonoids (Schreiner et al., 2012). The accumulation of phenolics in epidermal tissues acts as a sunscreen, and their innate antioxidant potential protects underlying sensitive tissues from UV-B-induced damage (Takshak and Agrawal, 2019). However, the localized accumulation may complicate the distribution of phenolics depending on developmental age and uneven UV-B exposure with leaf position (Csepregi et al., 2017; Yoon et al., 2021a).

Ultraviolet-B-induced metabolic changes are multifaceted in terms of optical, morphological, and physiological factors; therefore, the use of UV-B radiation requires more precise manipulation to enhance the phenolic content (Schreiner et al., 2012). The actual dose perceived by the plant tissue depends not only on UV-B intensity from the light source but also on various optical factors and the morphological structure of the plant (Schreiner et al., 2012). Even under natural light, the attenuation of UV radiation in the plant canopy is affected by the spatial distribution and angle of the leaves, which are difficult to mathematically describe (Aphalo et al., 2012). Even without plants, lighting conditions with various optical factors, such as lighting distance, physical light distribution, and spectral power distribution of light sources, affect the spatial light distribution simulated in a growth chamber (Hitz et al., 2019). In addition, the simulated light absorbed by leaves depends on planting density and lighting arrangement as well as the three-dimensional (3D) structure of the plant in a controlled environment (Kim et al., 2020).

The developmental stage of plants is a strong determinant of the stress response and susceptibility to various environmental stresses (Rankenberg et al., 2021). In some cases, physiologically young leaves showed higher sensitivity to UV-B radiation, resulting in higher amounts of phenolics, higher AOC, or a higher expression of phenylpropanoid pathway genes (Majer and Hideg, 2012; Rizi et al., 2021). Furthermore, phenolic changes were more affected by the developmental stage than by UV-B levels in pak choi plants (Heinze et al., 2018). However, young leaves, typically located near the top of the plant, are exposed to targeted lighting conditions, while older leaves rely on light penetration in the 3D structure of plants. The effect of the developmental stage cannot be separated from the positional light-exposure effect. For experimental purposes, positional UV-exposure effects can be avoided by selecting plants with a 2D structure (Majer and Hideg, 2012; Csepregi et al., 2017). The UV dose absorbed by the leaves in the 3D structure has been attempted to be quantified through simulation with a 3D-scanned plant model, and the UV exposure and developmental effects could be separately analyzed (Yoon et al., 2021a,b).

For the application of UV-B radiation to phenolic production, a common strategy is to find a combination of UV-B-related factors, such as UV-B dose (fluence rate and duration), timing (plant developmental stage at which UV-B exposure is initiated), or wavelength/type of UV-B (Schreiner et al., 2009; Sun et al., 2010; Rechner et al., 2016; Dou et al., 2019). Traditional UV-B lamps are prone to causing photosynthetic damage to plants due to their broadband wavelength range, including shorter wavelengths close to UV-C (100–280 nm) and excessive and difficult-to-control energy (Mosadegh et al., 2019; Yoon et al., 2020). Recently, the performance of light-emitting diodes (LEDs) has advanced enough to provide light of the desired wavelength and intensity for plants (Kneissl et al., 2019; Loi et al., 2020; Paradiso and Proietti, 2021). Narrowband UV-B LEDs have also been applied at low doses to enhance health-promoting compound accumulation without damaging plants (Wiesner-Reinhold et al., 2021). Since the application of UV-B radiation incurs additional energy costs, either UV-B energy efficiency or maximum phenolic production should be pursued in controlled environmental agriculture. Prediction of UV-B-induced phenolic content will allow us to find the optimal UV-B conditions for maximizing phenolic production.

Statistical modeling has widely been used because it is simple but powerful for predicting and quantifying the relationship between variables (Kim et al., 2016). The plant developmental stage affects plant structures as well as their sensitivity to UV-B radiation (Yoon et al., 2021b). Thus, the phenolic production could be quantified with the modeling based on developmental age and UV-B radiation on the plant structure. This study focused on preharvest UV-B exposure as an elicitor for the biosynthesis of phenolics in non-acclimated plants to rule out possible UV-B acclimation effects (Liao et al., 2020). This study aimed to analyze UV-B-induced phenolic accumulation with preharvest UV-B exposure based on UV-B radiation interception and developmental stage of plants, and ultimately aimed to develop statistical models and investigate the UV-B energy yield for the phenolic accumulation. For this purpose, the contents of phenolics, flavonoids, anthocyanin, UV-absorbing pigments, and chlorophylls were evaluated in individual leaves with UV-B radiation interception simulated with 3D-scanned plant models according to growth stage.

MATERIALS AND METHODS

Plant Materials and Experimental Conditions

Kale (*B. oleracea* L. var. *acephala*) seeds were sown on sponge cubes in water culture under fluorescent lamps at a photosynthetic photon flux density (PPFD) of 150 μmol m^{-2} s^{-1} over the waveband 400–700 nm for a 16-h light period (Yoon et al., 2021a,b). After true leaves appeared, seedlings were supplied with a nutrient solution for *Brassica* modified from a previous study (Choi et al., 2005): N 137.8, P 30.9, K 140.9, Ca 104.6, Mg 54.8, Fe 2.76, Cu 0.02, Zn 0.05, Mn

0.68, B 0.50, and Mo 0.01 mg L^{-1}, at an electrical conductivity (EC) of 0.6 dS m^{-1}. After the fourth true leaf appeared, the seedlings of uniform size were transplanted into plant factory modules with a deep flow technique system. The modules were maintained at an air temperature of 19–22°C, relative humidity of 65–75%, a CO_2 concentration of 500 μmol mol^{-1}, an EC of 1.18–1.22 dS m^{-1}, and a pH of 6.8–7.0. The plants were irradiated with red, blue, and white LEDs at a PPFD of 255 μmol m^{-2} s^{-1} (at 7 cm from the center of the ground) for a 16-h light period. In kale plants grown in plant factories (Yoon et al., 2019) or fields (Hagen et al., 2009) under normal conditions, the concentration of bioactive compounds was not significantly different depending on the harvest time. Therefore, the harvest time was determined as 4 weeks when the total fresh mass reached around 100 *g*, which is sufficient for sale (**Supplementary Figure 1**). The four plants per treatment were harvested separately at 23, 30, and 38 days after transplanting (DAT).

For UV treatment, UV-B LEDs with a spectral peak at approximately 310 nm were used, and the irradiance at 7 cm above the center of the bottom was 3.0 W m^{-2}. The spectrum and intensity of photosynthetically active radiation (PAR) and UV-B LEDs were measured using a spectroradiometer (BlueWave spectrometer, StellarNet Inc., Tampa, FL, United States) in the range of 250–900 nm (**Figure 1A**). The plants at 23, 30, and 38 DAT were irradiated with UV-B LEDs for 6 or 12 h (UV6h or UV12h) and then harvested after recovery for 4 h. The UV6h and UV12h treatments corresponded to 15.6 and 31.3 kJ m^{-2} day^{-1} biologically effective UV-B radiation ($UV\text{-}B_{BE}$), respectively, calculated using a biological spectral weighting function for plants (Flint and Caldwell, 2003). The arrangements of PAR and UV-B LEDs are shown in **Figure 1B**.

Three-Dimensional-Scanning to Optical Simulation for Radiation Interception Analysis

Ultraviolet radiation interception analysis with a 3D-scanned plant model and ray-tracing simulation was performed as previously described (Kim et al., 2020; Yoon et al., 2021a; **Figure 2**). In brief, plant models were directly obtained using a high-resolution portable 3D scanner (Go! SCAN50TM, Creaform Inc., Lévis, QC, Canada) and its software (Vxelement, Creaform Inc.). Four plants per treatment were 3D-scanned after the UV treatment at 23, 30, and 38 DAT. After repair for holes and noise, the 3D mesh data were segmented into leaf mesh data and reconstructed into individual surface models using reverse engineering software (Geomagic Design X, 3D Systems, Rock Hill, SC, United States). The virtual plant factory modules based on the dimensions measured were constructed using 3D computer-aided design software (Solidworks, Dassault Systèmes, Vélizy-Villacoublay, France). The 3D model arrangement and simulation parameters, including the optical properties of materials and plants, and the setting of light sources and detectors, are described in **Figure 2**. All 3D models were placed in the same position and orientation as the actual materials and plants. The ray-tracing simulation was performed using ray-tracing software (Optisworks, Optis Inc., La Farlède, France). The daily UV-B radiation interception on individual leaves was calculated from the simulation results with UV-exposure durations.

Growth Characteristics

Growth parameters, including total fresh mass, total leaf area, and root dry mass, were measured as shown in **Supplementary Figure 1**. Fresh masses of individual leaves were measured separately at harvest with four plants per treatment (**Supplementary Figure 2**). After photographing all leaves, the areas of individual leaves were calculated with an image analysis software (ImageJ 1.53, National Institutes of Health, Bethesda, MD, United States). Leaf order was determined as an absolute order of emergence (the first true leaf was set as 1) and was numbered from the oldest leaf at the bottom to the youngest at the top of the plant. Leaf groups at each growth stage were determined based on the relative growth rate of individual leaves, which are shown in **Supplementary Figure 3** and **Supplementary Table 1** (Behn et al., 2011; Pontarin et al., 2020). Leaf groups 1, 2, and 3 corresponded to leaf orders 1–3, 4–7, and 8–11, respectively, at 23 DAT, leaf orders 3–6, 7–9, and 10–14, respectively, at 30 DAT, and leaf orders 4–8, 9–12, and 13–18, respectively, at 38 DAT.

Phenolic Content, Antioxidant Capacity, and Photosynthetic Pigment Content

Sample Preparation

The whole leaves were sampled separately at harvest and frozen at −80°C. After lyophilization with a freeze dryer (FD8512, Ilshin Biobase Co., Yangju, South Korea) at −80°C under a vacuum of 0.007 mm Hg for 120 h, the leaf dry mass was determined. The lyophilized sample was pulverized in liquid nitrogen using a cryogenic grinder (SPEX 6875D Freezer/Mill, SPEX SamplePrep, Metuchen, NJ, United States), and then stored in the dark at 4°C until needed for analysis. The freeze-milled samples used for the analysis corresponded to leaf orders 5–9, 5–13, and 5–17 at 23, 30, and 38 DAT, respectively.

Total Phenolic Content and Total Flavonoid Content

For determining Total phenolic content (TPC) and total flavonoid content (TFC), aliquots of the powdered sample (50 mg) were mixed with 1 ml of 80% (v/v) methanol, incubated in the dark at 4°C for 18 h, and then centrifuged at 11,000 × *g* at 4°C for 10 min. TPC was determined according to the Folin–Ciocalteu colorimetric method (Ainsworth and Gillespie, 2007). The supernatant of 100 μl was collected in a 2-ml tube and mixed with 200 μl of 10% (v/v) Folin–Ciocalteu solution (Junsei Chemical Co., Ltd., Tokyo, Japan), and 400 μl of distilled water. After vortex mixing, 800 μl of 700 mM Na_2CO_3 was added. The mixture was shaken for 10 s and incubated in a water bath at 45°C for 15 min. The absorbance was read at 765 nm using a spectrophotometer (Photolavis, WTW,

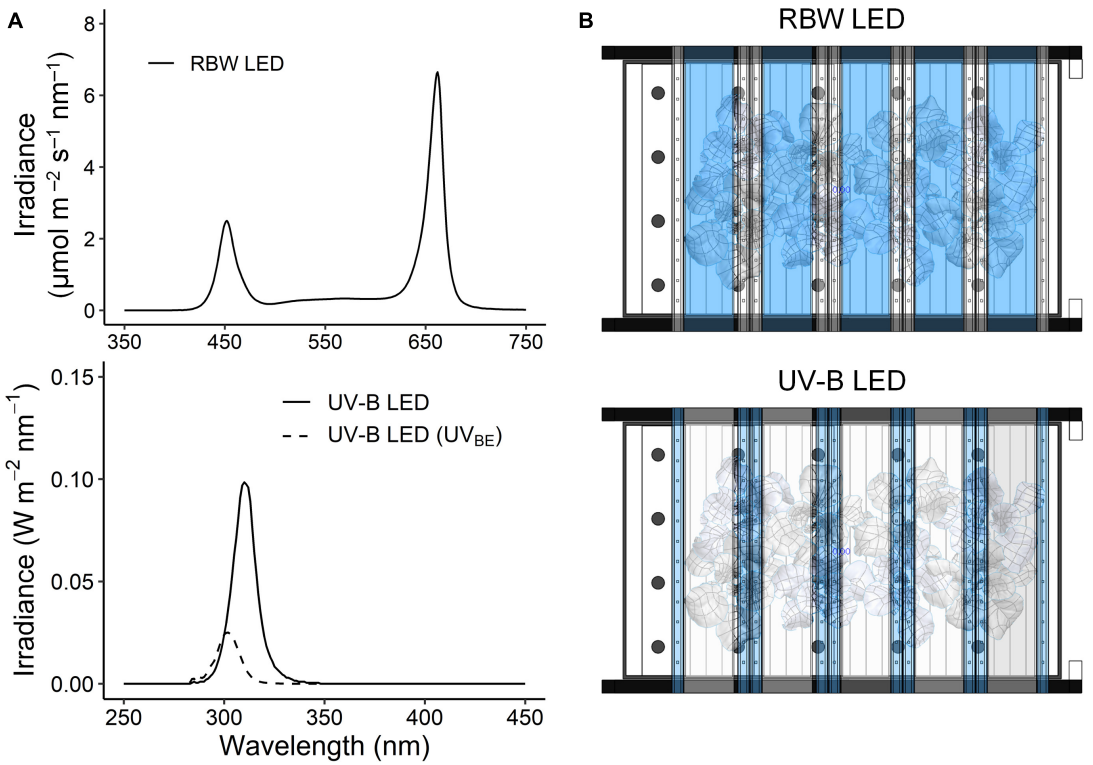

FIGURE 1 | Spectra **(A)** and arrangement **(B)** of red, blue, and white light-emitting diodes (RBW LED) and UV-B LED used in the plant factory. The irradiance of UV-B LEDs with a spectral peak at about 310 nm was 3.0 W m^{-2} at 280–400 nm. UV-B_{BE} indicates biologically effective UV-B calculated using a biological spectral weighting function for plants (Flint and Caldwell, 2003), and thereby its spectral peak was at about 302 nm. The RBW LEDs irradiated at a photosynthetic photon flux density of 255 μmol m^{-2} s^{-1}.

Weilheim, Germany), and the TPC was expressed as milligrams of gallic acid (Sigma–Aldrich Chemical Corp., St. Louis, MO, United States) equivalent per gram of dry mass (mg GAE g^{-1} DM). TFC was determined according to the aluminum chloride colorimetric method (Dewanto et al., 2002). The supernatant of 100 μl was collected in a 2-ml tube, and mixed with 500 μl of distilled water and 30 μl of 5% (w/v) $NaNO_2$. After 6 min, 60 μl of 10% (w/v) $AlCl_3$ was added. After 5 min, 200 μl of 1 M NaOH and 110 μl of distilled water were added, and all reactants were thoroughly mixed. After incubating for 5 min, the absorbance was read at 510 nm, and the TFC was expressed as milligrams of catechin acid (Supelco, Bellefonte, PA, United States) equivalent per gram of dry mass (mg CE g^{-1} DM).

Total Anthocyanin Content and UV-Absorbing Pigment Content

For determining total anthocyanin content (TAC) and UV-B absorbing pigment content (UAPC), the aliquots of the powdered sample (20 mg) were mixed with 1 ml of 1% acidified methanol, incubated in the dark at 4°C for 48 h, and then centrifuged at 11,000 × *g* at 4°C for 15 min. The supernatant of the extract was diluted two-fold, and the absorbance was read at 530 and 657 nm (A_{530} and A_{657}, respectively). TAC was determined with the corrected absorbance as A_{530}, $0.25A_{657}$ (Sytar et al., 2018) and expressed as milligrams of cyanidin 3-glucoside (Sigma–Aldrich Chemical Corp.) equivalent per gram of dry mass (mg C3GE g^{-1} DM). The supernatant of the extract was diluted 20-fold, and the absorbance was read at 285 and 330 nm (Si et al., 2015; Khudyakova et al., 2019). UAPC was determined as the average of two absorbances and expressed as an absorbance per gram of dry mass (OD g^{-1} DM).

Antioxidant Capacity

Antioxidant capacity can be determined depending on the choice of the assay, and analyzing phenol-rich samples by a single assay is recommended to be avoided (Csepregi et al., 2016). Thus, both the 2, 2'-azino-bis (3-ethylbenzothiazoline-6-sulfonic acid)-diammonium salt (ABTS) assay and the 2, 2-diphenyl-1-picrylhydrazyl (DPPH) assay were performed. The powdered sample of 50 mg was mixed with 1 ml of 80% (v/v) methanol, and the mixture was incubated in the dark at 4°C for 42 h and then centrifuged at 11,000 × *g* at 4°C for 10 min. The ABTS radical scavenging activity was determined as described by Re et al. (1999). Briefly, the ABTS radical cation ($ABTS^+$) reagent was produced by reacting 7 mM ABTS solution (Sigma–Aldrich Chemical Corp.) with 2.45 mM $K_2S_2O_8$ (1:1, v/v), and stored in the dark at 4°C for 18 h before use. The $ABTS^+$ solution was diluted with 80% methanol to obtain appropriate absorbance. The supernatant of 50 μl was added to 1.8 ml of diluted $ABTS^+$ solution. After 6 min of incubation in the dark

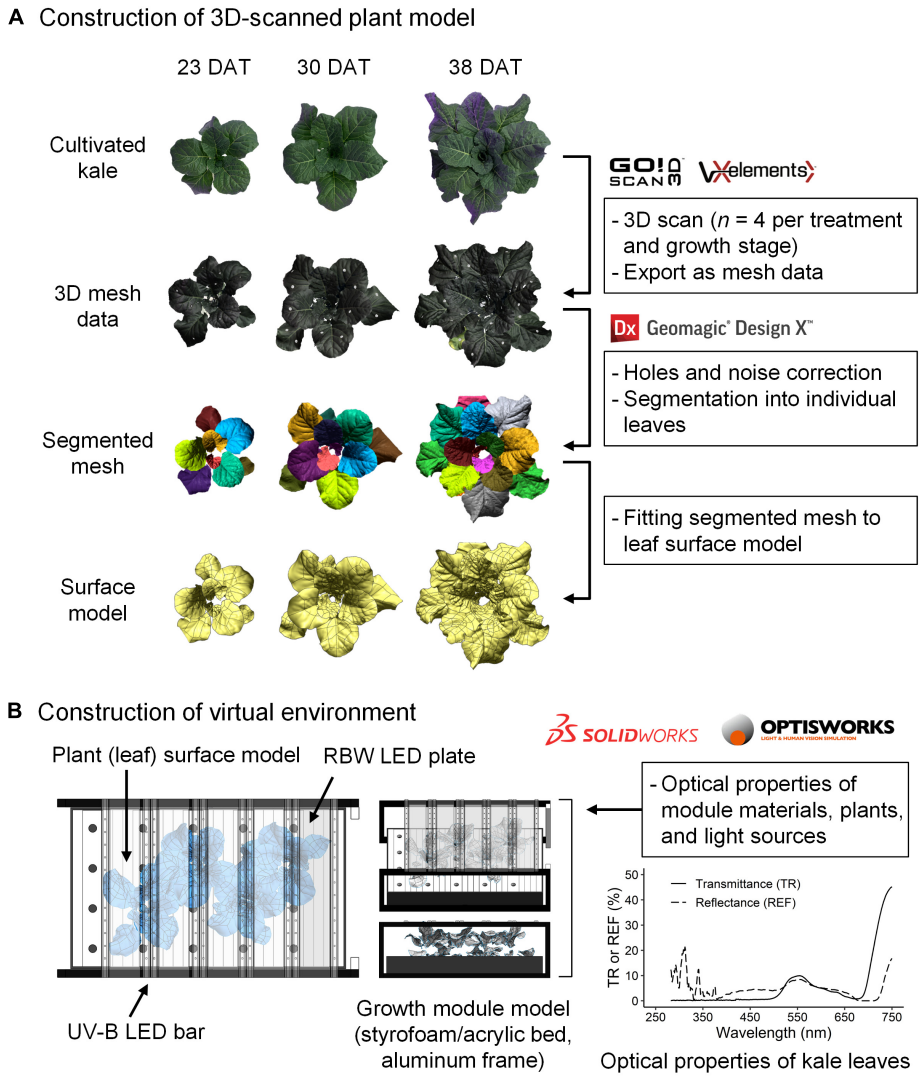

Light sources	UV-B LED bar (12 chips) × 10 bars
Spectral power distribution	Spectrum in Figure 1
Physical light distribution	Lambertian distribution with a half angle of 60°
Energy output	0.02139 W for each chip
Number of rays	1 Giga-rays
Detector	All leaf surface model

FIGURE 2 | Schematic diagram of 3D scanning to optical simulation for radiation interception analyzed in kale plants. After the construction of a 3D-scanned plant model **(A)**, the virtual environment for simulation **(B)** consisted of a 3D model of the growth module, light sources, and plants with actual dimensions and arrangement. A ray-tracing simulation **(C)** was conducted with these parameters. TR, transmittance; REF, reflectance.

at room temperature, the absorbance was read at 734 nm. The DPPH radical scavenging activity was determined as described by Brand-Williams et al. (1995). DPPH was purchased from Alfa Aesar (Ward Hill, MA, United States), and the DPPH solution was freshly made in methanol before use. The supernatant of 100 μl was added to 1.8 ml of 0.12 mM DPPH methanol solution. After incubation in the dark at room temperature for 30 min, the absorbance was read at 517 nm. A calibration curve for ABTS and DPPH assays was constructed using L-ascorbic acid (Samchun Pure Chemical Co., Ltd., Pyeongtaek, South Korea). The AOC_{ABTS} and AOC_{DPPH} were expressed as milligrams of ascorbic acid equivalent per gram of dry mass (mg AAE g^{-1} DM).

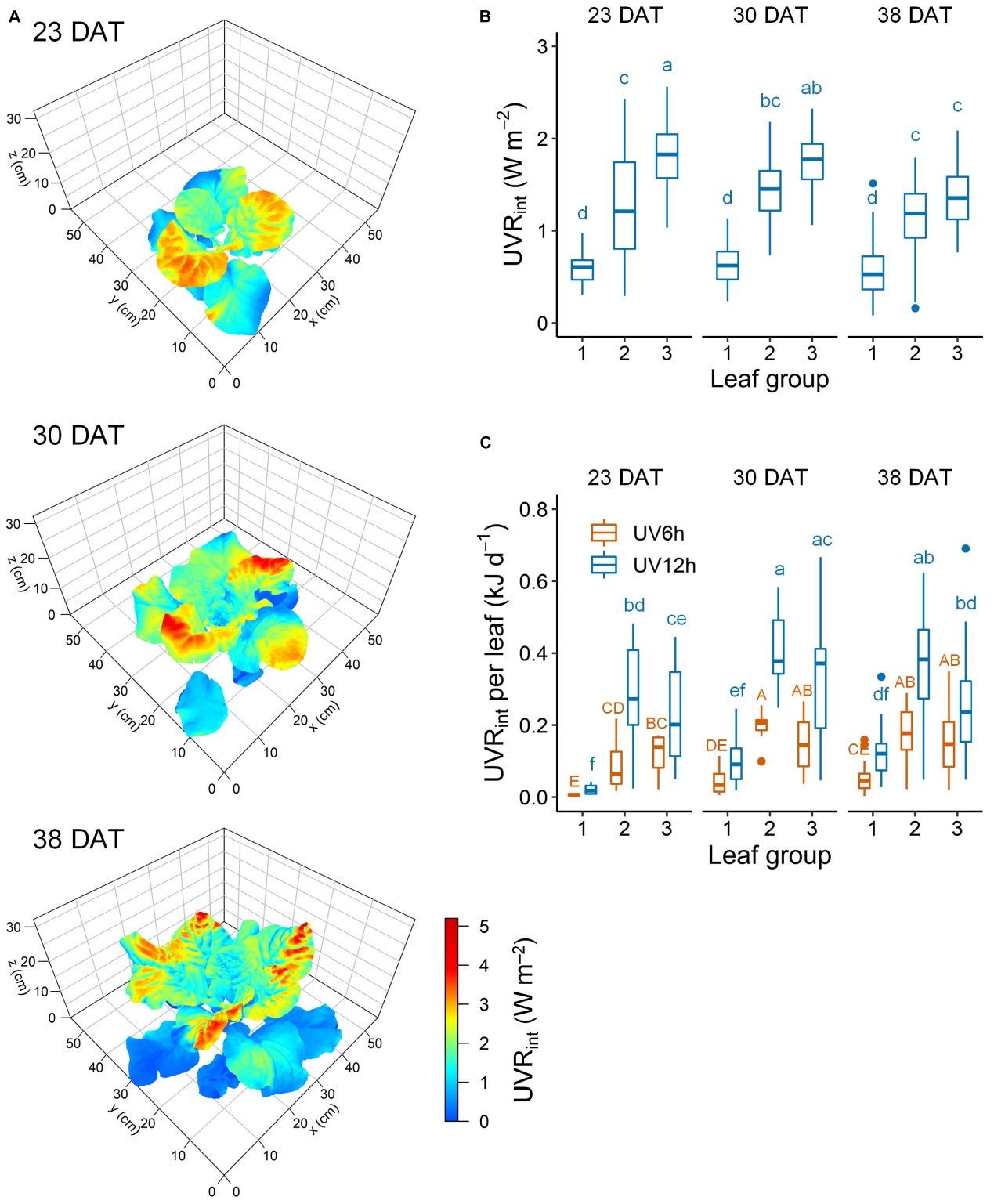

FIGURE 3 | Representative simulated UV-B radiation interception (UVR_{int}) on 3D-scanned models **(A)**, mean UVR_{int} **(B)**, and daily UVR_{int} per leaf **(C)** of kale plants according to UV-B radiation and leaf group at 23, 30, and 38 days after transplanting (DAT). Leaf groups were determined according to the order of leaf emergence and their relative growth state (**Supplementary Figure 3** and **Supplementary Table 1**). Different letters indicate significant differences at $P < 0.05$ for UVR_{int} value (n = 26–47) and daily UVR_{int} per leaf (n = 11–25) with growth stage and leaf group by two-way ANOVA and Tukey's HSD test.

Photosynthetic Pigment Content

For determining photosynthetic pigment, the aliquots of the powdered sample (50 mg) were mixed with 1 ml of 80% (v/v) acetone, incubated in the dark at room temperature for 24 h, and then centrifuged at 11,000 × *g* for 10 min. Chlorophyll *a*, Chlorophyll *b*, and carotenoid contents were calculated based on absorbance at 663, 647, and 470 nm according to the method of Lichtenthaler and Buschmann (2001) and expressed as milligrams of chlorophyll or carotenoid per gram of dry mass (mg g^{-1} DM).

Multiple Regression Model and Ultraviolet-B Yield

Total phenolic content, TFC, TAC, UAPC, and AOC per leaf were calculated by multiplying their concentrations (mg eq. g^{-1} DM) by the leaf dry mass (g DM). Stepwise multiple linear regressions were used to develop statistical models for predicting phenolic accumulation. The model was obtained by stepwise regression using the backward elimination method based on a second-order multi-polynomial (quadratic) model, including the single effect of leaf order and UV radiation interception and the interaction effect:

$$\mathbf{M}(\mathbf{L},\mathbf{U}) = \boldsymbol{\beta}_0 + \boldsymbol{\beta}_1\mathbf{L} + \boldsymbol{\beta}_2\mathbf{L}^2 + \boldsymbol{\beta}_3\mathbf{U} + \left(\boldsymbol{\beta}_4\mathbf{L} + \boldsymbol{\beta}_5\mathbf{L}^2\right)\mathbf{U} \quad (1)$$

where *M* is the phenolic content per leaf (mg eq. per leaf), *L* is leaf order numbered as an absolute order of leaf emergence, *U* is the daily UV radiation interception per leaf (kJ day^{-1} per leaf), and β_0–β_5 are the regression coefficients obtained by the regression analysis at each growth stage. The UV-B energy yield for phenolic accumulation per leaf was determined as the change in the phenolic content per absorbed UV-B energy and calculated as the slope of the multiple regression surface against UV interception as follows:

$$\mathbf{Y}(\mathbf{L},\mathbf{U}) = [\mathbf{M}(\mathbf{L},\mathbf{U}) - \mathbf{M}(\mathbf{L},\mathbf{0})]/\mathbf{U} = \boldsymbol{\beta}_3 + \boldsymbol{\beta}_4\mathbf{L} + \boldsymbol{\beta}_5 \quad (2)$$

where *Y* is UV-B energy yield for phenolic accumulation per leaf (mg eq. kJ^{-1} day) at each *L* and *U*.

Statistical Analysis

For all data, the homogeneity of variance was evaluated using Levene's test, and the normality was evaluated using the Shapiro–Wilk test. The mean values were compared using one-way or two-way ANOVA and Tukey's honestly significant difference (HSD) test to assess the effects of the UV-B treatment (control, UV6h, and UV12h), leaf group 1–3, or growth stage (23, 30, and 28 DAT). For data that failed the normality test, the Kruskal–Wallis and Dunn's tests were used, and for data that failed the homogeneity of variance, the Welch's ANOVA and Games-Howell tests were used.

For model development, nine plants per growth stage were used for the data set, which corresponded to a total of 250 data points, including 66, 74, and 110 data points at 23, 30, and 38 DAT, respectively, after removing outliers with the interquartile range. For accuracy of the multiple regression model, a data set (not used to develop the model) including nine plants and 76 data points was used for validation. The coefficient of determination (R^2), root mean squared error (RMSE), and normalized RMSE were selected. All visualization and statistical

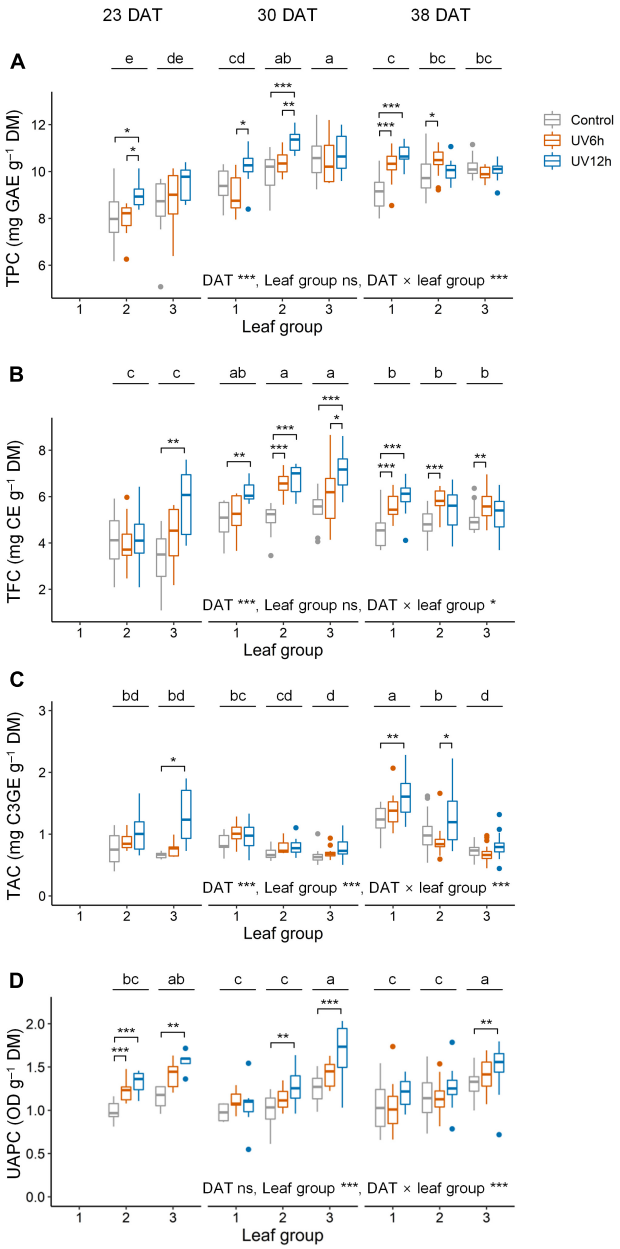

FIGURE 4 | Total phenolic content (TPC, **A)**, total flavonoid content (TFC, **B)**, total anthocyanin content (TAC, **C)**, and UV-absorbing pigment content (UAPC, **D)** in individual leaves of kale plants according to UV-B radiation and leaf group at 23, 30, and 38 days after transplanting (DAT). Leaf groups were determined according to the order of leaf emergence and their relative growth state (**Supplementary Figure 3** and **Supplementary Table 1**). Asterisks indicate significant differences between UV-B treatments at each growth stage and leaf group by one-way ANOVA and *post-hoc* test, $^*P < 0.05$; $^{**}P < 0.01$; $^{***}P < 0.001$; $n = 7$–22. Different letters indicate significant differences among growth stage and leaf group at $P < 0.05$ by two-way ANOVA and *post-hoc* test ($n = 22$–59) referring to the "Materials and Methods" section.

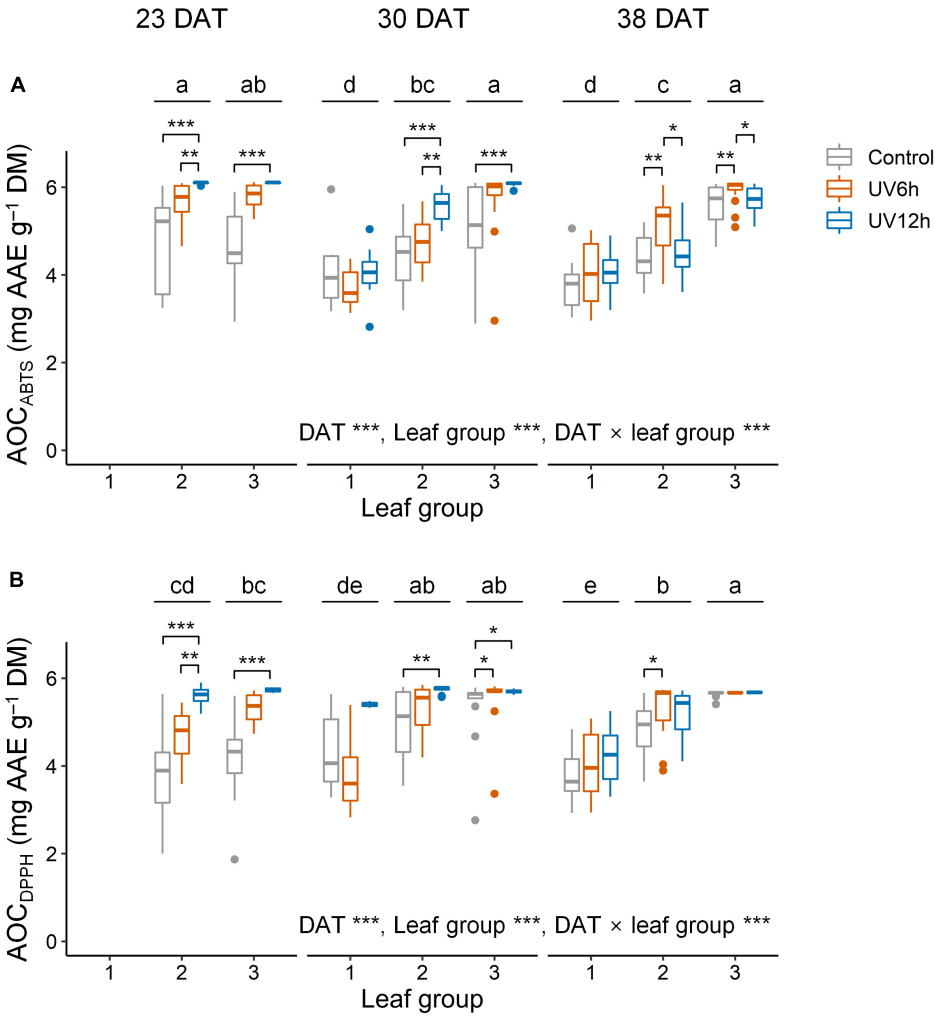

FIGURE 5 | Antioxidant capacity using ABTS (AOC_{ABTS}, **A)** and DPPH assays (AOC_{DPPH}, **B)** in individual leaves of kale plants according to UV-B radiation and leaf group at 23, 30, and 38 days after transplanting (DAT). Leaf groups were determined according to the order of leaf emergence and their relative growth state (**Supplementary Figure 3** and **Supplementary Table 1**). Asterisks indicate significant differences between UV-B treatments at each growth stage and leaf group by one-way ANOVA and *post-hoc* test, $^{*}P < 0.05$; $^{**}P < 0.01$; $^{***}P < 0.001$; $n = 7$–22. Different letters indicate significant differences among growth stage and leaf group at $P < 0.05$ by two-way ANOVA and *post-hoc* test ($n = 22$–59) referring to the "Materials and Methods" section.

analyses were performed using R software (R 4.0.2, R Foundation, Vienna, Austria).

RESULTS

Ultraviolet-B Radiation Interception According to Leaf Group and Growth Stage

Ultraviolet-B radiation interception with a 3D-scanned plant model was simulated along with the actual plant structure at each growth stage (**Figure 3A**). The UV radiation interception (UVR_{int}) was significantly higher in the order of leaf groups 3, 2, and 1 (**Figure 3B**). Across all stages, the UVR_{int} was significantly lower by 51.7% in leaf group 1 and significantly higher by 31.4% in group 3 than in group 2. At 23, 30, and 38 DAT, the mean UVR_{int} was 1.20, 1.28, and 1.05 W m^{-2}, respectively. The daily UVR_{int} per leaf did not significantly differ between the leaf groups 2 and 3 and was affected by individual leaf area (**Figure 3C**). Across all data, the daily UVR_{int} per plant was significantly higher with growth stage (1.7 ± 0.5, 2.2 ± 0.3, and 2.6 ± 0.4 kJ day^{-1} per plant at 23, 30, and 38 DAT, respectively).

Age-Dependent Changes in Phenolic Content According to Ultraviolet-B Radiation

Total phenolic content, TFC, TAC, and UAPC were significantly affected by UV-B radiation, growth stage, and leaf groups (**Figure 4**). Across all data, the contents of all the compounds were significantly higher in the UV12h treatment than in the control. TPC and TFC were significantly higher in the order of

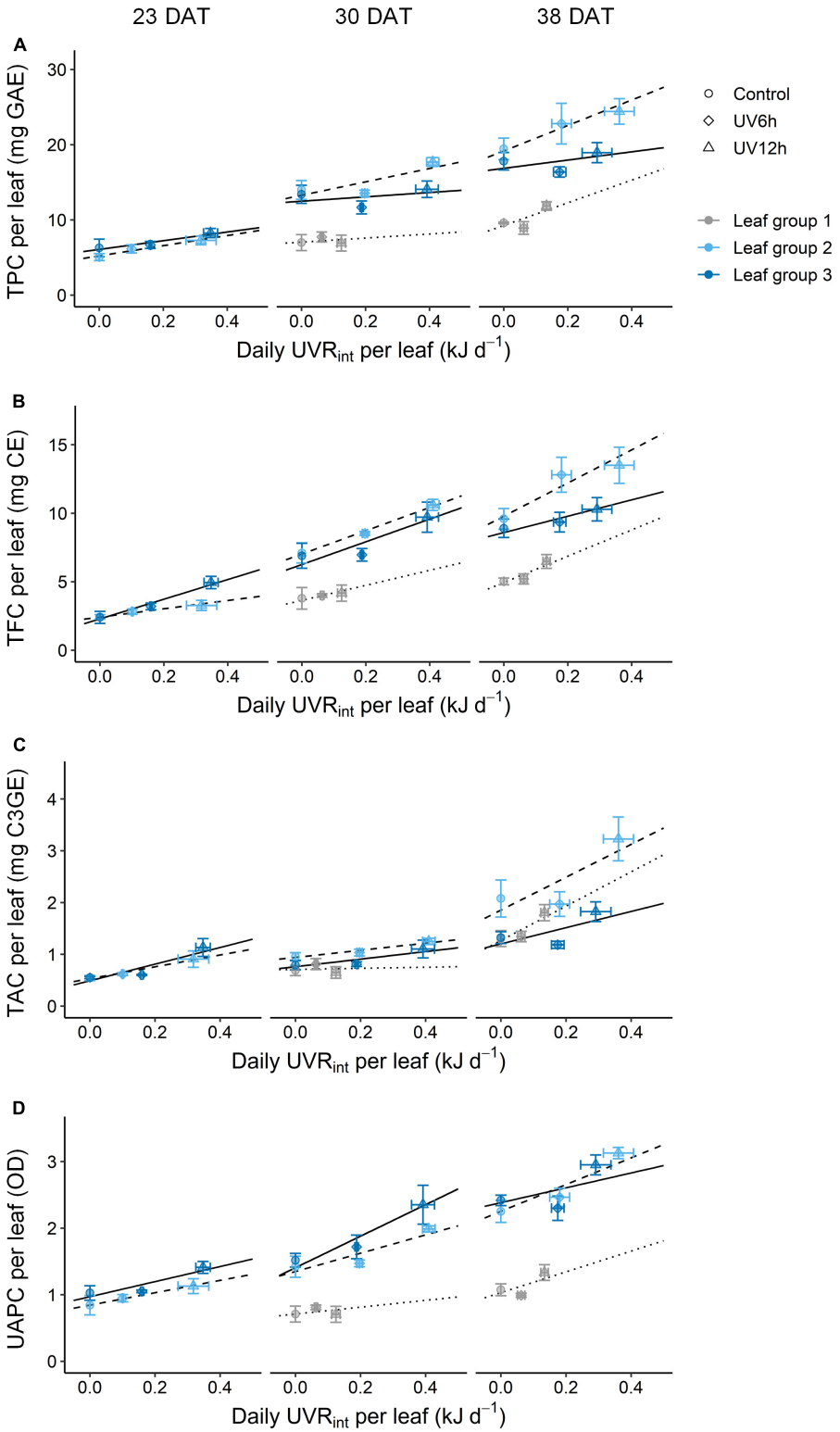

FIGURE 6 | Relationships between phenolic content and the daily UV-B radiation interception (UVR_{int}) per leaf of kales according to leaf group at 23, 30, and 38 days after transplanting (DAT); total phenolic content (TPC, **A)**, total flavonoid content (TFC, **B)**, total anthocyanin content (TAC, **C)**, and UV-absorbing pigment content (UAPC, **D)** in individual leaves. Leaf groups were determined according to the order of leaf emergence and their relative growth state (**Supplementary Figure 3** and **Supplementary Table 1**). The vertical and horizontal bars indicate SE (n = 4). The lines show linear fits of the leaf group 3, 2, and 1 data sets (solid, dashed, and dotted lines).

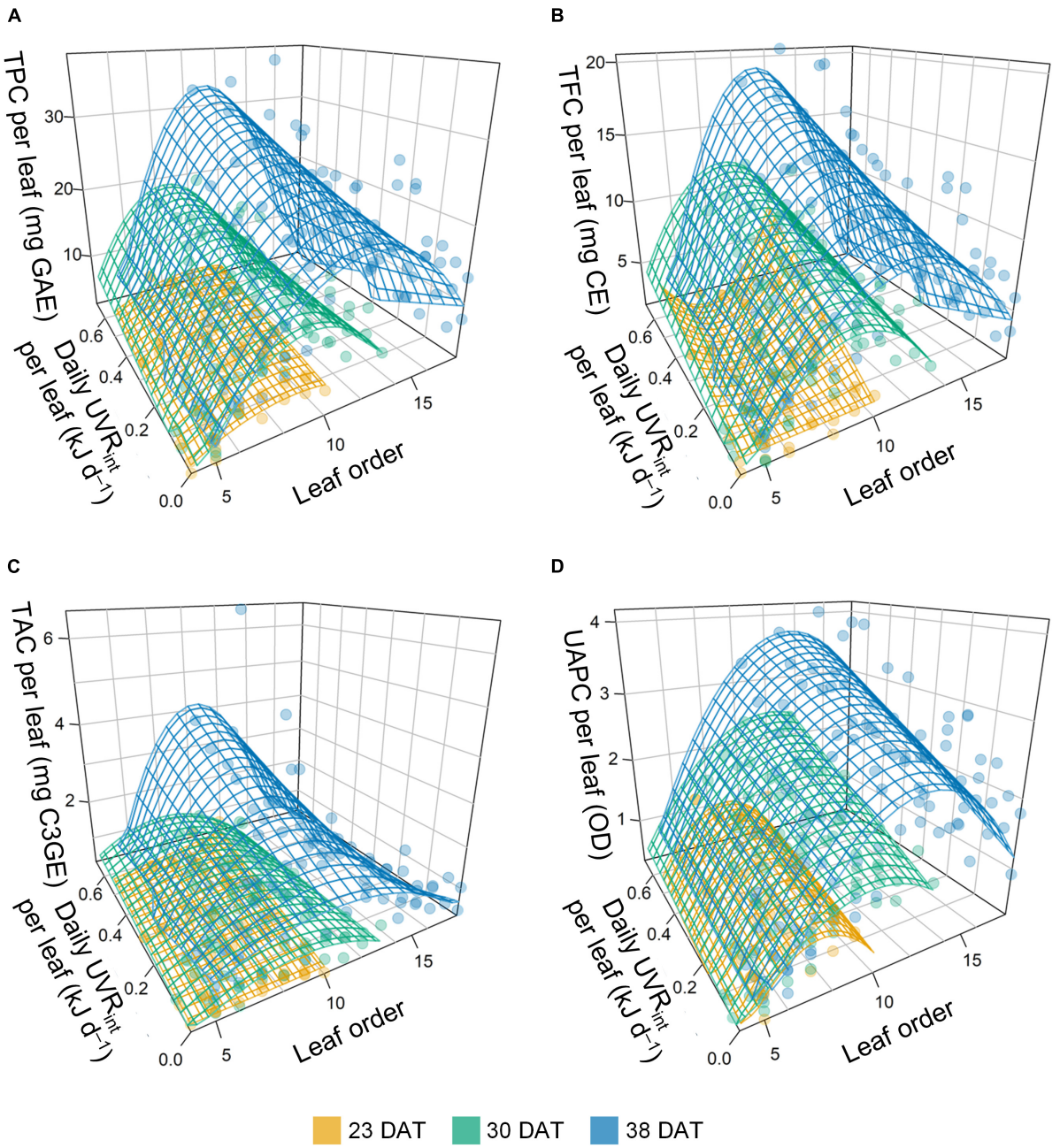

FIGURE 7 | Stepwise multiple linear regression model for phenolic content per leaf of kale plants with daily UV-B radiation interception (UVR_{int}) per leaf and leaf order at 23, 30, and 38 days after transplanting (DAT): TPC, total phenolic content **(A)**; TFC, total flavonoid content **(B)**; TAC, total anthocyanin content **(C)**; and UAPC, UV-absorbing pigment content **(D)**. The surfaces were obtained by stepwise multiple regression models referring to Eq. 1 and **Table 1**.

30, 38, and 23 DAT. They were the highest in leaf groups 2 and 3 at 30 DAT, respectively, in UV12h treatment (13.2 and 31.6% higher, respectively, than in the control).

Antioxidant capacity using ABTS and the AOC_{DPPH} were significantly higher in the UV12 treatment and leaf group 3 than in the others (**Figure 5**). The AOC_{ABTS} and AOC_{DPPH} were positively correlated with the UAPC, and their Pearson's correlation coefficients were 0.69 and 0.62, respectively, at $P < 0.001$ (data not shown). In contrast, the UAPC, AOC_{ABTS}, and AOC_{DPPH} were significantly higher in the order of leaf groups 3, 2, and 1, and the TAC was significantly higher in the reverse order. The UAPC was the highest in leaf group 3 at 30 DAT in the UV12h treatment (34.2% higher than in the control).

The TPC, TFC, TAC, and UAPC in individual leaves were increased with daily UVR_{int} per leaf, and the slopes were dependent on growth stage and leaf group (**Figure 6**). The slopes,

i.e., the increase rates of TPC and TFC with daily UVR_{int} per leaf in individual leaves, were highest in leaf group 2 at 38 DAT, followed by 30 DAT. Those of TPC and TFC in individual groups were increased as growth progressed. In contrast, the increase rates of TAC and UAPC were the highest in leaf group 3 at 23–30 DAT, and those were lower in leaf group 3 than in the others at 38 DAT.

Prediction Models of Phenolic Content Based on Ultraviolet-B Radiation Interception and Leaf Order According to Growth Stage

Multiple regression models for the phenolic contents per leaf were developed based on daily UVR_{int} per leaf and leaf order according to growth stage, and all models were significant at $P < 0.001$ (**Figure 7** and **Table 1**). The models for the TPC, TFC, and UAPC in individual leaves at each growth stage showed a high explanatory power, with $R^2 = 0.62–0.79$. However, the models for the TAC per leaf showed a low explanatory power, with $R^2 < 0.51$. All estimated coefficients were significant for the regression models. From the models, the spatial and intraindividual distributions of TPC and TFC on the 3D-scanned plant model were estimated (**Figure 8**). The R^2 values for the four models were higher in the data set integrated from the models across the whole growth stage than in the models at each growth stage (**Table 1** and **Supplementary Figure 5**).

The accuracies of the models for TPC, TFC, TAC, and UAPC per leaf were validated using test data sets (**Figure 9**). All models performed well for the whole growth stage, with $R^2 = 0.78–0.79$. The TPC, TFC, and UAPC models showed high performance with $R^2 > 0.7$, except for those at 23 DAT. The TAC model showed high performance with $R^2 > 0.6$ at all growth stages. The TPC model for the whole growth stage showed approximately 22.8% relative error, meaning that the model could predict the TPC per leaf with 77.2% accuracy during 23–38 DAT. Likewise, the models could predict TFC, TAC, and UAPC per leaf with 73.2, 75.0, and 64.9% accuracy, respectively, during 23–38 DAT.

Ultraviolet-B Energy Yields for Phenolic Content With Growth Stage

The UV-B energy yields for the TPC, TFC, TAC, and UAPC based on absorbed UV energy were significantly different depending on the growth stage and leaf group (**Table 2**).

The UV-B energy yields for the TPC and TFC significantly increased as growth progressed and were higher in leaf group 2 than in the others. As growth progressed, the UV-B energy yields for TPC and TFC decreased in leaf group 3 but increased in leaf group 2. Those for TPC and TFC were the highest in leaf group 2 at 38 DAT. The UV-B yield for the UAPC in both leaf groups 2 and 3 increased significantly as growth progressed and was the highest in leaf group 3 at 38 DAT. The UV-B energy yields for TAC were the highest in leaf group 2 at 38 DAT.

DISCUSSION

Narrowband Ultraviolet-B Radiation on Plants

Variables affecting the perception of UV-B radiation by plants, such as dose (fluence rate and duration), timing during a day or growth stages, light sources (solar, broadband, or narrowband UV lamp), and setup (greenhouse or chamber),

TABLE 1 | Stepwise multiple linear regression results and models to predict phenolic content per leaf of kale plants at 23, 30, and 38 days after transplanting (DAT) based on leaf order (*L*) and daily UV-B radiation interception per leaf (*U*) referring to Eq. 1.

Model	DAT	R^2	Adj R^2	RMSE	NRMSE (%)	*p-value*	Model equation
TPC	23	0.63	0.61	1.23	17.3	<0.001	$M(L, U) = -5.01 + 2.72\,L - 0.16L^2 + 6.54U$
	30	0.77	0.76	2.17	18.4	<0.001	$M(L, U) = -25.29 + 8.30\,L - 0.44L^2 + (4.54\,L - 0.38L^2)U$
	38	0.72	0.70	3.90	22.3	<0.001	$M(L, U) = -26.03 + 7.62\,L - 0.31L^2 - 73.52\,U + (17.18\,L - 0.80L^2)U$
	Integration	0.83		2.91	22.2		
TFC	23	0.62	0.60	0.73	21.4	<0.001	$M(L, U) = 2.42 + 39.67\,U + (-12.02\,L + 0.96L^2)U$
	30	0.78	0.77	1.35	19.6	<0.001	$M(L, U) = -3.38 + 4.52\,L - 0.25L^2 + (2.34\,L - 0.15L^2)U$
	38	0.74	0.73	2.16	23.3	<0.001	$M(L, U) = -12.23 + 3.80\,L - 0.16L^2 - 47.53\,U + (10.88\,L - 0.49L^2)U$
	Integration	0.83		1.65	23.5		
TAC	23	0.39	0.38	0.25	34.4	<0.001	$M(L, U) = 0.48 + 0.18LU$
	30	0.46	0.43	0.24	26.0	<0.001	$M(L, U) = -1.21 + 0.48\,L - 0.03L^2 + (0.30\,L - 0.03L^2)U$
	38	0.51	0.48	0.65	36.9	<0.001	$M(L, U) = -0.44 + 0.41\,L - 0.02L^2 - 17.19\,U + (3.92\,L - 0.19L^2)U$
	Integration	0.66		0.47	37.9		
UAPC	23	0.63	0.59	0.20	17.9	<0.001	$M(L, U) = -3.18 + 1.13\,L - 0.08L^2 + 1.05U$
	30	0.79	0.78	0.25	17.7	<0.001	$M(L, U) = -1.78 + 0.64\,L - 0.03L^2 + 0.17LU$
	38	0.72	0.71	0.48	23.1	<0.001	$M(L, U) = -3.67 + 0.99\,L - 0.04L^2 + 0.14LU$
	Integration	0.79		0.38	22.6		

TPC, total phenolic content per leaf (mg GAE per leaf); TFC, total flavonoid content per leaf (mg CE per leaf); TAC, total anthocyanin content per leaf (mg C3GE per leaf); and UAPC, UV-absorbing pigment content per leaf (OD per leaf).

R^2, the coefficient of determination; Adj R^2, adjusted R^2; RMSE, root mean squared error; and NRMSE, normalized RMSE (%).

Integration indicates results in the data set across all growth stages integrated from the models at each growth stage.

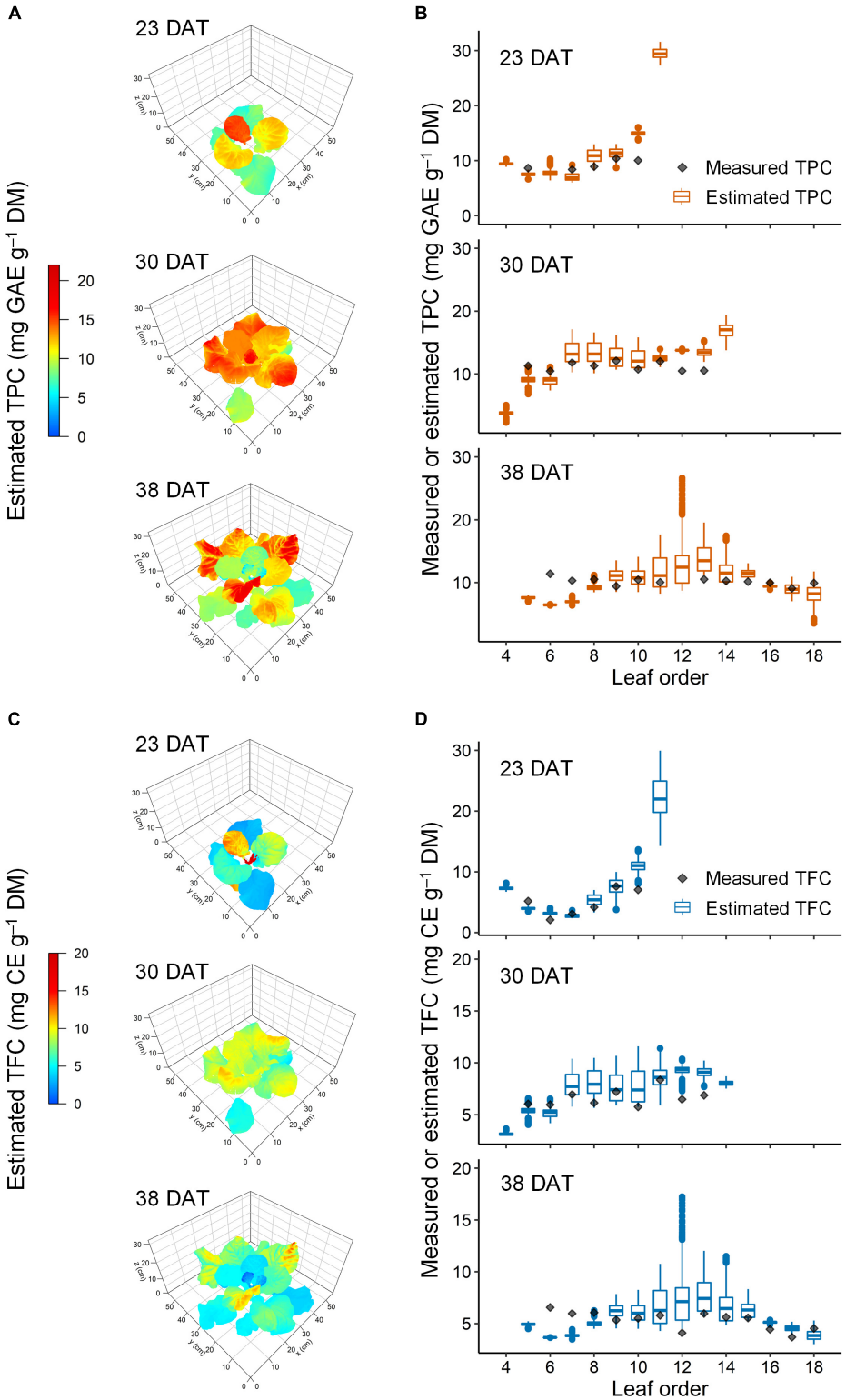

FIGURE 8 | Representative estimated distribution of total phenolic content (TPC, **A,B)** and total flavonoid content (TFC, **C,D)** in the leaves of kale plants under 12-h UV-B exposure at 23, 30, and 38 days after transplanting (DAT). The multiple regression models refer to in **Figure 4** and **Table 1**, and the 3D-scanned plant model refers to in **Figure 3**.

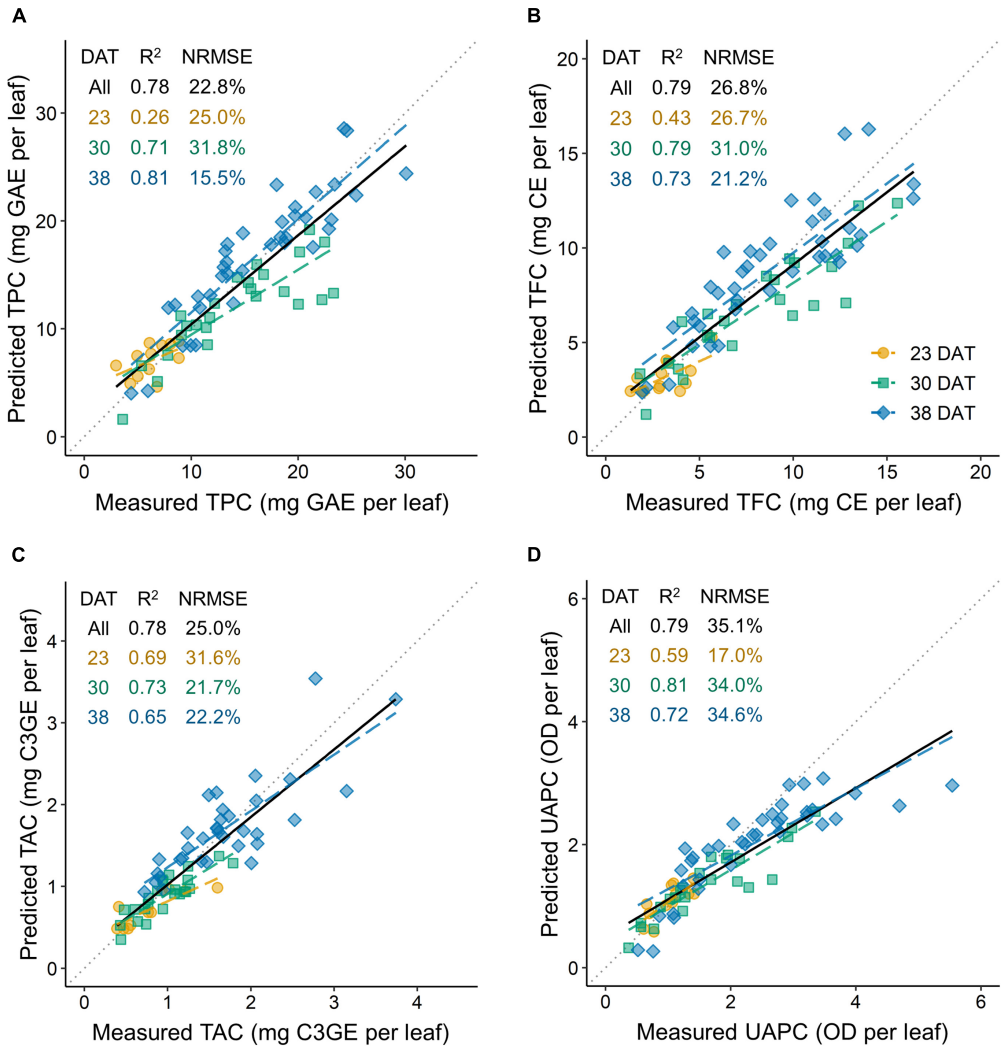

FIGURE 9 | Model accuracy for predicting phenolic content per leaf of kale plants using a test data set: TPC, total phenolic content per leaf **(A)**; TFC, total flavonoid content per leaf **(B)**; TAC, total anthocyanin content per leaf **(C)**; and UAPC, UV-absorbing pigment content per leaf **(D)**. The coefficient of determination (R^2) and the normalized root mean squared error (NRMSE) are presented inside each panel. The multiple regression models at 23, 30, and 38 days after transplanting (DAT) are shown in **Figure 4** and **Table 1**. All in DAT indicate the results in the data set across all growth stages integrated from the models at each growth stage.

make it hard to define the intensity or dose thresholds of UV-B radiation (Meyer et al., 2021). This confusion without coherence hampers understanding of plant physiology as well as commercial use of bioactive compound production. High doses of UV-B (high fluence rate, long duration, or shorter wavelength) cause metabolic disorders, such as chlorophyll degradation and the generation of reactive oxygen species (ROS), supporting the long-held opinion that UV-B radiation is harmful to plants (Jordan, 2002). Recent studies have highlighted the regulatory properties of moderate UV-B radiation (low and ecologically relevant level or longer wavelength) as a eustressor and numerous acclimation strategies, including changes in secondary metabolism (Hideg et al., 2013; Neugart and Schreiner, 2018). In general, plants perceive UV-B radiation by the specific receptor UV RESISTANCE LOCUS 8 (UVR8), leading to signal transduction of UVR8-COP1 (CONSTITUTIVE PHOTOMORPHOGENESIS1) with ELONGATED HYPOCOTYL5 (HY5) and HY5 HOMOLOG (HYH) transcription factors (Liang et al., 2019). O'Hara et al. (2019) reported that the expression of a gene encoding the transcription factor ARABIDOPSIS NAC DOMAIN PROTEIN 13 (ANAC13) was induced over a range of UV-B wavelengths at low doses, with a maximum response at 310 nm. Rácz and Hideg (2021) reported that the antioxidant enzyme activities under narrowband 311 nm UV-B radiation evoked opposite responses from broadband UV radiation. The contents of chlorophyll a and chlorophyll b, total chlorophyll, and carotenoid were significantly lower at 23 DAT and were significantly higher in UV6h radiation but lower in UV12h radiation than in the control (**Supplementary Figure 4**). These suggestions may support the

results in this study that the contents of bioactive compounds increased in kale plants exposed to UV-B radiation generated by the narrowband 310 nm UV-B LED for 6 h despite the high fluence rate without distinct damage to growth or chlorophyll content (**Figures 4**, **5** and **Supplementary Figures 1**, **4**).

Effect of Ultraviolet-B Radiation on Phenolic Content in Plants

Ultraviolet-B radiation has been reported to be effective in increasing phenolic contents and AOC. In this study, the TPC, TFC, TAC, UAPC, and AOC per DM and per leaf were significantly higher with longer UV-B exposure (**Figures 4–6**). As a response to UV-B radiation, the enhanced biosynthesis of phenylpropanoids has been well documented in *Brassica* species, including kale (Castillejo et al., 2021; Neugart and Bumke-Vogt, 2021). Under UV-B exposure, phenolics and flavonoids accumulate in epidermal tissues and act as direct UV screens, i.e., the main components of UAP (Neugart and Schreiner, 2018). The innate antioxidant potential of the compounds increases ROS scavenging activity and protects sensitive tissues from the high UV-B energy (Hideg et al., 2013). Dou et al. (2019) reported that AOC was positively correlated with UV-B dose, resulting from linear increases in the TPC and TFC in basil.

Plant and leaf developmental stages determine the UV-B-induced accumulation of bioactive compounds, but the relationships are not straightforward. In this study, leaf groups 1, 2, and 3 correspond to relatively old, intermediate, and young leaves at each growth stage, respectively, as determined by the order of leaf emergence and the relative growth state (**Supplementary Figure 3**). The increase rates of phenolic accumulation with UV-B radiation were highest in young leaves at 23 DAT, but those were not always higher in younger leaves than the other leaves at 30 and 38 DAT (**Figure 6**). Rizi et al. (2021) reported that UV-B-exposed young leaves of *Salvia verticillata* showed higher phenylpropanoid production than old leaves as higher gene expression of the key enzymes in their synthesis. However, young leaves are typically located near the top of the plant and are more exposed to UV-B radiation than the other leaves. At the plant canopy levels, higher canopy porosity was positively correlated with the contents of flavonoids such as kaempferol and quercetin in red wine grapes (Martínez-Lüscher et al., 2019). With simulated UVR_{int} in individual leaves, the increase rates of TPC and TFC were the highest in intermediate leaves at 30–38 DAT (**Figure 6**), which is consistent with the previous study (Yoon et al., 2021b). Therefore, at least locally accumulated UV-B-induced phenolics are determined by structural factors such as leaf position, area, and curvature as well as by developmental age.

Ultraviolet-B Radiation Interception on Plant Structures

The plant structure varies depending on its phyllotaxis and changes as the plant grows, but the plants are exposed to UV-B sources in a one-size-fits-all manner. The UV-B energy

TABLE 2 | UV-B energy yields for phenolic content per leaf of kale plants with leaf group at 23, 30, and 38 days after transplanting (DAT) referring to Eq. 2 and **Table 1**.

DAT	Leaf group	UV-B energy yield			
		TPC (mg GAE kJ^{-1} day)	TFC (mg CE kJ^{-1} day)	TAC (mg C3GE kJ^{-1} day)	UAPC (OD kJ^{-1} day)
23	2	6.54 c	3.14 d	1.05 bc	1.05 e
	3	6.54 c	7.68 b	1.53 b	1.05 e
30	1	13.1 b	7.91 b	0.89 bc	0.87 f
	2	11.6 b	8.70 b	0.81 bc	1.33 d
	3	2.47 c	6.63 bc	0.23 cd	1.86 b
38	1	3.80 c	2.16 d	0.32 cd	0.95 ef
	2	17.9 a	12.2 a	3.31 a	1.53 c
	3	3.65 c	5.05 cd	-0.28 d	2.15 a
DAT	23	6.54 B	4.91 B	1.22 A	1.05 C
	30	8.47 A	7.67 A	0.61 B	1.40 B
	38	8.02 A	6.31 A	1.00 A	1.58 A
Leaf group	1	7.40 B	4.39 C	0.54 B	0.91 C
	2	12.2 A	8.11 A	1.81 A	1.30 B
	3	3.69 C	6.06 B	0.23 B	1.83 A
Significance					
DAT		*	***	*	***
Leaf group		***	***	***	***
DAT × leaf group		***	***	***	***

TPC, yield for total phenolic content (mg GAE kJ^{-1} day); TFC, yield for total flavonoid content (mg CE kJ^{-1} day); TAC, yield for total anthocyanin content (mg C3GE kJ^{-1} day); and UAPC, yield for UV-absorbing pigment content (OD kJ^{-1} day).

*Leaf groups were determined according to the order of leaf emergence and their relative growth state (**Supplementary Figure 3** and **Supplementary Table 1**).*

Different letters indicate significant differences by two-way or one-way ANOVA and post-hoc test at $P < 0.05$ for each parameter referring to the "Materials and Methods" section.

$^{*}P < 0.05$; $^{***}P < 0.001$.

absorbed and its physiological interaction with individual leaves inevitably lead to a heterogeneous response in the plant. In this study, UV radiation interception was simulated well along with structural properties, including leaf height, angle, and surface curvature, using ray-tracing simulation and a 3D-scanned plant model (**Figure 3**). Previous studies on a light interception in plant structures have focused on the spatial distribution of PAR interception and photosynthesis using simulations (Sarlikioti et al., 2011; Shin et al., 2021). In controlled environments, the PAR interception was determined by the physical structures and arrangements of plants and artificial lighting (Kim et al., 2020; Saito et al., 2020). As growth progressed, plant height increased, but the UVR_{int} value of leaf group 3 decreased (**Figure 3B**). Reduced overlap of radiation at the position close to the UV-B LEDs with a narrow radiation area and the mutual shading by neighboring plants decreased the UVR_{int} despite growth progress (Yoon et al., 2021b).

Predicting Models of Phenolic Content in Three-Dimensional Plant Structures

In general, major environmental factors are controlled to optimize crop photosynthesis and growth in controlled environments (Carotti et al., 2021). Secondary metabolite production has been attempted to be maximized beyond biomass controlling environmental factors, including temperature, relative humidity, photoperiod, and light spectrum (Shim et al., 2018; Johnson et al., 2019; Appolloni et al., 2021). Unlike other environmental factors, supplementation with UV-B radiation near harvest could be more effective without growth loss or additional energy input (dos S. Nascimento et al., 2020; Yoon et al., 2020). Since UV-B exposure is a potent abiotic elicitor for the biosynthesis of secondary metabolites, its energy inputs should be optimized (Thakur et al., 2019; Toscano et al., 2019). Optimization of various elicitors has mostly been reported in the studies of *in vitro* plant tissue culture (Ghorbani et al., 2015; Farjaminezhad and Garoosi, 2021).

This study developed statistical models to assess how UV-B radiation as an elicitor enhances the phenolic accumulation in kale plants. For this purpose, the daily absorbed UV-B energy and the phenolic contents were analyzed as each value per leaf (**Figures 3C**, **6**). The developed models suitably explained the TPC, TFC, and UAPC as functions of UV-B radiation interception and leaf order according to growth stage (**Table 1** and **Figures 7**, **8**). These models showed high accuracies for predicting the TPC, TFC, TAC, and UAPC (**Figure 9**). The relatively low R^2 of the models at 23 DAT might be due to the small number of measured samples, which was less than half of the total (**Figures 9C,D** and **Supplementary Figure 2**).

Statistical modeling is an effective tool for quantifying the relationship between dependent and independent variables by the statistical significance of their correlations (Kim et al., 2016). Kim et al. (2018) developed a statistical model for glucosinolate content in Chinese cabbage using a second-order multi-polynomial equation with growth duration and temperature as independent variables. In this study, the model structure was determined according to the linear pattern of phenolic accumulation with UV-B dose as shown in the results from previous studies (Dou et al., 2019; Yoon et al., 2021a) or quadratic pattern with leaf group as shown in **Figure 6** and the results from a previous study (Yoon et al., 2021b). However, the developed models were limited to kale plants between 23 and 38 DAT in the UVR_{int} range below 2.5 W m^{-2} (**Figure 3**). Within the 3D plant structure, UV-B radiation further enhanced the intraindividual heterogeneity of phenolic contents (Yoon et al., 2021a). Using UV-B radiation interception on a 3D-scanned plant model, the developed models could extend the prediction of a phenolic accumulation from the intraindividual distribution level to the spatial distribution level (**Figure 7**). This approach to the distribution of metabolites in the 3D plant structure could provide the groundwork for plant metabolism and plant–environment interaction studies (Floros et al., 2017).

Application to Phenolic Production in the Food System

The main goal of controlled environment agriculture is to maximize plant productivity and minimize practical production costs, including energy costs (Kozai, 2018). The utilization efficiency of lighting systems on plant structures could be calculated using ray-tracing simulations and 3D-scanned plant models (Kim et al., 2020; Saito et al., 2020). The simulation results along with the photosynthesis model could be used to find out the optimal lighting system with the maximal light use efficiency for photosynthesis (Kim et al., 2020). In this study, the UV-B energy yield for phenolic content was calculated (**Table 2**). The annual production of bioactive compounds was simply estimated based on plant density (plant m^{-2}) and cultivation cycle per year according to harvest time (Yoon et al., 2019). From the data in this study, the optimal harvest time for the annual production of TFC was calculated as 30 DAT. Although the plant size and UV-B yield were high at 38 DAT, the annual production was high at 30 DAT because the shorter cultivation period increased the number of cultivations per year. We used kale as the representative plant because the phyllotaxis of the kale is a spiral pattern, which is a common pattern, and is widely cultivated around the world. This model approach could be extended to various plants and structures. Further steps in the modeling procedure for agriculture and food systems were model simulation and model-based analysis (Kim et al., 2016). These steps allow us to investigate numerous scenarios and predict the system responses with cost and input in an effective way (Kreutz and Timmer, 2009). Therefore, the developed model in this study could be used to predict the phenolic accumulation with effective UV-B energy input through model-based simulation in various environments.

CONCLUSION

This is the first study on the prediction of phenolic content with UV-B radiation interception and developmental age. Stepwise multiple linear regression models for the TPC, TFC, TAC, and UAPC were developed and validated with high accuracy. Preharvest UV-B radiation was also identified as a suitable strategy for the commercial production of secondary

metabolites in controlled environments. Ultimately, the model-based prediction will be used to find out the optimal conditions for the industrial production of secondary metabolites, saving production time and cost.

DATA AVAILABILITY STATEMENT

The original contributions presented in the study are included in the article/**Supplementary Material**, further inquiries can be directed to the corresponding author.

AUTHOR CONTRIBUTIONS

HY, M-MO, and JS designed the study and prepared the manuscript. HY and JK carried out the data collection. HY performed the model construction, simulation, statistical analysis, and visualization. All authors contributed to the article and approved the submitted version.

FUNDING

This study was supported by the Korea Institute of Planning and Evaluation for Technology in Food, Agriculture and Forestry (IPET) and Korea Smart Farm R&D Foundation (KosFarm) through the Smart Farm Innovation Technology Development Program, funded by the Ministry of Agriculture, Food and Rural Affairs (MAFRA), Korea government (MSIT), and Rural Development Administration (RDA; 421001-03).

ACKNOWLEDGMENTS

We thank Jewook Choi and Hyun Young Kim for their assistance with sample collection. We also thank Hee Jae Lee for helping with writing and proofreading.

SUPPLEMENTARY MATERIAL

The Supplementary Material for this article can be found online at: https://www.frontiersin.org/articles/10.3389/fpls.2022.918170/full#supplementary-material

Supplementary Figure 1 | Total fresh mass, leaf area, and root dry mass of kale plants.

Supplementary Figure 2 | Leaf fresh mass and leaf area of kale plants.

Supplementary Figure 3 | Leaf relative growth rate and expansion rate of leaf populations.

Supplementary Figure 4 | Chlorophyll and carotenoid contents in individual leaves of kale plants.

Supplementary Figure 5 | Comparison between measured and estimated phenolic contents per leaf of kale plants in the data set.

Supplementary Table 1 | Relative growth rate and expansion rate of leaf groups, and the assigned leaf order in kale plants at 23, 30, and 38 DAT.

REFERENCES

Ainsworth, E. A., and Gillespie, K. M. (2007). Estimation of total phenolic content and other oxidation substrates in plant tissues using Folin-Ciocalteu reagent. *Nat. Protoc.* 2, 875–877. doi: 10.1038/nprot.2007.102

Aphalo, P. J., Albert, A., Björn, L. O., McLeod, A. R., Robson, T. M., and Rosenqvist, E. (2012). *Beyond the visible : A Handbook of Best Practice in Plant UV Photobiology*, eds P. J. Aphalo, A. Albert, L. O. Björn, A. R. McLeod, T. M. Robson, and E. Rosenqvist (Helsinki: University of Helsinki), doi: 10.31885/9789521083631

Appolloni, E., Pennisi, G., Zauli, I., Carotti, L., Paucek, I., Quaini, S., et al. (2021). Beyond vegetables: effects of indoor LED light on specialized metabolite biosynthesis in medicinal and aromatic plants, edible flowers, and microgreens. *J. Sci. Food Agric.* 30, 472–487. doi: 10.1002/jsfa.11513

Behn, H., Schurr, U., Ulbrich, A., and Noga, G. (2011). Development-dependent UV-B responses in red oak leaf lettuce (*Lactuca sativa* L.): physiological mechanisms and significance for hardening. *Eur. J. Hortic. Sci.* 76, 33–40.

Brand-Williams, W., Cuvelier, M. E., and Berset, C. (1995). Use of a free radical method to evaluate antioxidant activity. *LWT Food Sci. Technol.* 28, 25–30. doi: 10.1016/S0023-6438(95)80008-5

Carotti, L., Graamans, L., Puksic, F., Butturini, M., Meinen, E., Heuvelink, E., et al. (2021). Plant factories are heating up: hunting for the best combination of light intensity, air temperature and root-zone temperature in lettuce production. *Front. Plant Sci.* 11:592171. doi: 10.3389/fpls.2020.592171

Castillejo, N., Martínez-Zamora, L., and Artés-Hernández, F. (2021). Periodical UV-B radiation hormesis in biosynthesis of kale sprouts nutraceuticals. *Plant Physiol. Biochem.* 165, 274–285. doi: 10.1016/j.plaphy.2021.05.022

Choi, K. Y., Seo, T. C., and Suh, H.-D. (2005). Development of nutrient solution for hydroponics of cruciferae leaf vegetables based on nutrient-water absorption rate and the cation ratio. *Prot. Hortic. Plant Fact.* 14, 288–296.

Csepregi, K., Coffey, A., Cunningham, N., Prinsen, E., Hideg, É, and Jansen, M. A. K. (2017). Developmental age and UV-B exposure co-determine antioxidant capacity and flavonol accumulation in *Arabidopsis* leaves. *Environ. Exp. Bot.* 140, 19–25. doi: 10.1016/j.envexpbot.2017.05.009

Csepregi, K., Neugart, S., Schreiner, M., and Hideg, É (2016). Comparative evaluation of total antioxidant capacities of plant polyphenols. *Molecules* 21:208. doi: 10.3390/molecules21020208

Dewanto, V., Xianzhong, W., Adom, K. K., and Liu, R. H. (2002). Thermal processing enhances the nutritional value of tomatoes by increasing total antioxidant activity. *J. Agric. Food Chem.* 50, 3010–3014. doi: 10.1021/jf0115589

dos S. Nascimento, L. B., Brunetti, C., Agati, G., Lo Iacono, C., Detti, C., et al. (2020). Short-term pre-harvest UV-B supplement enhances the polyphenol content and antioxidant capacity of *Ocimum basilicum* leaves during storage. *Plants* 9:797. doi: 10.3390/plants9060797

Dou, H., Niu, G., and Gu, M. (2019). Pre-harvest UV-B radiation and photosynthetic photon flux density interactively affect plant photosynthesis, growth, and secondary metabolites accumulation in basil (*Ocimum basilicum*) plants. *Agronomy* 9:434. doi: 10.3390/agronomy9080434

Farjaminezhad, R., and Garoosi, G. (2021). Improvement and prediction of secondary metabolites production under yeast extract elicitation of *Azadirachta indica* cell suspension culture using response surface methodology. *AMB Express* 11:43. doi: 10.1186/s13568-021-01203-x

Flint, S. D., and Caldwell, M. M. (2003). A biological spectral weighting function for ozone depletion research with higher plants. *Physiol. Plant.* 117, 137–144. doi: 10.1034/j.1399-3054.2003.1170117.x

Floros, D. J., Petras, D., Kapono, C. A., Melnik, A. V., Ling, T. J., Knight, R., et al. (2017). Mass spectrometry based molecular 3D-cartography of plant metabolites. *Front. Plant Sci.* 8:429. doi: 10.3389/fpls.2017.00429

Francisco, M., Tortosa, M., Martínez-Ballesta, M., del, C., Velasco, P., García-Viguera, C., et al. (2017). Nutritional and phytochemical value of *Brassica* crops from the agri-food perspective. *Ann. Appl. Biol.* 170, 273–285. doi: 10.1111/aab.12318

Ghorbani, M., Ghorbani, A., Omidi, M., and Hashemi, S. M. (2015). Response surface modelling of noradrenaline production in hairy root culture of purslane

(*Portulaca oleracea* L.). *Turkish J. Agric. Food Sci. Technol.* 3:349. doi: 10.24925/turjaf.v3i6.349-443.320

Hagen, S. F., Borge, G. I. A., Solhaug, K. A., and Bengtsson, G. B. (2009). Effect of cold storage and harvest date on bioactive compounds in curly kale (*Brassica oleracea* L. var. *acephala*). *Postharvest Biol. Technol.* 51, 36–42. doi: 10.1016/j.postharvbio.2008.04.001

Heinze, M., Hanschen, F. S., Wiesner-Reinhold, M., Baldermann, S., Gräfe, J., Schreiner, M., et al. (2018). Effects of developmental stages and reduced UVB and low UV conditions on plant secondary metabolite profiles in pak choi (*Brassica rapa* subsp. *chinensis*). *J. Agric. Food Chem.* 66, 1678–1692. doi: 10.1021/acs.jafc.7b03996

Hideg, É, Jansen, M. A. K., and Strid, Å (2013). UV-B exposure, ROS, and stress: inseparable companions or loosely linked associates? *Trends Plant Sci.* 18, 107–115. doi: 10.1016/j.tplants.2012.09.003

Hitz, T., Henke, M., Graeff-Hönninger, S., and Munz, S. (2019). Three-dimensional simulation of light spectrum and intensity within an LED growth chamber. *Comput. Electron. Agric.* 156, 540–548. doi: 10.1016/j.compag.2018.11.043

Johnson, A. J., Meyerson, E., de la Parra, J., Savas, T. L., Miikkulainen, R., and Harper, C. B. (2019). Flavor-cyber-agriculture: optimization of plant metabolites in an open-source control environment through surrogate modeling. *PLoS One* 14:e0213918. doi: 10.1371/journal.pone.0213918

Jordan, B. R. (2002). Review: Molecular response of plant cells to UV-B stress. *Funct. Plant Biol.* 29, 909. doi: 10.1071/FP02062

Khudyakova, A. Y., Kreslavski, V. D., Shmarev, A. N., Lyubimov, V. Y., Shirshikova, G. N., Pashkovskiy, P. P., et al. (2019). Impact of UV-B radiation on the photosystem II activity, pro-/antioxidant balance and expression of light-activated genes in *Arabidopsis thaliana hy4* mutants grown under light of different spectral composition. *J. Photochem. Photobiol. B Biol.* 194, 14–20. doi: 10.1016/j.jphotobiol.2019.02.003

Kim, D.-G., Cho, B.-K., and Lee, W.-H. (2016). A novel approach in analyzing agriculture and food systems: review of modeling and its applications. *Korean J. Agric. Sci.* 43, 163–175. doi: 10.7744/kjoas.20160019

Kim, D.-G., Shim, J.-Y., Ko, M.-J., Chung, S.-O., Chowdhury, M., and Lee, W.-H. (2018). Statistical modeling for estimating glucosinolate content in Chinese cabbage by growth conditions. *J. Sci. Food Agric.* 98, 3580–3587. doi: 10.1002/jsfa.8874

Kim, J., Kang, W. H., and Son, J. E. (2020). Interpretation and evaluation of electrical lighting in plant factories with ray-tracing simulation and 3D plant modeling. *Agronomy* 10:1545. doi: 10.3390/agronomy10101545

Kneissl, M., Seong, T.-Y., Han, J., and Amano, H. (2019). The emergence and prospects of deep-ultraviolet light-emitting diode technologies. *Nat. Photonics* 13, 233–244. doi: 10.1038/s41566-019-0359-9

Kozai, T. (2018). *Smart Plant Factory*, ed. T. Kozai Singapore (Cham: Springer). doi: 10.1007/978-981-13-1065-2

Kreutz, C., and Timmer, J. (2009). Systems biology: experimental design. *FEBS J.* 276, 923–942. doi: 10.1111/j.1742-4658.2008.06843.x

Liang, T., Yang, Y., and Liu, H. (2019). Signal transduction mediated by the plant UV-B photoreceptor UVR8. *New Phytol.* 221, 1247–1252. doi: 10.1111/nph.15469

Liao, X., Liu, W., Yang, H., and Jenkins, G. I. (2020). A dynamic model of UVR8 photoreceptor signalling in UV-B-acclimated *Arabidopsis*. *New Phytol.* 227, 857–866. doi: 10.1111/nph.16581

Lichtenthaler, H. K., and Buschmann, C. (2001). Chlorophylls and carotenoids: Measurement and characterization by UV-VIS spectroscopy. *Curr. Protoc. Food Anal. Chem.* 1, F4.3.1–F4.3.8. doi: 10.1002/0471142913.faf0403s01

Loconsole, D., and Santamaria, P. (2021). UV lighting in horticulture: A sustainable tool for improving production quality and food safety. *Horticulturae* 7:9. doi: 10.3390/horticulturae7010009

Loi, M., Villani, A., Paciolla, F., Mulè, G., and Paciolla, C. (2020). Challenges and opportunities of light-emitting diode (LED) as key to modulate antioxidant compounds in plants. A review. *Antioxidants* 10:42. doi: 10.3390/antiox10010042

Majer, P., and Hideg, É (2012). Developmental stage is an important factor that determines the antioxidant responses of young and old grapevine leaves under UV irradiation in a green-house. *Plant Physiol. Biochem* 50, 15–23. doi: 10.1016/j.plaphy.2011.09.018

Martínez-Lüscher, J., Brillante, L., and Kurtural, S. K. (2019). Flavonol profile is a reliable indicator to assess canopy architecture and the exposure of red wine grapes to solar radiation. *Front. Plant Sci.* 10:10. doi: 10.3389/fpls.2019.00010

Meyer, P., Van de Poel, B., and De Coninck, B. (2021). UV-B light and its application potential to reduce disease and pest incidence in crops. *Hortic. Res.* 8:194. doi: 10.1038/s41438-021-00629-5

Mosadegh, H., Trivellini, A., Lucchesini, M., Ferrante, A., Maggini, R., Vernieri, P., et al. (2019). UV-B physiological changes under conditions of distress and eustress in sweet basil. *Plants* 8:396. doi: 10.3390/plants8100396

Neugart, S., and Bumke-Vogt, C. (2021). Flavonoid glycosides in *Brassica* species respond to UV-B depending on exposure time and adaptation time. *Molecules* 26:494. doi: 10.3390/molecules26020494

Neugart, S., and Schreiner, M. (2018). UVB and UVA as eustressors in horticultural and agricultural crops. *Sci. Hortic.* 234, 370–381. doi: 10.1016/j.scienta.2018.02.021

O'Hara, A., Headland, L. R., Díaz-Ramos, L. A., Morales, L. O., Strid, Å, and Jenkins, G. I. (2019). Regulation of *Arabidopsis* gene expression by low fluence rate UV-B independently of UVR8 and stress signaling. *Photochem. Photobiol. Sci.* 18, 1675–1684. doi: 10.1039/C9PP00151D

Paradiso, R., and Proietti, S. (2021). Light-quality manipulation to control plant growth and photomorphogenesis in greenhouse horticulture: The state of the art and the opportunities of modern LED systems. *J. Plant Growth Regul.* 41, 742–780. doi: 10.1007/s00344-021-10337-y

Pontarin, N., Molinié, R., Mathiron, D., Tchoumtchoua, J., Bassard, S., Gagneul, D., et al. (2020). Age-dependent metabolic profiles unravel the metabolic relationships within and between flax leaves (*Linum usitatissimum*). *Metabolites* 10:218. doi: 10.3390/metabo10060218

Rácz, A., and Hideg, É (2021). Narrow-band 311 nm ultraviolet-B radiation evokes different antioxidant responses from broad-band ultraviolet. *Plants* 10:1570. doi: 10.3390/plants10081570

Rankenberg, T., Geldhof, B., van Veen, H., Holsteens, K., Van de Poel, B., and Sasidharan, R. (2021). Age-dependent abiotic stress resilience in plants. *Trends Plant Sci.* 26, 692–705. doi: 10.1016/j.tplants.2020.12.016

Re, R., Pellegrini, N., Proteggente, A., Pannala, A., Yang, M., and Rice-Evans, C. (1999). Antioxidant activity applying an improved ABTS radical cation decolorization assay. *Free Radic. Biol. Med.* 26, 1231–1237. doi: 10.1016/S0891-5849(98)00315-3

Rechner, O., Neugart, S., Schreiner, M., Wu, S., and Poehling, H.-M. (2016). Different narrow-band light ranges alter plant secondary metabolism and plant defense response to aphids. *J. Chem. Ecol.* 42, 989–1003. doi: 10.1007/s10886-016-0755-2

Rizi, M. R., Azizi, A., Sayyari, M., Mirzaie-Asl, A., and Conti, L. (2021). Increased phenylpropanoids production in UV-B irradiated *Salvia verticillata* as a consequence of altered genes expression in young leaves. *Plant Physiol. Biochem.* 167, 174–184. doi: 10.1016/j.plaphy.2021.07.037

Saito, K., Ishigami, Y., and Goto, E. (2020). Evaluation of the light environment of a plant factory with artificial light by using an optical simulation. *Agronomy* 10:1663. doi: 10.3390/agronomy10111663

Šamec, D., Urlić, B., and Salopek-Sondi, B. (2019). Kale (*Brassica oleracea* var. *acephala*) as a superfood: review of the scientific evidence behind the statement. *Crit. Rev. Food Sci. Nutr.* 59, 2411–2422. doi: 10.1080/10408398.2018.1454400

Sarlikioti, V., de Visser, P. H. B., and Marcelis, L. F. M. (2011). Exploring the spatial distribution of light interception and photosynthesis of canopies by means of a functional–structural plant model. *Ann. Bot.* 107, 875–883. doi: 10.1093/aob/mcr006

Schreiner, M., Krumbein, A., Mewis, I., Ulrichs, C., and Huyskens-Keil, S. (2009). Short-term and moderate UV-B radiation effects on secondary plant metabolism in different organs of nasturtium (*Tropaeolum majus* L.). *Innov. Food Sci. Emerg. Technol.* 10, 93–96. doi: 10.1016/j.ifset.2008.10.001

Schreiner, M., Mewis, I., Huyskens-Keil, S., Jansen, M. A. K., Zrenner, R., Winkler, J. B., et al. (2012). UV-B-induced secondary plant metabolites - Potential benefits for plant and human health. *CRC Crit. Rev. Plant Sci.* 31, 229–240. doi: 10.1080/07352689.2012.664979

Shim, J.-Y., Kim, H.-Y., Kim, D.-G., Lee, Y.-S., Chung, S.-O., and Lee, W.-H. (2018). Optimizing growth conditions for glucosinolate production in Chinese cabbage. *Hortic. Environ. Biotechnol.* 59, 649–657. doi: 10.1007/s13580-018-0084-1

Shin, J., Hwang, I., Kim, D., Moon, T., Kim, J., Kang, W. H., et al. (2021). Evaluation of the light profile and carbon assimilation of tomato plants in greenhouses with respect to film diffuseness and regional solar radiation using ray-tracing simulation. *Agric. For. Meteorol.* 296:108219. doi: 10.1016/j.agrformet.2020.108219

Si, C., Yao, X. Q., He, X. L., Chu, J. Z., Ma, C. H., and Shi, X. F. (2015). Effects of enhanced UV-B radiation on biochemical traits in postharvest flowers of medicinal chrysanthemum. *Photochem. Photobiol.* 91, 845–850. doi: 10.1111/php.12450

Sun, M., Gu, X., Fu, H., Zhang, L., Chen, R., Cui, L., et al. (2010). Change of secondary metabolites in leaves of *Ginkgo biloba* L. in response to UV-B induction. *Innov. Food Sci. Emerg. Technol.* 11, 672–676. doi: 10.1016/j.ifset.2010.08.006

Sytar, O., Bośko, P., Živèák, M., Brestic, M., and Smetanska, I. (2018). Bioactive phytochemicals and antioxidant properties of the grains and sprouts of colored wheat genotypes. *Molecules* 23:2282. doi: 10.3390/molecules23092282

Takshak, S., and Agrawal, S. B. (2019). Defense potential of secondary metabolites in medicinal plants under UV-B stress. *J. Photochem. Photobiol. B Biol.* 193, 51–88. doi: 10.1016/j.jphotobiol.2019.02.002

Thakur, M., Bhattacharya, S., Khosla, P. K., and Puri, S. (2019). Improving production of plant secondary metabolites through biotic and abiotic elicitation. *J. Appl. Res. Med. Aromat. Plants* 12, 1–12. doi: 10.1016/j.jarmap.2018.11.004

Toscano, S., Trivellini, A., Cocetta, G., Bulgari, R., Francini, A., Romano, D., et al. (2019). Effect of preharvest abiotic stresses on the accumulation of bioactive compounds in horticultural produce. *Front. Plant Sci.* 10:1212. doi: 10.3389/fpls.2019.01212

Wiesner-Reinhold, M., Dutra Gomes, J. V., Herz, C., Tran, H. T. T., Baldermann, S., Neugart, S., et al. (2021). Subsequent treatment of leafy vegetables with low doses of UVB-radiation does not provoke cytotoxicity, genotoxicity, or oxidative stress in a human liver cell model. *Food Biosci.* 43:101327. doi: 10.1016/j.fbio.2021.101327

Yoon, H. I., Kim, D., and Son, J. E. (2020). Spatial and temporal bioactive compound contents and chlorophyll fluorescence of kale (*Brassica oleracea* L.) under UV-B exposure near harvest time in controlled environments. *Photochem. Photobiol.* 96, 845–852. doi: 10.1111/php.13237

Yoon, H. I., Kim, H. Y., Kim, J., and Son, J. E. (2021b). Quantitative analysis of UV-B radiation interception and bioactive compound contents in kale by leaf position according to growth progress. *Front. Plant Sci.* 12:667456. doi: 10.3389/fpls.2021.667456

Yoon, H. I., Kim, H. Y., Kim, J., Oh, M., and Son, J. E. (2021a). Quantitative analysis of UV-B radiation interception in 3D plant structures and intraindividual distribution of phenolic contents. *Int. J. Mol. Sci.* 22:2701. doi: 10.3390/ijms22052701

Yoon, H. I., Kim, J. S., Kim, D., Kim, C. Y., and Son, J. E. (2019). Harvest strategies to maximize the annual production of bioactive compounds, glucosinolates, and total antioxidant activities of kale in plant factories. *Hortic. Environ. Biotechnol.* 60, 883–894. doi: 10.1007/s13580-019-00174-0

Conflict of Interest: The authors declare that the research was conducted in the absence of any commercial or financial relationships that could be construed as a potential conflict of interest.

Publisher's Note: All claims expressed in this article are solely those of the authors and do not necessarily represent those of their affiliated organizations, or those of the publisher, the editors and the reviewers. Any product that may be evaluated in this article, or claim that may be made by its manufacturer, is not guaranteed or endorsed by the publisher.

frontiers | Frontiers in Plant Science

ORIGINAL RESEARCH
published: 01 July 2022
doi: 10.3389/fpls.2022.929672

Technological Advancements and Economics in Plant Production Systems: How to Retrofit?

*Daniel Dooyum Uyeh[1,2,3], Rammohan Mallipeddi[4], Tusan Park[1,3], Seungmin Woo[1,2,3] and Yushin Ha[1,2,3]**

[1] Department of Bio-Industrial Machinery Engineering, Kyungpook National University, Daegu, South Korea, [2] Upland-Field Machinery Research Centre, Kyungpook National University, Daegu, South Korea, [3] Smart Agriculture Innovation Center, Kyungpook National University, Daegu, South Korea, [4] Department of Artificial Intelligence, School of Electronics Engineering, Kyungpook National University, Daegu, South Korea

Plant production systems such as plant factories and greenhouses can help promote resilience in food production. These systems could be used for plant protection and aid in controlling the micro- and macro- environments needed for optimal plant growth irrespective of natural disasters and changing climate conditions. However, to ensure optimal environmental controls and efficient production, several technologies such as sensors and robots have been developed and are at different stages of implementation. New and improved systems are continuously being investigated and developed with technological advances such as robotics, sensing, and artificial intelligence to mitigate hazards to humans working in these systems from poor ventilation and harsh weather while improving productivity. These technological advances necessitate frequent retrofits considering local contexts such as present and projected labor costs. The type of agricultural products also affects measures to be implemented to maximize returns on investment. Consequently, we formulated the retrofitting problem for plant production systems considering two objectives; minimizing the total cost for retrofitting and maximizing the yearly net profit. Additionally, we considered the following: (a) cost of new technologies; (b) present and projected cost for human labor and robotics; (c) size and service life of the plant production system; (d) productivity before and after retrofit, (e) interest on loans for retrofitting, (f) energy consumption before and after retrofit and, (g) replacement and maintenance cost of systems. We solved this problem using a multi-objective evolutionary algorithm that results in a set of compromised solutions and performed several simulations to demonstrate the applicability and robustness of the method. Results showed up to a 250% increase in annual net profits in an investigated case, indicating that the availability of all the possible retrofitting combinations would improve decision making. A user-friendly system was developed to provide all the feasible retrofitting combinations and total costs with the yearly return on investment in agricultural production systems in a single run.

Keywords: decision making, greenhouse, non-dominated sorting genetic algorithm, plant factory, return on investment, resilient food systems

OPEN ACCESS

Edited by:
Yuxin Tong,
Institute of Environment and Sustainable Development in Agriculture (CAAS), China

Reviewed by:
Toyoki Kozai,
Japan Plant Factory Association, Japan
Lixia Kang,
Xi'an Jiaotong University, China

***Correspondence:**
Yushin Ha
yushin72@knu.ac.kr

Specialty section:
This article was submitted to Technical Advances in Plant Science, a section of the journal Frontiers in Plant Science

Received: *27 April 2022*
Accepted: *06 June 2022*
Published: *01 July 2022*

Citation:
Uyeh DD, Mallipeddi R, Park T, Woo S and Ha Y (2022) Technological Advancements and Economics in Plant Production Systems: How to Retrofit? Front. Plant Sci. 13:929672. doi: 10.3389/fpls.2022.929672

INTRODUCTION

Plant production systems offer numerous opportunities and benefits for growers, such as year-round cultivation, improved growing conditions for ornamental crops and vegetables, and control of micro- and macro- environments (Gerson and Weintraub, 2007; Van Straten et al., 2010; Nordey et al., 2017). These systems have been serving communities for decades. They have transformed from simple structures to grow vegetables in temperate regions during the cold winter months to advanced facilities currently used to grow in tropics, including deserts (Wittwer and Castilla, 1995; Gullino et al., 1999; Shamshiri et al., 2018).

The advancement in these protected cultivation structures is still ongoing, with the world incessantly requiring improvements to cater to the fast-growing populace demanding healthier food. Top on this list is the diminishing skilled farm labor, rapidly changing climate, and disasters such as the COVID 19 outbreak caused by the SARS-CoV-2 virus (Wang et al., 2020) that became widespread at the beginning of 2020, leading to difficulties in international travels for migrant workers (Lima et al., 2020). Most countries were forced to close their borders or place stringent entry procedures (Barua, 2020; Wells et al., 2020). This has led to various farm losses (Galanakis, 2020; Helm, 2020; Nicola et al., 2020; Sahoo and Rath, 2020). Autonomous growing has been under investigation to resolve labor accessibility and precision issues. Also, the environment in plant production systems is toxic to humans because of the poor ventilation and high temperature and humidity content. Advanced plant production systems are complex multi-input structures that come at a high cost (Stanghellini and Montero, 2010; Baeza et al., 2011; Reddy, 2016). This necessitates the proper implementation of new and/or existing technologies.

Plant production systems existed for centuries (42 BC–37 AC), but the major advancement occurred in the early 1950s and has continuously improved to the current phase (Jensen and Malter, 1995; Paul and Gwynn-Jones, 2003; Raviv and Antignus, 2004; Nordey et al., 2017). Most plant production systems, such as plant factories and greenhouses, were not designed to adopt the new technologies. Furthermore, building new structures also needs proper planning and implementation. This contrasts with the open field cultivation system that requires less planning. Plant production systems could be catastrophic if proper planning and implementation are neglected despite having positive returns. With the current evolution in technologies, the grower should have an appropriate decision-making system that considers investment capital, interest on loans, market opportunities, and profit, which are critical to sustainability.

Structural upgrades are often required for implementing new technologies. Retrofitting is usually adopted as the choice approach. This has been applied majorly to residential buildings to save energy and limit greenhouse gas emissions (Dixon et al., 2008), simultaneously considering several environmental and economic criteria (Antipova et al., 2014), comparing internal and external thermal insulation systems for residential buildings (Kolaitis et al., 2013), and several other retrofitted buildings with focus on energy saving (Xu et al., 2011, 2015; Xu and Chan, 2013; Wu et al., 2016; El-Darwish and Gomaa, 2017; Fan and Xia, 2017, 2018; Liu et al., 2018). In this scenario, the combination of retrofitting measures and strategies has proven to be complex and requires tradeoffs. In residential buildings, the measures adopted to retrofit the buildings for energy efficiency are categorized into the following groups: (a) measures to reduce load; (b) measures to control and monitor loads; (c) enveloping measures such as insulation and sealing roofs or ceilings; (d) alter energy consumption patterns of the occupants; and (e) adoption of renewable energy sources (Diakaki et al., 2008; Marszal et al., 2011; Ma et al., 2012; Malatji et al., 2013).

Retrofitting plant production systems to cover the progress in efficient growing technologies is much more complex than residential buildings that focus primarily on energy. The energy retrofitting benefits could be social, which has to do with enhancing the health and comfort of the occupants, reducing air emissions hurting the environment, and economic perspective in reduction of operation costs (Jafari et al., 2016). The dynamics in plant production systems are numerous, requiring multi-objective optimization approach, and the strategy to adopt and/or retrofit the existing system is much more challenging and delicate. These include (a) plant production systems are far more extensive than regular residential houses reaching 215 square feet (Robinson, 2018); (b) the advancement in technologies used in growing are occurring simultaneously in different aspects of protected cultivation and at a much faster rate than residential houses (Uyeh et al., 2019b; Raviteja and Supriya, 2020; Rayhana et al., 2020); (c) unlike in residential buildings where the primary concern is energy consumption for heating and cooling (Jafari and Valentin, 2017), plant production systems require energy for similar purposes in addition to other technological advancements such as autonomous growing that needs to be retrofitted (Bogue, 2020; Kurtser and Edan, 2020); and (d) wrong retrofitting strategy would not result in discomfort as in residential buildings but an irreversible loss of the plants accompanied with substantial economic losses. These make the retrofitting problem in protected cultivation non-deterministic polynomial-time hard (NP-hard) (Bagnall et al., 2001).

Multi-objective optimization requires maximizing or minimizing multiple objective functions that are constrained. These include analyzing design, selecting process designs or optimal products, tradeoffs, or applications where optimal solutions are needed with tradeoffs between two or more conflicting objectives. The conventional approaches for this type of optimization include the Pareto front, goal attainment, and minimax. In Pareto fronts, noninferior solutions are found. These are solutions in which an improvement in one objective requires a degradation in another.

On the other hand, goal attainment reduces the values of a linear or nonlinear vector function to attain the goal values given in a goal vector. The comparative significance of the goals is shown by applying a weight vector, and goal fulfillment problems may also be subject to linear and nonlinear constraints. Finally, minimax, minimizes the worst-case values of a set of multivariate functions, probably subject to linear and nonlinear constraints (MathWorks, 2021).

Multi-objective techniques are popular due to their capabilities in solving a wide range of real-world problems (Saini and Saha, 2021). For example, Fonseca and Fleming (1993) Multiple Objective Genetic Algorithm enables decision-makers to progressively articulate their preferences while learning about the problem under consideration. Srinivas and Deb's (1994) Nondominated Sorting in Genetic Algorithms adopted Goldberg's notion of nondominated sorting in genetic algorithms and a niche and speciation method to find multiple Pareto-optimal points simultaneously. Horn et al.'s (1993) Niched Pareto genetic algorithm, a multi-objective optimization algorithm, is adopted to find the Pareto optimal set. The previously discussed algorithms are some of the elitist multi-objective methods that non-dominated sorting genetic algorithm II (NSGA II) used in this study have been proven to be better (Deb et al., 2002). These methods are limited in their computational complexity (the number of objectives and population size), non-elitism approach; and the need for specifying a sharing parameter that alleviates all the above three difficulties.

In summary, Pareto optimality which is the backdrop on which NSGA II is built, has been reported to be the best approach to describe multi-objective optimization since there is no single global solution. It is often necessary to determine a set of points that all fit a predetermined definition for an optimum (Marler and Arora, 2004). NSGA II is undoubtedly the elitist method (Deb et al., 2000; Kannan et al., 2008; Li and Zhang, 2008; Yusoff et al., 2011). NSGA-II, a multi-objective evolutionary algorithm, improves the difficulties of using multi-objective optimization. These include the need to specify a sharing parameter, computational complexity, and a non-elitism approach. It possesses a selection operator that generates a mating pool by merging the parent and offspring populations and selecting the best N solutions (Deb et al., 2002).

Consequently, in this study, we formulated the protected cultivation retrofitting problem considering; (a) cost of retrofitting items such as sensors and robots; (b) cost of labor and cost-benefits obtainable from replacing human labor with robots; (c) size and service life of the plant production system; (d) impact of retrofitting on productivity and consequently profit; and (e) category of retrofitting to be implemented which delivers tradeoff solutions that represent the possible retrofits associated with expenditure and benefits. This problem was then solved using NSGA-II. Parameters such as present and projected cost of labor and agricultural products can be set to the user's local context. Due to the conflicting nature of the objectives, NSGA-II can provide a tradeoff solution that can enable better decision-making when selecting retrofit measures. We demonstrated the applicability of this method by carrying out experimental simulations on different plant production system sizes.

RETROFITTING IN PLANT PRODUCTION SYSTEMS

Figure 1 shows the factors and options available for retrofitting a plant production system. In this study, a prospective retrofit is represented as "*RM*". Furthermore, some options are limited by constraints, as shown in **Figure 2**. Two options are available in retrofitting the plant production system to include a network controller (**Figure 2**). If an analogous network controller is selected, all sensors to be selected must be analog. A similar procedure would occur if a digital network controller were selected and with the type of layout and robots, respectively. Retrofit number 23 (Transportation robot) was considered nil only in Option 2 because a transport robot is not required in this situation. **Figure 3** shows the benefits derived from the combination of different retrofit measures.

The factors are represented with vector "*X*" as shown below:

$$X = [1,\ 2,\ 3,\ 4,\ 5,\ 6,\ 7,\ 8,\ 9,\ 10,\ 11,\ 12,\ 13,\ 14,\ 15,\ 16,\ 17,\ 18,\ 19,\ 20,\ 21,\ 22,\ 23]$$

X=	1	2	3	4	5	6	7	8	9	10	11	12
RM1=	[ℝ		ℝ		ℝ		ℝ		ℝ			
RM2=	[	ℝ		ℝ		ℝ		ℝ		ℝ		ℝ
.												
.												

X=	13	14	15	16	17	18	19	20	21	22	23
RM1=					ℝ		ℝ		ℝ		]
RM2=						ℝ		ℝ		ℝ	]
.											
.											

The prospective retrofit represented with vectors RM1, RM2,. . . above presents the feasible retrofit measures that could be implemented. The selected retrofit measure denoted with "ℝ" corresponds to the factor number (*X*) for a given feasible retrofit vector "RM".

The retrofitting problem in a plant production system differs from conventional residential buildings. In this study and referring to the scenario in the Republic of Korea, the following variables were considered:

(a) Size of the plant production system.
(b) The service life of the plant production system (m).
(c) Cost of the items for retrofitting (C_i).
(d) Cost of electricity per unit (*UCE*).
(e) Impact of retrofitting on electricity consumption (*ECC*).
(f) The initial estimated cost of energy consumption.
(g) Interest paid on loans for retrofitting items.
(h) The annual rate of increase in energy cost (e).
(i) Maintenance and replacement period for each retrofitted item (t_{RMi}).
(j) Number of maintenance and replacements needed to be done during the service life of the system (nRM_i).
(k) Production before and after retrofitting was done (*PBR*).
(l) Price per unit of production.
(m) Projections in the price of the product.

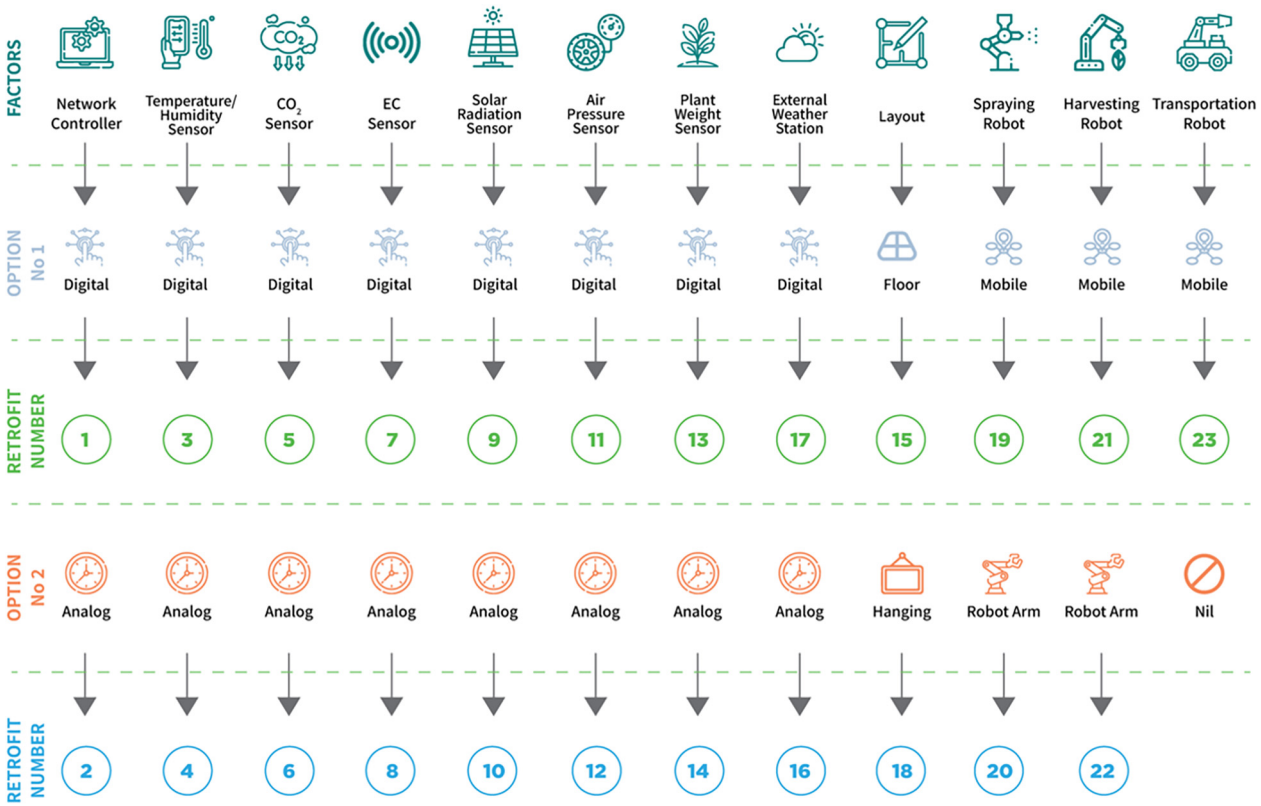

FIGURE 1 | Retrofit factors and options used in the experimental simulation.

(n) Labor cost before and after retrofit.
(o) Projections in the cost of labor.
(p) Profit (P).

PROBLEM FORMULATION

Expenditures in Retrofitting a Plant Production System

Initial Cost of Investment

To calculate the initial cost of investment (ICI) to retrofit in a plant production system, the cost of purchasing sensors (digital or analog) for precision and improved decision making, retrofitting the navigation system for the robots (mobile rail or hanging system), and purchase cost of robots were considered and computed in Eq. 1.

$$ICI = \sum_{i=1}^{n} C_i y_i \tag{1}$$

Where C_i is the cost of implementing the ith retrofitting measure, which is the cost of the items for retrofitting, and y_i is an indication variable demonstrating if the ith retrofitting measure is selected in the automation strategy. Furthermore, n is the total number of potential retrofitting measures.

Energy Consumption Cost

To compute the current energy consumption cost from retrofitting (ECC) the protected cultivation system, Eqs 2, 3 were used (Fan and Xia, 2018).

$$ECC = YEC \times \left[\frac{\left(1 + \left(\frac{Ir-e}{1+e}\right)\right)^m - 1}{\left(\frac{Ir-e}{1+e}\right) \times \left(1 + \left(\frac{Ir-e}{1+e}\right)\right)^m} \right] \tag{2}$$

Where YEC is the estimated yearly energy consumption cost of the plant production system in the first year, Ir is the interest rate, e is the annual rate of energy cost increase (a rate of 5% was considered), and m is the service life of the plant production system.

The yearly energy consumption of the plant production system in the first year can be calculated as the sum of the estimated electricity per year as follow:

$$AEC = \left(\sum_{i=1}^{n} EC_i \right) \times UCE \tag{3}$$

Where AEC is the annual energy consumption of the plant production system before implementing the energy retrofit, EC is the energy consumption of the items in retrofitting the plant production system, and UCE is the unit cost of electricity.

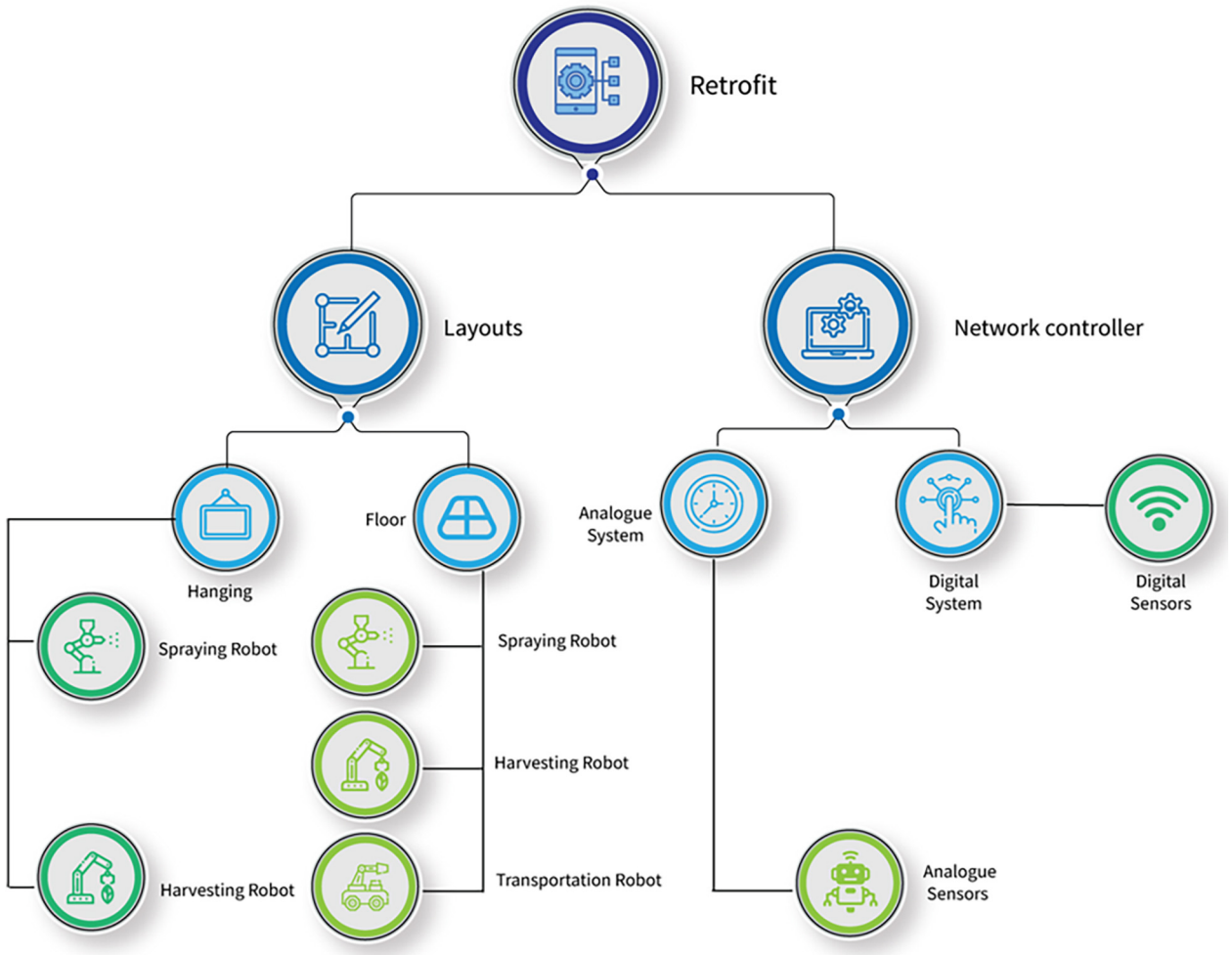

FIGURE 2 | Tree showing constraints for implementing retrofits.

Replacement and Maintenance Cost

To estimate the replacement and maintenance cost because of retrofitting the plant production system, the number of replacements during the service life of the system is calculated using Eqs 4, 5 (Fan and Xia, 2018):

$$nRM_i = Round\_Down\left[\frac{(t)}{t_{RM_i}}\right] \quad (4)$$

Where nRM_i is the number of times replacements and maintenance are required for the ith measure during the service life of the plant production system, and t_{RMi} is the replacement and maintenance period for the ith measure.

Furthermore, to compute the current replacement and maintenance cost from the retrofits, the equation below was used.

$$ECC_{Rc} = \sum_{i=1}^{n}\left[\left(\sum_{j=1}^{nRM_i}\frac{E_{MRi}}{(1+p)^j \times t_{RM_i}}\right)\right] \times x_i \quad (5)$$

Where E_{MRi} is the expenditure estimated from replacement and maintenance to implement the ith activity after its replacement and maintenance period.

Total Expenditure in Retrofitting a Plant Production System

The total expenditure is computed using Eq. 6:

$$Expenditure = CR + ECC + ECC_{RC} \quad (6)$$

Where CR is the cost of the systems used in the retrofits, ECC is the current energy consumption cost from retrofitting the system and ECC_{RC} is the replacement and maintenance cost for the retrofitted items.

The Net Profit Derived From Retrofitting a Plant Production System

The profit gotten from the retrofit is assumed from two perspectives in this study. These were computed using Eqs 7–10.

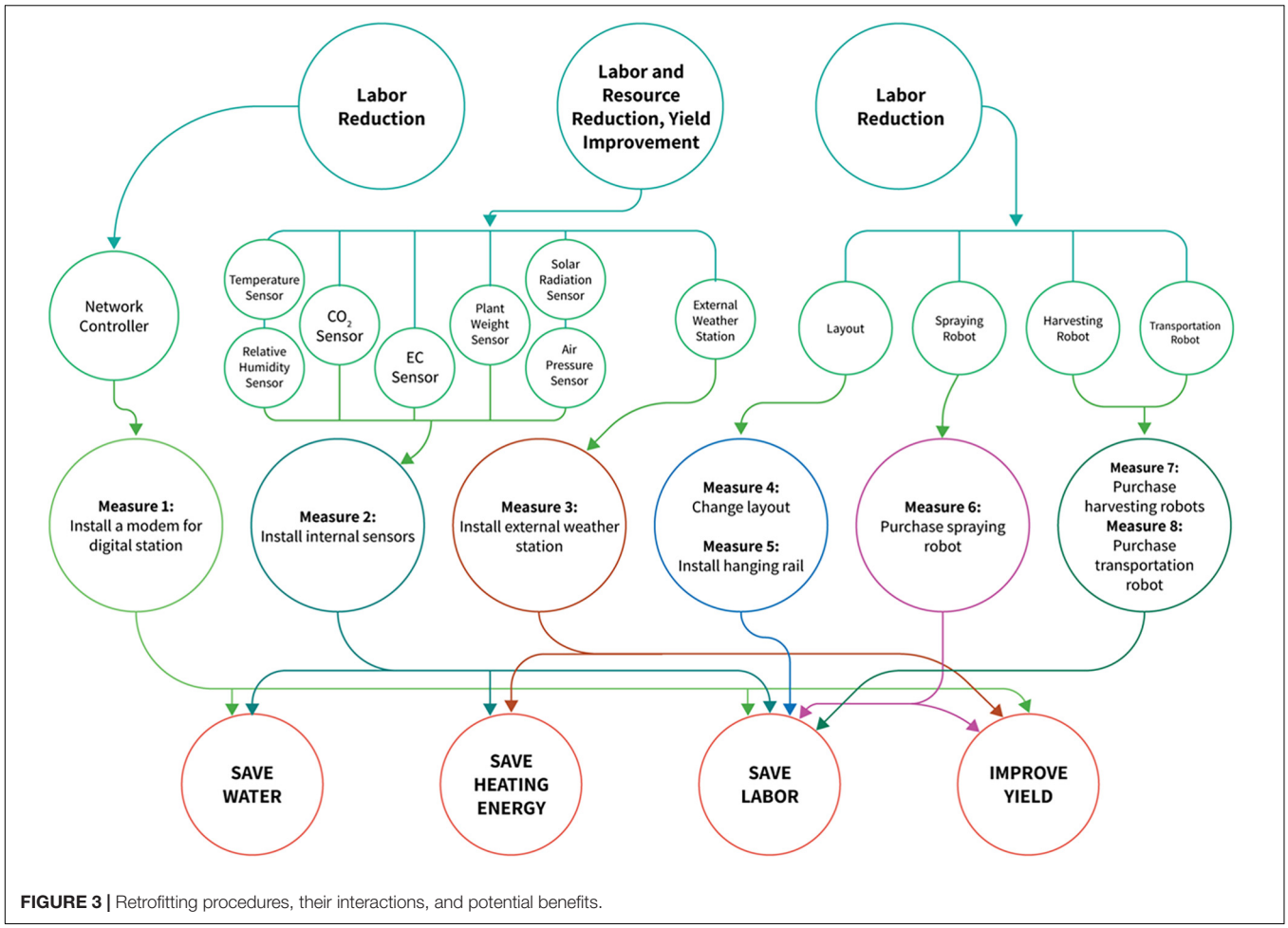

FIGURE 3 | Retrofitting procedures, their interactions, and potential benefits.

Net Profit From Improved Productivity

This was calculated as follows:

$$Profit_P = YEC - P \times \left[\frac{\left(I + \left(\frac{Ir-e}{1+e}\right)\right)^m - 1}{\left(\frac{Ir-e}{1+e}\right) \times \left(1 + \left(\frac{Ir-e}{1+e}\right)\right)^m} \right] \quad (7)$$

Where YEC is the estimated yearly energy consumption cost of the plant production system in the first year, P is profit from the retrofit, Ir is the interest rate, e is the annual rate of energy cost increase (a rate of 5%), and m is the service life of the plant production system.

$$YEC_P = EL_P \times UEL_P \quad (8)$$

Where YEC_P is the estimated yearly energy cost of production in the plant production system for the first year, EL_P is estimated annual production in the first year due to retrofit, and UEL_P is the price per unit productivity.

Net Profit From Savings in the Cost of Labor

$$Profit_L = YEC - L \times \left[\frac{\left(I + \left(\frac{Ir-e}{1+e}\right)\right)^m - 1}{\left(\frac{Ir-e}{1+e}\right) \times \left(1 + \left(\frac{Ir-e}{1+e}\right)\right)^m} \right] \quad (9)$$

Where YEC is the estimated yearly energy consumption cost of the plant production system in the first year, L is the Labor cost, Ir is the interest rate, e is the annual rate of energy cost increase (a rate of 5%), and m is the service life of the plant production system.

Consequently, the total net profit, which is the increased income from added productivity due to the new items used in retrofitting the plant production system and the money saved from labor spending because of the new systems that were retrofitted and replaced labor cost was calculated as:

$$Profit = Profit_P + Profit_L \quad (10)$$

Optimization Model

The optimization problem was formulated with two objectives: to minimize the total expenditure to retrofit for the lifespan of the plant production system (Eq. 11) while maximizing the yearly net profit derived from retrofitting the system (Eq. 12). This is shown below as objectives 1 and 2.

Objective 1: Expenditure for Retrofitting a Plant Production System

$$Minimize\ Expenditure = CR + ECC + ECC_{RC} \quad (11)$$

Where CR is the cost of the systems used in the retrofits, ECC is the energy consumption cost because of retrofitting new systems and ECC_{RC} is the replacement and maintenance cost for the retrofitted items.

Objective 2: Net Profit From Retrofitting a Plant Production System

$$Maximize\ Profit\ =\ Profit_P\ +\ Profit_L \tag{12}$$

The profit from the retrofit is the summation of the increased income from added productivity due to the new items used in retrofitting the plant production system and the money saved from labor spending because of the new systems that were retrofitted and replaced labor costs.

Constraints in Carrying Out Retrofits

In addition to the two objectives, the following constraints were implemented in this study, as shown earlier in **Figure 2**. The problem formulation could be tuned to incorporate other constraints depending on the system.

Selection of Sensors and Network Controller for Retrofitting

Since digital network controllers are meant to transmit data remotely, the type of sensors that could synchronize with it must have certain features. We formulated a constraint that only sensors with this capacity should be picked if a digital network controller is selected. This was also extended to the on-site network controller (Eq. 13).

$$x(2\,(i-1)\ x\,(2\,(i-1)\ +\ 2)\ =\ 0 \tag{13}$$

Given that, $i = 1. \ldots . \ldots 11$ (retrofitting number).

Selection of Layouts for Retrofitting

With the current advances in plant production systems, two types of robotic navigation systems have been studied. These are mobile robots that navigate on the floor of the plant production system (Uyeh et al., 2019b) and hanging types of robots suspended above the plants and hung to the roof of the plant production system. In this constraint, the problem is formulated that if the hanging type of layout is picked for retrofit, then the selected harvesting and spraying robots should be robot arms, and no transportation robot should be chosen. If otherwise, then all types of robots could be selected (Eqs 14, 15).

$$\max\,(x\,[19]\,,\ \ x\,[21]\,,\ \ x\,[23])\ \times\ x[17]^1\ =\ 0 \tag{14}$$

$$\max\,(x\,[20]\,,\ \ x\,[22])\ \times\ x[18]^1\ =\ 0 \tag{15}$$

Where x is the number of item for retrofit.

The Search Algorithm Used in This Study

The two objectives considered in the study – (a) minimization of investment cost and (b) maximizing the profit, are conflicting. In other words, minimizing investment costs results in lesser profits while maximization of profits demands more investments. Therefore, the optimization of multi-objective optimization problems does not provide a single optimal solution but a set of tradeoff solutions referred to as Pareto-optimal solutions. Population-based evolutionary algorithms are considered to solve the multi-objective problem due to their effectiveness and ability to provide the entire tradeoff solutions in a single run. Specifically, NSGA-II (Deb et al., 2002) is a more popular multi-objective evolutionary algorithm and has been widely adopted for real-world optimization problems. The general flowchart of NSGA-II is shown in **Figure 4**. NSGA-II starts with a randomly generated population of size (N), whose objective values are evaluated. The initialized population evolves over the generations through variation operators such as mutation, crossover, and environmental selection. The variation operators aim to produce effective solutions (referred to as offspring members) by using the information present in the solutions of the current population (referred to as the parent population).

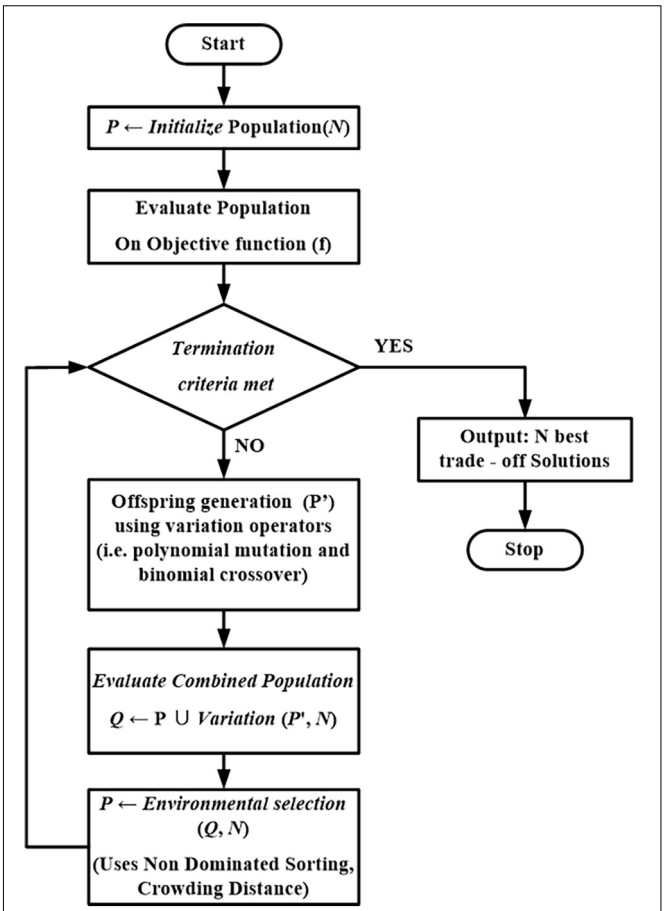

FIGURE 4 | Flowchart of non-dominated sorting genetic algorithm.

TABLE 1 | Cases used in the experimental simulations.

Case	Production before retrofits (kg)	Labor cost (USD)
1	1,000	1,000
2	2,000	1,000
3	1,000	2,000

On the other hand, environmental selection aims to select effective solutions from the combination of parent and offspring populations (P). In other words, environmental choice drives the entire population toward convergence to the Pareto-optimal solutions. The process of producing offspring members and environmental selection is repeated until the termination criteria are met. The variation operators considered in the current study are polynomial mutation and binomial crossover. Multi-objective optimization aims to obtain a set of converged well-spread diverse Pareto-optimal solutions. Thus, in NSGA-II, the environmental selection is made using non-dominated sorting followed by crowding distance, which is supposed to provide convergence and diversity. Non-dominated sorting and crowding distance are used in NSGA II to obtain the Pareto dominance of final tradeoff solutions (Uyeh et al., 2019a). The parameters of the optimization algorithm were set as follows:

Maximum number of generations (termination criteria): 500.
Population size (N): 500.
Crossover: Simulated binary crossover.
Constraint bond: 0–20.
Distribution indices for mutation (nm): 20.
Distribution indices for crossover (nc): 20.
Probability of crossover (Pc): 1.0.
Probability of mutation (Pm): 1/10.
Mutation: Polynomial mutation.

The average run time for the proposed algorithm was 180 s. The simulations were done on a 3.59 GHz AMD Ryzen 5 3500X 6-Core processor, 16 GB random access memory, and 256 GB solid-state drive with Windows 10 operating system in MATLAB (Matlab and Simulink, 2012). We conducted several simulations using guidelines from a previous manuscript (Deb et al., 2002) that proposed the algorithm and our experience working with this algorithm (Uyeh et al., 2018, 2019a,b). We finetuned and gradually increased the generations (iteration) until we got no further improvements. The number of generations that converged served as a termination value.

Experimental Design and Data Used in the Simulation

To evaluate the robustness of the proposed method, two sub-factors of the investigated factors were considered (**Table 1**) with three Cases and five sizes of a plant production system. The plant production system used for this study had five compartments of similar sizes. Size one represented one compartment, size two represented two compartments, and up to size five represented all compartments. The schematic is shown in **Figure 5**. Usually, growers have their systems divided into compartments of similar sizes for different reasons, such as ease of management. Protected cultivation systems are typically single large structures divided into smaller simple compartments. Depending on the local situation and resources of the grower, the system could be divided into various compartments (Research Wua, 2021). For example, The Radix Serre Plant production system in the Netherlands has 9,000 m^2 glass and comprises over 100 compartments (Research Wua, 2021). Each is considered and treated as an individual system. This study selected a plant production system with one to five compartments. Depending on the factor (type of equipment) and the number of compartments, the relationship between the variables at different sizes (compartments) would be linear as the compartments would require the same number of equipment such as the sensors (temperature and humidity). Since the compartments in the protected cultivation system have similar sizes, cost, impact on electricity consumption, production, and labor cost had a linear relationship. When it comes to the cost of maintenance and replacement, it can be linear in some situations and not linear in others, as there are ranges that these are priced. For example, only a single network controller is required

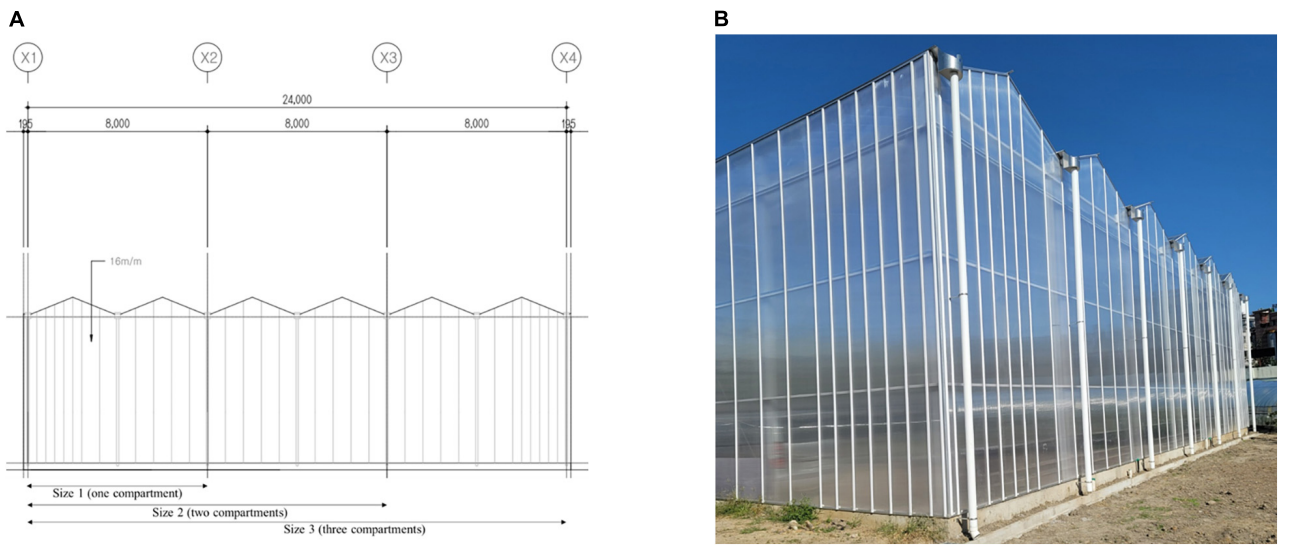

FIGURE 5 | Schematic of the experimental plant production system with one to three compartments (X1–X2: Size 1, X2–X3: Size 2, X3–X4: Size 3) **(A)**, and external view of the system **(B)**.

TABLE 2 | Data used in the experimental simulation.

Factor	Category	Size 1					Size 2					Size 3					Size 4					Size 5				
		Cost (USD)	IOEC	CMR	Ip	IL	Cost (USD)	IOEC	CMR	Ip	IL	Cost (USD)	IOEC	CMR	Ip	IL	Cost (USD)	IOEC	CMR	Ip	IL	Cost (USD)	IOEC	CMR	Ip	IL
Network controller	A	1800	200	100	2	0.9	3600	200	100	4	1.8	5400	210	100	6	2.7	7200	220	100	8	3.6	9000	230	100	10	4.5
	AN	1260	140	60	1	0.5	2520	280	90	2	1	3780	420	120	3	1.5	5040	560	120	4	2	6300	700	150	5	2.5
Temperature/ humidity	A	300	20	100	2	0.001	600	40	150	4	0.002	900	60	200	6	0.003	1200	80	200	8	0.004	1500	100	250	10	0.005
	AN	210	14	60	1	0.001	420	28	90	2	0.002	630	42	120	3	0.003	840	56	120	4	0.004	1050	70	150	5	0.005
CO_2	A	345	20	100	2	0.001	690	40	150	4	0.002	1035	60	200	6	0.003	1380	80	200	8	0.004	1725	100	250	10	0.005
	AN	241.5	14	60	1	0.001	483	28	90	2	0.002	724.5	42	120	3	0.003	966	56	120	4	0.004	1207.5	70	150	5	0.005
EC	A	320	20	100	1	0.001	640	40	150	2	0.002	960	60	200	3	0.003	1280	80	200	4	0.004	1600	100	250	5	0.005
	AN	224	14	60	0.5	0.001	448	28	90	1	0.002	672	42	120	1.5	0.003	896	56	120	2	0.004	1120	70	150	2.5	0.005
Solar radiation	A	420	20	100	2	0.001	840	40	150	4	0.002	1260	60	200	6	0.003	1680	80	200	8	0.004	2100	100	250	10	0.005
	AN	294	14	60	1	0.001	588	28	90	2	0.002	882	42	120	3	0.003	1176	56	120	4	0.004	1470	70	150	5	0.005
Air pressure	A	62	20	100	1	0.001	124	40	150	2	0.002	186	60	200	3	0.003	248	80	200	4	0.004	310	100	250	5	0.005
	AN	43.4	14	60	0.5	0.001	86.8	28	90	1	0.002	130.2	42	120	1.5	0.003	173.6	56	120	2	0.004	217	70	150	2.5	0.005
Plant weight	A	50	20	100	1	0.001	100	40	150	2	0.002	150	60	200	3	0.003	200	80	200	4	0.004	250	100	250	5	0.005
	AN	35	14	60	0.5	0.001	70	28	90	1	0.002	105	42	120	1.5	0.003	140	56	120	2	0.004	175	70	150	2.5	0.005
External weather station	A	2000	200	100	1	0.001	4000	400	150	2	0.002	6000	600	200	3	0.003	8000	800	200	4	0.004	10000	1000	250	5	0.005
	AN	1400	140	60	0.5	0.001	2800	280	90	1	0.002	4200	420	120	1.5	0.003	5600	560	120	2	0.004	7000	700	150	2.5	0.005
Layout	F	50000	0	10000	0	0.5	100000	0	15000	0	1	150000	0	20000	0	1.5	200000	0	20000	0	2	250000	0	25000	0	2.5
	H	25000	0	600	0	0.1	50000	0	900	0	0.2	75000	0	1200	0	0.3	100000	0	1200	0	0.4	125000	0	1500	0	0.5
Spraying robot	M	30000	1200	6000	1	0.95	60000	2400	9000	2	1.9	90000	3600	12000	3	2.85	120000	4800	12000	4	3.8	150000	6000	15000	5	4.75
	R	10000	840	3600	0.5	0.95	20000	1680	5400	1	1.9	30000	2520	7200	1.5	2.85	40000	3360	7200	2	3.8	50000	4200	9000	2.5	4.75
Harvesting robot	M	30000	1200	6000	0.01	0.95	60000	2400	9000	0.02	1.9	90000	3600	12000	0.03	2.85	120000	4800	12000	0.04	3.8	150000	6000	15000	0.05	4.75
	R	10000	840	3600	0.005	0.95	20000	1680	5400	0.01	1.9	30000	2520	7200	0.015	2.85	40000	3360	7200	0.02	3.8	50000	4200	9000	0.025	4.75
Transportation robot	M	15000	1200	3000	0.01	0.95	30000	2400	4500	0.02	1.9	45000	3600	6000	0.03	2.85	60000	4800	6000	0.04	3.8	75000	6000	7500	0.05	4.75

A, digital; AN, analogue; F, floor; H, hanging; M, mobile; R, rail; IOEC, impact on electricity consumption; CMR, cost of maintenance and replacement; IP, impact on production; IL, impact on labor. Source: Ubn (2021).

in a plant production system irrespective of the number of compartments; the cost of maintenance and replacement of the network controller would not be linear compared to temperature and relative humidity sensors. The number of sensors and other retrofitting measures in one compartment (Size 1) of the plant production system was selected based on Korean industrial standards (UBN, 2021; **Table 2**). A compartment of the system had a height of 6,700 mm, a width of 8,000 mm, and a length of 16,700 mm. This formed the basis for selecting the number of retrofitting measures required for the other system sizes (Sizes 2–5).

The yield data (**Table 1**) used was guided by visits to plant production system growers in the Republic of Korea to validate the optimization model. Strawberry yields are dependent on the environmental conditions, systems, techniques of production, and type of plant production system, which includes plant factories and greenhouses, as also reported by Kubota (2015).

Computation of Impact of Automation on Labor

Data were acquired using structured questionnaires from growers adopting plant production systems to demonstrate the importance of retrofitting robotics in a plant production system. The human category was divided into three groups based on their expertise. Finally, we considered a real-world scenario of the first-of-its-kind strawberry harvesting robot (**Table 3**) as a comparison.

TABLE 3 | Comparison between humans and robots in strawberry harvesting.

Factors	Category (s)			
	Robot	Human		
		Beginner	Average	Experienced
Platform movement/ Movement to fruit location	4.7	2	2	2
Fruit localization/ identification	3.7	10	10	10
Obstacle localization	3.0	1	1	1
Visual servoing/harvesting decision making	4.0	10	7.5	5
Detach fruit	2.2	2	1.5	1
Put fruit in the container	7.8	5	4	3
Working time (per h/day)	20	4	6	8
Success rate (%)	95	Uncertain	Uncertain	Uncertain
Cost of purchase (USD)	110,000	Not applicable	Not applicable	Not applicable
Lifespan (years)	7	Not applicable	Not applicable	Not applicable
Salvage cost (Purchase cost/ lifespan), USD	15,714	Not applicable	Not applicable	Not applicable

The factors (Sweeper, 2020) given in **Table 3** were considered in deciding the impact of operating a robot on labor cost and yield.

Additionally, there are numerous benefits of using robotics in a plant production system that is near impossible to quantify in terms of monetary benefits but rather impact. These include:

(i) Safety of products.

(ii) Availability of skilled workers.

(iii) Incessant increase in wages of skilled workers as seen in the context of the Republic of Korea and other OECD countries.

Also, the data for the sensors were collected from the UBN sensors company (UBN, 2021) and used in the simulation.

Overall, the developed system provides the user with the possibilities of specifying their local context (Size and service life of the plant production system, cost of the items for retrofitting, cost of electricity per unit and impact of retrofitting on electricity consumption, interest paid on loans for retrofitting items, the annual rate of increase in energy cost, maintenance, and replacement period for each retrofitted item, projected production before and after retrofitting, projections in the price of the product, labor cost before and after retrofit, projections in the cost of labor and profit).

SIMULATION RESULTS AND DISCUSSION

Measures, Cost of Expenditure, and Profit for Retrofitting Case 1 Plant Production Systems

The simulation results show feasible combinations at different sizes for Case 1, represented with different colors for the selected measures (**Figure 6**). Each combination shows the total expenditure required to carry out the retrofit for the lifespan of the plant production system and the projected net profit per year (**Figure 7**). The feasible retrofits and tradeoff total expenditure versus the net profit per year are presented for all sizes. In Case 1, in size 1 of the retrofitting combinations, multiple feasible combinations were obtained compared to sizes 2–5 (**Figure 6**). However, the few possible retrofit combinations in sizes 2–5 show more return on investments (ROI) than the multiple feasible combinations in size 1. This demonstrates that despite the grower with size 1 having numerous possible combinations, the size of a system is more critical for profitability (**Figure 7**). The results also indicate that introducing new technologies might not necessarily mean a return on investment in an optimum way without analyzing all possible factors, such as current and projected labor costs and electricity consumption. The results in **Figure 6** also show that despite a similar amount of money being spent to carry out the retrofit at a point across the different sizes of the plant production system, the net profit increased with the size of the system.

Further analyses of the return on investment in the size 1 (**Figure 7A**) in Case 1 showed a similar cost. Subsequently, retrofit combinations were available to be implemented that significantly increased the net profits. For example, there was

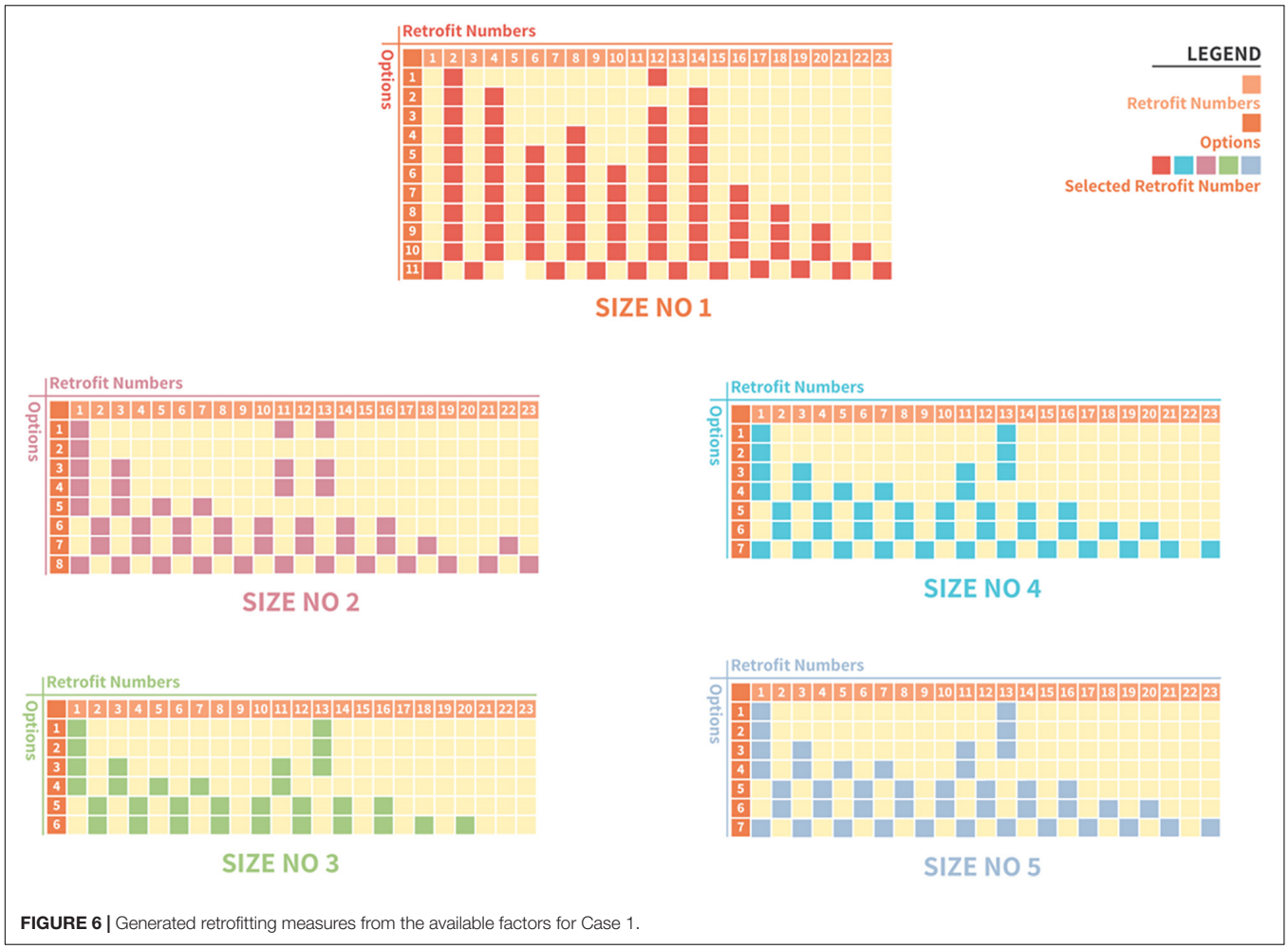

FIGURE 6 | Generated retrofitting measures from the available factors for Case 1.

a 4.03% increase in yearly net profit between two retrofit combinations with an investment cost of 4,990 and 5,700 USD (**Figure 7A**). An increase of 700 USD investment would result in about 280,000 USD or 4.03% in yearly net profit in this situation. In these combinations, the combination at the cost of 4,990 USD had selected retrofit measures 2 and 12 (**Figure 6**), which are analog network controller and temperature/humidity sensors (**Figure 1**). However, in the combination of 5,700 USD, the selected retrofit measures were 2, 4, 6, 8, 12, and 14 (**Figure 6**). This combination picked additional measures in addition to the two chosen at the cost of 4,990 USD. These were sensors for CO_2, solar radiation, air pressure, and plant weight (**Figure 6**). Both combinations picked only analog measures. The sensors picked at the cost of 5,700 USD facilitated improved decision-making, thus increasing yearly productivity and extension profit.

Further analysis showed that all cost combinations except one selected the analog category instead of the digital. However, despite the investment cost of about 133,984 USD compared to the closest cost combination of about 52,394 USD which is less than half, the return on investments is approximately 7,675,358 USD and 7,599,365 USD, respectively (**Figure 7A**). This was a 1% increase compared to the 155% increase in investment cost. This analysis shows the importance of this system and the need to consider various factors when carrying out retrofits.

Measures, Cost of Expenditure, and Profit for Retrofitting Case 2 Plant Production Systems

In Case 2 retrofitting measures for a plant production system (**Figure 8**), an increase in productivity at a similar labor cost in Case 1 was investigated. These analyses were done to ascertain the impact of production on retrofit. Despite the cost of investment was similar, there was a significant increase in the return on investment when the productivity was doubled. This was around a 100% increase in the return on investment in size 1 of the system (**Figure 8A**). However, as the size of the system increased (**Figures 8B–E**), despite the similarity in the investment cost for retrofitting between Case 1 and 2, and the doubling of the productivity, a different trend was seen with the return on investment of around 132% for sizes 2 (**Figures 7B**, **8B**), 121% for sizes 3 (**Figures 7C**, **8C**), 136% for sizes 4 (**Figures 7C**, **8D**), and 155% for size 5 (**Figure 8E**). This demonstrates that the size of the system and productivity are essential factors to consider in

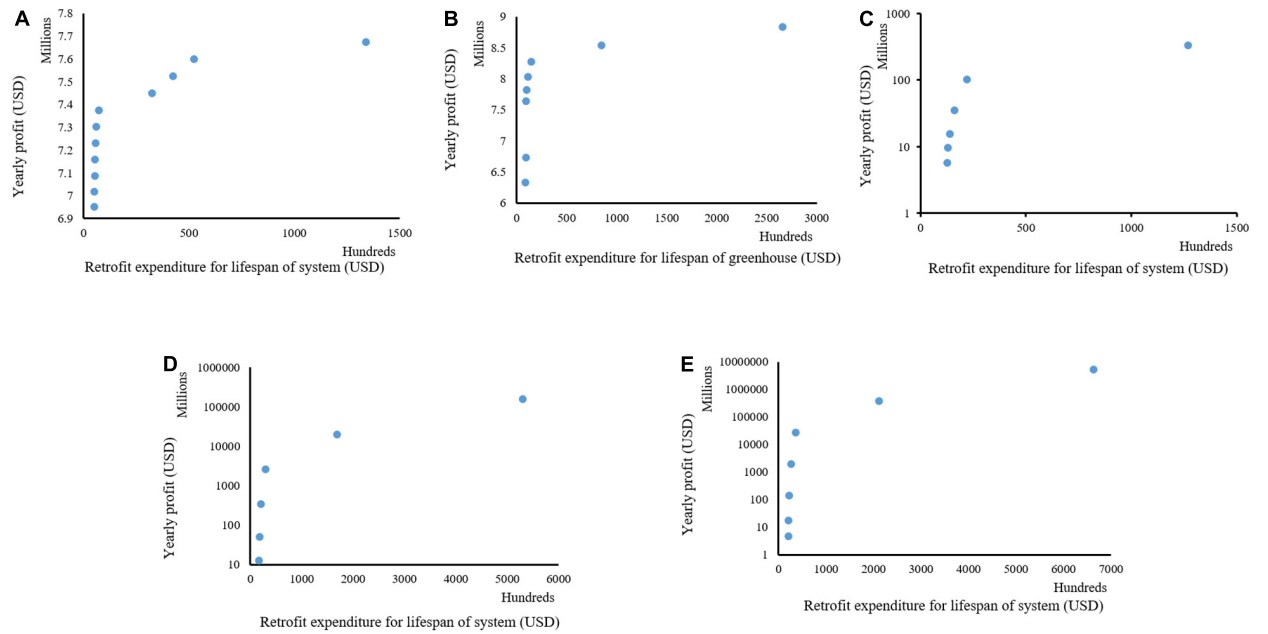

FIGURE 7 | Different combinations of cost of retrofitting and yearly profit derived at different sizes of a plant production system for Case 1; size 1 **(A)**, size 2 **(B)**, size 3 **(C)**, size 4 **(D)**, and size 5 **(E).**

retrofitting. A similar trend in combinations of retrofit measures to be implemented was seen between Case 1 and Case 2.

Measures, Cost of Expenditure, and Profit for Retrofitting Case 3 Plant Production Systems

Case 3 was designed to investigate the impact of labor cost on the retrofit measures, cost of investment, and return on investment. This case was investigated because of the similarities in productivity that are sometimes found in plant production systems from the optimal control of the micro- and macro-environments but the difference in the local contexts with labor cost because of the disparity in standard of living and development. In this Case, the productivity was kept like in Case 1, but the labor cost was doubled in Case 3. Size 1 (**Figure 9A**) showed no difference between Case 1 and Case 3 at comparable investment costs, even though the labor cost in Case 3 doubled that in Case 1. However, in the size 2 (**Figure 9B**) of Case 3, a different trend was seen compared to Case 1. The results show that the least amount of money for retrofit (around 9,000 USD) had a better return on investment than the most expensive combination (about 26,000 USD) for retrofits in Cases 1 and 3. These were a 29% increase in return on investment in Case 1 compared to Case 3 at the least combination of retrofit factors and around a 2% increase in return on investment in Case 1 compared to Case 3 for the maximum combination of retrofit factors. This was even more with the comparisons in investment cost and the cost of labor in Case 3 being a 100% increase from Case 1. To validate our method, we analyzed the components selected in both situations (least and highest cost of investment). Only two retrofit measures were selected at the least cost of investment: a digital network controller and an air pressure sensor for Case 1. In Case 2, only the digital network controller was selected. The selected retrofit measures in both Case 1 and Case 3 have minimal impact on productivity and cost of labor. This verifies the increase in return on investment of around 29% in Case 1, size 2 from that of Case 3. The increase was because of the savings from labor costs in Case 1. However, with the maximum investment cost, all the automated measures were selected in Case 1 and Case 3. With this, the labor cost did not significantly impact the return on investment, thus leading to only a 2% increase in return on investment of Case 1 compared to Case 3.

Impact of Labor Cost and Productivity on Return in Investment in Retrofitting

Figures 7–9 shows the combination of the total expenditure required to carry out the retrofit for the lifespan of the plant production system and the projected net profit per year for three investigated cases. These cases varied in the production quantity before retrofits and local labor costs. These were done to explore what would impact the retrofitting expenditure and profits as different yields are gotten across different systems depending on the cultivated variety and other inputs. The labor cost also varies with the local situation as systems closer to the urban centers would have more expenditure on labor costs than those located farther from the cities. Analyses of the results showed that despite having similar spending for the three investigated scenarios of labor cost and yields, the total maximum yearly profit was similar for Cases 1 and 3 but was double for Case 2 from what was recorded in Cases 1 and 3 for size 1. A similar scenario was recorded in Size 2. In sizes 3–5, a similar maximum profit was

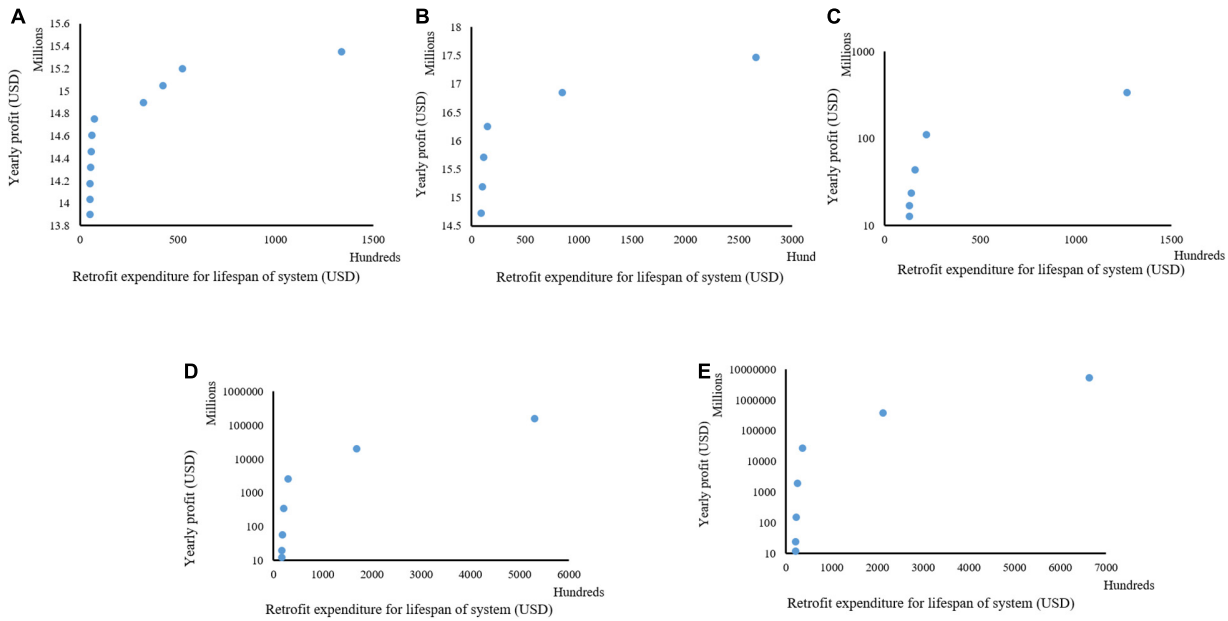

FIGURE 8 | Different combinations of cost of retrofitting and yearly profit derived at different sizes of a plant production system for Case 2; size 1 **(A)**, size 2 **(B)**, size 3 **(C)**, size 4 **(D)**, and size 5 **(E).**

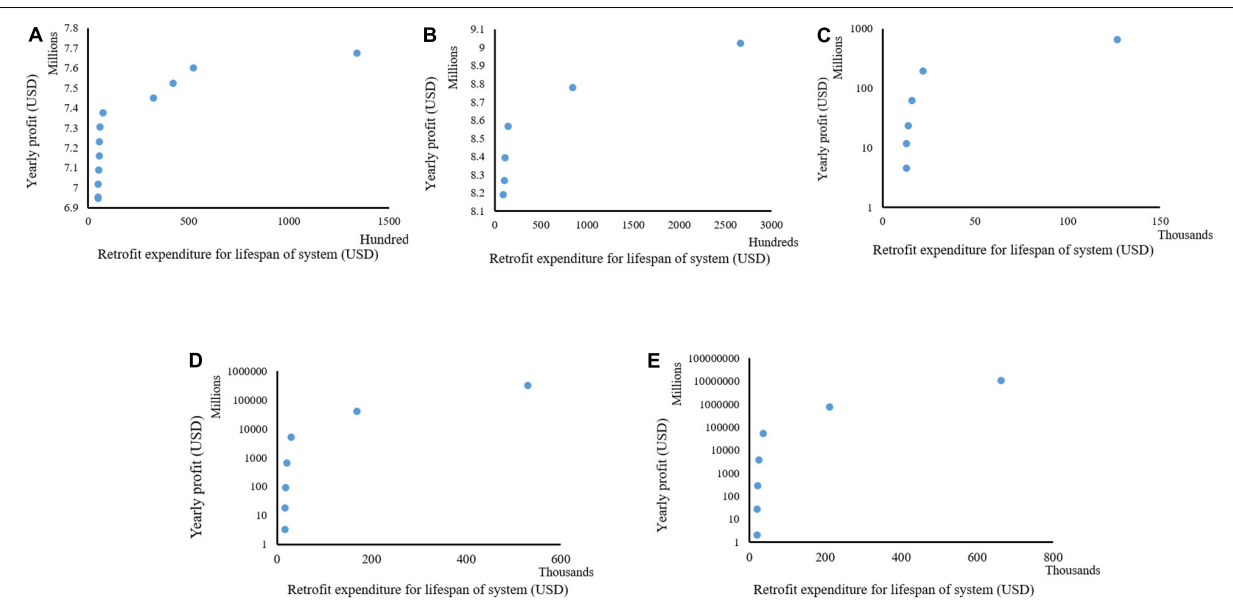

FIGURE 9 | Different combinations of cost of retrofitting and yearly profit derived at different sizes of a plant production system for Case 3; size 1 **(A)**, size 2 **(B)**, size 3 **(C)**, size 4 **(D)**, and size 5 **(E).**

recorded in all the investigated cases. This points out that despite the labor cost being double in Case 3, the similar productivity in Cases 1 and 3 would result in similar profits at a smaller production capacity, but this would change as the size of the production system increases. Also, our analyses show that at a smaller production capacity, the grower needs to pay attention to the best variety for productivity when retrofitting. This becomes less important when the size of the system increases. These analyses point to the importance of this decision-making tool when deciding to retrofit.

CONCLUSION

A user-friendly system to generate all the feasible tradeoff retrofit combinations for agricultural production systems such as

plant factories and greenhouses was developed in this study. Cost of new technologies, interest on loans for retrofitting, size and service life of the production system, the present and projected cost for human labor and robotics, productivity, energy consumption, and replacement and maintenance costs were considered in the developed system. The presentation of tradeoff solutions of possible retrofit combinations, total expenditure, and net profit per year that is made possible by the developed system would improve decision-making. For example, an investigated case showed an increase of up to 250% in net profits. We propose a multi-objective retrofitting method for agricultural production systems to minimize the total cost of investment and maximize the yearly net profit.

DATA AVAILABILITY STATEMENT

The original contributions presented in this study are included in the article/**Supplementary Material**, further inquiries can be directed to the corresponding author.

AUTHOR CONTRIBUTIONS

DU: conceptualization, methodology, software, investigation, formal analysis, data curation, visualization, and writing – original draft. RM: methodology, investigation, software, data curation, visualization, and writing – review and editing. TP and YH: validation, resources, writing – review and editing, supervision, and funding acquisition. SW: validation, visualization, funding acquisition, and project administration. All authors contributed to the article and approved the submitted version.

FUNDING

This work was supported by Korea Institute of Planning and Evaluation for Technology in Food, Agriculture, and Forestry (IPET) through the Agriculture, Food and Rural Affairs Convergence Technologies Program for Educating Creative Global Leader, funded by the Ministry of Agriculture, Food and Rural Affairs (MAFRA) (320001-4) and (716001-7), Republic of Korea and Rural Development Administration (RDA) through the development of data application technology for postharvest management of the agricultural & livestock product project, funded by the Ministry of Agriculture, Food and Rural Affairs (MAFRA) (PJ016981).

SUPPLEMENTARY MATERIAL

The Supplementary Material for this article can be found online at: https://www.frontiersin.org/articles/10.3389/fpls.2022.929672/full#supplementary-material

REFERENCES

Antipova, E., Boer, D., Guillén-Gosálbez, G., Cabeza, L. F., and Jiménez, L. (2014). Multi-objective optimization coupled with life cycle assessment for retrofitting buildings. *Energy Build.* 82, 92–99. doi: 10.1016/j.enbuild.2014.07.001

Baeza, E., Stanghellini, C., and Castilla, N, editors (2011). "Protected cultivation in Europe," in *Proceedings of the International Symposium on High Tunnel Horticultural Crop Production 987*. State College.

Bagnall, A. J., Rayward-Smith, V. J., and Whittley, I. M. (2001). The next release problem. *Inform. Softw. Technol.* 43, 883–890. doi: 10.1016/S0950-5849(01)00194-X

Barua, S. (2020). Understanding coronanomics: the economic implications of the coronavirus (COVID-19) pandemic. *SSRN Electr. J.* doi: 10.2139/ssrn.3566477

Bogue, R. (2020). Fruit picking robots: has their time come? *Ind. Robot* 47, 141–145. doi: 10.1108/IR-11-2019-0243

Deb, K., Agrawal, S., Pratap, A., and Meyarivan, T, editors (2000). "A fast elitist non-dominated sorting genetic algorithm for multi-objective optimization: NSGA-II," in *Proceedings of the International Conference on Parallel Problem Solving from Nature*. (Heidelberg: Springer). doi: 10.1007/3-540-45356-3_83

Deb, K., Pratap, A., Agarwal, S., and Meyarivan, T. (2002). A fast and elitist multiobjective genetic algorithm: NSGA-II. *IEEE Trans. Evol. Comput.* 6, 182–197. doi: 10.1109/4235.996017

Diakaki, C., Grigoroudis, E., and Kolokotsa, D. (2008). Towards a multi-objective optimization approach for improving energy efficiency in buildings. *Energy Build.* 40, 1747–1754. doi: 10.1016/j.enbuild.2008.03.002

Dixon, T., McNamara, P., Miller, E., and Buys, L. (2008). Retrofitting commercial office buildings for sustainability: tenants' perspectives. *J. Prop. Invest. Finance* 26, 552–561. doi: 10.1108/14635780810908398

El-Darwish, I., and Gomaa, M. (2017). Retrofitting strategy for building envelopes to achieve energy efficiency. *Alex. Eng. J.* 56, 579–589. doi: 10.1016/j.aej.2017.05.011

Fan, Y., and Xia, X. (2017). A multi-objective optimization model for energy-efficiency building envelope retrofitting plan with rooftop PV system installation and maintenance. *Appl. Energy.* 189, 327–335. doi: 10.1016/j.apenergy.2016.12.077

Fan, Y., and Xia, X. (2018). Energy-efficiency building retrofit planning for green building compliance. *Build. Environ.* 136, 312–321. doi: 10.1016/j.buildenv.2018.03.044

Fonseca, C. M., and Fleming, P. J. (1993). "Genetic algorithms for multiobjective optimization: formulation, discussion and generalization," in *Proceedings of the 5th International Conference on Genetic Algorithms (ICGA-93), 17-22 July 1993*, Vol. 93, San Mateo, CA, Urbana-Champaign. 416–423.

Galanakis, C. M. (2020). The food systems in the era of the coronavirus (COVID-19) pandemic crisis. *Foods.* 9:523. doi: 10.3390/foods9040523

Gerson, U., and Weintraub, P. G. (2007). Mites for the control of pests in protected cultivation. *Pest Manag. Sci. Form. Pestic. Sci.* 63, 658–676. doi: 10.1002/ps.1380

Gullino, M. L., Albajes, R., and van Lenteren, J. C. (1999). "Setting the stage: characteristics of protected cultivation and tools for sustainable crop protection," in *Integrated Pest and Disease Management in Greenhouse Crops Developments in Plant Pathology*, eds R. Albajes, M. Lodovica Gullino, J. C. van Lenteren, and Y. Elad (Dordrecht: Springer), 1–15. doi: 10.1007/0-306-47585-5_1

Helm, D. (2020). The environmental impacts of the coronavirus. *Environ. Resour. Econo.* 76, 21–38. doi: 10.1007/s10640-020-00426-z

Horn, J., Nafpliotis, N., and Goldberg, D. E. (1993). *Multiobjective Optimization Using the Niched Pareto Genetic Algorithm. IlliGAL Report 93005*. Urbana: University of Illinois.

Jafari, A., and Valentin, V. (2017). An optimization framework for building energy retrofits decision-making. *Build. Environ.* 115, 118–129. doi: 10.1016/j.buildenv.2017.01.020

Jafari, A., Valentin, V., and Bogus, SM, editors (2016). "Assessment of social indicators in energy housing retrofits," in *Proceedings of the Construction Research Congress 2016*. (San Juan). doi: 10.1061/9780784479827.109

Jensen, M. H., and Malter, A. J. (1995). *Protected Agriculture: a Global Review*. Washington, DC: World Bank Publications.

Kannan, S., Baskar, S., McCalley, J. D., and Murugan, P. (2008). Application of NSGA-II algorithm to generation expansion planning. *IEEE Trans. Power Syst.* 24, 454–461. doi: 10.1109/TPWRS.2008.2004737

Kolaitis, D. I., Malliotakis, E., Kontogeorgos, D. A., Mandilaras, I., Katsourinis, D. I., and Founti, M. A. (2013). Comparative assessment of internal and external thermal insulation systems for energy efficient retrofitting of residential buildings. *Energy Build.* 64, 123–131. doi: 10.1016/j.enbuild.2013.04.004

Kubota, C. (2015). *Strawberry Production Costs in Greenhouse*. Available online at https://cals.arizona.edu/strawberry/Hydroponic_Strawberry_Information_Website/Costs.html (accessed July 12, 2021).

Kurtser, P., and Edan, Y. (2020). Planning the sequence of tasks for harvesting robots. *Robot. Auton. Syst.* 131:103591. doi: 10.1016/j.robot.2020.103591

Li, H., and Zhang, Q. (2008). Multiobjective optimization problems with complicated Pareto sets. MOEA/D and NSGA-II. *IEEE Trans. Evol. Comput.* 13, 284–302. doi: 10.1109/TEVC.2008.925798

Lima, C. K. T., de Medeiros Carvalho, P. M., Lima, I. A. A. S., de Oliveira Nunes, J. V. A., Saraiva, J. S., de Souza, R. I., et al. (2020). The emotional impact of Coronavirus 2019-nCoV (new Coronavirus disease). *Psychiatry Res.* 287, 112915. doi: 10.1016/j.psychres.2020.112915

Liu, Y., Liu, T., Ye, S., and Liu, Y. (2018). Cost-benefit analysis for energy efficiency retrofit of existing buildings: a case study in China. *J. Clean. Prod.* 177, 493–506. doi: 10.1016/j.jclepro.2017.12.225

Ma, Z., Cooper, P., Daly, D., and Ledo, L. (2012). Existing building retrofits: methodology and state-of-the-art. *Energy Build.* 55, 889–902. doi: 10.1016/j.enbuild.2012.08.018

Malatji, E. M., Zhang, J., and Xia, X. (2013). A multiple objective optimisation model for building energy efficiency investment decision. *Energy Build.* 61, 81–87. doi: 10.1016/j.enbuild.2013.01.042

Marler, R. T., and Arora, J. S. (2004). Survey of multi-objective optimization methods for engineering. *Struct multidisciplinary Optimiz.* 26, 369–395. doi: 10.1007/s00158-003-0368-6

Marszal, A. J., Heiselberg, P., Bourrelle, J. S., Musall, E., Voss, K., Sartori, I., et al. (2011). Zero energy building – a review of definitions and calculation methodologies. *Energy Build.* 43, 971–979. doi: 10.1016/j.enbuild.2010.12.022

MathWorks (2021). *Minimize Multiple Objective Functions Subject to Constraints*. Natick, MA: MathWorks.

Matlab and Simulink (2012). *Matlab*. Natick, MA: The MathWorks.

Nicola, M., Alsafi, Z., Sohrabi, C., Kerwan, A., Al-Jabir, A., Iosifidis, C., et al. (2020). The socio-economic implications of the coronavirus pandemic (COVID-19): A review. *Int. J. Surg.* 78:185. doi: 10.1016/j.ijsu.2020.04.018

Nordey, T., Basset-Mens, C., De Bon, H., Martin, T., Déletré, E., Simon, S., et al. (2017). Protected cultivation of vegetable crops in sub-Saharan Africa: limits and prospects for smallholders. A review. *Agron. Sustain. Dev.* 37:53. doi: 10.1007/s13593-017-0460-8

Paul, N. D., and Gwynn-Jones, D. (2003). Ecological roles of solar UV radiation: towards an integrated approach. *Trends Ecol. Evol.* 18, 48–55. doi: 10.1016/S0169-5347(02)00014-9

Raviteja, K., and Supriya, M. (2020). "IoT-based agriculture monitoring system," in *Data Engineering and Communication Technology. Advances in Intelligent Systems and Computing*, Vol. 1079, eds K. Raju, R. Senkerik, S. Lanka, and V. Rajagopal (Singapore: Springer), 473–483.

Raviv, M., and Antignus, Y. (2004). UV radiation. *Photochem. Photobiol.* 79, 219–226. doi: 10.1562/SI-03-14.1

Rayhana, R., Xiao, G., and Liu, Z. (2020). Internet of Things Empowered Smart Greenhouse. *IEEE J. Radio Freq Identif.* 4, 195–211. doi: 10.1109/JRFID.2020.2984391

Reddy, P. P. (2016). *Sustainable Crop Protection Under Protected Cultivation*. Singapore: Springer. doi: 10.1007/978-981-287-952-3

Research Wua (2021). *Greenhouses*. Available online at: https://www.wur.nl/en/Research-Results/Projects-and-programmes/Unifarm-1/Facilities/Greenhouses.htm (accessed October 11, 2021).

Robinson, J. (2018). World's Largest Single-Domed Tropical Greenhouse is Coming to France. London: The Vinyl Factory Group.

Sahoo, P. P., and Rath, S. (2020). Potential impact of corona virus on agriculture sector. *Biotica Res. Today* 2, 64–65.

Saini, N., and Saha, S. (2021). Multi-objective optimization techniques: a survey of the state-of-the-art and applications. *Eur. Phys. J. Spec Top.* 230, 2319–2335. doi: 10.1140/epjs/s11734-021-00206-w

Shamshiri, R., Kalantari, F., Ting, K., Thorp, K. R., Hameed, I. A., Weltzien, C., et al. (2018). Advances in greenhouse automation and controlled environment agriculture: a transition to plant factories and urban agriculture. *Int. J. Agric. Biol. Eng.* 11, 1–22. doi: 10.25165/j.ijabe.20181101.3210

Srinivas, N., and Deb, K. (1994). Muiltiobjective optimization using nondominated sorting in genetic algorithms. *Evol. Comput.* 2, 221–248. doi: 10.1162/evco.1994.2.3.221

Stanghellini, C., and Montero, J. I. (2010). "Resource use efficiency in protected cultivation: towards the greenhouse with zero emissions," in *Proceedings of the XXVIII International Horticultural Congress on Science and Horticulture for People (IHC2010)*, Vol. 927, Lisbon, 91–100.

Sweeper (2020). *Sweet Pepper Harvesting Robot*. Available online at: http://www.sweeper-robot.eu/ (accessed February 13, 2021).

UBN (2021). *UBN Smartfarm System*. Available online at: http://farmlink.ubncorp.co.kr/eng/main.php (accessed December 10, 2021).

Uyeh, D. D., Mallipeddi, R., Pamulapati, T., Park, T., Kim, J., Woo, S., et al. (2018). Interactive livestock feed ration optimization using evolutionary algorithms. *Comput. Electr. Agric.* 155, 1–11. doi: 10.1016/j.compag.2018.08.031

Uyeh, D. D., Pamulapati, T., Mallipeddi, R., Park, T., Asem-Hiablie, S., Woo, S., et al. (2019a). Precision animal feed formulation: an evolutionary multi-objective approach. *Animal Feed Sci Technol.* 256, 114211. doi: 10.1016/j.anifeedsci.2019.114211

Uyeh, D. D., Ramlan, F. W., Mallipeddi, R., Park, T., Woo, S., Kim, J., et al. (2019b). Evolutionary greenhouse layout optimization for rapid and safe robot navigation. *IEEE Access.* 7, 88472–88480. doi: 10.1109/ACCESS.2019.2926566

Van Straten, G., van Willigenburg, G., van Henten, E., and van Ooteghem, R. (2010). *Optimal Control of Greenhouse Cultivation*. Boca Raton, FL: CRC press. doi: 10.1201/b10321

Wang, C., Horby, P. W., Hayden, F. G., and Gao, G. F. (2020). A novel coronavirus outbreak of global health concern. *Lancet* 395, 470–473. doi: 10.1016/S0140-6736(20)30185-9

Wells, C. R., Sah, P., Moghadas, S. M., Pandey, A., Shoukat, A., Wang, Y., et al. (2020). Impact of international travel and border control measures on the global spread of the novel 2019 coronavirus outbreak. *Proc. Natl Acad. Sci. U.S.A.* 117, 7504–7509. doi: 10.1073/pnas.2002616117

Wittwer, S. H., and Castilla, N. (1995). Protected cultivation of horticultural crops worldwide. *HortTechnology* 5, 6–23. doi: 10.21273/HORTTECH.5.1.6

Wu, Z., Wang, B., and Xia, X. (2016). Large-scale building energy efficiency retrofit: concept, model and control. *Energy* 109, 456–465. doi: 10.1016/j.energy.2016.04.124

Xu, P., and Chan, E. H. (2013). ANP model for sustainable building energy efficiency retrofit (BEER) using energy performance contracting (EPC) for hotel buildings in China. *Habit. Int.* 37, 104–112. doi: 10.1016/j.habitatint.2011.12.004

Xu, P., Chan, E. H., Visscher, H. J., Zhang, X., and Wu, Z. (2015). Sustainable building energy efficiency retrofit for hotel buildings using EPC mechanism in China: analytic network process (ANP) approach. *J. Clean. Prod.* 107, 378–388. doi: 10.1016/j.jclepro.2014.12.101

Xu, P., Chan, E. H.-W., and Qian, Q. K. (2011). Success factors of energy performance contracting (EPC) for sustainable building energy efficiency retrofit (BEER) of hotel buildings in China. *Energy Policy* 39, 7389–7398.

Yusoff, Y., Ngadiman, M. S., and Zain, A. M. (2011). Overview of NSGA-II for optimizing machining process parameters. *Proc. Eng.* 15, 3978–3983.

Conflict of Interest: The authors declare that the research was conducted in the absence of any commercial or financial relationships that could be construed as a potential conflict of interest.

Publisher's Note: All claims expressed in this article are solely those of the authors and do not necessarily represent those of their affiliated organizations, or those of the publisher, the editors and the reviewers. Any product that may be evaluated in this article, or claim that may be made by its manufacturer, is not guaranteed or endorsed by the publisher.

frontiers | Frontiers in Plant Science

TYPE Original Research
PUBLISHED 15 July 2022
DOI 10.3389/fpls.2022.944716

OPEN ACCESS

EDITED BY
Yuxin Tong,
Institute of Environment and Sustainable Development in Agriculture (CAAS), China

REVIEWED BY
Rongfang Guo,
Fujian Agriculture and Forestry University, China
Xueyan Zhang,
Ningxia University, China

*CORRESPONDENCE
Eiji Goto
goto@faculty.chiba-u.jp

SPECIALTY SECTION
This article was submitted to Technical Advances in Plant Science, a section of the journal Frontiers in Plant Science

RECEIVED 15 May 2022
ACCEPTED 27 June 2022
PUBLISHED 15 July 2022

CITATION
Wittayathanarattana T, Wanichananan P, Supaibulwatana K and Goto E (2022) A short-term cooling of root-zone temperature increases bioactive compounds in baby leaf *Amaranthus tricolor* L.
Front. Plant Sci. 13:944716.
doi: 10.3389/fpls.2022.944716

A short-term cooling of root-zone temperature increases bioactive compounds in baby leaf *Amaranthus tricolor* L.

Takon Wittayathanarattana[1,2], Praderm Wanichananan[3], Kanyaratt Supaibulwatana[2] and Eiji Goto[1,4]*

[1]Graduate School of Horticulture, Chiba University, Chiba, Japan, [2]Department of Biotechnology, Faculty of Science, Mahidol University, Bangkok, Thailand, [3]National Science and Technology Development Agency, Thailand Science Park, National Center for Genetic Engineering and Biotechnology, Pathum Thani, Thailand, [4]Plant Molecular Science Center, Chiba University, Chiba, Japan

Leafy vegetables that are offered as seedling leaves with petioles are referred to as baby leaf vegetables. One of the most nutritious baby leaves, amaranth (*Amaranthus tricolor* L.), contains several bioactive compounds and nutrients. Here, we investigated the growth and quality of baby leaf amaranth using a variety of short-term cooling root-zone temperatures (RZT; 5, 10, 15, and 20°C), periods (1, 3, 5, and 7days), and combinations thereof. We observed that exposing amaranth seedlings to RZT treatments at 5 and 10°C for 1–3days increased the antioxidant capacity and the concentrations of bioactive compounds, such as betalain, anthocyanin, phenolic, flavonoid, and ascorbic acid; however, extending the treatment period to 7days decreased them and adversely affected growth. For RZT treatments at 20°C, leaf photosynthetic pigments, bioactive compounds, nutrients, and antioxidant capacity increased gradually as the treatment period was extended to 7days. The integration of RZTs at 5 and 10°C for one day preceded or followed by an RZT treatment at 20°C for 2days had varied effects on the growth and quality of amaranth leaves. After one day of RZT treatment at 5°C followed by 2days of RZT treatment at 20°C, the highest concentrations of bioactive compounds, nutrients, and antioxidant capacity were 1.4–3.0, 1.7, and 1.7 times higher, respectively, than those of the control, and growth was not impaired. The short-term cooling RZT treatments under controlled environments were demonstrated to be adequate conditions for the improvement of target bioactive compounds in amaranth baby leaf without causing leaf abnormality or growth impairment.

KEYWORDS

abiotic stress, anthocyanin, antioxidant capacity, ascorbic acid, baby greens, betalain, flavonoids, seedling

Introduction

Consumption of food with health benefits, often called functional foods, is increasing. Functional foods could prevent lifestyle diseases, such as cancer, atherosclerosis, and Alzheimer's disease due to their bioactive compounds (Lee et al., 2009; Albuquerque et al., 2021). Vegetables represent affordable daily functional foods that contain various bioactive compounds, such as flavonoids, phenylpropanoids, and carotenoids.

Plants have been treated with biotic and abiotic stress to enhance the concentrations of their bioactive compounds. Root-zone temperature (RZT) is one of the abiotic factors that could enhance the contents of plant bioactive compounds (Calleja-Cabrera et al., 2020). The impact of RZT on growth and bioactive compound contents in relation to nutrition and water uptake functions in plants has been investigated (Qiuyan et al., 2012). Low or high RZT induces water stress in plants by altering the fluidity of the root membrane and the activity of aquaporin, a protein involved in water absorption (Carvajal et al., 1996; Maurel et al., 2015). In addition, calcium channels and lipid signaling are triggered as a consequence of such alterations, hence affecting intracellular calcium ions (Mittler et al., 2012). Subsequently, the calcium ion stimulates the activity of various temperature-sensitive elements, including calcium-dependent protein kinases and heat shock proteins. Additionally, reactive oxygen species (ROS), unstable oxidative products, are accumulated when certain thermal responsive mechanisms are altered (Raja et al., 2017). Numerous bioactive compounds that serve as ROS neutralizers, especially flavonoids and ascorbic acid, are synthesized and exploited to minimize ROS damage (Escobar-Bravo et al., 2017; Rácz and Hideg, 2021). Signal molecules are delivered from the roots to the shoots to trigger a bioactive compound synthesis pathway. However, when the ROS generated by low or high RZT exceed a threshold, cell death occurs (Mackerness, 2000). Moreover, a signal molecule is delivered to the shoots, signaling shoot-to-root nutrition transport, resulting in nutrient and biomass losses from the shoots (Heckathorn et al., 2013). Therefore, RZT treatment not only affects root physiology and activity but also shoot growth.

Root-zone temperature treatment is suitable for application in hydroponic systems. It facilitates a consistent nutrient solution temperature under controlled environments, such as in a plant factory with artificial light or a vertical farm. Ogawa et al. (2018) demonstrated that a 6-day RZT treatment at 10°C enhanced rosmarinic acid and luteolin concentrations in red perilla while decreasing shoot fresh weight. Cucumber plants were exposed to low RZT (10°C) for 4 weeks decreased leaf fresh weight and mineral content in addition to increasing leaf soluble sugar concentration (Chung et al., 2002). Similarly, a short-term RZT treatment (7 days) at 10–15°C enhanced total phenolic, anthocyanin, sugar, and antioxidant enzyme concentrations in red leaf lettuce, while decreasing fresh weight (Sakamoto and Suzuki, 2015). Furthermore, a high-temperature RZT treatment (30°C) increased the concentrations of bioactive compounds but decreased their antioxidant activity and appearance quality. Nguyen et al. (2020) applied RZT treatments to coriander for 3 and 6 days at 15, 25, 30, and 35°C. After 6 days, coriander treated with 15 or 35°C yielded relatively high concentrations of bioactive compounds, including ascorbic acid, chlorogenic acid, and carotenoids, while the highest biomass was observed in the treatments exposed to 30°C. The coriander treated for 3 days at 15°C exhibited decreased total phenolic contents, and no significant difference in fresh weight, when compared with that in the control group. The results of the study indicated that specific RZT levels and exposure periods influence the contents bioactive compounds differently.

Although high RZT treatment may enhance the contents of bioactive compounds in plants, it could have adverse effects on the appearance and shelf life of vegetable products due to increased respiration rates (Chun and Takakura, 1994; Falah et al., 2010; Masarirambi et al., 2018). Consequently, low RZT levels increase bioactive compounds in plants but decrease the water and minerals contents of the final product (Calatayud et al., 2008; Nxawe et al., 2009). Overall, RZT treatments at low and high levels influence bioactive compound characteristics, yield, and plant appearance. Consequently, low or high RZT could be employed considering the intended purpose of the product. Furthermore, rational RZT management could increase the contents of bioactive compounds in plants without adversely affecting growth and appearance.

Baby leaf vegetables, also known as baby greens, are commercial terms for leafy vegetables sold as seedling leaves with petioles. The leaf length, leaf area, color, texture, and flavor of baby leaf vegetables and the concentrations of certain bioactive compounds, such as ascorbic acid, anthocyanin, and β-carotene, are major quality criteria (Takahama et al., 2019). A seedling stage plant, on average, contains more bioactive compounds, nutrients, and minerals than a mature plant (Paradiso et al., 2018; Rakpenthai et al., 2019; Le et al., 2020).

Amaranth (*Amaranthus tricolor* L.) is a nutritious leafy vegetable with numerous and abundant bioactive compounds, such as ascorbic acid, betalain, β-carotene, phenolics, and flavonoids (Asao and Watanabe, 2010; Sarker and Oba, 2018; Sarker et al., 2020). Although amaranth baby leaf products are available on the market, no short-term treatment for manipulating the aerial or root-zone environment has been developed to enhance the contents of bioactive compounds in the leaves without causing leaf abnormality.

The aim of the present study was to establish a short-term cooling RZT under controlled environments that could be employed to improve bioactive compound accumulation in baby leaf amaranth without inducing abnormal appearance. RZT level, treatment period, and RZT combinations with different introduction times were investigated.

Materials and methods

Plant material and cultivation condition

The experiments were conducted at Chiba University, Japan, in a closed plant production system equipped with a

multi-layer cultivation shelf. *A. tricolor* L. (red amaranth) seeds were purchased from Nakahara Seed Product Co., Ltd. (Fukuoka, Japan). The cultivation procedure diagram is illustrated in Supplementary Figure S1. Two hundred seeds were germinated in the dark at 20°C. Ninety-six germinated seeds were sown on a polyurethane sponge (M urethane; M Hydroponics Laboratory Co. Inc., Aichi, Japan) which was placed in a 1.2-L polypropylene cultivation container. Once pairs of true leaves were visible, 56 uniform seedlings were transplanted to an 8-L cultivation container. A half-strength Otsuka A formulation (OAT house A treatment; OAT Agrio Co. Ltd., Tokyo, Japan) with an electrical conductivity of 0.10–0.12 S m^{-1} and pH of 6.3–6.5 was used as the nutrient solution and seedlings were irradiated with white LED lamps (LD40S-N/19/21; Panasonic Corporation, Osaka, Japan). The environmental condition until 26 days after sowing (DAS) is described in Table 1.

TABLE 1 Environmental conditions for *Amaranthus tricolor* L. seedling stage and test period.

Environmental factor	Setting value
PPFD (μmol m^{-2} s^{-1}) for seedling stage	200
PPFD (μmol m^{-2} s^{-1}) for test period	300
Light period (h)	16
Air temperature (light/dark, °C)	25/20
Nutrient solution temperature (°C)	Not controlled
Relative humidity (%)	70
CO_2 concentration (μmol mol^{-1})	1,000

PPFD, photosynthetic photon flux density.

Root-zone temperature treatments

Amaranth seedlings with four true leaves, approximately 27 DAS, were exposed to RZT treatments. Six seedlings selected from the average height seedlings grown in the 8-L container were transplanted into a 6-L hydroponic container (33 cm × 18 cm × 15 cm) for the treatment (Supplementary Figure S1). The RZT was controlled using a handy cooler (TRL-107NHF, Thomas Kagaku Co., Ltd., Tokyo, Japan) with a temperature control device (Supplementary Figures S2, S3). A 1.5-cm-diameter cooling coil and thermocouple connected to a temperature control device were installed in the treatment container. Aeration was performed using air pumps and air stones to ensure adequate supply of air to the roots and circulation of the nutrient solution in each container. The environmental conditions during the test period are described in Table 1. Seedlings in all treatments were exposed to similar aerial conditions.

Experiment 1 was carried out to determine the optimal RZT and treatment period. The seedlings were subjected to four RZT treatments for 1, 3, 5, and 7 days, including 5, 10, 15, and 20°C. Four seedlings were harvested after 1, 3, 5, and 7 days of treatment.

Experiment 2 was carried out to establish RZT integration regimes. The results from Experiment 1 demonstrated that RZT at 5 and 10°C for 1 day increased concentrations of targeted bioactive compounds. Furthermore, RZT at 20°C for one or 3 days increased or maintained photosynthetic pigment concentrations. Thus, we hypothesized that integrating RZT at 5 or 10°C for 1 day and 20°C for 2 days could synergistically enhance and maintain bioactive compounds of baby leaf amaranth. The seedlings were subjected to four RZT treatments (20 T5, 20 T10, 5 T20, and 10 T20°C). Table 2 and Supplementary Figure S4 show the RZT treatments and periods. Three days after treatment, four seedlings were harvested.

TABLE 2 Short-term root-zone temperature (RZT) conditions for the treatment of amaranth seedlings. The seedlings were irradiated under the same photosynthetic photon flux density of 300 μmol m^{-2} s^{-1} for 3 days (Experiment 2).

Treatment	RZT treatment (day/night, °C)		
	Day-1	Day-2	Day-3
20 T5	20/20	20/20	5/5
20 T10	20/20	20/20	10/10
5 T20	5/5	20/20	20/20
10 T20	10/10	20/20	20/20

Seedlings in all treatments were exposed to the same aerial conditions. The RZT of the control was maintained almost the same as the air temperature during a 25/20°C temperature cycle (day/night). The experiments were performed once.

Air temperatures in the canopy, cultivation shelf, and under cultivation foam were determined using a humidity and temperature recorder (TR-72wf, T&D Co., Ltd., Matsumoto, Japan; Supplementary Table S1). An infrared thermometer (830-T2, Testo, Inc.) was used to determine the surface temperature of the leaf and expanded polystyrene cultivation foam, whose emissivity was adjusted to 0.98 and 0.95, respectively (Chen, 2015; Krause and Nowoświat, 2019). The temperature of the nutrient solution was determined at different areas using thermocouples from the temperature control device on a handy cooler.

Yield, leaf water content, and leaf morphology

Four or five younger amaranth leaves 4.0–5.0 cm in length were harvested from four uniform seedlings, weighed, and subsequently freeze-dried (FDU-1110; Tokyo Rikakikai Co. Ltd., Tokyo, Japan) at −80°C for 24 h before being stored at −30°C for further analyses. Fresh (FW) and dry (DW) leaf weights were determined using a digital balance. The leaf water content (LWC) was calculated as previously described (Garnier and Laurent, 1994). Leaf morphology was visually recorded using a mobile camera.

Biochemicals determination

Sample preparation for biochemical determination was performed according to Wittayathanarattana et al. (2022). The leaves of each seedling were cold ground before being biochemically analyzed.

Chlorophyll and carotenoid concentrations

Powdered leaf samples (5 mg) were mixed with 1 ml of cold 80% acetone (v/v) and then homogenized using a 40 W ultrasonic machine. Samples were incubated overnight at 4°C and subsequently centrifuged (MX-307, TOMY Seiko Co., Ltd., Japan). The absorbance of the supernatants at 470, 480, 510, 645, and 663 nm was measured using a spectrophotometer (V-750; JASCO Corp., Japan). Total chlorophyll and carotenoid concentrations (conc.) were calculated using equations previously described by Sarker and Oba (2020).

Betalain concentration

Freeze-dried plant tissue samples (5 mg) were extracted with 1 ml of cold 80% methanol (v/v) containing 50 mM ascorbic acid. Samples were homogenized, then incubated overnight at 4°C and subsequently centrifuged. The absorbance of the β-cyanin and β-xanthin pigments were measured at 540 and 475 nm, respectively, using the spectrophotometer. Data were calculated as mg of betanin equivalent g^{-1} DW for β-cyanin and mg of indicaxanthin equivalent g^{-1} DW for β-xanthin. The concentrations were calculated by combining the β-cyanin and β-xanthin concentrations according to Sarker and Oba (2020).

Anthocyanin concentration

Anthocyanin determination was performed using a method modified from Mancinelli and Schwartz (1984). Powdered samples (5 mg) were mixed with 0.5 ml of chloroform, homogenized, and thereafter, centrifuged. Residues were collected and mixed with 1 ml of a 1% HCl-methanol (v/v) solution and subsequently centrifuged. The absorbance of supernatant was measured at 530 and 657 nm using the spectrophotometer. An appropriate dilution of cyanidin-3-glucoside (C3G) was used as the standard. The anthocyanin concentration was calculated using the equation described by Stanciu et al. (2009).

Total phenolic and flavonoid concentrations

Powdered leaf samples (5 mg) were mixed with 1 ml of cold 90% methanol (v/v), obtaining methanolic extract. The total phenolic concentration determination was performed as described by Jiménez-Aguilar and Grusak (2017). The extracts were mixed with 0.2 N of Folin-Ciocalteu reagent and 1 mol L^{-1} Na_2CO_3 at a ratio of 1:5:4. The absorbance of the solutions was measured at 760 nm using the spectrophotometer. Appropriate dilutions of gallic acid were used to plot a standard curve. Total phenolic concentrations were expressed as gallic acid equivalents (mg of GAE g^{-1} DW). Total flavonoid concentrations were determined based on the aluminum chloride reaction principle, as described in Sarker and Oba (2020). The extract was mixed with 5% $NaNO_2$ (w/v), 10% aluminum chloride (w/v) solution, and 1 mol L^{-1} NaOH at a ratio of 5:1.5:2:1.5. Absorbance was measured at 410 nm using the spectrophotometer. An appropriate dilution of rutin was used to create a standard curve. The total flavonoid concentrations were expressed as rutin equivalents (mg of RTE g^{-1} DW).

Total antioxidant capacity

An appropriate dilution of methanolic extract was mixed with 2,2-azino-bis (3-ethylbenzothiazoline-6-sulfonic acid; ABTS; Sigma-Aldrich, St. Louis, MO, United States of America) according to the method described by Miller and Rice-Evans (1996). The reduction in absorbance at 740 nm within 1 min was measured using the spectrophotometer. An appropriate dilution of Trolox was used to plot a standard curve. Total antioxidant capacity was expressed as Trolox equivalent antioxidant capacity (mM g^{-1} DW).

Ascorbic acid concentration

Powdered leaf samples (10 mg) were combined with 1 ml of 5% meta-phosphoric acid (w/v), then mixed well by vortexing for 1 min and centrifuged. Ascorbic acid determination was carried out using Reflectoquant® ascorbic acid test strips (Merck, Germany) and a reflectometer (RQflex®, Merck). Ascorbic acid concentration was expressed as mg g^{-1} DW.

Statistical analysis

Data were processed using IBM SPSS Statistics 24 (IBM Corp., Armonk, NY, United States of America). Tukey's honestly significant difference (Tukey's HSD) test was used to compare the means of the measured parameters among the treatments.

Results

The optimization of RZT and treatment period

Amaranth seedlings developed differently under various RTZs. At day 7, the seedlings from the control and RZT 20°C treatment conditions had 7–8 leaves, with 3–4 of the leaves being emerging new leaves (data not shown). The seedlings treated with RZTs of 5, 10, and 15°C showed minor leaf length and width changes, and only one emerging new leaf, resulting in five leaves at day seven. Younger leaves of 4.0–5.0 cm in length were harvested from the RZT and control conditions, and their morphology analyzed, as illustrated in Figure 1. The visible redness of the leaves increased with an increase in the period of the RZT treatment. However, on the first day of treatment, seedlings treated with RZTs of 5, 10, and 15°C showed leaf wilting. The amaranth leaf fresh and dry weights were

1.05–1.39 g and 0.12–0.21 g, respectively (Figure 2). The RZT treatments at 5 and 10°C had significantly reduced leaf fresh weight when compared with those observed following the treatments at 15 and 20°C. When the treatment period was prolonged from 3 to 7 days, considerable increases in leaf fresh and dry weights were observed; however, 1 day of treatment resulted in a decrease in fresh weight. Notably, extension of the treatment period from 3 to 7 days increased leaf dry weight in the RZT treatments at 15 and 20°C significantly when compared with that observed in the control group (Figure 2). Leaf water content in the control seedlings was consistently between 88 and 90%, while seedlings treated with RZTs of 5, 10, and 15°C exhibited reduced leaf water content since the first day of treatment, when compared with that in the control. However, as the treatment period was prolonged, leaf water content in seedlings treated with RZTs of 5, 10, and 15°C increased gradually.

Figure 3 indicates that the temperatures and periods used for the RZT treatments affected amaranth leaf pigments significantly. When the treatment period was extended from 1 to 7 days, chlorophyll concentrations in the leaves grown at RZTs of 5, 10, and 15°C were 1.25–2.25 times lower than those observed in control and an RZT of 20°C. For one-day treatments, the seedlings grown at RZTs of 5 and 10°C yielded significantly more carotenoids than those grown under control conditions; however, the carotenoid concentrations decreased with a longer treatment period. From 1 to 7 days of treatment, carotenoid concentrations in the leaves grown at an RZT of 20°C increased gradually. Betalain concentrations in the seedlings grown at RZTs of 5, 10, and 15°C increased dramatically 1.2–1.8 times for one-day treatments, and decreased gradually when the treatment period was extended to 7 days.

The anthocyanin concentrations of seedlings subjected to RZT treatments were 1.3–2.3 times higher than that in the control group (Figure 4). After 3 days of treatment, the anthocyanin concentrations in the seedlings grown at RZTs of 5 and 10°C were increased significantly, up to 16.23 and 15.65 mg g^{-1} DW, respectively. The anthocyanin concentrations of seedlings grown at RZTs of 15 and 20°C increased gradually from day one to day seven of the treatment. Following 3 days of RZT treatment, the total phenolic concentrations in the seedlings grown at n RZT of 5°C increased to 18.06 mg g^{-1} DW, and was the highest among the RZT treatments. However, after 7 days of treatment, total phenolic concentrations in seedlings grown at n RZT of 5°C decreased slightly, whereas the anthocyanin concentrations increased under RZT treatments of 10, 15, and 20°C.

The RZT treatments increased flavonoid concentrations in amaranth leaves significantly during the treatment period, excluding in the RZT of 20°C, in which the was not significant different with that in the control (Figure 4). Extending the treatment periods from 1 to 7 days enhanced leaf flavonoid concentrations, particularly in seedlings grown at RZTs of 5 and 10°C on day 3 to 5. From day 1 to 3, the antioxidant capacity of control seedlings was slightly altered, whereas those of seedlings subjected to RZT treatments were significantly changed. On the first day of treatment, both the 5 and 10°C RZT treatments exhibited the highest antioxidant capacity (11.23 and 10.97 mM g^{-1} DW, respectively), which eventually decreased by 15–20%. Antioxidant capacity increased gradually over 5 days after the start of the RZT treatments at 15 and 20°C.

The concentrations of ascorbic acid were influenced by RZTs and treatment periods (Figure 4). On day three, RZT treatments of 5 and 10°C significantly increased ascorbic acid concentrations in amaranth leaves, whereas the other RZT treatments only marginally increased ascorbic acid concentrations when treatment period was extended.

Exposing amaranth seedlings to RZTs of 5 and 10°C for 1 to 3 days could enhance the contents of bioactive compounds; however, prolonging the treatment period to 7 days reduced the contents of the compounds. From days three to seven, photosynthesis-related pigments and target bioactive compounds increased gradually under an RZT of 20°C. Combining the RZTs could enhance the concentrations of target bioactive compounds and with no leaf abnormalities.

The establishment of RZTs integration regime

The leaf was almost entirely red without wilting symptoms after 3 days of RTZ treatment, whereas the leaves of the 20 T5 and 20 T10 treatments were red and partially green (Figure 5). The leaf fresh weight of RZT-treated seedlings ranged between 1.04 and 1.09 g, which was significantly different from that of the control

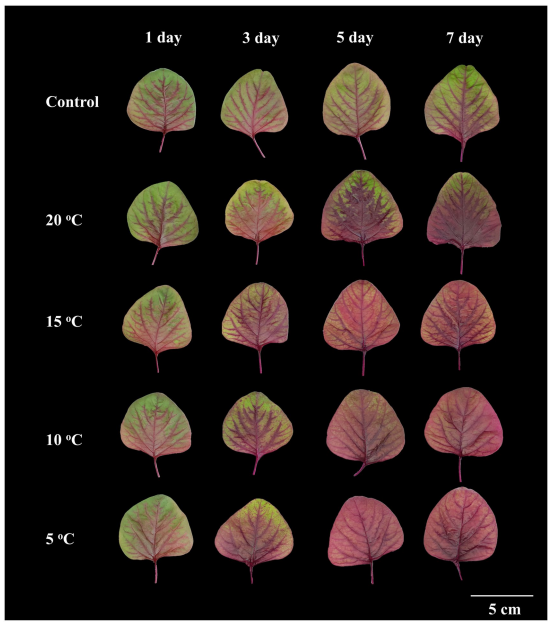

FIGURE 1
Morphology of amaranth leaves treated with different root-zone temperatures (RZT) for different periods (Experiment 1). The RZT at day/night-time: 5/5, 10/10, 15/15, and 20/20°C are indicated as: 5, 10, 15, and 20°C.

seedling (1.19 g; Table 3). Leaf dry weight was not significantly different between the RZT-treated seedlings and the control seedlings. In this experiment, the RZT treatment had no significant effect on leaf water content.

RZT treatment integration had no effect on photosynthetic pigments, including chlorophyll and carotenoid contents, in the present study (Table 4). The chlorophyll and carotenoid concentrations in the leaves of RZT-treated seedlings ranged from 7.44 to 8.08 and 2.48 to 2.53 mg g^{-1} DW, respectively, which were not significantly different from those of the control. Betalain concentrations in RZT-treated seedlings increased 1.5 to 1.8-times compared to that observed in the control; however, they did not differ significantly among the RZT treatments (3.81–4.21 mg g^{-1} DW).

Anthocyanin concentrations in the leaves of RTZ-treated seedlings ranged between 11.15 and 13.15 mg g^{-1} DW, which is approximately 1.3–1.5 times higher than that of the control (Table 5). In addition, RZT-treated seedlings had a phenolic concentration 1.2–1.4 times higher than that of control seedlings.

Integration of RZT treatments increased flavonoid concentrations significantly (2.7–3.0 times higher than that in the control). There were no significant differences in flavonoid concentrations among the RZT treatments. The highest phenolic concentrations (16.68 mg g^{-1} DW) were observed in leaves in the RZT 20 T10 treatment, whereas the lowest were observed in leaves in the RZT 10 T20 treatment. The findings are consistent with the antioxidant capacity of RZT-treated leaves, which was the highest in the 20 T10 treatment (15.51 mM g^{-1} DW) and the lowest in the 10 T20 treatment (11.85 mM g^{-1} DW), among the RZT treatments. Both phenolic concentration and antioxidant capacity of seedlings were significantly different between the RZT 20 T10 and RZT 10 T20 treatments. Interestingly, RZT 20 T10 and RZT 10 T20 protocols were designed using the same RZTs of 10 and 20°C, but different periods, implying that a different RZT introduction time at 10°C results in different phenolic concentration and antioxidant capacity. Conversely, a different RZT introduction time at 5°C showed a similar result.

The effects of RZTs integration treatments on ascorbic acid are listed in Table 5. The results indicate that both the 5 and 10°C RZTs can be used to increase ascorbic acid concentrations; however, the introduction period influenced the results considerably. RZT should be applied for 1 day at 5°C, followed by 2 days at 20°C (5 T20), whereas 10°C for 1 day should be used after seedlings have been treated for 2 days at 20°C (20 T10).

The results of the present study suggest that RZT integration could enhance the contents of target bioactive compounds. The application of an RZT of 5°C for one day, followed by an RZT of 20°C for two days (5 T20), represents a promising protocol for improving bioactive compound accumulation in baby leaf amaranth without inducing abnormal appearance.

Discussion

Numerous studies on RZT have examined its influence on hydroponically grown plants, with an emphasis on low RZTs. Low RZTs have been associated with adverse effects, such as reduced water and nutrient uptake, decreased root respiration and activity, retarded root development, or interruptions of the photosynthetic machinery, all of which result in loss in product yield, nutrients, and minerals (Aroca et al., 2001; Schwarz et al., 2010; Hao et al., 2012). Alternatively, low RZTs are considered beneficial since short- or long-term application can enhance the concentrations of bioactive compounds, such as rosmarinic acid (Lam et al., 2020), glucosinolates (He et al., 2020), ascorbic acid (Chadirin et al., 2011), total phenolics, and anthocyanin (Sakamoto and Suzuki, 2015), depending on the plant species.

Growth and photosynthesis-related pigments

Plant biomass is a growth indicator that reflects photosynthetic status and stress, so that a decrease in plant biomass implies poor growth or excessive stress. This study showed that the seedlings

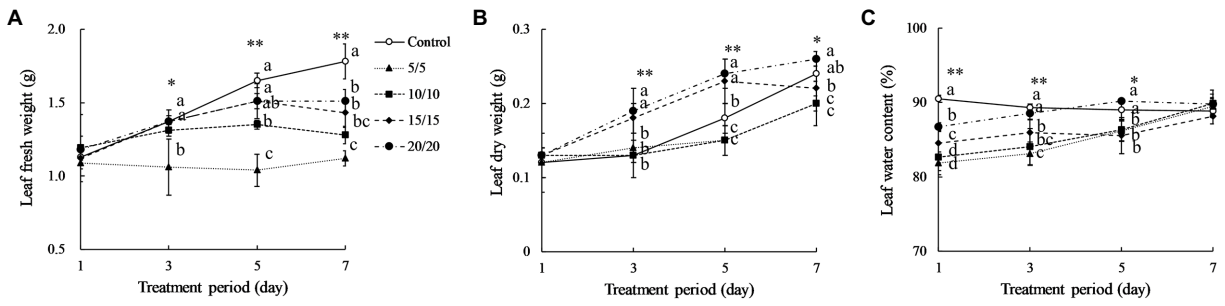

FIGURE 2
Amaranth leaf fresh weight **(A)**, dry weight **(B)**, and leaf water content **(C)** after treatment with different short-term RZTs for different periods (Experiment 1). Vertical bars indicate the standard error (n=4). Means were compared using Tukey's honestly significant difference (HSD) at a significance level at *p < 0.05 and **p < 0.01.

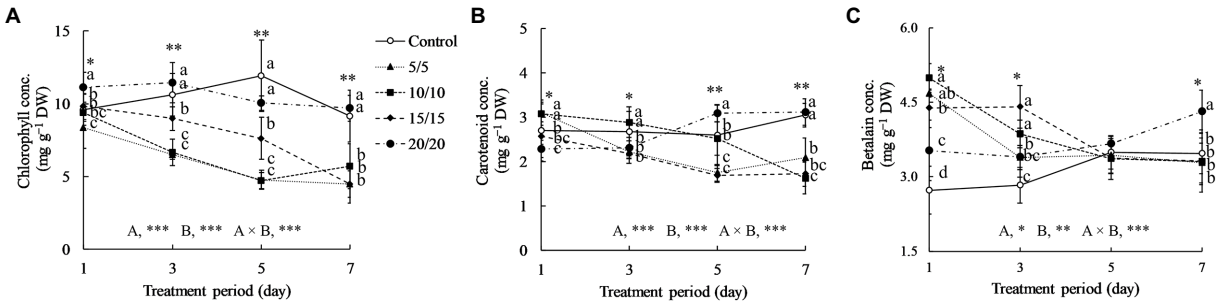

FIGURE 3
Total chlorophyll **(A)**, carotenoid **(B)**, and betalain **(C)** concentrations (conc.) in leaves of amaranth seedlings treated with different short-term RZTs for different periods (Experiment 1). Results of two-way analysis of variance for RZT (A), period (B), and their interaction (A×B) are shown. The asterisks indicate the significance levels (*p < 0.05, **p < 0.01, and ***p < 0.001). Vertical bars indicate the standard error (n=4). Means were compared using Tukey's HSD at a significance level at *p<0.05 and **p < 0.01. Betalain concentrations are expressed as β-cyanin and β-xanthin equivalents. DW, dry weight.

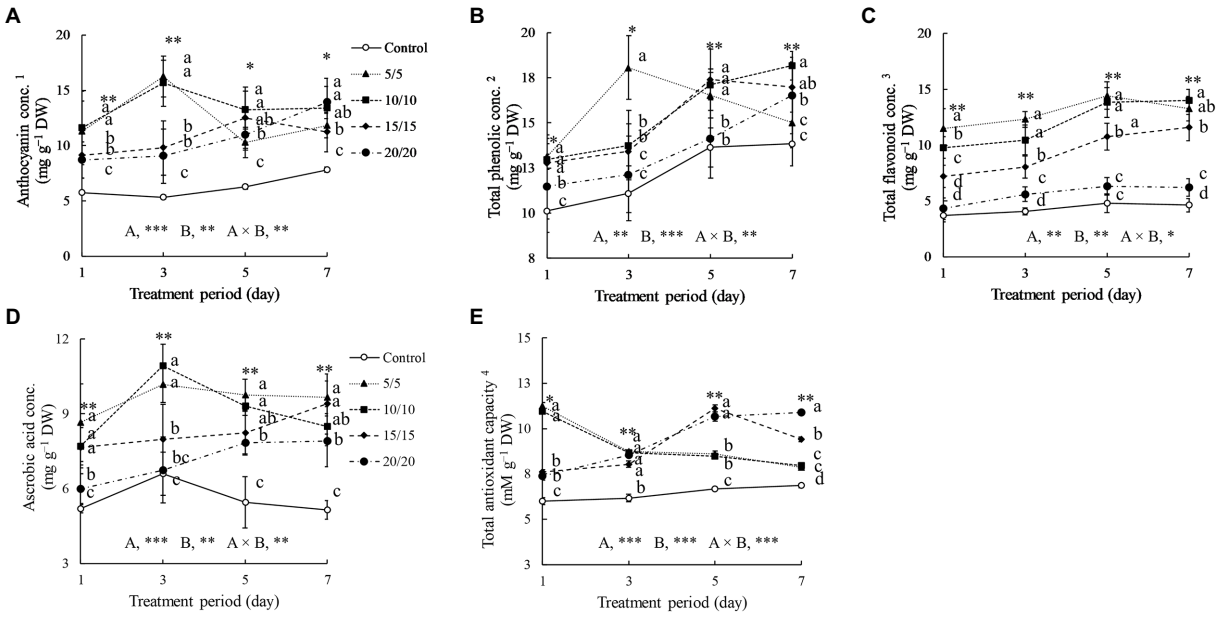

FIGURE 4
Anthocyanin **(A)**, total phenolic **(B)**, total flavonoid **(C)**, and ascorbic acid **(D)** concentrations, as well as total antioxidant capacity **(E)** of amaranth leaves treated with different short-term root-zone temperatures (RZT) for different periods (Experiment 1). Results of two-way analysis of variance for RZT (A), period (B), and their interaction (A×B) are shown. The asterisks indicate significance levels (*p < 0.05, **p < 0.01, and ***p < 0.001). Vertical bars indicate the standard error (n=4). Means were compared using Tukey's HSD at a significance level at *p < 0.05 and **p < 0.01. [1]Anthocyanin concentration is expressed as cyanidin-3-glucoside equivalents. [2]Total phenolic concentrations are expressed as gallic acid equivalents. [3]Total flavonoid concentrations are expressed as rutin equivalents. [4]Total antioxidant capacity is expressed as Trolox equivalents. DW, dry weight.

grown at RZTs of 5 and 10°C had a substantial decrease in fresh weight (Figure 2). Moreover, one-day treatments resulted in significant reduction in fresh weight. Sakamoto and Suzuki (2015) suggested that treating red leaf lettuce using an RZT of 10°C for 7 days noticeably decreased the fresh weight. According to Nguyen et al. (2020), although the fresh weight of coriander exposed to a 15°C RZT treatment did not change significantly after three days, it did after six days. The RZTs used and the treatment periods influenced plant fresh weight by inducing an imbalance in root water uptake. Li et al. (2019b) demonstrated that rice plants grown at an RZT of 17.5°C for two days increased malonaldehyde concentrations, reflecting oxidative status in the root and shoot, and decreasing shoot fresh and dry weights. Low RZT potentially disturbed redox balance, generating an overproduction of ROS that necessitated the synthesis of neutralizing antioxidant enzymes or bioactive compounds (Escobar-Bravo et al., 2017). Such activities

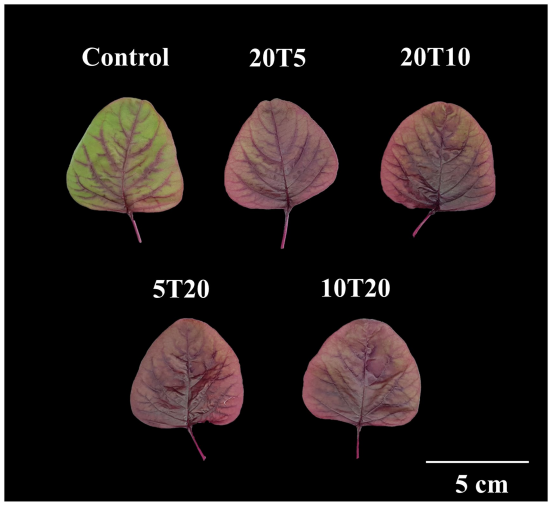

FIGURE 5
Morphology of amaranth leaves treated with different short-term root-zone temperatures (RZT) treatments for 3 days (Experiment 2). The seedlings that were subjected to 2 days of an RZT of 20°C followed by 1 day of RZTs of 5 or 10°C are designated as 20T5 and 20T10, respectively. The seedlings that were treated at 5 or 10°C for 1 day, then subjected to an RZT of 20°C for 2 days, are illustrated as 5T20 and 10T20.

TABLE 3 Amaranth leaves fresh weight (Leaf FW), dry weight (Leaf DW), and leaf water content (LWC) after treatment with different short-term root-zone temperatures (RZT) for 3 days (Experiment 2).

Treatment	Leaf FW (g)	Leaf DW (g)	LWC (%)
25/20°C (control)	1.19 ± 0.07[a]	0.19 ± 0.01	84.80 ± 1.23
20T5	1.06 ± 0.01[b]	0.16 ± 0.02	85.14 ± 0.88
20T10	1.04 ± 0.02[b]	0.17 ± 0.01	85.25 ± 1.03
5T20	1.07 ± 0.06[b]	0.16 ± 0.02	85.45 ± 1.18
10T20	1.09 ± 0.02[b]	0.18 ± 0.02	83.18 ± 1.43
Significant	**	NS	NS

NS indicates no statistical significance.
Data are mean ± standard error of four biological replicates. Means within columns were compared using Tukey's honestly significant difference (HSD). Different letters indicate significant differences within column. The asterisks indicate the significance level (**$p < 0.01$).

require energy to be performed; hence, respiration rate is increased. Due to the impairment of root water uptake, water is lost throughout respiration without being replenished by the root, resulting in loss of shoot fresh weight (Calleja-Cabrera et al., 2020). However, in the present study, the extended RZT treatment period increased leaf dry weight gradually, with a decrease observed only at the first day of treatment. The RZT treatments applied in the present study were potentially suboptimal and did not exceed amaranth's biological threshold, allowing the recovery process to proceed.

LWC is a parameter used to measure the leaf water stress status in response to drought, temperature, and nutrient limitation (Heinen et al., 2009). On the first day of treatment, RZT leaves exposed to 5, 10, and 15°C showed significant decreases in LWC (Figure 2). Therefore, the one-day RZT treatment may not

TABLE 4 Total chlorophyll (Chl conc.), carotenoid (Car conc.), and betalain (Bet conc.) concentrations in leaves of amaranth seedlings after treatment with different short-term root-zone temperatures (RZT) for 3 days (Experiment 2).

Treatment	Chl conc. (mg g^{-1} DW)	Car conc. (mg g^{-1} DW)	Bet conc. (mg g^{-1} DW)
25/20°C (control)	9.71 ± 0.90	2.41 ± 0.15	2.51 ± 0.35[b]
20T5	7.44 ± 0.83	2.48 ± 0.28	3.95 ± 0.54[a]
20T10	7.55 ± 1.01	2.49 ± 0.70	3.94 ± 0.56[a]
5T20	8.08 ± 1.04	2.51 ± 0.49	4.21 ± 0.19[a]
10T20	7.78 ± 0.97	2.53 ± 0.31	3.81 ± 0.35[a]
Significant	NS	NS	**

Data are mean ± standard error of four biological replicates. Means within columns were compared using Tukey's HSD. Different letters indicate significant differences within column. The asterisks indicate the significance level (**$p < 0.01$). NS indicates no statistical significance. DW, dry weight.

be appropriate for use prior to harvest. However, extension of RZT period increased LWC significantly, while seedlings grown in the control and under an RZT of 20°C exhibited minor changes in LWC (Figure 2). Various physiological responses are triggered, in general, to maintain water levels in plants during water stress, including alteration of stomata conductance (Tari, 2003; Yu et al., 2015) proline biosynthesis (Sperdouli and Moustakas, 2014; Zegaoui et al., 2017), and the accumulation of photosynthesis-related pigments (Sanchez et al., 1983; Mibei et al., 2017; Shah et al., 2017).

Decreases in chlorophyll concentrations in seedlings grown under RZTs of 5, 10, and 15°C may indicate poor light-harvesting ability for photosynthesis (Figure 3). Low RZT treatments cause lipid oxidation in the membrane, resulting in ROS production, most notably in the plastid. This ROS subsequently oxidizes the pigment, decreasing the chlorophyll content (León-Chan et al., 2017). The decrease may influence plant biomass, as previously described, by lowering seedling fresh and dry weights under low RZT treatments. The negative trends, especially for fresh weight, are more obvious when the treatment period is prolonged.

Carotenoids, in general, are synthesized in the same way as chlorophyll, highlighting their role in the photosynthetic machinery (Sagawa et al., 2016; Stanley and Yuan, 2019). Carotenoids are pigments accumulated in chloroplasts and crucial for photoprotection, capturing light, and stabilizing photosynthetic activities (Havaux, 1998), and have a high antioxidant capability, scavenging singlet oxygen and peroxyl radicals (Stahl and Sies, 2003). In the present study, carotenoid concentrations increased significantly in seedlings exposed to RZTs of 5 and 10°C on the first day but decreased thereafter, by 30–40%, when the treatment period was extended. Under cold temperatures, the elongated hypocotyl 5 (HY5), a protein that responds to cold and light stress, stabilized; however, the phytochrome interacting factor decreased antagonistically (Toledo-Ortiz et al., 2014). Both proteins interacted with the phytoene synthase enzyme associated with carotenoid biosynthesis under cold stress. However, plant age, leaf position, and phytohormone levels influence carotenoid stability.

TABLE 5 Anthocyanin (Ant conc.), total phenolic (Phl conc.), and total flavonoid (Flv conc.) concentrations, as well as total antioxidant capacity (TAC), and ascorbic acid (Asc conc.) concentration of amaranth seedling leaves treated with different short-term root-zone temperatures (RZT) for 3 days (Experiment 2).

Treatment	Ant conc.[1] (mg g^{-1} DW)	Phl conc.[2] (mg g^{-1} DW)	Flv conc.[3] (mg g^{-1} DW)	TAC[4] (mM g^{-1} DW)	Asc conc. (mg g^{-1} DW)
25/20°C (control)	8.11 ± 0.58^{b}	11.53 ± 0.58^{c}	4.10 ± 0.21^{b}	8.33 ± 0.97^{c}	6.78 ± 0.40^{c}
20 T5	13.15 ± 1.15^{a}	15.49 ± 1.13^{ab}	13.13 ± 0.93^{a}	13.45 ± 0.95^{ab}	9.90 ± 0.38^{b}
20 T10	13.14 ± 1.58^{a}	16.68 ± 0.80^{a}	12.00 ± 0.99^{a}	15.51 ± 1.22^{a}	11.05 ± 0.71^{a}
5 T20	12.61 ± 0.87^{a}	16.34 ± 0.83^{a}	12.45 ± 1.22^{a}	14.09 ± 1.08^{ab}	11.70 ± 0.84^{a}
10 T20	11.15 ± 1.04^{a}	14.40 ± 0.83^{b}	11.06 ± 0.94^{a}	11.85 ± 0.57^{b}	9.55 ± 0.51^{b}
Significant	**	**	**	**	**

[1]Anthocyanin concentrations are expressed as cyanidin-3-glucoside equivalents.
[2]Total phenolic concentrations are expressed as gallic acid equivalents.
[3]Total flavonoid concentrations are expressed as rutin equivalents.
[4]Total antioxidant capacity is expressed as Trolox equivalents.
Data are mean ± standard error of four biological replicates. Means within columns were compared using Tukey's HSD. Different letters indicate significant differences within column. The asterisks indicate the significance level (**$p < 0.01$). NS indicates no statistical significance. DW, dry weight.

Low RZTs suppress phytohormones such as gibberellins, auxin, and cytokinin in root apical meristems, in turn interfering with root-to-shoot hormonal transportation (Zhu et al., 2015; Müller and Munné-Bosch, 2021). Consequently, in amaranth seedlings, low RZT treatments lasting longer than 3 days may restrict the biosynthesis of photosynthesis-related pigments and reduce leaf growth.

Bioactive compounds

Betalain, a tyrosine-derived pigment, is required for homeostasis under abiotic stress. Betalain accumulates in the epidermis, mesophyll, and guard cell of leaves (Jain and Gould, 2015; Zhou et al., 2021). In amaranth leaves, especially red leaves, betalain concentrations are as much as 2–5 times higher than those in green leaves (Liu et al., 2019). Hayakawa and Agarie (2010) reported that cold stress enhanced betalain concentrations in *Suaeda japonica* leaves. Numerous cold-responsive bioactive compounds are synthesized to maintain photosynthetic machinery under cold stress. Betalain, rather than carotenoid, is a photoprotective compound strongly associated with cold stress (Li et al., 2019a). Betalain concentrations increased significantly in leaves under RZT treatments at 5, 10, and 15°C, and slightly reduced (Figure 3). In general, the biosynthesis of betalain requires nitrogen as a backbone, similar to chlorophyll, potentially explaining the observed decrease in chlorophyll and increase in betalain under RZT treatments. Jain and Gould (2015) showed that betalain concentrations increased 4-fold when exposed to water stress, while chlorophyll concentrations decreased dramatically. Under low RZT conditions, photosynthesis is restricted, which leads to the depletion of plant resources in tissues and forces them to preserve critical nutrients for survival. Chlorophyll may be less necessary in a resource-limited environment with excess ROS when compared with betalain and carotenoid (antioxidants; Polturak et al., 2016).

Anthocyanins have been commonly identified as plant stress-responsive bioactive molecules, acting as ROS scavengers and osmo-homeostatic agents (Stintzing and Carle, 2004). Numerous studies have showed that RZT treatments increase anthocyanins in leaves significantly. For example, anthocyanin concentrations increased in red leaf lettuce after exposure to low RZTs of 10 and 15°C for a certain period (Sakamoto and Suzuki, 2015). Similarly, the leaves of red perilla grown at an RZT of 10°C for 6 days exhibited a considerable increase in anthocyanin concentrations when compared with that in the control (Ogawa et al., 2018). In the present study, anthocyanin concentrations in amaranth leaves under RZT treatments responded variably depending on the RZT and treatment period (Figure 4). For instance, anthocyanin concentration increased dramatically, 2–3-fold, after treatment at 5 and 10°C for 3 days, when compared with that observed in the control, followed by a 15–20% decline on days 5 and 7. The leaves under 15 and 20°C treatments progressively produced anthocyanins as the treatment periods were extended, indicating that RZT treatments of 5 and 10°C may be the low threshold temperature level of amaranth, triggering the biosynthesis of anthocyanin components by activating chalcone synthase, chalcone isomerase, and flavanone-3-hydroxylase (Liu et al., 2018). However, the reduction in anthocyanin, known as anthocyanin degradation, may begin after day 3 of RZT treatment. During RZT treatment, photosynthesis is limited, with sugar lacking as an energy source, and plants are forced to recycle sugar to survive. Anthocyanins in general, which are present as glycosides, bonded with a sugar-backbone, may be targeted as alternative sugar sources. Therefore, the deglycosylation by β-glucosidase and oxidation by polyphenol oxidase or peroxidase may potentially result in anthocyanin degradation (Oren-Shamir, 2009). Anthocyanin performs its ROS scavenging function in a manner similar to betalain. Both bioactive compounds may be used initially during the RZT treatment; afterward, additional stress-responsive components will continue to perform the function. In the present study, anthocyanin and betalain reduction were observed on day 5 and 7 (Figures 3, 4).

Król et al. (2015) demonstrated that after a week of exposure to 10°C, total phenolic contents of *Vitis vinifera* L. leaves increased. However, the cold-sensitive cultivar had lower phenolic contents. The data suggest that the phenolic compounds play a role in cold tolerance. After 30 days of long-term low-temperature stress at 15°C, the accumulation of flavonoids and phenolic compounds in tomato leaves increased (Rivero et al., 2001). Rezaie et al. (2020) demonstrated that low RZTs induce transcription factors associated with phenylalanine ammonia-lyase and alter the expression of the cinnamate 4-hydroxylase gene, resulting in increased flavonoid and phenolic compound accumulation in sweet basil, which corroborate the findings of the present study, revealing that seedlings exposed to an RZT of 5°C for 3 days significantly enhanced their total phenolic concentration (Figure 4). The findings indicate that seedling leaves treated with different RZTs (5, 10, and 15°C) exhibited 3–5-fold increases in flavonoid concentrations when compared with those of the controls. When the treatment period was prolonged, total phenolic and flavonoid concentrations increased substantially, showing that both are required for homeostasis under low RZTs. Cold-tolerance capacity varies according to plant species, based on cold-responsive transcriptional factors. Moreover, different mechanisms may be adopted depending on the magnitude and period of the cold stress.

Lee and Oh (2015) reported that the antioxidant capacity of kale treated with an RZT of 4°C increased significantly on the first day after treatment. Consequently, the antioxidant capacity of leaves exposed to RZTs of 5 and 10°C increased dramatically by 1.5–1.8-fold, when compared with those observed after 1 day of treatment in the control (Figure 4). The antioxidant capacity of seedling leaves treated at 15 and 20°C increased gradually from day one to seven. Plant ROS defense mechanisms are diverse and include both enzymatic and non-enzymatic responses. Both are employed considering the quantity of ROS and the physiological status of the plant (Das and Roychoudhury, 2014). The antioxidant capacity of amaranth is strongly correlated with the concentration of bioactive compounds classified as non-enzymatic antioxidants, such as anthocyanin, betalain, phenolic, flavonoids, and ascorbic acid (Sarker et al., 2020). However, only betalain and carotenoid increased with an increase in antioxidant capacity, whereas phenolic, flavonoids, and ascorbic acid exhibited delayed responses (Figures 3, 4). Carotenoid and betalain antioxidant molecules may be the first line of defense against ROS damage in amaranth during RZT treatment. However, based on reactivity and structure, phenolic and flavonoid compounds are considered secondary ROS scavenging mechanisms in plants (Fini et al., 2011). Additionally, delayed synthesis resulting from delayed gene expression in response to abiotic stress has been described in other studies (Clayton et al., 2018; Qian et al., 2019).

Ascorbic acid is a water-soluble vitamin that is essential for the immune system and as a cellular ROS scavenger. Moreover, it is more effective in scavenging hydrogen peroxide than catalase and peroxidase (Dolatabadian and Jouneghani, 2009). Amaranth is a source of ascorbic acid, particularly from its leaves, containing 13 times the ascorbic acid content found in lettuce (Srivastava, 2011). In the present study, ascorbic acid increased significantly in leaves treated at 5°C from day one and remained constant until day seven, but it decreased slightly in leaves treated at 10°C after 7 days (Figure 4). Ascorbic acid functions as a scavenger in both enzymatic and non-enzymatic ROS defense mechanisms, implying that ascorbic acid biosynthesis may continue under abiotic stress (Barnes et al., 2002; Akram et al., 2017). Here, we showed that ascorbic acid increased in seedlings subjected to RZT treatments at 5 and 10°C for 3 days, and declined slightly thereafter. Subsequently, Ito and Shimizu (2020) observed that spinach (Amaranthaceae) exposed to 4°C treatment for 2–7 days exhibited enhanced levels of ascorbic acid. Moreover, Cheminant et al. (2011) reported that after 2 weeks of RZT treatment at 5°C, the ascorbic acid content in spinach increased. Although previous studies examined the influence of RZT treatments on ascorbic acid in spinach, the effects may differ based on the species analyzed. Ascorbic acid is produced from glucose, pectin, and myo-inositol; hence, higher ascorbic acid levels indicate increased utilization of the substrates (Wheeler et al., 1998; Smirnoff et al., 2001). Since these precursors influence plant growth and development, long-term RZT treatment of amaranth may not be appropriate, as demonstrated in the present study.

Effect of cooling root-zone temperature integration

Since each RZT level and period (Experiment 1) had distinct effects, an integration of varied RZTs for 3 days before harvest may be performed to enhance the concentrations of bioactive compounds. An RZT of 20°C may increase photosynthetic pigments, providing precursors of bioactive compounds and nutrients; hence, 2 days would be selected for this RZT. After the 20°C treatment, RZTs of 5 or 10°C would be used for a day to improve the bioactive compounds and nutrients before harvest. Conversely, RZTs of 5 and 10°C may be first used for a day to enhance the concentrations bioactive compounds and nutrients, followed by an RZT of 20°C to gradually increase and maintain them until harvest.

While cooling the root zone can enhance the concentrations of bioactive compounds (Ogawa et al., 2018; Nguyen et al., 2020), it also affects leaf fresh weight, in general, by interfering with root water uptake (Nxawe et al., 2009; Maurel et al., 2015). According to the results presented in Figure 2, the RZT of 20°C had no effect on leaf fresh weight when compared with that of the control group, and hence was employed in Experiment 2 to avoid leaf fresh weight reduction. However, the conclusion may not be valid, since the results indicated that seedlings treated with a combination of RZTs exhibited leaf fresh weight reductions of 10–15% compared to the control (Table 3). Notably, the combination of RZTs was observed to have a beneficial effect on plants by reducing water stress damage, as the dry weight and leaf water content indicated a water and nutrient balance

(Calleja-Cabrera et al., 2020; Zhou et al., 2021), which were not statistically different from those of the control (Table 3).

In experiment 1, chlorophyll may have been degraded by lipid oxidation (León-Chan et al., 2017) and reduced to a basal level for the maintenance of physiological processes under resource-constrained conditions induced by low RZTs (Figure 3). Notably, the findings in Experiment 2 suggest that the combination of RZTs had a beneficial effect on chlorophyll, despite the no significant difference between the RZT treatment and the control (Table 4). Chlorophyll may accumulate more when plants are under mild RZT stress, as shown in our experiment with an RZT of 20°C (Figure 3). Moreover, no reduction in chlorophyll concentration was observed when RZTs of 5 and 10°C were introduced (20 T5 and 20 T10, Table 4). The mild cooling RZTs of 15 to 20°C at 25/20°C air temperatures may promote chlorophyll accumulation, thereby increasing photosynthesis and ultimately bioactive compound concentrations or precursor biosynthesis (He et al., 2020). Therefore, when seedlings are exposed to low RZTs, the precursors are promptly converted to cooled RZT-responsive compounds, and the resulting bioactive chemical compounds immediately protect chlorophyll from lipid oxidation. Conversely, when RZTs of 5 and 10°C were introduced prior to the application of 20°C (5 T20 and 10 T20), the 20°C may serve as a recovery condition; various bioactive compounds increased during the recovery period (Lee and Oh, 2015).

RZT combinations had different effects on carotenoids, when compared to the effects observed during Experiment 1, where only a single RZT treatment was applied. The 5 and 10°C RZT treatments in Experiment 1 increased carotenoid concentrations for 1 day, and then decreased them over time (Figure 3); however, there was no significant difference between the RZT treatments and the control (Table 4). Carotenoids, as mentioned earlier, acts as ROS scavengers and photoprotective compounds (Stahl and Sies, 2003); cooling RZTs, in general, lead to increased carotenoid concentrations (Chadirin et al., 2011; Nguyen et al., 2020; He et al., 2021). A cooling RZT activates HY5, a switch for carotenoid biosynthesis (Catalá et al., 2011). However, the synthesis of several bioactive compounds, including flavonoids, is controlled by this protein (Kim et al., 2017). According to the results of the present study, RZT treatments may induce HY5, but carotenoids may not be the primary RZT stress-responsive compound.

In the present study, betalain, anthocyanins, phenolics, and flavonoids functioned as bioactive compounds in response to cooling RZTs (Table 5 and Figures 3, 4). RZTs, either single or in combination, improve these concentrations for a certain period when compared with the concentrations observed in control treatments. However, phenolic concentrations are affected by introduction of RZT treatments at 5 and 10°C followed by or before treatment at 20°C. Among RZT treatments, in the 10 T20 protocol, leaves had the lowest concentrations of phenolic compounds, and their antioxidant capacity was consequently reduced due to the lower phenolic concentrations (Table 5). The antioxidant capacity of amaranth leaves, on the other hand, demonstrates the total ROS scavenging ability (scavenging, neutralizing, and radical reaction chain inhibition; Rubio et al., 2016), which is highly correlated with betalain, phenolic, and flavonoid contents (Sarker and Oba, 2018, 2020).

The integration of RZTs had distinct effects on ascorbic acid contents in leaves (Table 5). Ascorbic acid concentration of seedlings under 20 T5 treatment was lower than that under the 20 T10. In comparison with other bioactive compounds examined following RZT combination treatments, only ascorbic acid concentrations were significantly decreased in leaves after 20 T5, indicating that the RZT of 5°C 1 day prior to harvest may induce cold stress and produce ROS, for which ascorbic acid is required as a first-line scavenger, resulting in the reduction in the ROS concentrations (Akram et al., 2017). However, leaves treated with 10 T20 showed reduced ascorbic acid concentrations, which is associated with decreased phenolic concentrations and antioxidant capacity. In the 10 T20 treatment, an RZT of 10°C induced cold-stress and generated ROS; however, the recovery period at 20°C could have masked the impact of stress, resulting in lower phenolic and ascorbic acid concentrations and antioxidant capacity than those in other combinations.

Pre-cooling, in general, is the application of 10–20°C of forced air to leafy vegetables to remove excess heat from the environment or metabolic process (Martínez and Artés, 1999). Numerous studies have shown that pre-cooling vegetables extends their shelf life by increasing the concentrations of bioactive compounds that function as radical scavengers and chelating agents (He et al., 2013; Garrido et al., 2015; Tian et al., 2016; Kongwong et al., 2019). Therefore, pre-cooling RZTs (20°C in this experiment), in contrast to the cold-RZT warning signal, may enhance bioactive compounds prior to the application of cold-RZTs (5 and 10°C). Alternatively, an RZT treatment of 20°C could be used after applying cold-RZTs (5 and 10°C; 5 T20 and 10 T20) where the RZT of 20°C may not act as a pre-cooling RZT but rather as a recovery-period RZT.

Our findings suggest that a one-day RZT treatment combination at 5°C followed by two-days treatment before harvest at 20°C can enhance the concentrations of target bioactive compounds and maintenance of nutrients in baby leaf amaranth without adversely affecting leaf appearance. Amaranth baby leaf responded differently to different RZT combinations, and this is the first study to report such findings. Further studies are required to demonstrate the relationship between pre-harvest treatment and post-harvest quality of baby leaf amaranth since physiological processes in plants change over time, even after harvest.

Conclusion

Our findings suggest that RZTs of 5 and 10°C for 1–3 days may increase the concentrations of bioactive compounds in baby leaf amaranth, with beneficial nutrients retained. An RZT of 20°C, conversely, would increase the concentrations of photosynthetic pigments and bioactive compounds without impairing growth,

when the treatment period is extended to 7 days. Furthermore, the combination of RZTs could enhance target bioactive components and maintain nutrients in amaranth baby leaf. Treatments for 1 day at 5°C and for 2 days at 20°C were associated with the highest concentrations of bioactive compounds and nutrients in the leaves. Therefore, treatment with an RZT of 5°C for 1 day followed by that for 20°C for 2 days may be the appropriate pre-harvest treatment for increasing bioactive compounds and maintaining nutrients in baby leaf amaranth without causing leaf appearance abnormalities.

Data availability statement

The original contributions presented in the study are included in the article/Supplementary material, further inquiries can be directed to the corresponding author.

Author contributions

EG and KS: conceptualization and supervision. TW: performing experiments. EG, KS, and PW: chemical analysis advice. TW: growth parameters and biochemical analysis, data analysis, and writing of manuscript. EG: review and editing of manuscript and funding acquisition. All authors contributed to the article and approved the submitted version.

Funding

This work was supported by JSPS KAKENHI Grant Number JP18H02301 and a Thailand Graduate Institute of Science and Technology (TGIST) Scholarship (SCA-CO-2560-4576-TH).

Acknowledgments

We would like to express our gratitude to the Laboratory of Environmental Control Engineering colleagues at Chiba University's Graduate School of Horticulture and Michiko Takagaki for their support. TW's research is part of a double degree program at Chiba University (Japan) and Mahidol University (Thailand). The authors are grateful for the support of the Excellent International Student Scholarship for Chiba University Graduate Programs (Type B) and Mahidol University.

Conflict of interest

The authors declare that the research was conducted in the absence of any commercial or financial relationships that could be construed as a potential conflict of interest.

Publisher's note

All claims expressed in this article are solely those of the authors and do not necessarily represent those of their affiliated organizations, or those of the publisher, the editors and the reviewers. Any product that may be evaluated in this article, or claim that may be made by its manufacturer, is not guaranteed or endorsed by the publisher.

Supplementary materials

The Supplementary materials for this article can be found online at: https://www.frontiersin.org/articles/10.3389/fpls.2022.944716/full#supplementary-material

References

Akram, N. A., Shafiq, F., and Ashraf, M. (2017). Ascorbic acid-A potential oxidant scavenger and its role in plant development and abiotic stress tolerance. *Front. Plant Sci.* 8:613. doi: 10.3389/fpls.2017.00613

Albuquerque, B. R., Heleno, S. A., Oliveira, M. B. P. P., Barros, L., and Ferreira, I. C. F. R. (2021). Phenolic compounds: current industrial applications, limitations and future challenges. *Food Funct.* 12, 14–29. doi: 10.1039/D0FO02324H

Aroca, R., Tognoni, F., Irigoyen, J. J., Sánchez-Díaz, M., and Pardossi, A. (2001). Different root low temperature response of two maize genotypes differing in chilling sensitivity. *Plant Physiol. Biochem.* 39, 1067–1073. doi: 10.1016/S0981-9428(01)01335-3

Asao, M., and Watanabe, K. (2010). Functional and bioactive properties of quinoa and amaranth. *Food Sci. Technol. Res.* 16, 163–168. doi: 10.3136/fstr.16.163

Barnes, J., Zheng, Y., and Lyons, T. (2002). "Plant resistance to ozone: the role of ascorbate," in *Air Pollution and Plant Biotechnology*. Tokyo: Springer Japan, 235–252.

Calatayud, Á., Gorbe, E., Roca, D., and Martínez, P. F. (2008). Effect of two nutrient solution temperatures on nitrate uptake, nitrate reductase activity, NH_4^+ concentration and chlorophyll a fluorescence in rose plants. *Environ. Exp. Bot.* 64, 65–74. doi: 10.1016/j.envexpbot.2008.02.003

Calleja-Cabrera, J., Boter, M., Oñate-Sánchez, L., and Pernas, M. (2020). Root growth adaptation to climate change in crops. *Front. Plant Sci.* 11:544. doi: 10.3389/fpls.2020.00544

Carvajal, M., Cooke, D. T., and Clarkson, D. T. (1996). Plasma membrane fluidity and hydraulic conductance in wheat roots: interactions between root temperature and nitrate or phosphate deprivation. *Plant Cell Environ.* 19, 1110–1114. doi: 10.1111/j.1365-3040.1996.tb00219.x

Catalá, R., Medina, J., and Salinas, J. (2011). Integration of low temperature and light signalling during cold acclimation response in Arabidopsis. *Proc. Natl. Acad. Sci.* 108, 16475–16480. doi: 10.1073/pnas.1107161108

Chadirin, Y., Hidaka, K., Takahashi, T., Sago, Y., Wajima, T., and Kitano, M. (2011). Application of temperature stress to roots of spinach I. effect of the low temperature stress on quality. *Environ. Control. Biol.* 49, 133–139. doi: 10.2525/ecb.49.133

Cheminant, S., Wild, M., Bouvier, F., Pelletier, S., Renou, J.-P., Erhardt, M., et al. (2011). DELLAs regulate chlorophyll and carotenoid biosynthesis to prevent photooxidative damage during seedling deetiolation in *Arabidopsis*. *Plant Cell* 23, 1849–1860. doi: 10.1105/tpc.111.085233

Chen, C. (2015). Determining the leaf emissivity of three crops by infrared thermometry. *Sensors* 15, 11387–11401. doi: 10.3390/s150511387

Chun, C., and Takakura, T. (1994). Rate of root respiration of lettuce under various dissolved oxygen concentrations in hydroponics. *Environ. Control. Biol.* 32, 125–135. doi: 10.2525/ecb1963.32.125

Chung, S. J., Chun, Y. T., Kim, K. Y., and Kim, T. H. (2002). Root zone temperature effect in hydroponically grown cucumber plants: growth and carbohydrate metabolism. *Acta Hortic.* 588, 53–57. doi: 10.17660/ActaHortic.2002.588.6

Clayton, W. A., Albert, N. W., Thrimawithana, A. H., McGhie, T. K., Deroles, S. C., Schwinn, K. E., et al. (2018). UVR8-mediated induction of flavonoid biosynthesis for UVB tolerance is conserved between the liverwort *Marchantia polymorpha* and flowering plants. *Plant J.* 96, 503–517. doi: 10.1111/tpj.14044

Das, K., and Roychoudhury, A. (2014). Reactive oxygen species (ROS) and response of antioxidants as ROS-scavengers during environmental stress in plants. *Front. Environ. Sci.* 2:53. doi: 10.3389/fenvs.2014.00053

Dolatabadian, A., and Jouneghani, R. S. (2009). Impact of exogenous ascorbic acid on antioxidant activity and some physiological traits of common bean subjected to salinity stress. *Not. Bot. Horti Agrobot. Cluj-Napoca* 37, 165–172. doi: 10.15835/NBHA3723406

Escobar-Bravo, R., Klinkhamer, P. G. L., and Leiss, K. A. (2017). Interactive effects of UV-B light with abiotic factors on plant growth and chemistry, and their consequences for defense against arthropod herbivores. *Front. Plant Sci.* 8:278. doi: 10.3389/fpls.2017.00278

Falah, M. A. F., Wajima, T., Kitano, M., Affan, M., and Falah, F. (2010). Responses of root uptake to high temperature of tomato plants (*Lycopersicon esculentum* mill.) in soil-less culture. *J. Agric. Sci. Technol.* 6, 543–558.

Fini, A., Brunetti, C., Di Ferdinando, M., Ferrini, F., and Tattini, M. (2011). Stress-induced flavonoid biosynthesis and the antioxidant machinery of plants. *Plant Signal. Behav.* 6, 709–711. doi: 10.4161/psb.6.5.15069

Garnier, E., and Laurent, G. (1994). Leaf anatomy, specific mass and water content in congeneric annual and perennial grass species. *New Phytol.* 128, 725–736. doi: 10.1111/j.1469-8137.1994.tb04036.x

Garrido, Y., Tudela, J. A., and Gil, M. I. (2015). Comparison of industrial precooling systems for minimally processed baby spinach. *Postharvest Biol. Technol.* 102, 1–8. doi: 10.1016/j.postharvbio.2014.12.003

Hao, H. P., Jiang, C.-D., Zhang, S. R., Tang, Y. D., and Shi, L. (2012). Enhanced thermal-tolerance of photosystem II by elevating root zone temperature in *Prunus mira* Koehne seedlings. *Plant Soil* 353, 367–378. doi: 10.1007/s11104-011-1037-y

Havaux, M. (1998). Carotenoids as membrane stabilizers in chloroplasts. *Trends Plant Sci.* 3, 147–151. doi: 10.1016/S1360-1385(98)01200-X

Hayakawa, K., and Agarie, S. (2010). Physiological roles of betacyanin in a halophyte, *Suaeda japonica* Makino. *Plant Prod. Sci.* 13, 351–359. doi: 10.1626/pps.13.351

He, F., Thiele, B., Kraus, D., Bouteyine, S., Watt, M., Kraska, T., et al. (2021). Effects of short-term root cooling before harvest on yield and food quality of Chinese broccoli (*Brassica oleracea* var. Alboglabra Bailey). *Agronomy* 11:577. doi: 10.3390/agronomy11030577

He, F., Thiele, B., Santhiraraja-Abresch, S., Watt, M., Kraska, T., Ulbrich, A., et al. (2020). Effects of root temperature on the plant growth and food quality of Chinese broccoli (*Brassica oleracea var. alboglabra* bailey). *Agronomy* 10:702. doi: 10.3390/agronomy10050702

He, S. Y., Zhang, G. C., Yu, Y. Q., Li, R. G., and Yang, Q. R. (2013). Effects of vacuum cooling on the enzymatic antioxidant system of cherry and inhibition of surface-borne pathogens. *Int. J. Refrig.* 36, 2387–2394. doi: 10.1016/j.ijrefrig.2013.05.018

Heckathorn, S. A., Giri, A., Mishra, S., and Bista, D. (2013). "Heat stress and roots," in *Climate Change and Plant Abiotic Stress Tolerance*. eds. N. Tuteja and S. S. Hedges (Weinheim: Wiley-VCH Verlag GmbH & Co. KGaA), 109–136.

Heinen, R. B., Ye, Q., and Chaumont, F. (2009). Role of aquaporins in leaf physiology. *J. Exp. Bot.* 60, 2971–2985. doi: 10.1093/jxb/erp171

Ito, A., and Shimizu, H. (2020). Effect of temperature and duration of root chilling on the balance between antioxidant activity and oxidative stress in spinach. *Environ. Control. Biol.* 58, 115–121. doi: 10.2525/ecb.58.115

Jain, G., and Gould, K. S. (2015). Functional significance of betalain biosynthesis in leaves of *Disphyma australe* under salinity stress. *Environ. Exp. Bot.* 109, 131–140. doi: 10.1016/j.envexpbot.2014.09.002

Jiménez-Aguilar, D. M., and Grusak, M. A. (2017). Minerals, vitamin C, phenolics, flavonoids and antioxidant activity of *Amaranthus* leafy vegetables. *J. Food Compos. Anal.* 58, 33–39. doi: 10.1016/j.jfca.2017.01.005

Kim, S., Hwang, G., Lee, S., Zhu, J. Y., Paik, I., Nguyen, T. T., et al. (2017). High ambient temperature represses anthocyanin biosynthesis through degradation of HY5. *Front. Plant Sci.* 8:1787. doi: 10.3389/fpls.2017.01787

Kongwong, P., Boonyakiat, D., and Poonlarp, P. (2019). Extending the shelf life and qualities of baby cos lettuce using commercial precooling systems. *Postharvest Biol. Technol.* 150, 60–70. doi: 10.1016/j.postharvbio.2018.12.012

Krause, P., and Nowoświat, A. (2019). Experimental studies involving the impact of solar radiation on the properties of expanded graphite polystyrene. *Energies* 13, 75. doi: 10.3390/en13010075

Król, A., Amarowicz, R., and Weidner, S. (2015). The effects of cold stress on the phenolic compounds and antioxidant capacity of grapevine (*Vitis vinifera* L.) leaves. *J. Plant Physiol.* 189, 97–104. doi: 10.1016/j.jplph.2015.10.002

Lam, V. P., Kim, S. J., Bok, G. J., Lee, J. W., and Park, J. S. (2020). The effects of root temperature on growth, physiology, and accumulation of bioactive compounds of *Agastache rugosa*. *Agriculture* 10, 162. doi: 10.3390/agriculture10050162

Le, T. N., Chiu, C.-H., and Hsieh, P.-C. (2020). Bioactive compounds and bioactivities of *Brassica oleracea* L. var. Italica sprouts and microgreens: an updated overview from a nutraceutical perspective. *Plan. Theory* 9, 946. doi: 10.3390/plants9080946

Lee, J.-H., and Oh, M.-M. (2015). Short-term low temperature increases phenolic antioxidant levels in kale. *Hortic. Environ. Biotechnol.* 56, 588–596. doi: 10.1007/s13580-015-0056-7

Lee, Y. K., Yuk, D. Y., Lee, J. W., Lee, S. Y., Ha, T. Y., Oh, K. W., et al. (2009). (−)-Epigallocatechin-3-gallate prevents lipopolysaccharide-induced elevation of beta-amyloid generation and memory deficiency. *Brain Res.* 1250, 164–174. doi: 10.1016/j.brainres.2008.10.012

León-Chan, R. G., López-Meyer, M., Osuna-Enciso, T., Sañudo-Barajas, J. A., Heredia, J. B., and León-Félix, J. (2017). Low temperature and ultraviolet-B radiation affect chlorophyll content and induce the accumulation of UV-B-absorbing and antioxidant compounds in bell pepper (*Capsicum annuum*) plants. *Environ. Exp. Bot.* 139, 143–151. doi: 10.1016/j.envexpbot.2017.05.006

Li, S., Jiang, H., Wang, J., Wang, Y., Pan, S., Tian, H., et al. (2019a). Responses of plant growth, physiological, gas exchange parameters of super and non-super rice to rhizosphere temperature at the tillering stage. *Sci. Rep.* 9, 10618. doi: 10.1038/s41598-019-47031-9

Li, G., Meng, X., Zhu, M., and Li, Z. (2019b). Research progress of betalain in response to adverse stresses and evolutionary relationship compared with anthocyanin. *Molecules* 24, 3078. doi: 10.3390/molecules24173078

Liu, Y., Tikunov, Y., Schouten, R. E., Marcelis, L. F. M., Visser, R. G. F., and Bovy, A. (2018). Anthocyanin biosynthesis and degradation mechanisms in Solanaceous vegetables: A review. *Front. Chem.* 6:52. doi: 10.3389/fchem.2018.00052

Liu, S., Zheng, X., Pan, J., Peng, L., Cheng, C., Wang, X., et al. (2019). RNA-sequencing analysis reveals betalains metabolism in the leaf of *Amaranthus tricolor* L. *PLoS One* 14:e0216001. doi: 10.1371/journal.pone.0216001

Mackerness, S. (2000). Plant responses to ultraviolet-B (UV-B: 280–320 nm) stress: what are the key regulators? *Plant Growth Regul.* 32, 27–39. doi: 10.1023/A:1006314001430

Mancinelli, A. L., and Schwartz, O. M. (1984). The photoregulation of anthocyanin synthesis IX. The photosensitivity of the response in dark and light-grown tomato seedlings. *Plant Cell Physiol.* 76, 281–283. doi: 10.1093/oxfordjournals.pcp.a076701

Martínez, J. A., and Artés, F. (1999). Effect of packaging treatments and vacuum-cooling on quality of winter harvested iceberg lettuce. *Food Res. Int.* 32, 621–627. doi: 10.1016/S0963-9969(99)00135-0

Masarirambi, M. T., Nxumalo, K. A., Musi, P. J., and Rugube, L. M. (2018). Common physiological disorders of lettuce (*Lactuca sativa*) found in Swaziland: a review. *J. Agric. Environ. Sci.* 18, 50–56. doi: 10.5829/idosi.aejaes.2018.50.56

Maurel, C., Boursiac, Y., Luu, D.-T., Santoni, V., Shahzad, Z., and Verdoucq, L. (2015). Aquaporins in plants. *Physiol. Rev.* 95, 1321–1358. doi: 10.1152/physrev.00008.2015

Mibei, E. K., Ambuko, J., Giovannoni, J. J., Onyango, A. N., and Owino, W. O. (2017). Carotenoid profiling of the leaves of selected African eggplant accessions subjected to drought stress. *Food Sci. Nutr.* 5, 113–122. doi: 10.1002/fsn3.370

Miller, N. J., and Rice-Evans, C. A. (1996). Spectrophotometric determination of antioxidant activity. *Redox Rep.* 2, 161–171. doi: 10.1080/13510002.1996.11747044

Mittler, R., Finka, A., and Goloubinoff, P. (2012). How do plants feel the heat? *Trends Biochem. Sci.* 37, 118–125. doi: 10.1016/j.tibs.2011.11.007

Müller, M., and Munné-Bosch, S. (2021). Hormonal impact on photosynthesis and photoprotection in plants. *Plant Physiol.* 185, 1500–1522. doi: 10.1093/plphys/kiaa119

Nguyen, D. T. P., Lu, N., Kagawa, N., Kitayama, M., and Takagaki, M. (2020). Short-term root-zone temperature treatment enhanced the accumulation of secondary metabolites of hydroponic coriander (*Coriandrum sativum* L.) grown in a plant factory. *Agronomy* 10, 413. doi: 10.3390/agronomy10030413

Nxawe, S., Laubscher, C., and Ndakidemi, P. (2009). Effect of regulated irrigation water temperature on hydroponics production of spinach (*Spinacia oleracea* L.). *Afr. J. Agric. Res.* 4, 1442–1446.

Ogawa, E., Hikosaka, S., and Goto, E. (2018). Effects of nutrient solution temperature on the concentration of major bioactive compounds in red perilla. *J. Agric. Meteorol.* 74, 71–78. doi: 10.2480/agrmet.D-17-00037

Oren-Shamir, M. (2009). Does anthocyanin degradation play a significant role in determining pigment concentration in plants? *Plant Sci.* 177, 310–316. doi: 10.1016/j.plantsci.2009.06.015

Paradiso, V. M., Castellino, M., Renna, M., Gattullo, C. E., Calasso, M., Terzano, R., et al. (2018). Nutritional characterization and shelf-life of packaged microgreens. *Food Funct.* 9, 5629–5640. doi: 10.1039/C8FO01182F

Polturak, G., Breitel, D., Sarrion-Perdigones, A., Grossman, N., Weithorn, E., Pliner, M., et al. (2016). Elucidation of the first step in betalain biosynthesis allows the heterologous production of betalain pigments in plants. *Planta Med.* 81, S1–S381. doi: 10.1055/s-0036-1596788

Qian, M., Kalbina, I., Rosenqvist, E., Jansen, M. A. K., Teng, Y., and Strid, Å. (2019). UV regulates the expression of phenylpropanoid biosynthesis genes in cucumber (*Cucumis sativus* L.) in an organ and spectrum dependent manner. *Photochem. Photobiol. Sci.* 18, 424–433. doi: 10.1039/C8PP00480C

Qiuyan, Y., Zengqiang, D., Jingdong, M., Xun, L., and Fei, D. (2012). Effects of root-zone temperature and N, P, and K supplies on nutrient uptake of cucumber (*Cucumis sativus* L.) seedlings in hydroponics. *Soil Sci. Plant Nutr.* 58, 707–717. doi: 10.1080/00380768.2012.733925

Rácz, A., and Hideg, É. (2021). Narrow-band 311 nm ultraviolet-B radiation evokes different antioxidant responses from broad-band ultraviolet. *Plan. Theory* 10, 1570. doi: 10.3390/plants10081570

Raja, V., Majeed, U., Kang, H., Andrabi, K. I., and John, R. (2017). Abiotic stress: interplay between ROS, hormones and MAPKs. *Environ. Exp. Bot.* 137, 142–157. doi: 10.1016/j.envexpbot.2017.02.010

Rakpenthai, A., Khaksar, G., Burow, M., Olsen, C. E., and Sirikantaramas, S. (2019). Metabolic changes and increased levels of bioactive compounds in white radish (*Raphanus sativus* L. cv. 01) sprouts elicited by oligochitosan. *Agronomy* 9, 467. doi: 10.3390/agronomy9080467

Rezaie, R., Abdollahi Mandoulakani, B., and Fattahi, M. (2020). Cold stress changes antioxidant defense system, phenylpropanoid contents and expression of genes involved in their biosynthesis in *Ocimum basilicum* L. *Sci. Rep.* 10, 5290. doi: 10.1038/s41598-020-62090-z

Rivero, R. M., Ruiz, J. M., García, P. C., López-Lefebre, L. R., Sánchez, E., and Romero, L. (2001). Resistance to cold and heat stress: accumulation of phenolic compounds in tomato and watermelon plants. *Plant Sci.* 160, 315–321. doi: 10.1016/S0168-9452(00)00395-2

Rubio, C. P., Hernández-Ruiz, J., Martinez-Subiela, S., Tvarijonaviciute, A., and Joaquin, J. (2016). Spectrophotometric assays for total antioxidant capacity (TAC) in dog serum: an update. *BMC Vet. Res.* 12:166. doi: 10.1186/s12917-016-0792-7

Sagawa, J. M., Stanley, L. E., LaFountain, A. M., Frank, H. A., Liu, C., and Yuan, Y. (2016). An R2R3-MYB transcription factor regulates carotenoid pigmentation in *Mimulus lewisii* flowers. *New Phytol.* 209, 1049–1057. doi: 10.1111/nph.13647

Sakamoto, M., and Suzuki, T. (2015). Effect of root-zone temperature on growth and quality of hydroponically grown red leaf lettuce (*Lactuca sativa* L. cv. Red wave). *Am. J. Plant Sci.* 6, 2350–2360. doi: 10.4236/ajps.2015.614238

Sanchez, R. A., Hall, A. J., Trapani, N., and de Hunau, R. C. (1983). Effects of water stress on the chlorophyll content, nitrogen level and photosynthesis of leaves of two maize genotypes. *Photosynth. Res.* 4, 35–47. doi: 10.1007/BF00041799

Sarker, U., Hossain, M. N., Iqbal, M. A., and Oba, S. (2020). Bioactive components and radical scavenging activity in selected advance lines of salt-tolerant vegetable amaranth. *Front. Nutr.* 7:587257. doi: 10.3389/fnut.2020.587257

Sarker, U., and Oba, S. (2018). Drought stress enhances nutritional and bioactive compounds, phenolic acids and antioxidant capacity of *Amaranthus* leafy vegetable. *BMC Plant Biol.* 18, 258. doi: 10.1186/s12870-018-1484-1

Sarker, U., and Oba, S. (2020). Leaf pigmentation, its profiles and radical scavenging activity in selected *Amaranthus tricolor* leafy vegetables. *Sci. Rep.* 10, 18617. doi: 10.1038/s41598-020-66376-0

Schwarz, D., Rouphael, Y., Colla, G., and Venema, J. H. (2010). Grafting as a tool to improve tolerance of vegetables to abiotic stresses: thermal stress, water stress and organic pollutants. *Sci. Hortic. (Amsterdam).* 127, 162–171. doi: 10.1016/j.scienta.2010.09.016

Shah, S., Houborg, R., and McCabe, M. (2017). Response of chlorophyll, carotenoid and SPAD-502 measurement to salinity and nutrient stress in wheat (*Triticum aestivum* L.). *Agronomy* 7:61. doi: 10.3390/agronomy7030061

Smirnoff, N., Conklin, P. L., and Loewus, F. A. (2001). Biosynthesis of ascorbic acid in plants: a renaissance. *Annu. Rev. Plant Physiol. Plant Mol. Biol.* 52, 437–467. doi: 10.1146/annurev.arplant.52.1.437

Sperdouli, I., and Moustakas, M. (2014). Leaf developmental stage modulates metabolite accumulation and photosynthesis contributing to acclimation of *Arabidopsis thaliana* to water deficit. *J. Plant Res.* 127, 481–489. doi: 10.1007/s10265-014-0635-1

Srivastava, R. (2011). Nutritional quality of some cultivated and wild species of *Amaranthus* L. *Int. J. Pharm. Sci.* 2, 3152–3156.

Stahl, W., and Sies, H. (2003). Antioxidant activity of carotenoids. *Mol. Asp. Med.* 24, 345–351. doi: 10.1016/S0098-2997(03)00030-X

Stanciu, G., Lupșor, S., and Sava, C. (2009). Spectrophotometric characterizations of anthocyans extracted from black grapes skin. *Ovidius Univ. Ann. Chem.* 20, 205–208.

Stanley, L., and Yuan, Y.-W. (2019). Transcriptional regulation of carotenoid biosynthesis in plants: so many regulators, so little consensus. *Front. Plant Sci.* 10:1017. doi: 10.3389/fpls.2019.01017

Stintzing, F. C., and Carle, R. (2004). Functional properties of anthocyanins and betalains in plants, food, and in human nutrition. *Trends Food Sci. Technol.* 15, 19–38. doi: 10.1016/j.tifs.2003.07.004

Takahama, M., Kawagishi, K., Sugawara, A., Araki, K., Munekata, S., Nicola, S., et al. (2019). Classification and screening of baby-leaf vegetables on the basis of their yield, external appearance and internal quality. *Hortic. J.* 88, 387–400. doi: 10.2503/hortj.UTD-033

Tari, I. (2003). Abaxial and adaxial stomatal density, stomatal conductances and water status of bean primary leaves as affected by Paclobutrazol. *Biol. Plant.* 46, 215–220. doi: 10.1023/B:BIOP.0000022254.63487.16

Tian, D., Fen, L., Jiangang, L., Mengli, K., Jingfen, Y., Xingqian, Y., et al. (2016). Comparison of different cooling methods for extending shelf life of postharvest broccoli. *Int. J. Agric. Biol.* 9, 178–185. doi: 10.3965/j.ijabe.20160906.2107

Toledo-Ortiz, G., Johansson, H., Lee, K. P., Bou-Torrent, J., Stewart, K., Steel, G., et al. (2014). The HY5-PIF regulatory module coordinates light and temperature control of photosynthetic gene transcription. *PLoS Genet.* 10:e1004416. doi: 10.1371/journal.pgen.1004416

Wheeler, G. L., Jones, M. A., and Smirnoff, N. (1998). The biosynthetic pathway of vitamin C in higher plants. *Nature* 393, 365–369. doi: 10.1038/30728

Wittayathanarattana, T., Wanichananan, P., Supaibulwatana, K., and Goto, E. (2022). Enhancement of bioactive compounds in baby leaf *Amaranthus tricolor* L. using short-term application of UV-B irradiation. *Plant Physiol. Biochem.* 182, 202–215. doi: 10.1016/j.plaphy.2022.04.003

Yu, M.-H., Ding, G.-D., Gao, G.-L., Zhao, Y. Y., Yan, L., and Sai, K. (2015). Using plant temperature to evaluate the response of stomatal conductance to soil moisture deficit. *Forests* 6, 3748–3762. doi: 10.3390/f6103748

Zegaoui, Z., Planchais, S., Cabassa, C., Djebbar, R., Belbachir, O. A., and Carol, P. (2017). Variation in relative water content, proline accumulation and stress gene expression in two cowpea landraces under drought. *J. Plant Physiol.* 218, 26–34. doi: 10.1016/j.jplph.2017.07.009

Zhou, H., Zhou, G., He, Q., Zhou, L., Ji, Y., and Lv, X. (2021). Capability of leaf water content and its threshold values in reflection of soil–plant water status in maize during prolonged drought. *Ecol. Indic.* 124:107395. doi: 10.1016/j.ecolind.2021.107395

Zhu, J., Zhang, K.-X., Wang, W.-S., Gong, W., Liu, W. C., Chen, H. G., et al. (2015). Low temperature inhibits root growth by reducing auxin accumulation via ARR1/12. *Plant Cell Physiol.* 56, 727–736. doi: 10.1093/pcp/pcu217

frontiers | Frontiers in Plant Science

TYPE Original Research
PUBLISHED 25 August 2022
DOI 10.3389/fpls.2022.980581

OPEN ACCESS

EDITED BY
Yuxin Tong,
Institute of Environment and Sustainable Development in Agriculture (CAAS), China

REVIEWED BY
Eri Hayashi,
Japan Plant Factory Association, Japan
Minjuan Wang,
China Agricultural University, China
Adel Bakhshipour,
University of Guilan, Iran

*CORRESPONDENCE
Tao Lin
lintao1@zju.edu.cn

SPECIALTY SECTION
This article was submitted to Technical Advances in Plant Science, a section of the journal Frontiers in Plant Science

RECEIVED 28 June 2022
ACCEPTED 03 August 2022
PUBLISHED 25 August 2022

CITATION
Lin Z, Fu R, Ren G, Zhong R, Ying Y and Lin T (2022) Automatic monitoring of lettuce fresh weight by multi-modal fusion based deep learning. *Front. Plant Sci.* 13:980581. doi: 10.3389/fpls.2022.980581

Automatic monitoring of lettuce fresh weight by multi-modal fusion based deep learning

Zhixian Lin[1], Rongmei Fu[1], Guoqiang Ren[1], Renhai Zhong[1], Yibin Ying[1,2] and Tao Lin[1,2]*

[1]College of Biosystems Engineering and Food Science, Zhejiang University, Hangzhou, China, [2]Key Laboratory of Intelligent Equipment and Robotics for Agriculture of Zhejiang Province, Hangzhou, China

Fresh weight is a widely used growth indicator for quantifying crop growth. Traditional fresh weight measurement methods are time-consuming, laborious, and destructive. Non-destructive measurement of crop fresh weight is urgently needed in plant factories with high environment controllability. In this study, we proposed a multi-modal fusion based deep learning model for automatic estimation of lettuce shoot fresh weight by utilizing RGB-D images. The model combined geometric traits from empirical feature extraction and deep neural features from CNN. A lettuce leaf segmentation network based on U-Net was trained for extracting leaf boundary and geometric traits. A multi-branch regression network was performed to estimate fresh weight by fusing color, depth, and geometric features. The leaf segmentation model reported a reliable performance with a mIoU of 0.982 and an accuracy of 0.998. A total of 10 geometric traits were defined to describe the structure of the lettuce canopy from segmented images. The fresh weight estimation results showed that the proposed multi-modal fusion model significantly improved the accuracy of lettuce shoot fresh weight in different growth periods compared with baseline models. The model yielded a root mean square error (RMSE) of 25.3 g and a coefficient of determination (R^2) of 0.938 over the entire lettuce growth period. The experiment results demonstrated that the multi-modal fusion method could improve the fresh weight estimation performance by leveraging the advantages of empirical geometric traits and deep neural features simultaneously.

KEYWORDS

growth monitoring, fresh weight, deep learning, lettuce, multi-modal fusion, convolution neural network

Introduction

Plant factories have recently gained vast popularity owing to the advantages of growing efficiently and controlled environment. Plant factory, also known as vertical farm, is an advanced stage of controlled environment agriculture (CEA) that features high yield, high quality, and high efficiency (Graamans et al., 2018; Shamshiri et al., 2018). Compared with traditional agriculture, the internal environmental factors of plant factories can be controlled precisely and automatically. Crop yield and quality are significantly correlated with genetic, environmental factors (physical, chemical, and biological) and cultivation methods during crop growth (Kozai et al., 2019). Growing crops in a plant factory can be regarded as a process of control and optimization, in which crop growth monitoring is a crucial step. Accurate and timely crop growth information can reveal the current growth status and yield potential of crops, which are essential for management decision-making.

Fresh weight is a widely used growth indicator for quantifying crop growth. Crop growth can be defined as a process of increment in biomass or dimensions of a plant (Bakker et al., 1995). The fresh weight is one important quantitative factor that dynamically changes during crop growth. Automatic quantitation of fresh weight can help researchers better understand the crop growth process and the dynamic relationship between crop and environment. For leafy vegetables like lettuce, the fresh weight of plant is composed of the root part and the shoot part. The fresh weight of the shoot part is more directly related to yield as the leaves and stems are harvested as final products. Traditional fresh weight measurement methods are mainly based on destructive sampling, which are time-consuming, laborious, and destructive. Nowadays, most commercial greenhouses and plant factories can grow over 10,000 individual plants per day. Traditional methods by manually operation are facing challenges at this large production scale. Thus, automatic and non-destructive monitoring of crop fresh weight is urgently needed.

Image-based approaches have been widely used in fresh weight monitoring of lettuce (**Table 1**). Images can provide non-destructive, convenient, and low-cost access to crop growth information (Lin et al., 2022). The main processing steps of image-based approaches include image preprocessing, feature extraction, and fresh weight regression. Constructing an appropriate feature extraction method is the key to improving the model performance. Relating size and shape to weight is a common empirical concept in the field of agriculture (Kashiha et al., 2014; Konovalov et al., 2019). Geometric features extracted from lettuce images can quantitatively describe the characteristic of the canopy, which is helpful in fresh weight estimating. Many image segmentation algorithms are developed to segment plant leaves and backgrounds from RGB images or 3D point clouds and then calculate geometric features such as leaf projection area, volume, and plant height from the segmented data to construct a fresh weight regression model (Jung et al., 2015; Jiang et al., 2018; Mortensen et al., 2018; Reyes-Yanes et al., 2020). These empirical feature extraction approaches show promising results, indicating the low-level features extracted from images have strong correlations with fresh weight.

Deep learning techniques such as deep convolutional neural networks (DCNNs) can extract and learn intricate relationships from data through multiple levels for representation (LeCun et al., 2015). End-to-end deep learning methods based on DCNNs have recently emerged and show opportunities to estimate fresh weight directly from input images (Zhang et al., 2020; Buxbaum et al., 2022). Although most DCNNs are initially designed for classification tasks, they can also perform regression tasks well because of their strong feature learning capability. These end-to-end approaches eliminate the cumbersome efforts of extracting features from plant segmentation results and show potential for the practical application of crop growth monitoring.

Some works demonstrate that combining empirical-constructed and deep neural features is an effective method for image-based applications (Nanni et al., 2017; Kan et al., 2019). The data-driven deep learning methods naturally meet their limits when sufficient training data are unavailable (von Rueden et al., 2021). The low-level features extracted by experience can help to provide complementary information for optimizing the initialization and filtering of proposals for deep learning networks, which leads to higher estimation accuracies.

Multi-modal fusion has received intensive research covering different application domains in recent years. Extracting and combining information from multiple modalities considered for a given learning task can produce an improved performance (Ramachandram and Taylor, 2017). Encouraged by the growing availability of image acquisition devices, RGB-D (Red, Green, Blue – Depth) data has attracted increasing attention in agriculture. As a typical multi-modal data, RGB-D images can provide not only color information but also depth information for each pixel. With the combination of color and depth information, the geometrical traits of targets (size, length, or width) can be accurately measured (Fu et al., 2020), which is more advantageous for describing crop growth status. Fusing color and depth features based on DCNNs is a promising approach for achieving better performance (Eitel et al., 2015; Zeng et al., 2019; Quan et al., 2021). However, existing depth sensors still have some limitations, and depth images are prone to holes on transparent or shiny surfaces (Song et al., 2015), which challenges applying multi-modal fusion for extracting and combining information in practical applications.

In this study, we proposed a multi-modal fusion based deep learning model for automatic monitoring of lettuce shoot fresh weight by utilizing RGB-D images. The model combined geometric traits from empirical feature extraction and deep

TABLE 1 An overview of existing image-based methods for lettuce fresh weight monitoring.

Method type	Input data types	Sample sizes	Methods	Descriptions	References
Empirical feature extraction	RGB	/	Traditional image processing + quadratic regression	Regression by projected area from top view images	Lee, 2008
	RGB	82	Traditional image processing + linear regression	Regression by pixel counting from top view images	Jung et al., 2015; Jiang et al., 2018
	RGB	/	OpenCV-based segmentation + linear regression	Regression by extracted 2D and 3D geometric features from a stereo-vision system	Yeh et al., 2014; Chen et al., 2016
	3D point clouds	230	Rule-based segmentation + linear regression	Regression by extracted geometric features from colored 3D point clouds.	Mortensen et al., 2018
	RGB	338	Optical flow analysis + gradient boost regression	Regression by extracted leaf movement features from top view images.	Nagano et al., 2019
	RGB	750	CNN segmentation + linear regression	Regression by extracted geometric features from the side and top view images	Reyes-Yanes et al., 2020
End-to-end deep learning	RGB	286	CNN regression	Regression directly by a CNN model	Zhang et al., 2020
	RGB-D	3,888	CNN regression	Regression directly by an RGB-D fusion CNN network	Buxbaum et al., 2022

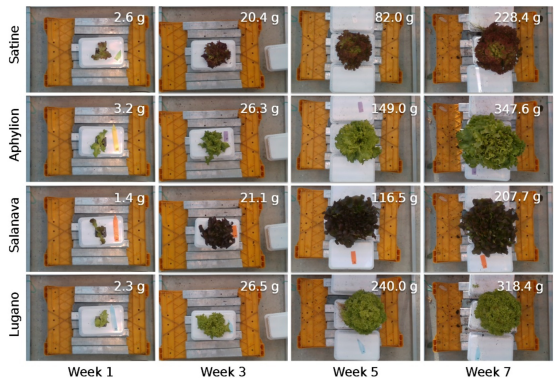

FIGURE 1
Examples of RGB images (cropped) of the AGC dataset.

neural features from CNN. A lettuce leaf segmentation network based on U-Net was trained for extracting leaf boundary and geometric traits. A multi-branch regression network was performed to estimate fresh weight by fusing color, depth, and geometric features. Specifically, the objectives of the study were to (1) achieve an accurate and automatic fresh weight estimation of lettuce by a multi-modal fusion based deep learning model; (2) quantify the benefits of combining geometric traits with deep neural features in improving the model performance; (3) investigate the performance variances of fresh weight estimation for different lettuce varieties in the entire growth period.

Materials and methods

Dataset

The 3rd Autonomous Greenhouse Challenge: Online Challenge Lettuce Images dataset (AGC dataset) was used in this study (Hemming et al., 2021). The dataset was generated for the needs of the 3rd International Autonomous Greenhouse Challenge, a famous international competition held by Wageningen University & Research. Top-view RGB images and aligned depth images of 388 lettuces were provided in the dataset. The dataset contains references to images and measured data on a lettuce crop growing in well-controlled greenhouse conditions. The sampled plants include four different lettuce varieties suitable for hydroponics: Aphylion, Salanova, Satine, and Lugano. Five crop traits were destructively measured at 7-day intervals, including fresh weight of shoot, height, diameter, leaf area, and dry weight of shoot. A total of seven batches of data were collected, covering the entire growth period of lettuce (**Figure 1**). The AGC dataset did not provide ground truth annotation for leaf segmentation. The CVAT tool (Sekachev et al., 2020) was used to label the leaves and background pixels from RGB images manually.

Data preprocessing and augmentation

The original top-view RGB and depth images of the AGC dataset were captured with an image size of 1,920 × 1,080 pixels. We applied the same preprocessing strategy for RGB and depth images of each sample. First, all images were cropped to

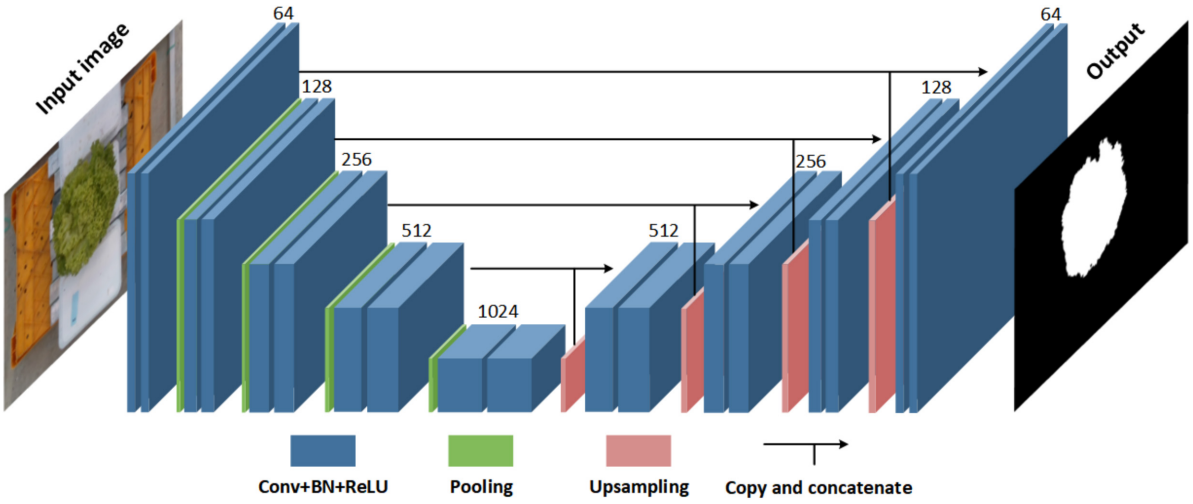

FIGURE 2
The structure of the U-Net based leaf segmentation network.

1,080 × 720 with the same position parameters (the x and y coordinate of the upper-left corner is 515 and 210) to remove invalid pixels at the edges. The cropped image dataset was used as the input of the proposed method. We used 70% of the image dataset for training and the rest for testing.

The proposed method consists of two independent networks, which used the same training set and test set, but their data preprocessing and data augmentation methods were different. For the segmentation network, each image is resized to 960 × 640 before being fed to the network. The Albumentations tool was used for data augmentation (Buslaev et al., 2020). Image rotation, rescale, flip, shift, brightness change, contrast change, and RGB change were used in this study. The input images of the segmentation network were augmented one-to-one during training without duplication. For the regression network, the original images of the cropped dataset were used. Since the image scale significantly affects the estimation of fresh weight, only spatial level transforms that maintain the image scale was applied. As a result, an augmented training set containing 2,439 images was constructed before network training.

Multi-modal fusion model

System pipeline for the model

The multi-modal fusion model composed of a lettuce segmentation network and a multi-branch regression network was developed for automatic estimation of the fresh weight of lettuce. The system pipeline of the proposed model included the following steps: (i) data preprocessing, (ii) geometric traits extraction, and (iii) fresh weight estimation. The model's input was the top-view RGB image, depth image, and empirical geometric traits of lettuce, and the output was the estimation of shoot fresh weight. In the model-building stage, we trained the leaf segmentation network and multi-branch regression network with the same dataset.

Leaf segmentation network

A leaf segmentation network based on U-Net architecture was employed to automatically segment lettuce leaves and backgrounds from RGB images (**Figure 2**). U-Net is a semantic segmentation network based on fully convolutional networks with a typical U-shaped encoder-decoder architecture (Ronneberger et al., 2015). The U-Net architecture used in this study consists of two parts: contractive path (encoder) and expanding path (decoder). The contractive path can extract feature maps of different resolutions by stacking convolutional layers and max-pooling layers, thereby capturing both global and local features of the input images. The expanding path combines features and spatial information at each level by a sequence of up-sampling and concatenation.

As a pixel-wise classification network, each pixel in the input image of the leaf segmentation network corresponds to one instance, where leaf pixels are labeled as 1, and background pixels are labeled as 0. The input image size is 960 × 640 × 3 to balance further processing requirements and the memory limitation. The number of levels, resolutions and channels of each feature map is shown in **Figure 2**. The Dice loss was used as the loss function (Milletari et al., 2016). The 2-class variant of the Dice loss function was calculated as follows (Equation 1):

$$Loss_{dice} = 1 - \frac{2\sum_i^N p_i g_i}{\sum_i^N p_i^2 + \sum_i^N g_i^2} \quad (1)$$

where N is the sum of pixels, p_i and g_i are the ground truth and prediction label at pixel i, $p_i, g_i \in [0, 1]$.

To quantitatively evaluate the performance of the leaf segmentation model, different metrics were used, including intersection over union (IoU), F1 score, pixel accuracy, precision, and recall.

Geometric traits extraction

A total of 10 geometric traits were defined to describe the structure of the lettuce canopy (**Table 2**). We used edge and contour detection methods based on OpenCV to extract geometric traits from segmented images, and the processing step were as follows: (1) removing blobs in the binary image by morphological operations, (2) detecting the largest contour, (3) detecting the minimal circumcircle, minimal area rectangle and convex hull of the contour, (4) calculating geometric traits. The size-related geometric traits (PA, PP, CA, CP, PCD, ARW, and ARH) were obtained directly by pixel counting, and the remaining morphology-related geometric traits (PPR, CPR, and CAR) were calculated by size-related geometric traits.

Multi-branch regression network

A multi-branch architecture regression network was built to fuse multi-modal data for lettuce fresh weight monitoring (**Figure 3**). The multi-branch regression network was made up of two blocks: feature extraction block and regression block. Min-max normalization was applied for all input variables to speed up the training process. We employed a late fusion architecture to effectively extract and fuse RGB, depth, and geometric features. For RGB and depth branches, we utilized ResNet-34 for feature extraction (He et al., 2015). As a popular network that is widely used in the field of image classification, ResNet can extract deep features from images and have good feature extraction performance. We removed the final 1,000 × 1 fully connected layer of ResNet and obtained the features of RGB and depth from the last flatten layer (average pool). As for geometric features extracted from the leaf segmentation network, we utilized a multilayer perception (MLP) for feature extraction. All outputs of three branches were flattened to ensure they have the same dimensions. Finally, these three feature sets were concatenated and passed to the regression block. The regression block consists of three sequential fully connected layers. In our tests, we found that increasing the depth or width of the regression blocks had little effect on the prediction results. We employed a retraining strategy to train the whole network since the dataset is quite different from ImageNet. The multi-branch regression network used the mean-squared-error (MSE) loss as the loss function (Equation 2).

$$Loss_{MSE} = \frac{1}{N}\sum_{i}^{N}(y_i - \hat{y}_i)^2 \quad (2)$$

where N is the number of samples, y_i and $\hat{y}_i$ are the ground truth fresh weight and predicted fresh weight for sample i.

Root mean square error (RMSE), mean absolute percentage error (MAPE), and coefficient of determination (R^2) were used as performance indicators for the multi-branch regression network.

TABLE 2 Geometric traits extracted from the segmented images.

Traits type	Traits	Description
Size related	PA	Projected area
	PP	Projected perimeter
	CA	Convex hull area
	CP	Convex hull perimeter
	PCD	Circumcircle diameter of the projected area
	ARW	Width of minimal area rectangle of the projected area
	ARH	Height of minimal area rectangle of the projected area
Morphology-related	PPR	Projected area/projected perimeter
	CPR	Convex hull area/convex hull perimeter
	CAR	Projected area/convex hull area

Experimental design and implementation

We performed a model ablation study to comprehensively evaluate the fresh weight estimation capability of the multi-modal fusion model. The multi-modal input of the model consists of RGB images, depth images, and geometric traits extracted from segmented images. It is worthwhile to investigate the performance variances of models with these inputs individually and in different combinations. Specifically, we built three dual-branch baseline models and three single-branch baseline models. The regression block and training configurations of baseline models were as same as the three-branch multi-modal fusion model. Moreover, the fresh weight estimation results of a dataset without data augmentation were presented to evaluate the performance of the model under insufficient data sizes.

All models were trained and tested on a Linux workstation (Ubuntu 16.04 LTS) with two Intel Xeon Gold Processors (2.1G/20 Core/27.5M), 128 GB of RAM, and four NVIDIA GeForce RTX 2080 Ti graphics cards (11 GB of RAM). All the deep learning models were implemented on the Python platform based on PyTorch.

Results and discussion

Analysis of the distribution of the lettuce dataset

The AGC dataset contains 388 lettuce samples of four varieties growing in 7 weeks. To better describe the dataset, we

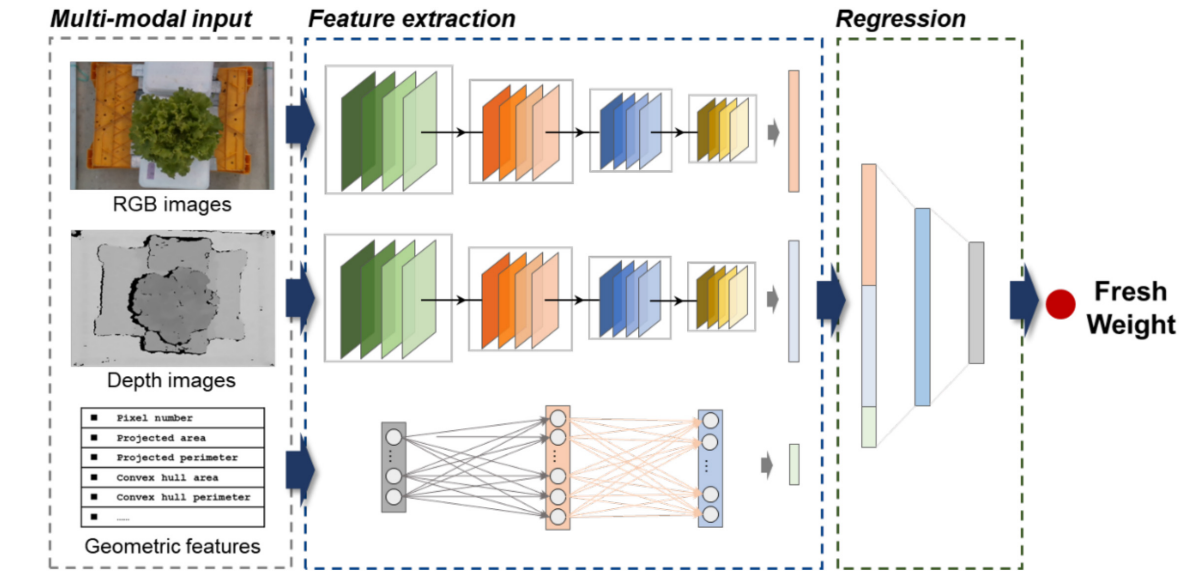

FIGURE 3
Overall structure of the multi-branch regression network.

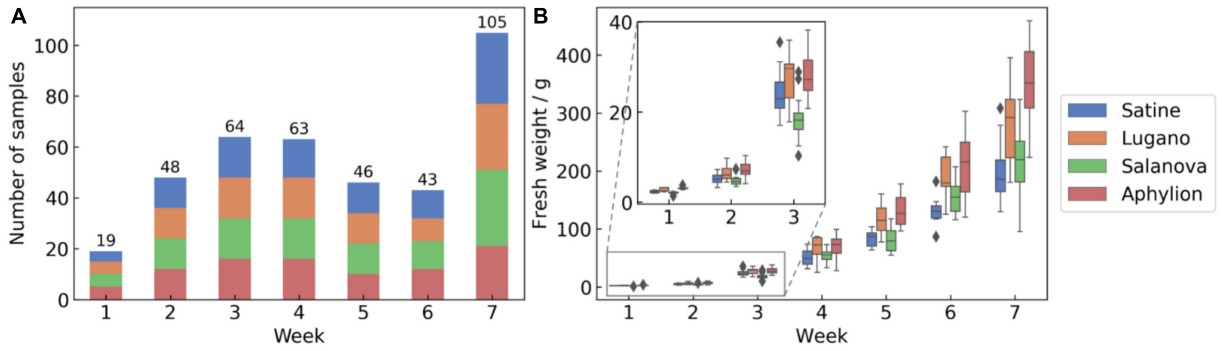

FIGURE 4
Data distribution of the AGC dataset: **(A)** sample size of the four varieties, and **(B)** fresh weight distribution of the four varieties.

TABLE 3 Pixel-level accuracy indices of the leaf segmentation network.

	Class	mIoU	Accuracy	IoU	F1 score	Precision	Recall
Training set	Leaf	0.988	0.998	0.978	0.989	0.989	0.989
	Background			0.998	0.999	0.999	0.999
Test set	Leaf	0.982	0.998	0.968	0.983	0.984	0.983
	Background			0.997	0.999	0.999	0.999

summarized the data frequency and fresh weight distribution (Figure 4). The sample size of four lettuce varieties was evenly distributed, with a maximum of 102 and a minimum of 92. However, the dataset distribution was skewed toward larger and older plants in terms of the growth period. Moreover, the fresh weight of lettuce varied significantly in different growth periods, ranging from 1.4 to 459.7 g. We also observed that the fresh weight varied across different lettuce varieties, especially in the maturity period. For example, the green leaf varieties (Lugano and Aphylion) were heavier than the red leaf varieties (Satine and Salanova). The unbalanced data distribution potentially challenged the fresh weight estimation of different lettuce varieties in the entire growth period.

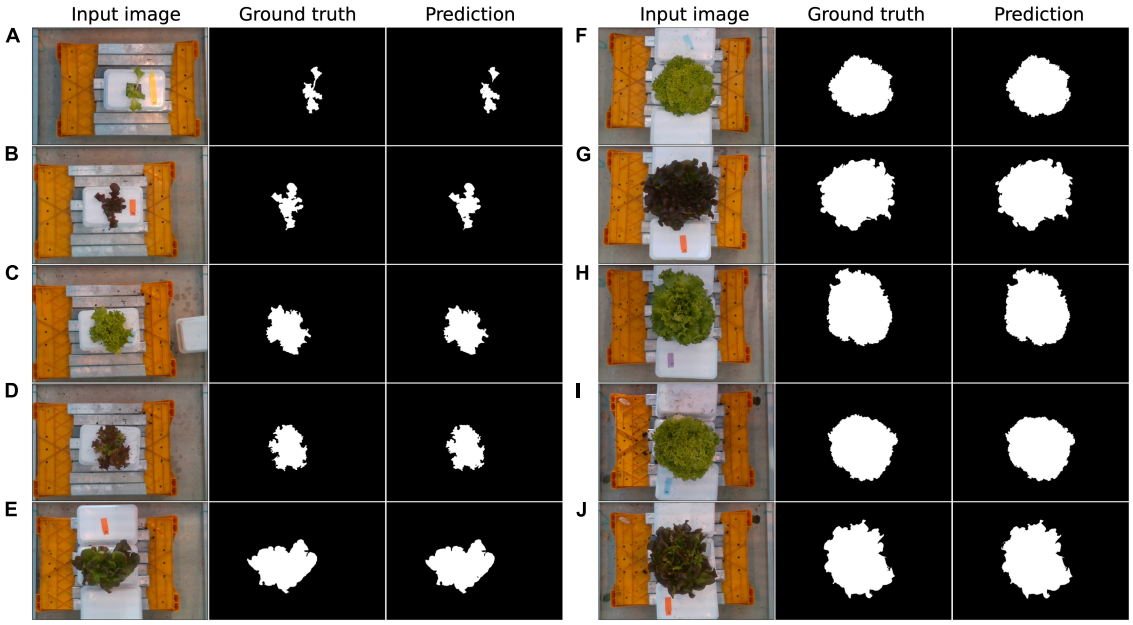

FIGURE 5
Qualitative results obtained by the leaf segmentation network. 10 samples **(A–J)** were randomly selected.

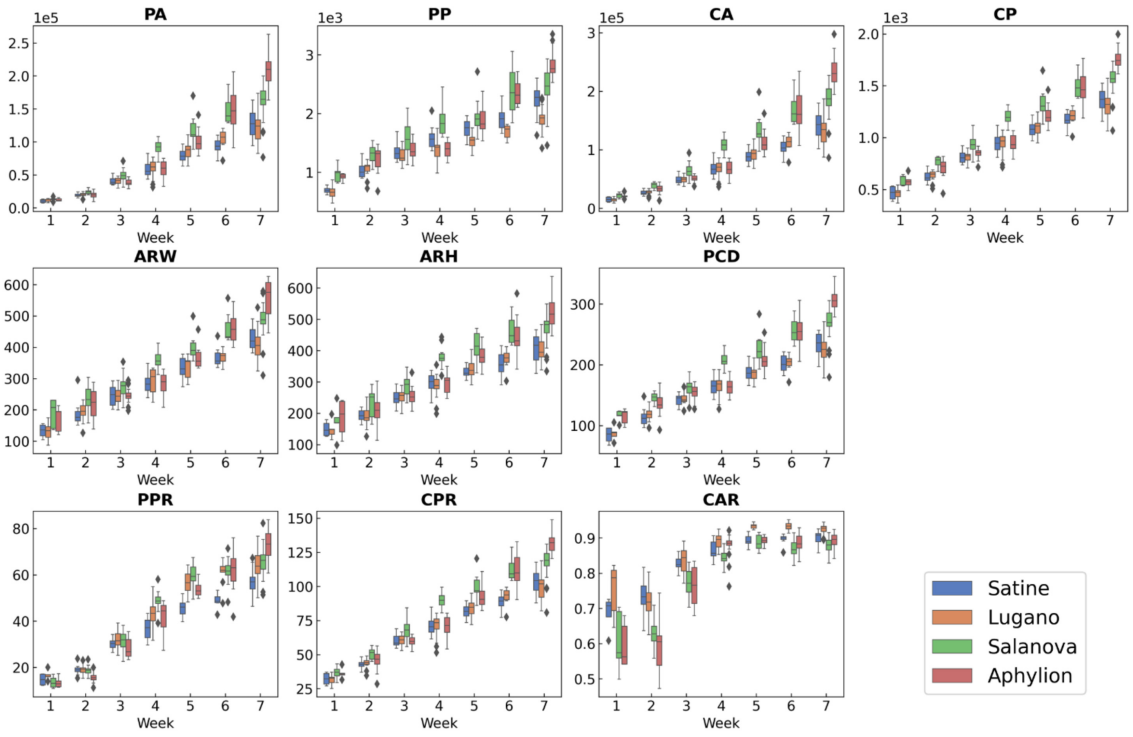

FIGURE 6
Data distribution of extracted geometric traits of the four lettuce varieties in 7 weeks.

Evaluation of leaf segmentation and geometric traits

The leaf segmentation network based on U-Net architecture showed good performance in the AGC dataset (Table 3). We evaluated the pixel-level classification performance of the leaf segmentation network. The leaf segmentation network achieved a mIoU of 0.982 and an accuracy of 0.998 in the test set. For background pixels, all indices were above 99% in the test set. The leaf pixels also obtain satisfactory performance, with an IoU of 0.968 and an F1 score of 0.983 for the test set. The background pixels were more accessible to classify than leaf pixels since background scenes vary less across the dataset. It is noteworthy that the network achieved similarly high results across the test and training sets, indicating that the network was well trained on the dataset without overfitting. Some representative results generated by the leaf segmentation network were also provided (Figure 5). We found the network performed slightly worse in small lettuce through visual appraisal. This may be caused by the relatively small proportion of leaf pixels in the image of small lettuce. The lighter color and loose shape of the leaves also can be factors that influence the performance. In general, the background and leaves were well segmented for lettuce images in different varieties and growth periods, demonstrating the geometric traits extracted from segmented images can accurately describe the morphology of the leaves.

We also analyzed the data distribution of extracted geometric traits of the four lettuce varieties (Figure 6). Both size-related and morphology-related geometric traits showed significant variance in different growth periods. We observed that the canopy size among different varieties had high variance at the maturity period. For example, Aphylion and Salanova had larger canopy sizes than the remaining varieties in weeks 6–7. However, compared with the distribution of fresh weight, Aphylion has a large fresh weight while the fresh weight of Salanova was relatively small. Inconsistencies in canopy size and fresh weight made it difficult for the model to learn comprehensive information for fresh weight estimation at maturity. The correlation between fresh weight and geometric traits of lettuce was analyzed (Table 4). All geometric traits showed significant positive correlations with fresh weight ($P < 0.001$). Such high correlations provide an opportunity for using canopy geometric features to improve fresh weight estimation.

TABLE 4 Correlation coefficients between fresh weight and geometric traits of lettuce.

	FW	PA	PP	ARW	ARH	PCD	CA	CP	PPR	CPR	CAR
FW	1										
PA	0.904***	1									
PP	0.799***	0.945***	1								
ARW	0.856***	0.963***	0.944***	1							
ARH	0.838***	0.955***	0.928***	0.896***	1						
PCD	0.862***	0.980***	0.967***	0.968***	0.962***	1					
CA	0.885***	0.997***	0.959***	0.964***	0.955***	0.985***	1				
CP	0.868***	0.986***	0.965***	0.973***	0.970***	0.994***	0.988***	1			
PPR	0.876***	0.933***	0.817***	0.906***	0.919***	0.908***	0.911***	0.932***	1		
CPR	0.873***	0.985***	0.954***	0.969***	0.971***	0.983***	0.982***	0.996***	0.950***	1	
CAR	0.607***	0.627***	0.500***	0.600***	0.632***	0.575***	0.579***	0.622***	0.807***	0.674***	1

FW, fresh weight. ***Correlation is significant at the 0.001 level.

TABLE 5 Fresh weight estimation result of different models in the test set.

	With data augmentation			Without data augmentation		
	RMSE/g	MAPE (%)	R^2	RMSE/g	MAPE (%)	R^2
RGB + D + G	25.3	17.7	0.938	30.3	21.6	0.910
RGB + G	25.5	18.2	0.936	29.3	23.1	0.916
D + G	31.2	21.2	0.905	35.9	48.2	0.874
RGB + D	29.5	19.6	0.915	36.0	27.8	0.873
RGB only	28.8	17.9	0.919	30.4	39.9	0.910
D only	32.0	25.8	0.900	37.8	44.6	0.861
G only	/	/	/	37.9	34.8	0.860

D, depth; G, geometric features.

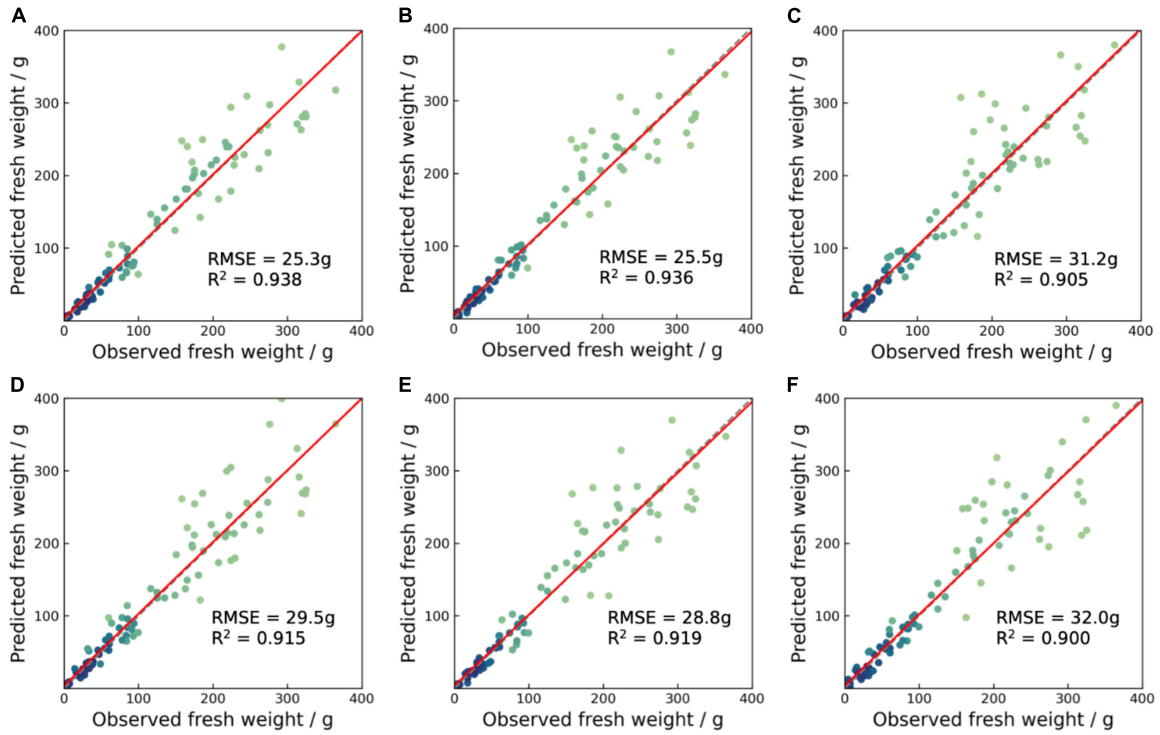

FIGURE 7
Scatter plots between predicted and observed fresh weight for the test set of augmented models **(A)** RGB + D + G, **(B)** RGB + G, **(C)** D + G, **(D)** RGB + D, **(E)** RGB only, and **(F)** D only. The red solid lines represent the fitting lines, and the gray dotted lines represent the 1:1 lines.

Fresh weight estimation results

The multi-branch regression network provided a good fresh weight estimation performance for different lettuce varieties in the entire growth period (Table 5). The triple-branch fusion architectures network with RGB, depth and geometric features exhibited the highest estimation performance with an RMSE of 25.3 g, a MAPE of 17.7%, and an R^2 of 0.938. Compared to the dual-branch fusion networks with RGB and depth images, the RMSE was reduced by 4.2 g (14.2%). This improvement mainly came from the late growth period samples (Figure 7). In addition, the models with geometric features showed higher estimation accuracies than the models without geometric features, with a reduction of RMSE by 0.8–4.2 g. The results indicate that fusing the geometric features with deep neural features can lead to a more accurate fresh weight estimation for the image-based deep learning model. Interestingly, the performance of the RGBG fusion model and RGB model was superior to the RGBD fusion model, which was different from prior knowledge. The main reason was that the inevitable noise of depth images made the learning process of the network difficult. Similar results have been found in the field of object detection (Sun et al., 2022). On the other hand, the results implied that the addition of geometric features could help the fusion of multi-modal features.

We also compared the impact of data augmentation on model performance. All models performed better when data augmentation techniques were applied, with a reduction of RMSE by 1.6–6.5 g. The noticeable improvements demonstrated that data augmentation techniques significantly improved the data generalization and reduced overfitting. We also observed that the models containing depth features were more sensitive to the dataset size. Similar results were found when comparing the performance of models with and without geometric features. The geometric features can improve model performance whether dataset size is limited or sufficient. The model only containing geometric features showed the worst performance among the models, and the performance difference became larger when the model was trained with sufficient data. The deep

TABLE 6 The triple-branch fusion network's performance of each lettuce varieties.

Variety	RMSE	MAPE (%)	R^2
Aphylion	29.9	17.4	0.927
Salanova	30.3	24.2	0.899
Lugano	21.3	14.0	0.964
Satine	16.6	15.3	0.956
All	25.3	17.7	0.938

neural features extracted from images are dominant, however, geometric features still provide complementary information that can help improve the model performance. The reliability of the multi-branch regression network was evaluated. We randomly produced another five different data partitions for training and testing the triple-branch fusion network, with a ratio of 7:3. The triple-branch fusion network showed high performance stability, with a standard deviation of RMSE equals 0.81 g (**Supplementary Table 1**). The results indicated that the proposed method provides reliable performance for lettuce fresh weight estimation.

Model performance across different varieties

We compared the model performance of the triple-branch fusion network of each lettuce variety to analyze the influence of varieties (**Table 6**). The results showed that the varieties with large leaf areas or canopy had poor fresh weight estimation performance. For example, the Satine showed the lowest RMSE of 16.6 g, while Salanova showed the highest RMSE of 30.3 g. As we mentioned in 3.2, Salanova had a large canopy size and a relatively small fresh weight, which affected the estimation performance. The variance in fresh weight distribution and leave color potentially led to inconsistencies in the complexity of model learning in different varieties that affect the model's generalization ability.

The proposed model with a flexible multi-modal fusion framework showed potential for automatic growth monitoring across different crops in the CEA. Although the model showed high estimation accuracy, many possibilities still remain to be further studied to improve the model, such as its robustness and interpretation capability. For example, the model's performance in larger lettuce should be further improved. The light environment in plant factories with artificial lighting could be inconsistent with the AGC dataset. It is worthwhile to further perform our model in practical agricultural applications. Enlarging the dataset with more scenarios and applying transfer learning algorithms will effectively improve the model's robustness. Another limitation is the interpretation capability of the model. Further work could be done to understand and evaluate the contribution of each modality to the performance of the multi-modal fusion model. Adopting model visualization tools such as Grad-CAM (Selvaraju et al., 2017) and SHAPley Additive exPlanations (Lundberg and Lee, 2017) will improve the understanding of the multi-modal fusion model.

Conclusion

This study proposed a multi-modal fusion based deep learning model for automatic estimation of lettuce shoot fresh weight by combining deep neural features and empirical geometric features. The model is composed of a lettuce segmentation network and a multi-branch regression network. A lettuce leaf segmentation network based on U-Net was trained for extracting leaf boundary and geometric traits. A multi-branch regression network was performed to estimate fresh weight by fusing color, depth, and geometric features. The results demonstrated that: (1) the multi-modal fusion showed good fresh weight estimation performance for different lettuce varieties in the entire growth period. (2) The triple-branch fusion regression network outperformed baseline models, suggesting that the combination of deep neural features and geometric features improves fresh weight estimation performance. (3) The empirical geometric features provided complementary information for improving the model learning ability of lettuce fresh weight estimation, especially for the lettuce with a complex canopy. This study highlights that the fusion of multi-modal data and the combination of deep neural and empirical geometric features are promising approaches for fresh weight estimation of lettuce. The flexible fusion framework can be further applied to the growth monitoring of other crops.

Data availability statement

Publicly available datasets were analyzed in this study. This data can be found here: https://data.4tu.nl/articles/dataset/3rd_Autonomous_Greenhouse_Challenge_Online_Challenge_Lettuce_Images/15023088.

Author contributions

ZL, YY, and TL: conception and design of the research. ZL: data preprocessing, model generation and testing, visualization, and writing—original draft. ZL, RZ, and TL: writing—review and editing. ZL, RF, and GR: validation. All authors contributed to manuscript revision, read, and approved the submitted version.

Funding

This research was partially funded by Key R&D Program of Zhejiang Province under Grant Number: 2022C02003.

Acknowledgments

We would like to thank the Wageningen University & Research for providing the lettuce images datasets.

Conflict of interest

The authors declare that the research was conducted in the absence of any commercial or financial relationships that could be construed as a potential conflict of interest.

Publisher's note

All claims expressed in this article are solely those of the authors and do not necessarily represent those of their affiliated organizations, or those of the publisher, the editors and the reviewers. Any product that may be evaluated in this article, or claim that may be made by its manufacturer, is not guaranteed or endorsed by the publisher.

Supplementary material

The Supplementary Material for this article can be found online at: https://www.frontiersin.org/articles/10.3389/fpls.2022.980581/full#supplementary-material

References

Bakker, J. C., Bot, G. P. A., Challa, H., and van de Braak, N. J. (1995). *Greenhouse Climate Control: an Integrated Approach*. Wageningen, NL: Wageningen Academic Publishers.

Buslaev, A., Iglovikov, V. I., Khvedchenya, E., Parinov, A., Druzhinin, M., and Kalinin, A. A. (2020). Albumentations: Fast and Flexible Image Augmentations. *Information* 11:125. doi: 10.3390/info11020125

Buxbaum, N., Lieth, J. H., and Earles, M. (2022). Non-destructive Plant Biomass Monitoring With High Spatio-Temporal Resolution via Proximal RGB-D Imagery and End-to-End Deep Learning. *Front. Plant Sci.* 13:758818. doi: 10.3389/fpls.2022.758818

Chen, W.-T., Yeh, Y.-H. F., Liu, T.-Y., and Lin, T.-T. (2016). An Automated and Continuous Plant Weight Measurement System for Plant Factory. *Front. Plant Sci.* 7:392. doi: 10.3389/fpls.2016.00392

Eitel, A., Springenberg, J. T., Spinello, L., Riedmiller, M., and Burgard, W. (2015). "Multimodal deep learning for robust RGB-D object recognition," in *2015 IEEE/RSJ International Conference on Intelligent Robots and Systems (IROS)*, (Hamburg: IEEE), 681–687. doi: 10.1109/IROS.2015.7353446

Fu, L., Gao, F., Wu, J., Li, R., Karkee, M., and Zhang, Q. (2020). Application of consumer RGB-D cameras for fruit detection and localization in field: A critical review. *Comput. Electr. Agric.* 177:105687. doi: 10.1016/j.compag.2020.105687

Graamans, L., Baeza, E., van den Dobbelsteen, A., Tsafaras, I., and Stanghellini, C. (2018). Plant factories versus greenhouses: Comparison of resource use efficiency. *Agric. Syst.* 160, 31–43. doi: 10.1016/j.agsy.2017.11.003

He, K., Zhang, X., Ren, S., and Sun, J. (2015). Deep Residual Learning for Image Recognition. *arXiv* [Preprint]. doi: 10.48550/arXiv.1512.03385

Hemming, S., de Zwart, H. F., Elings, A., Bijlaard, M., van Marrewijk, B., and Petropoulou, A. (2021). *3rd Autonomous Greenhouse Challenge: Online Challenge Lettuce Images*. 4TU.ResearchData. doi: 10.4121/15023088.v1

Jiang, J., Kim, H.-J., and Cho, W.-J. (2018). On-the-go Image Processing System for Spatial Mapping of Lettuce Fresh Weight in Plant Factory. *IFAC-PapersOnLine* 51, 130–134. doi: 10.1016/j.ifacol.2018.08.075

Jung, D.-H., Park, S. H., Han, X. Z., and Kim, H.-J. (2015). Image Processing Methods for Measurement of Lettuce Fresh Weight. *J. Biosyst. Eng.* 40, 89–93. doi: 10.5307/JBE.2015.40.1.089

Kan, S., Cen, Y., He, Z., Zhang, Z., Zhang, L., and Wang, Y. (2019). Supervised Deep Feature Embedding With Handcrafted Feature. *IEEE Trans. Image Proc.* 28, 5809–5823. doi: 10.1109/TIP.2019.2901407

Kashiha, M., Bahr, C., Ott, S., Moons, C. P. H., Niewold, T. A., Ödberg, F. O., et al. (2014). Automatic weight estimation of individual pigs using image analysis. *Comput. Electr. Agric.* 107, 38–44. doi: 10.1016/j.compag.2014.06.003

Konovalov, D. A., Saleh, A., Efremova, D. B., Domingos, J. A., and Jerry, D. R. (2019). "Automatic Weight Estimation of Harvested Fish from Images," in *2019 Digital Image Computing: Techniques and Applications (DICTA)*, (IEEE), 1–7. doi: 10.1109/DICTA47822.2019.8945971

Kozai, T., Niu, G., and Takagaki, M. (2019). *Plant Factory: An Indoor Vertical Farming System for Efficient Quality Food Production*. Cambridge, MA: Academic press.

LeCun, Y., Bengio, Y., and Hinton, G. (2015). Deep learning. *Nature* 521, 436–444. doi: 10.1038/nature14539

Lee, J. W. (2008). Machine vision monitoring system of lettuce growth in a state-of-the-art greenhouse. *Mod. Phys. Lett. B* 22, 953–958. doi: 10.1142/S0217984908015668

Lin, Z., Wang, S., Fu, R., Ting, K.-C., and Lin, T. (2022). "Data-Driven Modeling for Crop Growth in Plant Factories," in *Sensing, Data Managing, and Control Technologies for Agricultural Systems*, eds S. Ma, T. Lin, E. Mao, Z. Song, and K.-C. Ting (New York, NY: Springer International Publishing), 101–129. doi: 10.1007/978-3-031-03834-1_5

Lundberg, S. M., and Lee, S.-I. (2017). A unified approach to interpreting model predictions. *Adv. Neural Inf. Proc. Syst.* 30, 4765–4774.

Milletari, F., Navab, N., and Ahmadi, S.-A. (2016). "V-Net: Fully Convolutional Neural Networks for Volumetric Medical Image Segmentation," in *2016 Fourth International Conference on 3D Vision (3DV)*, (IEEE), 565–571. doi: 10.1109/3DV.2016.79

Mortensen, A. K., Bender, A., Whelan, B., Barbour, M. M., Sukkarieh, S., Karstoft, H., et al. (2018). Segmentation of lettuce in coloured 3D point clouds for fresh weight estimation. *Comput. Electro. Agric.* 154, 373–381. doi: 10.1016/j.compag.2018.09.010

Nagano, S., Moriyuki, S., Wakamori, K., Mineno, H., and Fukuda, H. (2019). Leaf-Movement-Based Growth Prediction Model Using Optical Flow Analysis and Machine Learning in Plant Factory. *Front. Plant Sci.* 10:227. doi: 10.3389/fpls.2019.00227

Nanni, L., Ghidoni, S., and Brahnam, S. (2017). Handcrafted vs. non-handcrafted features for computer vision classification. *Pattern Recognit.* 71, 158–172. doi: 10.1016/j.patcog.2017.05.025

Quan, L., Li, H., Li, H., Jiang, W., Lou, Z., and Chen, L. (2021). Two-Stream Dense Feature Fusion Network Based on RGB-D Data for the Real-Time Prediction of Weed Aboveground Fresh Weight in a Field Environment. *Remote Sensing* 13:2288. doi: 10.3390/rs13122288

Ramachandram, D., and Taylor, G. W. (2017). Deep Multimodal Learning: A Survey on Recent Advances and Trends. *IEEE Signal Proc. Magazine* 34, 96–108. doi: 10.1109/MSP.2017.2738401

Reyes-Yanes, A., Martinez, P., and Ahmad, R. (2020). Real-time growth rate and fresh weight estimation for little gem romaine lettuce in aquaponic grow beds. *Comput. Electr. Agric.* 179:105827. doi: 10.1016/j.compag.2020.105827

Ronneberger, O., Fischer, P., and Brox, T. (2015). U-Net: Convolutional Networks for Biomedical Image Segmentation. *arXiv*. 1505.04597 [cs].

Sekachev, B., Manovich, N., Zhiltsov, M., Zhavoronkov, A., Kalinin, D., Hoff, B., et al. (2020). *opencv/cvat: v1.1.0*. doi: 10.5281/zenodo.4009388

Selvaraju, R. R., Cogswell, M., Das, A., Vedantam, R., Parikh, D., and Batra, D. (2017). "Grad-cam: Visual explanations from deep networks via gradient-based localization," in *Proceedings of the IEEE International Conference on Computer Vision*, (Manhattan, NY: IEEE), 618–626.

Shamshiri, R. R., Kalantari, F., Ting, K. C., Thorp, K. R., Hameed, I. A., Weltzien, C., et al. (2018). Advances in greenhouse automation and controlled environment agriculture: A transition to plant factories and urban agriculture. *Int. J. Agric. Biol. Eng.* 11, 1–22. doi: 10.25165/j.ijabe.20181101.3210

Song, S., Lichtenberg, S. P., and Xiao, J. (2015). "Sun rgb-d: A rgb-d scene understanding benchmark suite," in *Proceedings of the IEEE Conference*

on Computer Vision and Pattern Recognition, (Manhattan, NY: IEEE), 567–576.

Sun, Q., Chai, X., Zeng, Z., Zhou, G., and Sun, T. (2022). Noise-tolerant RGB-D feature fusion network for outdoor fruit detection. *Comput. Electr. Agric.* 198:107034. doi: 10.1016/j.compag.2022.107034

von Rueden, L., Mayer, S., Beckh, K., Georgiev, B., Giesselbach, S., Heese, R., et al. (2021). Informed Machine Learning - A Taxonomy and Survey of Integrating Prior Knowledge into Learning Systems. *IEEE Trans. Knowl. Data Eng.* doi: 10.1109/TKDE.2021.3079836

Yeh, Y.-H. F., Lai, T.-C., Liu, T.-Y., Liu, C.-C., Chung, W.-C., and Lin, T.-T. (2014). An automated growth measurement system for leafy vegetables. *Biosyst. Eng.* 117, 43–50. doi: 10.1016/j.biosystemseng.2013.08.011

Zeng, J., Tong, Y., Huang, Y., Yan, Q., Sun, W., Chen, J., et al. (2019). "Deep Surface Normal Estimation With Hierarchical RGB-D Fusion," in *2019 IEEE/CVF Conference on Computer Vision and Pattern Recognition (CVPR)*, (Long Beach, CA: IEEE), 6146–6155. doi: 10.1109/CVPR.2019.00631

Zhang, L., Xu, Z., Xu, D., Ma, J., Chen, Y., and Fu, Z. (2020). Growth monitoring of greenhouse lettuce based on a convolutional neural network. *Hortic. Res.* 7:124. doi: 10.1038/s41438-020-00345-6

frontiers | Frontiers in Plant Science

TYPE Original Research
PUBLISHED 02 September 2022
DOI 10.3389/fpls.2022.978468

OPEN ACCESS

EDITED BY
Yuxin Tong,
Institute of Environment and Sustainable Development in Agriculture (CAAS), China

REVIEWED BY
Naser Karimi,
Razi University, Iran
Qingming Li,
Institute of Urban Agriculture (CAAS), China

*CORRESPONDENCE
Xuzhang Xue
xuexz@nercita.org.cn

†These authors have contributed equally to this work

SPECIALTY SECTION
This article was submitted to Technical Advances in Plant Science, a section of the journal Frontiers in Plant Science

RECEIVED 26 June 2022
ACCEPTED 17 August 2022
PUBLISHED 02 September 2022

CITATION
Li J, Guo X, Zhang S, Zhang Y, Chen L, Zheng W and Xue X (2022) Effects of light quality on growth, nutritional characteristics, and antioxidant properties of winter wheat seedlings (*Triticum aestivum* L.). *Front. Plant Sci.* 13:978468. doi: 10.3389/fpls.2022.978468

Effects of light quality on growth, nutritional characteristics, and antioxidant properties of winter wheat seedlings (*Triticum aestivum* L.)

Junyan Li[1,2†], Xiaolei Guo[1,2†], Siqi Zhang[1,2], Yinghua Zhang[2], Liping Chen[1], Wengang Zheng[1] and Xuzhang Xue[1*]

[1]National Research Center of Intelligent Equipment for Agriculture, Beijing, China, [2]College of Agronomy and Biotechnology, China Agricultural University, Beijing, China

Wheat seedlings are becoming popular for its high nutritional value. Effects of White (W), White + Red (WR), and White + Blue (WB) light-emitting diodes (LEDs) treatments on growth, nutritional characteristics and antioxidant properties of wheat seedlings were studied in a plant factory. The results showed that height, leaf area, shoot fresh, and shoot dry weight per wheat seedling were the highest under WR at 13 and 22 days after planting. Soluble sugar content in leaves and stems were 22.3 and 65% respectively higher under WB than those under W. Soluble protein content in leaves and stems were 36.8 and 15.2% respectively lower under WR than those under W. Contents of total flavonoids, glutathione (GSH) and ascorbic acid (ASA) in leaves were the highest under WB, whereas malondialdehyde (MDA) content in leaves was the lowest under WB. The activities of antioxidant enzymes [superoxide dismutase (SOD), peroxidase (POD), and ascorbate peroxidase (APX)] in leaves and 2,2-diphenyl-1-picrylhydrazyl (DPPH) radical scavenging ability were also the highest under WB. In conclusion, WR promoted the growth of wheat seedlings, and WB promoted antioxidant level and nutritional accumulation. This study provides guidance for wheat seedlings to carry out preferential production (biomass or quality).

KEYWORDS

wheat seedling, light quality, growth, nutritional characteristics, antioxidant property

Introduction

Wheat (*Triticum aestivum* L.) is the most widely cultivated crop in the world, providing carbohydrates and proteins for human beings (Nazim Ud Dowla et al., 2018; Hu et al., 2021). Except for the grains, the seedlings of wheat, also named wheatgrass have been proved to be rich in flavonoids and polyphenols, which have the capability of

scavenging reactive oxygen species (ROS) and are beneficial to human health (Durairaj et al., 2014; Bar-Sela et al., 2015; Jaiswal et al., 2018). Besides, wheat seedlings also contain proteins, sugars, triterpenes, and various antioxidant enzymes (Gawlik-Dziki et al., 2016; Ghumman et al., 2017; Kaur et al., 2021; Virdi et al., 2021). Adding wheat seedling juice to milk or meat can improve the nutritional value of the food (Devi et al., 2019). Wheat seedlings products are becoming widely used supplemental health foods (Kulkarni et al., 2006; Tsai et al., 2013; Choi et al., 2021).

Light is one of the most important variables affecting plant growth and development (Jiao et al., 2007; de Wit et al., 2016; Yadav et al., 2021). It not only provides energy source for photosynthesis, but also regulates seed germination, root architecture, shoot elongation, leaf expansion, circadian rhythms, phototropism, shade avoidance, flowering, chloroplast movement, and accumulation of phytochemical compounds such as phenolics (Bantis et al., 2018; Yadav et al., 2020). Modern agriculture has evolved towards the application of advanced technologies for plant cultivation in a controlled environment, exemplified with plant factories, in which light source is the most critical environment factor (Paradiso and Proietti, 2022). Light-emitting diodes (LEDs) are ideal light sources in plant factories, due to their advantages of small size, long service life, low energy consumption, low heat generation, and customized wavelengths compared with other artificial light sources (Lin et al., 2013; Bian et al., 2015; Ouzounis et al., 2015; Paradiso and Proietti, 2022). A white LED consists of a LED chip, which emits blue light with a narrow spectrum between 440 and 470 nm, and a coating of yellow phosphors. The light emitted by the phosphor, in combination with the remaining blue light leaking through the phosphor layer, result in a light which is perceived as white by the human eye (Gayral, 2017). White LEDs have been proven to maintain growth and development of plants (Singh et al., 2015; Guo et al., 2022a). However, the spectra of white LEDs are concentrated in the bluish visible light and other light qualities need to be added to meet the light needs of different plants at different growth stages (Cao et al., 2021).

Red and blue light account for the largest proportion of the total light received by plants (Nishio, 2000; Terashima et al., 2009). Proper combination of red and blue light can promote growth of *Oncidium*, perilla, lettuce, tomato, pepper, and *Lycoris longituba* (Liu et al., 2011; Goto et al., 2014; Zhang et al., 2018; Kaiser et al., 2019; Naznin et al., 2019; Li et al., 2022). Azad et al. (2020) demonstrated that red light promotes accumulation of carbohydrates in lettuce, while increasing blue light caused a decrease in fresh and dry weight in lettuce shoots (Son and Oh, 2013). It is worth noting that blue light has positive role in synthesis and accumulation of flavonoids and polyphenols (Lin et al., 2013; Zheng et al., 2019; Gao et al., 2021; Jung et al., 2021). In the study about *Salvia plebeian*, it has been found that the total phenolic and flavonoid contents were higher under red light supplemented with blue light (such as B:R = 3:7, B:R = 5:5, and B:R = 7:3) than in the monochromatic red light (Lee et al., 2020). Red and blue light induce changes of antioxidants level, including superoxide dismutase (SOD), peroxidase (POD), catalase (CAT), and ascorbate peroxidase (APX), ascorbic acid (ASA), and glutathione (GSH) (Mittler et al., 2004; You and Chan, 2015). Santos-Tierno et al. (2021) reported that red LEDs was effective in facilitating SOD and CAT activities in *Passiflora setacea*, while SOD and POD activities in ramie under red light were lower than those under white light (Rehman et al., 2020). According to Causin et al. (2006), blue light enhanced CAT activity in wheat compared with white light. Red and blue light lead to diverse morphological and physiological responses of plants, and these responses are species-specific. However, there are few studies on the roles of red and blue light in wheat seedlings, which is worth exploring.

In this experiment, three different LEDs light treatments (White, White + Red, and White + Blue) were designed to investigate the effects of red and blue light on the growth, nutritional quality and antioxidant capacity of wheat seedlings in a hydroponic system with the same light intensity and photoperiod in a plant factory. The results will provide some basic information for optimizing the spectral combinations of LEDs in production of wheat seedlings.

Materials and methods

Light treatments

Three spectral combinations, white LEDs (W, B:G:R = 34:46:20, **Figures 1A-a**), white plus red LEDs (WR, B:G:R = 19:25:56, **Figures 1A-b**), and white plus blue LEDs (WB, B:G:R = 70:21:9, **Figures 1A-c**) were applied and wheat seedlings were planted in a plant factory for 43 days. The spectral characteristics of different light treatments were measured with a portable spectroradiometer (Plant Lighting Analyzer, V 2.00, China), and showed in **Figure 1**. Light intensity was kept constant at 450 ± 20 μmol m^{-2} s^{-1} throughout the experiment by moving up the light sources above the plants every week, where the photosynthetic photon flux density (PPFD) was measured with a photo/radiometer (Plant Lighting Analyzer, V 2.00, China). Lighting time per day was set to 12 h (12/12 h light/dark).

Cultivation conditions

Winter wheat seeds (*T. aestivum* L., cv. 'JiMai22') were sterilized by 5% hydrogen peroxide (H_2O_2) for 30 min, then washed adequately 4 times in distilled water, and soaked in distilled water for 12 h. The seeds were imbibed in the dark on moistened germination paper at 25°C until plumule exposed 1 cm, and then vernalized for 15 days at 4°C. Before planting,

A

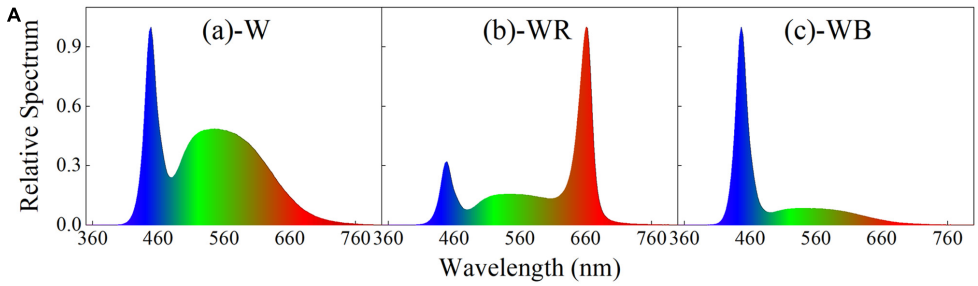

B Characteristics of different light treatments

Light treatments	PPFD (400-700nm) (μmol m^{-2} s^{-1})	Blue (%)	Green (%)	Red (%)
W	430.4	34.2	45.9	19.9
WR	463.6	18.8	25.3	55.8
WB	456.7	70.0	21.0	9.0

FIGURE 1
Spectral distribution **(A)** and characteristics **(B)** of different light treatments. **(A-a)** White light emitting diodes (LEDs) (W); **(A-b)** white plus red LEDs (WR); **(A-c)**, white plus blue LEDs (WB). Photosynthetic photon flux density (PPFD) for each light treatment was equal to 450 ± 20 μmol m^2 s^{-1}.

germinated seeds grew for 3 days under white LEDs light (spectrum same as white LEDs, Figures 1A-a) for uniform growth (PPFD = 100 μmol m^{-2} s^{-1}). The germinated seeds were planted into sponge cubes (2.0 cm × 2.0 cm × 2.0 cm) and hydroponically grown in a plant factory. Eighty-one plants spaced 8 cm apart were planted in a hydroponic box (80 cm × 80 cm × 10 cm). Each hydroponic box was used for one light treatment, and three hydroponic boxes as biological replicates in each light environment. During the experiment, wheat was grown for 43 days and randomly rotated every 5 days. A half-strength Hoagland's solution was used, the pH of which was kept between 5.5 and 6.5, and renewed weekly (Hoagland and Arnon, 1950). Temperature during the experiment was maintained at 22 ± 1°C, and relative humidity was controlled at 65 ± 5%.

Growth characteristics

Eight seedlings were taken from each treatment to measure plant height, leaf area and shoot dry weight at 13, 22, 31, and 40 days after planting (DAP). Plant height, length and width of all leaves of the samples were measured by a ruler, and the leaf area was calculated according to the coefficient method (Leaf area = Length × Width × 0.76) (Li et al., 2018; Guo et al., 2022b). Shoot fresh weight of the entire plant was determined by an electronic precision balance (CP224C, OHAUS, United States). After oven-dried at 105°C for 30 min, the samples were kept at 80°C for 72 h, and shoot dry weight was then measured by the electronic precision balance.

Sampling

Fresh samples of 30 wheat seedlings (10 plants from the same hydroponic box as a biological repeat) were collected from each treatment at 43 DAP, and immediately frozen in liquid nitrogen, and then stored in a laboratory refrigerator at −80°C. The chemical used in the experiment were all supplied by Sigma-Aldrich (United States).

Determination of soluble sugar and protein contents

Soluble sugar content was determined as described by Hanft and Jones (1986). Fresh sample (0.1 g) was ground in liquid nitrogen. After adding 3 ml deionized water, the grounded sample was heated in a boiling water bath for 20 min, centrifuged at 4,500 *g* for 10 min, and the supernatant was taken. A total of 3 ml deionized water was added to the residue, extracted twice repeatedly. After combining the resulting supernatants, deionized water was added to adjust the volume to 10 ml. Extract solution (1 ml) was mixed with 4 ml anthrone solution (2 g L^{-1}), and then soaked in a water bath at 45°C for 12 min. After cooling in the dark, the absorbance of the mixture was detected at 625 nm by a microplate reader (Multiskan FC, Thermo Scientific™, United States), and soluble sugar content was calculated using a sucrose standard curve with concentrations ranging from 0 to 2 mg ml^{-1} (R^2 = 0.9997).

Soluble protein content was measured by the Coomassie brilliant blue colorimetry method (Bradford, 1976). A total of 0.1 g fresh sample was homogenized in 2 ml distilled water. The mixture was centrifuged at 3,000 *g* for 10 min, and 1 ml supernatant was mixed with 5 ml Coomassie brilliant blue G-250 solution (0.1 g L^{-1}). After 2 min, the absorbance of the mixture was detected at 595 nm by the microplate reader, and soluble protein content was calculated from standard curves ($R^2 = 0.9968$).

Determinations of malondialdehyde, glutathione, and ascorbic acid contents

Fresh sample (0.2 g) was ground into homogenate with 5 ml trichloroacetic acid solution (TBA, 5%, w/v), and centrifuged at 15,000 *g* for 15 min. The supernatant was used for measurement of malondialdehyde (MDA) and GSH contents.

The method described by Hameed et al. (2021) was used to quantify MDA content, with slight modification. 1 ml supernatant was mixed with 1 ml TBA solution (0.67%, w/v), incubated in boiling water for 30 min and then quickly cooled in an ice-bath. The mixture was centrifuged and the absorbance was detected at 450, 532, and 600 nm. MDA content was determined using the following equation:

$$\text{MDA}\ (\mu\text{mol}\ g^{-1}\ \text{FW}) = \frac{(6.45 \times (\text{OD532} - \text{OD600}) - 0.56 \times \text{OD450}) \times \text{V}}{1000 \times \text{W}} \quad (1)$$

where V is the total volume of supernatant and W is the fresh weight of the sample.

Glutathione content was measured according to the method by Qiu et al. (2014) with slight modification. A total of 2 ml supernatant was added to 4 ml phosphate buffer (200 mM, pH 7.0) and 0.4 ml 5, 5-dithiobis (2-nitrobenzoic) solution (0.396 mg ml^{-1}, pH 7.0). After 5 min at 30°C, the absorbance was determined at 412 nm by the microplate reader and GSH content was calculated based on the GSH standard curve with concentrations ranging from 0 to 80 μg ml^{-1} ($R^2 = 0.9976$).

Ascorbic acid content was determined according to the method by He et al. (2020). Fresh sample (0.1 g) was extracted with 1 ml oxalic acid EDTA solution (1%, w/v), and centrifuged at 4,000 *g* for 10 min. 0.2 ml supernatant was mixed with 0.8 ml oxalic acid EDTA solution (1%, w/v), 0.1 ml phosphate-acetic acid solution (3%, w/v), 0.2 ml vitriol (5%, v/v), and 0.4 ml ammonium molybdate solution (5%, w/v). After 15 min, the absorbance of mixture solution was measured at 705 nm by the microplate reader, and ASA content was calculated based on the standard curve with concentration ranging from 0 to 1 mg ml^{-1} ($R^2 = 0.9977$).

Determination of total flavonoids, triterpenes, and polyphenols contents

Fresh sample (1.0 g) was ground in liquid nitrogen, and extracted with 25 ml methanol solution (80%, v/v) ultrasonically for 20 min, and centrifuged to obtain supernatant. The above process was repeated three times, and all supernatants were pooled and volume was adjusted to 100 ml with methanol solution (80%, v/v). The methanol extract was stored at −20°C for determination of the contents of flavonoids, triterpenes, and polyphenols, and the free radical scavenging abilities of 2,2′-azino-bis (3-ethylbenzthiazoline-6-sulfonic acid) (ABTS) and 2,2-diphenyl-1-picrylhydrazyl (DPPH).

The total flavonoids content was measured using the method described by Guo et al. (2013). A total of 2 ml extract, 0.2 ml $NaNO_2$ solution (5%, w/v), 0.2 ml $Al(NO_3)_3$ solution (10%, w/v), and 2 ml NaOH solution (1 M) were mixed adequately. The absorbance of the mixture was measured at 510 nm by the microplate reader after standing for 15 min. Total flavonoids content was expressed as milligram rutin equivalent $gram^{-1}$ in fresh weight (mg RE g^{-1} FW) through the calibration curve of rutin with the concentration ranging from 0 to 20 μg ml^{-1} ($R^2 = 0.9974$).

The total triterpenes content was measured by the method of Jiang et al. (2021). A total of 100 μl extract were mixed with 100 μl vanillin-acetic acid solution (2.5%, w/v) and 200 μl perchloric acid solution. After incubation at 60°C for 15 min, 650 μl glacial acetic acid was added and adequately mixed. The absorbance of mixture was detected at 550 nm by the microplate reader after standing for 10 min. The total triterpenes content was expressed as milligram ursolic acid equivalent $gram^{-1}$ in fresh weight (mg UAE g^{-1} FW) and calculated from the standard curve (concentration ranging from 20 to 120 μg ml^{-1}, $R^2 = 0.9918$).

The total polyphenols content was measured using the method described by Sarker and Oba (2020). A total of 100 μl extract was mixed with the Folin–Ciocalteu reagent (2 N, 50 μl). A total of 400 μl Na_2CO_3 solution (1 M) and 1 ml deionized water were added after 5 min. The mixture was incubated at 37°C for 90 min and the absorbance was measured at 740 nm by the microplate reader. The content of the total polyphenols was expressed as gallic acid equivalent standard of fresh weight (mg GAE g^{-1} FW) through the calibration curve of gallic acid with concentration ranging from 0 to 50 μg ml^{-1} ($R^2 = 0.9983$).

Determination of antioxidant activities

ABTS radical scavenging ability was measured using the method by Jiang et al. (2021). Equal volume of 7.4 mM ABTS solution and 2.6 mM $K_2S_2O_8$ solution were mixed at room temperature in the dark for 20 h to generate ABTS+

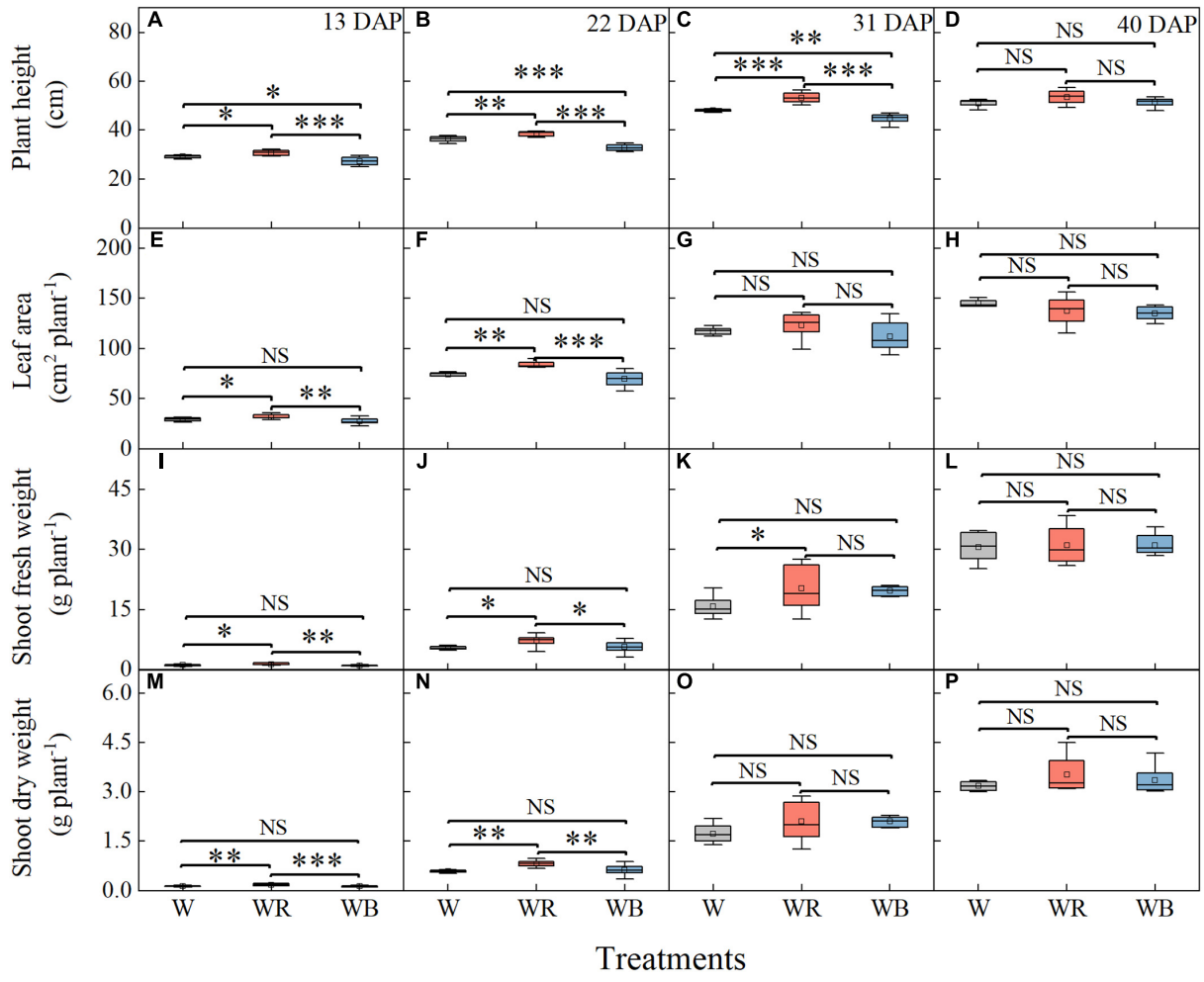

FIGURE 2
Plant height **(A–D)**, leaf area **(E–H)**, shoot fresh weight **(I–L)**, and shoot dry weight **(M–P)** of wheat seedlings under different treatments at 13, 22, 31, and 40 days after planting (DAP). Values represent the mean ± SE (n = 8). The symbols *, **, and *** indicate significance at the 0.05, 0.01, and 0.001 levels, respectively. NS, not significant, according to the Duncan's test.

stock solution. A total of 5 mM PBS solution (pH 7.4) was used to dilute ABTS+ stock solution to absorbance of 0.75 at 734 nm to prepare working solution. A total of 200 μl of working solution was mixed with 40 μl extract. After incubation in the dark for 6 min, the absorbance was read at 734 nm by the microplate reader. The ABTS radical scavenging ability was calculated from the Trolox calibration curve (concentration ranging from 0 to 0.05 mg ml^{-1}, R^2 = 0.999) and expressed as Trolox equivalent standard of fresh weight (mg TE g^{-1} FW).

2,2-Diphenyl-1-picrylhydrazyl radical scavenging ability was also measured using the method by Jiang et al. (2021) with small adjustment. A total of 200 μl DPPH solution (0.15 mM) was blended with 100 μl extract in a 96-well-plate. After incubation at 37°C for 30 min, the absorbance was read at 517 nm by the microplate reader. The result was expressed as ASA equivalent per gram of fresh weight (mg AE g^{-1} FW) based on the standard curve (concentration ranging from 0.005 to 0.4 mM, R^2 = 0.9976).

Antioxidant enzymes activities

Fresh sample (0.5 g) was ground in liquid nitrogen, and extracted into a homogenate with 3 ml of ice-cold extraction buffer, which contained phosphate buffer (50 mM, pH 7.8) and EDTA (1 mM). The homogenate was centrifuged at 15,000 g for 15 min at 4°C, and the supernatant was used to measure the activities of SOD, POD, CAT, and APX.

Superoxide dismutase activity was measured based on the method proposed by Giannopolitis and Ries (1977), with slight modifications. A total of 3 ml reaction mixture was composed of 0.1 ml supernatant, phosphate buffer (50 mM, pH 7.8), EDTA (0.1 mM), methionine (130 mM), nitroblue tetrazolium

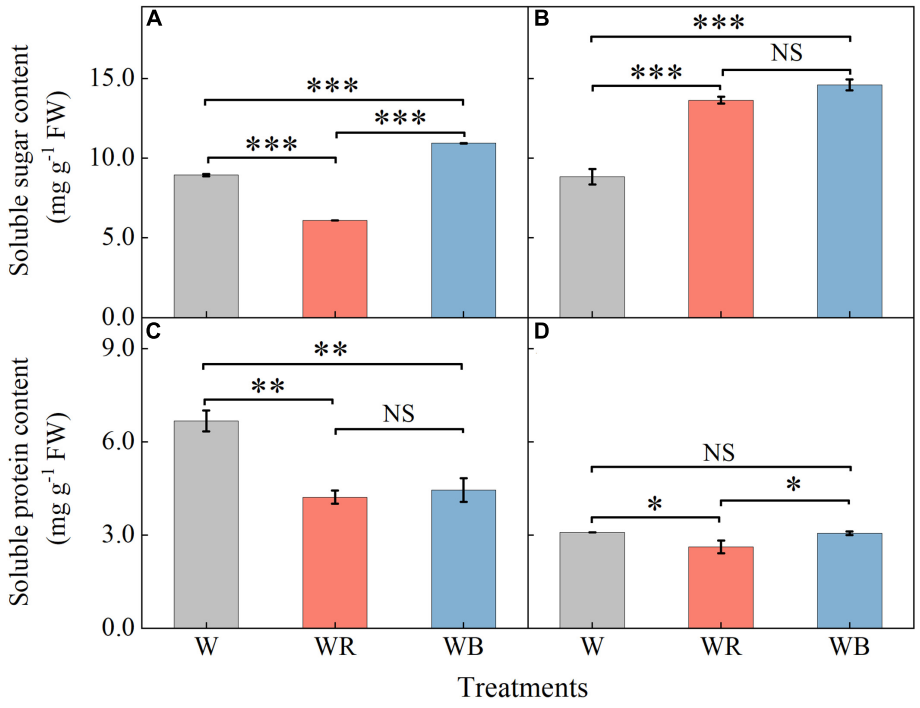

FIGURE 3
The contents of soluble sugar and soluble protein in extracts of wheat seedlings leaves **(A,C)** and stems **(B,D)** under different treatments. Values represent the mean ± SE (n = 3). The symbols *, ** and *** indicate significance at the 0.05, 0.01, and 0.001 levels, respectively. NS, not significant, according to the Duncan's test.

(NBT, 0.4 mM), and riboflavin (0.02 mM). The reaction was started by placing the reaction tube under two 40 W fluorescent lamps and stopped after 20 min by removing the reaction tube from the light source. Light reactions with no light and no supernatant were used as calibration standards. The absorbance of the reaction mixture was read at 560 nm. One unit of SOD activity (U) was defined as the amount of enzyme required to produce 50% inhibition of NBT reduction.

Peroxidase activity was measured based on the method of Qiu et al. (2011) with slight changes. Added 0.1 ml supernatant to a mixture consisting of phosphate buffer (50 mM, pH 7.0), guaiacol (0.05%, w/v), EDTA (0.1 mM), and H_2O_2 (2%, v/v). By tracking the increase in absorbance at 470 nm over 5 min and quantified by the amount of tetraguaiacol formed using its molar extinction coefficient (26.6 mM^{-1} cm^{-1}). One unit of POD activity (U) was defined as a decrease in absorbance value of 0.01 per minute.

Catalase activity was measured with the method of Cakmak and Marschner (1992). A total of 0.1 ml supernatant was added to a mixture of phosphate buffer (100 mM, pH 7.0), EDTA (0.1 μM), and H_2O_2 (0.1%, v/v). The reaction was measured by tracking the decrease in absorbance at 240 nm for 3 min and quantified by its molar extinction coefficient (39.4 mM^{-1} cm^{-1}). One unit of CAT activity (U) was defined as a decrease in absorbance value of 0.01 per minute.

Ascorbate peroxidase activity was measured with the method of Nakano and Asada (1981). A total of 3 ml reaction solution consisted of 0.1 ml supernatant, phosphate buffer (50 mM, pH 7.8), EDTA (0.1 mM), ascorbate (0.5 mM), and H_2O_2 (0.1 mM). The resulting mixture was quantified by tracking the increase in absorbance at 290 nm for 1 min and by its molar extinction coefficient (2.8 mM^{-1} cm^{-1}). One unit of APX activity (U) was defined as an increase in absorbance value of 0.01 per minute.

Statistical analysis

The data were subjected to one-way ANOVA using SPSS statistical software (PASW statistical version 26.0, SPSS Inc., Chicago, IL, United States). Duncan's new multiple range test was applied to identify differences between means at the $^{*}P < 0.05$, $^{**}P < 0.01$, and $^{***}P < 0.001$ level. Correlations between growth, quality characteristics, antioxidant properties of wheat seedlings and light environments were uncovered through Pearson correlation analysis based on the percentage composition of light quality in the treatments (**Figure 1B**). All figures were created using OriginPro 2022 (OriginLab Corp., United States) or Adobe Illustrator CC 242 2019 (Adobe Inc., United States).

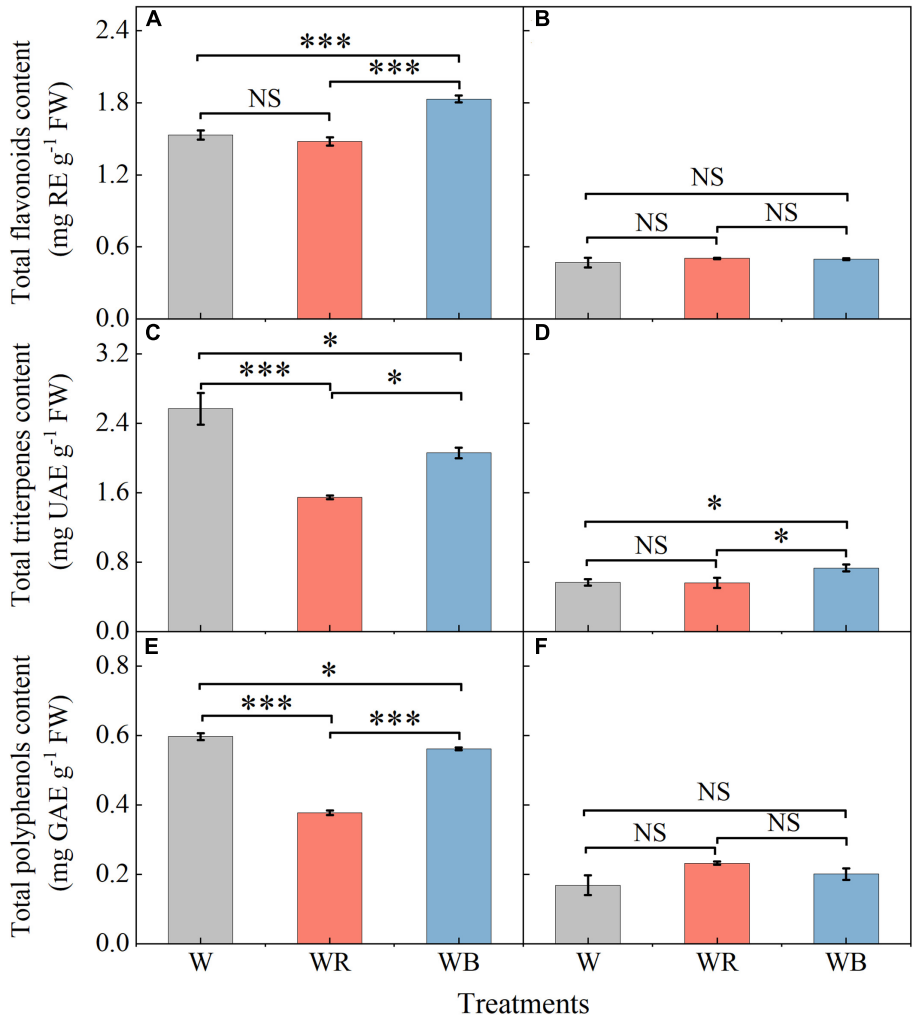

FIGURE 4
The contents of total flavonoids, triterpenes and polyphenols in extracts of wheat seedlings leaves **(A,C,E)** and stems **(B,D,F)** under different treatments. Values represent the mean ± SE (n = 3). The symbols * and *** indicate significance at the 0.05 and 0.001 levels, respectively. NS, not significant, according to the Duncan's test.

Results

Growth characteristics

As showed in Figure 2, growth of wheat seedlings was significantly influenced by light qualities. The highest plant height of wheat seedlings was observed under WR and lowest was observed under WB at 13, 22, and 31 DAP (Figures 2A–C). Leaf area, shoot fresh and dry weight per wheat seedling was highest under WR at 13 and 22 DAP (Figures 2E,F,I,J,M,N). Shoot fresh weight was higher under WR than that under W at 31 DAP (Figure 2K). Difference in plant height and shoot fresh weight among the three light treatments disappeared at 40 DAP (Figures 2D,L), and difference in leaf area and shoot dry weight disappeared at 31 and 40 DAP (Figures 2G,H,O,P).

Soluble sugar and soluble protein

The contents of soluble sugar and soluble protein in wheat seedling leaves and stems were shown in Figure 3. Soluble sugar contents under WB increased 22.3% in leaves and 65.0% in stems compared with those under W (Figures 3A,B). Soluble protein content under WB decreased 33.5% in leaves than that under W (Figure 3C). Soluble sugar contents under WR increased 54.1% in stems (Figure 3B), and decreased 31.8%

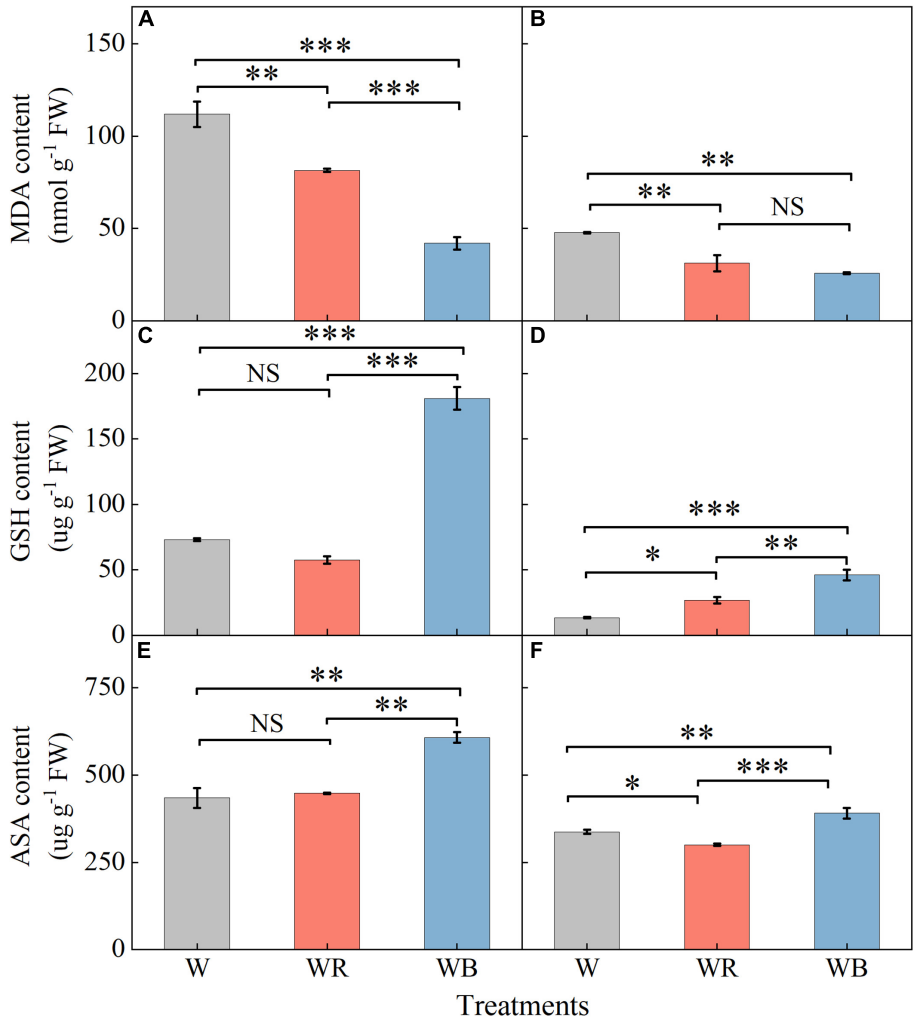

FIGURE 5
The contents of malondialdehyde, glutathione and ascorbic acid in extracts of wheat seedlings leaves **(A,C,E)** and stems **(B,D,F)** under different treatments. Values represent the mean ± SE (n = 3). The symbols *, ** and *** indicate significance at the 0.05, 0.01, and 0.001 levels, respectively. NS, not significant, according to the Duncan's test.

in leaves compared than those under W (Figure 3A). Soluble protein contents were 36.8% lower in leaves and 15.2% lower in stems than those under W (Figures 3C,D).

Total flavonoids, triterpenes, and polyphenols

The contents of total flavonoids, triterpenes and polyphenols in leaves and stems of wheat seedlings grown under different LEDs treatments were provided in Figure 4. Compared with W, WB enhanced total flavonoids content in leaves by 19.3% (Figure 4A), and total triterpenes content in stems by 29.4% (Figure 4D). Compared with W, WR, and WB resulted in a significant decrease in total triterpenes and polyphenols content in leaves (Figures 4C,E). There was no significant difference in the contents of total flavonoids and polyphenols in stems among all treatments (Figures 4B,F).

Lipid peroxidation and antioxidants

Contents of MDA, GSH, and ASA in leaves were higher than those in stems (Figure 5). MDA contents of leaves and stems under WB and WR were significantly lower than those under W (Figures 5A,B). Contents of GSH and ASA in leaves and stems were the highest under WB (Figures 5C–F). GSH content in stems increased 98.6% under WR than that under W (Figure 5D). ASA content in stems decreased 11.0% under WR than that under W (Figure 5F). Contents of GSH and ASA in leaves under WR and W were not significantly different (Figures 5C,E).

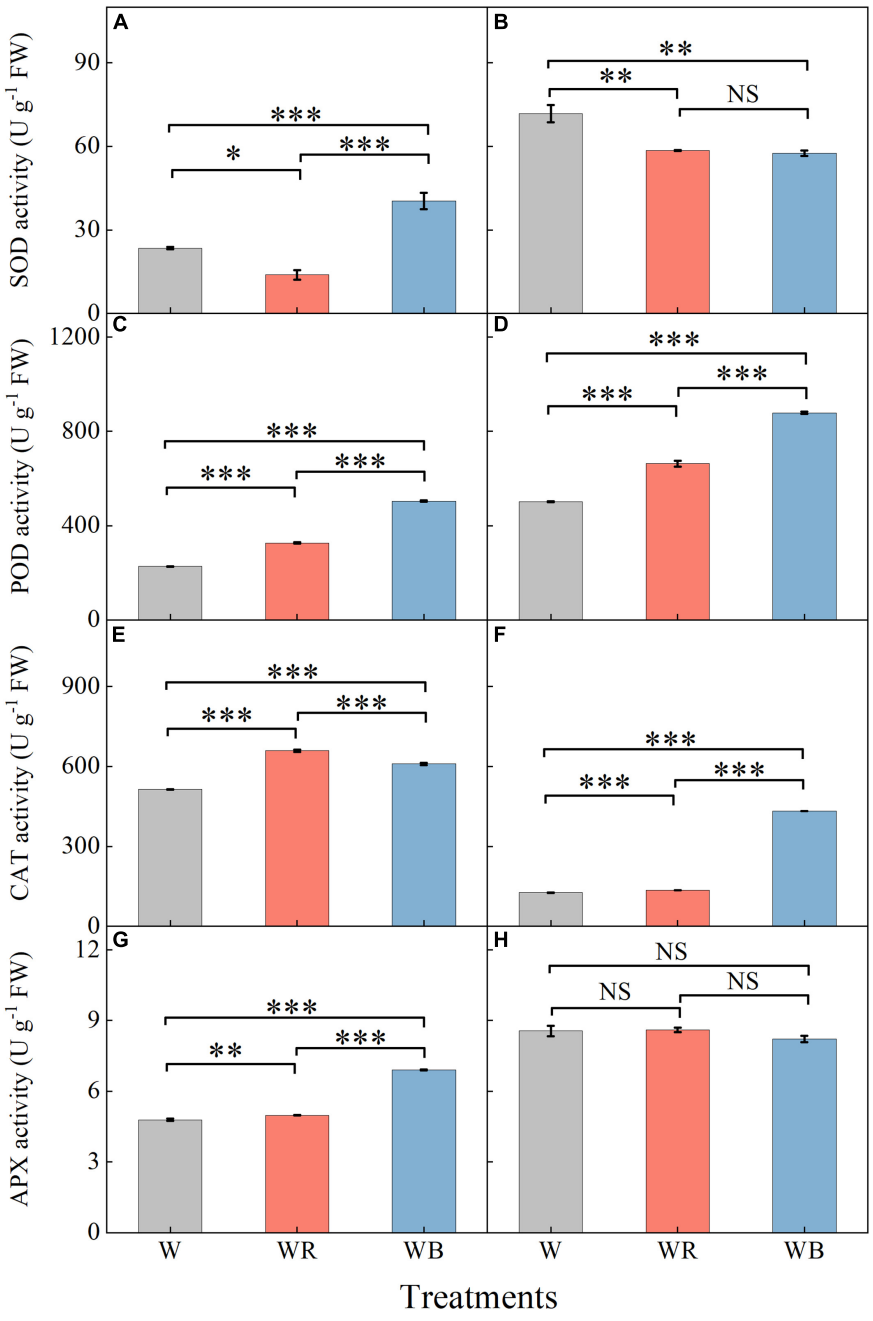

FIGURE 6
The activities of SOD, POD, CAT, and APX in extracts of wheat seedlings leaves **(A,C,E,G)** and stems **(B,D,F,H)** under different treatments. Values represent the mean ± SE (n = 3). The symbols *, ** and *** indicate significance at the 0.05, 0.01, and 0.001 levels, respectively. NS, not significant, according to the Duncan's test.

Antioxidant enzymes

The activities of antioxidant enzymes in leaves and stems were affected by light qualities (Figure 6). Compared with W, WB increased SOD activity of leaves by 72.1% (Figure 6A), and decreased SOD activity of stems by 19.8% (Figure 6B). SOD activity under WR decreased 40.9% in leaves and 18.3% in stems compared with those under W (Figures 6A,B). POD and CAT activities in leaves and stems under WR and WB were significantly higher than those under W (Figures 6C–F). APX activities in leaves under WR and WB were higher than that under W (Figure 6G). No significant difference in stem APX activity was observed among the three treatments (Figure 6H).

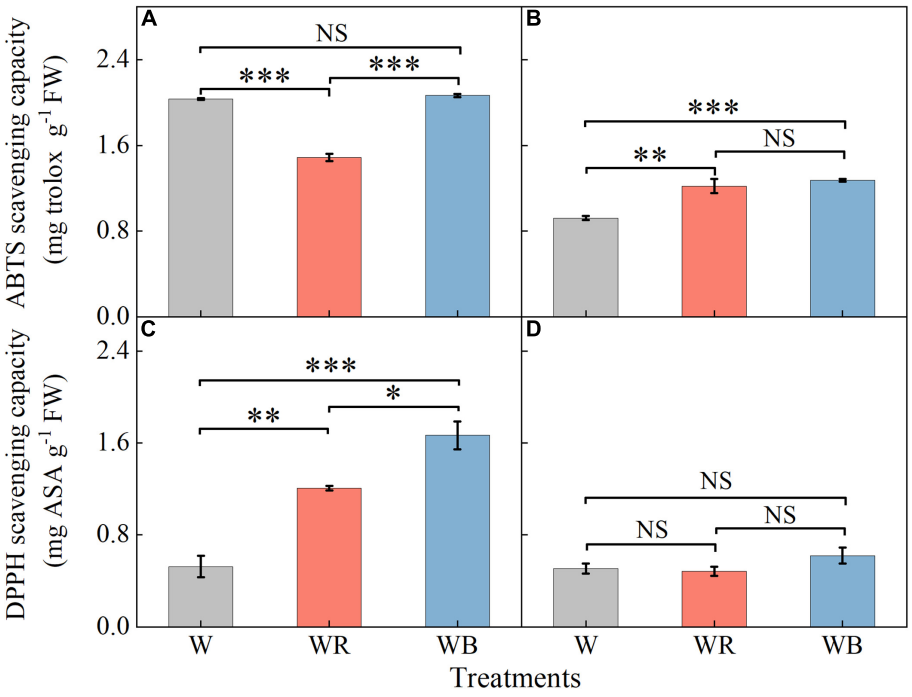

FIGURE 7
The values of ABTS and DPPH scavenging capacity in extracts of wheat seedlings leaves **(A,C)** and stems **(B,D)** under different treatments. Values represent the mean ± SE (n = 3). The symbols *, ** and *** indicate significance at the 0.05, 0.01, and 0.001 levels, respectively. NS, not significant, according to the Duncan's test.

Antioxidant capacity

The ABTS and DPPH radical scavenging capacities in leaves were higher than those in stems (Figure 7). Compared with W, WR reduced ABTS radical scavenging capacity in leaves by 26.7% (Figure 7A). Compared with W, WB, and WR increased ABTS radical scavenging capacity in stems by 32.1 and 37.9%, respectively (Figure 7B), and DPPH radical scavenging ability in leaves by 130.6 and 218.5%, respectively (Figure 7C). There was no significant difference in DPPH radical scavenging ability in stems among all the three treatments (Figure 7D).

Comprehensive effects of light qualities on plant growth, nutrition, and antioxidant properties

To explore the effects of light spectral qualities (blue, green, and red) of light treatments, correlation between light spectral qualities and growth characteristics (Figure 8), nutritional and antioxidant characteristics (Figure 9) of wheat seedlings was analyzed. Among the measured parameters of growth characteristics, blue light was significantly negatively correlated with most parameters, and red light was significantly positively correlated with most parameters (Figure 8). The situation was different when it came to parameters in terms of nutritional characteristics and antioxidant properties (Figure 9). In leaves, blue light was significantly positively correlated with SS (soluble sugar), TF (total flavonoids), GSH, ASA, SOD, POD, APX, and ABTS, and significantly negatively correlated with MDA. In stems, blue light was significantly positively correlated with TT (total triterpenes), GSH, ASA, POD, and CAT. Conversely, red light was significantly negatively correlated with SS, TF, TT, TP (total polyphenols), GSH, SOD, and ABTS in leaves, and was significantly negatively correlated with SP (soluble protein) and ASA in stems. In addition, there was a significant positive correlation among TF, GSH, ASA, SOD, POD, and APX in leaves. MDA was significantly negatively correlated with TF, GSH, ASA, POD, APX, and DPPH.

Discussion

Growth and development of plants are affected by wavelengths of light, among which red and blue light are regarded as the most influential wavelengths, attracting much attention (Zheng et al., 2019; Li et al., 2020; Jung et al., 2021). Our results showed that red light promoted the growth of wheat seedlings, mainly manifested as increased plant height, leaf area, shoot fresh, and dry weight per plant under WR (B:G:R = 19:25:56) (Figure 2). Similar results have been reported

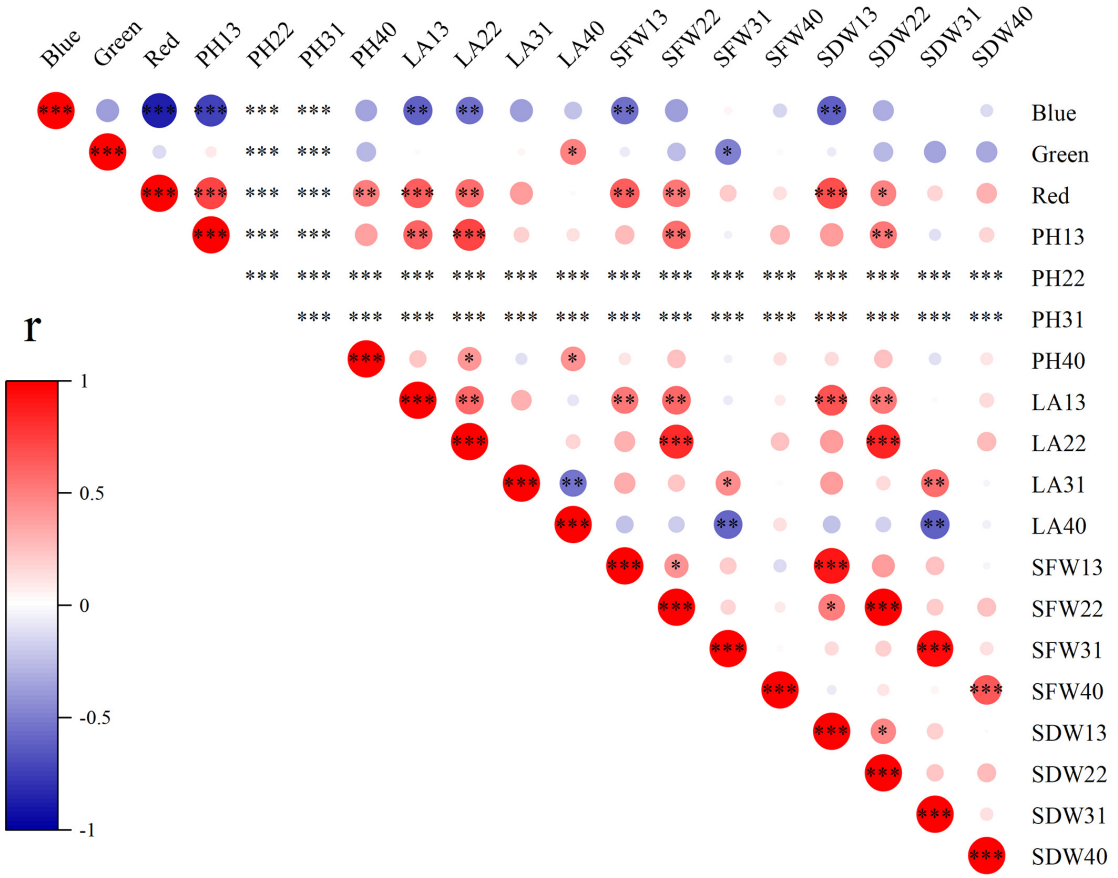

FIGURE 8
The correlation among light spectral quality (blue, green, and red) and growth indicators. PH, plant height; LA, leaf area; SFW, shoot fresh weight; SDW, shoot dry weight. Difference test at the $^{*}P < 0.05$, $^{**}P < 0.01$, and $^{***}P < 0.001$ level. The colors reflect the changes in correlation coefficient: red color represents correlation coefficient with high and positive correlation and blue indicates high and negative correlation.

in water spinach by Kitayama et al. (2019) that red LEDs light resulted in a high level of stem fresh weight and plant height. WB (B:G:R = 70:21:9) had a negative effect on wheat growth (**Figure 2**), which is similar to the result of Wollaeger and Runkle (2015). That might be because high proportion of blue light under WB inhibited stem elongation and leaf area expansion (Kalaitzoglou et al., 2021). Interestingly, the effect of red and blue light on growth of wheat seedlings diminished over time (**Figure 8**), which indicated that this effect might be related to the growth stage of wheat or an acclimation response to the new light conditions.

Soluble sugars, soluble proteins, flavonoids, triterpenoids, and polyphenols are important primary and secondary metabolites of plants, which have been proved to be beneficial for human health (Augustin et al., 2011; Kumar and Pandey, 2013; Jakobek, 2015; Rienth et al., 2021). It has been reported that light quality is an important factor affecting the synthesis and accumulation of these metabolites (Jeong et al., 2012; Bae et al., 2016; He et al., 2020; Jiang et al., 2021). In our study, the contents of soluble sugar and total flavonoids content in leaves were highest under WB (B:G:R = 70:21:9), and the contents of soluble protein, total triterpenoids, and polyphenols was highest under W (B:G:R = 34:46:20) (**Figures 3**, **4**), which is similar to the results of the study by Son and Oh (2013). However, Zhang et al. (2018) reported different results in lettuce. They found that soluble sugar content was the highest under red light and 1B:9R, while soluble protein content was the highest under blue light and 1B:4R. Different results may be related to species. Blue light was positively correlated with TF in leaves (**Figure 9A**), which may be because blue light enhances the activities of general phenylpropanoid and flavonoid pathways enzymes, thereby promoting the synthesis and accumulation of total flavonoids in leaves (Koyama et al., 2012; Zoratti et al., 2014).

Abiotic stress can break the balance of ROS production and elimination, resulting in excessive accumulation of ROS, and ultimately oxidative stress (Gill and Tuteja, 2010). MDA is the oxidation end product of lipid peroxidation caused by free radicals, which can indirectly reflect the degree of oxidative stress (Saleem et al., 2019). In our study, WB (B:G:R = 70:21:9) decreased MDA content in leaves and stems of wheat seedlings

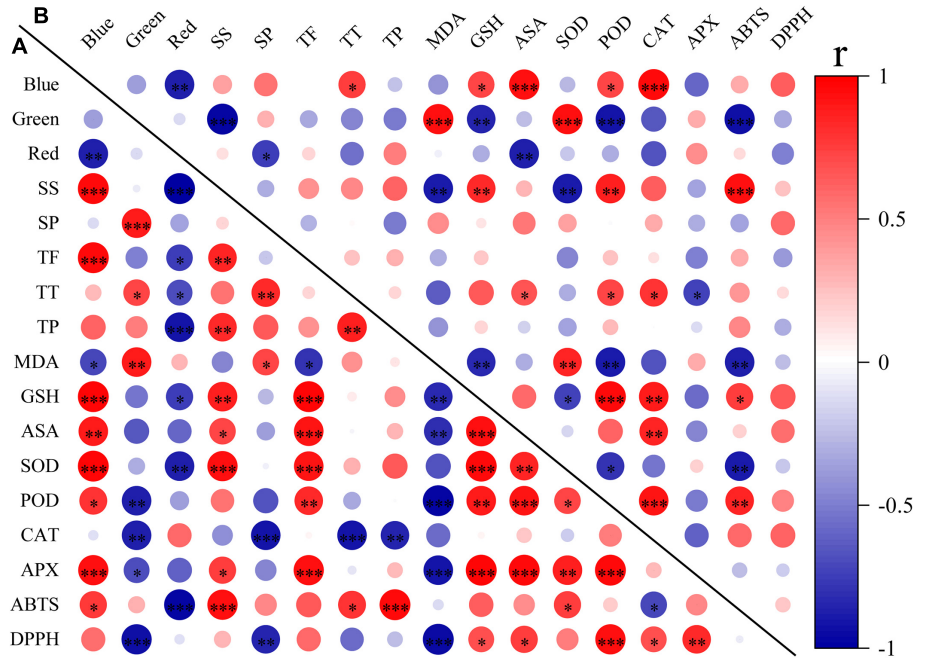

FIGURE 9
The correlation among light spectral quality (blue, green, and red) and nutritional and antioxidant indicators in leaves **(A)** and in stems **(B)**. SS, soluble sugar content; SP, soluble protein content; TF, total flavonoids; TT, total triterpenes; TP, total polyphenols; MDA, malondialdehyde; GSH, glutathione; ASA, ascorbic acid; SOD, superoxide dismutase; POD, peroxidase; CAT, catalase; APX, ascorbate peroxidase; ABTS, 2,2′-azino-bis (3-ethylbenzthiazoline-6-sulfonic acid); DPPH, 2,2-diphenyl-1-picrylhydrazyl. Difference test at the $^{*}P < 0.05$, $^{**}P < 0.01$, and $^{***}P < 0.001$ level. The colors reflect the changes in correlation coefficient: red color represents correlation coefficient with high and positive correlation and blue indicates high and negative correlation.

compared with W (B:G:R = 34:46:20) (**Figure 5**). Similar results have been reported that MDA content of wheatgrass under 75B:25R was lower in comparison with 18B:64G:18R (Bartucca et al., 2020).

Plants are well equipped with a variety of antioxidants to scavenge oxidative stress (Gill and Tuteja, 2010). Among them, GSH and ASA are important non-enzymatic antioxidant, which donate electrons for antioxidant enzymes to scavenge ROS (Noctor and Foyer, 1998; Akram et al., 2017; Zhitkovich, 2021). SOD, POD, CAT, and APX are crucial enzymatic antioxidants that cooperate to detoxify excessive ROS (You and Chan, 2015). Numerous studies have shown that the responses of antioxidants vary with the proportion of red and blue light, plant species, their genotypes and development stages (Choi et al., 2013; Manivannan et al., 2017; Ye et al., 2017; Yu et al., 2017; Liu et al., 2018). In our study, WB (B:G:R = 70:21:9) increased the contents of GSH and ASA (**Figure 5**), which may be due to blue light changes transcription signal transduction and metabolism of GSH and ASA metabolism (Liu and Zhang, 2021). WB also enhanced activities of antioxidant enzymes (SOD, POD, CAT, and APX) in leaves or stems of wheat seedlings (**Figure 6**), which is similar to the results reported by Kook et al. (2013), who found blue LEDs light improved CAT and APX activities of lettuce. Non-enzymatic antioxidants (ASA and GSH) were positively correlated with enzymatic antioxidants (SOD, POD, and APX) in leaves (**Figure 9A**), which is related to their synergistic cooperation in scavenging ROS (Mittler et al., 2004; Hasanuzzaman et al., 2020). In addition, TF was also positively correlated with these antioxidants (ASA, GSH, SOD, POD, and APX) in leaves (**Figure 9A**), which might be the antioxidant-induced change in cellular redox homeostasis that activates the biosynthesis of flavonoids (Agati et al., 2012).

ABTS and DPPH radical scavenging capacity are two commonly used parameters to indicate the total antioxidant capacity of plants (Floegel et al., 2011). WB could effectively improve the ABTS radical scavenging capacity in stems and DPPH radical scavenging capacity in leaves. Apparently, occurrence of higher contents of non-enzymatic antioxidants (ASA and GSH) and higher activities of antioxidant enzymes (SOD, POD, CAT, and APX) under the WB positively affected the ABTS and DPPH radical scavenging capacities in leaves and stems extract. Similar results were obtained in *Rehmannia glutinosa* (Manivannan et al., 2015) and *P. setacea* (Santos-Tierno et al., 2021). Consequently, our results suggest that WB (B:G:R = 70:21:9) have the capacity to enhance antioxidant defense mechanism and to elicit accumulation of potential secondary metabolites in wheat seedlings leaves.

Conclusion

This study investigated growth, nutrition, and antioxidant characteristics of wheat seedlings under LEDs sources with different spectra combinations. Plant height, leaf area, shoot fresh, and dry weight were the highest under WR at the early stage of planting. Contents of soluble sugar, soluble protein, triterpenoids, polyphenols, flavonoids, ASA, and GSH were higher and MDA content was lower under WB than those under W. Activities of antioxidant enzymes (SOD, POD, CAT, and APX) and ABTS and DPPH radical scavenging capacities in leaves or stems under WB were higher than those under W. LEDs with a high ratio of red light promoted growth of wheat seedlings, and LEDs with a high ratio of blue light reduced damage of membrane lipid peroxidation and improved antioxidant capacity by increasing activities of antioxidant enzymes and contents of antioxidants. Our study provides a basis for selecting appropriate ratio of red to blue according to the production aim.

Data availability statement

The raw data supporting the conclusions of this article will be made available by the authors, without undue reservation.

Author contributions

JL and XG performed the experiment, analyzed the data, and wrote the manuscript. SZ participated in the experiment. XX and YZ designed and supervised the research. LC and WZ reviewed and edited the manuscript. All authors have read and agreed to the published version of the manuscript.

Funding

This work was funded by China Agriculture Research System (CARS-03), National and Local Joint Engineering Laboratory for Agricultural Internet of Things (PT2022-23), and the National Natural Science Foundation of China (31871563).

Acknowledgments

We gratefully acknowledge TIANDINGXING Optoelectronics Technology Co., Ltd., located in Ningbo, Zhejiang Province, China for providing the LED lamps, and Yong Li, an engineer from the National Research Center of Intelligent Equipment for Agriculture, for his technical assistance on precise control of the plant factory.

Conflict of interest

The authors declare that the research was conducted in the absence of any commercial or financial relationships that could be construed as a potential conflict of interest.

Publisher's note

All claims expressed in this article are solely those of the authors and do not necessarily represent those of their affiliated organizations, or those of the publisher, the editors and the reviewers. Any product that may be evaluated in this article, or claim that may be made by its manufacturer, is not guaranteed or endorsed by the publisher.

References

Agati, G., Azzarello, E., Pollastri, S., and Tattini, M. (2012). Flavonoids as antioxidants in plants: Location and functional significance. *Plant Sci.* 196, 67–76. doi: 10.1016/j.plantsci.2012.07.014

Akram, N. A., Shafiq, F., and Ashraf, M. (2017). Ascorbic acid-a potential oxidant scavenger and its role in plant development and abiotic stress tolerance. *Front. Plant Sci.* 8:613. doi: 10.3389/fpls.2017.00613

Augustin, J. M., Kuzina, V., Andersen, S. B., and Bak, S. (2011). Molecular activities, biosynthesis and evolution of triterpenoid saponins. *Phytochemistry* 72, 435–457. doi: 10.1016/j.phytochem.2011.01.015

Azad, M. O. K., Kjaer, K. H., Adnan, M., Naznin, M. T., Lim, J. D., Sung, I. J., et al. (2020). The evaluation of growth performance, photosynthetic capacity, and primary and secondary metabolite content of leaf lettuce grown under limited irradiation of blue and red LED light in an urban plant factory. *Agriculture* 10:28. doi: 10.3390/agriculture10020028

Bae, J., Park, Y., Namiesnik, J., Gulcin, I., Kim, T., Ho-Cheol, K., et al. (2016). Effects of artificial lighting on bioactivity of sweet red pepper (*Capsicum annuum* L.). *Intl. J. Food Sci. Technol.* 51, 1378–1385. doi: 10.1111/ijfs.13116

Bantis, F., Smirnakou, S., Ouzounis, T., Koukounaras, A., Ntagkas, N., Radoglou, K., et al. (2018). Current status and recent achievements in the field of horticulture with the use of light-emitting diodes (LEDs). *Sci. Hortic.* 235, 437–451. doi: 10.1016/j.scienta.2018.02.058

Bar-Sela, G., Cohen, M., Ben-Arye, E., and Epelbaum, R. (2015). The medical use of wheatgrass: Review of the gap between basic and clinical applications. *Mini Rev. Med. Chem.* 15, 1002–1010. doi: 10.2174/1389557515121507311128 36

Bartucca, M. L., Guiducci, M., Falcinelli, B., Del Buono, D., and Benincasa, P. (2020). Blue:red LED light proportion affects vegetative parameters, pigment content, and oxidative status of einkorn (*Triticum monococcum* L. ssp. monococcum) wheatgrass. *J. Agric. Food Chem.* 68, 8757–8763.

Bian, Z. H., Yang, Q. C., and Liu, W. K. (2015). Effects of light quality on the accumulation of phytochemicals in vegetables produced in controlled environments: A review. *J. Sci. Food Agric.* 95, 869–877. doi: 10.1002/jsfa.6789

Bradford, M. M. (1976). A rapid and sensitive method for quantitation of microgram quantities of protein utilizing principle of protein-dye binding. *Anal. Biochem.* 72, 248–254. doi: 10.1006/abio.1976.9999

Cakmak, I., and Marschner, H. (1992). Magnesium deficiency and high light intensity enhance activities of superoxide-dismutase, ascorbate peroxidase, and glutathione-reductase in bean leaves. *Plant Phys.* 98, 1222–1227. doi: 10.1104/pp.98.4.1222

Cao, L., Zheng, Z., Zhang, H., Liang, P., Zhu, Q., Le, W., et al. (2021). Phosphor-converted white light-emitting diodes for plant lighting. *Spectros. Spectr. Anal.* 41, 1060–1065. doi: 10.3964/j.issn.1000-0593202104-1060-06

Causin, H. F., Jauregui, R. N., and Barneix, A. J. (2006). The effect of light spectral quality on leaf senescence and oxidative stress in wheat. *Plant Sci.* 171, 24–33. doi: 10.1016/j.plantsci.2006.02.009

Choi, C. Y., Kim, N. N., Shin, H. S., Park, H. G., Cheon, S., Kil, G., et al. (2013). The effect of various wavelengths of light from light-emitting diodes on the antioxidant system of marine cyanobacteria. *Synechococcus* sp. *Mol. Cell. Toxicol.* 9, 295–302. doi: 10.1007/s13273-013-0037-9

Choi, M., Lee, M. Y., Yang, S., Shin, H., and Jeon, Y. J. (2021). Hydrophobic fractions of *Triticum aestivum* L. Extracts contain polyphenols and alleviate inflammation by regulating nuclear factor-kappa B. *Biotechnol. Bioproc. Eng.* 26, 93–106. doi: 10.1007/s12257-020-0352-7

de Wit, M., Galvao, V. C., and Fankhauser, C. (2016). Light-mediated hormonal regulation of plant growth and development. *Annu. Rev. Plant Biol.* 67, 513–537. doi: 10.1146/annurev-arplant-043015-112252

Devi, C., Chatli, M. K., Bains, K., Kaur, H., and Rindhe, S. N. (2019). Enrichment of wheatgrass (*Triticum aestivum* L.) juice and powder in milk and meat-based food products for enhanced antioxidant potential. *Intl. J. Curr. Microbiol. Appl. Sci.* 8, 3259–3268. doi: 10.20546/ijcmas.2019.806.388

Durairaj, V., Hoda, M., Shakya, G., Babu, S. P. P., and Rajagopalan, R. (2014). Phytochemical screening and analysis of antioxidant properties of aqueous extract of wheatgrass. *Asian Pac. J. Trop. Med.* 71, S398–S404. doi: 10.1016/S1995-7645(14)60265-0

Floegel, A., Kim, D., Chung, S., Koo, S. I., and Chun, O. K. (2011). Comparison of ABTS/DPPH assays to measure antioxidant capacity in popular antioxidant-rich US foods. *J. Food Compos. Anal.* 24, 1043–1048. doi: 10.1016/j.jfca.2011.01.008

Gao, S., Liu, X., Liu, Y., Cao, B., Chen, Z., Xu, K., et al. (2021). Comparison of the effects of LED light quality combination on growth and nutrient accumulation in green onion (*Allium fistulosum* L.). *Protoplasma* 258, 753–763. doi: 10.1007/s00709-020-01593-y

Gawlik-Dziki, U., Dziki, D., Nowak, R., Swieca, M., Olech, M., Pietrzak, W., et al. (2016). Influence of sprouting and elicitation on phenolic acids profile and antioxidant activity of wheat seedlings. *J. Cereal Sci.* 70, 221–228. doi: 10.1016/j.jcs.2016.06.011

Gayral, B. (2017). LEDs for lighting: Basic physics and prospects for energy savings. *C R Phys.* 18, 453–461. doi: 10.1016/j.crhy.2017.09.001

Ghumman, A., Singh, N., and Kaur, A. (2017). Chemical, nutritional and phenolic composition of wheatgrass and pulse shoots. *Intl. J. Food Sci. Technol.* 52, 2191–2200. doi: 10.1111/ijfs.13498

Giannopolitis, C. N., and Ries, S. K. (1977). Superoxide dismutases: I. Occurrence in higher plants. *Plant Physiol.* 59, 309–314. doi: 10.1104/pp.59.2.309

Gill, S. S., and Tuteja, N. (2010). Reactive oxygen species and antioxidant machinery in abiotic stress tolerance in crop plants. *Plant Physiol. Biochem.* 48, 909–930. doi: 10.1016/j.plaphy.2010.08.016

Goto, E., Matsumoto, H., Ishigami, Y., Hikosaka, S., Fujiwara, K., Yano, A., et al. (2014). Measurements of the photosynthetic rates in vegetables under various qualities of light from light-emitting diodes. *Acta Hortic.* 1037, 261–268. doi: 10.17660/ActaHortic.2014.1037.30

Guo, L., Zhu, W., Liu, Y., Wu, J., Zheng, A., Yan-li, L., et al. (2013). Response surface optimized extraction of flavonoids from mimenghua and its antioxidant activities in vitro. *Food Sci. Biotechnol.* 22, 1285–1292. doi: 10.1007/s10068-013-0214-6

Guo, X., Xue, X., Chen, L., Li, J., Wang, Z., Zhang, Y., et al. (2022a). Effects of leds light spectra on the growth, yield, and quality of winter wheat (*Triticum aestivum* L.) Cultured in plant factory. *J. Plant Growth Regulation* doi: 10.1007/s00344-022-10724-z

Guo, X., Zhao, Q., Li, J., Wang, Z., Zhang, Y., Xue, X., et al. (2022b). Daily drip irrigation based on real-time weather improves winter wheat grain yield and water use efficiency. *Irrig. Drainage* 71, 589–603. doi: 10.1002/ird.2673

Hameed, A., Akram, N. A., Saleem, M. H., Ashraf, M., Ahmed, S., Ali, S., et al. (2021). Seed treatment with α-tocopherol regulates growth and key physio-biochemical attributes in carrot (*Daucus carota* L.) plants under water limited regimes. *Agronomy* 11, 469. doi: 10.3390/agronomy11030469

Hanft, J. M., and Jones, R. J. (1986). Kernel abortion in maize II. Distribution of 14C among kernel carbohydrates. *Plant Physiol.* 2, 511–515. doi: 10.1104/pp.81.2.511

Hasanuzzaman, M., Bhuyan, M. H. M. B., Zulfiqar, F., Raza, A., Mohsin, S. M., Mahmud, J. A., et al. (2020). Reactive oxygen species and antioxidant defense in plants under abiotic stress: Revisiting the crucial role of a universal defense regulator. *Antioxidants* 9:681. doi: 10.3390/antiox9080681

He, R., Gao, M., Shi, R., Song, S., Zhang, Y., Su, W., et al. (2020). The combination of selenium and LED light quality affects growth and nutritional properties of broccoli sprouts. *Molecules* 25:4788. doi: 10.3390/molecules25204788

Hoagland, D. R., and Arnon, D. I. (1950). The water culture method for growing plants without soil. *California Agric. Exp. Station Circ.* 347:32. doi: 10.1016/S0140-6736(00)73482-9

Hu, N., Li, W., Du, C., Zhang, Z., Gao, Y., Sun, Z., et al. (2021). Predicting micronutrients of wheat using hyperspectral imaging. *Food Chem.* 343:128473. doi: 10.1016/j.foodchem.2020.128473

Jaiswal, S. K., Prakash, R., Skalny, A. V., Skalnaya, M. G., Grabeklis, A. R., Skalnaya, A. A., et al. (2018). Synergistic effect of selenium and UV-b radiation in enhancing antioxidant level of wheatgrass grown from selenium rich wheat. *J. Food Biochem.* 42:e12577. doi: 10.1111/jfbc.12577

Jakobek, L. (2015). Interactions of polyphenols with carbohydrates, lipids and proteins. *Food Chem.* 175, 556–567. doi: 10.1016/j.foodchem.2014.12.013

Jeong, S. W., Park, S., Jin, J. S., Seo, O. N., Kim, G., Kim, Y., et al. (2012). Influences of four different light-emitting diode lights on flowering and polyphenol variations in the leaves of Chrysanthemum (*Chrysanthemum morifolium*). *J. Agric. Food Chem.* 60, 9793–9800. doi: 10.1021/jf302272x

Jiang, B., Gao, G., Ruan, M., Bian, Y., Geng, F., Yan, W., et al. (2021). Quantitative assessment of abiotic stress on the main functional phytochemicals and antioxidant capacity of wheatgrass at different seedling age. *Front. Nutr.* 8:731555. doi: 10.3389/fnut.2021.731555

Jiao, Y., Lau, O. S., and Deng, X. W. (2007). Light-regulated transcriptional networks in higher plants. *Nat. Rev. Genet.* 8, 217–230. doi: 10.1038/nrg2049

Jung, W., Chung, I., Hwang, M. H., Kim, S., Yu, C. Y., Ghimire, B. K., et al. (2021). Application of light-emitting diodes for improving the nutritional quality and bioactive compound levels of some crops and medicinal plants. *Molecules* 26:1477. doi: 10.3390/molecules26051477

Kaiser, E., Ouzounis, T., Giday, H., Schipper, R., Heuvelink, E., Marcelis, L. F. M., et al. (2019). Adding blue to red supplemental light increases biomass and yield of greenhouse-grown tomatoes, but only to an optimum. *Front. Plant Sci.* 9:2002. doi: 10.3389/fpls.2018.02002

Kalaitzoglou, P., Taylor, C., Calders, K., Hogervorst, M., van Ieperen, W., Harbinson, J., et al. (2021). Unraveling the effects of blue light in an artificial solar background light on growth of tomato plants. *Environ. Exp. Bot.* 184:104377. doi: 10.1016/j.envexpbot.2021.104377

Kaur, N., Singh, B., Kaur, A., Yadav, M. P., Singh, N., Ahlawat, A. K., et al. (2021). Effect of growing conditions on proximate, mineral, amino acid, phenolic composition and antioxidant properties of wheatgrass from different wheat (*Triticum aestivum* L.) Varieties. *Food Chem.* 341:128201. doi: 10.1016/j.foodchem.2020.128201

Kitayama, M., Nguyen, D. T. P., Lu, N., and Takagaki, M. (2019). Effect of light quality on physiological disorder, growth, and secondary metabolite content of water spinach (*Ipomoea aquatica* Forsk) cultivated in a closed-type plant production system. *Hortic. Sci. Technol.* 37, 206–218. doi: 10.12972/kjhst.20190020

Kook, H., Park, S., Jang, Y., Lee, G., Kim, J. S., Kim, H. M., et al. (2013). Blue led (light-emitting diodes)-mediated growth promotion and control ofbotrytisdisease in lettuce. *Acta Agric. Scand. Section B Soil Amp Plant Sci.* 63, 271–277. doi: 10.1080/09064710.2012.756118

Koyama, K., Ikeda, H., Poudel, P. R., and Goto-Yamamoto, N. (2012). Light quality affects flavonoid biosynthesis in young berries of cabernet sauvignon grape. *Phytochemistry* 78, 54–64. doi: 10.1016/j.phytochem.2012.02.026

Kulkarni, S. D., Tilak, J. C., Acharya, R., Rajurkar, N. S., Devasagayam, T., Reddy, A. V. M., et al. (2006). Evaluation of the antioxidant activity of wheatgrass (*Triticum aestivum* L.) As a function of growth under different conditions. *Phytother. Res.* 20, 218–227. doi: 10.1002/ptr.1838

Kumar, S., and Pandey, A. K. (2013). Chemistry and biological activities of flavonoids: An overview. *Sci. World J.* 2013:162750. doi: 10.1155/2013/162750

Lee, H. R., Kim, H. M., Jeong, H. W., and Hwang, S. J. (2020). Growth and bioactive compounds of salvia plebeia r. Br. Grown under various ratios of red and blue light. *Horticulturae* 6:35. doi: 10.3390/horticulturae6020035

Li, H., Li, H., Wang, H., Li, D., Li, R., and Li, Y. (2018). Further study on the method of leaf area calculation in winter wheat. *J. Triticeae Crops* 38, 455–459.

Li, Q., Xu, J., Yang, L., Sun, Y., Zhou, X., Yuhong, Z., et al. (2022). LED light quality affect growth, alkaloids contents, and expressions of amaryllidaceae alkaloids biosynthetic pathway genes in Lycoris longituba. *J. Plant Growth Regul.* 41, 257–270. doi: 10.1007/s00344-021-10298-2

Li, Y., Xin, G., Liu, C., Shi, Q., Yang, F., and Wei, M. (2020). Effects of red and blue light on leaf anatomy, CO2 assimilation and the photosynthetic electron transport capacity of sweet pepper (*Capsicum annuum* L.) seedlings. *BMC Plant Biol.* 20:4518. doi: 10.1186/s12870-020-02523-z

Lin, K., Huang, M., Huang, W., Hsu, M., Yang, Z., Yang, C., et al. (2013). The effects of red, blue, and white light-emitting diodes on the growth, development, and edible quality of hydroponically grown lettuce (*Lactuca sativa* L. var. capitata). *Sci. Hortic.* 150, 86–91. doi: 10.1016/j.scienta.2012.10.002

Liu, M., Xu, Z., Yang, Y., and Feng, Y. (2011). Effects of different spectral lights on Oncidium PLBs induction, proliferation, and plant regeneration. *Plant Cell Tissue Organ. Cult.* 106, 1–10. doi: 10.1007/s11240-010-9887-1

Liu, T., and Zhang, X. (2021). Comparative transcriptome and metabolome analysis reveal glutathione metabolic network and functional genes underlying blue and red-light mediation in maize seedling leaf. *BMC Plant Biol.* 21:593. doi: 10.1186/s12870-021-03376-w

Liu, Y., Wang, T., Fang, S., Zhou, M., and Qin, J. (2018). Responses of morphology, gas exchange, photochemical activity of photosystem II, and antioxidant balance in *Cyclocarya paliurus* to light spectra. *Front. Plant Sci.* 9:1704. doi: 10.3389/fpls.2018.01704

Manivannan, A., Soundararajan, P., Halimah, N., Ko, C. H., and Jeong, B. R. (2015). Blue LED light enhances growth, phytochemical contents, and antioxidant enzyme activities of *Relunannia glutinosa* cultured in vitro. *Hortic. Environ. Biotechnol.* 56, 105–113. doi: 10.1007/s13580-015-0114-1

Manivannan, A., Soundararajan, P., Park, Y. G., Wei, H., Kim, S. H., and Jeong, B. R. (2017). Blue and red light-emitting diodes improve the growth and physiology of in vitro-grown carnations 'Green Beauty' and 'Purple Beauty'. *Hortic. Environ. Biotechnol.* 58, 12–20. doi: 10.1007/s13580-017-0051-2

Mittler, R., Vanderauwera, S., Gollery, M., and Van Breusegem, F. (2004). Reactive oxygen gene network of plants. *Trends Plant Sci.* 9, 490–498. doi: 10.1016/j.tplants.2004.08.009

Nakano, Y., and Asada, K. (1981). Hydrogen peroxide is scavenged by ascorbate-specific peroxidase in spinach chloroplasts. *Plant Cell Physiol.* 22, 867–880. doi: 10.1093/oxfordjournals.pcp.a076232

Nazim Ud Dowla, M. A. N., Edwards, I., O'Hara, G., Islam, S., and Ma, W. (2018). Developing wheat for improved yield and adaptation under a changing climate: Optimization of a few key genes. *Engineering* 4, 514–522. doi: 10.1016/j.eng.2018.06.005

Naznin, M. T., Lefsrud, M., Gravel, V., and Azad, M. O. K. (2019). Blue light added with red LEDs enhance growth characteristics, pigments content, and antioxidant capacity in lettuce, spinach, kale, basil, and sweet pepper in a controlled environment. *Plants* 8:93. doi: 10.3390/plants8040093

Nishio, J. N. (2000). Why are higher plants green? Evolution of the higher plant photosynthetic pigment complement. *Plant Cell Environ.* 23, 539–548. doi: 10.1046/j.1365-3040.2000.00563.x

Noctor, G., and Foyer, C. H. (1998). Ascorbate and glutathione: Keeping active oxygen under control. *Ann. Rev Plant Physiol. Plant Mol. Biol.* 49, 249–279. doi: 10.1146/annurev.arplant.49.1.249

Ouzounis, T., Rosenqvist, E., and Ottosen, C. (2015). Spectral effects of artificial light on plant physiology and secondary metabolism: A review. *Hortscience* 50, 1128–1135. doi: 10.21273/HORTSCI.50.8.1128

Paradiso, R., and Proietti, S. (2022). Light-quality manipulation to control plant growth and photomorphogenesis in greenhouse horticulture: The state of the art and the opportunities of modern LED systems. *J. Plant Growth Regul.* 41, 742–780. doi: 10.1007/s00344-021-10337-y

Qiu, Z., Guo, J., Zhu, A., Zhang, L., and Zhang, M. (2014). Exogenous jasmonic acid can enhance tolerance of wheat seedlings to salt stress. *Ecotoxicol. Environ. Saf.* 104, 202–208. doi: 10.1016/j.ecoenv.2014.03.014

Qiu, Z., Li, J., Zhang, Y., Bi, Z., and Wei, H. (2011). Microwave pretreatment can enhance tolerance of wheat seedlings to CdCl2 stress. *Ecotoxicol. Environ. Saf.* 74, 820–825. doi: 10.1016/j.ecoenv.2010.11.008

Rehman, M., Fahad, S., Saleem, M. H., Hafeez, M., Rahman, M. H., Liu, F., et al. (2020). Red light optimized physiological traits and enhanced the growth of ramie (*Boehmeria nivea* L.). *Photosynthetica* 58, 922–931. doi: 10.32615/ps.2020.040

Rienth, M., Vigneron, N., Darriet, P., Sweetman, C., Burbidge, C., Bonghi, C., et al. (2021). Grape berry secondary metabolites and their modulation by abiotic factors in a climate change scenario-a review. *Front. Plant Sci.* 12:643258. doi: 10.3389/fpls.2021.643258

Saleem, M. H., Rehman, M., Zahid, M., Imran, M., Xiang, W., and Liu, L. (2019). Morphological changes and antioxidative capacity of jute (Corchorus capsularis. Malvaceae) under different color light-emitting diodes. *Braz. J. Bot.* 42, 581–590. doi: 10.1007/s40415-019-00565-8

Santos-Tierno, R., Garcia, R., Fonseca, E., Faleiro, F., Moreira, D., Pacheco, G., et al. (2021). Light quality and explant type modulate growth, antioxidant properties and bioactive compounds production of calluses of Passiflora setacea cv BRS Perola do Cerrado. *Plant Cell Tissue Organ. Cult.* 147, 635–646. doi: 10.1007/s11240-021-02188-y

Sarker, U., and Oba, S. (2020). Phenolic profiles and antioxidant activities in selected drought-tolerant leafy vegetable amaranth. *Sci. Rep.* 10:18287. doi: 10.1038/s41598-020-71727-y

Singh, D., Basu, C., Meinhardt-Wollweber, M., and Roth, B. (2015). LEDs for energy efficient greenhouse lighting. *Renew. Sustain. Energy Rev.* 49, 139–147. doi: 10.1016/j.rser.2015.04.117

Son, K. H., and Oh, M. (2013). Leaf shape, growth, and antioxidant phenolic compounds of two lettuce cultivars grown under various combinations of blue and red light-emitting diodes. *Hortscience* 48, 988–995. doi: 10.21273/HORTSCI.48.8.988

Terashima, I., Fujita, T., Inoue, T., Chow, W. S., and Oguchi, R. (2009). Green light drives leaf photosynthesis more efficiently than red light in strong white light: Revisiting the enigmatic question of why leaves are green. *Plant Cell Physiol.* 50, 684–697. doi: 10.1093/pcp/pcp034

Tsai, C., Lin, C., Tsai, H., Chen, C., Li, W., Yu, H. M., et al. (2013). The immunologically active oligosaccharides isolated from wheatgrass modulate monocytes via toll-like receptor-2 signaling. *J. Biol. Chem.* 288, 17689–17697. doi: 10.1074/jbc.M112.448381

Virdi, A. S., Singh, N., Bains, K. K., and Kaur, A. (2021). Effect of photoperiod and growth media on yield and antioxidant properties of wheatgrass juice of Indian wheat varieties. *J. Food Sci. Technol. Mysore* 58, 3019–3029. doi: 10.1007/s13197-020-04805-8

Wollaeger, H. M., and Runkle, E. S. (2015). Growth and acclimation of impatiens, salvia, petunia, and tomato seedlings to blue and red light. *Hortscience* 50, 522–529. doi: 10.21273/HORTSCI.50.4.522

Yadav, A., Singh, D., Lingwan, M., Yadukrishnan, P., Masakapalli, S. K., and Datta, S. (2020). Light signaling and UV-B-mediated plant growth regulation. *J. Integr. Plant Biol.* 62, 1270–1292. doi: 10.1111/jipb.12932

Yadav, S., Srivastava, A., Biswas, S., Basu, S., Singh, S. K., and Mishra, Y. (2021). Seasonal changes in the antioxidative defence system of a liverwort *Dumortiera hirsuta*. *J. Plant Growth Regul.* 41, 1265–1275. doi: 10.1007/s00344-021-10379-2

Ye, S., Shao, Q., Xu, M., Li, S., Wu, M., Tan, X., et al. (2017). Effects of light quality on morphology, enzyme activities, and bioactive compound contents in *Anoectochilus* roxburghii. *Front. Plant Sci.* 8:857. doi: 10.3389/fpls.2017.00857

You, J., and Chan, Z. (2015). ROS regulation during abiotic stress responses in crop plants. *Front. Plant Sci.* 6:1092. doi: 10.3389/fpls.2015.01092

Yu, W., Liu, Y., Song, L., Jacobs, D. F., Du, X., Ying, Y., et al. (2017). Effect of differential light quality on morphology, photosynthesis, and antioxidant enzyme activity in *Camptotheca* acuminata seedlings. *J. Plant Growth Regul.* 36, 148–160. doi: 10.1007/s00344-016-9625-y

Zhang, T., Shi, Y., Piao, F., and Sun, Z. (2018). Effects of different LED sources on the growth and nitrogen metabolism of lettuce. *Plant Cell Tissue Organ. Cult.* 134, 231–240. doi: 10.1007/s11240-018-1415-8

Zheng, L., He, H., and Song, W. (2019). Application of light-emitting diodes and the effect of light quality on horticultural crops: A review. *Hortscience* 54, 1656–1661. doi: 10.21273/HORTSCI14109-19

Zhitkovich, A. (2021). Ascorbate: Antioxidant and biochemical activities and their importance for in vitro models. *Arch. Toxicol.* 95, 3623–3631. doi: 10.1007/s00204-021-03167-0

Zoratti, L., Karppinen, K., Escobar, A. L., Haggman, H., and Jaakola, L. (2014). Light-controlled flavonoid biosynthesis in fruits. *Front. Plant Sci.* 5:534. doi: 10.3389/fpls.2014.00534

frontiers | Frontiers in Plant Science

TYPE Original Research
PUBLISHED 07 September 2022
DOI 10.3389/fpls.2022.978462

OPEN ACCESS

EDITED BY
Yuxin Tong,
Institute of Environment and Sustainable Development in Agriculture (CAAS), China

REVIEWED BY
Yun Kong,
Texas A&M University, United States
Sofia D. Carvalho,
Universidad San Francisco de Quito, Ecuador

*CORRESPONDENCE
Xuzhang Xue
xuexz@nercita.org.cn

†These authors have contributed equally to this work

SPECIALTY SECTION
This article was submitted to Technical Advances in Plant Science, a section of the journal Frontiers in Plant Science

RECEIVED 26 June 2022
ACCEPTED 18 August 2022
PUBLISHED 07 September 2022

CITATION
Zhang S, Guo X, Li J, Zhang Y, Yang Y, Zheng W and Xue X (2022) Effects of light-emitting diode spectral combinations on growth and quality of pea sprouts under long photoperiod.
Front. Plant Sci. 13:978462.
doi: 10.3389/fpls.2022.978462

Effects of light-emitting diode spectral combinations on growth and quality of pea sprouts under long photoperiod

Siqi Zhang[1,2†], Xiaolei Guo[1,2†], Junyan Li[1,2], Yinghua Zhang[2], Youming Yang[2], Wengang Zheng[1] and Xuzhang Xue[1*]

[1]National Research Center of Intelligent Equipment for Agriculture, Beijing, China, [2]College of Agronomy and Biotechnology, China Agricultural University, Beijing, China

Pea sprouts have rich nutrition and are considered good for heart health. In this study, the kaspa peas and black-eyed peas were chosen to clarify the effect of different LED spectral combinations on the growth, yield, and nutritional quality of pea sprouts under long photoperiod (22 h light/2 h dark). The results showed that the two pea varieties responded differently to light spectral combinations. Black-eyed pea sprouts had higher plant height, fresh weight per plant, dry weight per plant, soluble sugar content, and lower malondialdehyde (MDA) content than kaspa peas under the same light treatment. Compared with white light, red-to-blue ratio of 2:1 significantly increased peroxidase (POD) and superoxide dismutase (SOD) activity, soluble sugar and soluble protein content of kaspa pea sprouts, and decreased MDA content of black-eyed pea sprouts. Blue light was negatively correlated with the plant height of pea sprouts and positively correlated with SOD activity, vitamin C, soluble sugar, and soluble protein content. Antioxidant capacity, yield, and nutritional quality of black-eyed pea sprouts were higher than those of kaspa pea sprouts under the same light treatment. Blue light improved the nutritional quality of pea sprouts. Compared with other light treatments, the red-to-blue ratio of 2:1 was more conducive to improving the antioxidant capacity and nutritional quality of pea sprouts under long photoperiod.

KEYWORDS

pea sprout, LED spectral combination, growth, nutritional quality, plant factory

Introduction

With the improvement of people's living standards, healthy diet has attracted more and more attention. Vegetables are rich in nutrients needed by humans, and demands for vegetable yield and quality are getting higher (Kearney, 2010). Sprouts, which means the edible vegetables after seed germination (Benincasa et al., 2019), accumulate lots of bioactive substances, such as vitamins, polysaccharides, proteins and polyphenols (Gan et al., 2017). Sprouts are considered to have the function of anti-oxidation, anti-virus

and anti-inflammatory, and reduce risk of diseases (Geng et al., 2022). As a high-quality sprout vegetable, pea sprout is rich in vitamin C and protein, and conducive to improve human immunity (Zhao et al., 2020). Sprouts also have the advantages of short growth cycle, low production cost, and small land area needed (Zhang et al., 2020).

A plant factory is a closed plant production system that aims to achieve high-precision control of plant growth environment and high crop yield (Avgoustaki and Xydis, 2020). Plant factory can avoid the impact of outdoor extreme weather conditions on plant growth (Al-Kodmany, 2018). Light-emitting diode (LED) is an indispensable lighting system that can provide different light quality, light intensity, and photoperiod to control plant growth. Compared with traditional lighting equipment, LED has the advantages of small volume, low energy consumption, long service life, safe use, energy, and environmental protection (Olle and Virsile, 2013).

Light is not only the energy for photosynthesis but also a signal for plant morphogenesis (Chen et al., 2017). Light quality and photoperiod have an important impact on plant growth and development, as well as yield and quality. Photoperiod can regulate plant germination, growth, and flowering (Cao et al., 2014; Bian et al., 2015). Previous studies have shown that long photoperiod can promote flowering of horticultural crops, shorten growth time of wheat, and increase leaf area of many temperate grass species (Adams and Langton, 2005; Sulpice et al., 2014; Watson et al., 2018). But excessive long illumination time will lead to reduction of yield, chlorosis of leaves, and weakened growth activity in tomatoes, cucumbers, and wheat (Gonzalez et al., 2003; Lanoue et al., 2021a). Some studies found that suitable light quality can reduce the adverse effects of long photoperiod on crops (Lanoue et al., 2021b).

Light quality affects plant height, chlorophyll content, antioxidant capacity, yield, and quality (de Wit et al., 2016; van Gelderen et al., 2018). Red and blue light is the main absorption wavelengths of plants (Ptushenko et al., 2020). Studies found that red LED can promote seed germination and plant elongation (Sellaro et al., 2012), and blue LED influences phytochrome content and stomata conductance (Samuoliene et al., 2013). Compared with monochromatic light, a mixture of red and blue LEDs can stimulate various types of photoreceptors in plants and reduce light stress (Sabzalian et al., 2014). However, optimal red-to-blue ratio varies among different plant species, even among different cultivars of the same plant species.

Black-eyed pea (Vigna unguiculata), also known as southern pea, cow pea, and crowder pea, grows well in summer and is native to Asia and Africa and contains significant amounts of protein, calories, and some water-soluble vitamins (Bhandari et al., 2016). Kaspa pea is a semi-leafless field pea variety that flourishes well in cool seasons (Sudheesh et al., 2015). This study was carried out in a plant factory to determine growth, yield, and nutritional quality of pea sprouts of the two cultivars under different LED spectral combinations and long photoperiod (22 h light:2 h dark).

Materials and methods

Experimental design

The experiment was conducted in the plant factory of the national precision agriculture experimental station in Xiaotangshan Town, Changping District, Beijing in 2019. Two pea cultivars, kaspa peas and black-eyed peas, were grown under four LED spectral combinations, including white light (W), red-to-blue ratio 2:1 (R2B1), red-to-blue ratio 4:1 (R4B1), and red-to-blue ratio 7:1 (R7B1). The relative spectral distribution (**Figure 1**) and relative spectral content (**Table 1**) were measured with a plant light analyzer (PLA-20, Everfine, Hangzhou, China), and the photosynthetic photon flux density (PPFD) was kept at $190 \pm 25\ \mu mol \cdot m^{-2} \cdot s^{-1}$.

Plant growth condition

Seeds were soaked in clean water for 12 h and then were sown in four sprouters (32 cm × 25 cm). One-half of each sprouter was occupied by 40 seeds of kaspa peas, and another half was occupied by 40 seeds of black-eyed peas. The four sprouters were covered with wet germination paper and put into a constant temperature incubator at 22°C for dark germination for 3 days. The four sprouters were then transferred under four LED light panels in the plant factory for hydroponic culture, with one sprouter under one LED spectral combination. The temperature in the plant factory was kept at 21 ± 1°C/17 ± 1°C (day/night), the photoperiod was 22 h light: 2 h dark, and the hydroponic nutrient solution was updated every week (Hoagland and Arnon, 1950). The distance between the bottom of the sprouters and the LED panels was 40 cm initially and adjusted during the experiment to maintain approximately stable PPFD ($190 \pm 25\ \mu mol\ m^{-2}\ s^{-1}$) at the top of sprouts.

Measurement of growth characteristics

After 12 days of LED light treatment, six plants from each cultivar in each sprouter were selected for measurement of growth characteristics. The remaining plants were stored in a −80°C ultra-low temperature freezer for measurement of antioxidant capacity and nutrition parameters. SPAD values of the upper three leaves of the six plants were determined by a chlorophyll meter (SPAD-502; Minolta, Osaka, Japan). Plant height of the six plants was measured using a ruler, and fresh weight was measured with one ten-thousandth scale (JA1003; balance instrument, Shanghai, China). After sterilizing the six

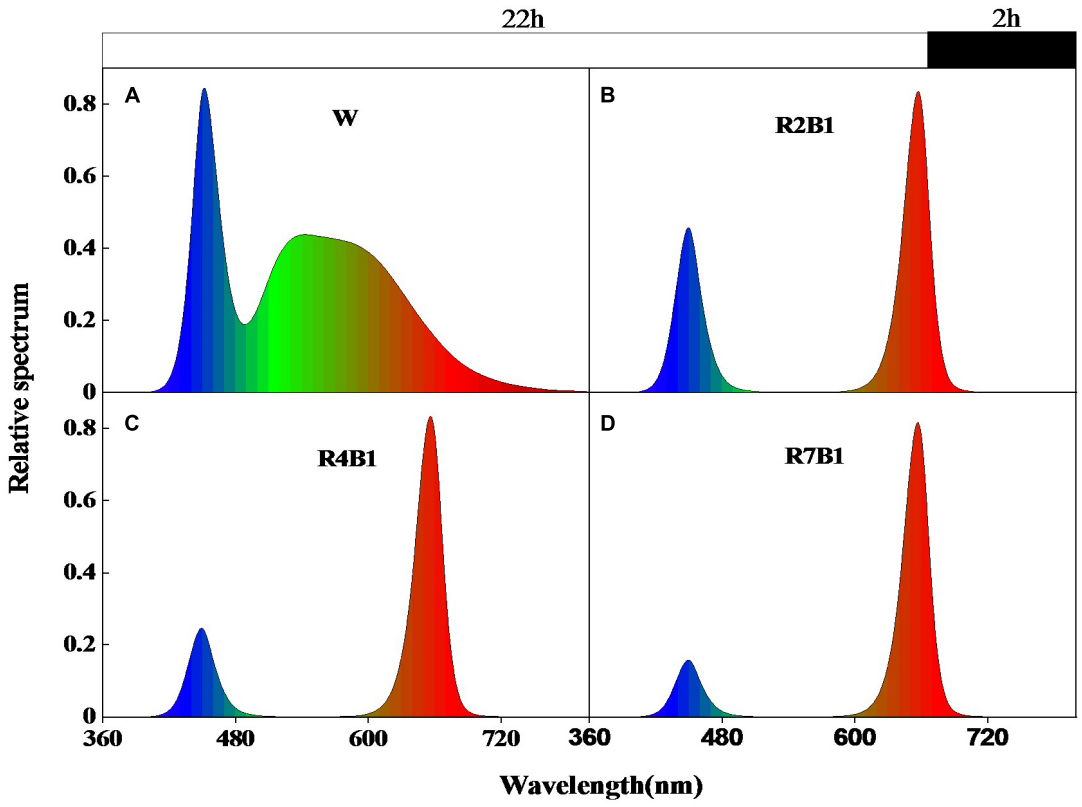

FIGURE 1
Relative spectrum distribution of the four LEDs' light quality combinations. **(A)** White light (W); **(B)** red-blue light ratio 2:1 (R2B1); **(C)** red-blue light ratio 4:1 (R4B1); **(D)** red-blue light ratio 7:1 (R7B1). The white box above the figure represents the light duration of 22 h, and the black box represents the dark time of 2 h.

plants at 105°C in a blast drying oven (DHG-9140a; Lakebo Instrument, Beijing, China) for 1 h, they were dried at 80°C to constant weight, and then the dry weight was measured by an electronic scale.

Antioxidant capacity

The plants were taken out from the ultra-low temperature freezer and ground into powder in liquid nitrogen. Three samples of fresh tissue (0.2 g) from each treatment were homogenized with 50 mmol/L phosphoric buffer (pH 7.8), then centrifuged at 15,000 r/min for 15 min, and the supernatant (enzyme solution) was extracted for POD, CAT, and SOD activity determination.

TABLE 1 Relative spectral content of the four LEDs' light quality combinations.

Light quality treatment	Blue light (%)	Green light (%)	Red light (%)
W	34.06	43.61	22.32
R2B1	35.64	0.42	63.93
R4B1	22.14	0.47	77.38
R7B1	15.87	0.38	83.74

POD and catalase (CAT) activities were determined by the guaiacol method (Liang et al., 2003). The POD activity was determined by the change rate of the absorbance value at 470 nm of the mixed assay of 0.05 ml enzyme solution, 2 ml 0.2% (w/v) H_2O_2, 0.95 ml 0.2% (w/v) guaiacol, and 1 ml pH7.0 phosphoric buffer; 1 ml 0.2% (w/v) H_2O_2 and 1.9 ml distilled water were added into 0.1 ml extracted solution, and the absorbance at 240 nm was measured to determine the CAT activity. The change of absorbance value of 0.01 per minute was token as an enzyme activity unit (U).

SOD activity was determined by nitroblue tetrazole (NBT) photochemical reduction method (Hassan et al., 2005). The 3 ml assay mixture contained 2.5 ml 13 μmol methionine, 0.25 ml 63 μmol/L NBT, 0.15 ml 13 μmol/L riboflavin, 0.05 ml phosphate buffer (pH 7.8), and 0.05 ml enzyme solution. Then it was exposed to light in a 4000-lx light incubator for 20 min, and the absorbance value at 560 nm was measured. One unit of enzyme activity was defined as inhibition of NBT photoreduction by 50%.

The content of malondialdehyde (MDA) was determined by thiobarbituric acid method (Al-Aghabary et al., 2004). Three samples of fresh tissue (0.3 g) from each treatment were homogenized in 0.5% (w/v) thiobarbituric acid and then heated in a boiling water bath for 10 min. After cooling, the homogenate was centrifuged at 3,000 *g* for 15 min. The absorbance value of supernatant was measured at 532, 600, and 450 nm, and the MDA content was calculated by the following formula:

$$MDA(mmol \bullet g^{-1}FW) = [6.452 \times (A_{532} - A_{600}) - 0.559 \times A_{450}] \times V_t/(V_s \times FW)$$

In the formula, V_t represents the total volume of the extract (ml), V_s represents the volume of the extract for measurement (ml), and FW represents the fresh weight of the sample (g).

Nutrition parameters

The content of vitamin C was determined by molybdenum blue colorimetry (Li, 2000). Three samples of fresh tissue (0.2 g) from each treatment were homogenized with 5 ml oxalic acid-EDTA solution, then centrifuged at 3,000 *g* for 10 min. The assay mixture contained 1 ml supernatant, 5 ml oxalic acid EDTA, 0.5 ml metaphosphoric acid-acetic acid, 3.5% (w/v) H_2SO_4, and 5% ammonium molybdate, then the absorbance value was determined at 760 nm, and the content was calculated by a standard curve.

The content of soluble sugar was determined by the anthrone-sulfuric acid method (Fairbairn, 1953). Three dry samples (0.3 g) from each treatment were added to 5 ml distilled water and heated in an 85°C water bath and then centrifuged at 3,500 g for 10 min. After 5 ml anthrone and sulfuric acid were added to the 2 ml supernatant, the absorbance value at 620 nm was measured to determine the content of soluble sugar.

The content of soluble protein was determined by Coomassie brilliant blue G-250 method (Bradford, 1976). Three samples of fresh tissue (0.2 g) from each treatment were homogenized with 2 ml distilled water and centrifuged at 5,000 r/min for 10 min. Then 0.9 ml distilled water and 5 ml coomassie brilliant blue G-250 solution were added to 0.1 ml of the supernatant. The absorbance at 595 nm was measured to determine the content of soluble protein.

Statistical analysis

In plant factories, spatial variability of hydroponic nutrient solution is neglectable and spatial variability of micro-climate is restricted by uniform ventilation from ventilation wall. So spatial replications of LED light treatments are not needed, especially when the LED panels are at the same height in the same level. We regarded this experiment as a completely randomized design. Six plants per treatment were used to measure the growth characteristics, and the determination of antioxidant capacity and nutritional parameters was repeated three times. Excel 2010 was used for data entry and processing. Variance analysis and principal component analysis were conducted using SPSS Statistics 25.0. The comprehensive scores in the principal component analysis of each treatment were calculated through the formula "comprehensive score = variance contribution rate of PC1 × variance contribution rate of FAC1 + PC2 × variance contribution rate of FAC2 + PC3 × variance contribution rate of FAC3" (Li et al., 2022). We used raw data and Origin 2020 for correlation analysis. Graphpad prism 8.0 was used for the creation of histograms. Duncan's multiple range test was used for multiple comparisons in this experiment.

Results

Effects of light spectral combinations on growth characteristics of pea sprouts

As shown in **Figure 2**, the growth characteristics of the two pea sprout cultivars were significantly different. Plant height of black-eyed pea sprouts was significantly higher than that of kaspa peas, and SPAD values of the upper three leaves of kaspa peas were significantly higher than those of black-eyed peas. LED light treatment had significant effects on plant height and SPAD value of the upper third leaf and the interaction of variety and LED light treatment had a significant effect on the SPAD3 (**Supplementary Table 1**). Compared with white light, plant height of black-eyed pea sprouts increased significantly under R4B1. For the kaspa pea sprouts, plant height under R4B1 was slightly higher than that under white light, without significant difference (**Figure 2A**). There was no significant difference in SPAD values of the upper two leaves of kaspa pea sprouts among all the treatments, but the SPAD value of the third leaf under R2B1 and R7B1 was significantly lower than that under white light treatment. For black-eyed pea sprouts, the SPAD value of the upper three leaves showed little difference among different treatments (**Figures 2B–D**).

Effects of different light quality combinations on antioxidant capacity of pea sprouts

Red and blue light ratios significantly affected the antioxidant capacity of pea sprouts (**Figure 3**). There was

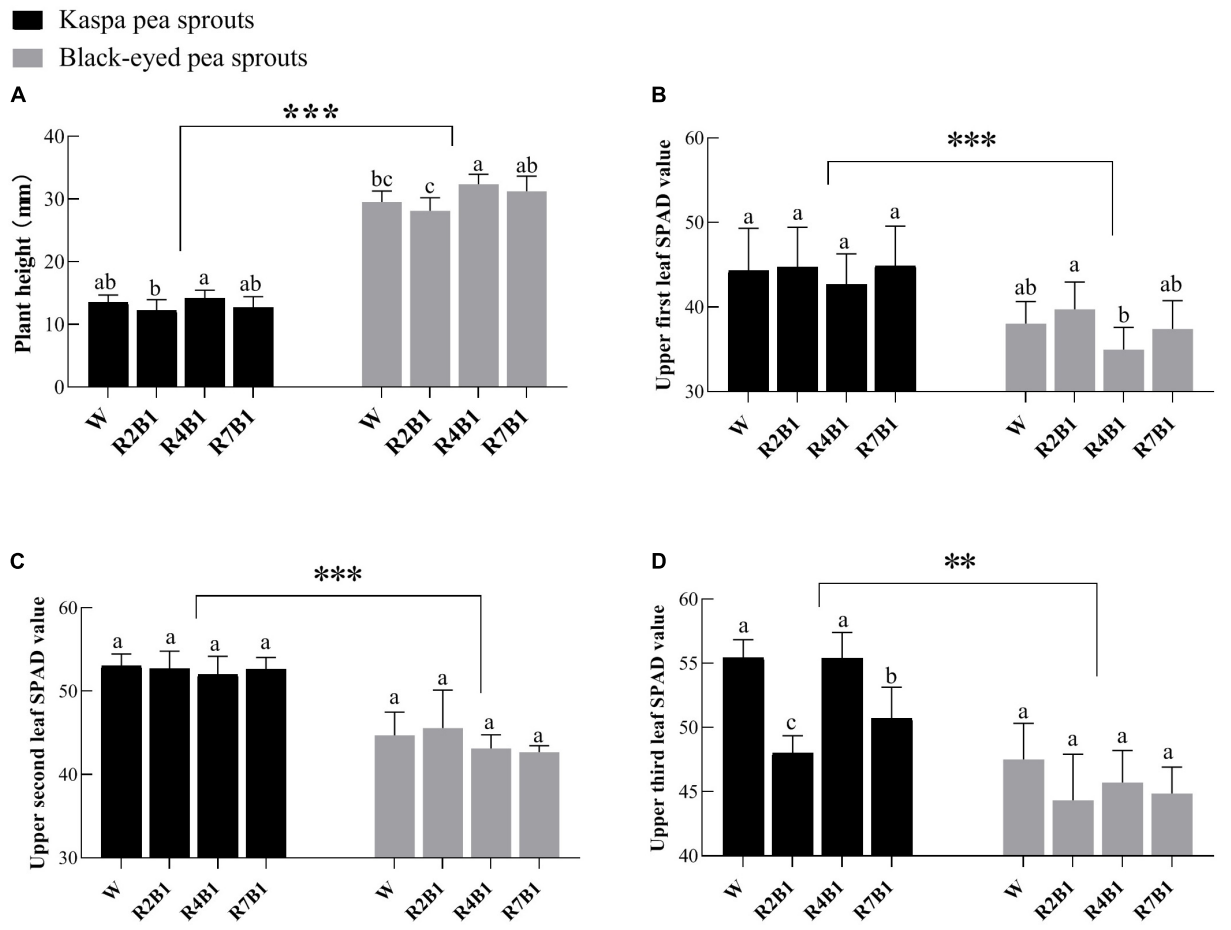

FIGURE 2
Effects of four LEDs' light quality combinations on the plant height and SPAD value of the two cultivars of pea sprouts. **(A)** Plant height; **(B)** upper first leaf SPAD value; **(C)** upper second leaf SPAD value; **(D)** upper third leaf SPAD value. Different letters indicate significant differences at $P \leq 0.05$ of the same variety among treatments. ** and *** denote significant differences at $P \leq 0.01$ and $P \leq 0.001$ of different varieties. Error bars represent six replicates.

no significant difference in POD, SOD, and CAT activities between the two cultivars, while the MDA content of kaspa pea sprouts was two times higher than that of black-eyed pea sprouts. LED light treatment has no significant effect on CAT only and the interaction of variety and LED light treatment had a significant effect on antioxidant capacity (Supplementary Table 1). Activities of POD and SOD of kaspa pea sprouts were significantly higher under R2B1 than those under white light treatment, while there was no significant difference among different light treatments in activities of POD and SOD of black-eyed pea sprouts (Figures 3A,B). There was no significant difference in CAT activity between the two cultivars (Figure 3C). MDA content of black-eyed pea sprouts was significantly lower under R2B1 than that under white light. As the ratio of red light further increased, MDA content was still slightly lower than that under white light (Figure 3D).

Effects of different light quality combinations on yield and quality of pea sprouts

As shown in Figure 4, fresh weight, dry weight, and soluble sugar content of black-eyed pea sprouts were significantly higher than those of kaspa pea sprouts, while there was no significant difference in vitamin C content and soluble protein content between the two cultivars. LED light treatment had significant effects on yield and nutritional quality except for dry weight, and the interaction of variety and LED light treatment had a significant effect on dry weight, soluble sugar content, and soluble protein content (Supplementary Table 1). Fresh weight of kaspa pea sprouts was significantly lower under R2B1 than that under white light, and dry weight of kaspa pea sprouts was significantly lower under R2B1 and R7B1 than that under white light. There was no significant difference in fresh weight

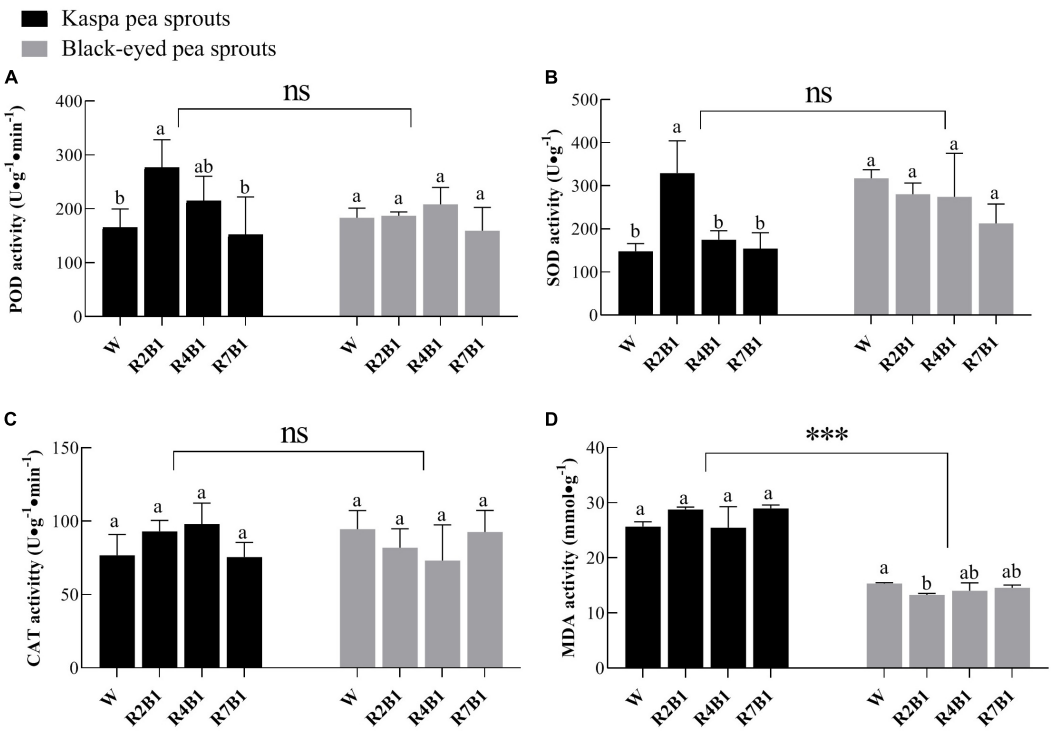

FIGURE 3
Effects of four LEDs' light quality combinations on antioxidant capacity of two cultivars of pea sprouts. **(A)** Peroxidase (POD) activity; **(B)** superoxide dismutase (SOD) activity; **(C)** catalase (CAT) activity; **(D)** malondialdehyde (MDA) content. Different letters indicate significant differences at $P \leq 0.05$ of the same variety among treatments. ***Denotes significant differences at $P \leq 0.001$ of different varieties, and ns means no significant difference. Error bars represent six replicates.

and dry weight of black-eyed pea sprouts among different light treatments (Figures 4A,B).

There was no significant difference in vitamin C content between the two varieties. Soluble sugar content of the two varieties was significantly higher under R2B1 than that under white light. Soluble sugar content decreased with an increase in the proportion of red light, leading to the significantly lower soluble sugar content of kaspa pea sprouts under R4B1 than that under white light. Soluble protein content of kaspa pea sprouts was significantly higher under R2B1 than that under white light, but soluble protein content of black-eyed pea sprouts was significantly lower under R2B1 and R4B1 than that under white light.

Principal component analysis of indicators of pea sprouts under different light quality combinations

Principal component analysis was carried out on 13 parameters including plant height, SPAD value of the upper three leaves, POD, SOD, and CAT activity, MDA content, fresh weight per plant, dry weight per plant, vitamin C, soluble sugar, and soluble protein content of pea sprouts under different light quality combinations. Three principal components PC1, PC2, and PC3 with eigenvalues greater than 1 were extracted, with contribution rates of 49.18, 17.35, and 9.27%, respectively, and a cumulative contribution rate of 75.80%. Plant height, SPAD value of the upper three leaves, MDA, fresh weight, dry weight, and soluble sugar had higher loadings on PC1, indicating that the PC1 basically reflected the information of these eight parameters. In addition, POD, SOD, and soluble protein had higher loadings on PC2, and CAT and VC have higher loadings on PC3. Therefore, these three principal components can be used to represent all indicators for analysis. The comprehensive score results showed (Table 2) that the score of R2B1 was the highest, which is 0.277, indicating that this treatment had the greatest impact on these three principal components. The second was R4B1, with a comprehensive score of 0.063, while R7B1 had the lowest score of −0.208.

Correlation analysis between R: B ratio and various indicators of pea sprouts

The correlations between R: B ratio and various indicators of pea sprouts are shown in Figure 5. Among the growth

10.3389/fpls.2022.978462

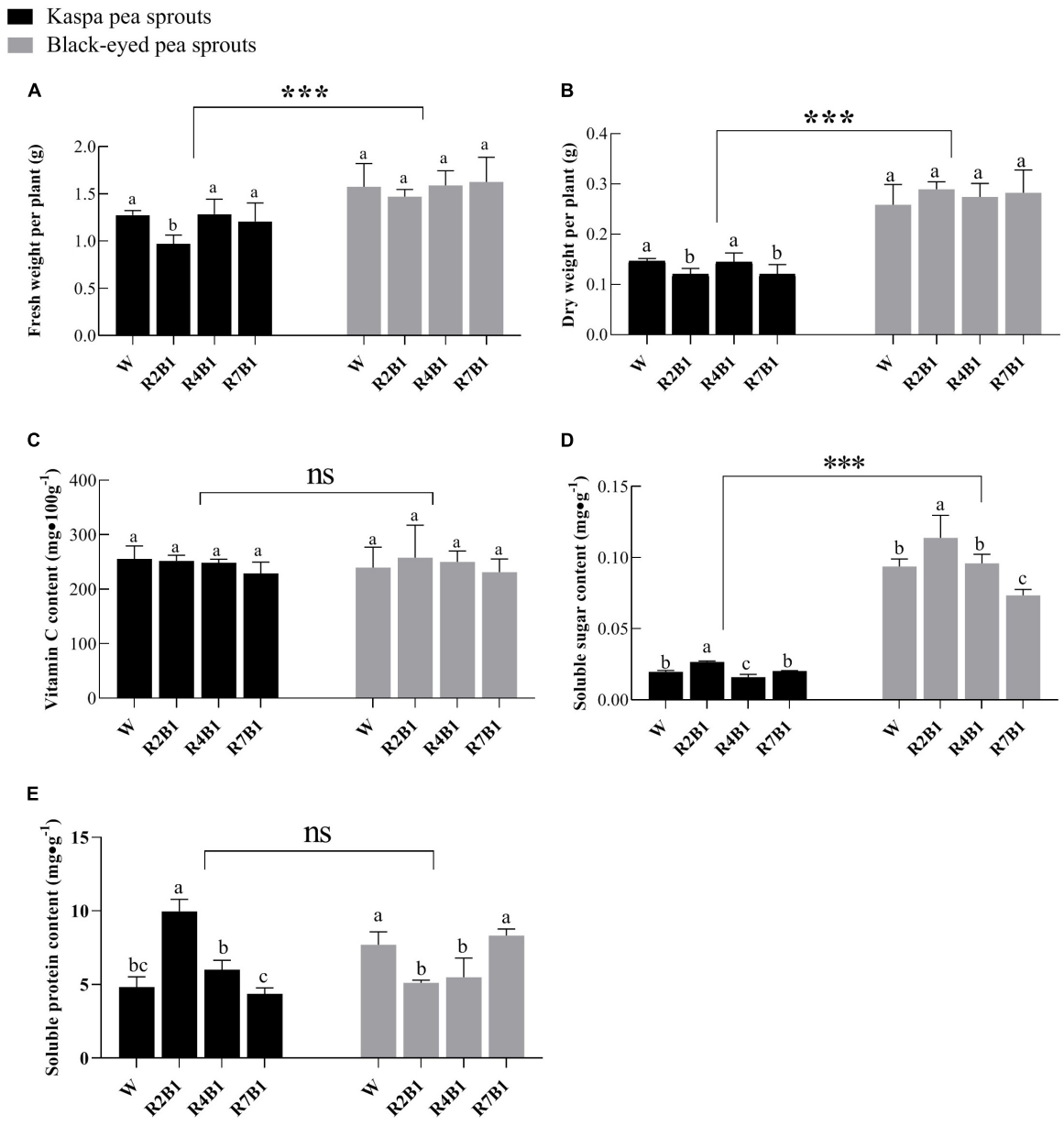

FIGURE 4
Effects of different light quality combinations on the yield and quality of two varieties of pea sprouts. **(A)** Fresh weight per plant; **(B)** dry weight per plant; **(C)** vitamin C content; **(D)** soluble sugar content; **(E)** soluble protein content. Different letters indicate significant differences at $P \leq 0.05$ of the same variety among treatments. ***Denotes significant differences at $P \leq 0.001$ of different varieties, and ns means no significant difference. Error bars represent six replicates.

parameters, blue light was significantly negatively correlated with the plant height of pea sprouts, and red light was significantly negatively correlated with the SPAD value of the upper three leaves. Blue light was positively correlated with SOD activity. Red light was positively correlated with POD activity and MDA content but negatively correlated with SOD and CAT activity, and the correlations were not significant. There was no significant correlation between light quality and yield. Blue light was significantly and positively correlated with vitamin C, soluble sugar, and soluble protein. Red light was negatively correlated with vitamin C, soluble sugar and soluble protein, but the correlation was not significant.

Discussion

With the emergence of LEDs, people can choose different wavelengths of light to regulate the growth of plants. Effects of

TABLE 2 Factor analysis and comprehensive scores of 4 LEDs light treatments.

Treatments	FAC1	FAC2	FAC3	Composite scores
R2B1	0.024	0.780	0.667	0.277
R4B1	0.113	−0.003	0.200	0.063
W	−0.102	−0.189	−0.188	−0.132
R7B1	0.035	−0.639	−0.678	−0.208

FAC1, FAC2, and FAC3 represent the analysis factor scores of the three principal components, respectively.

light quality on vegetables such as lettuce, peppers, tomatoes, and cucumbers have been extensively studied (Li and Kubota, 2009; Su et al., 2014; Kaiser et al., 2019). Red and blue light have an important impact on plant height, chlorophyll, biomass, and photosynthetic capacity (Son and Oh, 2013; Liu and van Iersel, 2021; Liu et al., 2022). A mixture of red and blue light is more conducive to plant growth and development than monochromatic light, but the optimal ratio varies by plant species (Yu, 2021).

In this study, the plant height, antioxidant capacity, yield, and nutritional quality of black-eyed pea sprout were higher than those of kaspa pea sprout, indicating that the effect of light quality on plants was influenced by genotypes. Therefore, in production, it is not only necessary to select optimal light quality but also to choose suitable varieties according to the practical needs. The growth characteristics of pea sprouts under different ratios of red to blue showed that the plant height of pea sprouts was higher under R4B1 than that under white light (**Figure 2**). This was related to the fact that blue light was significantly negatively correlated with the plant height of pea sprouts in the correlation analysis (**Figure 5**). Therefore, the plant height of sprouts was higher when the ratio of red to blue was low, which was consistent with the previous study (Inoue and Kinoshita, 2017). However, the results of the principal component analysis showed that the comprehensive score of R7B1 was the lowest, indicating that it had the least impact on the indexes. Therefore, the plant height of sprouts was the highest under R4B1 instead of R7B1.

Chlorophyll is an important pigment for photosynthesis in green plants, so its content is significantly related to plant growth. The results showed that the SPAD value of the upper three leaves of pea sprouts decreased or did not change significantly under different ratios of red to blue light compared with white light (**Figure 2**). According to previous research reports, blue light can promote the synthesis of chlorophyll because blue light can induce the expression of key genes for chlorophyll synthesis (Liu et al., 2022). But red light reduces chlorophyll content because red light reduces 5-aminolevulinic acid, a precursor to chlorophyll synthesis (Sood et al., 2005). Therefore, the higher proportion of red light than blue light in the treatment of this experiment may be the reason why the SPAD value does not increase.

Under aerobic conditions, the production of reactive oxygen species (ROS) will hurt plant cells. In order to avoid ROS damage, plants have evolved defense systems to eliminate free radicals, including antioxidant and antioxidant enzyme systems (Logan et al., 2006). POD, SOD, and CAT are the main components in the plant antioxidant enzyme system and play important roles in regulating cellular redox state and responding to adverse environmental conditions (Loi et al., 2021). MDA is one of the most important products of membrane lipid peroxidation, and its content can indirectly reflect the degree of damage to the membrane system and the strength of plant stress resistance (Yamauchi et al., 2008). A number of studies have shown that blue light can improve the activity of antioxidant enzymes in many plants (Xu et al., 2014; Ye et al., 2017; Yu et al., 2017). Consistent with the above results, this study indicated that blue light was positively correlated with antioxidant enzyme activities (**Figure 5**), and R2B1 significantly enhanced POD and SOD activities of pea sprouts (**Figure 4**). Compared with white light, R2B1 reduced the MDA content of black-eyed pea sprouts and enhanced the antioxidant capacity of pea sprouts. Cryptochrome absorbing blue light can transmit the signal of stress response and then resist the damage of ROS by improving the activity of antioxidant enzymes (Jourdan et al., 2015).

The differences seen in growth, yield, and nutritional qualities between the two cultivars and among the different light treatments are not only a result of the light qualities tested. In this study, fresh weight and dry weight of kaspa pea sprouts were significantly lower under R2B1 than that under white light, which was consistent with a decrease of SPAD value in leaves under R2B1 (**Figure 2**). Results of previous studies on the effect of light quality on plant nutritional quality are contradictory. Some studies believe that the content of soluble sugar, soluble protein, and vitamin C in pea sprouts was higher when the R:B ratio was 3:1 or higher (Geng et al., 2017; Ban et al., 2019), while others found that the quality of tomato is better when blue light accounts for 60% of total light (Liu et al., 2010). In the study of tomato by Dong et al. (2019), it was found that the sugar content was the highest when the ratio of red to blue was 3:1, because light quality regulated the expression of protein genes related to glucose metabolism. In addition, studies have found that the soluble protein content of radish was higher under blue light than red light, because the nitrate reductase activity was stronger under blue light, which improves the nitrogen assimilation rate of plants (Maevskaya and Bukhov, 2005). However, it was also found that strawberry had higher contents of soluble protein, total sugar, and anthocyanin under red light (Peng et al., 2020). This study found that the content of soluble sugar and soluble protein of kaspa pea sprouts was significantly higher under R2B1 than that of white light, but the soluble protein content of black-eyed pea sprouts decreased under this treatment (**Figure 4**). Therefore, it can be seen that the effect of light quality on crop nutritional quality varies with different crop types and varieties.

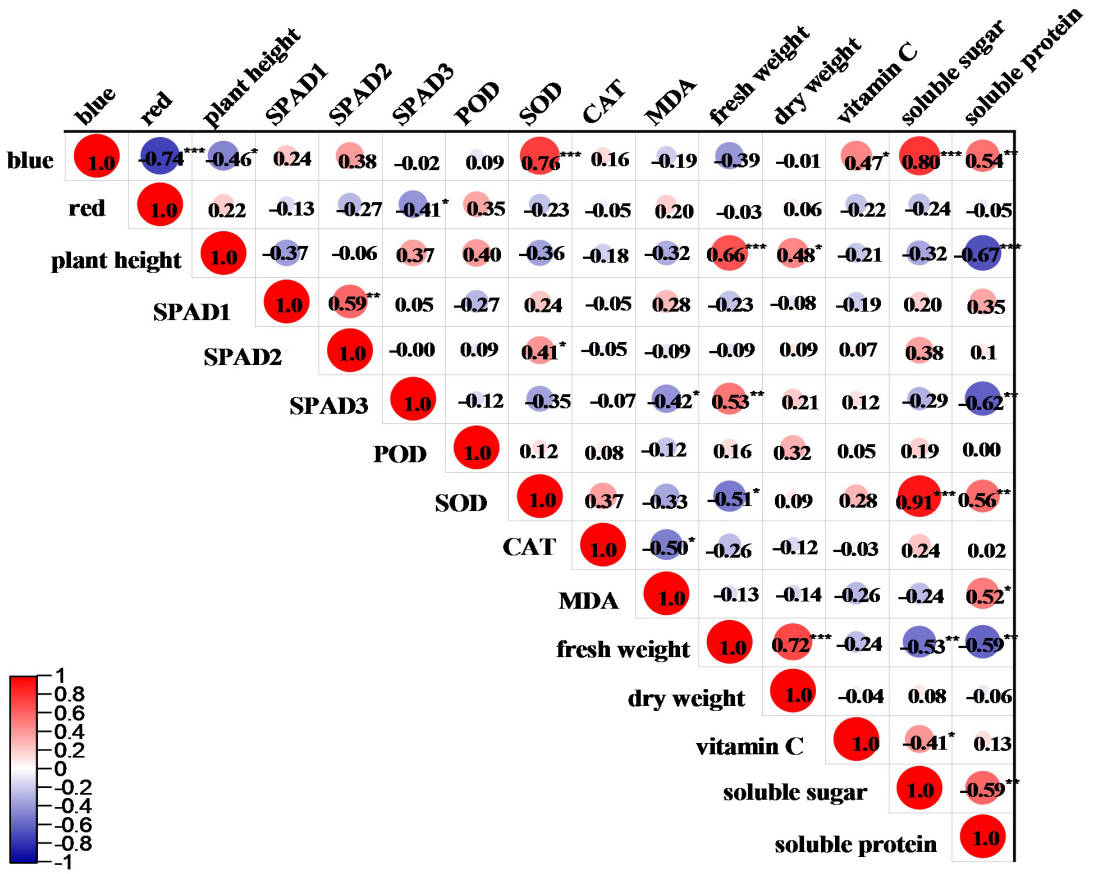

FIGURE 5
Correlation analysis between different light qualities and various indicators of pea sprouts. *, **, and ***Denote significant differences at $P \leq 0.05$, $P \leq 0.01$, and $P \leq 0.001$ of different species. Numbers are correlation coefficients. SPAD1, SPAD2, and SPAD3 denote upper first leaf, upper second leaf, and upper third leaf. Blue and red, respectively, represent the percentage of blue and red light.

Conclusion

Black-eyed pea sprouts had higher plant height, while kaspa pea sprouts had higher SPAD values. Compared with white light, R4B1 significantly increased plant height of black-eyed pea sprouts and slightly increased plant height of kaspa pea sprouts.

MDA content of black-eyed pea sprouts was significantly lower than that of kaspa pea sprouts. R2B1 was optimal to improve POD and SOD activities of kaspa pea sprouts and reduced the MDA content of black-eyed pea sprouts. Antioxidant enzyme activities of black-eyed pea sprouts were not significantly affected by light treatments.

Black-eyed pea sprouts had a higher yield and soluble sugar content than kaspa pea sprouts. Compared with white light, R2B1 reduced the yield but increased the content of soluble sugar and soluble protein of kaspa pea sprouts. Yield of black-eyed pea sprouts was not significantly affected by light quality treatment. R2B1 increased the content of soluble sugar but decreased the content of soluble protein of black-eyed pea sprouts.

Black-eyed pea sprouts have a higher yield and better nutritional quality than kaspa pea sprouts. Among different R:B ratios, R2B1 was the best spectral composition for the nutritional quality of pea sprouts, significantly increased antioxidant enzyme activity, reduced content of MDA, and increased content of soluble sugar of pea sprouts.

Data availability statement

The raw data supporting the conclusions of this article will be made available by the authors, without undue reservation.

Author contributions

SZ and XG performed the experiment, analyzed the data, wrote the manuscript, and equally contributed to the research. JL participated in the experiment. XX and YZ designed and supervised the research. YY and WZ reviewed and edited the

manuscript. All authors have read and agreed to the published version of the manuscript.

Funding

This work was funded by the National and Local Joint Engineering Laboratory for Agricultural Internet of Things (PT2022-23), the National Natural Science Foundation of China (31871563), and China Agriculture Research System of MOF and MARA (CARS-03), and supported by China Agriculture Research System of MOF and MARA Grant CARS-23-D07.

Acknowledgments

We gratefully acknowledge Tiandingxing Optoelectronics Technology Co., Ltd., located in Ningbo, Zhejiang Province, China, for providing the LED lamps, and Yong Li, an engineer from the National Research Center of Intelligent Equipment for Agriculture, for his technical assistance on the precise control of the environment in the control room.

Conflict of interest

The authors declare that the research was conducted in the absence of any commercial or financial relationships that could be construed as a potential conflict of interest.

Publisher's note

Supplementary material

The Supplementary Material for this article can be found online at: https://www.frontiersin.org/articles/10.3389/fpls.2022.978462/full#supplementary-material

References

Adams, S. R., and Langton, F. A. (2005). Photoperiod and plant growth: A review. *J. Hortic. Sci. Biotechnol.* 80, 2–10. doi: 10.1080/14620316.2005.11511882

Al-Aghabary, K., Zhu, Z., and Shi, Q. H. (2004). Influence of silicon supply on chlorophyll content, chlorophyll fluorescence, and antioxidative enzyme activities in tomato plants under salt stress. *J. Plant Nutr.* 27, 2101–2115. doi: 10.1081/LPLA-200034641

Al-Kodmany, K. (2018). The vertical farm: A review of developments and implications for the vertical city. *Buildings* 8:24. doi: 10.3390/buildings8020024

Avgoustaki, D. D., and Xydis, G. (2020). Plant factories in the water-food-energy Nexus era: A systematic bibliographical review. *Food Secur.* 12, 253–268. doi: 10.1007/s12571-019-01003-z

Ban, T. T., Li, X. H., and Ma, C. (2019). Effects of different light qualities on the growth and quality of pea sprouts. *North. Hortic.* 13, 77–82.

Benincasa, P., Falcinelli, B., Lutts, S., Stagnari, F., and Galieni, A. (2019). Sprouted grains: A comprehensive review. *Nutrients* 11:421. doi: 10.3390/nu11020421

Bhandari, L., Sodhi, N. S., and Chawla, P. (2016). Effect of acidified methanol modification on physico chemical properties of black-eyed pea (*Vigna unguiculata*) starch. *Int. J. Food Properties* 19, 2635–2648. doi: 10.1080/10942912.2016.1171236

Bian, Z. H., Yang, Q. C., and Liu, W. K. (2015). Effects of light quality on the accumulation of phytochemicals in vegetables produced in controlled environments: A review. *J. Sci. Food Agric.* 95, 869–877. doi: 10.1002/jsfa.6789

Bradford, M. M. (1976). A rapid and sensitive method for the quantitation of microgram quantities of protein utilizing the principle of protein-dye binding. *Anal. Biochem.* 72, 248–254. doi: 10.1016/0003-2697(76)90527-3

Cao, S., Kumimoto, R. W., Gnesutta, N., Calogero, A. M., Mantovani, R., and Holt, B. F. (2014). A distal CCAAT/NUCLEAR FACTOR y complex promotes chromatin looping at the FLOWERING LOCUS t promoter and regulates the timing of flowering in *Arabidopsis*. *Plant Cell* 26, 1009–1017. doi: 10.1105/tpc.113.120352

Chen, X., Yang, Q., Song, W., Wang, L., Guo, W., and Xue, X. (2017). Growth and nutritional properties of lettuce affected by different alternating intervals of red and blue LED irradiation. *Sci. Hortic.* 223, 44–52. doi: 10.1016/j.scienta.2017.04.037

de Wit, M., Galvao, V. C., and Fankhauser, C. (2016). Light-Mediated hormonal regulation of plant growth and development. *Annu. Rev. Plant Biol.* 67, 513–537. doi: 10.1146/annurev-arplant-043015-112252

Dong, F., Wang, C. Z., Sun, X. D., Bao, Z. L., Dong, C., Sun, C., et al. (2019). Sugar metabolic changes in protein expression associated with different light quality combinations in tomato fruit. *Plant Growth Regul.* 88, 267–282. doi: 10.1007/s10725-019-00506-1

Fairbairn, N. J. (1953). A modified enthrone reagent. *Chem. India.* 31:86

Gan, R., Lui, W., Wu, K., Chan, C., Dai, S., Sui, Z.-Q., et al. (2017). Bioactive compounds and bioactivities of germinated edible seeds and sprouts: An updated review. *Trends Food Sci. Technol.* 59, 1–14. doi: 10.1016/j.tifs.2016.11.010

Geng, J., Li, J., Zhu, F., Chen, X., Du, B., Tian, H., et al. (2022). Plant sprout foods: Biological activities, health benefits, and bioavailability. *J. Food Biochem.* 46:e13777. doi: 10.1111/jfbc.13777

Geng, L. L., Chen, H. T., Qs, L. I., Chen, X., Cui, J., and Yuan, X.-X. (2017). Effects of LED red and blue compound light on yield and nutritional quality of pea sprouts. *Fujian Agric. J.* 32, 1091–1095. doi: 10.19303/j.issn.1008-0384.2017.10.009

Gonzalez, F. G., Slafer, G. A., and Miralles, D. J. (2003). Grain and floret number in response to photoperiod during stem elongation in fully and slightly vernalized wheats. *Field Crops Res.* 81, 17–27. doi: 10.1016/S0378-4290(02)00195-8

Hassan, M. J., Shao, G. S., and Zhang, G. P. (2005). Influence of cadmium toxicity on growth and antioxidant enzyme activity in rice cultivars with different grain cadmium accumulation. *J. Plant Nutr.* 28, 1259–1270. doi: 10.1081/PLN-200063298

Hoagland, D. R., and Arnon, D. I. (1950). The water-culture method for growing plants without soil. *California Agricultural Experimental Station Circular.* 347, 1–32.

Inoue, S., and Kinoshita, T. (2017). Blue light regulation of stomatal opening and the plasma membrane H^+-ATPase. *Plant Physiol.* 174, 531–538. doi: 10.1104/pp.17.00166

Jourdan, N., Martino, C. F., El-Esawi, M., Witczak, J., Bouchet, P. E., d'Harlingue, A., et al. (2015). Blue-light dependent ROS formation by *Arabidopsis* cryptochrome-2 may contribute toward its signaling role. *Plant Signal. Behav.* 10:e1042647. doi: 10.1080/15592324.2015.1042647

Kaiser, E., Ouzounis, T., Giday, H., Schipper, R., Heuvelink, E., and Marcelis, L. F. M. (2019). Adding blue to red supplemental light increases biomass and yield of greenhouse-grown tomatoes, but only to an optimum. *Front. Plant Sci.* 9:2002. doi: 10.3389/fpls.2018.02002

Kearney, J. (2010). Food consumption trends and drivers. *Philos. Trans. R. Soc. B Biol. Sci.* 365, 2793–2807. doi: 10.1098/rstb.2010.0149

Lanoue, J., Thibodeau, A., Little, C., Zheng, J. M., Grodzinski, B., and Hao, X. (2021a). Light spectra and root stocks affect response of greenhouse tomatoes to long photoperiod of supplemental lighting. *Plants* 10:1674. doi: 10.3390/plants10081674

Lanoue, J., Zheng, J. M., Little, C., Grodzinski, B., and Hao, X. M. (2021b). Continuous light does not compromise growth and yield in mini-cucumber greenhouse production with supplemental LED light. *Plants* 10:378. doi: 10.3390/plants10020378

Li, J. (2000). Determination of reduced vitamin C by molybdenum blue colorimetry. *Food Sci.* 8, 42–45. doi: 10.1016/j.talanta.2015.01.024

Li, Q., and Kubota, C. (2009). Effects of supplemental light quality on growth and phytochemicals of baby leaf lettuce. *Environ. Exp. Bot.* 67, 59–64. doi: 10.1016/j.envexpbot.2009.06.011

Li, Y. F., Zhang, H. H., Duan, H. M., Wan, M. L., Ma, X. K., and Wang, Y. P. (2022). Comprehensive evaluation of processed tomato fruit quality in Hexi desert oasis area. *J. Northwest A&F Univ.* 1–10.

Liang, Y. C., Chen, Q., Liu, Q., Zhang, W. H., and Ding, R. X. (2003). Exogenous silicon (Si) increases antioxidant enzyme activity and reduces lipid peroxidation in roots of salt-stressed barley (*Hordeum vulgare* L.). *J. Plant Physiol.* 160, 1157–1164. doi: 10.1078/0176-1617-01065

Liu, J., and van Iersel, M. W. (2021). Photosynthetic physiology of blue, green, and red light: Light intensity effects and underlying mechanisms. *Front. Plant Sci.* 12:619987. doi: 10.3389/fpls.2021.619987

Liu, X. Y., Chang, T. T., Guo, S. R., Xu, Z. G., and Chen, W. H. (2010). Effects of red and blue LED light irradiation on fruit quality of cherry tomato. *Chin. Veg.* 22, 21–27.

Liu, X. Y., Yang, M. J., Xie, X. D., Khaldun, A., Atak, A., Caihong, Z., et al. (2022). Effect of light on growth and chlorophyll development in kiwifruit ex vitro and in vitro. *Sci. Hortic.* 291:110599. doi: 10.1016/j.scienta.2021.110599

Logan, B. A., Kornyeyev, D., Hardison, J., and Holaday, A. S. (2006). The role of antioxidant enzymes in photoprotection. *Photosynth. Res.* 88, 119–132. doi: 10.1007/s11120-006-9043-2

Loi, M., Villani, A., Paciolla, F., Mulè, G., and Paciolla, C. (2021). Challenges and opportunities of light-emitting diode (LED) as key to modulate antioxidant compounds in plants. A review. *Antioxidants* 10:42. doi: 10.3390/antiox10010042

Maevskaya, S. N., and Bukhov, N. G. (2005). Effect of light quality on nitrogen metabolism of radish plants. *Russ. J. Plant Physiol.* 52, 304–310. doi: 10.1007/s11183-005-0046-1

Olle, M., and Virsile, A. (2013). The effects of light-emitting diode lighting on greenhouse plant growth and quality. *Agric. Food Sci.* 22, 223–234. doi: 10.23986/afsci.7897

Oyaert, E., Volckaert, E., and Debergh, P. C. (1999). Growth of chrysanthemum under coloured plastic films with different light qualities and quantities. *Sci. Hortic.* 79, 195–205. doi: 10.1016/S0304-4238(98)00207-6

Peng, X., Wang, B., Wang, X. L., Ni, B. B., and Zuo, Z. J. (2020). Effects of different colored light-quality selective plastic films on growth, photosynthetic abilities, and fruit qualities of strawberry. *Hortic. Sci. Technol.* 38:462. doi: 10.7235/HORT.20200044

Ptushenko, O. S., Ptushenko, V. V., and Solovchenko, A. E. (2020). Spectrum of light as a determinant of plant functioning: A historical perspective. *Life* 10:25. doi: 10.3390/life10030025

Sabzalian, M. R., Heydarizadeh, P., Zahedi, M., Boroomand, A., Agharokh, M., Sahba, M. R., et al. (2014). High performance of vegetables, flowers, and medicinal plants in a red-blue LED incubator for indoor plant production. *Agron. Sustain. Dev.* 34, 879–886. doi: 10.1007/s13593-014-0209-6

Samuoliene, G., Brazaityte, A., Jankauskiene, J., Virsile, A., Sirtautas, R., Noviėkovas, A., et al. (2013). LED irradiance level affects growth and nutritional quality of *Brassica microgreens*. *Cent. Eur. J. Biol.* 8, 1241–1249. doi: 10.2478/s11535-013-0246-1

Sellaro, R., Pacín, M., and Casal, J. J. (2012). Diurnal dependence of growth responses to shade in *Arabidopsis*: Role of hormone, clock, and light signaling. *Mol. Plant* 5, 619–628. doi: 10.1093/mp/ssr122

Son, K., and Oh, M. (2013). Leaf shape, growth, and antioxidant phenolic compounds of two lettuce cultivars grown under various combinations of blue and red light-emitting diodes. *Hortscience* 48, 988–995.

Sood, S., Gupta, V., and Tripathy, B. C. (2005). Photoregulation of the greening process of wheat seedlings grown in red light*. *Plant Mol. Biol.* 59, 269–287. doi: 10.1007/s11103-005-8880-2

Su, N., Wu, Q., Shen, Z., Xia, K., and Cui, J. (2014). Effects of light quality on the chloroplastic ultrastructure and photosynthetic characteristics of cucumber seedlings. *Plant Growth Regul.* 73, 227–235. doi: 10.1007/s10725-013-9883-7

Sudheesh, S., Sawbridg, T. I., Cogan, N. O., Kennedy, P., Forster, J. W., and Kaur, S. (2015). De novo assembly and characterisation of the field pea transcriptome using RNA-Seq. *BMC Genomics* 16:611. doi: 10.1186/s12864-015-1815-7

Sulpice, R., Flis, A., Ivakov, A. A., Apelt, F., Krohn, N., Encke, B., et al. (2014). *Arabidopsis* coordinates the diurnal regulation of carbon allocation and growth across a wide range of photoperiods. *Mol. Plant* 7, 137–155. doi: 10.1093/mp/sst127

van Gelderen, K., Kang, C. K., and Pierik, R. (2018). Light signaling, root development, and plasticity. *Plant Physiol.* 176, 1049–1060. doi: 10.1104/pp.17.01079

Watson, A., Ghosh, S., Williams, M. J., Cuddy, W. S., Simmonds, J., Rey, M.-D., et al. (2018). Speed breeding is a powerful tool to accelerate crop research and breeding. *Nat. Plants* 4, 23–29. doi: 10.1038/s41477-017-0083-8

Xu, F., Shi, L. Y., Chen, W., Cao, S. F., Su, X. G., and Yang, Z. (2014). Effect of blue light treatment on fruit quality, antioxidant enzymes and radical-scavenging activity in strawberry fruit. *Sci. Hortic.* 175, 181–186. doi: 10.1016/j.scienta.2014.06.012

Yamauchi, Y., Furutera, A., Seki, K., Toyoda, Y., Tanaka, K., and Sugimoto, Y. (2008). Malondialdehyde generated from peroxidized linolenic acid causes protein modification in heat-stressed plants. *Plant Physiol. Biochem.* 46, 786–793. doi: 10.1016/j.plaphy.2008.04.018

Ye, S. Y., Shao, Q. S., Xu, M. J., Li, S. L., Wu, M., Tan, X., et al. (2017). Effects of light quality on morphology, enzyme activities, and bioactive compound contents in *Anoectochilus roxburghii*. *Front. Plant Sci.* 8:857. doi: 10.3389/fpls.2017.00857

Yu, T. (2021). *Effects of light environment on the growth and quality of pea and radish sprouts*. Ürümqi: Xinjiang Agricultural University. doi: 10.27431/d.cnki.gxnyu.2021.000025

Yu, W. W., Liu, Y., Song, L. L., Jacobs, D. F., Du, X. H., Ying, Y., et al. (2017). Effect of differential light quality on morphology, photosynthesis, and antioxidant enzyme activity in *Camptotheca acuminata* seedlings. *J. Plant Growth Regul.* 36, 148–160. doi: 10.1007/s00344-016-9625-y

Zhang, X., Bian, Z., Yuan, X., Chen, X., and Lu, C. (2020). A review on the effects of light-emitting diode (LED) light on the nutrients of sprouts and microgreens. *Trends Food Sci. Technol.* 99, 203–216. doi: 10.1016/j.tifs.2020.02.031

Zhao, T., Wang, L., Jiang, H., and Kang, Y. (2020). Study on nutritional quality, functional components and antioxidant activity of bean seeds and their sprouts. *Food Ferment. Ind.* 46, 83–90. doi: 10.13995/j.cnki.11-1802/ts.022141

frontiers | Frontiers in Plant Science

TYPE Original Research
PUBLISHED 08 September 2022
DOI 10.3389/fpls.2022.992194

OPEN ACCESS

EDITED BY
Wei Fang,
National Taiwan University, Taiwan

REVIEWED BY
Genhua Niu,
Texas A&M University, United States
Jung Eek Son,
Seoul National University, South Korea

*CORRESPONDENCE
Masao Kikuchi
m.kikuchi@faculty.chiba-u.jp

†These authors have contributed equally to this work

SPECIALTY SECTION
This article was submitted to Technical Advances in Plant Science, a section of the journal Frontiers in Plant Science

RECEIVED 12 July 2022
ACCEPTED 08 August 2022
PUBLISHED 08 September 2022

CITATION
Zhuang Y, Lu N, Shimamura S, Maruyama A, Kikuchi M and Takagaki M (2022) Economies of scale in constructing plant factories with artificial lighting and the economic viability of crop production. *Front. Plant Sci.* 13:992194. doi: 10.3389/fpls.2022.992194

Economies of scale in constructing plant factories with artificial lighting and the economic viability of crop production

Yunfei Zhuang[1†], Na Lu[2†], Shigeharu Shimamura[3], Atsushi Maruyama[1], Masao Kikuchi[2*] and Michiko Takagaki[1]

[1]Graduate School of Horticulture, Chiba University, Matsudo, Japan, [2]Center for Environment, Health, and Field Sciences, Chiba University, Kashiwa, Japan, [3]HANMO Co., Ltd., Kashiwa, Japan

Since the introduction of LED lamps a decade ago, the plant factory with artificial lighting (PFAL) has been expected to be a savior that overcomes the food crisis, brings food safety, and enhances environmental friendliness. Despite such high expectations, the diffusion of commercial crop production in PFALs has been slow. It has been said that the main reason for this is the huge initial investment required to construct PFALs. This situation has attracted studies to access the economic feasibility of the crop production in PFALs. One thing strange in these studies is that they pay little attention to the scale of their PFALs. PFALs are factories so that they would be subject to economies of scale. If so, the scale of PFALs is an important factor that determines the economic feasibility of plant production in PFALs. However, no study has thus far attempted to examine whether economies of scale exist in the construction of PFALs. To fill this gap, this paper tries to examine, based on the data on the investment cost of PFAL construction collected from various countries and regions in the world, whether economies of scale exist in PFAL construction and, if yes, how it affects the economic viability of the plant production in PFALs by searching for the minimum scale that ensures PFAL crop production economically viable. The results show that economies of scale exist in PFAL construction, and that the production of lettuce, PFALs' most popular crop, is now well on a commercial basis with the technology level of the most advanced PFAL operators, but strawberries has not reached that stage yet. It is also shown that crop production in PFALs is highly sensitive to changes in the yield and the price of the crops: A 30% decline either in the yield or the price of lettuce would easily bring PFALs bankruptcy. It is discussed that the optimum scale of PFALs would depend not only on the economies of scale but also on the transaction costs, such as the costs of searching and keeping a sufficient number of buyers who offer good and stable crop prices.

KEYWORDS

benefit-cost ratio, breakeven scale, lettuce, strawberries, transaction cost, urban agriculture

Introduction

The plant factory with artificial lighting (PFAL), also called synonymously the vertical farm, controlled environment agriculture, and indoor agriculture, grows plants with artificial light in a shielded space like a factory. Although its origin may be traced back to the Hanging Gardens of Babylon in ancient times (Crumpacker, 2018), the PFAL today has only 20–30 years of history (Despommier, 2010; Kozai et al., 2022). Because of its high productivity, high resource use efficiency, high environmental gain, and characteristics that can be located in urban or semi-urban areas, crop production in PFALs has been expected to be an important solution to food security as well as food safety in the urban-overpopulated world in the 21st century (van Delden et al., 2021).

In the early stages of development, commercial production of crops in PFALs was going slowly, mainly because the initial investment needs were prohibitively high (Kozai, 2017). The emergence and introduction of LED lamps at the end of the last century drastically changed the situation (Bantis et al., 2018). It seems that the rapid progress in LEDs and the development of technology associated with the crop production in PFALs since the beginning of this century, especially since the early 2010s, have made the crop production, in particular leafy vegetable production, in PFALs a feasible commercial proposition (Benke and Tomkins, 2017; Pinstrup-Andersen, 2018; Shamshiri et al., 2018; Kozai et al., 2019, 2022).

On the other hand, however, harsh criticism against the PFAL still remains. As late as in 2020, an article appeared in an internationally renowned daily newspaper, questioning "Vertical farming: hope or hype?" (Terazono, 2020). It is pointed out in the article, referring to a Rabobank analyst in Netherlands as the source of information, that "Vertical farming occupies the equivalent of 30 hectares of land worldwide, . . ., compared with outdoor cultivation of about 50 m ha and 500,000 ha for greenhouses." Asia, particularly in Japan, is the region where the commercial operation of PFALs has been going relatively better (Newbean Capital, 2016; Kozai et al., 2019; Harding, 2020). A large-scale survey of greenhouses and PFALs in Japan reveals that the number of PFALs under commercial operation had increased from 64 in 2011 to 197 in 2017 and has been stagnant since then (Japan Greenhouse Horticulture Association [JGHA], 2015-2022). It is estimated that the total cultivated area of these PFALs in 2021 is less than 60 ha, compared with 2 million ha of open upland field and 420,000 ha of greenhouse area in Japan. It could be said that, as in the world, the production of commercial crops by PFALs is hardly widespread even in Japan.

The gap between the hopeful future and the reality of commercial crop production in PFALs appears to be deep worldwide.

Certainly, such circumstances have induced studies on the economic feasibility of vegetable production in PFALs. For example, Eaves and Eaves (2018) and Avgoustaki and Xydis (2020) compare, respectively, the profitability of leafy vegetable production in a PFAL with that in a greenhouse with the conclusion that the PFAL production is more profitable, and the latter gives the internal rate of return to the investment in the construction of the PFAL as high as 35%. Lu et al. (2022) estimate the rate of return for constructing two different walk-in type mini PFALs: 61%/year and 22%/year, respectively. Another study by de Souza et al. (2022) also reports the internal rate of return of 14% for a PFAL. All these studies guarantee the optimistic prospect of PFAL production in terms of economic viability. One exception is Zeidler et al. (2017), which concludes that the production of lettuce and tomato in their PFAL has no economic advantage over the production in greenhouses.

It should be mentioned that the PFALs assessed by these studies are all fixed sizes, all different from small (the PFAL floor area of 3 m^2: Lu et al., 2022) to large (2,625 m^2: Zeidler et al., 2017). A plant factory is a "factory," and in this respect, it is no different from a factory in any industrial sector. One of the most classical findings in industrial economics is that "factories (plants)" are subject to strong economies of scale (e.g., Moore, 1959; Haldi and Whitcomb, 1967). This means that the scale in the construction of PFALs could be an important factor in determining the economic performance of PFAL investments and operations. Almost all the literature on the PFAL, regardless of whether in favor of it or not, points out that the high initial investment cost is the most serious barrier to commercial crop production in PFALs. Though much less, many authors in the literature recognize that economies of scale exist in the construction cost of PFALs (e.g., Burton, 2019; Dahlberg and Lindén, 2019; Harding, 2020; Cambridge HOK, 2021; de Souza et al., 2022). None of them, however, gives any idea as to the degree of economies of scale in the construction of PFALs. If the construction cost of PFALs is subject to economies of scale, what scale of PFALs should we assume in assessing the economic viability of crop production in PFALs?

We have tried to find out some studies that attempt to estimate the economies of scale in PFAL construction but failed thus far. Shao et al. (2016) present a computational model to estimate the possible scale of PFALs for a given budget but give no information on the scale economies at all. In assessing the profitability of lettuce production in a PFAL, de Souza et al. (2022) provide two scenarios as to the scale of the PFAL, in addition to the base scenario, one if the scale is 50% and the other if it is twice as large. However, they assume constant return to scale in the PFAL construction: The capital cost of constructing the PFAL is assumed to be half in the former, and two times in the latter, of the base scenario. They succeed in detecting economies of scale in the current production of lettuce in the PFAL, but not in the PFAL construction.

To fill this gap, in this paper, we first try to estimate the degree of economies of scale in PFAL construction,

using data on PFAL construction costs in Asia, North America, and Europe, and then we examine how the economies of scale affect the economic viability of crop production in PFALs, by estimating the minimum PFAL scale that brings about break-even in the crop production for a few typical crops grown in PFALs. This examination is expected to shed light on, and fill in, the deep gap that exists between the proponents in favor of, and critics against, the future prospect of commercial crop production in PFALs.

Materials and methods

We first explain the methods we adopt in this study and then the data used in the analysis.

Methods

Economies of scale

We are interested in whether investment costs to construct PFALs are subject to economies of scale. Haldi and Whitcomb (1967) find that plant investment costs in many industries are characterized by strong economies of scale. They measure economies of scale empirically as follows:

$$K = a' S^{b'}, \quad (1)$$

where K is the investment cost (US $) to construct a plant, S is the scale of the plant (in terms of output capacity; an example is the total ground area of the plant in m^2), a' is a constant, and the exponent b' is a constant, called the "scale coefficient." Since $(dK/dS)(S/K) = b'$, a value of $b' < 1$ implies that, as the scale increases, the cost increases at a rate of increase less than that of the scale variable, hence increasing returns to scale, in other words, scale economies. Likewise, $b' = 1$ means constant returns and $b' > 1$ implies decreasing returns, or in other words, scale diseconomies.

In our study, we take the total plantable area (the total area of trays on which plants are grown; see sub-section 1-1 of **Supplementary Material** for the definition of this variable) of a PFAL as the variable to measure the scale of the PFAL and see sub-section 1-5 of **Supplementary Material** how different the degree of scale economies if we use PFALs' building total floor are, instead of PFALs' total plantable area.

Dividing through Eq. 1 by S, we obtain

$$(K/S) = a' S^{(b'-1)}, \text{ or}$$
$$I = a' A^{b}, \quad (2)$$

where A (= S) is the total plantable area (m^2), I (= K/S = K/A) is the unit investment cost per plantable area (US $/$m^2$), and $b = b' - 1$. Note that b' is a constant so is b. With this modification, the criterion for economies of scale becomes $b < 0$ for scale economies, $b = 0$ for constant returns, and $b > 0$ for scale diseconomies. We do use the unit investment cost for convenience to compare with the unit benefit obtained from the plant production in PFALs. Taking logarithm for both sides of Eq. 2, we obtain

$$\text{Ln } I = \text{Ln } a' + b\text{Ln } A$$
$$= a + b\text{Ln } A, \quad (3)$$

where a = Ln a'. By estimating this equation by means of the regression method, the *t*-test as to the "scale elasticity" b will tell us whether the PFAL construction cost follows economies of scale.

The actual estimation of this equation is made with several additional variables that control the variances in the dependent variable "I" due to years, countries, and technology levels of sample PFALs. Of these variables, "years" (when sample PFALs were constructed, planned, or uploaded online) is a continuous variable, and all others are dummy variables.

The breakeven minimum scale of PFALs

First, let us define the benefit-cost (B/C) ratio of the investment in the construction of a PFAL in the annual flow term as follows:

$$B/C = P_y Y / \left\{ \left[\sum_i P_i \text{Input}_i \right] + \left[\sum_j w_j \text{Labor}_j \right] + [I/LS] + [\alpha I] + [rI] \right\}, \quad (4)$$

where B = the benefit of the PFAL (US $/plantable area/year), Y = the quantity of the output produced and sold by the PFAL operator (kg/plantable area/year), P_y = the unit price (US $/kg) at which the output is sold ($P_y Y$ is called the revenue), C = the total cost of the PFAL (US $/plantable area/year), Input_i = the quantity of i-th current input used in the production per plantable area per year, P_i = the unit price of i-th current input, Labor_j = labor inputs (person-hours/plantable area/year) used in the production for j-th labor activity, w_j = the wage rate of type j labor (US $/person-hour), I = the unit investment cost of constructing the PFAL (US $/plantable area), LS = the lifespan of the PFAL (years), α = maintenance costs of the PFAL (in % share of the total investment), and r = the interest rate (%/year). Note that the benefit and cost are all defined in terms of "per plantable area."

At B/C = 1, B = C, so that no economic loss. Set B/C = 1 and solve the equation for I,

$$I^* = (P_y Y - \sum_i P_i \text{Input}_i - \sum_j w_j \text{Labor}_j)/(1/LS + \alpha + r)$$
$$= \text{Surplus}/(1/LS + \alpha + r), \quad (5)$$

where I* is the (breakeven) investment that ensures no economic loss in producing the crop in question, and Surplus = $(P_y Y - \sum_i P_i Input_i - \sum_j w_j Labor_j)$. Note that "Surplus" is the profit in the current crop production, with no regard of tax and subsidy. Also note that Eq. 5 requires the following conditions:

$$I^* \geq 0 \text{ and } Surplus \geq 0. \quad (6)$$

Solving Eq. 3 in the previous sub-section with respect to A, we obtain the following equation:

$$A = \text{Exp}\left[(\text{Ln } I - a)/b\right], \quad (7)$$

Inserting I* into Eq. 7, we obtain

$$A^* = \text{Exp}\left\{\left\langle \text{Ln}\left[\text{Surplus}/(1/LS + \alpha + r)\right] - a\right\rangle /b\right\}, \quad (8)$$

A*, thus estimated, is the scale of PFAL that ensures neither economic loss nor profit in producing the crop in question.

Crops to be examined

As crops for which the economically viable minimum scale is examined, we select two crops: lettuce and strawberry.

Leafy vegetables are the most popular crops commercially grown in PFALs worldwide, of which lettuce dominates taking an overwhelmingly large share. The large-scale PFAL surveys in Japan, mentioned earlier, show that more than 90% of commercially operating PFALs have been growing leafy vegetables, and more than 90% of which are made up of lettuce (Japan Greenhouse Horticulture Association [JGHA], 2018, 2019, 2020, 2021, 2022). Lettuce is the first crop to be examined in the context of this paper.

Strawberry is a fruit vegetable. Tomato is the most preferred fruit vegetable in greenhouses and solar-using plant factories, followed by strawberry (Japan Greenhouse Horticulture Association [JGHA], 2015-2022; Costa and Heuvelink, 2018). According to the PFAL surveys, no PFAL operator in Japan had dare tried to grow any fruit vegetable until 2020. In 2021, however, a PFAL operator began to grow strawberry. It is eagerly expected that strawberry is soon added to the list of crops stably produced in PFALs (Kozai et al., 2018, O'Sullivan et al., 2020, Nikkei, 2021, SPREAD, 2021). Strawberry is thus worth to be examined its breakeven minimum scale of PFALs.

Data requirements and data collection

We need three groups of data in this paper. First, data on the unit investment cost, I, and the total plantable area, A, of as many PFALs as possible, to estimate Eq. 3. Second, data on the revenues, costs, and "surplus" in current production of lettuce and strawberry in PFALs, required to estimate I*, the breakeven investment, in Eq. 5 and A*, the breakeven scale of PFALs, in Eq. 8. Third, data on the lifespan of PFAL facilities, the maintenance cost rate, and the capital interest rate in Eqs 5 and 8.

For the first group, we collect data through searching the internet for sites that contain information on PFAL construction costs; monographs, journal papers, survey/project reports, homepages of various organizations, advertisements, online shops, etc. In addition, we design six PFALs of different scales and estimate their construction costs, based on our experiences in designing PFALs.

For the second and the third groups, we obtain necessary data by reviewing the past studies and surveys, including our own data.

Results

Estimation of economies of scale in PFAL construction

PFAL construction cost

We have collected data for 26 PFALs from 14 sources, including ours, for which the necessary data, i.e., the unit investment cost per plantable area (I) and the total plantable area (A), are duly available (**Table 1**). The data sources of these PFALs are presented in **Supplementary Table S1**.

It should be noted that this main dataset is not without problems. Firstly, the dataset consists of data of very different quality. Some data sources give very accurate and highly detailed estimates of the construction costs, while others do give very rough data only. Secondly, the confidentiality of technology and patent information, tax consideration, etc., not only limit the cases where PFAL construction costs are disclosed, but even if information is available, it might possibly give certain undesirable biases to the information disclosed. Thirdly, the dataset includes PFALs constructed and those at design level. The design-level PFALs, though deliberately designed for good performances not only engineeringly, biologically and environmentally but also economically, some revisions might be required if actually built. The number of observations of this dataset, 26, may or may not be sufficient to cancel out biases and errors, if any, caused by these problems. In any case, we should be aware of these problems when interpreting the results.

The 26 sample PFALs in **Table 1** are from five different countries and regions, with relevant years ranging from 2011 to 2021. The construction costs in the table are shown in terms of the current United States dollars, converted from respective local currencies using the exchange rate in respective years. Since the value of the United States dollar has fluctuated little during this period and the use of United States dollars in constant prices has altered the results only slightly without

changing any of our conclusions, we use the cost data in United States dollars in current prices throughout this paper.

Economies of scale

Data on the unit investment cost, I, and the total plantable area, A, in Table 1 are depicted in Figure 1A and the results of regression estimation of Eq. 3 are presented in Table 2. The dataset reveals significant economies of scale, with the scale elasticity of – 0.201 (Regression #1 in Table 2). The dotted line drawn in Figure 1A is the Regression #1, the intercept term of which is adjusted for by evaluating seven non-slope variables from "Year" to "Canada" at their respective means.

Among the 26 sample PFALs, the cost differentials for PFALs of similar scale are large (Figure 1A). At the scale around 100 m^2, the differential in the unit cost is as large as US $ 1,700/m^2 between high cost PFALs and low cost PFALs. Similarly, at the scale around 3,500–4,000 m^2, the unit cost differentials are about US $ 1,300/m^2.

The significant positive regression coefficient of "Year" in Regression #1 in Table 2 suggests that there is a tendency that the unit construction cost of PFALs in recent years is higher than

TABLE 1 List of sample PFALs included in this study, in the order of the scale of PFALs' total plantable area.

PFAL ID	Total plantable area[a]	Cultivation-zone floor area[b]	PFAL building floor area	Planting rack tiers	Total construction cost	Unit construction cost	Technology level[c]	Year[d]	Country	Source ID[e]
	(1) = (2)*(3)	(2)		(3)	(4)	(5) = (4)/(1)				
	m^2	m^2	m^2		US $ 000	US $/$m^2$				
1	100,000	10,000	19,491	10	115,891	1,159	High	2020	United States	1
2	26,013	2,008	6,410	13	39,000	1,499	High	2019	United States	2
3	20,000	1,250	2,625	16	32,635	1,632	High	2015	EU	3
4	4,000	1,000	2,500	4	2,673	668		2011	Japan	4
5	3,780	315	930	12	6,295	1,665		2021	Japan	5
6	3,600	360	1,800	10	2,727	758		2019	Japan	6
7	3,528	321	1,000	11	7,136	2,023	High	2017	Japan	7
8	3,500	292	1,319	12	4,545	1,299		2013	Japan	6
9	3,380	338	676	10	3,591	1,062		2010	Japan	8
10	2,520	315	930	8	5,418	2,150		2021	Japan	5
11	2,184	364	1,000	6	3,208	1,469		2016	Japan	9
12	1,500	167	782	9	3,182	2,121	High	2018	Japan	6
13	1,370	274	391	5	2,500	1,825		2021	Canada	10
14	1,300	130	498	10	2,364	1,818		2013	Japan	11
15	1,225	175	350	7	1,400	1,143		2013	Japan	12
16	1,050	88	357	12	2,007	1,911		2021	Japan	5
17	700	88	357	8	1,744	2,492		2021	Japan	5
18	525	44	165	12	1,209	2,304		2021	Japan	5
19	400	100	417	4	1,364	3,409	High	2016	Japan	6
20	350	44	165	8	1,051	3,004		2021	Japan	5
21	134	22	28	6	145	1,080	Low	2021	Canada	10
22	112	22	28	5	100	893	Low	2021	China	13
23	89	22	28	4	237	2,652		2021	Canada	10
24	61	20	28	3	160	2,609		2021	Canada	10
25	52	10	15	5	60	1,152	Low	2020	China	14
26	12	3	3	4	50	4,167		2020	Japan	14

[a]The summation of the area of planting trays. For definitions of this and other variables, see sub-section 1-1 of Supplementary Material.
[b]The total floor area taken by planting racks = the total bottom area of planting racks.
[c]The level of technology related to the systems of hydroponic production, environment control, and automation of cultivation works, adopted by PFALs. Three levels are distinguished: high (highly advanced, highly automated), average, and low (more primitive, more dependent on manual labor). The PFALs with high technology are those so announced in the data sources. PFALs with low technology are partly those so announced in the sources and partly so identified by the authors. The PFALs, for which this column is blank are of the average technology or those with no information on the technology level.
[d]The year the PFAL was constructed or designed, or its information was uploaded online.
[e]IDs showing data sources, which are explained in Supplementary Table S1.

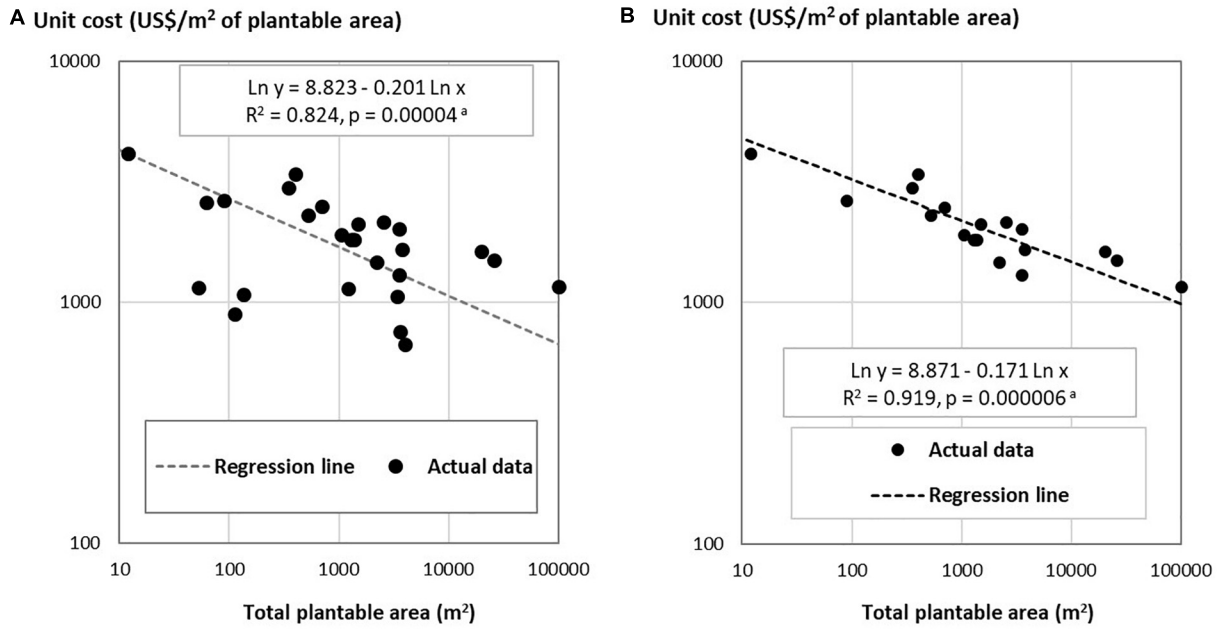

FIGURE 1
The relationship between the unit cost of PFAL construction and the scale of PFAL's total plantable area: panel **(A)** for all sample PFALs (n = 26) and panel **(B)** for above-average PFALs (n = 18). [a]For each chart, the regression line drawn is obtained by inserting the respective means to the seven variables from "Year" to "Canada" of Regression #1 **(A)** and Regression #2 **(B)** in **Table 2**. The probability shown is the probability that the null hypothesis of no slope is accepted.

in earlier years. The significant positive coefficient of "High-tech PFAL" dummy and the significant negative coefficient of "Low-tech PFAL" dummy also suggest that the unit construction cost reflects difference in the technology levels embodied in PFALs. The type of PFAL, such as shipping-container PFAL or ordinary-factory-type PFAL, may also affect the unit-construction cost.

For example, there are three PFALs at the scale around 100 m^2 far below the regression line (**Figure 1A**). These PFALs are of shipping container type, one is using a 20-foot container and the other two each using a 40-foot container. One of these 40-foot container type PFALs, you can buy in an online shop. These are indeed low-cost PFALs, as you may conceive (Alberta Agriculture and Forestry, 2017; Alibaba.com, 2022; Lu et al., 2022). It should be noted, however, that shipping-container type PFALs are not always cheap. There are two PFALs of similar scales, straight above these three PFALs in **Figure 1A**, just on or only slightly below the regression line. These two are of the 40-foot container type, with some advanced technology (Alberta Agriculture and Forestry, 2017).

At the scale around 3,500–4,000 m^2, there are two PFALs, located far below the regression line. One of them is a PFAL, which was planned as early as 2011 by a city government in Japan but ended up unsuccessfully. Straight above this PFAL at a similar scale, three PFALs are found lining up along the top frontier line or just below it. One of them is a PFAL operated by one of the largest PFAL company in Japan well known for its successful vegetable production (Hayashi, 2020). The other two are among those we designed, which could attain the best crop growing performance within the purview of the present PFAL technology with minimum automation.

These observations indicate that the PFALs located below the regression line tend to be those with relatively simpler technology, whereas those on and above the line are of relatively better technology. The regression estimations applied to 18 above-average PFALs and 8 below-average PFALs both show reasonably good fitting, but R^2 of Regression #2 for the above-average PFALs is as high as 0.919, with the sample PFALs that are less scattered, centering around the regression line, as shown in **Figure 1B**. The partial R^2 of the scale variable ("Ln Plantable area") is estimated 0.916 (not shown in **Table 2**), i.e., more than 99% of the R^2 (0.916/0.919) of this regression equation is accounted for by the variance in the scale variable in log transformation. It is rather surprising that the variation in the scale of PFAL alone accounts for nearly 100% of the variation in the unit construction costs of PFAL in different countries explained by the explanatory variables. We will use Regression #2 for the above-average PFALs as the main equation to estimate the economically viable minimum scale of PFALs, with Regression #1 as a reference equation (for a supplementary analysis to check if the PFALs in the main dataset aptly belong to the PFAL population, see sub-section 1.4 of **Supplementary Material**).

10.3389/fpls.2022.992194

TABLE 2 The results of regression analyses applied to the PFAL construction cost data: Regressing Ln (Unit construction cost) on Ln (Plantable area), year and other dummy variables.[a]

Regression number	Regression #1		Regression #2		Regression #3	
	For all PFAL samples (n = 26)[b]		For PFALs above average (n = 18)[c]		For PFALs below average (n = 8)[d]	
	Coeffi.	Prob.	Coeffi.	Prob.	Coeffi.	Prob.
Ln (Plantable area)	**−0.201**	**8.3E−05**	**−0.171**	**5.9E-06**	**−0.283**	**0.001**
Year	**0.048**	**0.008**	**0.030**	**0.028**		
High-Tech PFAL	**0.426**	**0.011**	**0.278**	**0.005**		
Low-Tech PFAL	**−0.844**	**0.006**			**−0.806**	**0.005**
China	-0.345	0.319				
EU	0.243	0.413	0.125	0.417		
United States	0.003	0.992	−0.061	0.669		
Canada	−0.192	0.267	−0.169	0.105		
Intercept	**−87.7**	**0.014**	−50.8	0.054	**9.03**	**1.2E−06**
R^2	0.824		0.919		0.890	
Degree of freedom	17		11		5	

[a]The estimation results of Eq. 3, with the following additional explanatory variables to control "errors and biases." The regression equation to be estimated for the full model of Regression #1 is as follows:

Ln (Unit construction cost) = a + b Ln (Plantable area) + c_1 Year + c_2 High-Tech PFAL + c_3 Low-Tech PFAL + c_4 China + c_5 EU + c_6 United States + c_7 Canada,

where Year = the year the PFAL was constructed, designed, or referred to; High-Tech PFAL = a dummy variable taking 1 if a sample PFAL is said to be with high-technology and 0 if not; Low-Tech PFAL = a dummy variable taking 1 if a sample PFAL is said to be with low-technology and 0 if not; China, EU, United States, and Canada are all dummy variables taking 1 if a sample PFAL is from China, EU, United States, or Canada, respectively, and 0 if not; and a, b, and c_1–c_7 are regression coefficients to be estimated. The base country for the country dummy variables is Japan.

In the table, "Coeffi" stands for regression coefficients estimated and "Prob." for the provability that the null hypothesis that the estimated regression coefficient is not statistically different from 0 is accepted. The probability that is smaller than 0.001 is shown in the index form, e.g., 8.3 E-05 = 8.3×10^{-5}. The coefficients that are shown in bold letters are statistically significant at $p < 0.05$.

[b]R^2 of the simple regression (n = 26) is 0.160 (p = 0.0428).

[c]For the 18 PFALs which are located on and above the regression line in Figure 1A. The PFALs "on" the regression line are defined as those which are located below the regression line but within the neighborhood less than US$ 100/m^2 in the vertical distance. R^2 of the simple regression (n = 18) is 0.754 (p = 3.0E-06).

[d]For the 8 PFALs which are located below the regression line in Figure 1A. Because of the small degree of freedom, the regression equation shown is the only one which gives significant results. R^2 of the simple regression (n = 8) is 0.374 (p = 0.107).

The economically viable minimum scale of PFALs

We estimate the minimum scale of PFALs for lettuce and strawberry, using Eq. 8.

Crop performance in PFALs and other assumptions

For the second and the third data groups, we obtain necessary data by reviewing the past studies and surveys, including our own data. The crop performance of lettuce and strawberries in PFALs are assumed as shown in Table 3.

The yield of lettuce is assumed to be 115 kg/m^2/year. This is a high yield, which used to be challenging to attain several years ago. Thanks to the rapid improvements in LED in recent years, developments of new lettuce varieties suited to the production in PFALs, and PFAL operators' efforts to improve crop growing technology, the yield of lettuce has increased dramatically in the last 5 years or so. The assumed yield level is the level that PFAL operators with advanced growing technology can attain stably (for details, see sub-section 2.1 of Supplementary Material).

The yield of strawberry is assumed to be 20 kg/m^2/year. This is the highest yield level attained in PFALs by researchers in their experiments. The kind of yield revolution, which has happened to lettuce, seems not to have happened yet to strawberry. Unlike in the case of lettuce, we have failed to find out data on the revenue-cost structure of strawberries cultivation in PFALs. We estimate it by referring to the cases of lettuce and other fruit vegetables. Another handicap for strawberry to be grown in PFALs is that its cultivation requires more space than lettuce cultivation for the needs of labor works (for details, see sub-section 2.2 of Supplementary Material).

It should be noted that no subsidy as well as no tax are assumed in the production costs. Taxes are not included because the rates of taxes differ across countries. Subsidies are not included because we are interested in the economic viability of crop production in PFALs without any subsidy. A more important note to make is that no scale economies are assumed in the production costs for lettuce and strawberry production. It is assumed that all cost items are divisible and freely variable without any fixed factor. The production costs could be subject to economies of scale because of such fixed factors as permanent employees paid with monthly or yearly salaries. We make this

assumption for the sake of simplicity in order to focus on the scale economies in PFAL construction.

Equation 8 requires the lifespan of PFAL building and other durable facilities (LS), the rate of maintenance expenses (α), and interest rate (r). We assume LS = 15 years, α = 1.5%, and r = 5% (see section 3 of **Supplementary Material** for more details in these assumptions).

PFALs' breakeven minimum scales

The estimated breakeven scales are presented in **Table 4** for the two crops for the above-average PFALs (**Figure 1B**) and for the average PFALs (**Figure 1A**).

Lettuce

The above-average scale equation gives the scale of 38 m^2 as the breakeven scale. Investing in setting up a PFAL of this scale for lettuce cultivation, you would attain breakeven in your business of lettuce production. The corresponding breakeven investment cost, I* (Eq. 5), is computed as US $ 3,821/m^2, so that the total investment amounts to US $ 145,198 per PFAL. Suppose your planting rack is 5 tiers, then the cultivation-zone floor area in this case is 7.6 m^2. This cultivation-zone floor area, in turn, leads to the PFAL building floor area of about 11 m^2, if we assume that the cultivation-zone area takes up 70% of the building floor area (see sub-section 1.4 of **Supplementary Material**). This scale is close to the scale of PFAL #25 in **Table 1**, which is a 20-foot shipping container type PFAL.

Any PFAL of the scale larger than this breakeven scale gives a positive profit to the operator who grows lettuce. Suppose you invest in constructing a PFAL of 3,000 m^2 of total plantable area (the average scale of commercially operating PFALs in Japan in 2021: Japan Greenhouse Horticulture Association [JGHA], 2015-2022), the unit investment cost of the above-average PFAL of this scale is US $ 1,808/m^2 and the B/C ratio (Eq. 4) is calculated as 1.28, i.e., the annual rate of return of 28%. If we apply the average scale equation (**Figure 1A**), the breakeven scale is reduced to 17 m^2. This scale is a bit larger than 12 m^2 of PFAL #26 (**Table 1**). On this average scale equation, the rate of return for the investment to construct a PFAL of 3,000 m^2 increases to 37% per annum.

Whichever is the case, it is evident that lettuce has established a solid status as a commercially cultivated crop for PFAL operators who attain the level of the revenue-cost performance in lettuce production specified in **Table 3**.

TABLE 3 Assumed levels of lettuce and strawberry production in PFALs and their production costs.[a]

		Lettuce	Strawberries
Plant/fruit weight (1)	g/plant	180	800
Planting density (2)	no. of plant/m^2	80	10
Crops harvested per year (3)		8	2.5
Yield per year (4) = (1)*(2)*(3)/1000	kg/m^2/year	115	20
Harvest loss (5)	%	5	5
Output selling price (6)	US$/kg	11	50
Revenue (7) = (4)*(1−(5))*(6)	US$/$m^2$/year	1,204	950
Current production costs			
Labor	US$/$m^2$/year	279	175
Electricity	US$/$m^2$/year	166	199
Seeds and nutrients	US$/$m^2$/year	86	201
Water and others	US$/$m^2$/year	12	12
Packaging and logistics	US$/$m^2$/year	157	205
Total (8)	US$/$m^2$/year	700	791
Surplus (9) = (7)−(8)	US$/$m^2$/year	**504**	**127** [b]

[a]For details of the estimation and sources of the data, see the second section of **Supplementary Material**.
[b]Adjusted for the 20% reduction in the planted area due to the labor work setting for strawberry production.

TABLE 4 The minimum PFAL scale (total plantable area) at which the break-even is brought about in the commercial vegetable production: lettuce and strawberries.[a]

	Lettuce		Strawberries	
The above-average PFALs[b]	38	m^2	115,697	m^2
The average PFALs[c]	17	m^2	16,131	m^2

[a]Estimated as A* in Eq. 8 in the text. The surplus in lettuce and strawberries production are given in **Table 3**. The assumed levels of LS (life span of PFALs), a (the ratio of maintenance expenditures to the total investment), and r (interest rate) are 15 years, 1.5%, and 5%, respectively. For details, see the third section of **Supplementary Material**.
[b]Based on Regression #2 in **Table 2**, as depicted in **Figure 1B**.
[c]Based on Regression #1 in **Table 2**, as depicted in **Figure 1A**.

Strawberries

The minimum scale for strawberry production in PFALs is estimated to be 115,697 m^2 if the above-average scale equation is applied and 16,131 m^2 if the average scale equation is applied. The former scale is larger than the scale of the largest PFAL that has ever been conceived (PFAL #1 in **Table 1**; Asseng et al., 2020). Even the latter scale is very large if compared to the average scale of commercially operating PFALs. There would be few people who dare want to construct an "above-average" PFAL of a scale greater than the breakeven minimum scale to grow strawberries under the given conditions. You may want to construct an "average" PFAL of the scale larger than the breakeven scale to obtain a positive profit from strawberry production, but the guaranteed annual rate of return on the investment to build a 50,000 m^2 PFAL is estimated to be mere 3.5%. These results suggest that strawberry is still premature to be a crop grown in PFALs on a commercial base.

Sensitivity tests

How the breakeven minimum scale changes as one of the assumed parameters changes? We present the results of sensitivity tests conducted for "the above-average PFALs" to examine how the minimum scale changes, for lettuce, if the

revenue or the labor cost changes, and for strawberries, if the revenue or the electricity cost changes. Since revenue = unit yield × unit output price, a change in revenue by, say, 10%, means either of unit yield or unit price changes by 10% while the other remains constant. Likewise, a positive change in labor cost or in electricity cost means that either the input requirement of labor or electricity increases while the corresponding price remains constant or the price (the wage rate or the electricity charge) changes while the corresponding input requirement remains constant.

The results are shown in **Figure 2** for lettuce and in **Figure 3** for strawberries. It is apparent for both crops that changes in revenue give larger impacts on the minimum scale than changes in a cost item. This is because changes in revenue gives larger impacts on "surplus" than changes in one of cost items (see Eq. 5). For lettuce, if the output price declines by 20% (from US $ 11/kg to US $ 8.8/kg), the breakeven minimum scale increases sharply from 38 to 1,700 m^2. Corresponding to this decline in the lettuce price, the B/C ratio of the investment to build a PFAL of 38 m^2 declines from 1.0 to 0.8. With this lower lettuce price, the PFAL operator of this small scale PFAL faces to a negative rate of return (-20%/year). Should the lettuce price decline by 35% to US $ 7.2/kg, the breakeven minimum scale would increase to more than 100 ha (**Figure 2**).

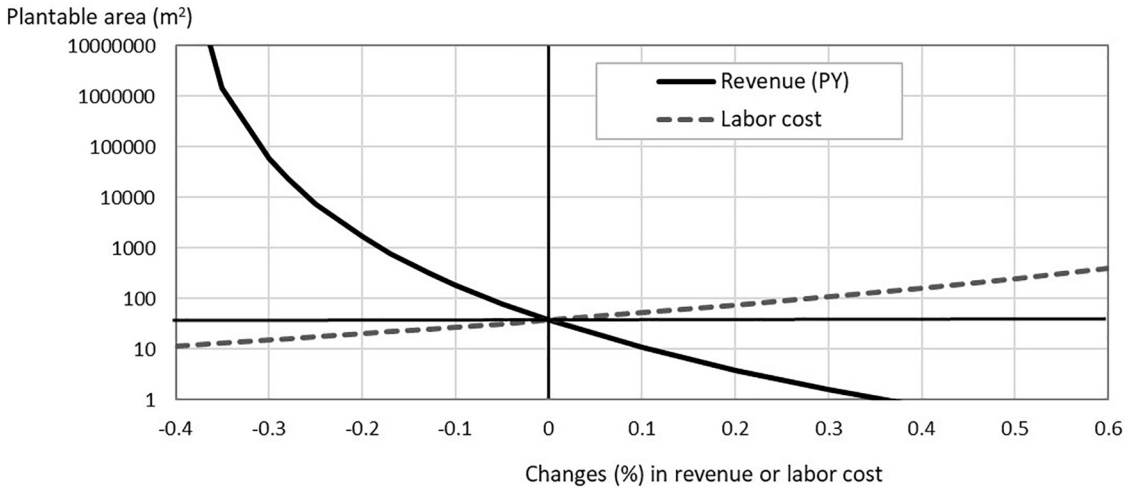

FIGURE 2
Sensitivity analyses for lettuce production in PFALs: How the minimum plantable area, which satisfies (B/C) = 1 in lettuce production, changes when the revenue (PY) or labor cost changes (for the above-average PFALs). The starting point before the change is *the minimum plantable area = 38 m^2, Y = 115 kg/m^2/year, P = US$ 11/kg, and labor cost = US$ 279/m^2/year*.

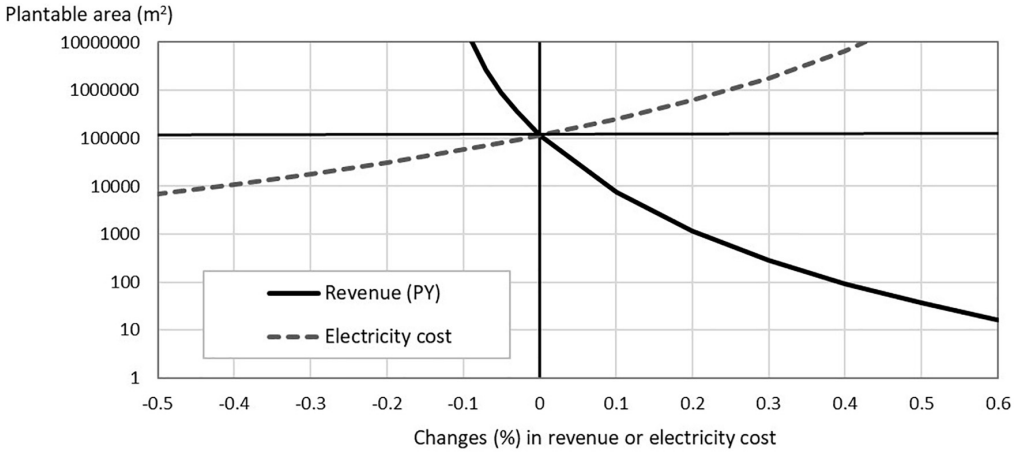

FIGURE 3
Sensitivity analyses for strawberry production in PFALs: How the minimum plantable area, which satisfies (B/C) = 1 in strawberry production, changes when the revenue (PY) or electricity cost changes (for the above-average PFALs). The starting point before the change is *the minimum plantable area = 115,697 m^2, Y = 20 kg/m^2/year, P = US$ 50/kg, and electricity cost = US$ 199/m^2/year*.

In the case of strawberries, a 20% increase in the unit yield from 20 kg/m^2/year to 24 kg/m^2/year by technological advances, or the same rate of increase in the output price because of higher quality of the output, brings about a drastic decline in the breakeven minimum scale from 115,697 to 1,200 m^2 (**Figure 3**), which would convert strawberries to economically viable crop to be grown in PFALs.

Changes in production costs, such as labor cost and electricity cost affect the profitability of crops in PFALs and therefore the breakeven minimum scale. Compared to the degree of impact that changes in the revenue give to the profitability, however, the degree of the impact becomes lower as the cost share of the cost item in the total current production cost becomes lower. For example, a 30 % increase in the wage rate increases the breakeven minimum scale from 38 to 110 m^2 for lettuce (**Figure 2**). Similarly, a 40% decrease in the electricity cost reduces the minimum scale for strawberries, but only down to 10,000 m^2 (**Figure 3**).

Discussions

Economies of scale in PFAL construction

The relatively better-quality subset of the main dataset gives the degree of economies of scale (the scale elasticity) in PFAL construction of -0.17 (**Figure 1B**), with its 95% confidence interval of "-0.12 – -0.22." Another simplest way to estimate the scale elasticity would be to check the slope of the straight line that connects the PFAL of the smallest size (PFAL #26) and that of the largest size (PFAL #1) in **Figure 1B**, which is -0.14. All other sample PFALs are located in between the two PFALs, in the neighborhood around the straight line. It would be highly probable that the true value of the scale elasticity is within this 95% confidence interval.

How economies of scale of PFAL construction are compared with those of other industries? The distribution of the scale elasticity ("b" in Eqs 2 and 3) of industrial plant investment estimated by Haldi and Whitcomb (1967) has the mode for the elasticity class of [-0.2 > b > -0.3], with the mean of -0.27. In the case of infrastructure project such as irrigation scheme construction, this elasticity is as large as -0.7 (Inocencio et al., 2007). Comparing to these industries, the scale elasticity of -0.17 is not large. One reason for this observation may be that the PFAL construction cost in this paper includes not only the costs of constructing the factory building but also the costs of installing various facilities and equipment in the factory, such as hydroponic cultivation systems, LED lighting systems, planting racks, etc. These facilities and equipment, though fixed production factors, may be more "divisible" than the factory building, which reduces the degree of scale economies for the total investment.

Though not so large compared to other industries, the mean estimate of the scale elasticity of -0.17 still means that, when the scale of PFALs increases 10, 100, and 1,000 times, say from 100 to 1,000 m^2, to 10,000, and to 100,000 m^2, the unit cost of PFAL construction decreases by 33, 55, and 80%, respectively.

Economically viable crops in PFAL production

A basic implication derived from the results of our exercise is that the list of crops that can be grown commercially in PFALs is very short at present.

It must be clear that grain crops, such as wheat, are out of question. Asseng et al. (2020) concluded in their highly intensive study that wheat production in PFAL of 10 ha scale, or even of 100 ha scale, cannot be economically viable under the present price conditions for wheat and production inputs. It should be noted that their conclusion does not depend on the oft-mentioned barrier to the commercial crop production in PFALs, i.e., "high initial investment cost." In their case, wheat is not an economically viable crop simply because the current production of wheat in PFALs cannot generate any positive profit, or "surplus" in our Eq. 5: The cost of constructing the PFAL and its scale are nothing to do with their conclusion. In this respect, their wheat case is different from our strawberry case. In the latter case, the current production of strawberries in PFALs can generate "surplus," but it is not enough to justify the investment to construct a PFAL: The case the "initial investment cost" matters.

Lettuce is an economically viable crop in PFAL production. It should be pointed out again that such a status of lettuce has been established by the yield revolution that occurred in recent years because of improvements in LED technology, new lettuce varieties, and efforts made by PFAL operators to advance lettuce growing technology in PFALs. This point cannot be overemphasized. Until 2017, the unit yield of lettuce in PFAL production in Japan had been less than 60 kg/m^2/year (see subsection 2.1 in **Supplementary Material**). **Table 3** in the text, after simple calculations, tells that the unit yield of lettuce less than 67 kg/m^2/year fails to give any positive surplus. Under such a condition, lettuce is no difference with the wheat case above as far as commercial production in PFALs is concerned: They are equally economically not viable, regardless of the cost of PFAL construction.

The results of our exercise suggest that strawberry production in PFALs under present conditions is not economically viable yet but about to be added to the list of PFAL crops. The sensitivity test shows that a 20% increase in the unit yield transforms it to a crop that is profitably grown. A breakthrough in cultivation technology to increase its yield

or to reduce its production costs is expected to come soon, as in lettuce production.

Vulnerability in crop production in PFALs

The sensitivity tests show that the PFAL's breakeven minimum scale for lettuce production quickly approaches infinity as the decline in the revenue progresses beyond the decline rate of 30% (**Figure 2**). This is because the "surplus" approaches zero as the revenue continues to decline. In the case of crop production in PFALs, yield may increase, but not likely to decrease significantly. In contrast, the risk that the output price declines significantly could be high for PFAL operators. Their market outlets are generally not ordinary wholesale markets (see **Supplementary Table S7**) but direct off-market shipments to supermarkets, ready-to-eat food manufacturers, delicatessens, and restaurants under contracts. To the extent less dependent on the ordinary markets, they face to less risk in seasonal price fluctuations in the markets. Instead, they would have to face to the risk of losing some contracts or requests from contractors for downward price revisions. Such risks could be high because they have many contacts with business partners. In the case of PFAL operators in Japan, on average, each PFAL operator has as many as 30 contracts with buyers, and 30% of them have more than 50 contracts (see **Supplementary Table S7**). Demand for vegetables of the off-market buyers such as supermarkets, delicatessens, and restaurants may not be subject to seasonal fluctuations, but could be affected by rapidly changing end-consumers' teste and preference, and these shops and restaurants themselves are operating in tightly competitive markets where the rise and fall of stores and shops is fierce.

The high sensitivities of the rate of return to the investment in PFAL construction to changes in basic parameters related to the crop performance are reported by some past studies. The internal rate of return to the investment on PFAL construction for growing basil ranges wide from 0.04 to 98% among nine scenarios tested (Avgoustaki and Xydis, 2020). Similarly, another case of PFAL construction for growing lettuce, the rate of return to the investment varies among nine scenarios examined from -0.5 to 38% (de Souza et al., 2022). A recent paper by Baumont de Oliveira et al. (2022), assessing financial risk for PFALs, reports that a PFAL actually constructed in the United Kingdom goes bankrupt with p = 100% (the case of a negative surplus in the current lettuce production account), if without any intervention, and that the other designed PFAL in Japan (the same PFAL assessed by de Souza et al., 2022 = our PFAL #11) would face, in its 15-year life span, a negative financial balance at about p = 30% and below-threshold rates of returns to the investment at about p = 50%.

While vegetable production by PFALs is highly touted as "promising," it is still said to be "hype" (Terazono, 2020; Gordon-Smith, 2021). A reason for this could be the fact that many commercial PFALs have been built so far, many of which have ended up in bankruptcy. As mentioned earlier in this paper, the number of PFALs in Japan has been stagnant since 2017. This does not mean that the PFAL vegetable production industry is in a stationary state. On the contrary, there has been substantial number of new entries in this industry but there has been nearly the same number of exits. Available data suggest that, within a period of 10 years since 2012, nearly 80% of PFALs in Japan have disappeared, being replaced with nearly the same number of new ones (see section 4.2 of **Supplementary Material**).

One of the most likely causes of this bankruptcy is the high risk associated with the instability in price and contract, which gives serious adverse impacts on profitability. The results of the sensitivity test suggest that lettuce production in PFALs is economically viable, but it is subject to high vulnerability. When planning to establish a PFAL for commercial engagement, it is necessary to have an ample leeway or measures that can sufficiently withstand the risk of instability in output and input prices and in sales and cultivation contracts.

PFALs' optimum scale?

The construction of PFALs is subject to economies of scale: The larger the scale, the lower the unit investment cost. As everyone points out, the initial investment cost is the most serious entry barrier. Then, does the scale of PFALs continue to increase to enjoy ever lower initial unit investment costs? In some industries characterized by huge facilities and structures of public nature, such as the power generation and gas supply industries, the scale of plants continues to increase to the extent that the industry becomes a regional monopoly consisting of only one huge company. In many industries, however, this does not occur: The ever-increasing scale is checked at somewhere before this stage. The checking factor is generally called "transaction costs."

Transaction costs are non-monetary costs that are associated with economic transactions (Williamson, 1979). For example, a PFAL operator has to search if there are someone who buy crops produced by the PFAL, find them out, negotiate with them about the prices and quantities, make contracts, enforce the contracts, and take appropriate actions in case of breach in the contracts: All these actions (transactions) are not costless, or rather often very costly to the PFAL operator. As the number of contractors increases, the transaction costs could increase, even disproportionally. The PFAL operator has to hire laborers and you may have to monitor to have them work carefully with plants. This cost for monitoring and enforcing labor contracts is another example of transaction costs, which would become more costly as the scale of your

PFAL becomes larger. Fund markets are prone to market failures, and you may face difficulties in raising funds when planning to construct a PFAL of large scale, which is also a transaction cost.

In Asia, the proliferation of delicatessens, ready-to-eat food manufactures, and restaurants have made themselves good customers of vegetable-producing PFALs. Small- to medium-scale PFALs sell their vegetables, which do not need to be washed before cooking, to many of these customers in small individual packages so that the customers can use them immediately without the hassle of arranging them into small units. As a result, they enjoy a higher unit price for their vegetables than they sell to the ordinary wholesale market. Large-scale PFALs, on the other hand, tend to sell their mass-produced vegetables in bulk to buyers, such as regional centers of large supermarket chains, at low prices. Such a difference should result from high transaction costs associated with dealing with a large number of customers by delivering vegetables in small packaging (often tailor-made for individual customers). The price difference between individual packaging delivery and bulk sales often exceeds 30% (for more details, see sub-section 2.1 of **Supplementary Material**).

These transaction costs would work to counterbalance the merit of economies of scale. It is an important research agenda to study how these transaction costs and economies of scale in PFAL construction interact, or counteracts, in determining the scale of PFALs and how the optimal scale differs among the type of crops grown and among the various modes of PFAL management.

Conclusion

In this paper, for the first time in this research field, we have explored whether economies of scale exist in the construction of PFALs and how it affects to the economic viability of vegetable production in PFALs.

We find that economies of scale exist in the costs to construct and set up PFALs. The relatively better-quality subset of our datasets gives the 95% confidence interval of the scale elasticity as "-0.12 to -0.22" with the mean estimate of -0.17. Not a large elasticity compared with other industries, but with this mean elasticity the unit construction cost declines by as much as 55%, to a level less than half, when the scale of PFALs increases 100 times.

The minimum scale, which ensures the breakeven in the crop production in PFALs, is estimated to be less than 40 m^2 for lettuce and more than 100,000 m^2 for strawberries, suggesting that the former is an established PFAL crop, but the latter is not yet. The recent revolutionary increase in the yield due to improvements in LED technology, new lettuce varieties, and PFAL operators' efforts to finetune these new "inputs" toward higher yields has helped lettuce to establish this status. It would be almost certain that such technological advances do occur, sooner or later, for strawberries and other candidate crops for PFAL production.

The breakeven minimum scale is extremely sensitive to changes in the variables to determine the profitability of crop production in PFALs. The impacts of changes in the unit yield of the crop and its price, which together determine the revenue, are particularly large. A 30% decline in the lettuce price puts most lettuce producing PFALs on the brink of bankruptcy, while a 20% increase in the unit yield or the price of strawberries transforms strawberries into an economically viable PFAL crop. This overly sensitive nature of the commercial crop production in PFALs is behind the current state of the crop production in PFALs where many PFALs go bankrupt while being replaced by many newcomers every year. Both pros and cons of PFALs have the grounds for their claims. If you make a claim by looking at only one side of the fact, not knowing or ignoring the other side, however, it could be called "hype."

The existence of economies of scale may transform the PFAL crop production industry into an industry where large PFALs are more popular than today. However, the emergence of excessively large-scale PFALs would be restricted by transaction costs that are inherent in various aspects of the management of PFAL crop production. Transaction costs typical of the plant factory business would arise from the needs to develop and maintain stable and good-price-offering buyers and to manage the workforce for high-quality plant production. How these transaction costs and economies of scale in PFAL construction interact in determining the optimum scale of PFALs is an important research agenda to be addressed in the future.

Data availability statement

The sources of all the data used in this article are presented either in the main text or in the **Supplementary material**. Further inquiries are entertained upon request to the corresponding author.

Author contributions

MK, YZ, NL, and MT: conceptualization. YZ, MK, SS, and AM: methodology, data preparation, and investigation. MK: writing—rough draft. YZ, MK, NL, AM, and MT: writing—final draft, review, and editing. MK, MT, and NL: supervision. All authors contributed to the article and approved the submitted version.

Acknowledgments

We would like to thank Toyoki Kozai for lecturing us about the early development history of PFALs, including the information on PFALs' construction costs and their secret nature. Possible errors and mistakes in this manuscript, if any, are due solely to us.

Conflict of interest

SS was employed by HANMO Co., Ltd.

The remaining authors declare that the research was conducted in the absence of any commercial or financial relationships that could be construed as a potential conflict of interest.

Publisher's note

Supplementary material

The Supplementary Material for this article can be found online at: https://www.frontiersin.org/articles/10.3389/fpls.2022.992194/full#supplementary-material

References

Alberta Agriculture and Forestry (2017). *Vertical farming case study*. Available Online at: https://open.alberta.ca/dataset/1c1f48a2-63b9-4dcb-823c-aa49a9a7c810/resource/b0cdfe26-7058-4ee9-a40a-7a3dcff2fe89/download/af-vertical-farming-case-study-2021-04.pdf [accessed January 2, 2022].

Alibaba.com (2022). *Hydroponic vertical plant factory 40ft container greenhouse for agriculture LED plant growing system. On-line shop*. Available Online at: https://www.alibaba.com/productdetail/Hydroponic-vertical-plantfactory-40ftcontainer_1600118796279.html?spm=a2700.7724857.normal_offer.d_image.2e38243avbl9Mj [accessed January 12, 2022].

Asseng, S., Guarin, J. R., Raman, M., Monje, O., Kiss, G., Despommier, D. D., et al. (2020). Wheat yield potential in controlled-environment vertical farms. *Proc. Natl. Acad. Sci. U.S.A.* 117, 19131–19135. doi: 10.1073/pnas.2002655117

Avgoustaki, D. D., and Xydis, G. (2020). Indoor vertical farming in the urban nexus context: Business growth and resource savings. *Sustainability* 12:1965. doi: 10.3390/su12051965

Bantis, F., Smirnakou, S., Ouzounis, T., Koukounaras, A., Ntagkas, N., and Radoglou, K. (2018). Current status and recent achievements in the field of horticulture with the use of light-emitting diodes (LEDs). *Sci. Hortic.* 235, 437–451. doi: 10.1016/j.scienta.2018.02.058

Baumont de Oliveira, F. J., Ferson, S., Dyer, R. A. D., Thomas, J. M. H., Myers, P. D., and Gray, N. C. (2022). How high is high enough? Assessing financial risk for vertical farms using imprecise probability. *Sustainability* 14:5676. doi: 10.3390/su14095676

Benke, K., and Tomkins, B. (2017). Future food-production systems: Vertical farming and controlled-environment agriculture. *Sustain. Sci. Pract. Policy* 13, 13–26. doi: 10.1080/15487733.2017.1394054

Burton, R. (2019). *The future of vertical farming: The intelligent ecosystem*. Cambridge: Cambridge Consultants.

Cambridge HOK (2021). *How much does vertical farming cost?*. Available Online at: https://cambridgehok.co.uk/news/how-much-does-vertical-farming-cost [accessed January 3, 2022].

Costa, J. M., and Heuvelink, E. P. (2018). "The global tomato industry," in *Tomatoes*, ed. E. Heuvelink (Boston, MA: CABI), 1–26.

Crumpacker, M. (2018). *A look at the history of vertical farming*. Available Online at: https://medium.com/@MarkCrumpacker/a-look-at-the-history-of-verticalfarming-f4338df5d0f4 [accessed May 18, 2022].

Dahlberg, A., and Lindén, A. (2019). *Can vertical farms outgrow their cost?-An analysis of the competitive strength of vertical*. Available Online at: https://odr.chalmers.se/bitstream/20.500.12380/256972/1/256972.pdf [accessed May 18, 2022].

de Souza, S. V., Peterson, H. C., and Seong, J. (2022). "Emerging economics and profitability of PFALs," in *Plant factory basics, applications and advances*, eds T. Kozai, G. Niu, and J. Masabni (Amsterdam: Elsevier), 251–270. doi: 10.1016/B978-0-323-85152-7.00025-2

Despommier, D. (2010). *The vertical farm: Feeding the world in the 21st century*. London: Macmillan.

Eaves, J., and Eaves, S. (2018). Comparing the profitability of a greenhouse to a vertical farm in Quebec. *Can. J. Agric. Econ.* 66, 43–54. doi: 10.1111/cjag.12161

Gordon-Smith, H. (2021). *Vertical farming is headed for the 'trough of disillusionment.' Here's why that's a good thing*. Available Online at: https://agfundernews.com/vertical-farming-is-headed-for-the-trough-of-disillusionment-heres-why-thats-a-good-thing [accessed March 13, 2022].

Haldi, J., and Whitcomb, D. (1967). Economies of scale in industrial plants. *J. Polit. Econ.* 75, 373–385.

Harding, R. (2020). *Vertical farming finally grows up in Japan*. London: Financial Times.

Hayashi, E. (2020). "Selected PFALs in Japan," in *Plant Factory*, (Amsterdam: Elsevier), 437–454. doi: 10.1016/B978-0-12-816691-8.00030-3

Inocencio, A., Kikuchi, M., Tonosaki, M., Maruyama, A., Merrey, D., Sally, H., et al. (2007). *Costs and performance of irrigation projects: A comparison of sub-Saharan Africa and other developing regions*. Anand: International Water Management Institute.

Japan Greenhouse Horticulture Association [JGHA] (2015-2022). *Survey and case report on large-scale greenhouses and plant factories (each-year edition) (in Japanese)*. Available Online at: https://jgha.com/dl [accessed March 1, 2022].

Kozai, T. (2017). "Benefits, problems and challenges of plant factories with artificial lighting (PFALs): A short review," in *Proceedings of the international symposium on new technologies for environment control, energy-saving and crop production in greenhouse and plant*, Vol. 1227, Beijing, 25–30.

Kozai, T., Hayashi, E., and Amagai, Y. (2018). "Plant factories with artificial lighting (PFALs) toward sustainable plant production," in *Proceedings of the XXX international horticultural congress IHC2018: II international symposium on soilless culture and VIII international*, Vol. 1273, Istanbul, 251–260.

Kozai, T., Niu, G., and Masabni, J. G. (2022). *Plant factory basics, applications and advances*. Cambridge, MA: Academic Press.

Kozai, T., Niu, G., and Takagaki, M. (2019). *Plant factory: An indoor vertical farming system for efficient quality food production*. Cambridge, MA: Academic Press. doi: 10.1016/C2018-0-00969-X

Lu, N., Kikuchi, M., Keuter, V., and Takagaki, M. (2022). "Business model and cost performance of mini-plant factory in downtown," in *Plant factory basics, applications and advances*, eds T. Kozai, G. Niu, and J. Masabni (Amsterdam: Elsevier), 271–293. doi: 10.1016/B978-0-323-85152-7.00002-1

Moore, F. T. (1959). Economies of scale: Some statistical evidence. *Q. J. Econ.* 73, 232–245. doi: 10.2307/1883722

Newbean Capital (2016). *The rise of Asia's indoor agriculture industry*. Available Online at: http://agfundernews.com/wp-content/uploads/2016/01/The-Rise-of-Asias-Indoor-Agriculture-Industry-White-Paper_FinalProtected.pdf [accessed March 13, 2022].

Nikkei (2021). *NTT West (Nippon Telegraph and Telephone West Corporation) sells strawberries: Year-round harvest at a plant factory (in Japanese)*. Available Online at: https://www.nikkei.com/article/DGXZQOUF105BK0Q1A810C2000000/ [accessed June 20, 2022].

O'Sullivan, C. A., McIntyre, C. L., Dry, I. B., Hani, S. M., Hochman, Z., and Bonnett, G. D. (2020). Vertical farms bear fruit. *Nat. Biotechnol.* 38, 160–162.

Pinstrup-Andersen, P. (2018). Is it time to take vertical indoor farming seriously? *Glob. Food Sec.* 17, 233–235.

Shamshiri, R., Kalantari, F., Ting, K. C., Thorp, K., Hameed, I. A., Weltzien, C., et al. (2018). Advances in greenhouse automation and controlled environment agriculture: A transition to plant factories and urban agriculture. *Int. J. Agric. Biol. Eng.* 11, 1–22. doi: 10.25165/j.ijabe.20181101.3210

Shao, Y., Heath, T., and Zhu, Y. (2016). Developing an economic estimation system for vertical farms. *Int. J. Agric. Environ. Inf. Syst.* 7, 26–51.

SPREAD (2021). *SPREAD establishes a mass-production technology of strawberries in plant factories (in Japanese)*. Available Online at: https://www.spread.co.jp/files/news_20210518.pdf [accessed June 20, 2022].

Terazono, E. (2020). *Vertical farming: Hope or hype?*. London: Financial Times.

van Delden, S. H., SharathKumar, M., Butturini, M., Graamans, L. J. A., Heuvelink, E., Kacira, M., et al. (2021). Current status and future challenges in implementing and upscaling vertical farming systems. *Nat. Food* 2, 944–956. doi: 10.1038/s43016-021-00402-w

Williamson, O. E. (1979). Transaction-cost economics: The governance of contractual relations. *J. Law Econ.* 22, 233–261.

Zeidler, C., Schubert, D., and Vrakking, V. (2017). *Vertical farm 2.0: Designing an economically feasible vertical farm-A combined European endeavor for sustainable urban agriculture*. Available Online at: https://elib.dlr.de/116034/ [accessed April 8, 2022].

frontiers | Frontiers in Plant Science

TYPE Original Research
PUBLISHED 30 September 2022
DOI 10.3389/fpls.2022.983222

OPEN ACCESS

EDITED BY
Yuxin Tong,
Institute of Environment and Sustainable Development in Agriculture (CAAS), China

REVIEWED BY
Jung Eek Son,
Seoul National University, South Korea
Viktorija Vastakaite-Kairiene,
Lithuanian Research Centre for Agriculture and Forestry, Lithuania

*CORRESPONDENCE
Xiuming Hao
Xiuming.Hao@agr.gc.ca

SPECIALTY SECTION
This article was submitted to Technical Advances in Plant Science, a section of the journal Frontiers in Plant Science

RECEIVED 30 June 2022
ACCEPTED 12 September 2022
PUBLISHED 30 September 2022

CITATION
Lanoue J, St. Louis S, Little C and Hao X (2022) Continuous lighting can improve yield and reduce energy costs while increasing or maintaining nutritional contents of microgreens. *Front. Plant Sci.* 13:983222. doi: 10.3389/fpls.2022.983222

Continuous lighting can improve yield and reduce energy costs while increasing or maintaining nutritional contents of microgreens

Jason Lanoue, Sarah St. Louis, Celeste Little and Xiuming Hao*

Harrow Research and Development Centre, Agriculture & Agri-Food Canada, Harrow, ON, Canada

Microgreens represent a fast growing segment of the edible greens industry. They are prized for their colour, texture, and flavour. Compared to their mature counterparts, microgreens have much higher antioxidant and nutrient content categorizing them as a functional food. However, current production practices in plant factories with artificial light are energy intensive. Specifically, the lack of sunlight within the indoor structure means all of the light must be provided *via* energy consuming light fixtures, which is energy intensive and costly. Plant growth is usually increased with the total amount of light provided to the plants - daily light integral (DLI). Long photoperiods of low intensity lighting (greater than 18h) providing the desired/target DLI can reduce the capital costs for light fixtures and electricity costs. This is achieved by moving the electricity use from peak daytime hours (high price) to off-peak hours (low price) during the night in regions with time-based pricing scheme and lowering the electricity use for air conditioning, if plant growth is not compromised. However, lighting with photoperiods longer than tolerance thresholds (species/cultivar specific) usually leads to plant stress/damage. Therefore, we investigated the effects of continuous 24h white light (CL) at two DLIs (~14 and 21 mol m^{-2} d^{-1}) on plant growth, yield, and antioxidant content on 4 types of microgreens - amaranth, collard greens, green basil, and purple basil to see if it compromises microgreen production. It was found that amaranth and green basil had larger fresh biomass when grown under CL compared to 16h when the DLIs were the same. In addition, purple basil had higher biomass at higher DLI, but was unaffected by photoperiods. Plants grown under the CL treatments had higher energy-use-efficiencies for lighting (10-42%) than plants grown under the 16h photoperiods at the same DLI. Notably, the electricity cost per unit of fresh biomass ($ g^{-1}) was reduced (8-38%) in all microgreens studied when plants were grown under CL lighting at the same

10.3389/fpls.2022.983222

DLIs. Amaranth and collard greens also had higher antioxidant content. Taken together, growing microgreens under CL can reduce electricity costs and increase yield while maintaining or improving nutritional content.

KEYWORDS

continuous lighting, microgreens, antioxidant, phenolics, anthocyanin, energy efficiency, plant factory with artificial light, indoor vertical farming

1 Introduction

Microgreens are a fast growing specialty crop within the edible greens industry (Kyriacou et al., 2016). They are prized for their colour, texture, and flavour. Microgreens are typically harvested within 3 weeks of sowing and can be harvested before or at the first true leaf stage depending on desired use. Although smaller in size, microgreens have higher nutritional content than their mature counterparts, and thus are considered a functional food (Xiao et al., 2012; Choe et al., 2018; Kyriacou et al., 2019).

Due to their small size and compact growing strategy, microgreens are typically grown in indoor vertical farms or plant factories with artificial light to maximize yield per unit of land area (Graamans et al., 2018). The terms indoor vertical farm and plant factory are typically used synonymously but usage varies based on geographical location. Generally, indoor vertical farm is used in North America whereas plant factories with artificial light (PFAL) is used in Europe and Asia. Both refer to the use of multi-layer growing platforms (i.e., vertical farming) inside warehouses or insulated shipping containers for production with artificial light as the sole light source (Kozai and Niu, 2016). Throughout this manuscript we will use the term plant factory. While this type of growing system can have very high yield per unit of land area, it is energy intensive. All the light required for plant growth and photosynthesis needs to come from artificial lighting with the use of electricity (Shibaeva et al., 2022b). Even if the adoption of the energy-efficient light-emitting diode (LED) fixtures can reduce the electricity use (van Delden et al., 2021), the electricity used by LED lighting still represents upwards of 20% of operating costs in plant factories; second only to labour (Kozai and Niu, 2019). Furthermore, this type of growing system is also capital intensive. It not only uses expensive LED lighting systems (even though their price has come down) but also uses heating, ventilation, and air conditioning (HVAC) to control temperature and humidity. The majority of input electricity to the lighting system will eventually becoming heat since plants typically only convert 1-5% of the incoming radiation to biomass (Zhu et al., 2008; Kozai and Niu, 2019). The excessive heat load and the high humidity from plant transpiration requires its removal and dehumidification *via* air conditioning systems to maintain an optimal growing environment for the plants, which, in addition to lighting, increases electricity costs (Goto, 2012; Kozai and Niu, 2016). These high input costs are in part why only 50% of plant factories in Japan were profitable in 2018 (Kozai and Niu, 2019), and why plant factories struggle to be used as a mainstream producer of edible greens elsewhere in the world (Kozai, 2018). Based on the poll conducted by Indoor AgTech Innovation Virtual Summit 2021 (https://indooragcenter.org/indoor-agtech-virtual-summit-2021/), high energy cost is the main limiting factor for profitable production with plant factories. Therefore, innovation in lighting systems and strategies is the key to reduce energy costs and improve energy efficiency.

Plant growth and yield are usually determined by the amount of light intercepted by the plant during a day - daily light integral (DLI; photosynthetic photon flux density (PPFD) x photoperiod duration). Both the increase in PPFD (Samuoliene et al., 2013) and an extension in photoperiod (Demers and Gosselin, 2002) can increase DLIs and have been shown to increase biomass production up to a saturation point. With respect to PPFD, beyond a certain species-specific limit, no further increase in biomass is observed and further increases to the PPFD can be detrimental to the plant (Demmig-Adams and Adams, 1992; Szymańska et al., 2017) since as PPFD increases, the quantum yield (i.e., the increase in CO_2 fixed per additional photon) decreases (Lanoue et al., 2017). Furthermore, the use of high PPFD can increase the transpiration rate of plants, exacerbating the aforementioned humidity issue (Goto, 2012; Lanoue et al., 2018).

Similar to an increase in PPFD, photoperiod extension can be used to increase DLI and biomass (Demers and Gosselin, 2002). The ultimate goal in photoperiod extension is 24h lighting/continuous lighting (CL). It is more economical to use long photoperiods (18h up to 24h) of low PPFD (<200 μmol m^{-2} s^{-1}) to achieve the target/desired DLIs because it reduces the capital cost of light fixtures (Hao et al., 2018). The longer the photoperiod, the lower the PPFD that can be used to reach the desired DLI. It should be noted that the DLI requirements vary between plant species and cultivars. Therefore the definition of a long photoperiod, low PPFD lighting strategy will be species-specific.

In many regions of the world which employ time-of-use pricing (TOUP) such as Ontario, Canada, some states in the USA, 17 European countries including France, Sweden, Germany, Finland, as well as South Korea, the price of electricity is much higher in the peak hours during daytime (when demand is highest) compared to the price in the off-peak hours during the night (IRENA, 2019; IESO, 2022). It is important to note that the form in which TOUP is utilized in each country may be different (i.e., static time-of-use pricing, real-time pricing, variable peak pricing, or critical peak pricing), but regardless of strategy, off peak pricing is always cheaper than on peak. Therefore, long photoperiod, low PPFD lighting such as CL can also reduce electricity costs by moving part of electricity use from daytime to nighttime when prices are at their lowest in these regions (Hao et al., 2018; IESO, 2022). At lower PPFD, both the heat load from lighting and plant transpiration decrease, reducing the usage of electricity by the air conditioning system to remove heat and moisture to maintain optimal growing environment for plants (Kozai and Niu, 2016).

The use of long photoperiod lighting such as 24h CL means constant photon energy is provided to the plant allowing for 24h CO_2 fixation and growth. In this way, it has been hypothesized that the use of CL can increase plant production (Sysoeva et al., 2010; Velez-Ramirez et al., 2011; Velez-Ramirez et al., 2012; Shibaeva et al., 2022a). However, exceeding the tolerable photoperiod limits, which are species-specific, can lead to diminished yield, photoperiod-related leaf injury, and an economic disadvantage for growers (Demers and Gosselin, 2002; Hao et al., 2018). Some plant species such as tomato and pepper have reduced yield and leaf injury characterized by chlorosis when grown under CL (Murage and Masuda, 1997; Velez-Ramirez et al., 2017). It is hypothesized that CL-injury is due to a mismatch between environmental cues and endogenous circadian rhythms (Velez-Ramirez et al., 2017; Marie et al., 2022). Specifically, since the plant is under constant light, it seems that components of the light harvesting complex are negatively affected causing reduced transcription leading to inadequate use and/or dissipation of light (Velez-Ramirez et al., 2014). More recent research in these two crops have provided evidence that dynamic CL, which involves a change in light spectrum between daytime and nighttime, can result in injury-free production (Lanoue et al., 2019; Lanoue et al., 2022). Some cultivars of lettuces and some members of the Brassicaceae microgreen family have also been shown to have positive interactions with CL (Ohtake et al., 2018; Shibaeva et al., 2022b). Since the production period of microgreens is short, and CL-injury in tomatoes and peppers tends to take more than a month to have noticeable reductions in yield (Lanoue et al., 2021a), we hypothesize that CL may not compromise the production of microgreens and could be a viable production strategy.

However, CL can increase harmful reactive oxygen species (ROS) due to the stress from constant light exposure to the plant (Haque et al., 2015; Huang et al., 2019). Subsequently, the concentration of ROS scavenging molecules such as antioxidants can also be increased during CL (Haque et al., 2015). The extent of injury is largely linked to the interplay between ROS production and scavenging ability. If this homeostatic balance becomes too heavily skewed by elevated ROS production, then leaf injury will occur, resulting in detrimental plant growth and yield. However, if one can balance the oxidative pressure with the antioxidant synthesis, injury-free production is feasible. Therefore, the prospect of injury-free production under CL coupled with the hormetic impact can increase antioxidants/health promoting compounds in plants; which is an intriguing possibility for microgreen production in plant factories.

As such, we studied the impact of PPFD and photoperiod (including CL) on plant growth, yield and nutritional content of 4 types of microgreens in order to assess if long photoperiod (CL) and low intensity lighting can be used to improve the sustainability/energy efficiency in indoor production of microgreens grown in plant factories.

2 Materials and methods

2.1 Plant materials and lighting treatments

Four types of microgreens were used in the study. Two hundred seeds each of amaranth (*Amaranthus tricolor*) cv. 'Garnet Red', collard greens (*Brassica oleracea* var. *viridis*) cv. 'Vates', as well as basil (*Ocimum basilicum*) cv. 'Genovese' and cv. 'Red Rubin' (henceforth referred to as green and purple basil respectively; Johnny's Select Seeds, Fairfield, Maine, USA) were sown into individual trays filled with Berger BM6 All-Purpose potting soil (Berger, Saint-Modeste, Quebec, Canada). Once sown, the trays were placed in a germination chamber at Agriculture & Agri-Food Canada's Harrow Research and Development Centre with a constant temperature of 24°C and a relative humidity of 90% in complete darkness. Amaranth and collard greens remained in the chamber for 3 days while basil was in the germination chamber for 5 days. Upon germination, trays of each cultivar were placed into four different growth areas (1.93 m^2) within Conviron walk-in growth chambers (PGW40; Conviron, Winnipeg, MB, Canada) each containing one of four lighting treatments (Table 1). The growth chamber temperature was maintained at 22°C (24 hour) while the relative humidity was kept between 60-70%. Plants were irrigated as needed. Harvest occurred 11 days after sowing for amaranth and collard greens and 19 days after sowing for both basil cultivars.

The four light treatments consisted of 2 levels of DLIs (14 and 21 mol m^{-2} day^{-1}) and 2 photoperiods (16h and 24h; Table 1). Throughout the manuscript, the lighting treatments will be represented using the following notation: DLI/

TABLE 1 Light treatments provided by the Flexstar 645W dimmable LED fixtures (Flexstar, California, USA) in Conviron walk-in growth chambers (PGW40; Conviron, Winnipeg, MB, Canada) measured at the height of the top of the tray in 6 different locations within the chamber.

Treatment (DLI/photoperiod)	PPFD (μmol m^{-2} s^{-1})	DLI (mol m^{-2} d^{-1})	Photoperiod (h)
14DLI/16h	250.8 ± 2.1	14.5 ± 0.1	16
14DLI/24h	166.6 ± 2.7	14.4 ± 0.2	24
21DLI/16h	376.8 ± 1.7	21.7 ± 0.1	16
21DLI/24h	247.6 ± 7.9	21.4 ± 0.7	24

photoperiod. Lighting treatments were chosen based on similar PPFD and photoperiods in other studies where between 200-300 μmol m^{-2} s^{-1} was the typical PPFD used with 16h photoperiods (Samuoliene et al., 2013; Viršilė et al., 2019; Pennisi et al., 2020; Shibaeva et al., 2022b; Sutulienė et al., 2022; Vaštakaitė-Kairienė et al., 2022). Using that as a baseline for the 14DLI/16h treatment, the other treatments we determined by controlling either DLI but extending the photoperiod or controlling the PPFD and extending the photoperiod. All light treatments were provided by Flexstar 645W dimmable LED fixtures (Flexstar, California, USA) and were the same broad/white spectrum (Figure 1). The growth chamber trials were replicated 3 times in 2022.

2.2 Growth measurements

The plants were harvested by cutting them at the junction where their base meets the growth media. Plant height was measured on five random plant samples from each treatment of each cultivar during each replicate (i.e., 15 total samples per microgreen per treatment). Total fresh weight was obtained then a subsample was flash frozen in liquid nitrogen and placed in a -80°C freezer until analysis. Another subsample was weighed, then placed in a 70°C oven for 1 week then re-weighed to obtain the dry matter percentage of the sample. Energy-use-efficiency of the lights (EUEL) only was calculated using the total fresh biomass obtained and dividing it by the cumulative input of energy into the lighting fixtures during the production period (g FW MJ^{-1}).

2.3 Photosynthetic pigment analysis

Frozen tissue was lyophilized then ground. One mL of 95% ethanol was then added to the sample and the tube was placed in a water bath at 50°C for 3 hours. The tube was centrifuged at 13000 rpm for 1 minute before the supernatant was removed and placed in a clean tube. The process was repeated and both aliquots were combined for a total extract volume of 2 mL.

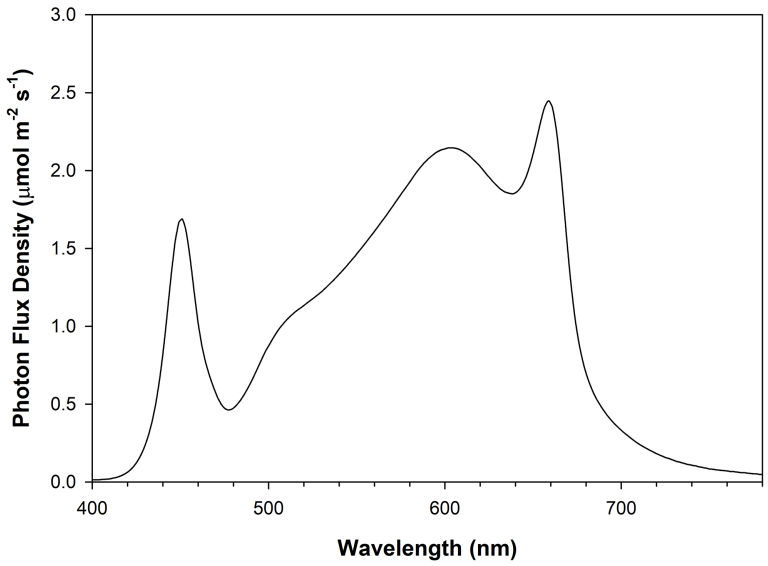

FIGURE 1
Photon flux density (PFD) distribution of Flexstar 645W dimmable LED fixtures (Flexstar, California, USA) measured using a Li-180 spectrometer (Li-COR Biosciences Inc. Lincoln, Nebraska, USA).

Samples were then analyzed at 664 nm, 649 nm, and 470 nm in a UV/VIS spectrophotometer (UV-1600PC. VWR. Mississauga, Ontario, Canada). Concentrations of chlorophyll *a*, *b*, and carotenoids were determined using the equations from Lichtenthaler (1987).

2.4 Antioxidant assays

2.4.1 DPPH (2,2-diphenyl-1-picrylhydrazyl) assay

The antiradical activity in microgreen tissue was determined based on a modified version of a previously reported method (Alrifai et al., 2020). Tissue samples that were previously frozen in liquid nitrogen and stored in a -80°C freezer were removed and lyophilized. Lyophilized tissue was ground in a homogenizer then 1 mL of 100% methanol was added to the microfuge tube. The sample was then left on a nutator overnight at room temperature. The next morning, the samples were centrifuged at 13,000 rpm for 5 minutes. The supernatant was collected in a clean tube before re-suspending the pellet in 1 mL of fresh 100% methanol. The sample was placed on a nutator for 3 hours before being centrifuged and having the supernatant removed. Both supernatant fractions were mixed in a single tube and placed in -20°C freezer until analysis. Fresh 2,2-diphenyl-1-picrylhydrazyl (DDPH; 350 µM) was prepared immediately before analysis. In a cuvette, 1 mL of DPPH was mixed with 125 µL of sample and placed in the dark to incubate for 30 minutes before the absorbance was measured at 517 nm. This procedure was completed in duplicate. A standard curve was completed in triplicate using the same assay technique with ascorbic acid used in place of the tissue sample.

2.4.2 FRAP (ferric reducing antioxidant power) assay

The ferric reducing antioxidant power (FRAP) assay of microgreen tissue was determined using a modified version of a previously reported method (Alrifai et al., 2020). Samples were extracted using a method similar to the DPPH analysis. FRAP reagent was made at the time of analysis and consisted of 300 mM acetate buffer (pH 3.6), 20 mM $FeCl_3$, and 10 mM 2, 4, 6-Tris (2-pyridyl)-s-triazine (TPTZ) in 40 mM HCl. 100 µL of methanolic sample extract was mixed with 900 µL of FRAP reagent and incubated at 37°C for 2h before reading the absorbance at 593 nm. A standard curve was completed using the same assay technique with ascorbic acid used in place of the tissue sample.

2.4.3 Total phenolic content

Total phenolic content was determined using a modified protocol from Ainsworth and Gillespie (2007). Briefly, 100 µL of methanolic sample extract was combined with 200 µL of Folin-Ciocalteu's reagent (Thermo Fisher Scientific, MA, USA) and 800 µL of 700 mM sodium carbonate. The tubes were vortexed for 30 seconds then allowed to stand at room temperature for 2h. The absorbance was measured at 765 nm using a UV/VIS spectrophotometer. Total phenolic content was expressed as gallic acid equivalents.

2.4.4 Total anthocyanin

Determination of total anthocyanin content was done using a slightly modified protocol from Lee et al. (2005). The assay began by adding 100 µL of methanolic sample to both 1 mL of potassium chloride (0.025 M; pH = 1.0) and 1 mL of sodium acetate (0.4 M; pH = 4.5) separately. The mixtures were incubated at room temperature for 30 minutes before the absorbance was measured at both 520 nm and 700 nm. Anthocyanin contents were then calculated using the following equation:

$$Anthocyanin\ \ content = \frac{\left(A \star MW \star DF \star 10^3\right)}{\epsilon \star l}$$

Where A is the absorbance ($A=(A_{520nm}\text{-}A_{700nm})_{pH1.0} - (A_{520nm}\text{-}A_{700nm})_{pH4.5}$), MW is the molecular weight of cyanidin-3-glucoside (449.2 $gmol^{-1}$), DF was the dilution factor, 10^3 is the factor to convert g to mg, $\epsilon$is the molar extinction coefficient of cyanidin-3-glucoside (26900 L mol^{-1}) and l is the path length of 1 cm.

2.5 Electricity Cost Calculation

The electricity cost (\$ g^{-1} FW) from LED lighting only during each production period of all microgreens was calculated using the following equation:

$$Electicity\ \ cost = \frac{\left[\sum_{n=0}^{n}\left(\left(\frac{Lu}{Lm}\right)\left(\frac{P}{10^6}\right)\right)E_n\right]}{FW}$$

Where n is the hour, Lu is the PPFD used, Lm is the maximum PPFD of the fixture, P is the input wattage of the fixture (W), 10^6 is a conversion factor from W to MW, E_n is the electricity price at a given hour (n) as determined from IESO, 2022, and FW is the fresh weight (g) produced for a given microgreen during a specific production period. Fresh weight was a measure of total biomass produced by each microgreen under each light treatment at the end of the growth period.

2.6 Statistics

For each microgreen, the experiment was replicated 3 times. For each of the pigment analyses and antioxidant analyses, 2 subsamples were taken from each destructive harvest. All statistics were performed using SAS studio 3.5. A two-way

10.3389/fpls.2022.983222

ANOVA was performed and a multiple means comparison was done using a Tukey-Kramer adjustment with a $p<0.05$ indicating a significant difference.

3 Results

3.1 Plant growth and yield

Amaranth plants were observed to be shortest in height under the 21DLI/16h treatment which was a result of the high PPFD used (Table 2). Both light treatments that ran for 24h produced the tallest plants regardless of DLI (Table 2; Figure 2). Fresh weight, a determination of yield for microgreens, was highest under the 21DLI/24h light treatment andlowest under the 14DLI/16h lighting treatment. Although the DLI was the same, both lighting treatments which utilized a 24h photoperiod produced more plant fresh biomass than did plants grown under the 16h photoperiod (Table 2). The energy-use-efficiency of the lights (EUEL) only is a measure of biomass accumulation normalized for the input energy of the lighting fixture. For amaranth, both 24h lighting treatments had the highest EUEL indicating that the input energy produced a higher biomass than the 16h treatment (Table 2). The percentage of dry matter was also highest under the 21DLI/24h light treatment while both light treatments with a low DLI had the lowest percentage of dry matter.

Similar to amaranth, collard greens grown under 14DLI/24h which utilized the lowest PPFD produced the tallest plants while plants grown under the highest PPFD (21DLI/16h) were the shortest (Table 3; Figure 3). Fresh weight was the lowest in plants grown under the 14DLI/16h treatment and the highest under the 21DLI/24h treatment (Table 3). Interestingly, although the DLI was lower, plants grown under the 14DLI/24h light treatment produced similar fresh weight to both treatments with high DLIs of approximately 21 mol m^{-2} d^{-1} (Table 3). Collard green plants grown under the 14DLI/24h treatment had the highest EUEL as more biomass was produced with the least amount of input energy (Table 3). Plants grown under both high DLI treatments had the lowest EUEL regardless of photoperiods. Percentage of dry matter was the highest in both 21DLI/16h and 21DLI/24h compared to treatments with low DLIs of approximately 14 mol m^{-2} d^{-1}.

Green basil plants were tallest when grown under 21DLI/24h, while those grown under 14DLI/16h were the shortest (Table 4; Figure 4). The same trend was noticed in fresh weight production where plants under 21DLI/24h produced the highest biomass while those under 14DLI/16h produced the least (Table 4). In green basil, both 24h lighting treatments had higher EUEL than did their 16h counterparts which is both a factor of increased biomass production and the lower input energy required by these treatments (Table 4). Notably, plants grown under the 14DLI/24h treatment produced the highest EUEL among all treatments. While the fresh weight produced was not the highest, the input energy required to produce the fresh weight was the lowest of all treatments, resulting in the highest EUEL. However, while plant height, fresh weight, and EUEL were impacted by the lighting treatments, the percentage of dry matter was similar between all treatments indicating no increase in water uptake under different light treatments (Table 4).

Similar to green basil, purple basil plants were shortest under 14DLI/16h and the tallest under 21DLI/24h (Table 5; Figure 5). Total fresh weight was observed to be the highest when plants were grown under the high DLI of approximately 21 mol m^{-2} d^{-1} and the lowest under the low DLI of approximately 14 mol m^{-2} d^{-1} regardless of photoperiods. Consistent with the green basil results, purple basil plants grown under the 14DLI/24h light treatment had the highest EUEL due to having the lowest input energy. Notably, both 24h lighting treatments had higher EUEL than the 16h treatments at the same DLI (Table 5). Coinciding with the results from green basil, the percentage of dry matter of purple basil was similar regardless of treatments. Interestingly, although both green and purple basils are the same species, both fresh weight and percentage of dry matter were lower in purple basil compared to green basil (Tables 4, 5).

TABLE 2 Growth measurement summary of Amaranth cv. 'Garnet Red' grown under various lighting DLI and photoperiods.

Daily Light Integral (mol m^{-2} d^{-1})	Photoperiod (h)	Height (cm)	Fresh Weight (g)	EUEL (g FW MJ^{-1})	% Dry Matter
		Amaranth cv. 'Garnet Red'			
14	16	4.32 ± 0.16^{AB}	6.47 ± 0.29^{C}	0.26 ± 0.01^{B}	7.12 ± 0.12^{C}
	24	4.65 ± 0.19^{A}	8.53 ± 0.58^{B}	0.35 ± 0.02^{A}	7.38 ± 0.25^{BC}
21	16	3.91 ± 0.32^{B}	8.90 ± 0.59^{B}	0.24 ± 0.02^{B}	7.92 ± 0.17^{B}
	24	4.55 ± 0.09^{A}	12.47 ± 0.61^{A}	0.34 ± 0.02^{A}	8.76 ± 0.13^{A}
Daily Light Integral		0.0624	<0.0001	0.2441	0.0004
Photoperiod		0.0048	0.0001	0.0001	0.0111
Daily Light Integral*Photoperiod		0.2126	0.0628	0.5036	0.1062

Height was subsampled at five locations within the tray at the end of each of the three respective growth trials. Values presented are the means of three replicates, one from each trial ± the standard error of the means. Different letter groups (A, B, C) represent statistical differences as determined by a two-way ANOVA within each parameter at $p<0.05$.

10.3389/fpls.2022.983222

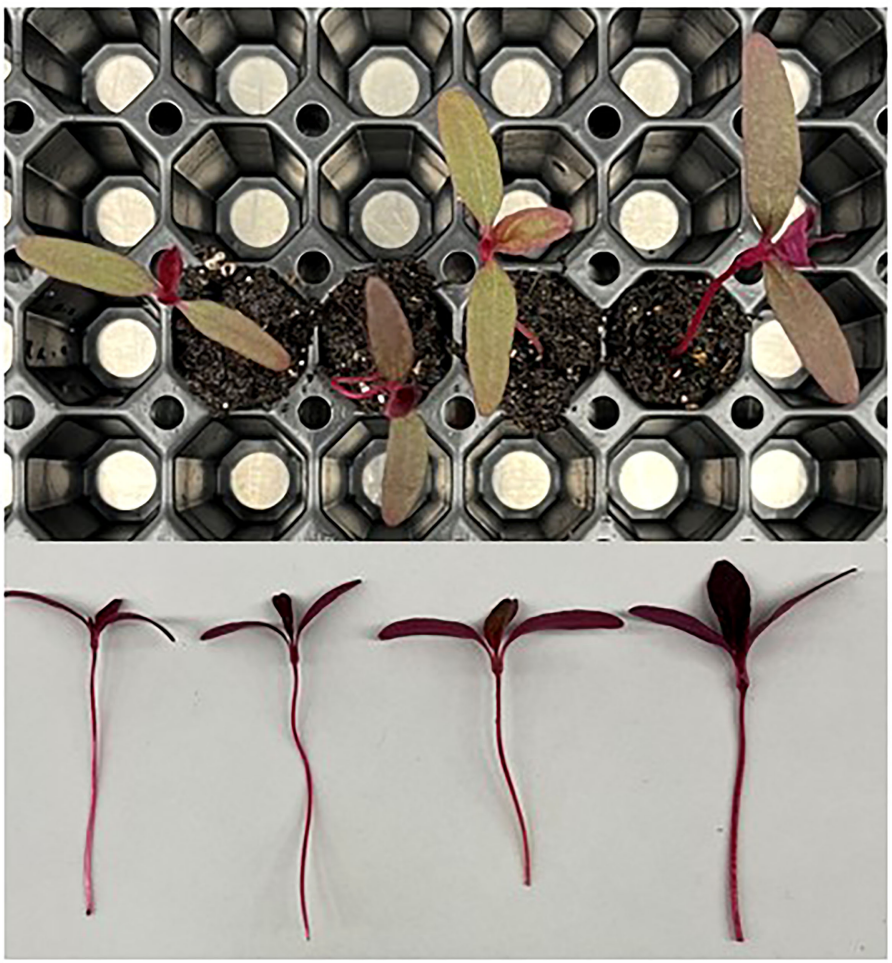

FIGURE 2
Amaranth plants grown under various lighting DLI and photoperiods. Top photo is an overhead picture, while the bottom is a side profile. From left to right, the lighting treatments are as follows (DLI/photoperiod): 14DLI/16h, 14DLI/24h, 21DLI/16h, and 21DLI/24h.

TABLE 3 Growth measurement summary of Collard greens cv. 'Vates' grown under various lighting DLI and photoperiods.

Daily Light Integral (mol m^{-2} d^{-1})	Photoperiod (h)	Height (cm)	Fresh Weight (g)	EUEL (g FW MJ^{-1})	% Dry Matter
		Collard Greens cv. 'Vates'			
14	16	3.44 ± 0.22^{AB}	20.40 ± 1.81^{B}	0.82 ± 0.07^{B}	9.87 ± 0.04^{B}
	24	3.88 ± 0.06^{A}	23.37 ± 2.28^{AB}	0.95 ± 0.09^{A}	9.98 ± 0.47^{B}
21	16	3.09 ± 0.22^{B}	22.40 ± 2.29^{AB}	0.60 ± 0.06^{C}	11.95 ± 0.11^{A}
	24	3.64 ± 0.22^{AB}	24.70 ± 2.39^{A}	0.67 ± 0.07^{C}	13.23 ± 0.24^{A}
Daily Light Integral		0.0888	0.0420	<0.0001	<0.0001
Photoperiod		0.0153	0.0066	0.0061	0.0425
Daily Light Integral*Photoperiod		0.7032	0.6248	0.2994	0.0757

Height was subsampled at five locations within the tray at the end of each of the three respective growth trials. Values presented are the means of three replicates, one from each trial± the standard error of the means. Different letter groups (A, B, C) represent statistical differences as determined by a two-way ANOVA within each parameter at $p<0.05$.

FIGURE 3
Collard greens plants grown under various lighting DLI and photoperiods. Top photo is an overhead picture, while the bottom is a side profile. From left to right, the lighting treatments are as follows (DLI/photoperiod): 14DLI/16h, 14DLI/24h, 21DLI/16h, and 21DLI/24h.

3.2 Photosynthetic pigments

Chlorophyll, as well as carotenoids, play a role in light harvesting for photosynthesis. However, in microgreens, they also provide vibrant green, yellow, and red colours which are sought after by chefs. In amaranth, green basil, and purple basil, growth under both 24h lighting treatments produced the highest chlorophyll *a* content (Figure 6A). In collard greens, chlorophyll *a* was the highest in the 14DLI/24h treatment but observed to be the lowest in the 21DLI/24h treatment. Chlorophyll *b* was not affected by light treatments in both amaranth and green basil (Figure 6B). In collard greens, similar to chlorophyll *a*, chlorophyll *b* was observed to be the highest in the 14DLI/24h treatments and the lowest in the 21DLI/24h treatment. In addition, both high DLI treatments were observed to have lower chlorophyll *b* content than the 14DLI/24h light treatments. In purple basil, both 24h light treatments had higher chlorophyll *b* content than did the 16h treatments (Figure 6B). The chlorophyll *a*:*b* was observed to be similar between light treatments in amaranth and both basil microgreens (Figure 6C). However, in collard greens, the chlorophyll *a*:*b* was the lowest in the 14DLI/16h treatment and the highest in both high DLI treatments. Carotenoids were the highest in both 24h lighting treatments in amaranth but the other three microgreens were unaffected by light treatments (Figure 6D).

3.3 Antioxidants

Microgreens are prized for their antioxidant and nutrient densities in comparison to their mature counterparts. Here we see that the antioxidant activity as measured by 2,2-diphenyl-1-picrylhydrazyl (DPPH) assay was increased in both 24h lighting treatments compared to their 16h counterparts at the same DLI in green basil (Figure 7A). Furthermore, plants grown under the 14DLI/24h light treatment had the highest DPPH activity of all light treatments in green basil. DPPH activity was unaffected by light treatments in all other microgreens. Similarly, ferric reducing antioxidant power (FRAP) was observed to be unaffected by light treatments in all microgreens (Figure 7B). Phenolics, which can provide resistance against various biotic and abiotic stress conditions the plant is under, were unaffected by the different light treatments (Figure 7C). In amaranth, the anthocyanin content was observed to be the highest under the 21DLI/16h treatment and the lowest under the 14DLI/16h treatment (Figure 7D). Anthocyanin content was unaffected by light treatments in all other microgreens (Figure 7D). A trend which can be observed is that there is higher antioxidant activity and phenolic and anthocyanin content in both basil microgreens in comparison to amaranth and collard greens. Notably, purple basil tends to have the highest antioxidant capacity as well as

10.3389/fpls.2022.983222

TABLE 4 Growth measurement summary of green basil cv. 'Genovese' grown under various lighting DLI and photoperiods.

Daily Light Integral (mol m^{-2} d^{-1})	Photoperiod (h)	Height (cm)	Fresh Weight (g)	EUEL (g FW MJ^{-1})	% Dry Matter
		Green Basil cv. 'Genovese'			
14	16	2.75 ± 0.12^{C}	16.33 ± 1.05^{C}	0.66 ± 0.04^{B}	10.17 ± 1.20^{A}
	24	2.99 ± 0.13^{B}	20.30 ± 0.97^{B}	0.82 ± 0.04^{A}	10.29 ± 0.50^{A}
21	16	2.98 ± 0.08^{B}	19.30 ± 0.47^{B}	0.52 ± 0.01^{C}	11.73 ± 0.44^{A}
	24	3.28 ± 0.15^{A}	23.37 ± 0.58^{A}	0.64 ± 0.02^{B}	10.93 ± 0.75^{A}
Daily Light Integral		0.0003	0.0010	0.0002	0.0378
Photoperiod		0.0003	0.0002	0.0005	0.4453
Daily Light Integral*Photoperiod		0.4284	0.9245	0.3046	0.3040

Height was subsampled at five locations within the tray at the end of each of the three respective growth trials. Values presented are the means of three replicates, one from each trial ± the standard error of the means. Different letter groups (A, B, C) represent statistical differences as determined by a two-way ANOVA within each parameter at $p<0.05$.

phenolic and anthocyanin concentrations, which is in part a cause of its deep purple colouration.

4 Discussion

4.1 Continuous lighting and microgreen growth

Both PPFD and photoperiod are known to impact plant morphology. Growth under low PPFD will increase leaf area in order to maximize the area capable of intercepting incoming light (Palmer and van Iersel, 2020). Conversely, high PPFD will lead to a reduction in specific leaf area (i.e., smaller, thicker leaves) to protect the plant from high irradiance levels in order to minimize damage due to excessive light (Matos et al., 2009; Fan et al., 2013). Extended photoperiods including CL have led to smaller leaf area in tomatoes (Velez-Ramirez et al., 2014), which is a similar attribute seen in plants grown under high PPFD in order to avert damage due to excess light.

In this study, with the exception of collard greens, we observed that plants grown under the 21DLI/24h treatment were the tallest (Tables 2–5). Furthermore, and again with the exception of collard greens, leaf area was visually larger when plants were grown under the 21DLI/24h treatment (Figures 2–5). Increases in both plant height and leaf area are traits typically associated with growth in low light environments (Poorter et al., 2019). However, there is an interplay between leaf expansion due to low light and photosynthesis driven by adequate PPFD. Compared to the 21DLI/16h treatment, the 21DLI/24h treatment used lower PPFD which enabled greater leaf expansion. In turn, the larger leaf expansion allowed for greater light interception and thus higher overall plant photosynthesis leading to increased biomass. This notation is supported by an increased EUEL of plants grown under the 24h photoperiods compared to their respective 16h counterparts. It should also be noted that all 24h lighting treatments in amaranth, green basil, and purple basil had elevated levels of chlorophyll (Figure 5). Being the major photosynthetic pigment, a strong correlation can be drawn between chlorophyll content

TABLE 5 Growth measurement summary of purple basil cv. 'Red Rubin' grown under various lighting DLI and photoperiods.

Daily Light Integral (mol m^{-2} d^{-1})	Photoperiod (h)	Height (cm)	Fresh Weight (g)	EUEL (g FW MJ^{-1})	% Dry Matter
		Purple Basil cv. 'Red Rubin'			
14	16	3.02 ± 0.18^{B}	10.67 ± 0.50^{B}	0.43 ± 0.02^{BC}	7.20 ± 0.51^{A}
	24	3.17 ± 0.13^{AB}	12.07 ± 0.32^{B}	0.49 ± 0.01^{A}	7.05 ± 0.88^{A}
21	16	3.21 ± 0.15^{AB}	14.77 ± 0.67^{A}	0.40 ± 0.01^{C}	7.53 ± 0.58^{A}
	24	3.30 ± 0.10^{A}	15.53 ± 0.71^{A}	0.44 ± 0.01^{B}	7.75 ± 0.77^{A}
Daily Light Integral		0.0104	0.0001	0.0330	0.0398
Photoperiod		0.0329	0.0480	0.0197	0.8678
Daily Light Integral*Photoperiod		0.5624	0.4964	0.5373	0.3966

Height was subsampled at five locations within the tray at the end of each of the three respective growth trials. Values presented are the means of three replicates, one from each trial ± the standard error of the means. Different letter groups (A, B, C) represent statistical differences as determined by a two-way ANOVA within each parameter at $p<0.05$.

FIGURE 4
Green basil plants grown under various lighting DLI and photoperiods. Top photo is an overhead picture, while the bottom is a side profile. From left to right, the lighting treatments are as follows (DLI/photoperiod): 14DLI/16h, 14DLI/24h, 21DLI/16h, and 21DLI/24h.

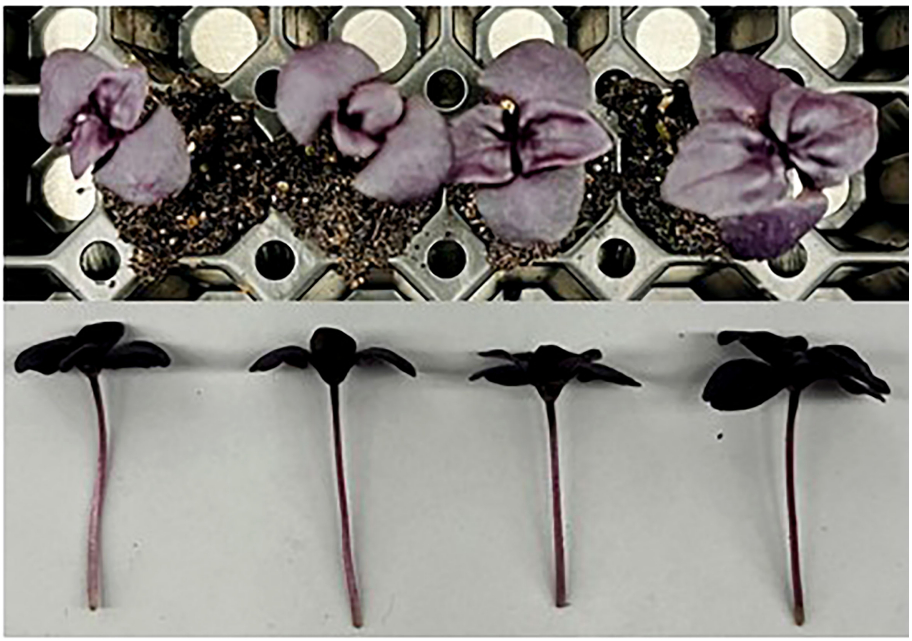

FIGURE 5
Purple basil plants grown under various lighting DLI and photoperiods. Top photo is an overhead picture, while the bottom is a side profile. From left to right, the lighting treatments are as follows (DLI/photoperiod): 14DLI/16h, 14DLI/24h, 21DLI/16h, and 21DLI/24h.

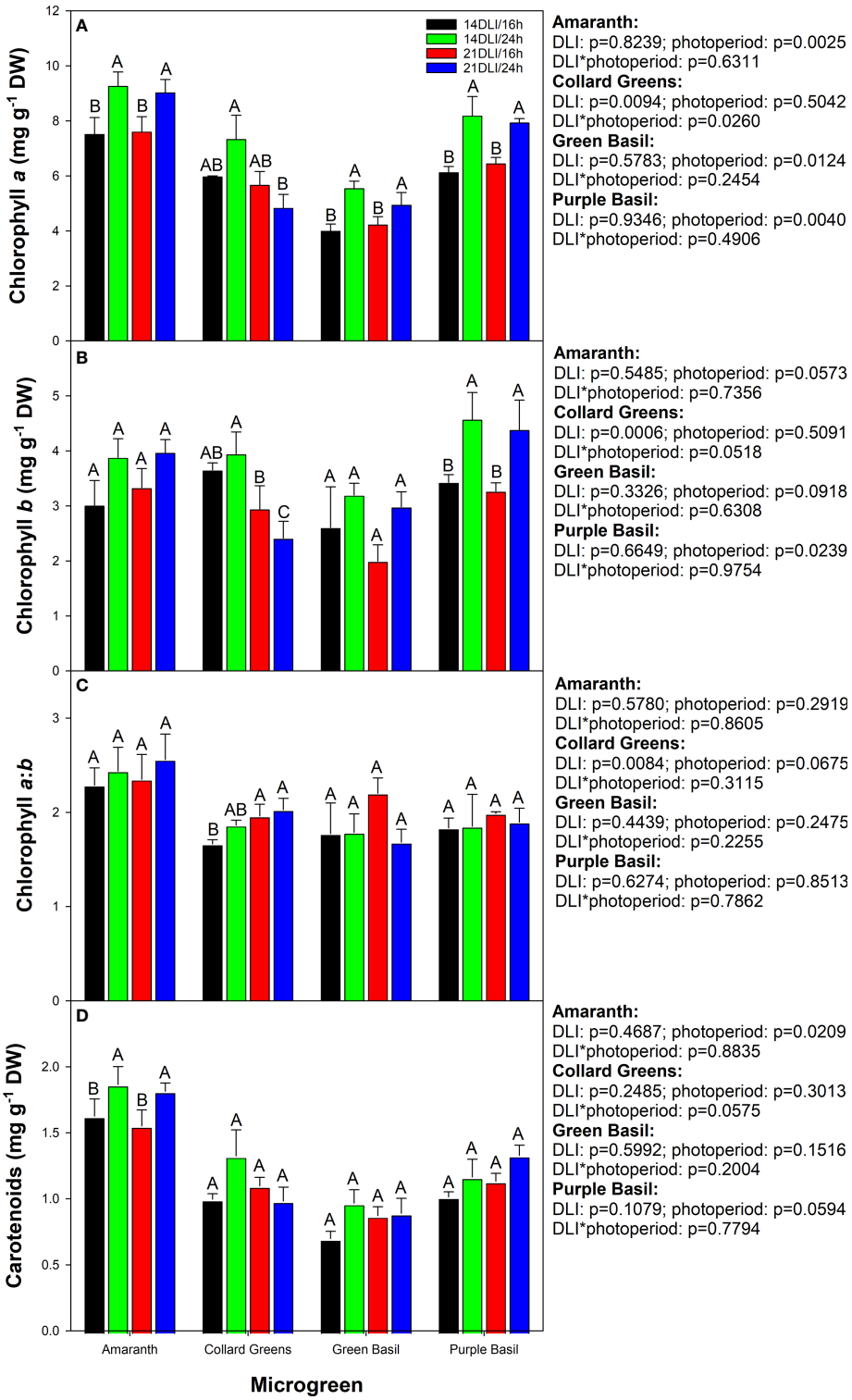

FIGURE 6
Photosynthetic pigment analysis of amaranth, collard greens, green basil, and purple basil grown under 14DLI/16h, 14DLI/24h, 21DLI/16h, and 21DLI/24h lighting treatments. Chlorophyll *a*, chlorophyll *b*, chlorophyll *a*:*b*, and carotenoids are shown in panels **(A–D)** respectively. Values presented are the means of two subsamples from each of the three replicates ± the standard error of the means. Different letter groups (A–C) represent statistical differences with microgreen type and panel as determined by a two-way ANOVA within each parameter at $p<0.05$. P-values are shown to the right of their respective panels for each microgreen.

and increased photosynthesis leading to greater biomass accumulation (Buttery and Buzzell, 1977). It has been observed that amaranth growth under a 20h photoperiod had the highest fresh biomass while also having increased levels of chlorophyll *a* (Meas et al., 2020). Interestingly, collard greens do not show the same obvious enhancement in leaf size or biomass accumulation under CL. This also coincided with similar or lower chlorophyll content when comparing the 24h treatments to the 16h treatments (Figure 6). Photosynthetic pigment concentration was observed to increase in basil, rocket, and chicory plants grown under a similar 24h light treatment as used in this manuscript (Pennisi et al., 2020). Similar to the results in amaranth and both basil cultivars, Weaver and van Iersel (2020) observed that lettuce had increased leaf area and dry biomass when the photoperiod was extended, but the DLI stayed the same. In contrast to our study, Pennisi et al. (2020) did not observe an increase in fresh biomass accumulation in basil when grown under a 24h photoperiod with a DLI of 21.6 mol m^{-2} d^{-1}. The difference in observations could be a result of differences in plant age. In Pennisi et al. (2020) the 24h treatment began when the plants were 21 days old whereas in our study, the 24h treatment began when the plants were only 5 days old. In this way, no mutual shading had occurred in our study (due to the small size of the plants) allowing maximum photon capture by the plant which resulted in greater biomass accumulation. Accordingly, an increase in photon capture and biomass accumulation would be negated when the canopy is fully matured and vegetation is dense. Since microgreens are typically harvested before or at the first true leaf stage, this competitive advantage when plants are young would lead to larger plants as observed in this study, or reduced production times as the plants would reach the desired size more quickly when grown under a long photoperiod with low PPFD (i.e., 21DLI/24h) as opposed to a shorter photoperiod and higher PPFD (i.e., 21DLI/16h).

In contrast to traditional morphological responses to CL, generally speaking, the microgreens in this study grown under 24h lighting had visually larger leaves than those grown under 16h. Reduced leaf size due to CL has been seen in tomatoes (Velez-Ramirez et al., 2014; Pham et al., 2019). However, microgreens grown under CL have been shown to have increased leaf area (Figures 2–4; Shivaeva et al., 2022b). This may indicate that microgreens have a higher PPFD threshold before morphological adaptation occurs to reduce light capture. In a model analysis on tomatoes, a theoretical increase in yield of 22-26% (depending on PPFD) has been predicted when grown under CL if injury could be averted (Velez-Ramirez et al., 2012). In this study, yield increases were 92.7%, 21.1%, 43.1%, and 45.5% for amaranth, collard greens, green basil, and purple basil, respectively when the photoperiod was extended from 16h to 24h at the same PPFD (i.e., comparing 14DLI/16h and 21DLI/24h). Our results show equal or higher yield increases compared to the theoretical model analysis for tomatoes. This difference in result is likely two-fold. Firstly, as opposed to the complex canopy of tomatoes, microgreens in this study had very little mutual shading during their production and consequently all of the leaf area was able to absorb light, maximizing photosynthesis. Secondly, unlike tomatoes which produce fruit, all of the above ground biomass of the microgreen is edible and therefore all of the assimilated carbon contributes to yield increase. Therefore, due to the simplicity of microgreens, a greater yield return is observed during CL when compared to the more complex crop of tomatoes.

4.2 Maintaining nutritional content during CL production

Microgreens are prized for their nutrient profile, vibrant colours, and flavour which often allow chefs to add new dimensions to their dishes. Microgreens are also increasingly becoming popular as an everyday leafy green due to their high antioxidant content making them a functional food (Xiao et al., 2012; Kyriacou et al., 2019). Here we see that, generally speaking, antioxidant, phenolic, and anthocyanin content remained similar or increased when microgreens were grown under a high DLI or an extended photoperiod. Coupling this with the reduced electricity cost of microgreens grown under 24h lighting, utilizing CL for microgreen production can produce plants at a reduced cost without sacrificing nutrient density.

Both amaranth and collard greens showed improved dry matter content under the high DLI treatment regardless of photoperiods (Tables 2 and 3). Additionally, amaranth was observed to have improved dry matter content under the 24h photoperiod compared to the 16h photoperiod at the high DLI. Since DPPH and FRAP activities (Figures 7A, B) as well as phenolic (Figure 7C) and anthocyanin (Figure 7D) content were expressed on a dry weight basis and were similar, it then stands to reason that under the high DLI treatment, both amaranth and collard greens have improved antioxidant, phenolic, and anthocyanin content due to their higher dry matter content. Amaranth has also been shown to have increased anthocyanin production when grown under 280 μmol m^{-2} s^{-1} compared to lower PPFD values (Meas et al., 2020). What's more is that for amaranth, growth under CL at the high DLI also improved overall nutrient content compared to the 21DLI/16h treatment.

Both an increase in DLI and photoperiod extension are known to impact the secondary metabolite concentrations within plants (Samuoliene et al., 2013). Increasing the PPFD during growth and/or extending the photoperiod can cause an abiotic stress response within plants as additional light is being provided, and, in this study, the plant is under CL (Demmig-Adams and Adams, 1992; Sairam et al., 2001; Brazaityte et al., 2015; Haque et al., 2015; Gharibi et al., 2016; Szymańska et al., 2017). The stress response is characterized by an increase in reactive oxygen species (ROS) and free radicals which can be detrimental to plant health if not properly addressed,

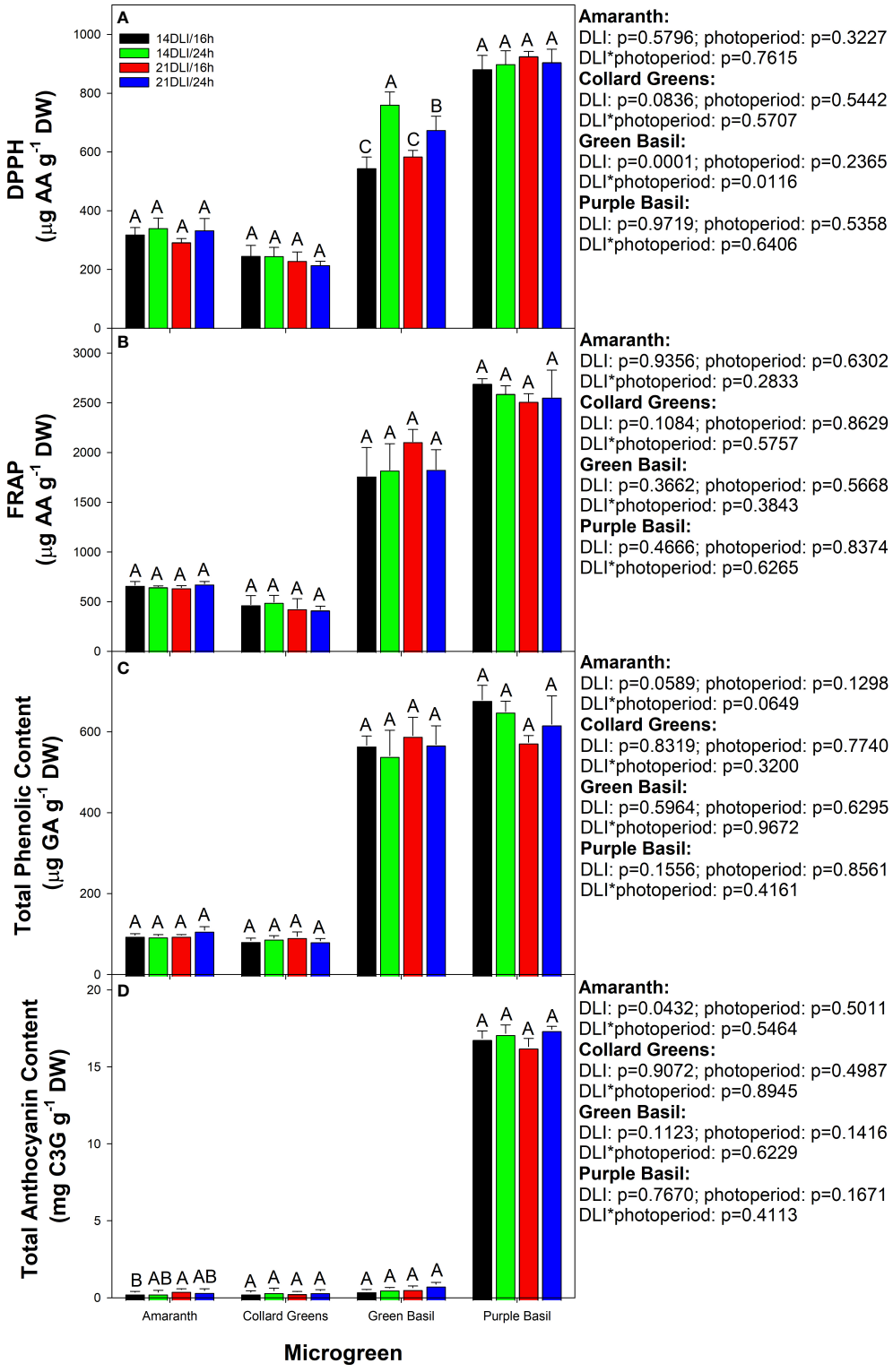

FIGURE 7
Antioxidant activities in microgreens as measured by 2,2-diphenyl-1-picrylhydrazyl (DPPH; Panel **A**), ferric reducing antioxidant power (FRAP; Panel **B**), total phenolic content (Panel **C**), and total anthocyanin content (Panel **D**) of all microgreens grown under 14DLI/16h, 14DLI/24h, 21DLI/16h, and 21DLI/24h lighting treatments. Values presented are the means of two subsamples from each of the three replicates ± the standard error of the means. Different letter groups (A–C) represent statistical differences with microgreen type and panel as determined by a two-way ANOVA within each parameter at $p<0.05$. P-values are shown to the right of the panel.

causing damage to the photosynthetic machinery (Arora et al., 2002; Pospisil et al., 2016; Huang et al., 2019). To counter the increase in free radicals, an increase in antioxidants is needed. Here, we see that under the high DLI conditions for collard greens and under high DLI and CL in amaranth, an increase in DPPH and FRAP activities was observed (Figures 7A, B). This, coupled with increased phenolic and anthocyanin levels, helps to reduce oxidative stress in the plant by channeling extra light energy away from the light harvesting complex and removing free radicals (Huang et al., 2019). Similar responses have been noted in tomatoes (Haque et al., 2015), lettuces (Zha et al., 2019), mung beans (Kumar et al., 2022), and *Brassicaceae* microgreens (Shibaeva et al., 2022b).

Notably, the increase in DPPH, FRAP, phenolics, and anthocyanins was only observed to occur in amaranth and collard greens and was absent in both basil microgreens with the exception of DPPH in green basil which was higher in the 24h treatments than the 16h treatments. However, green and purple basil had higher levels of all secondary metabolites compared to amaranth and collard greens (Figures 7). Basil is known for its incredible aroma and antioxidant concentration (Ciriello et al., 2021). Due to its already high secondary metabolic concentrations, further enhancement due to any hormetic effect of increased PPFD/DLI or photoperiod was not observed. Sutulienė et al. (2022) also observed no increase in FRAP and DPPH activity as well as total phenolic and anthocyanin content in basil when the PPFD was increased from 150 to 250 μmol m^{-2} s^{-1}. Samuoliene et al. (2013) noted the impact of PPFD is species-specific with respect to secondary metabolite concentrations. This suggests that further studies need to be done to identify species-specific secondary metabolite responses to various lighting conditions.

While increases in antioxidants, phenolics, and anthocyanins can have a beneficial response in plants under environment stressors, they can also be advantageous to humans during consumption. Similar to their radical-scavenging abilities in plants, these compounds have been shown to reduce the risk of cardiovascular disease, diabetes, cancer, and even mitigate age-related diseases in humans (Lobo et al., 2010; Engwa, 2018). Therefore, growing microgreens under high DLI and CL can produce a hormetic effect in which the plant responds to the stress of high light and/or a long photoperiod by increasing the production of important secondary metabolites which also happen to be health promoting compounds for humans.

4.3 Continuous lighting can improve yield and lower electricity cost

Since microgreens are sold on a fresh weight basis, the main goal of plant factories producing microgreens is to increase fresh biomass while minimizing inputs and maintaining nutritional content. A traditional way to increase biomass is to increase the DLI either through increased PPFD or extended photoperiods (Samuoliene et al., 2013; Meas et al., 2020). In this study, all microgreens tested, with the exception of collard greens, showed an increase in fresh weight when the DLI increased from approximately 14 mol m^{-2} d^{-1} to approximately 21 mol m^{-2} d^{-1} when the photoperiod was 16h. In general, as the DLI increases, one would expect biomass to increase as well (up to a saturation point) because more light means more photo-assimilation (Poorter et al., 2019). The increase in biomass seen here with an increase in DLI is in-line with results from previous works with other microgreen species including broccoli, arugula, mizuna, radish, tatsoi, and red pak choi (Samuoliene et al., 2013; Shibaeva et al., 2022b). However, in all microgreens studied, an increase in production due to increased DLI during a 16h photoperiod was associated with the same or increased electricity cost due to the additional light needed (Table 6). In this way, resource-use-efficiency actually decreased as DLI increased.

In this study, the continuous 24h lighting uses low intensity light throughout the production period of the plant. In this way, the plant is under constant illumination and is continuously photosynthesizing; thereby negating dark respiration and therefore, no loss of carbon occurs during the night. In fact, most plants are observed to have elevated leaf carbohydrate levels when grown under CL when nighttime light intensities are above the light compensation point (Globig et al., 1997; Matsuda et al., 2014; Pham et al., 2019). In microgreens which do not export fixed carbon to a growing fruit, CL-injury did not occur in any of the four microgreens which were studied. The extended photoperiod translated to an increase in biomass due to the accumulation of carbohydrates in the leaves – increasing resource-use-efficiency of the production system (Table 6). In fact, EUEL was increased by 10-42% and electricity cost of the light fixtures was decreased by 8-38% depending on DLIs and microgreens, when transitioning from a 16h to a 24h photoperiod.

Due to the nature of plant factories being inside buildings, all lighting requirements needed by the plant must be achieved through sole-source lighting such as LEDs. Electricity is then one of the largest input cost components for plant factories (Kozai and Niu, 2019; van Delden et al., 2021). CL can reduce the number of lighting fixtures needed (compared to a similar DLI at a 16h photoperiod) which will reduce the initial fixture cost – often a large barrier to entry into controlled environment agriculture, specifically plant factories (Hao et al., 2018). Furthermore, CL can reduce electrical costs *via* the use of lower nighttime electricity prices in regions of the world which use TOUP (Supplementary Table 1). While the data provided in Table 6 is for Ontario, Canada, other regions of the world such as some US states, 17 European nations, and South Korea use time-of-use electricity pricing, so this concept would also provide a good potential to reduce electricity costs in those regions (IRENA, 2019; IESO, 2022). In regions which do not utilize TOUP, the reduction in initial fixture cost due to the lower PPFD used during CL as well as the reduced need for heat and humidity dissipation would still provide growers with financial

TABLE 6 Electricity cost from LED lighting only of microgreens under various DLI and photoperiods.

Daily Light Integral (mol m^{-2} d^{-1})	Photoperiod (h)	Electricity Cost ($ g^{-1} FW)			
		Amaranth	Collard Greens	Green Basil	Purple Basil
14	16	0.41 ± 0.01^{A}	0.13 ± 0.02^{B}	0.65 ± 0.01^{B}	0.44 ± 0.03^{AB}
	24	0.27 ± 0.02^{B}	0.10 ± 0.01^{C}	0.60 ± 0.01^{C}	0.34 ± 0.02^{C}
21	16	0.45 ± 0.02^{A}	0.18 ± 0.02^{A}	0.76 ± 0.02^{A}	0.48 ± 0.04^{A}
	24	0.28 ± 0.02^{B}	0.14 ± 0.01^{B}	0.66 ± 0.02^{B}	0.39 ± 0.03^{B}
Daily Light Integral		0.2999	0.0001	0.0003	0.0085
Photoperiod		<0.0001	0.0005	<0.0001	0.0002
Daily Light Integral*Photoperiod		0.5666	0.2023	0.1729	0.1824

All electrical prices are for Ontario, Canada and were obtained from the Independent Electricity System Operator (IESO, 2022) for the given production periods (Supplementary Table 1). All prices are in Canadian dollars. Electricity usage was calculated using the Flexstar 645W with appropriate dimming capabilities to reach the desired light intensities (Table 1). Electricity costs are calculated by using the total electricity costs related to lighting for each production period (i.e., replicate) and dividing that by the actually fresh biomass produced in said production period. Values presented are the means of three growth trials, each representing one replicate ± the standard error of the means. Different letter groups (A, B, C) represent statistical differences as determined by a two-way ANOVA within each parameter at $p<0.05$.

gains (Goto, 2012; Kozai and Niu, 2016; Kozai et al., 2016; Graamans et al., 2018). Plant factories typically require extensive air conditioning in order to maintain proper temperature and humidity for plants; mostly to overcome heat generated by the LED fixtures (Wang et al., 2014; Graamans et al., 2018) and to remove the moisture from plant transpiration. The use of CL not only reduces the overall amount of fixtures, but allows the grower to reduce the PPFD by 33% at the same DLI (Table 1). Together, both the reduction in overall fixtures and lower PPFD used means less heat and moisture will be produced within the plant factory which in turn translates to less need for energy consuming air conditioning. The use of CL and subsequent reduction in fixtures needed, heat emittance, and moisture generation can also be useful for space travel as power consumption and heat loss can be large challenges in self-supporting food production (Stutte, 2015).

In this study, at the same DLI, amaranth and green basil produced higher fresh biomass when grown under CL when compared to the 16h lighting treatments (Tables 2, 4). Even in collard greens and purple basil, the use of reduced electrical prices during the night lowered electricity cost in 24h treatments making them more cost effective than their 16h counterparts (Table 6). The microgreens studied here join a growing list of plants which can tolerate CL including other microgreen species (Shibaeva et al., 2022b), lettuces (Ohtake et al., 2018), cucumbers (Lanoue et al., 2021b), peppers (Lanoue et al., 2022), and tomatoes (Haque et al., 2017; Lanoue et al., 2019).

5 Conclusion

Plant factories require the use of sole-source lighting with intensive energy input. It usually requires high capital investment due to the high costs of LED and HVAC equipment. CL has been studied in many plant systems and represents a potential strategy to lower fixture needs and reduce PPFD during prolonged photoperiods; resulting in reduced electricity costs. Here we show that four microgreens, amaranth, collard greens, green basil, and purple basil have increased fresh biomass accumulation and/or reduced electricity costs when grown under CL regardless of DLIs. Furthermore, the use of high DLI in collard greens and high DLI and CL in amaranth increased DPPH and FRAP activities as well as phenolic and anthocyanin content. Green basil and purple basil maintained their secondary metabolite concentrations while still having reduced electricity costs when grown under CL. In this way, the use of CL for microgreen production can improve energy efficiency while maintaining or increasing antioxidants, phenolics, and anthocyanins making it a more sustainable lighting strategy than high intensity short photoperiod lighting.

Data availability statement

The original contributions presented in the study are included in the article/Supplementary Material. Further inquiries can be directed to the corresponding author.

Author contributions

JL and XH were involved in the conceptualization, methodology development, and writing. JL, XH, and CL edited the manuscript. JL SS and CL were involved in data curation and day-to-day upkeep of the experiment. JL performed data analysis. XH was responsible for funding

acquisition. All authors have read and agreed to the submitted manuscript.

Funding

The project is funded by the Foundation Science Program of Agriculture and Agri-Food Canada to XH (J-002228.001.04).

Conflict of interest

The authors declare that the research was conducted in the absence of any commercial or financial relationships that could be construed as a potential conflict of interest.

Publisher's note

Supplementary material

The Supplementary Material for this article can be found online at: https://www.frontiersin.org/articles/10.3389/fpls.2022.983222/full#supplementary-material

References

Ainsworth, E. A., and Gillespie, K. M. (2007). Estimation of total phenolic content and other oxidation substrates in plant tissues using folin-ciocalteu reagent. *Nat. Protoc.* 2, 875–877. doi: 10.1038/nprot.2007.102

Alrifai, O., Hao, X., Liu, R., Lu, Z., Marcone, M. F., and Tsao, R. (2020). Amber, red and blue LEDs modulate phenolic contents and antioxidant activities in eight cruciferous microgreens. *J. Food Bioact.* 11, 95–109. doi: 10.31665/jfb.2020.11241

Arora, A., Sairam, R. K., and Srivastava, G. C. (2002). Oxidative stress and antioxidative system in plants. *Curr. Sci.* 82, 1227–1238.

Brazaityte, A., Viršile, A., Jankauskiene, J., Sakalauskiene, S., Samuoliene, G., Sirtautas, R., et al. (2015). Effect of supplemental UV-a irradiation in solid-state lighting on the growth and phytochemical content of microgreens. *Int. Agrophysics* 29, 13–22. doi: 10.1515/intag-2015-0004

Buttery, B. R., and Buzzell, R. I. (1977). The relationship between chlorophyll content and rate of photosynthesis in soybeans. *Can. J. Plant Sci.* 57, 1–5. doi: 10.4141/cjps77-001

Choe, U., Yu, L. L., and Wang, T. T. Y. (2018). The science behind microgreens as an exciting new food for the 21st century. *J. Agric. Food Chem.* 66, 11519–11530. doi: 10.1021/acs.jafc.8b03096

Ciriello, M., Formisano, L., El-Nakhel, C., Corrado, G., Pannico, A., De Pascale, S., et al. (2021). Morpho-physiological responses and secondary metabolites modulation by preharvest factors of three hydroponically grown genovese basil cultivars. *Front. Plant Sci.* 12. doi: 10.3389/fpls.2021.671026

Demers, D. A., and Gosselin, A. (2002). Growing greenhouse tomato and sweet pepper under supplemental lighting: Optimal photoperiod, negative effects of long photoperiod and their causes. *Acta Hortic.* 580, 83–88. doi: 10.17660/ActaHortic.2002.580.9

Demmig-Adams, B., and Adams, W. W. (1992). Photoprotection and other responses of plants to high light stress. *Annu. Rev. Plant Physiol. Plant Mol. Biol.* 43, 599–626. doi: 10.1146/annurev.pp.43.060192.003123

Engwa, G. A. (2018). "Free radicals and the role of plant phytochemicals as antioxidants against oxidative stress-related diseases," in *Phytochemicals*. Eds. T. Asao and M. Asaduzzaman, 13 BoD- Books on Demand; Norderstedt Germany. doi: 10.5772/intechopen.76719

Fan, X. X., Xu, Z. G., Liu, X. Y., Tang, C. M., Wang, L. W., and Han, X. (2013). Effects of light intensity on the growth and leaf development of young tomato plants grown under a combination of red and blue light. *Sci. Hortic. (Amsterdam).* 153, 50–55. doi: 10.1016/j.scienta.2013.01.017

Gharibi, S., Tabatabaei, B. E. S., Saeidi, G., and Goli, S. A. H. (2016). Effect of drought stress on total phenolic, lipid peroxidation, and antioxidant activity of achillea species. *Appl. Biochem. Biotechnol.* 178, 796–809. doi: 10.1007/s12010-015-1909-3

Globig, S., Rosen, I., and Janes, H. W. (1997). Continuous light effects on photosynthesis and carbon metabolism in tomato. *Acta Hortic.* 418, 141–151. doi: 10.17660/actahortic.1997.418.19

Goto, E. (2012). Plant production in a closed plant factory with artificial lighting. *Acta Hortic.* 956, 37–49. doi: 10.17660/ActaHortic.2012.956.2

Graamans, L., Baeza, E., van den Dobbelsteen, A., Tsafaras, I., and Stanghellini, C. (2018). Plant factories versus greenhouses: Comparison of resource use efficiency. *Agric. Syst.* 160, 31–43. doi: 10.1016/j.agsy.2017.11.003

Hao, X., Guo, X., Lanoue, J., Zhang, Y., Cao, R., Zheng, J., et al. (2018). A review on smart application of supplemental lighting in greenhouse fruiting vegetable production. *Acta Hortic.* 1227, 499–506. doi: 10.17660/ActaHortic.2018.1227.63

Haque, M. S., de Sousa, A., Soares, C., Kjaer, K. H., Fidalgo, F., Rosenqvist, E., et al. (2017). Temperature variation under continuous light restores tomato leaf photosynthesis and maintains the diurnal pattern in stomatal conductance. *Front. Plant Sci.* 8. doi: 10.3389/fpls.2017.01602

Haque, M. S., Kjaer, K. H., Rosenqvist, E., and Ottosen, C. O. (2015). Continuous light increases growth, daily carbon gain, antioxidants, and alters carbohydrate metabolism in a cultivated and a wild tomato species. *Front. Plant Sci.* 6. doi: 10.3389/fpls.2015.00522

Huang, H., Ullah, F., Zhou, D. X., Yi, M., and Zhao, Y. (2019). Mechanisms of ROS regulation of plant development and stress responses. *Front. Plant Sci.* 10. doi: 10.3389/fpls.2019.00800

IESO (2022) *Independent electricity system operator - power data*. Available at: https://www.ieso.ca/power-data.

IRENA (2019) *International renewable energy agency - time-of-Use tariffs*. Available at: https://www.irena.org/-/media/Files/IRENA/Agency/Publication/2019/Feb/IRENA_Innovation_ToU_tariffs_2019.pdf.

Kozai, T. (2018). Benefits, problems and challenges of plant factories with artificial lighting (PFALs): A short review. *Acta Hortic.* 1227, 25–30. doi: 10.17660/ActaHortic.2018.1227.3

Kozai, T., Fujiwara, K., and Runkle, E. S. (2016). doi: 10.1007/978-981-10-1848-0_1

Kozai, T., and Niu, G. (2016). "Plant Factory: An Indoor Vertical Farming System for Efficient Quality Food Production," (Elsevier Inc) Cambridge, Massachusetts, USA. doi: 10.1016/B978-0-12-801775-3.00004-4

Kozai, T., and Niu, G. (2019). "Plant Factory: An Indoor Vertical Farming System for Efficient Quality Food Poduction:," (Elsevier Inc) Cambridge, Massachusetts, USA. doi: 10.1016/B978-0-12-816691-8.00002-9

Kumar, D., Singh, H., Bhatt, U., and Soni, V. (2022). Effect of continuous light on antioxidant activity, lipid peroxidation, proline and chlorophyll content in vigna radiata l. *Funct. Plant Biol.* 49, 145–154. doi: 10.1071/FP21226

Kyriacou, M. C., El-Nakhel, C., Graziani, G., Pannico, A., Soteriou, G. A., Giordano, M., et al. (2019). Functional quality in novel food sources: Genotypic variation in the nutritive and phytochemical composition of thirteen microgreens species. *Food Chem.* 277, 107–118. doi: 10.1016/j.foodchem.2018.10.098

Kyriacou, M. C., Rouphael, Y., Di Gioia, F., Kyratzis, A., Serio, F., Renna, M., et al. (2016). Micro-scale vegetable production and the rise of microgreens. *Trends Food Sci. Technol.* 57, 103–115. doi: 10.1016/j.tifs.2016.09.005

Lanoue, J., Leonardos, E. D., and Grodzinski, B. (2018). Effects of light quality and intensity on diurnal patterns and rates of photo-assimilate translocation and transpiration in tomato leaves. *Front. Plant Sci.* 9. doi: 10.3389/fpls.2018.00756

Lanoue, J., Leonardos, E. D., Ma, X., and Grodzinski, B. (2017). The effect of spectral quality on daily patterns of gas exchange, biomass gain, and water-use-efficiency in tomatoes and lisianthus: An assessment of whole plant measurements. *Front. Plant Sci.* 8. doi: 10.3389/fpls.2017.01076

Lanoue, J., Little, C., and Hao, X. (2022). The power of far-red light at Night : Photomorphogenic , physiological , and yield response in pepper during dynamic 24 hour lighting. *Frontiers in Plant Science* 13, 1–19. doi: 10.3389/fpls.2022.857616

Lanoue, J., Thibodeau, A., Little, C., Zheng, J., Grodzinski, B., and Hao, X. (2021a). Light spectra and root stocks affect response of greenhouse tomatoes to long photoperiod of supplemental lighting. *Plants* 10, 1–23. doi: 10.3390/plants10081674

Lanoue, J., Zheng, J., Little, C., Grodzinski, B., and Hao, X. (2021b). Continuous light does not compromise growth and yield in mini-cucumber greenhouse production with supplemental led light. *Plants* 10, 1–18. doi: 10.3390/plants10020378

Lanoue, J., Zheng, J., Little, C., Thibodeau, A., Grodzinski, B., and Hao, X. (2019). Alternating red and blue light-emitting diodes allows for injury-free tomato production with continuous lighting. *Front. Plant Sci.* 10. doi: 10.3389/fpls.2019.01114

Lee, J., Durst, R. W., and Wrolstad, R. E. (2005). Determination of total monomeric anthocyanin pigment content of fruit juices, beverages, natural colorants, and wines by the pH differential method: Collaborative study. *J. AOAC Int.* 88, 1269–1278. doi: 10.1093/jaoac/88.5.1269

Lichtenthaler, H. K. (1987). Chlorophylls and carotenoids: Pigments of photosynthetic biomembranes. *Methods Enzymol.* 148, 350–382. doi: 10.1016/0076-6879(87)48036-1

Lobo, V., Patil, A., Phatak, A., and Chandra, N. (2010). Free radicals, antioxidants and functional foods: Impact on human health. *Pharmacogn. Rev.* 4, 118–126. doi: 10.4103/0973-7847.70902

Marie, T. R. J. G., Leonardos, E. D., Lanoue, J., Hao, X., Micallef, B. J., and Grodzinski, B. (2022). A perspective emphasizing circadian rhythm entrainment to ensure sustainable crop production in controlled environment agriculture: Dynamic use of LED cues. *Front. Sustain. Food Syst.* 6. doi: 10.3389/fsufs.2022.856162

Matos, F. S., Wolfgramm, R., Gonçalves, F. V., Cavatte, P. C., Ventrella, M. C., and DaMatta, F. M. (2009). Phenotypic plasticity in response to light in the coffee tree. *Environ. Exp. Bot.* 67, 421–427. doi: 10.1016/j.envexpbot.2009.06.018

Matsuda, R., Ozawa, N., and Fujiwara, K. (2014). Leaf photosynthesis, plant growth, and carbohydrate accumulation of tomato under different photoperiods and diurnal temperature differences. *Sci. Hortic. (Amsterdam).* 170, 150–158. doi: 10.1016/j.scienta.2014.03.014

Meas, S., Luengwilai, K., and Thongket, T. (2020). Enhancing growth and phytochemicals of two amaranth microgreens by LEDs light irradiation. *Sci. Hortic. (Amsterdam).* 265, 109204. doi: 10.1016/j.scienta.2020.109204

Murage, E. N., and Masuda, M. (1997). Response of pepper and eggplant to continuous light in relation to leaf chlorosis and activities of antioxidative enzymes. *Sci. Hortic. (Amsterdam).* 70, 269–279. doi: 10.1016/S0304-4238(97)00078-2

Ohtake, N., Ishikura, M., Suzuki, H., Yamori, W., and Goto, E. (2018). Continuous irradiation with alternating red and blue light enhances plant growth while keeping nutritional quality in lettuce. *HortScience* 53, 1804–1809. doi: 10.21273/HORTSCI13469-18

Palmer, S., and van Iersel, M. W. (2020). Increasing growth of lettuce and mizuna under sole-source LED lighting using longer photoperiods with the same daily light integral. *Agronomy* 10 1–12. doi: 10.3390/agronomy10111659

Pennisi, G., Orsini, F., Landolfo, M., Pistillo, A., Crepaldi, A., Nicola, S., et al. (2020). Optimal photoperiod for indoor cultivation of leafy vegetables and herbs. *Eur. J. Hortic. Sci.* 85, 329–338. doi: 10.17660/eJHS.2020/85.5.4

Pham, M. D., Hwang, H., Park, S. W., Cui, M., Lee, H., and Chun, C. (2019). Leaf chlorosis, epinasty, carbohydrate contents and growth of tomato show different responses to the red/blue wavelength ratio under continuous light. *Plant Physiol. Biochem.* 141, 477–486. doi: 10.1016/j.plaphy.2019.06.004

Poorter, H., Niinemets, Ü., Ntagkas, N., Siebenkäs, A., Mäenpää, M., Matsubara, S., et al. (2019). A meta-analysis of plant responses to light intensity for 70 traits ranging from molecules to whole plant performance. *New Phytol.* 223, 1073–1105. doi: 10.1111/nph.15754

Pospisil, P. (2016). Production of reactive oxygen species by photosystem II as a response to light and temperature stress. *Front. Plant Sci.* 7: 1950. 1–2 doi: 10.3389/fpls.2016.01950

Sairam, R. K., Chandrasekhar, V., and Srivastava, G. C. (2001). Increased antioxidant acitivity under elevated temperatures: a mechanism of heat stress tolerance in wheat genotypes. *Biol. Plant* 44, 89–94.

Samuoliene, G., Brazaityte, A., Jankauskiene, J., Viršile, A., Sirtautas, R., Novičkovas, A., et al. (2013). LED irradiance level affects growth and nutritional quality of brassica microgreens. *Cent. Eur. J. Biol.* 8, 1241–1249. doi: 10.2478/s11535-013-0246-1

Shibaeva, T. G., Mamaev, A. V., Sherudilo, E. G., and Titov, A. F. (2022a). The role of photosynthetic daily light integral in plant response to extended photoperiods. *Russ. J. Plant Physiol.* 69, 1–8. doi: 10.1134/s1021443722010216

Shibaeva, T. G., Sherudilo, E. G., Rubaeva, A. A., and Titov, A. F. (2022b). Continuous LED lighting enhances yield and nutritional value of four genotypes of brassicaceae microgreens. *Plants* 11, 1–14. doi: 10.3390/plants11020176

Stutte, G. W. (2015). Commercial transition to leds: A pathway to high-value products. *HortScience* 50, 1297–1300. doi: 10.21273/hortsci.50.9.1297

Sutulienė, R., Laužikė, K., Pukas, T., and Samuolienė, G. (2022). Effect of light intensity on the growth and antioxidant activity of sweet basil and lettuce. *Plants* 11 1–14. doi: 10.3390/plants11131709

Sysoeva, M., Markovskaya, E., and Shibaeva, T. (2010). Plants under continuous light: A review. *Plant Stress* 4, 5–17.

Szymańska, R., Ślesak, I., Orzechowska, A., and Kruk, J. (2017). Physiological and biochemical responses to high light and temperature stress in plants. *Environ. Exp. Bot.* 139, 165–177. doi: 10.1016/j.envexpbot.2017.05.002

van Delden, S. H., SharathKumar, M., Butturini, M., Graamans, L. J. A., Heuvelink, E., Kacira, M., et al. (2021). Current status and future challenges in implementing and upscaling vertical farming systems. *Nat. Food* 2, 944–956. doi: 10.1038/s43016-021-00402-w

Vaštakaitė-Kairienė, V., Brazaitytė, A., Miliauskienė, J., Sutulienė, R., Lauzike, K., Viršilė, A., et al. (2022). Photon distribution of sole-source lighting affects the mineral nutrient content of microgreens. *Agric.* 12 1–14. doi: 10.3390/agriculture12081086

Velez-Ramirez, A. I., Dünner-Planella, G., Vreugdenhil, D., Millenaar, F. F., and Van Ieperen, W. (2017). On the induction of injury in tomato under continuous light: Circadian asynchrony as the main triggering factor. *Funct. Plant Biol.* 44, 597–611. doi: 10.1071/FP16285

Velez-Ramirez, A. I., Van Ieperen, W., Vreugdenhil, D., and Millenaar, F. F. (2011). Plants under continuous light. *Trends Plant Sci.* 16, 310–318. doi: 10.1016/j.tplants.2011.02.003

Velez-Ramirez, A. I., Van Ieperen, W., Vreugdenhil, D., Van Poppel, P. M. J. A., Heuvelink, E., and Millenaar, F. F. (2014). A single locus confers tolerance to continuous light and allows substantial yield increase in tomato. *Nat. Commun.* 5, 1–13. doi: 10.1038/ncomms5549

Velez-Ramirez, A. I., Vreugdenhil, D., Heuvelink, E., Van Ieperen, W., and Millenaar, F. F. (2012). Continuous light as a way to increase greenhouse tomato production: Expected challenges. *Acta Hortic.* 956, 51–57. doi: 10.17660/ActaHortic.2012.956.3

Viršilė, A., Brazaitytė, A., Vaštakaitė-Kairienė, V., Miliauskienė, J., Jankauskienė, J., Novičkovas, A., et al. (2019). Lighting intensity and photoperiod serves tailoring nitrate assimilation indices in red and green baby leaf lettuce. *J. Sci. Food Agric.* 99, 6608–6619. doi: 10.1002/jsfa.9948

Wang, J., Yang, Q., Tong, Y., and Wei, L. (2014). Reduction in electric-energy consumption for cooling in a plant factory with artificial light. *Acta Hortic.* 1037, 293–298. doi: 10.17660/actahortic.2014.1037.34

Weaver, G., and van Iersel, M. W. (2020). Longer photoperiods with adaptive lighting control can improve growth of greenhouse-grown 'Little gem' lettuce (Lactuca sativa). *HortScience* 55, 573–580. doi: 10.21273/HORTSCI14721-19

Xiao, Z., Lester, G. E., Luo, Y., and Wang, Q. (2012). Assessment of vitamin and carotenoid concentrations of emerging food products: Edible microgreens. *J. Agric. Food Chem.* 60, 7644–7651. doi: 10.1021/jf300459b

Zha, L., Liu, W., Zhang, Y., Zhou, C., and Shao, M. (2019). Morphological and physiological stress responses of lettuce to different intensities of continuous light. *Front. Plant Sci.* 10. doi: 10.3389/fpls.2019.01440

Zhu, X. G., Long, S. P., and Ort, D. R. (2008). What is the maximum efficiency with which photosynthesis can convert solar energy into biomass? *Curr. Opin. Biotechnol.* 19, 153–159. doi: 10.1016/j.copbio.2008.02.004

frontiers | Frontiers in Plant Science

TYPE Review
PUBLISHED 21 October 2022
DOI 10.3389/fpls.2022.1029901

OPEN ACCESS

EDITED BY
Yuxin Tong,
Institute of Environment and Sustainable Development in Agriculture (CAAS), China

REVIEWED BY
Toyoki Kozai,
Japan Plant Factory Association, Japan
Bruce Dunn,
Oklahoma State University, United States

*CORRESPONDENCE
Kai Shi
kaishi@zju.edu.cn

SPECIALTY SECTION
This article was submitted to Technical Advances in Plant Science, a section of the journal Frontiers in Plant Science

RECEIVED 28 August 2022
ACCEPTED 07 October 2022
PUBLISHED 21 October 2022

CITATION
Wang A, Lv J, Wang J and Shi K (2022) CO_2 enrichment in greenhouse production: Towards a sustainable approach.
Front. Plant Sci. 13:1029901.
doi: 10.3389/fpls.2022.1029901

CO_2 enrichment in greenhouse production: Towards a sustainable approach

Anran Wang[1], Jianrong Lv[1], Jiao Wang[1] and Kai Shi[1,2]*

[1]Department of Horticulture, Zhejiang University, Hangzhou, China, [2]Yazhou Bay Science and Technology City, Hainan Institute, Zhejiang University, Sanya, China

As the unique source of carbon in the atmosphere, carbon dioxide (CO_2) exerts a strong impact on crop yield and quality. However, CO_2 deficiency in greenhouses during the daytime often limits crop productivity. Crucially, climate warming, caused by increased atmospheric CO_2, urges global efforts to implement carbon reduction and neutrality, which also bring challenges to current CO_2 enrichment systems applied in greenhouses. Thus, there is a timely need to develop cost-effective and environmentally friendly CO_2 enrichment technologies as a sustainable approach to promoting agricultural production and alleviating environmental burdens simultaneously. Here we review several common technologies of CO_2 enrichment in greenhouse production, and their characteristics and limitations. Some control strategies of CO_2 enrichment in distribution, period, and concentration are also discussed. We further introduce promising directions for future CO_2 enrichment including 1) agro-industrial symbiosis system (AIS); 2) interdisciplinary application of carbon capture and utilization (CCU); and 3) optimization of CO_2 assimilation in C_3 crops *via* biotechnologies. This review aims to provide perspectives on efficient CO_2 utilization in greenhouse production.

KEYWORDS

carbon dioxide, elevated CO_2, controlled environment agriculture, horticulture, agro-industrial symbiosis system, carbon capture and utilization, CO_2 assimilation

Introduction

Food security requires greater and more consistent crop production against a backdrop of climate change and population growth (Bailey-Serres et al., 2019). Greenhouses offer solutions for protecting crops from extreme weather events and provide more suitable conditions for crop growth than open field cropping (Syed and Hachem, 2019). However, crops grown in greenhouses still suffer from multiple suboptimal conditions, one of which is frequent insufficient CO_2 availability, limiting crop yield and quality (Poudel and Dunn, 2017). Due to a relatively airtight environment and crop uptake of CO_2, the CO_2 concentration in greenhouse drops to

only 100~250 μmol mol^{-1} in the daytime, which is below the ambient CO_2 level of 350~450 μmol mol^{-1} even with effective ventilation, and is far below the optimal concentration required for crop growth, 800~1000 μmol mol^{-1} (Figure 1; Pascale and Maggio, 2008; Zhang et al., 2014; Merrill et al., 2016).

Although various CO_2 enrichment technologies have been developed for applications in protected cultivation for decades, CO_2 concentration around the crop canopy is still a complex variate in modern agricultural environment control systems (Table 1; Linker et al., 1999; Kläring et al., 2007; Li et al., 2018). Unlike other environmental factors, CO_2 needs to be controlled at a micro level (10^2 ~10^3 μmol mol^{-1}), and is highly affected by ventilation, plant growth period, and weather (Wang et al., 2016; Li et al., 2018).

Currently, the ongoing global climate warming brings challenges to innovating and upgrading existing agricultural CO_2 enrichment systems. Several key issues need to be addressed in terms of carbon reduction, such as direct CO_2 emissions caused by an imbalance between CO_2 supply, crop uptake, and ventilation operation (Vermeulen, 2014; Kozai et al., 2015), and resource consumption during the generation, transportation, storage of pure CO_2 (Vermeulen, 2014). Moreover, the promotion of clean energy uses forces greenhouses that obtain CO_2 from boiler heating systems to seek new enrichment solutions (Marttila et al., 2021).

Increasing endeavors are being devoted to improving CO_2 enrichment in greenhouse production, while comprehensive articles on various techniques and solutions explored in production practices and scientific research are few. Here we review CO_2 enrichment technologies and strategies applied in current greenhouse production or laboratory, focusing on their advantages and obstacles, and further summarize three promising directions for future agricultural CO_2 enrichment, aiming to provide a sustainable approach to ensure food and climate security through agriculture.

Effects of CO_2 enrichment on greenhouse crops

The crops grown in greenhouses are mainly C_3 plants, such as tomatoes and cucumbers (Sage, 2017). Due to a lack of efficient mechanisms to cope with CO_2 scarcity, C_3 crops are more sensitive to changes in CO_2 concentrations compared with C_4 plants and CAM plants (Long et al., 2015). Importantly, C_3 crops have a more positive response to increased CO_2 concentrations (Ainsworth and Long, 2020). For instance, a moderate CO_2 elevation of 550 ~ 650 μmol mol^{-1} improves the yield of various C_3 crops by an average of 18% (Ainsworth and Long, 2020). Moreover, the CO_2 concentration of around 1000 μmol mol^{-1} promotes the contents of soluble sugar and some nutrients of leafy, fruit and root vegetables by around 10% ~ 60% (Dong et al., 2018). As summarized in Figure 2, elevated CO_2 is involved in a multitude of physiological activities in C_3 crops including photosynthesis, signaling pathway, organ development, as well as the resistance to biotic and abiotic stresses, and CO_2 enrichment further improves the yield and quality, and enhances the utilization efficiency of light and water (Zhang et al., 2015; Hu et al., 2021; Ahammed and Li, 2022). More detailed descriptions can be found in reviews by Xu et al. (2015); Dong et al. (2018); Kazan (2018); Ahammed et al. (2021); Poorter et al. (2021); Roy and Mathur (2021), and Chaudhry and Sidhu (2022).

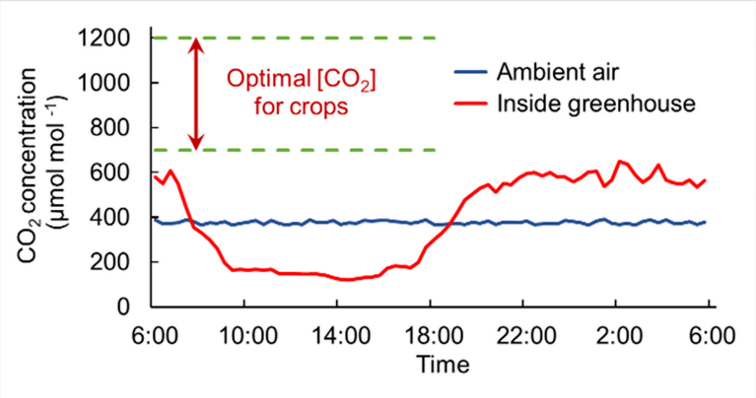

FIGURE 1
Schematic diagram of CO_2 deficiency in greenhouse production. CO_2 in the greenhouse (red curve) accumulates at night due to crop respiration, while the CO_2 concentration decreases sharply after light exposure due to CO_2 absorption by crops through photosynthesis, which is far below the crop demand (the range within green dotted lines), almost the whole daytime. The blue curve represents the CO_2 level in the ambient air outside. The data for plotting the line graphs refer to the text in Zhang et al. (2014); Noctor and Mhamdi (2017); Dong et al. (2018); Li et al. (2018), and figures in Sánchez-Guerrero et al. (2005) and Kläring et al. (2007).

TABLE 1 Application examples of different CO_2 enrichment technologies reported in scientific articles.

Enrichment technology	Principle	Crops	Treatment/control	Production effects of CO_2 enrichment	References
Compressed CO_2 injection	Physical diffusion	Lettuce	700/400 ± 20 mol mol^{-1}	Higher growth rates; Enhanced antioxidant capacity	Pérez-López et al., 2015
Injection & Ventilation	Physical diffusion	Cucumber	400-500/285-300 mol mol^{-1} average throughout the day	Increased fruit biomass; slightly effect on leaf area index	Sánchez-Guerrero et al., 2005
Biogas burning	Chemical reaction	Rose	800~2500 mol mol^{-1}/ normal atmosphere	Enhanced fresh mass of cut flowers	Jaffrin et al., 2003
Mixing baking soda with acid	Chemical reaction	Mostly mentioned in reviews			Syed and Hachem, 2019
Composting	Biological activity	Tomato	800–900 mol mol^{-1}/ not mentioned	Increased nutritional and sensory quality of fruits	Zhang et al., 2014

Current CO_2 enrichment technologies

Atmosphere ventilation

Ventilation allows exchanges of heat and CO_2 inside and outside the greenhouse by means of natural ventilation with roof/side windows or forced ventilation (Ishii et al., 2014; Yasutake et al., 2017). Although ventilation can supply CO_2 into greenhouses from atmosphere continuously, it is typically to regulate temperature preferentially, and an extra supply of CO_2 is necessary for geographically cold regions with restricted ventilation (Stanghellini et al., 2008). Moreover, ventilation alone is not enough to maintain CO_2 concentration around crops at an ambient air level (Pascale and Maggio, 2008), and crop yield is more heavily dependent on CO_2 at a lower concentration (below 450 μmol mol^{-1}) than a higher concentration (Vermeulen, 2014).

Compressed CO_2

The direct supply of compressed CO_2 ensures a stable and clean airflow. However, due to the high market price and transportation cost, it is more commonly used as a complement to other techniques or in scientific research such as Free-Air CO_2 Enrichment (FACE) (Sánchez-Guerrero et al., 2005; Allen et al., 2020). In addition, compressed CO_2 needs to be equipped with devices for gas storage and pressure control that most often occupy some space in greenhouses (Kuroyanagi et al., 2014; Poudel and Dunn, 2017; Li et al., 2018).

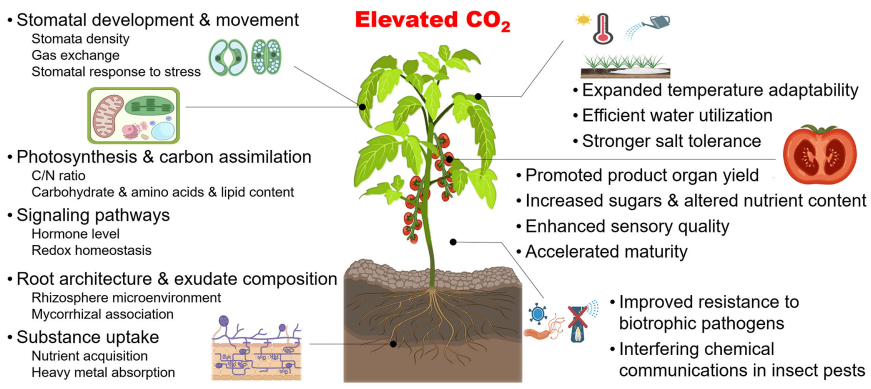

FIGURE 2
Schema illustrating effects of elevated CO_2 on C_3 crops. Elevated CO_2 affects a series of plant biological processes (left) in C_3 crops, including stomatal development and movement, photosynthesis, and carbon assimilation, signaling pathways, root development and exudate composition, and nutrient acquisition. Meanwhile, macro-production effects (right) can also contribute to promoted yield and quality, enhanced tolerance to abiotic stress and improved resistance to several biotic stresses, which invigorate efficient and safe agricultural production to a certain extent. Created with BioRender.com.

Carbonaceous fuel burning

When heating the greenhouse by combustion of natural gas, coal, biomass, and other carbonaceous fuels, CO_2 generated during the processes can be delivered to crops or collected and stored for further use (Vermeulen, 2014). As a relatively effective approach to the reduction of carbon emissions and production costs, this technique is adopted widely in current greenhouse production (Dion et al., 2011; Marchi et al., 2018). Moreover, ventilation is often closed during heating, which ensures a better effect of CO_2 enrichment (Kläring et al., 2007). A major limitation, however, is that for areas or seasons that do not require heating, burning fuel for CO_2 is undesirable.

Given that the gas obtained from the combustion boiler carries too much heat and harmful gases, such as NO_x, SO_2 and CO, efficient procedures of cooling and purification are essentially required (Roy et al., 2014; Li et al., 2018). In addition, the time and dosage requirements often mismatch between CO_2 and heat, resulting in a need for collection and storage devices and flow controllers of CO_2 (Dion et al., 2011). Takeya et al. (2017) proposed a system to collect an appropriate amount of CO_2 at night when the heating system is turned on and the gas can be released in the daytime when crops have a strong demand for CO_2.

Notably, it is an increasingly urgent issue to replace carbonaceous fuels with clean energy to reduce carbon emissions, such as solar energy, hydrogen energy, geothermal energy, and even industrial waste heat (Vermeulen, 2014; Marttila et al., 2021). Meanwhile, the cost of production activities generating carbon emissions has increased drastically. Therefore, greenhouses obtaining CO_2 from heating systems are facing a challenge to find alternative CO_2 enrichment techniques (Vermeulen, 2014).

Chemical reaction

The chemical reactions of bicarbonate (such as baking soda) with acid and the decomposition by direct heating are relatively cheap and fast to obtain pure CO_2 quantitatively (Syed and Hachem, 2019). The CO_2 production rate can be controlled theoretically while the operation in practice is complicated, and a large amount of CO_2 generated out of control is wasted and can damage plants (Poudel and Dunn, 2017). Besides, ammonia bicarbonate is sometimes used as a raw material, which can produce by-products used as fertilizers. However, there is a threat of ammonia gas poisoning, so NH_3 filtration is mandatory in such cases (Sun et al., 2016).

Compost fermentation

Decomposition of carbon-rich agricultural wastes by microbial fermentation to release CO_2 for crop production is considered a beneficial technology to increase production, reduce agricultural carbon emissions, and lower environmental pollution at the same time (Karim et al., 2020). But there are strict restrictions on C/N ratio, pH, temperature, materials, and other conditions (Jin et al., 2009; Karim et al., 2020). Technologies that use crop-residues and animal-manure composting (CRAM) to increase CO_2 were developed to improve vegetable yield and quality (Jin et al., 2009; Karim et al., 2020). Secondary fermentation products could also be reused as a source of CO_2 (Liu et al., 2021). Necessary measures should be taken to deal with several weaknesses in compost fermentation, such as 1) associated unpleasant odors; 2) threat of ammonia poisoning (Li et al., 2018); 3) unstable rate of generated CO_2 (Karim et al., 2020); and 4) a larger space and more labor input requirements compared with other enrichment techniques (Tang et al., 2022).

Control strategies of CO_2 enrichment

The CO_2-use efficiency (CUE), defined as the ratio of net photosynthetic rate to CO_2 supply rate, suffers from various factors, such as excess supply, natural leakage, sensitive growth state of plants, and other environmental and biological components (Sánchez-Guerrero et al., 2005; Kuroyanagi et al., 2014; Li et al., 2018). The values of CUE in greenhouses are generally lower than 60%, which means that a considerable amount of CO_2 is released into the ambient atmosphere (Kozai, 2013; Kuroyanagi et al., 2014). Thereby, numerous attempts have been made on control strategies of CO_2 enrichment from various aspects to improve the CUE in the greenhouse.

Spatial distribution

The uniformity of environmental elements contributes to a unified and efficient management of greenhouse cultivation, while the spatially uneven distribution of CO_2 is universal in almost all greenhouse cultivation (Li et al., 2018). Due to the lack of air circulation and the relatively slow diffusion, CO_2 concentration is extremely low around the canopy with high leaf density where CO_2 is in most demand (Hidaka et al., 2022). Enrichment systems, with single-point outlet, make CO_2 more uneven in space, resulting in great waste and failure to meet the production demand (Zhang et al., 2020). Thus, some conveying pipes with holes around the leaves need to be assembled. Hidaka et al. (2022) applied pipe-delivered crop-local CO_2 enrichment in strawberry cultivation and achieved increased yield with CO_2 supply savings. Another option is by means of internal airflow stirring devices, which is also feasible (Boulard et al., 2017; Syed and Hachem, 2019).

Period setting

There are various modes in the period setting of CO_2 enrichment, such as throughout the day and night, during the daytime, and only in the morning or nighttime. Enrichment throughout the day and night or the whole daytime is generally adopted in controlled chambers for experimental purposes (e.g., Mamatha et al., 2014; Hu et al., 2021). Apparently, it is high energy-consuming and carbon-emitting to elevate CO_2 all day in production, especially since the carbon assimilation is typically most intense in the morning of the whole day (Xu et al., 2014). More critically, photosynthetic acclimation can occur with crops over prolonged periods of exposure to elevated CO_2 (Wang et al., 2013). Thus, strategies of enriching CO_2 only in the morning rather than all daytime have been explored. Treatments of elevating CO_2 only in the morning promoted biomass accumulation and flower/fruit quality with no difference from enriching throughout the daytime in some cases (Caliman et al., 2009; Xu et al., 2014). However, another similar strategy of CO_2 enrichment with intermittence was found to suppress the promotion of photosynthesis and yield in cotton, wheat, chrysanthemums, soybeans, and tomatoes (Mortensen et al., 1987; Bunce, 2012; Allen et al., 2020). Besides, the effects of nighttime CO_2 enrichment are still unclear, which may be species- or cultivar-dependent (Baker et al., 2022).

Concentration control

The concentration gaps between inside and outside the greenhouse (C_{in}-C_{out}) and the air exchange rate (dominated by ventilation) are two key factors affecting CUE, besides the crop intrinsic photosynthetic capacity (Kozai et al., 2015; Yasutake et al., 2017). When the setting C_{in} is higher, e.g., 1000 μmol mol^{-1}, the CUE is less than 50% even in an unventilated greenhouse due to a massive leakage of CO_2 (Kuroyanagi et al., 2014). Moderate control systems of CO_2 enrichment based on crop absorption rate or C_{in}-C_{out}, with a CUE close to 100%, have been reported to improve the yield of cucumbers and tomatoes (Kläring et al., 2007; Kozai et al., 2015). Thus, it is a feasible and sustainable strategy to keep a moderate CO_2 concentration slightly higher than the ambient concentration in the cultivation environment, e.g., 550 ~ 650 μmol mol^{-1}, considering economic cost and environmental protection (Vermeule, 2014; Kozai et al., 2015). The resulting gaps in yield and quality compared with crops cultivated in optimal CO_2 concentration might be alleviated by controlling other environmental conditions and imposing moderate environmental stresses (Kozai et al., 2015; Dong et al., 2018).

Notably, unlike the consistent conclusion of an increase in yield, the effects of elevated CO_2 on crop quality are diverse (Dong et al., 2018), suggesting that the optimal CO_2 concentration should be determined by specific production requirements rather than a constant value. Compared with ambient CO_2 and a lower CO_2 elevation (550 μmol mol^{-1}), the synthesis of glucose and fructose are promoted under higher CO_2 concentration (700 - 1000 μmol mol^{-1}), while some amino acids and minerals are deceased (Högy and Fangmeier, 2009; Dong et al., 2018). The changes in health-promoting compounds and flavor substances under elevated CO_2, such as flavonoids, lycopene, and ascorbic acid, carotene, are controversial in different vegetable crops, perhaps due to characteristics of different product organs and disturbance of synthesis processes by other environmental conditions (Mamatha et al., 2014; Dong et al., 2018; Hao et al., 2020).

Directions for future CO_2 enrichment

In addition to the challenge of increasing yields and improving quality, the global agricultural production system also faces tremendous pressure to reduce its carbon footprint to mitigate climate change. Even though photosynthesis of crops largely consumes CO_2 as the endogenous driving force of agriculture, protected agriculture in various countries and regions is still a carbon emission-intensive process (Marttila et al., 2021; Northrup et al., 2021). Thus, taking full advantage of the crop ability of carbon fixation and combining the advantages of various disciplines should be a sustainable strategy to meet challenges in global food production and climate change simultaneously. In this regard, three novel and potentially feasible directions for future CO_2 enrichment (Figure 3) are summarized and discussed as follows.

Agro-industrial symbiosis system (AIS)

Burning fossil fuels and the operation of non-renewable energy-based industries are being restricted gradually due to their intensive contribution to the majority of global carbon emissions. Strategic management of the agricultural production system has the potential to provide beneficial contributions to the global carbon budget (Marchi et al., 2018; Northrup et al., 2021; Friedlingstein et al., 2022). Thus, a novel agro-industrial symbiosis system (AIS) of channeling industrial waste heat and CO_2 to greenhouse productions through pipeline networks is proposed as a viable solution (Marttila et al., 2021). Compared with traditional AIS systems which only transfer heat, this system reduces carbon taxes related to CO_2 emissions in industrial processes while increasing revenues of agricultural production (Marchi et al., 2018). Bottlenecks are the initial construction cost and design. The

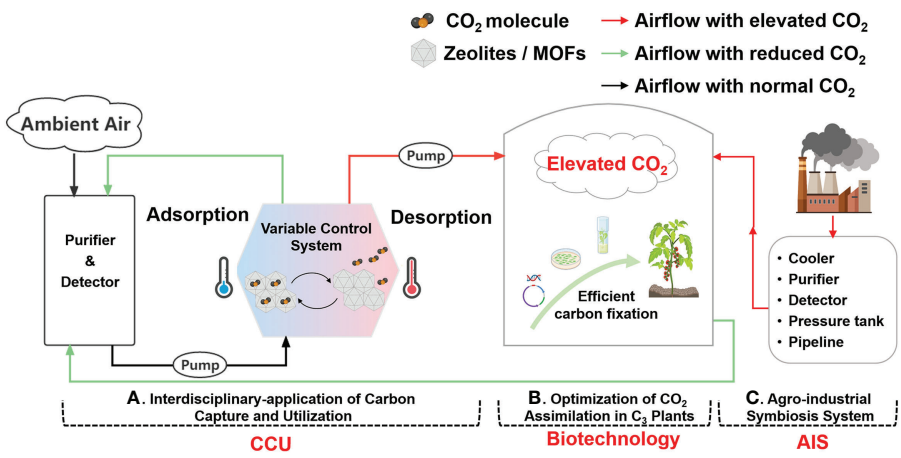

FIGURE 3
Overview of directions for future CO_2 enrichment in greenhouse production. **(A)** Interdisciplinary application of carbon capture and utilization. Zeolites/MOFs as carbon adsorption materials can adsorb CO_2 molecules from ambient air at low temperatures and desorb them at high temperatures to enrich CO_2 into greenhouses. **(B)** Optimization of CO_2 assimilation in C_3 crops. Limited CO_2 assimilation ability in C_3 crops can be improved *via* biotechnological approaches including gene manipulation and genetic transformation. **(C)** Agro-Industrial Symbiosis system. A direct connection between the energy industry and greenhouses can be built through a pipeline network to convey CO_2 and heat. Created with BioRender.com.

greenhouse needs to be within a limited distance (e.g., 10 km) of the factory, with a matching demand dosage of CO_2; and the change of CO_2 concentration during the delivery and purification of source gas needs to be considered (Vermeulen, 2014; Marchi et al., 2018).

Interdisciplinary-application of carbon capture and utilization (CCU)

Carbon dioxide capture, utilization, and storage technologies (CCUS) are being vigorously researched. Compared with the huge cost and risk of leakage of carbon storage, converting CO_2 into substances that people need, that is, carbon capture and utilization (CCU), is more attractive (Hepburn et al., 2019). Agriculture has an inherent advantage in this regard owing to the original demand for CO_2. But there is a long way to go from now to real applications in agricultural production.

Physical adsorption, with lower energy consumption and milder reaction conditions, may be the most suitable for agricultural production among various methods of carbon capture including absorption solution, calcium looping, membrane technology and microalgal bio-fixation (Ben-Mansour et al., 2016). Target fluid molecules like CO_2, can be selectively adsorbed through the huge surface area, specific pore structures, and ions inside the adsorbents (Zhou et al., 2021). Processes of reversible adsorption and desorption are controlled by changing conditions such as temperature and pressure (Ben-Mansour et al., 2016; Zhou et al., 2021).

There are two sources of CO_2 capture: 1) industrial exhaust, which is confined and high in concentration; and 2) natural atmosphere, which is widespread and low in concentration. The latter, which is called direct air capture (DAC), is more challenging but also more practically meaningful (Maina et al., 2021). However, the desorption capacity especially required in agricultural production is often overlooked in studies on DAC (Bao et al., 2018). And though there are kinds of adsorbents with various properties for options, the adsorption and desorption capacities are often antagonistic (Zhou et al., 2021). Therefore, the suitable CCU material for agricultural production remains to be explored or transformed.

Most of the control methods of utilizing CCU materials for CO_2 enrichment practices in agriculture production are based on variable temperature, as shown in Figure 2. Bao et al. (2018) used a water bath to control the temperature, and calculated that the cost of using 13X zeolite was close to that of the cheapest way of burning natural gas (halved because of the supply of heat), and can be lower considering the carbon tax. Araoz et al. (2021) developed conductive carbon tubes which could realize rapid temperature control of zeolite or metal-organic frameworks (MOFs) filled therein with voltage, providing an application model for greenhouse CO_2 enrichment. Tang et al. (2022)

reversed the temperature *via* a rotary regenerative wheel (RAW) loaded with carbon adsorbents, and analyzed the influence of gas flow, rotational speed, and other parameters on its CO_2 enrichment performance.

Although related studies are only theoretically feasible with parts of the devices or designs, this direction deserves great attention owing to the carbon neutrality as no CO_2 is freshly generated in the whole process. Besides, technological exploration of DAC is receiving increasing interest, and promisingly to play a breakthrough role in agriculture CO_2 enrichment technology in the future (Bao et al., 2018).

The requirements of CCU in agriculture systems in future applications can be summarized as follows: 1) strong adsorption in ambient CO_2 to provide sufficient pure CO_2; 2) sustained desorption to generate a controllable flow of CO_2; 3) low energy consumption in desorption or regeneration, such as lower temperature; 4) high adaptability to the agricultural environment with much water vapor and dust to ensure a stable effect in reusing (Wang et al., 2014; Bao et al., 2018).

Optimization of CO_2 assimilation in C_3 crops *via* biotechnologies

Except for controlling the environment, modifying plant intrinsic carbon utilization efficiency by altering hereditary substances is a more efficient and revolutionary approach. The capability of CO_2 fixation based on photosynthesis is limited especially in C_3 plants (Yang et al., 2021). Great efforts have been put into the optimization of the photosynthesis system of C_3 crops for decades (Raines, 2011). At present, the complicated mechanism of photosynthesis has been elucidated comprehensively and deeply (Long et al., 2015), preparing the foundation for improving plant carbon fixation *via* increasingly powerful biotechnologies.

As a crucial restriction enzyme of the C_3 cycle, Rubisco catalyzes the binding of CO_2 and its receptor ribulose 1,5-bisphosphate (RUBP), with a low activity and competitive dual functions of carboxylation and oxygenation (Long et al., 2015). The latter causes a loss of carbon and nitrogen fixation through photorespiration (Tcherkez, 2013). C_4 plants have evolved a transcellular carbon concentration mechanism (CCM) that increases CO_2 around rubisco, promoting photosynthetic carbon assimilation and reducing photorespiration significantly; and photosynthetic algae also have CCMs with different organelle structures (Zabaleta et al., 2012). Despite the tall order to introduce a whole CCM into C_3 plants, both C_4 plants and photosynthetic algae provide vital references and genetic materials for transforming the photosynthetic carbon fixation of C_3 crops (Raines, 2011; Rae et al., 2017). For example, overexpression operations of phosphoenolpyruvate carboxylase (PEPC, an enzyme catalyzing the entry of bicarbonate into the C_4 cycle), Sedoheptulose-1,7-bisphosphatase (SBPase, an enzyme involved in the regeneration of RUBP) and carbonic anhydrase (CA, an enzyme catalyzing conversion of intracellular CO_2 into bicarbonate reversibly) from C_4 plants or cyanobacteria, were all found effective to promote photosynthetic capacity in C_3 crops (Köhler et al., 2017; Liu et al., 2021; Kandoi et al., 2022).

Naturally, what can be done to improve the CO_2 utilization of C_3 crops is far beyond modifying the C_3 cycle, as listed below:

1) Searching for biological parts of metabolic processes from other organisms (Yang et al., 2021). For example, introducing photorespiratory bypasses from bacteria into rice increased photosynthesis by reducing energy losses in metabolism and releasing CO_2 around Rubisco (Wang et al., 2020).

2) Improving the light utilization efficiency by expanding the absorption spectrum of light-harvesting pigments and the photosynthetic electron transport chain, which provide energy to the C_3 cycle (Long et al., 2015).

3) Combining with computational modeling. Scientific prediction and analysis would accelerate the understanding and manipulation of complex life activities (Raines, 2011). e.g., Zhao et al. (2021) explained the underlying mechanism of mutual interference of enzymes in the C_3 cycle by a dynamic systems model, and pointed out the requirement of balanced activities of enzymes to gain a greater photosynthetic efficiency, which would be further explored by an iterative design-built-test-learn approach (Patron, 2020).

Outlook

Optimal CO_2 concentration has great potential to further improve the yield and quality of agricultural products, especially nowadays when technologies of controlling temperature, light, water, and fertilizer are quite advanced and efficient. Meanwhile, with those intrinsic and emerging conundrums in current CO_2 enrichment systems being overcome by multidisciplinary supports, efficient agricultural carbon utilization in greenhouse production would be a promising and sustainable advantageous solution to alleviating the pressure of food security and global warming.

In addition to those mentioned above, directions of improvement in the future agricultural CO_2 enrichment can be expanded, such as exploring technologies suitable for open field production, and developing more sensitive sensors and more intelligent CO_2 control models on period and concentration for greater CUE. Apart from photosynthesis, the important role of CO_2 in plants also needs in-depth studies on mechanisms and improvements of photoadaptation and reduced nutrients requirement under elevated CO_2.

Author contributions

KS conceived the paper. AW wrote the paper. KS, JL, and JW revised the paper. All authors contributed to the article and approved the submitted version.

Funding

This work was supported by the Natural Science Foundation of Zhejiang Province (LR19C150001), the National Natural Science Foundation of China (32172650), and the Starry Night Science Fund of Zhejiang University Shanghai Institute for Advanced Study (SN-ZJU-SIAS-0011).

Conflict of interest

The authors declare that the research was conducted in the absence of any commercial or financial relationships that could be construed as a potential conflict of interest.

Publisher's note

References

Ahammed, G. J., Guang, Y., Yang, Y., and Chen, J. (2021). Mechanisms of elevated CO_2-induced thermotolerance in plants: the role of phytohormones. *Plant Cell Rep.* 40, 2273–2286. doi: 10.1007/s00299-021-02751-z

Ahammed, G. J., and Li, X. (2022). Elevated carbon dioxide-induced regulation of ethylene in plants. *Environ. Exp. Bot.* 202, 105025. doi: 10.1016/j.envexpbot.2022.105025

Ainsworth, E. A., and Long, S. P. (2020). 30 years of free-air carbon dioxide enrichment (FACE): What have we learned about future crop productivity and its potential for adaptation? *Global Change Biol.* 27, 27–49. doi: 10.1111/gcb.15375

Allen, L. H., Kimball, B. A., Bunce, J. A., Yoshimoto, M., Harazono, Y., Baker, J. T., et al. (2020). Fluctuations of CO2 in free-air CO2 enrichment (FACE) depress plant photosynthesis, growth, and yield. *Agr For. Meteorol.* 284, 107899. doi: 10.1016/j.agrformet.2020.107899

Araoz, M., Marcial, A., Gonzalez, J., and Avila, A. (2021). Renewable and electroactive biomass-derived tubes for CO_2 capture in agroindustrial processes. *ACS Sustain. Chem. Eng* 9, 7759–7768. doi: 10.1021/acssuschemeng.1c00547

Bailey-Serres, J., Parker, J. E., Ainsworth, E. A., Oldroyd, G. E. D., and Schroeder, J. I. (2019). Genetic strategies for improving crop yields. *Nature* 575, 109–118. doi: 10.1038/s41586-019-1679-0

Baker, J. T., Lascano, R. J., Yates, C., and Gitz, III, D. C. (2022). Nighttime CO_2 enrichment did not increase leaf area or shoot biomass in cotton seedlings. *Agr For. Meteorol.* 320, 108931. doi: 10.1016/j.agrformet.2022.108931

Bao, J., Lu, W.-H., Zhao, J., and XXXT.Bi, X. (2018). Greenhouses for CO_2 sequestration from atmosphere. *Carbon Res. Conversion* 1, 183–190. doi: 10.1016/j.crcon.2018.08.002

Ben-Mansour, R., Habib, M., Bamidele, O., Basha, M., Qasem, N., Peedikakkal, A., et al. (2016). Carbon capture by physical adsorption: Materials, experimental investigations and numerical modeling and simulations – A review. *Appl. Energ.* 161, 225–255. doi: 10.1016/j.apenergy.2015.10.011

Boulard, T., Roy, J.-C., Pouillard, J.-B., Fatnassi, H., and Grisey, A. (2017). Modelling of micrometeorology, canopy transpiration and photosynthesis in a closed greenhouse using computational fluid dynamics. *Biosyst. Eng* 158, 110e133. doi: 10.1016/j.biosystemseng.2017.04.001

Bunce, J. A. (2012). Responses of cotton and wheat photosynthesis and growth to cyclic variation in carbon dioxide concentration. *Photosynthetica* 50, 395–400. doi: 10.1007/s11099-012-0041-7

Caliman, F. R. B., da Silva, D. J. H., Alves, D. P., de Sa Cardoso, T., and Mattedi, A. P. (2009). Intermittent CO_2 enrichment and analysis of dry matter accumulation and photoassimilate partitioning in tomato. *Acta. agronómica.* 58, 133–139.

Chaudhry, S., and Sidhu, G. (2022). Climate change regulated abiotic stress mechanisms in plants: a comprehensive review. *Plant Cell Rep.* 41, 1–31. doi: 10.1007/s00299-021-02759-5

Dion, L.-M., Lefsrud, M., and Orsat, V. (2011). Review of CO_2 recovery methods from the exhaust gas of biomass heating systems for safe enrichment in greenhouses. *Biomass Bioenergy* 35, 3422–3432. doi: 10.1016/j.biombioe.2011.06.013

Dong, J., Gruda, N., Lam, S. K., Li, X., and Duan, Z. (2018). Effects of elevated CO_2 on nutritional quality of vegetables: a review. *Front. Plant Sci.* 9. doi: 10.3389/fpls.2018.00924

Friedlingstein, P., Jones, M. W., O'Sullivan, M., Andrew, R. M., Bakker, D. C., Hauck, J., et al. (2022). Global carbon budget 2021. *Earth Syst. Sci. Data* 14, 1917–2005. doi: 10.5194/essd-14-1917-2022

Hao, P., Qiu, C., Ding, G., Vincze, E., Zhang, G., Zhang, Y., et al. (2020). Agriculture organic wastes fermentation CO_2 enrichment in greenhouse and the fermentation residues improve growth, yield and fruit quality in tomato. *J. Clean Prod.* 275, 123885. doi: 10.1016/j.jclepro.2020.123885

Hepburn, C., Adlen, E., Beddington, J., Carter, E. A., Fuss, S., Dowell, N., et al. (2019). The technological and economic prospects for CO_2 utilization and removal. *Nature* 575, 87–97. doi: 10.1038/s41586-019-1681-6

Hidaka, K., Nakahara, S., Yasutake, D., Zhang, Y., Okayasu, T., Dan, K., et al. (2022). Crop-local CO_2 enrichment improves strawberry yield and fuel use efficiency in protected cultivations. *Sci. Hortic.* 301 (111104), 1–10. doi: 10.1016/j.scienta.2022.111104

Högy, P., and Fangmeier, A. (2009). Atmospheric CO_2 enrichment affects potatoes: 2. tuber quality traits. *Eur. J. Agron.* 30, 85–94. doi: 10.1016/j.eja.2008.07.006

Hu, Z., Ma, Q., Foyer, C. H., Lei, C., Choi, H. W., Zheng, C., et al. (2021). High CO_2-and pathogen-driven expression of the carbonic anhydrase βCA3 confers basal immunity in tomato. *New Phytol.* 229, 2827–2843. doi: 10.1111/nph.17087

Ishii, M., Okushima, L., Moriyama, H., Sase, S., and Fukuchi, N. (2014). And both, a Experimental study of natural ventilation in an open-roof greenhouse during the summer. *J XXIX Int. Hortic. Congress Horticulture: Sustaining Lives Livelihoods Landscapes (IHC2014): Int. Symposium Innovation New Technol. Protected Cropping* 1107, 67–74. doi: 10.17660/ActaHortic.2015.1107.8

Jaffrin, A., Bentounes, N., Joan, A. M., and Makhlouf, S. (2003). Landfill biogas for heating greenhouses and providing carbon dioxide supplement for plant growth. *Biosyst. Eng* 86, 113–123. doi: 10.1016/s1537-5110(03)00110-7

Jin, C., Du, S., Wang, Y., Condon, J., Lin, X., and Zhang, Y. (2009). Carbon dioxide enrichment by composting in greenhouses and its effect on vegetable production. *J. Plant Nutr. Soil Sci.* 172, 418–424. doi: 10.1002/jpln.200700220

Kandoi, D., Ruhil, K., Govindjee, G., and Tripathy, B. C. (2022). Overexpression of cytoplasmic C_4 *Flaveria bidentis* carbonic anhydrase in C_3 *Arabidopsis thaliana* increases amino acids, photosynthetic potential, and biomass. *Plant Biotechnol. J.* 20, 1518–1532. doi: 10.1111/pbi.13830

Karim, M. F., Hao, P., Nordin, N. H. B., Qiu, C., Zeeshan, M., Khan, A. A., et al. (2020). Effects of CO_2 enrichment by fermentation of CRAM on growth, yield and physiological traits of cherry tomato. *Saudi J. Biol. Sci.* 27, 1041–1048. doi: 10.1016/j.sjbs.2020.02.020

Kazan, K. (2018). Plant-biotic interactions under elevated CO_2: A molecular perspective. *Environ. Exp. Bot.* 153, 249–261. doi: 10.1016/j.envexpbot.2018.06.005

Kläring, H. P., Hauschild, C., Heißner, A., and Bar-Yosef, B. (2007). Model-based control of CO_2 concentration in greenhouses at ambient levels increases cucumber yield. *Agr For. Meteorol.* 143, 208–216. doi: 10.1016/j.agrformet.2006.12.002

Köhler, I. H., Ruiz-Vera, U. M., VanLoocke, A., Thomey, M. L., Clemente, T., Long, S. P., et al. (2017). Expression of cyanobacterial FBP/SBPase in soybean prevents yield depression under future climate conditions. *J. Exp. Bot.* 68, 715–726. doi: 10.1093/jxb/erw435

Kozai, T. (2013). Resource use efficiency of closed plant production system with artificial light: Concept, estimation and application to plant factory. *Proc. Jpn. Acad. Ser. B Phys. Biol. Sci.* 89, 447–461. doi: 10.2183/pjab.89.447

Kozai, T., Kubota, C., Takagaki, M., and Maruo, T. (2015). Greenhouse environment control technologies for improving the sustainability of food production. *Acta Hortic.* 1107, 1–13. doi: 10.17660/ActaHortic.2015.1107.1

Kuroyanagi, T., Yasuba, K., Higashide, T., Iwasaki, Y., and Takaichi, M. (2014). Efficiency of carbon dioxide enrichment in an unventilated greenhouse. *Biosyst. Eng* 119, 58–68. doi: 10.1016/j.biosystemseng.2014.01.007

Li, Y., Ding, Y., Li, D., and Miao, Z. (2018). Automatic carbon dioxide enrichment strategies in the greenhouse: A review. *Biosyst. Eng* 171, 101–119. doi: 10.1016/j.biosystemseng.2018.04.018

Linker, R., Gutman, P. O., and Seginer, I. (1999). Robust controllers for simultaneous control of temperature and CO_2 concentration in greenhouses. *Control Eng Pract.* 7, 851–862. doi: 10.1016/S0967-0661(99)00042-8

Liu, D., Hu, R., Zhang, J., Guo, H. B., Cheng, H., Li, L., et al. (2021). Overexpression of an *Agave* phosphoenolpyruvate carboxylase improves plant growth and stress tolerance. *Cells* 10, 582. doi: 10.3390/cells10030582

Long, S. P., Marshall-Colon, A., and Zhu, X. G. (2015). Meeting the global food demand of the future by engineering crop photosynthesis and yield potential. *Cell* 161, 56–66. doi: 10.1016/j.cell.2015.03.019

Maina, J. W., Pringle, J. M., Razal, J. M., Nunes, S., Vega, L., Gallucci, F., et al. (2021). Strategies for integrated capture and conversion of CO_2 from dilute flue gases and the atmosphere. *ChemSusChem* 14, 1805–1820. doi: 10.1002/cssc.202100010

Mamatha, H., Rao, N. S., Laxman, R., Shivashankara, K., Bhatt, R., and Pavithra, K. (2014). Impact of elevated CO_2 on growth, physiology, yield, and quality of tomato (*Lycopersiconesculentum mill*) cv. *ArkaAshish Photosynthetica* 52, 519–528. doi: 10.1007/s11099-014-0059-0

Marchi, B., Zanoni, S., and Pasetti, M. (2018). Industrial symbiosis for greener horticulture practices: the CO_2 enrichment from energy intensive industrial processes. *Proc. CIRP* 69, 562–567. doi: 10.1016/j.procir.2017.11.117

Marttila, M. P., Uusitalo, V., Linnanen, L., and Mikkilä, M. H. (20219040). Agro-industrial symbiosis and alternative heating systems for decreasing the global warming potential of greenhouse production. *Sustainability-Basel* 13, 9040. doi: 10.3390/su13169040

Merrill, B. F., Lu, N., Yamaguchi, T., Takagaki, M., Maruo, T., Kozai, T., et al. (2016). Next evolution of agriculture: a review of innovations in plant factories. *Handb. Photosynthesis*, 723–740.

Mortensen, L. M. (1987). Review: CO_2 enrichment in greenhouses. crop responses. *Sci. Hortic.* 33, 1–25. doi: 10.1016/0304-4238(87)90028-8

Noctor, G., and Mhamdi, A. (2017). Climate change, CO_2, and defense: the metabolic, redox, and signaling perspectives. *Trends Plant Sci.* 22, 857–870. doi: 10.1016/j.tplants.2017.07.007

Northrup, D. L., Basso, B., Wang, M. Q., Morgan, C. L. S., and Benfey, P. N. (2021). Novel technologies for emission reduction complement conservation agriculture to achieve negative emissions from row-crop production. *Proc. Natl. Acad. Sci. U. S. A.* 118, e2022666118. doi: 10.1073/pnas.2022666118

Pascale, S., and Maggio, A. (2008). Plant stress management in semiarid greenhouse. international workshop on greenhouse environmental control and crop production. *Semi-Arid Regions* 797, 205–215. doi: 10.17660/ActaHortic.2008.797.28

Patron, N. J. (2020). Beyond natural: synthetic expansions of botanical form and function. *New Phytol.* 227, 295–310. doi: 10.1111/nph.16562

Pérez-López, U., Miranda-Apodaca, J., Lacuesta, M., Mena-Petite, A., and Muñoz-Rueda, A. (2015). Growth and nutritional quality improvement in two differently pigmented lettuce cultivars grown under elevated CO_2 and/or salinity. *Sci. Hortic.* 195, 56–66. doi: 10.1016/j.scienta.2015.08.034

Poorter, H., Knopf, O., Wright, I., Temme, A., Hogewoning, S., Graf, A., et al. (2021). A meta-analysis of responses of C_3 plants to atmospheric CO_2: dose–response curves for 85 traits ranging from the molecular to the whole-plant level. *New Phytol.* 223, 1560–1596. doi: 10.1111/nph.17802

Poudel, M., and Dunn, B. (2017). Greenhouse carbon dioxide supplementation. *Oklahoma Cooperative Extension Service*, HLA–6723.

Rae, B. D., Long, B. M., Förster, B., Nguyen, N. D., Velanis, C. N., Atkinson, N., et al. (2017). Progress and challenges of engineering a biophysical CO_2-concentrating mechanism into higher plants. *J. Exp. Bot.* 68, 3717–3737. doi: 10.1093/jxb/erx133

Raines, C. A. (2011). Increasing photosynthetic carbon assimilation in C_3 plants to improve crop yield: current and future strategies. *Plant Physiol.* 155, 36–42. doi: 10.1104/pp.110.168559

Roy, Y., Lefsrud, M., Orsat, V., Filion, F., Bouchard, J., Nguyen, Q., et al. (2014). Biomass combustion for greenhouse carbon dioxide enrichment. *Biomass Bioenergy* 66, 186e196. doi: 10.1016/j.biombioe.2014.03.001

Roy, S., and Mathur, P. (2021). Delineating the mechanisms of elevated CO_2 mediated growth, stress tolerance and phytohormonal regulation in plants. *Plant Cell Rep.* 40, 1345–1365. doi: 10.1007/s00299-021-02738-w

Sage, R. (2017). A portrait of the C_4 photosynthetic family on the 50th anniversary of its discovery: species number, evolutionary lineages, and hall of fame. *J. Exp. Bot.* 68, e11–e28. doi: 10.1093/jxb/erx005

Sánchez-Guerrero, M. C., Lorenzo, P., Medrano, E., Castilla, N., Soriano, T., and Baille, A. (2005). Effect of variable CO_2 enrichment on greenhouse production in mild winter climates. *Agr For. Meteorol.* 132, 244–252. doi: 10.1016/j.agrformet.2005.07.014

Stanghellini, C., Incrocci, L., Gázquez, J. C., and Dimauro, B. (2008). Carbon dioxide concentration in Mediterranean greenhouses: How much lost production? *Acta Hortic.* 801, 1541–1550. doi: 10.17660/ActaHortic.2008.801.190

Sun, Q., Cui, S., Song, Y., Yang, Z., Dong, Q., Sun, S., et al. (2016). Impact of illumination and temperature performance of blanket-inside solar greenhouse and CO_2 enrichment on cuumber growth and development. *Coll. Agronomy Inner Mongolia Agric. Univ. Agricultural Science & Technology*. 17, 1757–1761+1776. doi: 10.16175/j.cnki.1009-4229.2016.08.001

Syed, A., and Hachem, C. (2019). Review of design trends in lighting, environmental controls, carbon dioxide supplementation, passive design, and renewable energy systems for agricultural greenhouses. *J. Biosyst. Eng.* 44, 28–36. doi: 10.1007/s42853-019-00006-0

Takeya, S., Muromachi, S., Maekawa, T., Yamamoto, Y., Mimachi, H., Kinoshita, T., et al. (2017). Design of ecological CO_2 enrichment system for greenhouse production using TBAB + CO_2 semi-clathrate hydrate. *Energies* 10, 927. doi: 10.3390/en10070927

Tang, C., Gao, X., Shao, Y., Wang, L., Liu, K., Gao, R., et al. (2022). Investigation on the rotary regenerative adsorption wheel in a new strategy for CO_2 enrichment in greenhouse. *Appl. Therm Eng* 205 (118043), 1–13. doi: 10.1016/j.applthermaleng.2022.118043

Tcherkez, G. (2013). Modelling the reaction mechanism of ribulose-1,5-bisphosphate carboxylase/oxygenase and consequences for kinetic parameters. *Plant Cell Environ.* 36, 1586–1596. doi: 10.1111/pce.12066

Vermeulen, P. (2014). Alternative sources of CO_2 for the greenhouse horticulture. *Proc. 2nd Int. Symposium Energy Challenges Mechanics (ISECM2)* (Aberdeen, UK) 19–21.

Wang, L., Feng, Z., and Schjoerring, J. (2013). Effects of elevated atmospheric CO_2 on physiology and yield of wheat (*Triticum aestivum l.*): A meta-analytic test of current hypotheses. *Agric. Ecosyst. Environ.* 178, 57–63. doi: 10.1016/j.agee.2013.06.013

Wang, T., Huang, J., He, X., Wu, J., Fang, M., and Cheng, J. (2014). CO_2 fertilization system integrated with a low-cost direct air capture technology. *Energy Proc.* 63, 6842–6851. doi: 10.1016/j.egypro.2014.11.718

Wang, J., Niu, X., Zheng, L., Zheng, C., and Wang, Y. (20161941). Wireless mid-infrared spectroscopy sensor network for automatic carbon dioxide fertilization in a greenhouse environment. *Sensors* 16 (1941), 1–20. doi: 10.3390/s16111941

Wang, L.-M., Shen, B.-R., Li, B.-D., Zhang, C.-L., Lin, M., Tong, P.-P., et al. (2020). A synthetic photorespiratory shortcut enhances photosynthesis to boost biomass and grain yield in rice. *Mol. Plant* 13, 1802–1815. doi: 10.1016/j.molp.2020.10.007

Xu, Z., Jiang, Y., and Zhou, G. (2015). Response and adaptation of photosynthesis, respiration, and antioxidant systems to elevated CO_2 with environmental stress in plants. *Front. Plant Sci.* 6. doi: 10.3389/fpls.2015.00701

Xu, S., Zhu, X., Li, C., and Ye, Q. (2014). Effects of CO_2 enrichment on photosynthesis and growth in *Gerbera jamesonii*. *Sci. Hortic.* 177, 77–84. doi: 10.1016/j.scienta.2014.07.022

Yang, X., Liu, D., Lu, H., Weston, D., Chen, J.-G., Muchero, W., et al. (2021). Biological parts for plant biodesign to enhance land-based carbon dioxide removal. *BioDesign Res.* 2021, 1–22. doi: 10.34133/2021/9798714

Yasutake, D., Tanioka, H., Ino, A., Takahashi, A., Yokoyama, T., Mori, M., et al. (2017). Dynamic evaluation of natural ventilation characteristics of a greenhouse with CO_2 enrichment. *Acad. J. Agric. Res.* 5, 312–319. doi: 10.15413/ajar.2017.0164

Zabaleta, E., Martin, V., and Braun, H.-P. (2012). A basal carbon concentrating mechanism in plants? *Plant Sci.* 187, 97–104. doi: 10.1016/j.plantsci.2012.02.001

Zhang, S., Li, X., Sun, Z., Shao, S., Hu, L., Ye, M., et al. (2015). Antagonism between phytohormone signalling underlies the variation in disease susceptibility of tomato plants under elevated CO_2. *J. Exp. Bot.* 66, 1951–1963. doi: 10.1093/jxb/eru538

Zhang, Z., Liu, L., Zhang, M., Zhang, Y., and Wang, Q. (2014). Effect of carbon dioxide enrichment on health-promoting compounds and organoleptic properties of tomato fruits grown in greenhouse. *Food Chem.* 153, 157–163. doi: 10.1016/j.foodchem.2013.12.052

Zhang, Y., Yasutake, D., Hidaka, K., Kitano, M., and Okayasu, T. (2020). CFD analysis for evaluating and optimizing spatial distribution of CO_2 concentration in a strawberry greenhouse under different CO_2 enrichment methods. *Comput. Electron. Agric.* 179, 105811. doi: 10.1016/j.compag.2020.105811

Zhao, H., Tang, Q., Chang, T., Xiao, Y., and Zhu, X.-G. (2021). Why an increase in activity of an enzyme in the Calvin–Benson cycle does not always lead to an increased photosynthetic CO_2 uptake rate?–a theoretical analysis. *silico Plants* 3, diaa009. doi: 10.1093/insilicoplants/diaa009

Zhou, Y., Zhang, J., Wang, L., Cui, X., Liu, X., Wong, S. S., et al. (2021). Self-assembled iron-containing mordenite monolith for carbon dioxide sieving. *Science* 373, 315–320. doi: 10.1126/science.aax5776

frontiers | Frontiers in Plant Science

TYPE Original Research
PUBLISHED 21 November 2022
DOI 10.3389/fpls.2022.1044976

OPEN ACCESS

EDITED BY
Yuxin Tong,
Chinese Academy of Agricultural Sciences, China

REVIEWED BY
Tao Lin,
Zhejiang University, China
Ana Carolina Silva Siquieroli,
Federal University of Uberlandia, Brazil

*CORRESPONDENCE
Laura Cammarisano
cammarisano@igzev.de

SPECIALTY SECTION
This article was submitted to Technical Advances in Plant Science, a section of the journal Frontiers in Plant Science

RECEIVED 15 September 2022
ACCEPTED 25 October 2022
PUBLISHED 21 November 2022

CITATION
Cammarisano L, Graefe J and Körner O (2022) Using leaf spectroscopy and pigment estimation to monitor indoor grown lettuce dynamic response to spectral light intensity. *Front. Plant Sci.* 13:1044976. doi: 10.3389/fpls.2022.1044976

Using leaf spectroscopy and pigment estimation to monitor indoor grown lettuce dynamic response to spectral light intensity

Laura Cammarisano*, Jan Graefe and Oliver Körner

Next-Generation Horticultural Systems, Leibniz-Institute of Vegetable and Ornamental Crops (IGZ), Großbeeren, Germany

Rising urban food demand is being addressed by plant factories, which aim at producing quality food in closed environment with optimised use of resources. The efficiency of these new plant production systems could be further increased by automated control of plant health and nutritious composition during cultivation, allowing for increased produce value and closer match between plant needs and treatment application with potential energy savings. We hypothesise that certain leaf pigments, including chlorophylls, carotenoids and anthocyanins, which are responsive to light, may be good indicator of plant performance and related healthy compounds composition and, that the combination of leaf spectroscopy and mathematical modelling will allow monitoring of plant cultivation through noninvasive estimation of leaf pigments. Plants of two lettuce cultivars (a green- and a red-leaf) were cultivated in hydroponic conditions for 18 days under white light spectrum in climate controlled growth chamber. After that period, plant responses to white light spectrum ('W') with differing blue wavelengths ('B', 420 - 450 nm) percentage (15% 'B15', and 40% 'B40') were investigated for a 14 days period. The two light spectral treatments were applied at photon flux densities (PFDs) of 160 and 240 µmol m^{-2} s^{-1}, resulting in a total of four light treatments (160WB15, 160WB40, 240WB15, 240WB40). Chlorophyll *a* fluorescence measurements and assessment of foliar pigments, through destructive (*in vitro*) and non-destructive (*in vivo*) spectrophotometry, were performed at 1, 7 and 14 days after treatment initiation. Increase in measured and estimated pigments in response to WB40 and decrease in chlorophyll:carotenoid ratio in response to higher PFD were found in both cultivars. Cultivar specific behavior in terms of specific pigment content stimulation in response to time was observed. Content ranges of modelled and measured pigments were comparable, though the correlation between both needs to be improved. In conclusion, leaf pigment estimation may represent a potential noninvasive and real-time technique to monitor, and control, plant growth and nutritious quality in controlled environment agriculture.

KEYWORDS

indoor farming, precision farming, plant performance control, lettuce, leaf optical properties, pigments, blue light

1 Introduction

1.1 Semi- and fully- controlled environment agriculture for predictable crop yield and quality

Increased yield and nutritional quality of crop food are currently some of the main targets in horticulture and plant science due to rising world human population. The extreme and unpredictable climate events occurring all around the world threaten field crop production besides reducing crop quality (Maggiore et al., 2020). In greenhouses, the disturbances from the outside climate are minimised compared to open field production, while climate can be controlled to the desired set-point targets only to a certain extend (Gurban and Andreescu, 2018; Choab et al., 2019). The strong impact of solar radiation entering the greenhouse through the transparent cover material is the major driver for short-term greenhouse micro-climate dynamics (Körner and Challa, 2003a), often yielding in growth and quality reduction (Körner and Challa, 2003b). Moreover, the semi-controlled environment of greenhouses is more susceptible to influence from outdoor weather, thus a constant and highly predictable crop yield and quality is difficult to obtain throughout the year (Graamans et al., 2017). A nearly constant and controlled climate can be obtained when totally refraining from energy input by solar radiation in indoor farms. In these closed and fully controlled environments, artificial light substitutes solar radiation and climate can be controlled close to the desired set-points (Kozai, 2013; van Delden et al., 2021). Fluctuation in climate variables as temperature and humidity is avoided, which reduces the risks for several diseases and physiological disorders (Körner and Challa, 2003b). Actively controlling the cultivation light by only applying artificial light, in addition to air conditions, is therefore the key for predictable yield and quality. Since their first applications in indoor farming in the 2000s (Goto, 2012), light emitting diodes (LEDs) allowed their dominance in horticulture over conventional light sources, e.g. high-pressure sodium lamps or fluorescent lamps (Paucek et al., 2020). The fast evolving LED technology enables precision light control (Neo et al., 2022) with highly targeted narrow bandwidths and tuneable intensity (Van Iersel, 2017).

1.2 Controlled light stress application to enhance morphological and nutritional plant quality

Morphological and nutritional enhancements in plants can result from defensive mechanisms effected in response to stress conditions caused by high light energy. For instance, compaction of lettuce rosette, which could be considered as a desirable morphological trait for consumers, occurs in response to increased radiative energy allowing for the regulation of light capture and prevention of photo-damage (Cammarisano et al., 2021). Likewise, leaf thickness, which increases in response to light intensity and spectrum (Kang et al., 2014; Cioć and Pawłowska, 2020), can represent a demanded trait for marketability and for improved shelf life of lettuce (Clarkson et al., 2003). And, similarly, antioxidants, e.g., β-carotene and phenolics, represent effective protective compounds against oxidative stress both in plants (Dumanovic et al., 2020) and humans (Sharifi-Rad et al., 2020). Another plant bioactive compound, which rapidly fluctuates in response to light, with stimulation by excess light energy (Havaux et al., 2004), and which has been proved to have beneficial effect on human eye and brain health, is zeaxanthin (Demmig-Adams and Adams, 1992). Increased radiative energy effects can be triggered by light intensity and/or by high energy photons, i.e. short wavebands photons (Cammarisano et al., 2020). Light intensity has stimulating effect on antioxidant compounds (Sutuliene et al., 2022). In fact, light treatment with increased intensity applied at the end-of-production is proposed as a strategies to enhance nutritional quality of basil (Larsen et al., 2022) and lettuce (Gómez and Jiménez, 2020) indoor farming. The use of higher energy wavebands such as blue triggers plant photomorphogenic responses and allows the stimulation of secondary metabolites synthesis (Jung et al., 2021); thence, increasing plant morphological and nutritional quality. Blue radiation has been reported as highly effective in promoting accumulation of chlorophylls, carotenoids and anthocyanins in several plant species (Johkan et al., 2010; Xu et al., 2014; Taulavuori et al., 2016; Frede and Baldermann, 2022; Liu et al., 2022). Stress conditions can be beneficial for increasing plant defensive strategies, which in some cases are considered quality traits by consumers, i.e. antioxidants, though when the stress exceeds certain tolerance thresholds plant biomass could be negatively affected (Zhang et al., 2020).

1.3 Detection of changes in leaf biochemistry to monitor plant performance and quality

Detectable changes of compounds synthesized by the plant in response to stress could be used to monitor stress extent and hence, the balance between plant performance and nutritional quality in order to obtain predictable quality yield. Compounds such as phenolics, e.g. anthocyanins, which are considered to be beneficial to human health (Sen and Chakraborty, 2011) and which increase in presence of excessive radiative energy (Demmig-Adams and Adams, 1992), could be used as markers to monitor nutritional quality in terms of antioxidant content. Besides antioxidants, photosynthetic pigments, i.e., chlorophylls (chl) and carotenoids (car), can be indicative of plant performance (Ling et al., 2011; Croft et al., 2017). Total chlorophyll content (chl a+b) and the ratio between

chlorophylls a and b (chl a/b) positively correlate with photosynthetic capacity of plants (Croft et al., 2017) and are adjusted to the surrounding environment to enhance plant growth. For instance, chl a/b increases with higher light intensity as strategy to intensify light absorption of photosystem I in order to achieve a more balanced excitation state (Hogewoning et al., 2012). Content of photosynthetic and photoprotective pigments is rapidly adjusted by the plant in response to the environment and could be used as markers in noninvasive procedures, which would allow instant monitoring of plant nutritional quality adjustments and early warning for stress through spectroscopy and radiation transfer models (Blackburn, 2007).

Most non-destructive techniques to measure leaf biochemical composition found in literature are based on optical spectroscopy. The latter allows to measure the interaction of matter with electromagnetic radiation and has been used for studying properties of all kinds of materials for centuries (Baudelet, 2014). In plant research, such technique is widely proposed for remote sensing of physiological traits of forests and agricultural fields. Several studies propose leaf spectroscopy to detect, with different degree of spatial resolution, e.g. leaf to canopy, based on the specific technology, content of water (Ceccato et al., 2001), nitrogen (Wang et al., 2016), pigments (Blackburn, 2007), secondary compounds (Jayapal et al., 2022) and signs of abiotic (Grzesiak et al., 2009) and biotic (Mahlein et al., 2012) stresses (Jacquemoud and Ustin, 2001).

Leaf spectroscopy combined with physical based leaf radiation transfer models, with given technical adaptations, could be used to monitor leaf pigments in real-time and within the growth environment, giving the possibility to adjust the micro-climate in case of stress detection or harvest the crop at the exact quality status. Ideally, dynamic biochemical changes influenced by various abiotic parameters, e.g. spectral light intensity, temperature, humidity, and their combined effects, should be characterised in order to define pigment dynamics for each stress type and their combination to be used as target values for controlling plant growth and nutritional quality in indoor farming.

In this study, we aimed at 1) inducing leaf pigment changes by using light intensity and spectral composition, 2) characterising these changes during light treatment duration, and 3) developing a non-destructive procedure to detect the dynamic changes. For that, we applied a blue wavelength enhanced white light spectrum at two photon flux densities (PFDs) for 14 days on a typical green lettuce cultivar and a lettuce cultivar with strong red coloration from anthocyanins and determined leaf pigments including chlorophylls, carotenoids and anthocyanins in response to light in time.

2 Materials and methods

2.1 Experimental design

The experiment was executed at the Leibniz-Institute of Vegetable and Ornamental Crops IGZ (Grossbeeren, Germany) in a growth chamber with controlled atmosphere regarding temperature and relative humidity. The experimental system consisted of two double-layer shelving units providing four growing areas of 0.27 m^2 each (separated by white reflective plastic sheets). Each layer was equipped with two dimmable LEDs arrays (LightDNA8, Valoya, Finland) and hosted twelve plants, six per cultivar (plant density of 44.4 plants m^{-2}). Two light spectral treatments (white light spectrum with 15% blue (WB15) and with 40% blue (WB40)) were tested at two photon flux densities, PFDs, (160 and 240 µmol m^{-2} s^{-1}). The resulting four light treatments (160WB15, 160WB40, 240WB15, 240WB40; cf. Table 1) were applied on two lettuce cultivars (green leaf lettuce 'Aquino' cv. (CV_g), red leaf lettuce 'Barlach' cv. (CV_r), Rijk Zwaan, The Netherlands). The two light spectra were simultaneously tested in two distinct growing compartments of the chamber each (i.e. four compartments were used), and the experiment was repeated twice (sowing on 26 January and 7 March 2022) at 160 µmol m^{-2} s^{-1} and twice (sowing on 27 December 2021 and 7 April 2022) at 240 µmol m^{-2} s^{-1}.

2.2 Plant growth conditions and light treatments

Seeds of each of the two lettuce cultivars 'Barlach' (CV_r) and 'Aquino' (CV_g) were sown in stone-wool cubes (4 cm,

TABLE 1 Treatment codes and their spectral composition (in percentage) for the four light treatments: White light control and white-blue light at 160 (160WB15, 160WB240) and at 240 (240WB15, 240WB40) µmol m^{-2} s^{-1}.

Treatment code	Waveband percentage		PFD, µmol m^{-2} s^{-1}
	White [Green:Red:FR]	Blue	
160WB15	75 [40:29:16]	15	160
160WB40	60 [35:16:9]	40	160
240WB15	75 [40:29:16]	15	240
240WB40	60 [35:16:9]	40	240

Blue (400-480 nm, with peaks at 420 & 450 nm), Green (481-599 nm), Red (600-669 nm), FR (670-780 nm).

Rockwool®, Grodan, Roermond, The Netherlands) and kept at 4°C in the dark for 24 hours. Afterwards, the cubes were moved to the experimental unit and kept under white light spectrum (PFD of 160 μmol m^{-2} s^{-1} and photoperiod of 18 h) for 18 days. Temperature and relative humidity were controlled to 20°C (day and night) and 60% (day and night), respectively, for the whole duration of the experiments. Controlled environmental parameters were monitored (logging every 5 minutes) within each growing area (Tinytag Ultra 2, Gemini Data Loggers, Chichester, UK). Growing areas were automatically irrigated for 1 minute five times a day, using lettuce nutrient solution (Sonneveld and Straver, 1994) (EC: 1.9 dS m^{-1}, pH: 5.5–6). On day 18, 48 homogeneously germinated plants (≥ 6 expanded leaves) were selected from each of the two cultivars, including the substrate, were embedded into larger stone-wool cubes (10 cm, Rockwool®, Grodan, The Netherlands) and positioned onto the four growing areas (12 in each). From day 19, light treatments (160WB15, 160WB40, 240WB15, 240WB40) were applied for the following 14 days. The two spectral light treatments were composed of four main channels: blue (400-480 nm), green (481-599 nm), red (600-669 nm) and far-red (670-800 nm). WB15 resulted in 15% blue, 40% green, 29% red, 16% far red. WB40 resulted in 40% blue, 35% green, 16% red, 9% far-red, (Table 1). Spectral light intensity (PFD) was measured at canopy level (distance from lamps: 40 cm) using a spectroradiometer (UPRtek PG200N, 350–800 nm; UPRtek Corp., Taiwan).

2.3 Plant measurements

Time course measurements of the same plant samples were performed at three points during treatment application, one day (D1), seven days (D7) and fourteen days (14D) after treatments begun (Figure 1). Chlorophyll *a* fluorescence measurements and assessment of leaf pigments, through destructive (*in vitro*) and non-destructive (*in vivo*) spectrophotometry, were performed. Same leaf was used both for estimating pigment content through optical measurements followed by mathematical modeling and pigment quantification through laboratory procedure. Pigment extraction and quantification was done for total chlorophylls and carotenoids, while pigment estimation was feasible for anthocyanins, chlorophylls, carotenoids and their zeaxanthin fraction. Measurements started with excising one leaf for optical readings, followed by sampling of the same leaf in liquid nitrogen for subsequent pigments extraction and quantification. Assessed leaf area for optical properties was approx. 1 cm^2, while the whole leaf was sampled for pigment extraction. Leaf numbers 6, 9 and 12 were chosen for leaf measurements on D1, D7 and D14, respectively, being the youngest and most expanded ones. At the same time, the rest of the plant was measured for chlorophyll *a* fluorescence. Same plant was measured on the three sampling dates. On each sampling date, twenty-four plants were measured from 9:00 a.m. to 1:00 p.m. Consecutive measurements were alternated between cultivars and light treatments accordingly.

2.3.1 Measurements of leaf optical properties

In-vivo leaf spectroscopy was used to measure leaf optical properties. Immediately after excision, each leaf was assessed on the two sides of the midrib (adaxial side) for reflectance and transmittance using a double-beam spectrophotometer (V-670, Jasco, Japan) equipped with an internal integration sphere (ILN-925, inner diameter: 150 mm). Measuring range was set between 340 and 900 nm. Each instrument scan over this range required less than 2 minutes. A certified white reflective standard was used to calibrate reflectance readings.

2.3.2 Estimation of leaf pigments from leaf reflectance and transmittance

Using the leaf spectral models PROSPECT-D and Fluspect-CX, we estimated several leaf properties using least squares minimization of the difference between PROSPECT-D predicted and measured reflectances and transmittances (400 nm - 900 nm). Among the estimated leaf properties were the leaf content of chlorophyll, carotenoid and anthocyanin as well as the zeaxanthin +antheraxanthin to total xanthophyll ratio. Least square minimization was done using a trust region algorithm (fmincon matlab function, 1990-2019, The MathWorks, Inc.) with box-

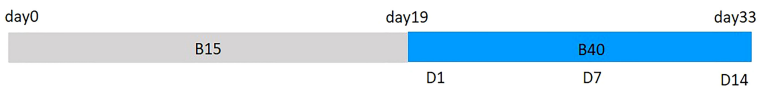

FIGURE 1
Scheduled growth periods of lettuce plants from sowing date (day 0) to harvest day (day 33). Plants were grown under white light spectrum (B15) for 18 days and treated with blue-enriched spectrum (B40) from day 19 for the following 14 days. Plant measurements were performed at 1 day, 7 days and 14 days after treatment start.

constraints on parameters (i.e. leaf properties) and an additional constraint on the chlorophyll to carotenoid ratio (4.4 < chl/car < 6.4), which corresponds to the observed range from lab analysis (see next section).

2.3.3 Extraction and quantification of leaf pigments

Chlorophyll and carotenoid content of leaves was determined through the wet chemistry procedure reported in (Cammarisano et al., 2021). Prior extraction, leaf samples were freeze-dried for 5 days and ground to fine powder. For the extraction, 1.6 – 2.8 mg of leaf tissue powder was weighed in triplicates in 2 ml green centrifuge tubes. 0.6 ml of 95% ethanol were added to each tube. After being vortexed and left in the fridge for the consecutive 24 hours, tubes were centrifuged and extracts were collected. The same extraction procedure was repeated 3 times, with three washes (0.6, 0.6 and 0.5 ml, respectively) in three following days. The combined extract for each sample was then read (at 470, 649, and 664 nm) in triplicates against the same amount (170 µl) of blank solution using a UV/VIS spectrophotometer (Infinite M200PRO, Tecan, Switzerland). Samples were measured in a 96-well half area microplate (UV-STAR, flat bottom, Greiner bio-one Gmbh, Austria), which was used to ensure a 1 cm pathlength. Chlorophylls a and b and total carotenoids concentration was determined using equations reported in Lichtenthaler and Buschmann (2001).

2.3.4 Measurements of chlorophyll *a* fluorescence

Light adapted plants were measured for chlorophyll a fluorescence using the modulated fluorescence imaging FluorCam system (Photon Systems Instruments, Brno, Czech Republic). Shutter time and sensitivity of the charge-coupled device (CCD) camera were chosen based on a spare sample and kept the same for all measurements. The distance between the camera lens and the upper leaves was maintained at 24 cm. A horizontal spot of 5380 pixels was used on the youngest and most expanded leaf to ensure comparable assessed area between measured plants. Calculated parameters are given in the Table 2.

2.4 Plant growth

Fresh and dry weight of the lettuce rosettes were determined at 14 days after treatment start, which coincided with the end of the experiment, following procedure described by (Cammarisano et al., 2021). A total of six intact plants per spectral light intensity treatment were harvested.

2.5 Data processing and statistics

Data were processed and statistically analyzed using Microsoft Excel Standard 2013 and R studio (R version 2022.02.2, "Prairie Trillium") with package "agricolae" (Mendiburu, 2010). Repeated measures ANOVA could not be used as sample size between different measuring dates was uneven. Three-way ANOVA was used to determine whether duration of treatment, light spectrum, PFD and their interactions significantly ($p \leq 0.05$) affected the measured response variables. Each cultivar was separately analysed. All determined variables (estimated chlorophylls, carotenoids and anthocyanins, lab quantified chlorophylls and carotenoids, chlorophyll a fluorescence parameters) were individually analysed. Two-way ANOVA was used for fresh and dry weights of lettuce heads to test for the effect of light spectrum and PFD. Least Significance Difference (LSD) was used as *post hoc* test to localize the differences between means at 5% significance level. Student's t-test was then performed at individual measuring days to locate specific means where the light spectrum had a significant effect. Correlation between modelled and quantified chlorophylls and carotenoids was performed after converting the area based estimated pigment content to dry mass based content.

3 Results

3.1 Leaf pigments

3.1.1 Leaf pigment content

The increased percentage of blue radiation (B40) used in the study significantly affected the leaf pigments quantified through wet chemistry procedure in the red-leaf lettuce cultivar samples. Both chlorophyll and carotenoid content was found to be significantly

TABLE 2 Chlorophyll *a* fluorescence parameters (steady state quantum yield, QY, φPSII; Lichtenberger vitality index, Rfd; energy-dependent quenching, qE) assessed 1, 7 and 14 days after high blue light treatment start on two lettuce cultivars, cv. 'Aquino' and cv. 'Barlach'.

Parameter	Formula	Description
QY, φPSII	$(F_{M}\_Lss - F_{t}\_Lss)/F_{M}\_Lss^{*}$	Steady state Quantum Yield
Rfd	$(F_{P} - F_{t}\_Lss)/F_{t}\_Lss^{*}$	Lichtenberger vitality index
qE	$(F_{M}\_D3 - F_{M}\_Lss)/F_{M}\_D3^{*}$	Energy-dependent quenching

*where F_{M}_Lss is the steady-state maximum fluorescence in light, F_{t}_Lss is the steady-state fluorescence in light, F_{P} is the peak fluorescence during the initial phase of the Kautsky effect, F_{M}_D3 is the instantaneous maximum fluorescence during dark relaxation.

greater in leaves of CV_r treated with B40 compared to B15 samples. In particular, statistical increase in chlorophylls was detected at D1 both in 160WB40 (13%) and 240WB40 (12%) red-leaf samples ($p = 0.03$ and $p = 7x10^{-6}$, respectively). A general increasing trend in chlorophyll content over the treatment duration was observed in both cultivars at higher PFD. Total carotenoid content resulted significantly greater in CV_r leaves at D1 (15%) and D7 (7%) in 160WB40 samples and only at D1 (15%) in 240WB40 samples (Figures 2E–H). At higher PFD (240), carotenoids tended to generally increase over time (from D1 to D14) in both lettuce cultivars. For both cultivars, the chl/car ratio was significantly different under the two tested PFD levels, 160 and 240 µmol m^{-2} s^{-1}, showing opposite behavior. If under lower PFD the greatest chl:car ratio was detected at D14, the greatest ratio under the highest PFD was detected at D1 (Figures 2I–L).

3.1.2 Leaf pigment estimation

Estimated leaf pigment was significantly affected by the increased percentage of blue radiation (B40) in the two investigated lettuce cultivars (Figures 2, 3). Estimated leaf pigments showed similar behavior to that of measured ones. In addition to chlorophylls and carotenoids, zeaxanthin fraction, defined as (Z+A)/(Z+A+V), and anthocyanins were estimated. In CV_r, the estimated zeaxanthin fraction was significantly decreased by blue enriched light spectrum (B40, Figures 3M–P) at lower PFD, while it was increased by B40 at 240 µmol m^{-2} s^{-1} (27 to 47% increase from D1 to D14 in 160B40 compared to 240B15). Estimated anthocyanins were only detectable in CV_r, in which, they were increased by light spectrum (B40) with stronger effect at lower PFD (maximum of 50% increase at 160 µmol m^{-2} s^{-1} and 19% at 240 µmol m^{-2} s^{-1}) (Figure 4).

3.1.3 Correlation between estimated and quantified leaf pigments

In spite of the similar ranges of chlorophylls and carotenoids observed in the measured and the estimated leaf pigments, the correlation analysis determined low association between the two procedures. Overall, greater correlation was detected for chlorophylls than carotenoids (Figure 5). In addition, correlation coefficient was very variable when grouping the different levels of each factor. For instance, when considering chlorophylls, greatest correlation coefficients were found for B15 ($r = 0.72$) and for CV_r ($r = 0.70$). A lowering of correlation coefficients was observed with the progress of the treatment duration, with r decreasing from 0.68 for day 1 and 7 to 0.34 for day 14.

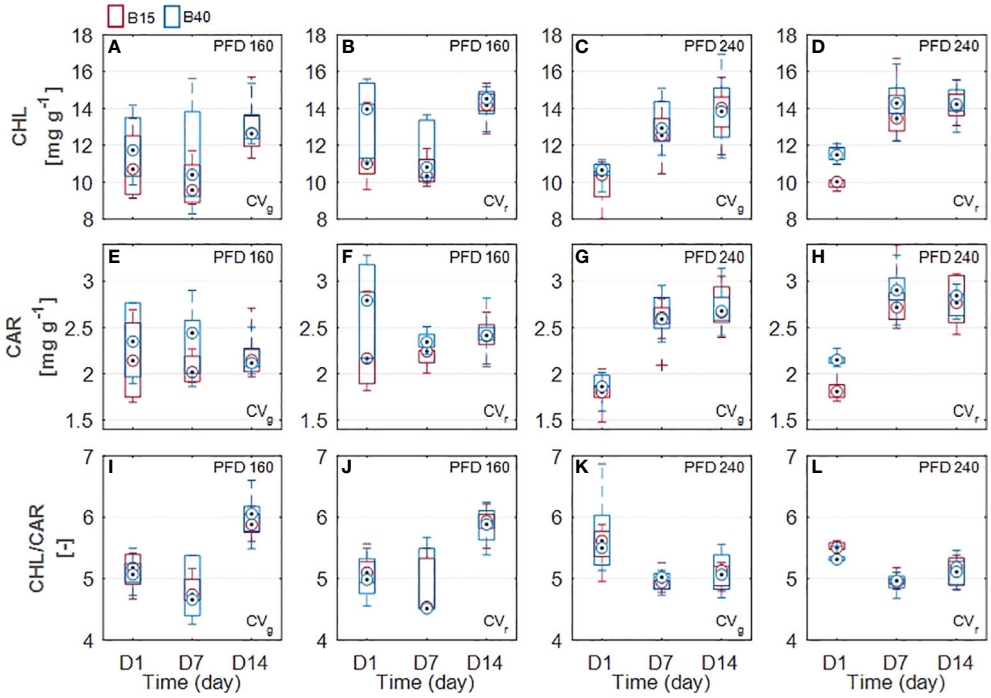

FIGURE 2
Measured leaf pigments of two lettuce cultivars (Aquino cv., CV_g and Barlach cv., CV_r) grown under two photon flux densities (PFDs; 160 and 240 µmol m^{-2} s^{-1}) and treated with two light spectra (white light spectrum with 15% blue, B15, in red; white light spectrum with 40% blue, B40, in blue) for 14 days. Pigment content was determined over three time points (day 1, day 7, and day 14 after treatment start) for total chlorophylls **(A-D)**, total carotenoids **(E-H)**, and chlorophyll/carotenoid ratio **(I-L)**. Boxplot whisker (W) was set to 2.5, and points were drawn as outliers if they were larger than Q25+W(Q75-Q25) or smaller than Q25-W(Q75-Q25).

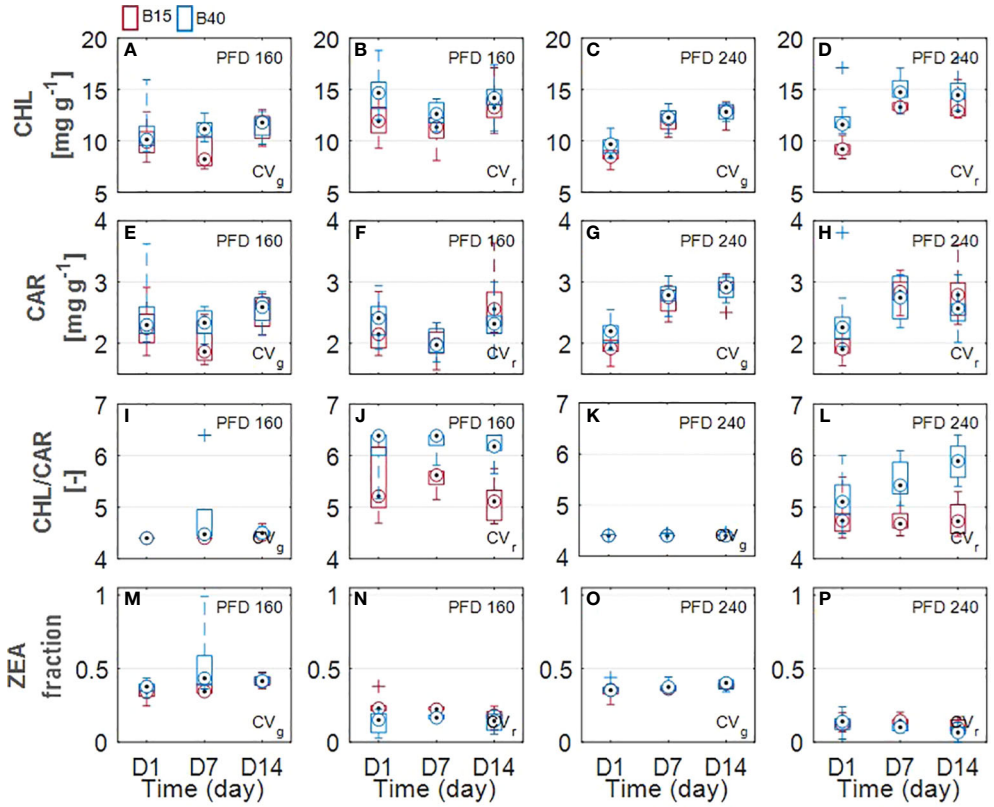

FIGURE 3
Estimated leaf pigments of two lettuce cultivars (Aquino cv., CV_g and Barlach cv., CV_r) grown under two photon flux densities (PFDs; 160 and 240 µmol m^{-2} s^{-1}) and treated with two light spectra (white light spectrum with 15% blue, B15, in red; white light spectrum with 40% blue, B40, in blue) for 14 days. Pigment content was determined at three time points (day 1, day 7, and day 14 after treatment start) for total chlorophylls **(A–D)**, total carotenoids **(E–H)**, chlorophyll-carotenoid ratio **(I–L)**, and fraction zeaxanthin **(M–P)**. Boxplot whisker (W) was set to 2.5, and points were drawn as outliers if they were larger than Q25+W(Q75-Q25) or smaller than Q25-W(Q75-Q25).

3.2 Chlorophyll *a* fluorescence

All measured chlorophyll *a* fluorescence parameters tended to increase with time in all analysed samples (Figure 6). QY was not significantly affected by the light treatments. Statistically greater Rfd and qE values were identified between samples treated with differing percentage of blue radiation. Greatest Rfd and qE occurred in B40 samples at D7 and D14, with same behavior observed for both used lettuce cultivars and PFDs. Only exception was the CV_g under the lower PFD which did not show any significant effect of light spectrum (Figure 6).

3.3 Plant growth

Fresh and dry weights of the lettuce rosette were significantly affected by PFD in both cultivars (Table 3). Fresh weight was increased of 56% for CV_g and of 42% for CV_r under the higher PFD, compared to the lower one. Significantly lower dry weight (-23%) was observed for lettuce heads of CV_g treated with increased percentage of blue radiation (B40) compared to control rosettes.

4 Discussion

The estimation of leaf pigments through non-destructive techniques such as the combination of leaf optical measurements and PROSPECT-D model inversion used in this study could represent a potential method for the *in vivo* monitoring of leaf biochemical changes indicative of plant abiotic stress progress and relative nutritional quality improvements. Parameters indicative of a rise in the plant stress level in response to light, as for instance the increasing ratio of zeaxanthin over carotenoids (Xie et al., 2020) and anthocyanins over chlorophylls (Kim et al., 2012; Zheng et al., 2021), could be used both for detecting exacerbation of stress response and increase of bioactive compounds. In contrast to strategies using portable leaf reflectance meter (Jiménez-Lao et al., 2021),

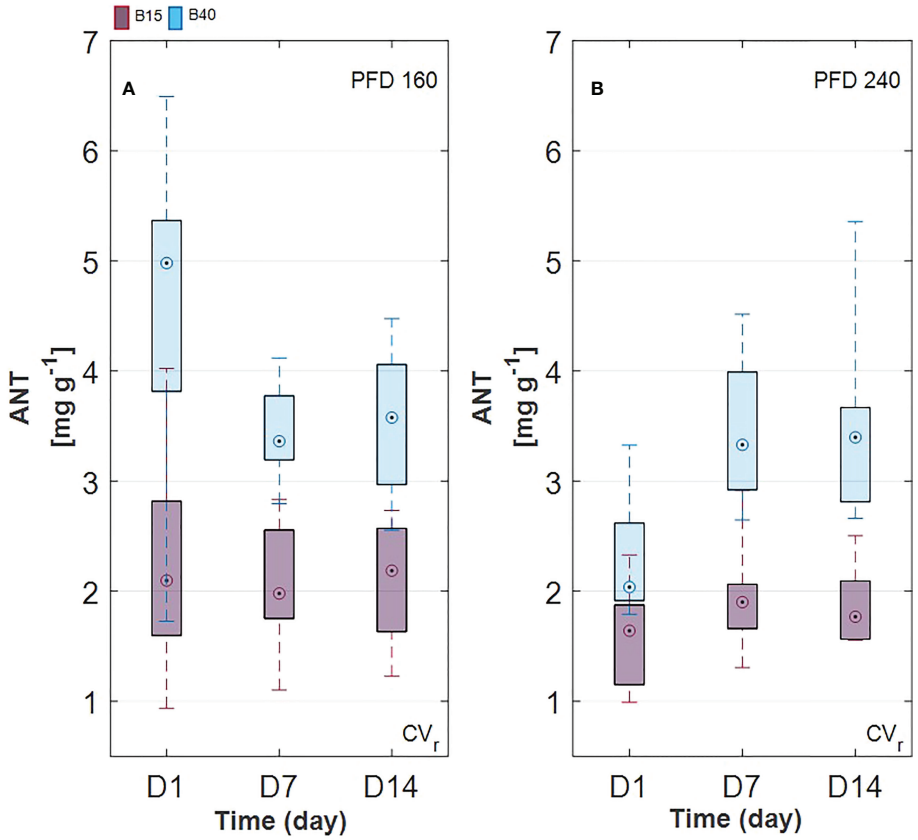

FIGURE 4
Estimated anthocyanin content in Barlach cv. (CV_r) grown under two photon flux densities (PFDs; 160 **(A)** and 240 **(B)** μmol m^{-2} s^{-1}) and treated with two light spectra (white light spectrum with 15% blue, B15, in red; white light spectrum with 40% blue, B40, in blue) for 14 days. Pigment content was determined over three time points (day 1, day 7, and day 14 after treatment start). Boxplot whisker (W) was set to 2.5, and points were drawn as outliers if they were larger than Q25+W(Q75-Q25) or smaller than Q25-W(Q75-Q25).

this technique offers potentials for continuous monitoring of plant pigment content within the growth environment for instance by using hyperspectral cameras (Jayapal et al., 2022). The advantage of *in vivo* monitoring of leaf pigments is essential for detection of the dynamic plant response in adjusting the content of these compounds in response to the surrounding environment. Indeed, content of pigments, including chlorophylls, carotenoids and flavonoids, has been found to vary according to the radiation dose and duration. For instance, applying low dose of UV-B radiation for 30 minutes to basil caused a fast decrease in zeaxanthin content followed by a strong increase in the next 48 hours during recovery time. When applying high dose of UV-B, zeaxanthin content decreased continuously from the first minutes of application to reach values close to zero after 24 hours (Mosadegh et al., 2019).

Chlorophylls have a key role in photosynthesis and their content has been found to change in response to various stresses (Muhammad et al., 2020), with rising behaviour under low-level stress and decreasing behaviour under more severe stress (Agathokleous and Penuelas, 2020). Otherwise, carotenoids and anthocyanins, which can be considered as protective pigments for their photoprotective and antioxidant properties, show increasing response to several stresses (Chalker-Scott, 1999; Havaux, 2014). From the results obtained in the current study, we could observe a pigment response to light spectrum with increased blue radiation (B40) which was similar between measured and estimated pigments (Figures 2, 3). Total chlorophylls and carotenoids were significantly greater in B40 but only during the first days of treatment application. When considering the ratio of chl/car though, a dual behaviour could be observed. While at lower PFD (160 μmol m^{-2} s^{-1}) the greatest chl/car ratio was detected in B40 samples at D14, at higher PFD (240 μmol m^{-2} s^{-1}) the greatest chl/car ratio was at D1 followed by constant decline with treatment duration. Such opposite trend could confirm the response of chlorophylls to mild versus more severe stress reported in literature (Agathokleous and Penuelas, 2020). At low PFD, the plant stress level might have been low enough to allow for mitigation through increased

potential for light use (> chlorophylls). The higher PFD was probably close to the threshold tolerance range for the plant, which invested in increasing protective pigments (> carotenoids) to acclimate to the extended exposure to B40 light treatment. Likewise, CV_r invested in anthocyanins over the duration of 240B40, with the ratio ANT/CHL rising over time meaning that the net rate of anthocyanins biosynthesis was increasing over that of chlorophylls (Figure 7). However, PFD of 240 µmol m^{-2} s^{-1} was far from the maximum saturating light level (400-700 µmol m^{-2} s^{-1}) reported for lettuce cultivated at temperatures of 20°C (Weigou et al., 2012; Cammarisano et al., 2020; Zhou et al., 2022). Indeed, the optimal vitality index (Rfd, Figures 6E-H), which expresses the potential photosynthetic activity of PSII, was never below the critical value of 1.0 (Haitz and Lichtenthaler, 1988). Rather it constantly raised reaching values indicative of high photosynthetic efficiency (< 3.0) at D14 in all treatments, with relative greater increase in response to higher PFD and to greater percentage of blue light. The observed pigment dual behaviour under the two tested PFDs and their dynamics highlight the significant need of characterising pigment changes to 1) varying climate and 2) over time.

Though, the trend in the pigment dynamics was similar between the two monitoring procedures, the absolute values did not match precisely (Figure 5). The r coefficient tended to lower with time (D1+D7>D14).This could be due to the fact that later measuring time corresponds to much larger portions of leaf sampled for lab analysis (the whole leaf was sampled, including veins and leaf area not uniformly exposed to the light) compared to portions used for optical measurements (a standard area of 1 cm^2 of leaf tips was used for optical readings). In addition, it needs to be considered that varied correlation between differently aged leaves may be expected as leaf structure is modified with leaf growth and consequently leaf spectral properties change (Gara et al., 2019). PROSPECT versions for estimating pigments have been optimised during the years, going from exclusively considering chlorophylls, to inclusion of carotenoids with PROSPECT-5 (Feret et al., 2008) and addition of anthocyanins with PROSPECT-D (Féret et al., 2017). Further improvements of PROSPECT model inversion allow to estimate leaf biochemical composition with sole use of reflectance or transmittance data (Sun et al., 2018). Future attempts to improve correlation could regard the sampling procedure by exactly matching the leaf portion used for optical measurement to that used for quantifying pigments. In this study, in order to match units, area based pigment estimates obtained by PROSPECT-D where converted to mass based estimates using independent estimates of leaf mass per area, which are usually known at best at the treatment level and not for each leaf spot. Unexpectedly, correlation for CV_r resulted to be greater compared to CV_g (Figure 5). Such result endorses the use of physical based models like PROSPECT-D under more general conditions, i.e. having low and high anthocyanin containing cultivars without prior calibration (Féret et al., 2017) which would be required with empirical regression models.

Additionally, species and cultivars differences should be taken into account. In fact, variability in pigments and their ratios can be very high between plant species and also between cultivars of the same plant species as reported in (Kowalczyk et al., 2016; Mastilović et al., 2020), where different cultivars of lettuce grown under the same conditions showed significant

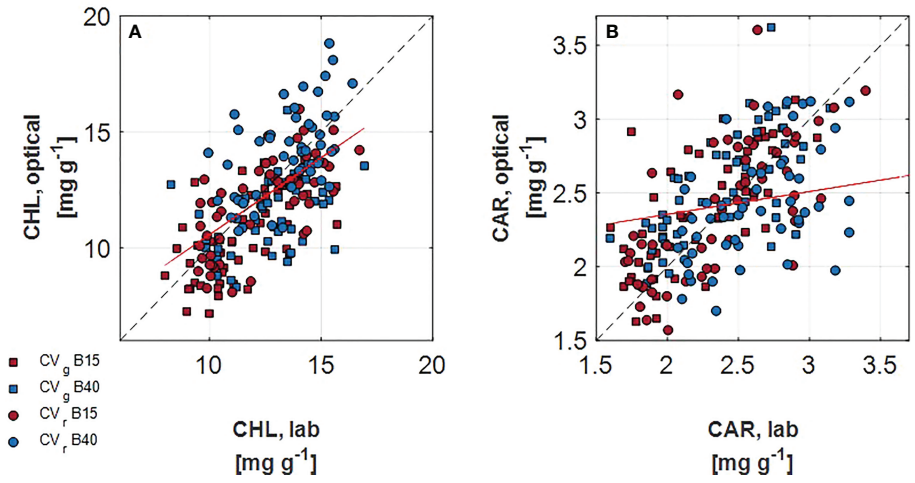

FIGURE 5
Correlation of lab measured and optically assessed total chlorophylls **(A)** and total carotenoids **(B)** for two lettuce cultivars (Aquino cv., CV_g, squares, and Barlach cv., CV_r, circles) treated with two light spectra (white light spectrum with 15% blue, in red, B15; white light spectrum with 40% blue, in blue, B40) after 14 days of treatment. The red line indicated the regression line over all data points. The 1:1 response is indicated as dashed line.

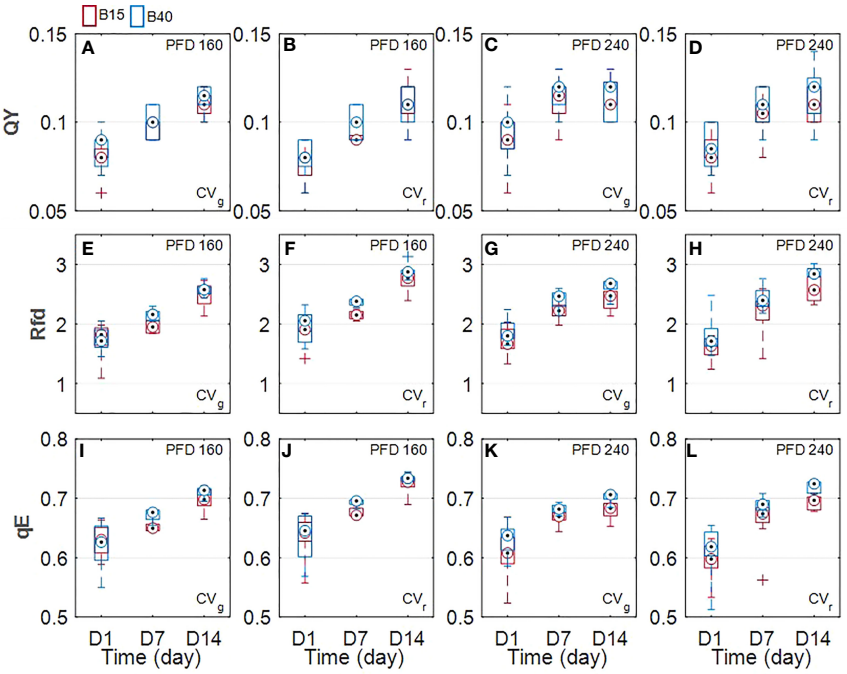

FIGURE 6
Measured light-adapted chlorophyll *a* fluorescence parameters 1. steady state quantum yield (QY; φPSII; **A-D**), 2. Lichtenberger vitality index (Rfd; **E-H**), and 3. energy-dependent quenching (qE, **I-L**) of two lettuce cultivars (Aquino cv., CV_g and Barlach cv., CV_r) grown under two photon flux densities (PFDs; 160 and 240 μmol m^{-2} s^{-1}) and treated with two light spectra (white light spectrum with 15% blue, B15, in red; white light spectrum with 40% blue, B40, in blue) for 14 days. Chlorophyll *a* fluorescence was determined over three time points (day 1, day 7, and day 14 after treatment start). Boxplot whisker (W) was set to 2.5, and points were drawn as outliers if they were larger than Q25+W(Q75-Q25) or smaller than Q25-W(Q75-Q25).

variability in chlorophyll and carotenoid content. In our study, distinct response of the two lettuce cultivars to light spectral intensity was observed. Most of the significant pigment changes were spotted in CV_r, confirming its greater adaptability to light compared to green leaf cultivars. In fact, no negative effect of the B40 treatment was observed in fresh and dry weight of CV_r, instead dry weight of CV_g was statistically diminished under B40 suggesting a less tolerating nature toward this light treatment. These results agree with the study of (Frąszczak and Kula-Maximenko, 2021), where red leaf lettuce cultivars accumulated more biomass and performed better compared to green leaf cultivars under blue-rich light spectrum. Due to the observed divergence in pigment changes between CV_g and CV_r, future works should address solutions to the issue of cultivar- and species- specific responses when defining stress indicators. For instance, the increase in the ANT/CHL ratio could be suggested as a stress versus quality indicator specific for red leaf cultivars (Figure 7).

Another important discussion point regards how to adapt spectra acquisition hardware and software for such a monitoring system for practical conditions, e.g. using PROSPECT-D with imaging data (Procosine), (Jay et al., 2016) and optimized settings for retrieval if only reflectance data are available (Spafford et al., 2021).

5 Conclusion

The current study proposes the combination of leaf optical measurements and PROSPECT-D model inversion as a potential approach for the *in vivo* monitoring of dynamic leaf biochemical changes indicative of plant abiotic stress and relative nutritional quality improvements in indoor farming. Still, there is some necessary progress to consider in future works for the development of such a system, including 1) improvement of the correlation between measured and estimated pigments to exactly estimate leaf pigment content, 2) study of the pigment responses in various plant species and cultivars to help characterising the range of responses, and 3) investigation of the responses to varying climate and nutrient solutions in order to determine stress type effects. A potential solution to develop an effective monitoring system would be to combine different detection methods, e.g.

TABLE 3 Growth response (fresh and dry weights determined 33 days after sowing) of two lettuce cultivars (cv. Aquino, CV_g and cv. Barlach, CV_r) treated for the last 14 days with blue-enriched white light spectrum (B40) compared to plants grown under white light spectrum (B15).

Treatments	Fresh weight (g) (g/head)	Dry weight (g) (g/head)
Cultivar Aquino, CV_g		
160B15	11.14 ± 0.64^{b}	0.63 ± 0.03^{b}
160B40	10.18 ± 0.28^{b}	0.49 ± 0.05^{c}
240B15	24.89 ± 2.24^{a}	1.16 ± 0.09^{a}
240B40	23.08 ± 1.85^{a}	1.07 ± 0.07^{a}
Cultivar Barlach, CV_r		
160B15	14.72 ± 1.14^{b}	0.83 ± 0.06^{b}
160B40	13.53 ± 0.51^{b}	0.77 ± 0.02^{b}
240B15	25.83 ± 1.98^{a}	1.17 ± 0.07^{a}
240B40	22.95 ± 1.98^{a}	1.07 ± 0.08^{a}

Values are reported as mean ± standard error. Different letters within columns indicate significant treatment differences at $P < 0.05$, as determined by Fisher's least significant difference (LSD) test, with a > b > c. Light spectral treatments were applied at two PFDs of 160 and 240 µmol m^{-2} s^{-1}. Tested factors were PFD, blue percentage and their interactions. Only PFD was significant at $p < 0.001$.

spectroscopy, imaging, thermography, fluorescence, to facilitate the distinction of species- and stress type- influence. And, connecting such sensing systems to a decision support system would allow the automated adjustment of the environment according to what is needed to reach the predicted target produce yield and nutritional content, additionally contributing to increase of resource use efficiency by more accurate match between plant needs and resource application.

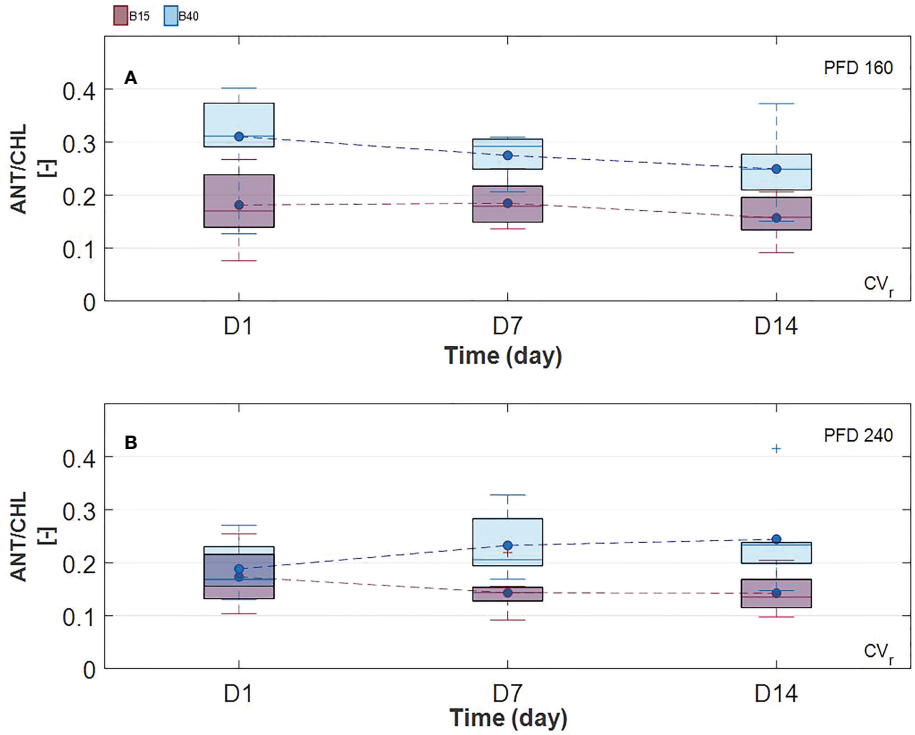

FIGURE 7
Ratio of estimated anthocyanins over chlorophylls, ANT/CHL, in time in Barlach cv. (CV_r). Plants were grown under two photon flux densities (PFDs; 160, **A**, and 240, **B**, µmol m^{-2} s^{-1}) and treated with two light spectra (white light spectrum with 15% blue, B15, in red; white light spectrum with 40% blue, B40, in blue) for the last 14 days of growth. Pigment content was determined over three time points (day 1, day 7, and day 14 after treatment start).

Data availability statement

The original contributions presented in the study are included in the article/supplementary material. Further inquiries can be directed to the corresponding author.

Author contributions

LC, JG, and OK contributed to conception and design of the study. LC performed the experimental investigation, LC, JG cured data, OK cured data visualization, LC performed the statistical analysis and wrote the first draft of the manuscript, LC, OK and JG wrote sections of the manuscript. OK acquired funding. All authors contributed to the article and approved the submitted version.

Conflict of interest

The authors declare that the research was conducted in the absence of any commercial or financial relationships that could be construed as a potential conflict of interest.

Publisher's note

All claims expressed in this article are solely those of the authors and do not necessarily represent those of their affiliated organizations, or those of the publisher, the editors and the reviewers. Any product that may be evaluated in this article, or claim that may be made by its manufacturer, is not guaranteed or endorsed by the publisher.

References

Agathokleous, E., and Penuelas, J. (2020). Chlorophyll hormesis: Are chlorophylls major components of stress biology in higher plants? *Sci. Total Environ.* 726, 138637. doi: 10.1016/j.scitotenv.2020.138637

Baudelet, M. (2014). *Introduction. laser spectroscopy for sensing: xxi-xxiv*. (Woodhead: Elsevier).

Blackburn, G. A. (2007). Hyperspectral remote sensing of plant pigments. *J. Exp. Bot.* 58 (4), 855–867. doi: 10.1093/jxb/erl123

Cammarisano, L., Donnison, I. S., and Robson, P. R. H. (2020). Producing enhanced yield and nutritional pigmentation in lollo rosso through manipulating the irradiance, duration, and periodicity of LEDs in the visible region of light. *Front. Plant Sci.* 11, 598082. doi: 10.3389/fpls.2020.598082

Cammarisano, L., Donnison, I. S., and Robson, P. R. H. (2021). The effect of red & blue rich LEDs vs fluorescent light on lollo rosso lettuce morphology and physiology. *Front. Plant Sci.* 12, 603411. doi: 10.3389/fpls.2021.603411

Ceccato, P., Flasse, S., Tarantola, S., Jacquemoud, S., and Grégoire, J.-M. (2001). Detecting vegetation leaf water content using reflectance in the optical domain. *Remote Sens. Environ.* 77, 22–33. doi: 10.1016/S0034-4257(01)00191-2

Chalker-Scott, L. (1999). Environmental significance of anthocyanins in plant stress responses. *Photochem. Photobiol.* 70 (1), 1–9. doi: 10.1111/j.1751-1097.1999.tb01944.x

Choab, N., Allouhi, A., El Maakoul, A., Kousksou, T., Saadeddine, S., and Jamil, A. (2019). Review on greenhouse microclimate and application: Design parameters, thermal modeling and simulation, climate controlling technologies. *Solar Energy* 191, 109–137. doi: 10.1016/j.solener.2019.08.042

Cioć, M., and Pawłowska, B. (2020). Leaf response to different light spectrum compositions during micropropagation of gerbera axillary shoots. *Agronomy* 10 (11), 1832. doi: 10.3390/agronomy10111832

Clarkson, G., O'Byrne, E., Rothwell, S., and Taylor, G. (2003). Identifying traits to improve postharvest processability in baby leaf salad. *Postharvest Biol. Technol. - POSTHARVEST Biol. Technol.* 30, 287–298. doi: 10.1016/S0925-5214(03)00110-8

Croft, H., Chen, J. M., Luo, X., Bartlett, P., Chen, B., and Staebler, R. M. (2017). Leaf chlorophyll content as a proxy for leaf photosynthetic capacity. *Glob Chang Biol.* 23 (9), 3513–3524. doi: 10.1111/gcb.13599

de Mendiburu, F. (2010). Agricolae: Statistical procedures for agricultural research. *R Package Version 1, 1–8* (CRAN repository). https://cran.r-project.org/web/packages/agricolae/agricolae.pdf

Demmig-Adams, B., and Adams, W. W. (1992). Photoprotection and other responses of plants to high light stress. *Plant Phvsiol. Plant Mol. Bioi* 43, 599–626. doi: 10.1146/annurev.pp.43.060192.003123

Dumanovic, J., Nepovimova, E., Natic, M., Kuca, K., and Jacevic, V. (2020). The significance of reactive oxygen species and antioxidant defense system in plants: A concise overview. *Front. Plant Sci.* 11, 552969. doi: 10.3389/fpls.2020.552969

Feret, J.-B., François, C., Asner, G. P., Gitelson, A. A., Martin, R. E., Bidel, L. P. R., et al. (2008). PROSPECT-4 and 5: Advances in the leaf optical properties model separating photosynthetic pigments. *Remote Sens. Environ.* 112 (6), 3030–3043. doi: 10.1016/j.rse.2008.02.012

Féret, J.-B., Gitelson, A., Noble, S. D., and Jacquemoud, S. (2017). PROSPECT-d: Towards modeling leaf optical properties through a complete lifecycle. *Remote Sens. Environ.* 193, 204–215. doi: 10.1016/j.rse.2017.03.004

Frąszczak, B., and Kula-Maximenko, M. (2021). The preferences of different cultivars of lettuce seedlings (Lactuca sativa l.) for the spectral composition of light. *Agronomy* 11 (6), 1211. doi: 10.3390/agronomy11061211

Frede, K., and Baldermann, S. (2022). Accumulation of carotenoids in brassica rapa ssp. chinensis by a high proportion of blue in the light spectrum. *Photochem. Photobiol. Sci* 21, 1947–1959. doi: 10.1007/s43630-022-00270-8

Gara, T., Darvishzadeh, R., Skidmore, A., and Heurich, M. (2019). Evaluating the performance of PROSPECT in the retrieval of leaf traits across canopy throughout the growing season. *Int. J. Appl. Earth Observation Geoinformat.* 83, 101919. doi: 10.1016/j.jag.2019.101919

Gómez, C., and Jiménez, J. (2020). Effect of end-of-production high-energy radiation on nutritional quality of indoor-grown red-leaf lettuce. *HortScience* 55 (7), 1055–1060. doi: 10.21273/HORTSCI15030-20

Goto, E. (2012). Plant prod in a closed plant factory with artificial lighting. *Acta Hortic.* 956, 37–49 . doi: 10.17660/ActaHortic.2012.956.2

Graamans, L., Baeza, E., Dobbelsteen, A., Tsafaras, I., and Stanghellini, C. (2017). Plant factories versus greenhouses: Comparison of resource use efficiency. *Agric. Syst.* 160, 31–43. doi: 10.1016/j.agsy.2017.11.003

Grzesiak, M. T., Filek, W., Hura, T., Kocurek, M., and Pilarski, J. (2009). Leaf optical properties during and after drought stress in triticale and maize genotypes differing in drought tolerance. *Acta Physiologiae Plantarum* 32 (3), 433–442. doi: 10.1007/s11738-009-0400-6

Gurban, E. H., and Andreescu, G.-D. (2018). Greenhouse environment monitoring and control: state of the art and current trends. *Environ. Eng. Manage. J.* 17, 399–416. doi: 10.30638/eemj.2018.041

Haitz, M., and Lichtenthaler, A. K. (1988). The measurement of rfd-values as plant vitality indices with the portable field chlorophyll fluoremeter and the PAM-fluorometer. *Appl. oj Chlorophyll Fluorescence*, 249–254. doi: 10.1007/978-94-009-2823-7_31

Havaux, M. (2014). Carotenoid oxidation products as stress signals in plants. *Plant J.* 79 (4), 597–606. doi: 10.1111/tpj.12386

Havaux, M., Dall'Osto, L., Cuine, S., Giuliano, G., and Bassi, R. (2004). The effect of zeaxanthin as the only xanthophyll on the structure and function of the photosynthetic apparatus in arabidopsis thaliana. *J. Biol. Chem.* 279 (14), 13878–13888. doi: 10.1074/jbc.M311154200

Hogewoning, S. W., Wientjes, E., Douwstra, P., Trouwborst, G., van Ieperen, W., Croce, R., et al. (2012). Photosynthetic quantum yield dynamics: from photosystems to leaves. *Plant Cell* 24 (5), 1921–1935. doi: 10.1105/tpc.112.097972

Jacquemoud, S., and Ustin, S. (2001). "Leaf optical properties: A state of the art," in *Proceedings 8th International Symposium Physical Measurements & Signatures in Remote Sensing*. (Aussois (France): CNES), 223–232.

Jay, S., Bendoula, R., Hadoux, X., Féret Gorretta, J. B., and Gorretta, N. (2016). A physically-based model for retrieving foliar biochemistry and leaf orientation using close-range imaging spectroscopy. *Remote Sensing of Environment* 177, 220–236.

Jayapal, P. K., Joshi, R., Sathasivam, R., Van Nguyen, B., Faqeerzada, M. A., Park, S. U., et al. (2022). Non-destructive measurement of total phenolic compounds in arabidopsis under various stress conditions. *Front. Plant Sci.* 13, 982247. doi: 10.3389/fpls.2022.982247

Jiménez-Lao, R., García-Caparrós, P., Pérez-Saiz, M., Llanderal, A., and Lao, M. (2021). Monitoring optical tool to determine the chlorophyll concentration in ornamental plants. *Agronomy* 11,2197. doi: 10.3390/agronomy11112197

Johkan, M., Shoji, K., Goto, F., Hashida, S. N., and Yoshihara, T. (2010). Blue light-emitting diode light irradiation of seedlings improves seedling quality and growth after transplanting in red leaf lettuce. *HortSci.: Publ. Am. Soc. Hortic. Sci.* 45, 1809–1814. doi: 10.21273/HORTSCI.45.12.1809

Jung, W. S., Chung, I. M., Hwang, M. H., Kim, S. H., Yu, C. Y., and Ghimire, B. K. (2021). Application of light-emitting diodes for improving the nutritional quality and bioactive compound levels of some crops and medicinal plants. *Molecules* 26 (5), 1477. doi: 10.3390/molecules26051477

Kang, J. H., KrishnaKumar, S., Atulba, S. L. S., Jeong, B. R., and Hwang, S. J. (2014). Light intensity and photoperiod influence the growth and development of hydroponically grown leaf lettuce in a closed-type plant factory system. *Horticul. Environment Biotechnol.* 54 (6), 501–509. doi: 10.1007/s13580-013-0109-8

Kim, J., Kang, S. W., Pak, C. H., and Kim, M. S. (2012). Changes in leaf variegation and coloration of English ivy and polka dot plant under various indoor light intensities. *HortTechnology* 22 (1), 49–55. doi: 10.21273/HORTTECH.22.1.49

Körner, O., and Challa, H. (2003a)Design for an improved temperature integration concept in greenhouse cultivation. *Comput. Electron. Agric.* 39, 39–59. doi: 10.1016/S0168-1699(03)00006-1

Körner, O., and Challa, H. (2003b)Process-based humidity control regime for greenhouse crops. *Comput. Electron. Agric.* 39, 173–192. doi: 10.1016/S0168-1699(03)00079-6

Kowalczyk, K., Mirgos, M., Bączek, K., Niedzińska, M., and Gajewski, M. (2016). Effect of different growing media in hydroponic culture on the yield and biological quality of lettuce (Lactuca sativa var. capitata). *Acta Hortic.* 1142), 10–110. doi: 10.17660/ActaHortic.2016.1142.17

Kozai, T. (2013). Sustainable plant factory: Closed plant production systems with artificial light for high resource use efficiencies and quality produce. *Acta Hortic.* 1004, 27–40. doi: 10.17660/ActaHortic.2013.1004.2

Larsen, D. H., Li, H., van de Peppel, A. C., Nicole, C. C. S., Marcelis, L. F. M., and Woltering, E. J. (2022). High light intensity at end-Of-Production improves the nutritional value of basil but does not affect postharvest chilling tolerance. *Food Chem.* 369, 130913. doi: 10.1016/j.foodchem.2021.130913

Ling, Q., Huang, W., and Jarvis, P. (2011). Use of a SPAD-502 meter to measure leaf chlorophyll concentration in arabidopsis thaliana. *Photosynth Res.* 107 (2), 209–214. doi: 10.1007/s11120-010-9606-0

Lichtenthaler, H. K., and Buschmann, C. (2001). Chlorophylls and Carotenoids: Measurement and Characterization by UV-VIS Spectroscopy. *Curr. Protocols in Food Analytical Chem.* 1, F4.3.1–F4.3.8. doi: 10.1002/0471142913.faf0403s01

Liu, Y., Schouten, R. E., Tikunov, Y., Liu, X., Visser, R. G. F., Tan, F., et al. (2022). Blue light increases anthocyanin content and delays fruit ripening in purple pepper fruit. *Postharvest Biol. Technol.* 192, 112024. doi: 10.1016/j.postharvbio.2022.112024

Maggiore, A., Afonso, A., Barrucci, F., and Sanctis, G. D. (2020). Climate change as a driver of emerging risks for food and feed safety, plant, animal health and nutritional quality. *EFSA Support. Publicat.* 17 (6), 42–69. doi: 10.2903/sp.efsa.2020.EN-1881

Mahlein, A.-K., Steiner, U., Hillnhütter, C., Dehne, H.-W., and Oerke, E.-C. (2012). Hyperspectral imaging for small-scale analysis of symptoms caused by different sugar beet diseases. *Plant Methods* 8 (1), 3. doi: 10.1186/1746-4811-8-3

Mastilović, J., Kevrešan, Ž., Stanojević, L., Cvetković, D., Barać, S., Šunić, L., et al. (2020). Bioactive constituents of red and green lettuce grown under colour shade nets. *Emirates J. Food Agric* 31 (12), 937–944. doi: 0.9755/ejfa.2019.v31.i12.2043

Mosadegh, H., Trivellini, A., Lucchesini, M., Ferrante, A., Maggini, R., Vernieri, P., et al. (2019). UV-B physiological changes under conditions of distress and eustress in sweet basil. *Plants (Basel)* 8 (10), 396. doi: 10.3390/plants8100396

Muhammad, I., Shalmani, A., Ali, M., Yang, Q. H., Ahmad, H., and Li, F. B. (2020). Mechanisms regulating the dynamics of photosynthesis under abiotic stresses. *Front. Plant Sci.* 11, 615942. doi: 10.3389/fpls.2020.615942

Neo, D. C. J., Ong, M. M. X., Lee, Y. Y., Teo, E. J., Ong, Q., Tanoto, H., et al. (2022). Shaping and tuning lighting conditions in controlled environment agriculture: A review. *ACS Agric. Sci. Technol.* 2 (1), 3–16. doi: 10.1021/acsagscitech.1c00241

Paucek, I., Pennisi, G., Pistillo, A., Appolloni, E., Crepaldi, A., Calegari, B., et al. (2020). Supplementary LED interlighting improves yield and precocity of greenhouse tomatoes in the Mediterranean. *Agronomy* 10 (7), 1002. doi: 10.3390/agronomy10071002

Sen, S., and Chakraborty, R. (2011). The role of antiox in human health. *Am. Chem. Society* 1083, 1–37. doi: 10.1021/bk-2011-1083.ch001

Sharifi-Rad, M., Anil Kumar, N. V., Zucca, P., Varoni, E. M., Dini, L., Panzarini, E., et al. (2020). Lifestyle, oxidative stress, and antioxidants: Back and forth in the pathophysiology of chronic diseases. *Front. Physiol.* 11, 694. doi: 10.3389/fphys.2020.00694

Sonneveld, C., and Straver, N. (1994). Nutrients solutions for vegetables and flowers grown in wateror substrates. *Voedingsoplossingen Glastuinbouw (Netherlands)* 8, 21.

Sun, J., Shi, S., Yang, J., Du, L., Gong, W., Chen, B., et al. (2018). Analyzing the performance of PROSPECT model inversion based on different spectral information for leaf biochemical properties retrieval. *ISPRS J. Photogrammet. Remote Sens.* 135, 74–83. doi: 10.1016/j.isprsjprs.2017.11.010

Sutuliene, R., Lauzike, K., Pukas, T., and Samuoliene, G. (2022). Effect of light intensity on the growth and antioxidant activity of sweet basil and lettuce. *Plants (Basel)* 11 (13), 1709. doi: 10.3390/plants11131709

Spafford, L., Maire, G., MacDougall, A., Boissieu, F., and Féret, J.-B. (2021). Spectral subdomains and prior estimation of leaf structure improves PROSPECT inversion on reflectance or transmittance alone. *Remote Sensing of Environ.* 252

Taulavuori, K., Hyöky, V., Oksanen, J., Taulavuori, E., and Julkunen-Tiitto, R. (2016). Species-specific differences in synthesis of flavonoids and phenolic acids under increasing periods of enhanced blue light. *Environ. Exp. Bot.* 121, 145–150. doi: 10.1016/j.envexpbot.2015.04.002

van Delden, S. H., SharathKumar, M., Butturini, M., Graamans, L. J. A., Heuvelink, E., Kacira, M., et al. (2021). Current status and future challenges in implementing and upscaling vertical farming systems. *Nat. Food* 2 (12), 944–956. doi: 10.1038/s43016-021-00402-w

Van Iersel, M. (2017). Light Emitting Diodes for Agriculture. *Optimizing LED lighting in controlled environment agriculture* 59–80 (Singapore: Springer). doi: 10.1007/978-981-10-5807-3_4

Wang, Z., Wang, T., Darvishzadeh, R., Skidmore, A., Jones, S., Suarez, L., et al. (2016). Vegetation indices for mapping canopy foliar nitrogen in a mixed temperate forest. *Remote Sens.* 8 (6), 250. doi: 10.3390/rs8060491

Weigou, F., Pingping, L., Yanyou, W., and Juanjuan, T. (2012). Effects of different light intensities on anti-oxidative enzyme activity, quality and biomass in lettuce. *Hortic. Sci.* 39, 129–134. doi: 10.17221/192/2011-HORTSCI

Xie, X., Lu, X., Wang, L. C., He, L., and Wang, G. (2020). High light intensity increases the concentrations of β-carotene and zeaxanthin in marine red macroalgae. *Algal Res.* 47, 101852. doi: 10.1016/j.algal.2020.101852

Xu, F., Shi, L., Chen, W., Cao, S., Su, X., and Yang, Z. (2014). Effect of blue light treatment on fruit quality, antioxidant enzymes and radical-scavenging activity in strawberry fruit. *Scientia Hortic.* 175, 181–186. doi: 10.1016/j.scienta.2014.06.012

Zhang, H., Zhao, Y., and Zhu, J. K. (2020). Thriving under stress: How plants balance growth and the stress response. *Dev. Cell* 55 (5), 529–543. doi: 10.1016/j.devcel.2020.10.012

Zheng, X. T., Yu, Z. C., Tang, J. W., Cai, M. L., Chen, Y. L., Yang, C. W., et al. (2021). The major photoprotective role of anthocyanins in leaves of arabidopsis thaliana under long-term high light treatment: antioxidant or light attenuator? *Photosynth Res.* 149 (1-2), 25–40. doi: 10.1007/s11120-020-00761-8

Zhou, J., Li, P., and Wang, J. (2022). Effects of light intensity and temperature on the photosynthesis characteristics and yield of lettuce. *Horticulturae* 8 (2), 178. doi: 10.3390/horticulturae8020178

frontiers | Frontiers in Plant Science

TYPE Original Research
PUBLISHED 05 December 2022
DOI 10.3389/fpls.2022.1045239

OPEN ACCESS

EDITED BY
Yuxin Tong,
Institute of Environment and Sustainable Development in Agriculture (CAAS), China

REVIEWED BY
Laura Cammarisano,
Leibniz Institute of Vegetable and Ornamental Crops, Germany
Luca Vitale,
Institute for Agricultural and Forestry Systems in the Mediterranean (CNR), Italy

*CORRESPONDENCE
Eiji Goto
goto@faculty.chiba-u.jp

†PRESENT ADDRESS
Jin-Hui Lee,
Department of Practical Arts Education, Jeonju National University of Education, Jeonju, South Korea

SPECIALTY SECTION
This article was submitted to Technical Advances in Plant Science, a section of the journal Frontiers in Plant Science

RECEIVED 15 September 2022
ACCEPTED 07 November 2022
PUBLISHED 05 December 2022

CITATION
Lee J-H and Goto E (2022) Ozone control as a novel method to improve health-promoting bioactive compounds in red leaf lettuce (*Lactuca sativa* L.). *Front. Plant Sci.* 13:1045239. doi: 10.3389/fpls.2022.1045239

Ozone control as a novel method to improve health-promoting bioactive compounds in red leaf lettuce (*Lactuca sativa* L.)

Jin-Hui Lee[1†] and Eiji Goto[1,2*]

[1]Graduate School of Horticulture, Chiba University, Chiba, Japan, [2]Plant Molecular Research Center, Chiba University, Chiba, Japan

In this study, we determined the short-term effects of ozone exposure on the growth and accumulation of bioactive compounds in red lettuce leaves grown in a controlled environment plant factory with artificial light, also known as a vertical farm. During cultivation, twenty-day-old lettuce (*Lactuca sativa* L. var. Redfire) seedlings were exposed to 100 and 200 ppb of ozone concentrations for 72 h. To find out how plants react to ozone and light, complex treatments were done with light and ozone concentrations (100 ppb; 16 h and 200 ppb; 24 h). Ozone treatment with 100 ppb did not show any significant difference in shoot fresh weight compared to that of the control, but the plants exposed to the 200 ppb treatment showed a significant reduction in fresh weight by 1.3 fold compared to the control. The expression of most genes in lettuce plants exposed to 100 and 200 ppb of ozone increased rapidly after 0.5 h and showed a decreasing trend after reaching a peak. Even when exposed to a uniform ozone concentration, the pattern of accumulating bioactive compounds such as total phenolics, antioxidant capacity and total flavonoids varied based on leaf age. At a concentration of 200 ppb, a greater accumulation was found in the third (older) leaf than in the fourth leaf (younger). The anthocyanin of lettuce plants subjected to 100 and 200 ppb concentrations increased continuously for 48 h. Our results suggest that ozone control is a novel method that can effectively increase the accumulation of bioactive compounds in lettuce in a plant factory.

KEYWORDS

air pollution, antioxidant capacity, environmental stress, ozone detoxification and repair, ozone sensitivity, phytochemical, vertical farm

Introduction

Phytochemicals are naturally occurring bioactive compounds found in plants. Numerous forms of antioxidant phytochemicals in plants have been linked to the prevention of chronic diseases including cancer and cardiovascular disease (Rajashekar et al., 2009). The emergence of several diseases are linked to oxidative stress induced by reactive oxygen species (ROS). Antioxidant phytochemicals are known for their neutralization effect on free radicals with high oxidation potential. Consequently, the popularity of diets containing antioxidant phytochemicals continues to rise (Tomasetti et al., 2017).

Tropospheric-level ozone (O_3) is a major air contaminant. The oxidative damage caused by ozone to the physiological and biochemical processes of plants is a serious global concern (Booker et al., 2012). According to a previous study, exposure to ozone concentrations of 80 ppb for 6.6 h resulted in decreased lung function and an increased inflammatory response in humans (Brown, 2009). Ozone induces substantial alterations in plant as well as human metabolism due to its strong oxidizing capacity (Lorenzini and Nali, 2018). Consequently, it affects plant growth, quality, and yield (Overmyer et al., 2003; Kangasjärvi et al., 2005). When plants are exposed to ozone, they trigger the expression of genes and subsequently accumulate ROS-scavengers and other metabolites as part of their antioxidant defense mechanism (Booker et al., 2012). In response to oxidative stress caused by ground-level ozone concentrations, an increase in antioxidant-related enzyme activity is observed in plants (Shao et al., 2007; Burkart et al., 2013; Sarkar et al., 2015). An increase in phenylpropanoid metabolites and the formation of various phenolic compounds have been reported in plants exposed to ozone. This further stimulates plant cell metabolism to restore and maintain cellular structure (Dizengremel, 2001; Andersen, 2003).

Since ROS are generated when plants are exposed to oxidative stress, especially after ozone uptake, the antioxidant capacity of the leaf apoplast is crucial for determining ozone tolerance (Podila et al., 2001). The response of plants to ozone varies depending on ozone concentration, duration of exposure, plant developmental stage, and stomatal conductance (De Temmerman et al., 2002). In addition to ascorbic acid and glutathione, various substances including phenols help scavenge ROS (Podila et al., 2001; De Temmerman et al., 2002). However, unlike other stress inducing substances, ozone acts as an elicitor and decomposes into oxygen, leaving no toxic residue behind (Pellegrini et al., 2018). In atmospheric systems, UV and ozone are closely correlated and have been reported to have similar effects on the mRNA accumulation of antioxidant genes in *Nicotiana plumbaginifolia* L. plants (Willekens et al., 1994). Unlike UV radiation, which is absorbed only on the leaf surface, ozone is easily absorbed by plant organs through the stomata and cuticular layers. After ozone penetrates the leaf tissue, O3 immediately interacts with extracellular antioxidants, which appear to stimulate ascorbate synthesis and/or its transport between compartments (Heath, 2008). Therefore, it could be said that ozone boosts the accumulation of bioactive antioxidants in plants (Sandermann et al., 1998).

A plant factory with artificial light (PFAL), also called a vertical farm, is an advanced plant cultivation system which is used for the production of commercial leafy vegetables such as leaf lettuce (Zhang et al., 2018; He et al., 2021). The system is airtight without windows and completely controls such as light, temperature, humidity, as well as CO_2 and O_2 gases. To date, many research on the effects of light, air, and root temperatures, humidity, and CO_2 concentration on dry mass production in lettuce and other leafy vegetables have been carried out in PFAL systems (Choi et al., 2000; Zhang et al., 2018; Carotti et al., 2021; He et al., 2021). As for the enhancement of health-promoting bioactive compounds in the plants, a variety of environmental parameters have been proposed as preharvest treatments which were effective in increasing the value of indoor farming produce (Lee et al., 2021). Ozone concentration can be controlled in a PFAL using a simple control unit with an ozone generator and a sensor. Compared to other chemical substances, the use of ozone is advantageous as it does not leave a residue; once generated, ozone is easily decomposed to O_2 and H_2O (Pellegrini et al., 2018). In addition, the plant factory has the advantage of being able to control the photoperiod because it uses artificial light. According to the results of previous studies, growth, net photosynthesis, and chlorophyll content were significantly decreased in unshaded-treated hybrid poplar (*Populus tristis* Fisch. × *P. balsamifera* L. cv. Tristis) compared to shaded-treated plants when combined treatment with light treatment (unshaded and shaded) and ozone was applied (Volin et al., 1993). Ozone induces stomata closure in leaves, which reduces CO_2 absorption and ultimately increases sensitivity to photoinhibition in ozonated plants (Fredericksen et al., 1996; Topa et al., 2001). This means that ozone and the light environment can exhibit strong interactions, and light conditions can cause further damage to plants exposed to ozone stress (Hurry et al., 1992; Guidi et al., 2000). Therefore, if light and ozone are treated for 24 hours without a dark period, it is possible to stimulate the antioxidant system in a shorter time than with photoperiodic treatment. If ozone induces the production of health-promoting bioactive compounds in plants, it can very well be incorporated in a preharvest treatment plan in a PFAL for value-added plant production.

Plant defense mechanisms against ozone vary based on factors, such as the leaf growth stage (leaf age) and thickness, plant species, and ozone exposure dynamics. In addition, environmental conditions affect the morphological and physiological response of plants to ozone (Guderian, 1985). For example, woody plants upon exposure to ozone have shown differential changes in antioxidant levels at different stages of plant development or have shown changes at the

same stage in a given day (Schupp and Rennenberg, 1988; Hausladen et al., 1990; Wieser et al., 2002; Nogués et al., 2008). Because it is difficult to expose large trees to ozone experimentally, studies have been conducted on woody plants mainly to determine the effect of age (developmental stages) on the response of trees to ozone. But only a few studies have shown that ozone has an effect on the stages of growth in herbaceous plants such as leafy vegetables. In the case of leafy vegetables such as Brassica (mustard, oilseed rape), there have been many studies related to ozone response based on crop or cultivars (Abedi and Pakniyat, 2010; Singh et al., 2011). When growing lettuce in a PFAL, it is important to monitor the ozone response as an elicitor because lettuce has a high economic and commercial value. Calatayud and Barreno (2004) confirmed that two lettuce varieties exhibited different chlorophyll a fluorescence reactions, photosynthetic pigmentations, and lipid peroxidation reactions when exposed to ozone. In addition, changes in photosynthetic CO_2 exchange, chlorophyll a fluorescence, and yield of lettuce exposed to ozone at different growth stages have also been reported (Calatayud et al., 2002; Goumenaki and Barnes, 2009). Apart from photosynthetic parameters and yield/growth responses (Temple et al., 1986; Goumenaki et al., 2007; Kleiber et al., 2017), biochemical parameters such as the accumulation of antioxidant enzymes have been identified upon exposure to ozone before harvest (Calatayud et al., 2002). To the best of our knowledge, there is no information on age-dependent defense responses of lettuce plants exposed to various ozone concentrations.

This study aims to determine the effect of ozone concentrations on the accumulation of secondary metabolites in red leaf lettuce plants grown in a plant factory-like system. The objectives of this study were to determine: (1) changes in secondary metabolite pathways upon ozone exposure monitored throughout the day before harvest, (2) effects of short-term ozone exposure on the levels of antioxidant bioactive compounds, and (3) effects of photoperiod and ozone concentrations on the accumulation of bioactive compounds.

Materials and methods

Plant materials and environmental conditions

Red leaf lettuce (*Lactuca sativa* L. var. Redfire) seeds were placed in a wet paper towel (Kimtowel, Nippon Paper Crecia Co. Ltd., Tokyo, Japan) in a Petri plate, wrapped using a plastic wrap. The following day, germinated seeds were moved to a urethane sponge for seedling growth. Distilled water was supplied until 6 days after sowing (DAS). The seedlings were then transferred to a hydroponic system with an air pump and subsequently cultivated until 20 DAS. Thirty-two plants were grown per tray with a deep flow technique hydroponic system, and three trays were grown per experiment. Lettuce plants were grown in the plant factory until 20 DAS, after which a uniform plant was selected and transferred to the ozone chamber. One-fourth concentration of Otsuka A (OAT house A treatment; OAT Agrio Co. Ltd., Tokyo, Japan) nutrient recipe solution was supplied (EC: 1.0 ds m^{-1} and pH: 6.5). The environmental conditions for growing red leaf lettuce was set as follows: white LED lamps (LDL40S-N/19/21; Panasonic Corp., Osaka, Japan), at 200 µmol m^{-2} s^{-1} photosynthetic photon flux density (PPFD), 16 h light, 25°C/20°C (day/night) air temperature, 70% relative humidity (RH), and 1000 µmol mol^{-1} CO_2 concentration. PPFD was measured at 12 points per tray, with a measurement range of 200 ± 10 µmol m^{-2} s^{-1}. The PPFD of the white LED light was adjusted to be 200 PPFD on average.

Ozone treatment

The 20-day-old seedlings (20 DAS; about four true leaves appeared) were subjected to 100 and 200 ppb of ozone treatment and non-ozonated treatment (control). The environment of the ozone chamber remained the same as the plant factory's cultivation area (200 PPFD, 25°C/20°C (day/night) air temperature, 70% RH, and 1000 µmol mol^{-1} CO_2). Ozone treatment was given to the seedlings for 72 h. Figure 1 and Supplementary Figure S1 show the schematic diagram of the ozone chamber and the ozone treatment given in this experiment. Ozone concentration was controlled using the light ozone generator (WOR1040-Z1; Ushio Inc., Tokyo, Japan) and an ozone monitor (EG-700EIII; Ebara Jitsugyo Co. Ltd., Tokyo, Japan) in a growth chamber with white LEDs (FLI-2010H-LED; Tokyo Rikakikai Co. Ltd., Tokyo, Japan). Two experiments were conducted to confirm the effect of light period and ozone concentration (Table 1). In the case of 100 ppb, the light period was set to 16 h, the same as in the current cultivation environment. To exclude plant reactions owing to ozone absorption during the light and dark periods, the following ozone experiment at a concentration of 200 ppb was conducted using continuous light conditions. The control plants were also grown in the same model chamber as the ozone chamber of which ozone concentration was controlled zero. At each time point, both ozonated plants and control plants were taken at the same time for the analysis of bioactive compounds. Fresh weight of shoot and root were determined immediately before treatment and at 72 h of ozone treatment.

Determination of total phenolics, antioxidant capacity, total flavonoids and anthocyanin

For the analysis of bioactive compounds, lettuce plants grown in ozone chambers or control chambers were randomly selected at every sampling point. Each leaf sample was collected at 0, 0.25, 0.5, 1, 2, 5, 8, 12, 16, 24, 48, and 72 hours after ozone

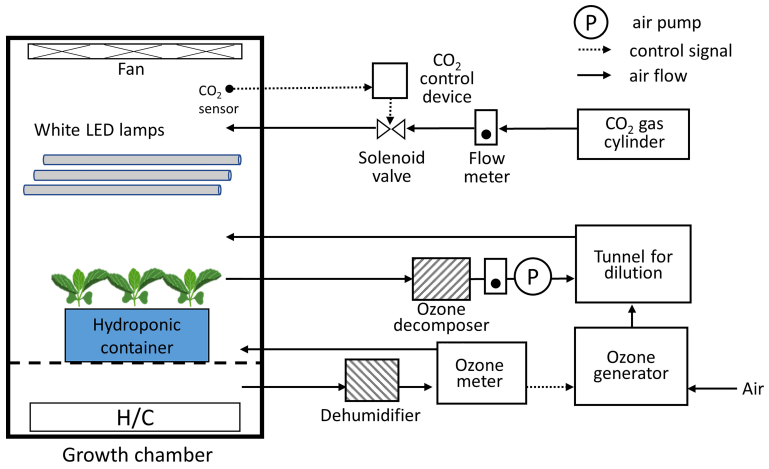

FIGURE 1
Schematic diagram of the growth chamber with an ozone concentration control equipment. The light period, photosynthetic photon flux density, CO_2 concentration, O_3 concentration, air temperature, and relative humidity in the chamber can be controlled.

exposure. In order to confirm the response according to the leaf age, the third and fourth leaves were sampled. Leaves were counted starting from bottom, excluding cotyledons. The collected leaf samples were stored in a deep freezer (-80°C) until further analysis. Total phenolic concentration and Trolox equivalent antioxidant capacity were analyzed using a slightly modified method by Miller and Rice-Evans (1996) and Ainsworth and Gillespie (2007). Approximately 50 mg of fresh leaf samples were used for the analyses. The remaining analytical procedures of the total phenolic concentration and antioxidant capacity were investigated as described (Lee et al., 2021).

Flavonoid concentration was determined using the method of Zhishen et al. (1999). One milliliter of 80% acetone was added to the powdered leaf sample and extracted at 16 Hz for 1 min using a MM400 ball mill (Retsch GmbH, Haan, Germany), and then sonicated at 30 Hz for 6 min. The extract was incubated overnight under darkness at 4°C. The assay mixture for the determination of total flavonoid concentration comprised distilled water, 5% $NaNO_2$, leaf extract, 10% (w/v) $AlCl_3$, 1M NaOH in a final mixture volume of 1.5 mL. The absorbance of flavonoid concentration was measured at 510 nm using a spectrophotometer (V-750; JASCO Corp., Tokyo, Japan) (mg catechin g^{-1} FW).

Anthocyanins concentration in red lettuce was measured with slight modifications to the analytical method of Mancinelli and Schwartz (1984). Leaves were used for the extraction of anthocyanin (50 mg fresh samples/400 mL of 1% (v/v) HCl in methanol). Briefly, the extracted samples were mixed with 200 µL distilled water and 500 µL chloroform and centrifuged for 2 min at 13,000 × g at 4°C. A 400 µL aliquot of the aqueous fraction of the sample was then mixed with 600 µL of 1% (v/v) HCl in methanol. The absorbance was read at 530 and 657 nm (A530-0.25 × A657) using a spectrophotometer (V-750; JASCO Corp., Tokyo, Japan). Results were expressed in ug C3G g^{-1} FW.

Hydrogen peroxide (H_2O_2) determination

Hydrogen peroxide accumulation in red lettuce leaves exposed to two ozone concentrations was analyzed using the

TABLE 1 Environmental conditions during ozone treatment.

	Seedling stage		Ozone treatment
Light period (h d^{-1}) [100 ppb]		16	
Light period (h d^{-1}) [200 ppb]		24	
PPFD* (µmol m^{-2} s^{-1})	100		200
Air temperature (°C)		25/20	
Relative humidity (%)		70	
CO_2 concentration (µmol mol^{-1})		1000	

*Photosynthetic photon flux density on culture panels.

method of Velikova et al. (2000). The collected fresh leaf samples were ground and then extracted with 1 mL 0.1% (w/v) trichloroacetic acid. An aliquot (0.5 mL) of the supernatant of the extract was mixed with 10 mM potassium phosphate buffer (pH 7.0, 0.5 mL) and 1M KI (1 mL). The absorbance of hydrogen peroxide mixture was measured at 390 nm using a spectrophotometer (V-750; JASCO Corp., Tokyo, Japan). Results were expressed in H_2O_2 g^{-1} FW.

Gene expression quantification

Total RNA was extracted from red leaf lettuce leaves (approximately 100–150 mg) using the RNeasy Plant Mini Kit (Qiagen N.V., Venlo, The Netherlands) after homogenization in liquid nitrogen. The fourth leaf from the bottom was sampled at 0, 0.25, 0.5, 1, 2, 5, 8, 12, 16, and 24 h of ozone exposure to examine time-dependent gene expression variations. The oligonucleotide primers used in this study were designed using data from the GenBank database (Table 2). The remaining analytical procedures (complementary DNA synthesis and PCR) were followed as described by Lee et al. (2021). The following mRNA transcripts were quantified: phenylalanine ammonia-lyase (*PAL*), cinnamic acid 4-hydroxylase (*C4H*), 4-coumaroyl-CoA ligase (*4CL*), chalcone synthase (*CHS*), chalcone isomerase (*CHI*), flavanone 3-hydroxylase (*F3H*), flavonoid 3′-hydroxylase (*F3′H*), flavonol synthase (*FLS*), dihydroflavonol 4-reductase (*DFR*), anthocyanidin synthase (*ANS*), and anthocyanidin reductase (*ANR*). The expression of each target mRNA transcript was compared to that of the reference actin gene. Log2 Ratio (relative gene expression) was computed as the ratio of treatment to control gene expression.

Statistical analysis

Statistical analyses were performed using SPSS software (version 24; IBM Corp., Armonk, NY, USA). To evaluate the effect of two ozone concentrations (100 and 200 ppb) and exposure time (0, 0.25, 0.5, 1, 2, 5, 8, 12, 16, 24, 48, and 72 hours), a one-way analysis of variance (ANOVA) was conducted to compare differences in variance between the treatment. Data shown in all figures are means ± standard error (± SE) (biological experimental replicates; n = 4 for each parameter), $p < 0.05$ was considered as statistically significant (T-test).

Results

Growth and morphology of red leaf lettuce

Figure 2 shows the shoot fresh weight differences between ozone treated and control lettuce plants over time. The growth of the ozone treated-red lettuce seedlings at 100 ppb was almost the same as the control until 48 h of exposure and almost negligible at 72 h. At 200 ppb ozone exposure, the shoot fresh weight was significantly decreased by 1.3 times compared to that of the control at 72 h of treatment.

Plants were evaluated visually for their appearance, and the size of the ozone-treated plants at 100 and 200 ppb did not differ significantly in comparison to the size of the control plants until 24 h after ozone exposure (Figure 3). In comparison to other treatments (control and 100 ppb concentration) lettuce leaves exposed to 200 ppb turned visibly red 24 hours after exposure 24 hours after ozone exposure. The leaves of lettuce exposed to 200

TABLE 2 Primers for internal standard gene and genes used in real time PCR.

Gene symbol	Gene name		Primer sequence (5' - 3')	Product length (bp)
ACT	Actin	Forward	TGGTAGGTATGGGCCAGAAA	113
		Reverse	GTCATCCCAGTTGCTCACAA	
PAL	Phenylalanin ammonia-lyase	Forward	AAGGGAAGCCGGAGTTTAC	286
		Reverse	GGAAACGTCGATCAATGG	
C4H	Cinnamic acid 4-hydroxylase	Forward	GGAGTCGATTGGCACAGAGCT	198
		Reverse	GGCGCATTTCAGTTGATTGTTC	
CHS	Chalcone synthase	Forward	GGAGGTGGGGCTAACTTTTC	169
		Reverse	GAGCTCCACCTGGTCCAATA	
F3H	Flavanone 3-hydroxylase	Forward	CTACTCAAGGTGGCCCGATA	210
		Reverse	AATGTGAGATCGGGTTGAGG	
FLS	Flavonol synthase	Forward	GGTTTGGCCACCTTCTGCTAAG	182
		Reverse	TCTTCACCACCCAACCCT	
DFR	Dihydroflavonol 4-reductase	Forward	GACAGTGAACGTGCACGGAA	152
		Reverse	CCTTTGTTGCTTCAAATGCTGCT	
UFGT	Flavonoid 3-O-glucosyltransferase	Forward	AAGAGACCAGAACCCCGTTT	203
		Reverse	AGCTCCAATGCTCTCCGATA	

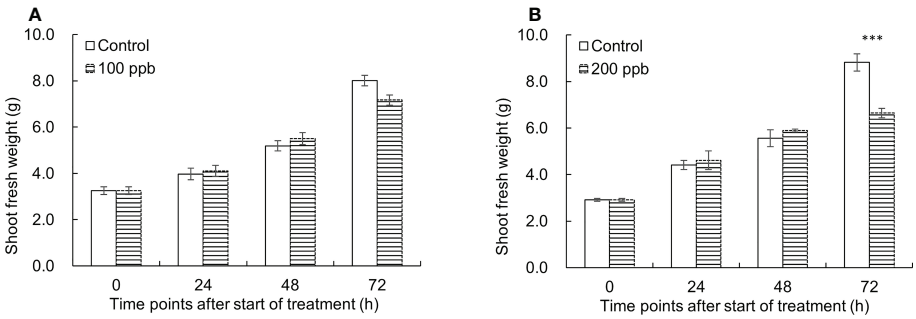

FIGURE 2
Changes of shoot fresh weight of the control and 100 ppb **(A)** and 200 ppb **(B)** ozone treatments used in this experiment. The vertical vars indicate SE (n=4). Statistically significant differences are indicated at ***$p < 0.001$ by T-test.

ppb treatment turned red at 24 h compared to those of other treatments (control and 100 ppb concentration).

Plants were visually assessed for appearance and severity, and when plants were exposed to 100 ppb ozone for 72 hours, there was no discernible difference in appearance compared to the control (Figure 3). The size of the plants exposed to the 200-ppb ozone treatment appeared smaller.

Gene expression of phenylpropanoid and flavonoid biosynthetic pathway

Relative gene expression in the fourth leaf of red lettuce exposed to both ozone concentrations (100 and 200 ppb) showed an increasing trend with ozone exposure time (Figures 4, 5). The *PAL* and *C4H* relative expression levels reached maxima after 0.5 and 1 h of 100 ppb ozone exposure (Figure 4). *PAL* and *C4H* encode the first and second essential enzymes of the phenylpropanoid pathway, respectively. *CHS* and *F3H* expression peaked after 0.5 h of ozone exposure and increased again after 16 h of ozone exposure. *FLS* expression levels peaked after 1 h and decreased thereafter. *UFGT* expression reached a maximum at 0.5 h of ozone exposure and increased once again after 16 h of exposure.

In response to a 200 ppb concentration, relative gene expression exhibited an upward trend compared to 100 ppb (Figure 5). All gene expression levels reached maxima at 0.5 h of ozone exposure and decreased thereafter. The *C4H*, *F3H*, *FLS*, *DFR*, and *UFGT* genes showed an increase again between 12 and 24 h of ozone exposure.

FIGURE 3
Red leaf lettuce plants exposed to 100 and 200 ppb ozone for 72 h.

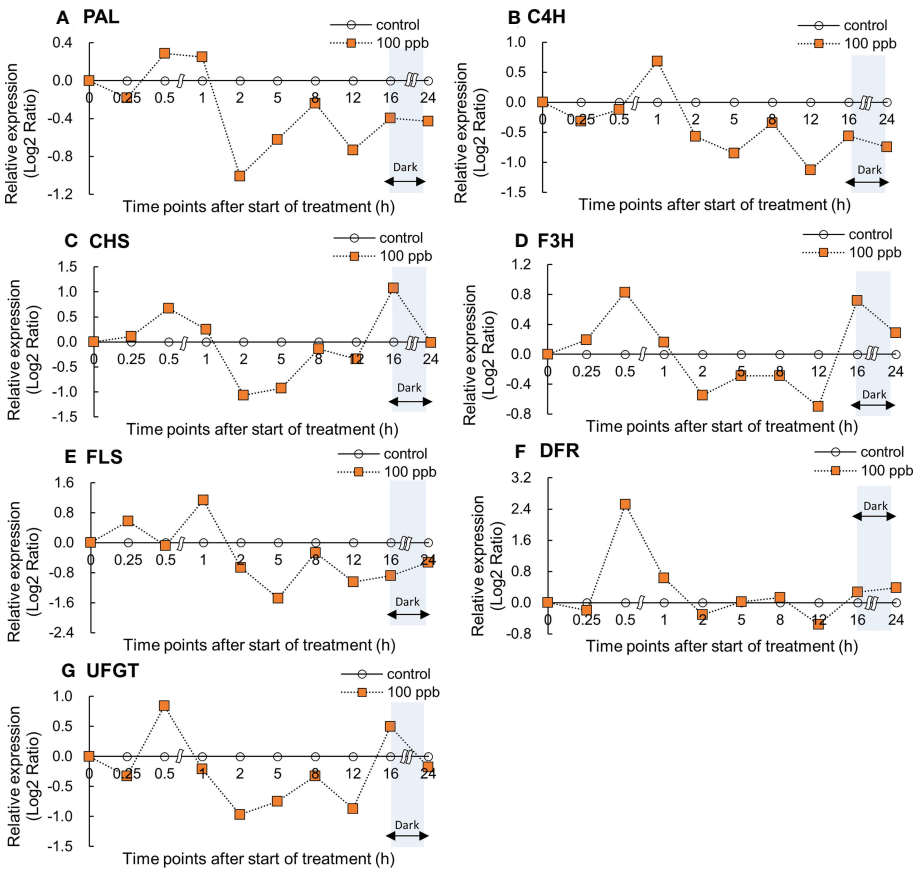

FIGURE 4
Effect of 100-ppb ozone exposure on relative gene expression (Log2 Ratio) of *PAL* **(A)**, *C4H* **(B)**, *CHS* **(C)**, *F3H* **(D)**, *FLS* **(E)** and *DFR* **(F)**, and *UFGT* **(G)** mRNA in fourth leaf of lettuce plant. The vertical vars indicate SE (n=4). The line graphs indicate Log2 fold change (treatment/control) levels of gene expression.

Total phenolics, antioxidant capacity, anthocyanin, and total flavonoid

The concentration of bioactive compounds (total phenolics, anthocyanin, and flavonoids) and the antioxidant capacity in the third and fourth leaves of the red lettuce plants exposed to 100 ppb of ozone were also determined at different times (Figures 6, 7).

A significant increase was observed in the total phenolic concentration of the third leaf compared to that of the control at 2 and 48 h of exposure to 100 ppb of ozone (Figure 6). No significant increase was observed in antioxidant capacity and flavonoid concentrations. The anthocyanin concentration of the third leaf showed a significant increase after 2 h of ozone exposure, and a marked increase was observed after 12 h of treatment.

The total phenolics, flavonoids, and anthocyanin concentrations and antioxidant capacity of the fourth leaf exposed to 100 ppb showed an increase immediately after ozone exposure (at 0.25 h) (Figure 7). A significant increase was observed in the total phenolic concentration after 0.5 h of treatment, after which it continued to show a higher value than the control. Thereafter, a significant increase was observed at 12 h of ozone exposure. The antioxidant capacity also showed similar results to the total phenolic concentrations. The flavonoid concentration showed a significant increase after 8 h of exposure but showed a tendency to decrease over time. As the ozone exposure time increased, the anthocyanin concentration in lettuce plants exposed to 100 ppb ozone continued to increase. In particular, at 72 h of exposure, anthocyanin concentration significantly increased by about 2.8-fold when compared to that of the control.

The bioactive compound concentrations (total phenolic, anthocyanin, and flavonoid) and antioxidant capacity in the third and fourth leaves of the red lettuce plants exposed to 200 ppb of ozone were also determined at different intervals (Figures 8, 9).

Right after exposure to 200 ppb ozone, the concentrations of total phenolics, flavonoids, and anthocyanins and antioxidant capacity in the third leaf were slightly higher than those of the control (Figure 8). Bioactive compounds as well as antioxidant

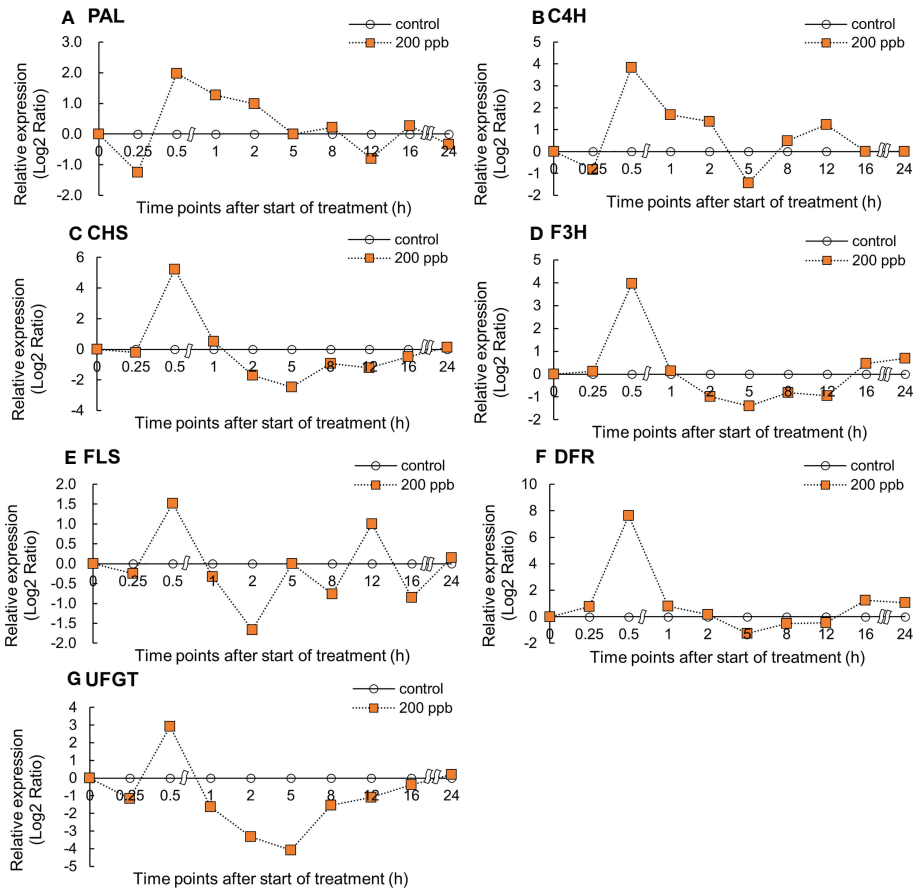

FIGURE 5
Effect of 200-ppb ozone exposure on relative gene expression (Log2 Ratio) of *PAL* **(A)**, *C4H* **(B)**, *CHS* **(C)**, *F3H* **(D)**, *FLS* **(E)** and *DFR* **(F)**, and *UFGT* **(G)** mRNA in fourth leaf of lettuce plant. The vertical vars indicate SE (n=4). The line graphs indicate Log2 fold change (treatment/control) levels of gene expression.

capacity exhibited an increasing tendency over time until 48 h. There was a slight decrease after 72 h of exposure to ozone. At 48 h of exposure, the total phenolics, antioxidant capacity, flavonoids, and anthocyanin concentrations were all significantly higher than those in the control by 2.1- 1.07-, 1.83-, and 5.23-fold, respectively.

Bioactive compound concentrations in the fourth leaf exposed to 200 ppb of ozone were also high compared to those of the control (Figure 9). Total phenolic concentration was significantly increased after 16 h of exposure. Flavonoid concentration was significantly increased at 8, 16, and 24 h of ozone exposure (1.42-, 1.58-, and 1.88-times). Anthocyanin concentration started to increase after 1 h; the highest value was obtained at 24 h after exposure to ozone (3.31-times) compared to the control.

Hydrogen peroxide

Hydrogen peroxide accumulation in red leaf lettuce varied depending on the ozone concentration and the order of the exposed leaves (Figure 10). The H_2O_2 content of lettuce leaves exposed to 100 ppb of ozone did not show any increase in both the third and fourth leaves. However, a significant increase was observed in the H_2O_2 content of the third leaf exposed to 200 ppb ozone after 0.5 h of ozone exposure compared to the control. The H_2O_2 content continued to show a higher value than the control; the highest value was obtained at 72 h of exposure (1.73-fold). The fourth leaf also showed a significant increase in H_2O_2 content in the leaves exposed to 200 ppb ozone after 0.25 h and showed a 1.11-times higher value compared to that of the control at 72 h of exposure.

Discussion

Effect of ozone concentration on growth

Both 100 and 200 ppb ozone treatments did not show a significant effect on growth until 48 h of ozone exposure

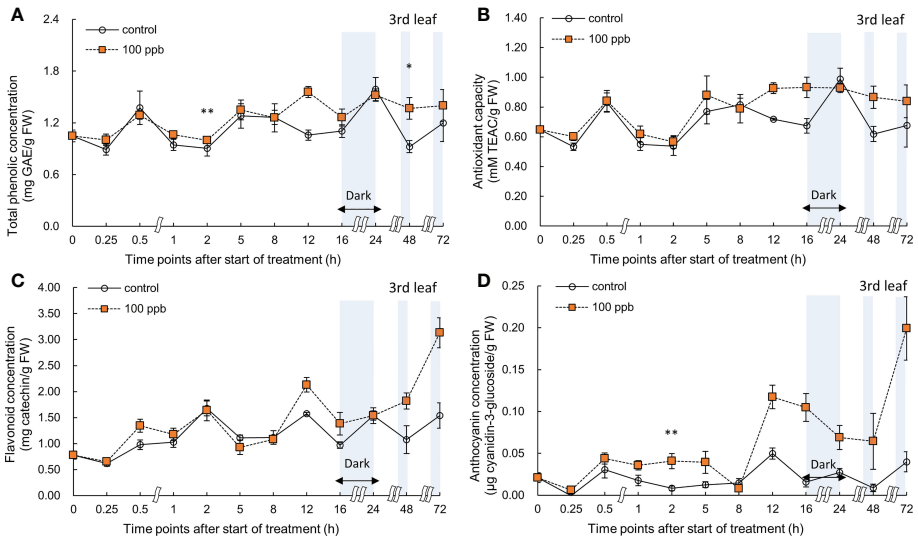

FIGURE 6
Total phenolic concentration **(A)**, antioxidant capacity **(B)**, total flavonoid concentration **(C)**, and anthocyanin concentration **(D)** of third red leaf lettuce subjected to 100–ppb ozone treatment for 72 h. The vertical vars indicate SE (n=4). Statistically significant differences are indicated at $*p < 0.05$ and $**p < 0.01$ by T-test.

(Figures 2, 3). As the ozone exposure continued for up to 72 h, there was a significant reduction in the growth of the ozonated seedlings. In particular, 200 ppb treatment significantly decreased the shoot fresh weight of red leaf lettuce plants. Damages caused by ozone exposure to plants depend on the ozone regime and plant species (Ferdinand et al., 2000; Singh et al., 2018). However, under conditions of chronic ozone exposure, increasing oxidative stress would cause damage to plant growth and quality (Khaling et al., 2015; Pandey et al., 2018). During respiration, the leaf absorbs ozone through its

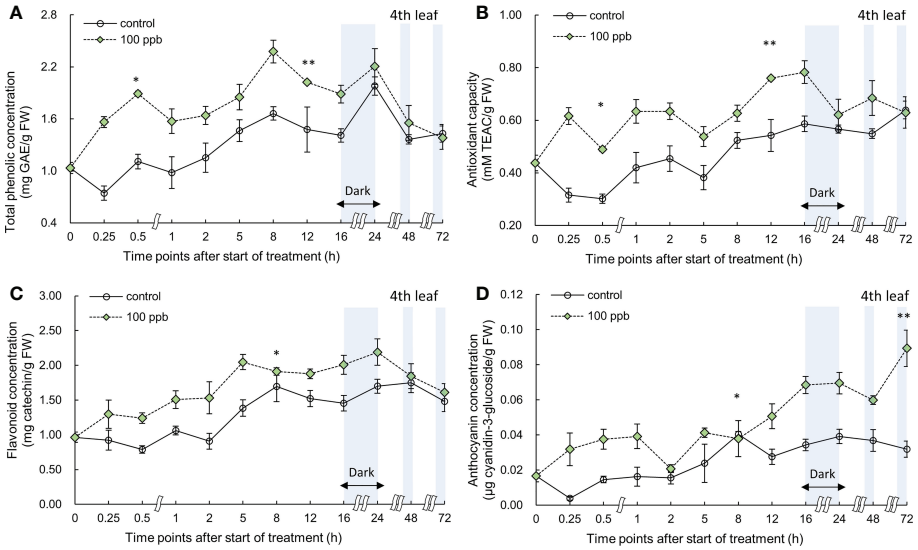

FIGURE 7
Total phenolic concentration **(A)**, antioxidant capacity **(B)**, total flavonoid concentration **(C)**, and anthocyanin concentration **(D)** of fourth red leaf lettuce subjected to 100–ppb ozone treatment for 72 h. The vertical vars indicate SE (n=4). Statistically significant differences are indicated at $*p < 0.05$ and $**p < 0.01$ by T-test.

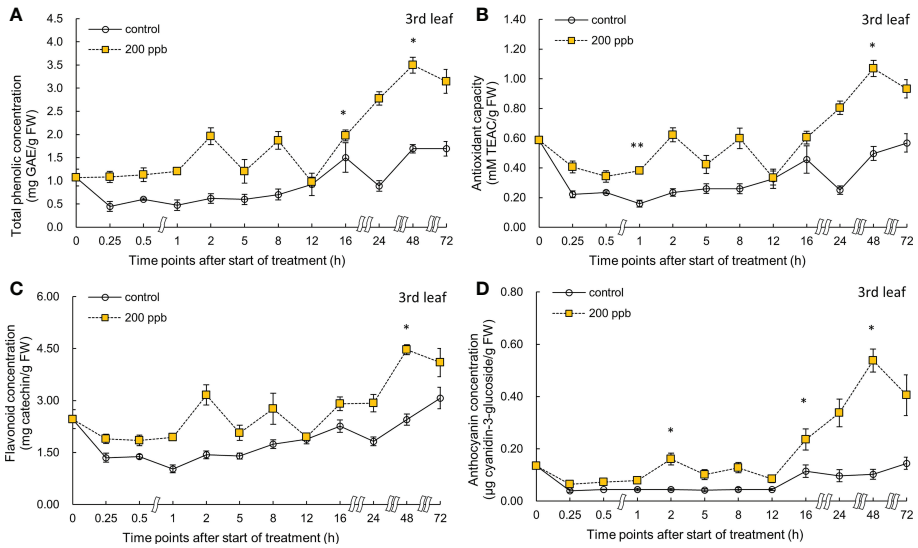

FIGURE 8
Total phenolic concentration **(A)**, antioxidant capacity **(B)**, total flavonoid concentration **(C)**, and anthocyanin concentration **(D)** of third red leaf lettuce subjected to 200-ppb ozone treatment for 72 h. The vertical vars indicate SE (n=4). Statistically significant differences are indicated at $*p < 0.05$ and $**p < 0.01$ by T-test.

stomata; this ozone can alter the chemical composition of cells as a whole (Lee, 1968). As ozone reacts, there is an instantaneous increase in the activity of reactive oxygen species (ROS) (Mehlhorn et al., 1990; Buchanan-Wollaston and Morris, 2000; Booker et al., 2009). Many studies have reported the effects of ozone stress-induced ROS on plants (Podila et al., 2001; De Temmerman et al., 2002).

In other studies, ozone has significantly reduced the overall development, leaf area, and biomass (yield) of most plants (Oksanen et al., 2001; Menéndez et al., 2017; Singh et al.,

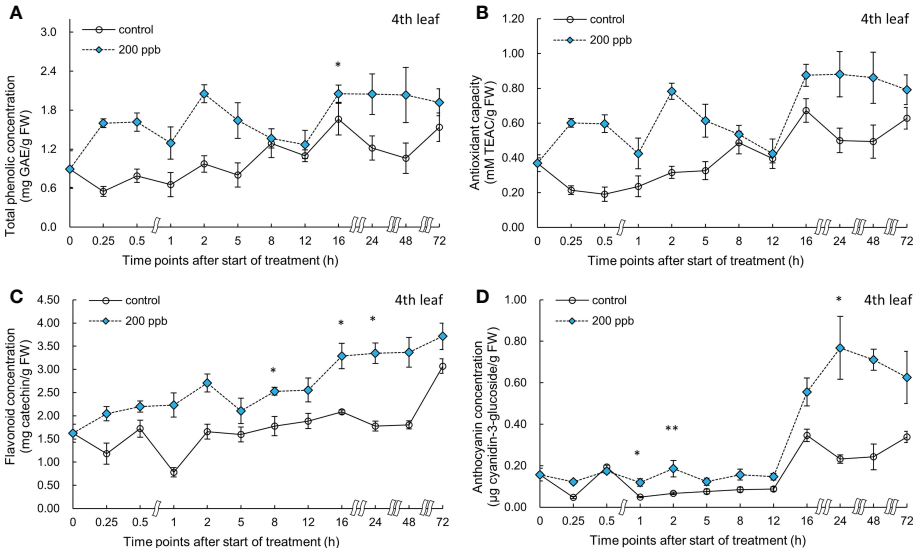

FIGURE 9
Total phenolic concentration **(A)**, antioxidant capacity **(B)**, total flavonoid concentration **(C)**, and anthocyanin concentration **(D)** of fourth red leaf lettuce subjected to 200-ppb ozone treatment for 72 h. The vertical vars indicate SE (n=4). Statistically significant differences are indicated at $*p < 0.05$ and $**p < 0.01$ by T-test.

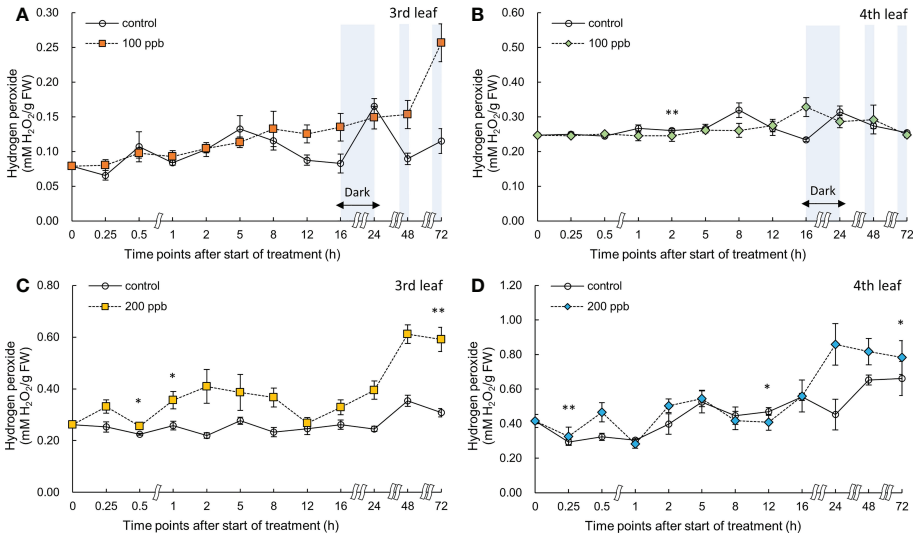

FIGURE 10
Hydrogen peroxide of third **(A, C)** and fourth **(B, D)** red leaf lettuce subjected to 100- and 200-ppb ozone treatment for 72 h. The vertical vars indicate SE (n=4). Statistically significant differences are indicated at $*p < 0.05$ and $**p < 0.01$ by T-test.

2018). However, some plants exhibit either negative or positive photopigment responses to extreme ozone stress (Pääkkönen et al., 1998a; Woo et al., 2004; Singh et al., 2009; Singh, 2017). The critical ozone concentration may vary depending on the dosage of ozone exposure, environmental conditions, leaf thickness, leaf age, leaf development stages, and plant varieties or cultivars (Karlsson et al., 1995; Calatayud et al., 2007; Sarkar and Agrawal, 2012) In the present study, no significant changes were observed in the fresh weight of red leaf lettuce after 3 days of exposure to 100 ppb ozone, but a significant decrease was observed in the 200 ppb ozonated plants compared with the control. These results suggest that a dose of approximately 200 ppb × 48 h is a critical dose in the red leaf lettuce cultivar and experimental conditions used in this study. It has been reported that due to a reduction in photosynthetic capacity, carbon assimilation and a reduced leaf lifetime, ozone-induced senescence acceleration contributes to economic yield losses of plants (Ainsworth, 2017; Emberson et al., 2018). The ROS produced in the plant by ozone concentration of 200 ppb for 3 days probably decreased the photosynthetic capacity of lettuce, thereby inhibiting its growth.

In a previous study, ozone exposure of 150 ppb for 1 h had no effect on dry matter growth of Pak-Choi plants, whereas 4 h of exposure resulted in growth reduction (Han et al., 2020). Seventy ppb ozone for 2 days had no effect on growth parameters such as leaf area and reproductive development, whereas 10 d ozone exposure reduced the whole growth of *Brassica campestris* plants (Black et al., 2007). When plants are exposed to extreme levels of ozone, injury such as tissue damage (cell necrosis), chlorosis and stomata closure occur due to excessive accumulation of ROS (Jacobson and Hill, 1970; Heath, 2008). Moeder et al. (2002) demonstrated that the regions/tissue where hydrogen peroxide is produced and chlorosis occurs are similar. However, in our study no tissue injury was observed in lettuce leaves even after exposure to 200 ppb for 3 days. These results indicate that the hydrogen peroxide generated during the 3 days was not at a level that would cause serious damage to the leaves.

Gene expression of phenylpropanoid and flavonoid pathways

Immediately after ozone exposure, the expression of genes involved in the phenylpropanoid and flavonoid biosynthetic pathways in red leaf lettuce plants increased in both 100 and 200 ppb ozone treatments (Figures 4, 5). Except for the *C4H* and *FLS* genes, gene expression in lettuce plants exposed to 100 ppb ozone reached a peak after 0.5 h of ozone exposure. However, the expression of all genes in lettuce plants exposed to 200 ppb of ozone increased rapidly after 0.5 h and showed a tendency to decrease after reaching a peak (Figure 5). Plants respond to ozone stress by inducing a variety of defense responses. Active defense mechanisms include an increase in phenylpropanoid pathway gene transcripts, such as those encoding *PAL* and *CHS* (Eckey-Kaltenbach et al., 1997; Pääkkönen et al., 1998b). When plants are exposed to low levels of ozone, physiological and metabolic changes are observed. With the exception of serious injuries such as tissue injury or stomata closure, the great majority of these disruptive changes generally begin at the level of gene expression (Heath, 2008). Previous studies found

that the increase in the gene expression of secondary metabolites in plants exposed to ozone followed different patterns depending on the type of crops (species or cultivar), ozone concentration, and exposure time. *PAL* gene expression in *Salvia officinalis* plants exposed to 120 ppb (5 h day^{-1}) significantly increased after 5 h of ozone exposure (Marchica et al., 2020); *PAL* mRNA in *Arabidopsis* leaves exposed to 300 ppb of ozone dramatically increased after 3 h (Sharma et al., 1996). According to Tuomainen et al. (1996), when birch plants were exposed to 150 ppb ozone for 96 h (8 h of pulse treatment), *PAL* was rapidly but transiently induced after 8 h of ozone exposure. *PAL* is an upstream gene that directs phenylpropanoid metabolism to its primary branch (Supplementary Figure S2). These results indicate that the expression of many genes encoding secondary metabolite pathways increased rapidly within 1 h of ozone exposure.

The phenylpropanoid and flavonoid biosynthetic pathways are certainly the most important pathways for the synthesis of antioxidant phytochemical compounds in plants, such as phenols, flavonoids, and lignin (Guidi et al., 2005). In our study, the expression of genes related to phenylpropanoid and flavonoid biosynthetic pathways increased immediately after ozone exposure (Figures 4, 5). It is possible that secondary metabolite compounds such as total phenolics, antioxidant capacity, flavonoids, and anthocyanins were increased. In several ozonated plants, an increase in the expression of genes related to secondary metabolites has been linked to an increase in the production of bioactive compounds (Eckey-Kaltenbach et al., 1994; Booker and Miller, 1998; Cabané et al., 2004).

Changes in bioactive compounds in relation to ozone concentrations according to leaf age

The concentration of bioactive compounds in red leaf lettuce leaves exposed to ozone showed different responses according to the ozone concentration (Figures 6–9). The total phenolic concentration, antioxidant capacity, and total flavonoid concentration of third leaves exposed to ozone did not show a significant difference in the 100-ppb ozone treatment compared to that of the control. The fourth leaf treated with 100 ppb ozone exhibited a relatively greater increase than the third leaf. However, in the case of lettuce leaves exposed to 200 ppb ozone, the bioactive compounds, except for anthocyanins, showed a tendency to increase rapidly immediately after ozone exposure regardless of leaf position (third or fourth). Thus, the ozone concentration affected the accumulation of bioactive compounds in red leaf lettuce. Antioxidant enzymes such as APX and CAT in wheat plants of the jointing stage exposed to various ozone concentrations showed increased activities at 40 ppb ozone treatment and decreased in other treatments (Liu et al., 2015). In addition, the concentrations of ascorbate and glutathione were significantly higher at 40 ppb than at 80 ppb in two soybean plants with different tolerances to ozone (Tiwari and Agrawal, 2011). Thus, there is an effective ozone concentration for the accumulation of antioxidants in different plants.

To confirm the effect of the light period, an experiment of 100 ppb of ozone concentration was performed with 16 h light period (Figures 6, 7). During the 8 h dark period, the plant failed to photosynthesize and did not accumulate new carbohydrates or precursors for the synthesis of secondary metabolite compounds, including antioxidants. Therefore, 100 ppb ozone treatment with an 8 h dark period may have a smaller positive effect on the accumulation of bioactive compounds than 200 ppb with continuous lighting. In addition, there was a significant reduction in the ascorbic acid content in both varieties of lettuce (*Lactuca sativa* and *Lactuca serriola*) which were exposed to ozone under dark conditions (Goumenaki et al., 2021). However, when the plants were transferred to the light conditions, the ascorbic acid content increased rapidly, showing twice the concentration of that under the dark condition (Goumenaki et al., 2021). These results indicate that plants are substantially more impacted by equivalent ozone flux absorbed at night than during the day, and that the detoxification potential of plants is compromised at night time (Wieser and Havranek, 1995; Lloyd et al., 2018). In addition, the nighttime reduction of ascorbate content and/or redox homeostasis may increase the sensitivity of the plants to ozone (Maddison et al., 2002; Sanmartin et al., 2003; Höller et al., 2015). For this reason, it is thought that the accumulation of bioactive compounds under 100 ppb ozone with a light period did not increase when compared to that treated with 200 ppb ozone (Figures 6–9). In addition, in the case of a control plant treated with a photoperiod of 16 hours in a 100 ppb treatment, it was observed that the total phenolic concentration, antioxidant capacity, and flavonoid concentration were increased at 24 hours after dark period compared to 16 hours after light period (Figures 6–7). This increase may be the result of daily rhythms of phytochemicals. Previous studies have shown that photosynthesis, carbohydrate, and amino acid levels can depend on circadian clock patterns (Vazirifar et al., 2021; Francisco and Rodriguez, 2021). Vazirifar et al. (2021) reported that the photoperiod (light/dark period) controls the carbon and energy flows involved in the production and consumption of starch and the activation of phenylalanine-related enzymes. Typically, at the end of the dark period/or at the beginning of the light period, phenolic compounds exhibiting antioxidant properties are accumulated higher in plants (Hasperué et al., 2011; Soengas et al., 2018). The polyphenols in plants are raised to protect them from damage caused by too much light, and plants adjust their biological clocks based on the daily cycle (Francisco and Rodriguez, 2021). It is also possible that the antioxidant accumulation pattern of plants may have changed due to the combined action of the

circadian rhythm of phytochemicals and ozone concentration according to the photoperiod. The increasing pattern of bioactive compounds was different according to the leaf age, even with the same ozone concentration (Figures 6–9). A higher accumulation was observed at 200 ppb concentration in the third leaf (older) than in the fourth leaf (younger). Therefore, the response to ozone exposure can vary greatly with leaf position. However, the opposite has been reported in soybean plants exposed to ozone (70 ppb for 5 days). In soybeans, older leaves are first exposed to stressors than younger leaves (Bailey et al., 2019). While considering the effects of ozone in plants, these observations emphasize the importance of understanding the age of the leaves. Leaf age could be related to the ability to modulate stomatal conductance, oxidative signaling, and activation of defense mechanisms (Vingarzan, 2004; Mill et al., 2011; Schneider et al., 2017). However, studies on the effect of ozone on the accumulation of bioactive compounds in different-aged leaves remain limited.

The ozone concentration of 200 ppb may have acted as a strong stressor on the third and fourth leaves of lettuce (Figure 9). The H_2O_2 concentration in the third leaf was approximately 1.9-fold higher than that in the control at 72 h of ozone exposure. However, the concentration in the fourth leaf was approximately 1.3-fold higher than that in the control. These results suggest that a constant 200 ppb ozone concentration can have a different effect on the accumulation of bioactive compounds according to leaf age. The ozone concentration of 100 ppb in the third leaf showed no significant difference compared to the control in the total phenolic concentration, flavonoid concentrations, and antioxidant capacity during all of the treatment periods. However, in the fourth leaf, a significant increase was observed in the antioxidant capacity compared to the control at 0.5 and 12 h of 100 ppb ozone exposure (Figure 7). These results indicate that the 100-ppb concentration in the fourth leaf can also help bioactive compound accumulation. The total phenolics, antioxidant capacity, flavonoids, and anthocyanin concentrations of the third leaf exposed to 200 ppb ozone continued to increase until 48 h and then decreased after 72 h of ozone exposure. In previous studies, researchers have also found that bioactive compounds increase and then decrease up to a certain treatment level (Taulavuori et al., 2016; Cammarisano et al., 2020). Thus, under high levels of ozone, the third leaf of lettuce plants gradually lose the ability to activate secondary metabolism. This time-dependent decrease in the accumulation of antioxidant properties was also observed in *Salvia officinalis* exposed to 120 ppb ozone (5 h day^{-1}) (Marchica et al., 2021).

Relationship between ROS and bioactive compounds in red leaf lettuce plants

The phytotoxic effects of ozone are mostly attributable to the ozone-induced generation of ROS that exceed the capacity of plants to maintain ROS below the tolerance threshold. Ozone impacts on plants are determined by the balance between ozone uptake and cellular antioxidant potential (Di Baccio et al., 2008). After ozone penetrates the leaf tissue, it interacts with extracellular antioxidants, which appear to stimulate ascorbate synthesis and/or its transport between compartments. The antioxidants in the apoplast will respond to ozone within the cell wall space, thereby protecting the membrane from ozone damage. The generation of H_2O_2 near the membrane appears to initiate both a pathogen-like response with an increase in H_2O_2 production (Zheng et al., 2000; Conklin and Barth, 2004; Heath, 2007; Heath, 2008). The effects of ozone can be characterized as either acute or chronic, based on the exposure intensity and duration of ozone treatment. Long-term exposure to relatively low ozone concentrations reduces photosynthesis and growth and promotes leaf senescence, but short-term exposure to high ozone concentrations induces leaf injuries reminiscent of the hypersensitive cell death triggered during plant-pathogen interactions (Schlagnhaufer et al., 1995; Mahalingam et al., 2003; Castagna and Ranieri, 2009).

In our study, it is possible that ROS (especially, H_2O_2) continued to increase as a result of the plant-pathogen interaction reaction caused by the short-term exposure of high ozone concentrations (Figure 10). Ascorbic acid and glutathione in the apoplast are two antioxidants that regulate ROS generated through ozone treatment, and are found in high concentrations in the leaves of all plant species (Iriti and Faoro, 2007; Foyer and Noctor, 2011). Regardless of leaf order, H_2O_2 concentration started to increase significantly immediately after 200 ppb ozone exposure (0.25 h) in the present study (Figure 10). After ozone enters the plant leaves, it is possible that H_2O_2 reacted with apoplastic antioxidants such as ascorbic acid and glutathione. In our results, the bioactive compounds of lettuce accumulated under both ozone treatments (100 and 200 ppb) and showed up-and-down mobility regardless of leaf order. These results may be due to the rapid oxidation-reduction reactions between antioxidants and ROS in cells. As ozone exposure time increased, ROS burst appeared; it is possible that antioxidants were generated as a defense mechanism (Bolwell, 1996). In 200 ppb ozonated third leaf, a rapid increase in the production of secondary metabolites as a defense mechanism in response to ozone entry into leaves was observed after 24 h of exposure.

Under conditions of oxidative stress, the phenolic compounds generated by the phenylpropanoid and flavonoid biosynthetic pathways are strong antioxidants in plant tissues (Taiz and Zeiger, 2002). Anthocyanins, which are flavonoids, are water-soluble pigments that concentrate in the vacuole (Chalker-Scott, 1999). According to the results of previous studies, ozone can stimulate the biosynthesis of anthocyanins in plants. Various stress factors, including water stress (osmotic), UV-irradiation, nutrient deficiency, low temperature, and ozone, strongly promote the production of anthocyanin (Chalker-Scott, 1999). Purified anthocyanin solutions are four times more

effective in scavenging ROS than α-tocopherol and ascorbate, indicating that these components have a significant antioxidant capacity (Gould et al., 2000; Feild et al., 2001; Gould, 2004). Thus, the accumulation of anthocyanins may be essential for ozone stress tolerance (or sensitivity), since it may protect ozonated leaves from damage caused by ozone-induced ROS (Bortolin et al., 2014). The anthocyanin content varies among different cultivars or species in vegetable plants exposed to ozone. Broccoli plants exposed to 70 μg m^{-3} of ozone did not show a significant difference in anthocyanin content compared to that of the control, but a significant 2.5-fold increase was observed in Chinese cabbage (Rozpądek et al., 2015). It could be said that the lettuce used in this experiment responded immediately to ozone because it was a red leaf lettuce accumulating anthocyanins as it matures. However, when plants are exposed to high ozone concentrations, ozone may destroy chlorophyll and decompose anthocyanins (Rathore and Chaudhary, 2019). In our results, anthocyanin concentrations decreased from 48 to 72 h of ozone exposure (Figures 6–9). These results suggest that ozone exposure for longer than 72 h may adversely affect anthocyanin biosynthesis. Three days of ozone exposure with 200 ppb inhibited the fresh weight of lettuce significantly, but did not show the difference at 2 days of ozone exposure (Figure 2). A significant accumulation of bioactive compounds both in the third and fourth leaves may have been observed at around 48 h of ozone exposure. Therefore, it can be concluded that 2 days of ozone exposure with 200 ppb can be useful for the production of photochemical-rich leaf lettuce. Our results suggest that ozone control is a novel method as preharvest treatment effective for increasing antioxidant bioactive compounds in lettuce in a PFAL.

Conclusions

A PFAL, also known as a vertical farm, is an advanced plant production system for the commercial production of leafy vegetables. Ozone concentration can be controlled easily using a simple control apparatus in a PFAL. This study was conducted to confirm the complex effect of ozone on red leaf lettuce. In the case of 100 ppb, the concentrations of bioactive compounds and antioxidant capacity were increased in the relatively young fourth leaf. However, with 200 ppb, those were found to be considerably high in the third leaf. Therefore, the sensitivity of red leaf lettuce plants to ozone-induced oxidative stress is determined by apoplast antioxidants and/or redox homeostasis. Although the degree of accumulation of antioxidant-bioactive compounds may vary between leaf age depending on the ozone concentration, it was confirmed that the concentrations of phytochemicals such as anthocyanins could be effectively increased in a few days. Also, in this study, a complex reaction between photoperiod and ozone was confirmed. These results suggest that if the ozone treatment is applied immediately prior to harvest (e.g., by progressively increasing the ozone concentration for 2 days and combined treatment of photoperiod and ozone), the amount of bioactive compounds can be enhanced without inhibiting growth. Our results suggest that ozone control is a novel method effective for increasing antioxidant bioactive compounds in lettuce in a PFAL or a vertical farm.

Data availability statement

The original contributions presented in the study are included in the article/Supplementary Material. Further inquiries can be directed to the corresponding authors.

Author contributions

Performance of experiments, sample collection, analyses of chemical data, writing-original draft preparation: J-HL; writing-review and editing, conceptualization, experimental design, supervision and funding acquisition: EG. All authors read and agreed to the final version of the manuscript.

Funding

This work was supported by the Ministry of Economy, Trade, and Industry of Japan in the form of a grant-in-aid from the project <*Development of Fundamental Technologies for the Production of High-Value Materials Using Transgenic Plants*> and funded by the Program on Open Innovation Platform with Enterprises, Research Institute and Academia, Japan Science and Technology Agency (JST-OPERA, JPMJOP1851).

Conflict of interest

The authors declare that the research was conducted in the absence of any commercial or financial relationships that could be construed as a potential conflict of interest.

Publisher's note

Supplementary material

The Supplementary Material for this article can be found online at: https://www.frontiersin.org/articles/10.3389/fpls.2022.1045239/full#supplementary-material

SUPPLEMENTARY FIGURE 1
The control and different ozone treatments used in this experiment.

SUPPLEMENTARY FIGURE 2
Phenylpropanoid, flavonoid, and anthocyanin biosynthetic pathways. The genes analyzed in this study are marked in red.

References

Abedi, T., and Pakniyat, H. (2010). Antioxidant enzymes changes in response to drought stress in ten cultivars of oilseed rape (*Brassica napus* l.). *Czech J. Genet. Plant Breed.* 46, 27–34. doi: 10.17221/67/2009-CJGPB

Ainsworth, E. A. (2017). Understanding and improving global crop response to ozone pollution. *Plant J.* 90, 886–897. doi: 10.1111/tpj.13298

Ainsworth, E. A., and Gillespie, K. M. (2007). Estimation of total phenolic content and other oxidation substrates in plant tissues using folin–ciocalteu reagent. *Nat. Protoc.* 2, 875–877. doi: 10.1038/nprot.2007.102

Andersen, C. P. (2003). Source–sink balance and carbon allocation below ground in plants exposed to ozone. *New Phytol.* 157, 213–228. doi: 10.1046/j.1469-8137.2003.00674.x

Bailey, A., Burkey, K., Taggart, M., and Rufty, T. (2019). Leaf traits that contribute to differential ozone response in ozone-tolerant and sensitive soybean genotypes. *Plants (Basel).* 8, 235. doi: 10.3390/plants8070235

Black, V. J., Stewart, C. A., Roberts, J. A., and Black, C. R. (2007). Ozone affects gas exchange, growth and reproductive development in *Brassica campestris* (Wisconsin fast plants). *New Phytol.* 176, 150–163. doi: 10.1111/j.1469-8137.2007.02163.x

Bolwell, G. P. (1996). The origin of the oxidative burst in plants. *Biochem. Soc Trans.* 24, 438–442. doi: 10.1042/bst0240438

Booker, F. L., Burkey, K. O., and Jones, A. M. (2012). Re-evaluating the role of ascorbic acid and phenolic glycosides in ozone scavenging in the leaf apoplast of *Arabidopsis thaliana* l. *Plant Cell Environ.* 35, 1456–1466. doi: 10.1111/j.1365-3040.2012.02502.x

Booker, F. L., and Miller, J. E. (1998). Phenylpropanoid metabolism and phenolic composition of soybean [*Glycine max* (L.) merr.] leaves following exposure to ozone. *J. Exp. Bot.* 49, 1191–1202. doi: 10.1093/jxb/49.324.1191

Booker, F., Muntifering, R., McGrath, M., Burkey, K., Decoteau, D., Fiscus, E., et al. (2009). The ozone component of global change: potential effects on agricultural and horticultural plant yield, product quality and interactions with invasive species. *J. Integr. Plant Biol.* 51, 337–351. doi: 10.1111/j.1744-7909.2008.00805.x

Bortolin, R. C., Caregnato, F. F., Divan, J. A.M., Reginatto, F. H., Gelain, D. P., and Moreira, J. C. F. (2014). Effects of chronic elevated ozone concentration on the redox state and fruit yield of red pepper plant *Capsicum baccatum*. ecotoxicol. *Environ. Saf.* 100, 114–121. doi: 10.1016/j.ecoenv.2013.09.035

Brown, J. S. (2009). Acute effects of exposure to ozone in humans: how low can levels be and still produce effects? *Am. J. Respir. Crit. Care Med.* 180, 200–201. doi: 10.1164/rccm.200906-0834ed

Buchanan-Wollaston, V., and Morris, K. (2000). Senescence and cell death in *Brassica napus* and *Arabidopsis*. *Symp. Soc Exp. Biol.* 52, 163–174. doi: 10.1201/9781003076889-11

Burkart, S., Bender, J., Tarkotta, B., Faust, S., Castagna, A., Ranieri, A., et al. (2013). Effects of ozone on leaf senescence, photochemical efficiency and grain yield in two winter wheat cultivars. *J. Agro. Crop Sci.* 199, 275–285. doi: 10.1111/jac.12013

Cabané, M., Pireaux, J. C., Léger, E., Weber, E., Dizengremel, P., Pollet, B., et al. (2004). Condensed lignins are synthesized in poplar leaves exposed to ozone. *Plant Physiol.* 134, 586–594. doi: 10.1104/pp.103.031765

Calatayud, A., and Barreno, E. (2004). Response to ozone in two lettuce varieties on chlorophyll a fluorescence, photosynthetic pigments and lipid peroxidation. *Plant Physiol. Biochem.* 42, 549–555. doi: 10.1016/j.plaphy.2004.05.002

Calatayud, V., Cerveró, J., and Sanz, M. J. (2007). Foliar, physiologial and growth responses of four maple species exposed to ozone. *Water Air Soil pollut.* 185, 239–254. doi: 10.1007/s11270-007-9446-5

Calatayud, A., Ramirez, J. W., Iglesias, D. J., and Barreno, E. (2002). Effects of ozone on photosynthetic CO2 exchange, chlorophyll a fluorescence and antioxidant systems in lettuce leaves. *Physiol. Plant* 116, 308–316. doi: 10.1034/j.1399-3054.2002.1160305.x

Cammarisano, L., Donnison, I. S., and Robson, P. R.. (2020). Producing enhanced yield and nutritional pigmentation in lollo rossothrough manipulating the irradiance, duration, and periodicity of LEDsin the visible region of light. *Front. in Plant Sci.* 11, 598082. doi: 10.3389/fpls.2020.598082

Carotti, L., Graamans, L., Puksic, F., Butturini, M., Meinen, E., Heuvelink, E., et al. (2021). Plant factories are heating up: Hunting for the best combination of light intensity, air temperature and root-zone temperature in lettuce production. *Front. Plant Sci.* 11. doi: 10.3389/fpls.2020.592171

Castagna, A., and Ranieri, A. (2009). Detoxification and repair process of ozone injury: from O3 uptake to gene expression adjustment. *Environ. pollut.* 157, 1461–1469. doi: 10.1016/j.envpol.2008.09.029

Chalker-Scott, L. (1999). Environmental significance of anthocyanins in plant stress responses. *Photochem. Photobiol.* 70, 1–9. doi: 10.1111/j.1751-1097.1999.tb01944.x

Choi, K. Y., Paek, K. Y., and Lee, Y. B. (2000). "Effect of air temperature on tipburn incidence of butterhead and leaf lettuce in a plant factory," in *Transplant production in the 21st century* (Dordrecht: Springer), 166–171. doi: 10.1007/978-94-015-9371-7_27

Conklin, P. L., and Barth, C. (2004). Ascorbic acid, a familiar small molecule intertwined in the response of plants to ozone, pathogens, and the onset of senescence. *Plant Cell Environ.* 27, 959–970. doi: 10.1111/j.1365-3040.2004.01203.x

De Temmerman, L., Vandermeiren, K., and D'Haese, D. (2002). Ozone effects on trees, where uptake and detoxification meet. *Dendrobiology* 47, 9–19.

Di Baccio, D., Castagna, A., Paoletti, E., Sebastiani, L., and Ranieri, A. (2008). Could the differences in O_3 sensitivity between two poplar clones be related to a difference in antioxidant defense and secondary metabolic response to O_3 influx? *Tree Physiol.* 28, 1761–1772. doi: 10.1093/treephys/28.12.1761

Dizengremel, P. (2001). Effects of ozone on the carbon metabolism of forest trees. *Plant Physiol. Biochem.* 39, 729–742. doi: 10.1016/S0981-9428(01)01291-8

Eckey-Kaltenbach, H., Ernst, D., Heller, W., and Sandermann, J. H. (1994). Biochemical plant responses to ozone (IV. cross-induction of defensive pathways in parsley (*Petroselinum crispum* l.) plants). *Plant Physiol.* 104, 67–74. doi: 10.1104/pp.104.1.67

Eckey-Kaltenbach, H., Kiefer, E., Grosskopf, E., Ernst, D., and Sandermann, H. (1997). Differential transcript induction of parsley pathogenesis-related proteins and of a small heat shock protein by ozone and heat shock. *Plant Mol. Biol.* 33, 343–350. doi: 10.1023/a:1005786317975

Emberson, L. D., Pleijel, H., Ainsworth, E. A., Van den Berg, M., Ren, W., Osborne, S., et al. (2018). Ozone effects on crops and consideration in crop models. *Eur. J. Agron.* 100, 19–34. doi: 10.1016/j.eja.2018.06.002

Feild, T. S., Lee, D. W., and Holbrook, N. M. (2001). Why leaves turn red in autumn. the role of anthocyanins in senescing leaves of red-osier dogwood. *Plant Physiol.* 127, 566–574. doi: 10.1104/pp.010063

Ferdinand, J. A., Fredericksen, T. S., Kouterick, K. B., and Skelly, J. M. (2000). Leaf morphology and ozone sensitivity of two open pollinated genotypes of black cherry (*Prunus serotina*) seedlings. *Environ. pollut.* 108, 297–302. doi: 10.1016/s0269-7491(99)00078-0

Foyer, C. H., and Noctor, G. (2011). Ascorbate and glutathione: the heart of the redox hub. *Plant Physiol.* 155, 2–18. doi: 10.1104/pp.110.167569

Francisco, M., and Rodríguez, V. M. (2021). Importance of daily rhythms on *Brassicaceae* phytochemicals. *Agronomy* 11, 639. doi: 10.3390/agronomy11040639

Fredericksen, T. S., Kolb, T. E., Skelly, J. M., Steiner, K. C., Joyce, B. J., and Savage, J. E. (1996). Light environment alters ozone uptake per net photosynthetic rate in black cherry trees. *Tree Physiol.* 16, 485–490. doi: 10.1093/treephys/16.5.485

Gould, K. S. (2004). Nature's Swiss army knife: the diverse protective roles of anthocyanins in leaves. *J. Biomed. Biotechnol.* 2004, 314–320. doi: 10.1155/S1110724304406147

Gould, K. S., Markham, K. R., Smith, R. H., and Goris, J. J. (2000). Functional role of anthocyanins in the leaves of *Quintinia serrata* a. *Cunn. J. Exp. Bot.* 51, 1107–1115. doi: 10.1093/jexbot/51.347.1107

Goumenaki, E., and Barnes, J. (2009). Impacts of tropospheric ozone on growth and photosynthesis of lettuce. *Acta Hortic.* 817, 169–176. doi: 10.17660/ActaHortic.2009.817.16

Goumenaki, E., Fernandez, I. G., Papanikolaou, A., Papadopoulou, D., Askianakis, C., Kouvarakis, G., et al. (2007). Derivation of ozone flux-yield relationships for lettuce: a key horticultural crop. *Environ. pollut.* 146, 699–706. doi: 10.1016/j.envpol.2006.08.009

Goumenaki, E., González-Fernández, I., and Barnes, J. D. (2021). Ozone uptake at night is more damaging to plants than equivalent day-time flux. *Planta* 253, 75. doi: 10.1007/s00425-021-03580-w

R. Guderian (Ed.) (1985). "Effects of photochemical oxidants on plants. air pollution by photochemical oxidants: formation, transport, control, and effects on plants," in *Ecol. stud*, vol. 52 (Berlin: Springer-Verlag), 346.

Guidi, L., Degl'Innocenti, E., Genovesi, S., and Soldatini, G. F. (2005). Photosynthetic process and activities of enzymes involved in the phenylpropanoid pathway in resistant and sensitive genotypes of *Lycopersicon esculentum* l. *exposed to ozone*. *Plant Sci.* 168, 153–160. doi: 10.1016/j.plantsci.2004.07.027

Guidi, L., Tonini, M., and Soldatini, G. F. (2000). Effects of high light and ozone fumigation on photosynthesis in *Phaseolus vulgaris.* plant physiol. *Biochememistry* 38, 717–725. doi: 10.1016/s0981-9428(00)01172-4

Han, Y. J., Gharibeshghi, A., Mewis, I., Förster, N., Beck, W., and Ulrichs, C. (2020). Plant responses to ozone: effects of different ozone exposure durations on plant growth and biochemical quality of *Brassica campestris* l. ssp. chinensis. *Sci. Hortic.* 262, 108921. doi: 10.1016/j.scienta.2019.108921

Hasperué, J. H., Chaves, A. R., and Martínez, G. A. (2011). End of day harvest delays postharvest senescence of broccoli florets. *Postharvest Biol. Technol.* 59, 64–70. doi: 10.1016/j.postharvbio.2010.08.005

Hausladen, A., Madamanchi, N. R., Fellows, S., Alscher, R. G., and Amundson, R. G. (1990). Seasonal changes in antioxidants in red spruce as affected by ozone. *New Phytol.* 115, 447–458. doi: 10.1111/j.1469-8137.1990.tb00470.x

Heath, R. L. (2007). Alterations of the biochemical pathways of plants by the air pollutant ozone: which are the true gauges of injury? *Sci. World J.* 7 Supplement 1, 110–118. doi: 10.1100/tsw.2007.19

Heath, R. L. (2008). Modification of the biochemical pathways of plants induced by ozone: what are the varied routes to change? *Environ. pollut.* 155, 453–463. doi: 10.1016/j.envpol.2008.03.010

He, R., Zhang, Y., Song, S., Su, W., Hao, Y., and Liu, H. (2021). UV-A and FR irradiation improves growth and nutritional properties of lettuce grown in an artificial light plant factory. *Food Chem.* 345, 128727. doi: 10.1016/j.foodchem.2020.128727

Höller, S., Ueda, Y., Wu, L., Wang, Y., Hajirezaei, M. R., Ghaffari, M. R., et al. (2015). Ascorbate biosynthesis and its involvement in stress tolerance and plant development in rice (*Oryza sativa* l.). *Plant Mol. Biol.* 88, 545–560. doi: 10.1007/s11103-015-0341-y

Hurry, V. M., Krol, M., Öquist, G., and Huner, N. P. A. (1992). Effect of long-term photoinhibition on growth and photosynthesis of cold-hardened spring and winter wheat. *Planta* 188, 369–375. doi: 10.1007/bf00192804

Iriti, M., and Faoro, F. (2007). Oxidative stress, the paradigm of ozone toxicity in plants and animals. *Water Air Soil pollut.* 187, 285–301. doi: 10.1007/s11270-007-9517-7

Jacobson, J. S., and Hill, A. C. (1970). *Recognition of air pollution injury to vegetation: a pictorial atlas* (Pittsburgh, PA: Air Pollution Control Association). doi: 10.1016/0013-9327(71)90010-3

Kangasjärvi, J., Jaspers, P., and Kollist, H. (2005). Signalling and cell death in ozone-exposed plants. *Plant Cell Environ.* 28, 1021–1036. doi: 10.1111/j.1365-3040.2005.01325.x

Karlsson, G. P., Sellden, G., Skärby, L., and Pleijel, H. (1995). Clover as an indicator plant for phytotoxic ozone concentrations: visible injury in relation to species, leaf age and exposure dynamics. *New Phytol.* 129, 355–365. doi: 10.1111/j.1469-8137.1995.tb04306.x

Khaling, E., Papazian, S., Poelman, E. H., Holopainen, J. K., Albrectsen, B. R., and Blande, J. D. (2015). Ozone affects growth and development of *Pieris brassicae* on the wild host plant *Brassica nigra*. environ. *Pollution* 199, 119–129. doi: 10.1016/j.envpol.2015.01.019

Kleiber, T., Borowiak, K., Schroeter-Zakrzewska, A., Budka, A., and Osiecki, S. (2017). Effect of ozone treatment and light colour on photosynthesis and yield of lettuce. *Sci. Hortic.* 217, 130–136. doi: 10.1016/j.scienta.2017.01.035

Lee, T. T. (1968). Effect of ozone on swelling of tobacco mitochondria. *Plant Physiol.* 43, 133–139. doi: 10.1104/pp.43.2.133

Lee, J. H., Shibata, S., and Goto, E. (2021). Time-course of changes in photosynthesis and secondary metabolites in canola (*Brassica napus*) under different UV-b irradiation levels in a plant factory with artificial light. *Front. Plant Sci.* 12. doi: 10.3389/fpls.2021.786555

Liu, X., Sui, L., Huang, Y., Geng, C., and Yin, B. (2015). Physiological and visible injury responses in different growth stages of winter wheat to ozone stress and the protection of spermidine. *Atmos. pollut. Res.* 6, 596–604. doi: 10.5094/APR.2015.067

Lloyd, K. L., Davis, D. D., Marini, R. P., and Decoteau, D. R. (2018). Effects of night time ozone treatment at ambient concentrations on sensitive and resistant snap bean genotypes. *J. Amer. Soc Hortic. Sci.* 143, 23–33. doi: 10.21273/JASHS04253-17

Lorenzini, G., and Nali, C. (2018). Editorial-ozone and plant life: the Italian state-of-the-art. *Environ. Sci. pollut. Res. Int.* 25, 8069–8073. doi: 10.1007/s11356-018-1387-6

Maddison, J., Lyons, T., Plöchl, M., and Barnes, J. (2002). Hydroponically cultivated radish fed l-galactono-1,4-lactone exhibit increased tolerance to ozone. *Planta* 214, 383–391. doi: 10.1007/s004250100625

Mahalingam, R., Gomez-Buitrago, A., Eckardt, N., Shah, N., Guevara-Garcia, A., Day, P., et al. (2003). Characterizing the stress/defense transcriptome of arabidopsis. *Genome Biol.* 4, 1–14. doi: 10.1186/gb-2003-4-3-r20

Mancinelli, A. L., and Schwartz, O. M. (1984). The photoregulation of anthocyanin synthesis IX. the photosensitivity of the response in dark and light-grown tomato seedlings. *Plant Cell Physiol.* 25, 93–105. doi: 10.1093/oxfordjournals.pcp.a076701

Marchica, A., Ascrizzi, R., Flamini, G., Cotrozzi, L., Tonelli, M., Lorenzini, G., et al. (2021). Ozone as eustress for enhancing secondary metabolites and bioactive properties in *Salvia officinalis*. *Ind. Crops Prod.* 170, 113730. doi: 10.1016/j.indcrop.2021.113730

Marchica, A., Cotrozzi, L., Detti, R., Lorenzini, G., Pellegrini, E., Petersen, M., et al. (2020). The biosynthesis of phenolic compounds is an integrated defence mechanism to prevent ozone injury in *Salvia officinalis*. *Antioxidants (Basel).* 9, 1274. doi: 10.3390/antiox9121274

Mehlhorn, H., Tabner, B. J., and Wellburn, A. R. (1990). Electron spin resonance evidence for the formation of free radicals in plants exposed to ozone. *Physiol. Plant* 79, 377–383. doi: 10.1111/j.1399-3054.1990.tb06756.x

Menéndez, A. I., Gundel, P. E., Lores, L. M., and Martínez-Ghersa, M. A. (2017). Assessing the impacts of intra- and interspecific competition between *Triticum aestivum* and *Trifolium repens* on the species' responses to ozone. *Bot. Botany.* 95, 923–932. doi: 10.1139/cjb-2016-0275

Miller, N. J., and Rice-Evans, C. A. (1996). Spectrophotometric determination of antioxidant activity. *Redox Rep.* 2, 161–171. doi: 10.1080/13510002.1996.11747044

Mills, G., Pleijel, H., Braun, S., Büker, P., Bermejo, V., Calvo, E., et al. (2011). New stomatal flux-based critical levels for ozone effects on vegetation. *Atmos. Environ.* 45, 5064–5068. doi: 10.1016/j.atmosenv.2011.06.009

Moeder, W., Barry, C. S., Tauriainen, A. A., Betz, C., Tuomainen, J., Utriainen, M., et al. (2002). Ethylene synthesis regulated by biphasic induction of 1-aminocyclopropane-1-carboxylic acid synthase and 1-aminocyclopropane-1-carboxylic acid oxidase genes is required for hydrogen peroxide accumulation and cell death in ozone-exposed tomato. *Plant Physiol.* 130, 1918–1926. doi: 10.1104/pp.009712

Nogués, I., Fares, S., Oksanen, E., and Loreto, F. (2008). "Ozone effects on the metabolism and the antioxidant system of poplar leaves at different stages of development," in *Photosynthesis. energy from the sun* (Dordrecht: Springer), 1317–1321. doi: 10.1007/978-1-4020-6709-9_284

Oksanen, E., Amores, G., Kokko, H., Amores, J. M., and Kärenlampi, L. (2001). Genotypic variation in growth and physiological responses of Finnish hybrid aspen (*Populus tremuloides* × p. *tremula*) to elevated tropospheric ozone concentration. *Tree Physiol.* 21, 1171–1181. doi: 10.1093/treephys/21.16.1171

Overmyer, K., Brosché, M., and Kangasjärvi, J. (2003). Reactive oxygen species and hormonal control of cell death. *Trends Plant Sci.* 8, 335–342. doi: 10.1016/S1360-1385(03)00135-3

Pääkkönen, E., Günthardt-Goerg, M. S., and Holopainen, T. (1998a). Responses of leaf processes in a sensitive birch (*Betula pendula roth*) clone to ozone combined with drought. *Ann. Bot.* 82, 49–59. doi: 10.1006/anbo.1998.0656

Pääkkönen, E., Seppänen, S., Holopainen, T., Kokko, H., Kärenlampi, S., Kärenlampi, L., et al. (1998b). Induction of genes for the stress proteins PR-10 and PAL in relation to growth, visible injuries and stomatal conductance in birch (*Betula pendula*) clones exposed to ozone and/or drought. *New Phytol.* 138, 295–305. doi: 10.1046/j.1469-8137.1998.00898.x

Pandey, A. K., Ghosh, A., Agrawal, M., and Agrawal, S. B. (2018). Effect of elevated ozone and varying levels of soil nitrogen in two wheat (*Triticum aestivum* l.) cultivars: growth, gas-exchange, antioxidant status, grain yield and quality. *Ecotoxicol. Environ. Saf.* 158, 59–68. doi: 10.1016/j.ecoenv.2018.04.014

Pellegrini, E., Campanella, A., Cotrozzi, L., Tonelli, M., Nali, C., and Lorenzini, G. (2018). Ozone primes changes in phytochemical parameters in the medicinal herb hypericum perforatum (St. john's wort). *Ind. Crops Prod.* 126, 119–128. doi: 10.1016/j.indcrop.2018.10.002

Podila, G. K., Paolacci, A. R., and Badiani, M. (2001). "The impact of greenhouse gases on antioxidants and foliar defence compounds," in *The impact of carbon dioxide and other greenhouse gases on forest ecosystems*. Eds. D. F. Karnosky, R. Ceulemans, G. E. Scarascia-Mugnozza and J. L. Innes (Vienna: CABI Publishing), 57–125. doi: 10.1079/9780851995519.0057

Rajashekar, C. B., Carey, E. E., Zhao, X., and Oh, M.-M. (2009). Health-promoting phytochemicals in fruits and vegetables: impact of abiotic stresses and crop production practices. *Funct. Plant Sci. Biotechnol.* 3, 30–38.

Rathore, D., and Chaudhary, I. J. (2019). Ozone risk assessment of castor (*Ricinus communis* l.) cultivars using open top chamber and ethylenediurea (EDU). *Environ. pollut.* 244, 257–269. doi: 10.1016/j.envpol.2018.10.036

Rozpądek, P., Nosek, M., Ślesak, I., Kunicki, E., Dziurka, M., and Miszalski, Z. (2015). Ozone fumigation increases the abundance of nutrients in brassica vegetables: broccoli (*Brassica oleracea* var. italica) and Chinese cabbage (*Brassica pekinensis*). *Eur. Food Res. Technol.* 240, 459–462. doi: 10.1007/s00217-014-2372-z

Sandermann, J. H., Ernst, D., Heller, W., and Langebartels, C. (1998). Ozone: an abiotic elicitor of plant defence reactions. *Trends Plant Sci.* 3, 47–50. doi: 10.1016/S1360-1385(97)01162-X

Sanmartin, M., Drogoudi, P. A., Lyons, T., Pateraki, I., Barnes, J. D., and Kanellis, A. K. (2003). Over-expression of ascorbate oxidase in the apoplast of transgenic tobacco results in altered ascorbate and glutathione redox states and increased sensitivity to ozone. *Planta* 216, 918–928. doi: 10.1007/s00425-002-0944-9

Sarkar, A., and Agrawal, S. B. (2012). Evaluating the response of two high yielding Indian rice cultivars against ambient and elevated levels of ozone by using open top chambers. *J. Environ. Manage.* 95 Supplement, 19–24S19–S24. doi: 10.1016/j.jenvman.2011.06.049

Sarkar, A., Singh, A. A., Agrawal, S. B., Ahmad, A., and Rai, S. P. (2015). Cultivar specific variations in antioxidative defense system, genome and proteome of two tropical rice cultivars against ambient and elevated ozone. *Ecotoxicol. Environ. Saf.* 115, 101–111. doi: 10.1016/j.ecoenv.2015.02.010

Schlagnhaufer, C. D., Glick, R. E., Arteca, R. N., and Pell, E. J. (1995). Molecular cloning of an ozone-induced 1-aminocyclopropane-1-carboxylate synthase cDNA and its relationship with a loss of rbcS in potato (*Solanum tuberosum* l.) plants. *Plant Mol. Biol.* 28, 93–103. doi: 10.1007/BF00042041

Schneider, G. F., Cheesman, A. W., Winter, K., Turner, B. L., Sitch, S., and Kursar, T. A. (2017). Current ambient concentrations of ozone in Panama modulate the leaf chemistry of the tropical tree *Ficus insipida*. *Chemosphere* 172, 363–372. doi: 10.1016/j.chemosphere.2016.12.109

Schupp, R., and Rennenberg, H. (1988). Diurnal changes in the glutathione content of spruce needles (*Picea abies* l.). *Plant Sci.* 57, 113–117. doi: 10.1016/0168-9452(88)90076-3

Shao, H. B., Chu, L. Y., Lu, Z. H., and Kang, C. M. (2007). Primary antioxidant free radical scavenging and redox signaling pathways in higher plant cells. *Int. J. Biol. Sci.* 4, 8–14. doi: 10.7150/ijbs.4.8

Sharma, Y. K., León, J., Raskin, I., and Davis, K. R. (1996). Ozone-induced responses in *Arabidopsis thaliana*: the role of salicylic acid in the accumulation of defense-related transcripts and induced resistance. *Proc. Natl. Acad. Sci. U. S. A.* 93, 5099–5104. doi: 10.1073/pnas.93.10.5099

Singh, R. N. (2017). Micrometeorological and biophysical parameters of chick pea under the interaction of elevated surface ozone and carbon dioxide. *[dissertation/doctor's thesis]*. [India(BHC)]: Banaras Hindu University.

Singh, P., Agrawal, M., and Agrawal, S. B. (2009). Evaluation of physiological, growth and yield responses of a tropical oil crop (*Brassica campestris* l. var. kranti) under ambient ozone pollution at varying NPK levels. *Environ. pollut.* 157, 871–880. doi: 10.1016/j.envpol.2008.11.008

Singh, P., Agrawal, M., and Agrawal, S. B. (2011). Differences in ozone sensitivity at different NPK levels of three tropical varieties of mustard (*Brassica campestris* l.): photosynthetic pigments, metabolites, and antioxidants. *Water Air Soil pollut.* 214, 435–450. doi: 10.1007/s11270-010-0434-9

Singh, A. A., Fatima, A., Mishra, A. K., Chaudhary, N., Mukherjee, A., Agrawal, M., et al. (2018). Assessment of ozone toxicity among 14 Indian wheat cultivars under field conditions: growth and productivity. *Environ. Monit. Assess.* 190, 190. doi: 10.1007/s10661-018-6563-0

Soengas, P., Cartea, M. E., Velasco, P., and Francisco, M. (2018). Endogenous circadian rhythms in polyphenolic composition induce changes in antioxidant properties in brassica cultivars. *J. Agric. Food Chem.* 66, 5984–5991. doi: 10.1021/acs.jafc.8b01732

Taiz, L., and Zeiger, E. (2002). *Sinauer associates* (Sunderland, MA: Inc. Plant Physiology, third ed. Publishers), 283–308.

Taulavuori, K., Hyöky, V., Oksanen, J., Taulavuori, E., and Julkunen-Tiitto, R.. (2016). Species-specific differences in synthesis of flavonoidsand phenolic acids under increasing periods of enhanced blue light. *Environ. Exp.* 121, 145–150. doi: 10.1016/j.envexpbot.2015.04.002

Temple, P. J., Taylor, O. C., and Benoit, L. F. (1986). Yield response of head lettuce (*Lactuca sativa* L.) to ozone. *Environ. Exp. Bot.* 26, 53–58. doi: 10.1016/0098-8472(86)90052-3

Tiwari, S., and Agrawal, M. (2011). Assessment of the variability in response of radish and brinjal at biochemical and physiological levels under similar ozone exposure conditions. *Environ. Monit. Assess.* 175, 443–454. doi: 10.1007/s10661-010-1542-0

Tomasetti, C., Li, L., and Vogelstein, B. (2017). Stem cell divisions, somatic mutations, cancer etiology, and cancer prevention. *Science* 355, 1330–1334. doi: 10.1126/science.aaf9011

Topa, M. A., Vanderklein, D. W., and Corbin, A. (2001). Effects of elevated ozone and low light on diurnal and seasonal carbon gain in sugar maple. *Plant Cell Environ.* 24, 663–677. doi: 10.1046/j.0016-8025.2001.00722.x

Tuomainen, J., Pellinen, R., Roy, S., Kiiskinen, M., Eloranta, T., Karjalainen, R., et al. (1996). Ozone affects birch (*Betula pendula roth*) phenylpropanoid, polyamine and active oxygen detoxifying pathways at biochemical and gene expression level. *J. Plant Physiol.* 148, 179–188. doi: 10.1016/S0176-1617(96)80312-9

Vazirifar, S., Samari, E., and Sharifi, M. (2021). Daily dynamics of intermediate metabolite profiles lead to time-dependent phenylethanoid glycosides production in *Scrophularia striata* during the day/night cycle. *J. Photochem. Photobiol. B: Biol.* 225, 112326. doi: 10.1016/j.jphotobiol.2021.112326

Velikova, V., Yordanov, I., and Edreva, A. (2000). Oxidative stress and some antioxidant systems in acid rain-treated bean plants. *Plant Sci.* 151, 59–66. doi: 10.1016/S0168-9452(99)00197-1

Vingarzan, R. (2004). A review of surface ozone background levels and trends. *Atmos. Environ.* 38, 3431–3442. doi: 10.1016/j.atmosenv.2004.03.030

Volin, J. C., Tjoelker, M. G., Oleksyn, J., and Reich, P. B. (1993). Light environment alters response to ozone stress in seedlings of acer saccharum marsh, and hybrid populus l. II. diagnostic gas exchange and leaf chemistry. *New Phytol.* 124, 637–646. doi: 10.1111/j.1469-8137.1993.tb03853.x

Wieser, G., and Havranek, W. M. (1995). Environmental control of ozone uptake in *Larix decidua* mill.: a comparison between different altitudes. *Tree Physiol.* 15, 253–258. doi: 10.1093/treephys/15.4.253

Wieser, G., Tegischer, K., Tausz, M., Häberle, K. H., Grams, T. E., and Matyssek, R. (2002). Age effects on Norway spruce (*Picea abies*) susceptibility to ozone uptake: a novel approach relating stress avoidance to defense. *Tree Physiol.* 22, 583–590. doi: 10.1093/treephys/22.8.583

Willekens, H., Van Camp, W., Van Montagu, M., Inze, D., Langebartels, C., and Sandermann, J. H. (1994). Ozone, sulfur dioxide, and ultraviolet b have similar effects on mRNA accumulation of antioxidant genes in *Nicotiana plumbaginifolia* l. *Plant Physiol.* 106, 1007–1014. doi: 10.1104/pp.106.3.1007

Woo, S. Y., Kwon, K. W., Lee, J. C., and Lee, S. H. (2004). Chlorophyll contents and glutathione reductase activity of *Ailanthus altissima*, *Liriodendron tulipifera* and *Platanus occidentalis* seedlings to the ozone exposure. *J. Kor Soc* 93, 423–427.

Zhang, X., He, D., Niu, G., Yan, Z., and Song, J. (2018). Effects of environment lighting on the growth, photosynthesis, and quality of hydroponic lettuce in a plant factory. *Int. J. Agric. Biol. Eng.* 11, 33–40. doi: 10.25165/j.ijabe.20181102.3240

Zheng, Y., Lyons, T., Ollerenshaw, J. H., and Barnes, J. D. (2000). Ascorbate in the leaf apoplast is a factor mediating ozone resistance in plantago major. *Plant Physiol. Biochem.* 38, 403–411. doi: 10.1016/S0981-9428(00)00755-5

Zhishen, J., Mengcheng, T., and Jianming, W. (1999). The determination of flavonoid contents in mulberry and their scavenging effects on superoxide radicals. *Food Chem.* 64, 555–559. doi: 10.1016/S0308-8146(98)00102-2

frontiers | Frontiers in Plant Science

TYPE Original Research
PUBLISHED 07 February 2023
DOI 10.3389/fpls.2022.984051

OPEN ACCESS

EDITED BY
Wei Fang,
National Taiwan University, Taiwan

REVIEWED BY
Yogesh Kumar Ahlawat,
University of Florida, United States
Yaroslav B. Blume,
National Academy of Sciences of Ukraine (NAN Ukraine), Ukraine

*CORRESPONDENCE
Yan Li
edmonlee@hotmail.com
Min Wei
minwei@sdau.edu.cn

SPECIALTY SECTION
This article was submitted to Technical Advances in Plant Science, a section of the journal Frontiers in Plant Science

RECEIVED 01 July 2022
ACCEPTED 19 December 2022
PUBLISHED 07 February 2023

CITATION
Li Y, Xin G, Shi Q, Yang F and Wei M (2023) Response of photomorphogenesis and photosynthetic properties of sweet pepper seedlings exposed to mixed red and blue light.
Front. Plant Sci. 13:984051.
doi: 10.3389/fpls.2022.984051

Response of photomorphogenesis and photosynthetic properties of sweet pepper seedlings exposed to mixed red and blue light

Yan Li[1,2]*, Guofeng Xin[1], Qinghua Shi[1], Fengjuan Yang[1] and Min Wei[1,2]*

[1]College of Horticultural Science and Engineering, Shandong Agricultural University, Tai'an, Shandong, China, [2]Scientific Observing and Experimental Station of Environment Controlled Agricultural Engineering in Huang-Huai-Hai Region, Ministry of Agriculture, Tai'an, Shandong, China

Various light spectra, especially red (RL) and blue light (BL), have great effects on physiological processes and growth of plants. Previously, we revealed that the plant photomorphogenesis and photosynthesis of sweet pepper was significantly altered under BL or mixed RL and BL. The present study aimed to elucidate how mixed RL and BL influences plant photosynthesis during photomorphogenesis. We examined the growth, plant morphology, photosynthetic response of sweet pepper seedlings under monochromatic RL, BL, different ratios of mixed RL and BL (9R1B, 6R1B, 3R1B, 1R1B, 1R3B) with the same photosynthetic photon flux density of 300 μmol·m^{-2}·s^{-1}. White light (WL) were used as a control. The findings showed that the elongation of hypocotyl and first internode as well as leaf expansion were all stimulated by RL, while significantly restrained by BL compared with WL. Conversely, the leaf development, biomass accumulation and photosynthetic properties were inhibited by RL but promoted by BL. Additionally, compared with WL and other treatments, 3R1B could significantly improve the net photosynthetic rate, gas exchange, photosynthetic electron transport capacity, photochemical efficiency, shoot and root biomass accumulation. Furthermore, seedlings grew robustly and exhibited the greatest value of seedling index when exposed to this treatment. Overall, these results suggested that pepper seedlings grown under 3R1B performed better, possibly due to the more balanced light spectrum. It was more conducive to improve the plant photomorphogenesis and photosynthesis of sweet pepper, and a higher biomass accumulation and energy utilization efficiency could be achieved simultaneously under this mixed light spectrum.

KEYWORDS

sweet pepper, light spectrum, growth, plant morphology, photosynthesis

Introduction

Plants have different morphological and physiological responses to specific light spectra, and among the different light spectra, red (RL) and blue light (BL), which focus on more light absorption by chlorophyll than other wavelengths, are most efficiently utilized for the photosynthesis and phytochemical metabolism in plants (Han et al., 2017; Monostori et al., 2018). RL is generally regarded as the fundamental spectrum for plant growth and RL-absorbing phytochromes (phys) plays a key role in regulating leaf morphogenesis, photosynthetic apparatus formation and carbohydrate accumulation (Rehman et al., 2017). BL is recognized by photoreceptors such as cryptochromes (crys) and phototropins (phots), and these photoreceptors regulate chloroplast development, chlorophyll biosynthesis and stomata opening (Savvides et al., 2012).

However, monochromatic RL or BL could not satisfy the requirement of normal plant growth. Various studies have found that the mixed RL and BL was an effective lighting source to plant development and a suitable proportion of RL and BL accelerate photosynthesis and growth of sweet pepper and tomato (Li et al., 2017; Li et al., 2020). Therefore, the mixed RL and BL is used nowadays more and more in research and can be applied for the commercial cultivation of horticultural crops in controlled and semi-controlled environments (Miao et al., 2016).

Sweet pepper (*Capsicum annuum* L.) is one of economically important vegetables and widely cultivated in greenhouses worldwide. A prolonged period of RL and BL treatment has an apparent impact on growth and physiology of pepper seedlings (Tang et al., 2019). Moreover, in recent years, plant factories have developed rapidly, and light-emitting diodes (LEDs) as a kind of artificial light with the characteristics of high light efficiency, narrowly-centered spectrum and low energy consumption, have been frequently applied to manipulate the plant growth, development and metabolism in plant factories (Matsuda et al., 2016; Liu et al., 2018). In a previous study, we found that a suitable proportion of mixed RL and BL accelerated sweet pepper seedlings' photosynthesis and growth (Li et al., 2020). However, the mechanism of how light spectra of mixed RL and BL regulate leaf photosynthesis and plant photomorphogenesis, as well as the optimal ratio of RL and BL, which could benefit pepper seedling growth remains unclear. Therefore, in this study, we investigated photosynthesis capacity, biomass accumulation and morphological acclimation of pepper seedlings under various proportions of mixed RL and BL.

Materials and methods

Plant material and climate conditions

The experiment was performed from May to September, 2016 in a Chinese solar greenhouse (China, 36°N, 117°E) in Shandong Agricultural University. The germinated sweet pepper (*Capsicum annuum* L. cv. HA-2502) seeds were sown in plastic trays with 50 holes (54 cm length × 30 cm width × 4.4 cm depth) filled with a mixture of peat and vermiculite (2:1, v/v). Three weeks later, when their second true leaf expanded fully, seedlings were transplanted into plastic pots (8 cm length × 8 cm width × 10 cm depth, one plant per pot). After that, 320 seedlings were selected and moved into an environmentally controlled growth chamber, where the average air temperature, relative humidity (RH), photoperiod and CO_2 concentration were 26/18 °C (day/night), 70%, 12 h/12 h and 400 μmol·mol^{-1}, respectively, and then, randomized into eight groups and were cultured under eight light spectra treatments for 30 d. From each light treatment, randomly five plants were sampled after periods of 6, 12, 18, 24 and 30 d after treatment (DAT) by LEDs. There were three replicates with a total of 40 seedlings for each treatment.

Light treatments

All the mixed LEDs had the uniform spectra of RL and BL, and were designed by Chunying Optoelectronics Technology Co., Ltd., Guangdong, China. All treatments were performed in different layers of cultivation racks, which were covered by opaque silver plastic reflective cloth to prevent the light disturbance from the adjacent treatments (Li et al., 2021). Plants were subjected under different light conditions: monochromatic BL (peak intensity: 457 nm) and RL (peak intensity: 657 nm), mixed RL and BL (9:1, 9R1B; 6:1, 6R1B; 3:1, 3R1B; 1:1, 1R1B; 1:3, 1R3B: 90%, 85%, 75%, 50%, 25% RL at a wavelength of 657 nm and 10%, 15%, 25%, 50%, 75% BL at a wavelength of 457 nm, respectively), and a multiwavelength white light (WL, as control) with the same photosynthetic photon flux density (PPFD) of 300 μmol·m^{-2}·s^{-1}. PPFD was recorded using a light meter with a quantum sensor (LI-250 and LI-190R, Li-Cor Inc., Lincoln, NE, USA) and was 10 cm away from the top of seedling canopy to the bottom of LED lighting panels. The spectral photon flux density distributions (SPDs) of RL, BL and WL was measured using a spectroradiometer (Unispec-SC Spectral Analysis System, PP Systems Inc., Haverhill, MA, USA) (Figure 1).

Measurements of plant morphological parameters

Plant height, first internode length and hypocotyl length were measured by a meter rule (cm), respectively, whereas the stem diameter was determined at the internode 1 cm above the cotyledona using a digital vernier caliper (mm, CD-20CPX, Mitutoya Corp., Kawasaki, Japan). The fully expanded true leaves and second fully expanded true leaves were collected to determine leaf number and leaf length, respectively. The

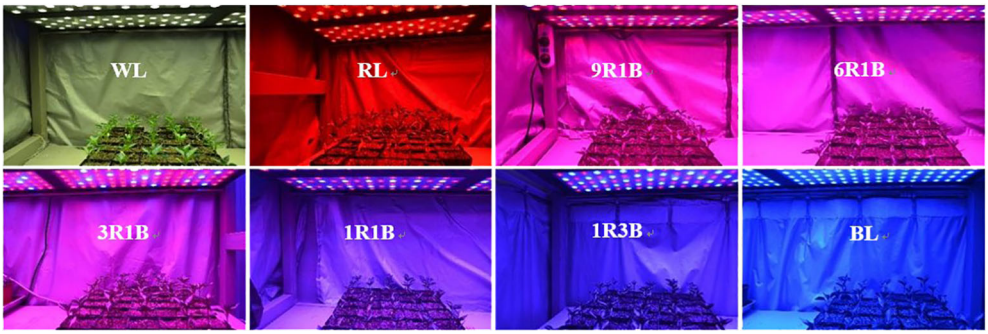

FIGURE 1
General view and spectral distribution of eight light spectra treatments.

seedlings including shoots and roots were dried to a constant weight at 75°C to measure the dry weight (DW). Before this measurement, the substrate particles attached to the roots were washed gently in distilled water. Root configuration indexes at 15 and 30 DAT, including total root length, root surface area, root volume, average diameter and tips number, were scanned with scanner (Epson Expression 10000G J181A, Japan) and leaf area (LA) of the fully developed young leaves at 15 and 30 DAT were monitored by a CI-202 leaf area measurer (CID Bio-Science Inc., Camas, WA, USA), and then, the data were analyzed with WinRHIZO (Model LA600, Regent Instruments Inc., Quebec, QC, Canada). The specific leaf area (SLA) and seedling index were determined using the following formulas:

$$\mathrm{SLA}\left(\mathrm{cm}^2 \cdot \mathrm{mg}^{-1}\mathrm{DW}\right) = \text{total LA}\ \left(\mathrm{cm}^2\right)/\text{leaf DW(mg)}$$

Seedling index
= (Stem diameter(mm)/Plant height (cm) + Root DW(g)/Shoot DW (g)) × DW (g)

Photosynthetic pigment concentration measurement

On 15 and 30 DAT, samples (0.5 g) from the fresh second fully expanded leaves were collected and incubated in 25 mL of 95% (v/v) ethanol reagent in darkness for 24-36 h at room temperature until the leaves became completely colorless. Afterwards, absorbance of the supernatant at 663, 646 and 470 nm were recorded by a spectrophotometer (UV-2450, Shimadzu Corp., Japan), respectively, and the concentration of chlorophyll *a* (Chl *a*), *b* (Chl *b*) and total carotenoid (Car) were measured based on the methods described by Sartory and Grobbelaar (1984).

Gas exchange parameters measurement

Gas exchange parameters including net photosynthetic rate (*Pn*), stomatal conductance (*Gs*), intercellular CO_2 concentration (*Ci*), transpiration rate (*Tr*) and stomatal limitation (*Ls*) of the second functional leaf of pepper seedlings were determined by a LI-6400 gas exchange analyzer (Li-Cor Inc., Lincoln, NE, USA) at 30 DAT. The conditions in the assimilation chamber of the LI-6400XT equipment such as PPFD with 90% RL and 10% BL, RH, CO_2 concentration, leaf temperature and flow rate were 300 $\mu mol \cdot m^{-2} \cdot s^{-1}$, 70%, 400 $\mu mol \cdot mol^{-1}$, 25°C and 400 $mL \cdot min^{-1}$, respectively.

Chlorophyll a fluorescence parameters measurement

Chl *a* fluorescence was investigated on same leaf and position mentioned above at 30 DAT using a FMS-2 chlorophyll fluorometer (Hansatech Instruments Ltd., King Lynn, Norfolk, UK). To standardize the measuring conditions and ensure that all of the photosynthesis system II (PSII) reaction centers were open when the maximal photochemical quenching was determined, seedlings were dark-adapted for 20 min prior to the evaluations, and then, minimum fluorescence (F_o) and maximum fluorescence (F_m) were recorded. Chl a fluorescence parameters, maximal quantum yield of PSII (F_v/F_m), effective quantum yield of PSII (Φ_{PSII}), electron transport rates (ETR) and photochemical quenching (*qP*) were calculated according to Li et al. (2021).

Root vigor measurement

Root vigor was analyzed by the triphenyl tetrazolium chloride (TTC, Sinopharm Chemical Reagent Co., Ltd., Shanghai, China) method (Wang et al., 2006). In brief, 0.5 g fresh root was immersed in 10 mL of equally mixed solution of 0.4% TTC and phosphate buffer and kept in the dark at 37°C for 2 h. Subsequently, 2 mL of 1 mol/L H_2SO_4 was added to stop the reaction with the root. The root was dried with filter paper and then extracted with ethyl acetate. The red extractant was

transferred into the volumetric flask to reach 10 mL by adding ethyl acetate. The absorbance of the extract at 485 nm was read. Root vigor was expressed as TTC reduction intensity and TTC reduction was calculated using the following formula:

Root vigor =

amount of TTC reduction (μg)/fresh root weight (g)time (h)

Statistical analysis

All values were presented as the mean ± standard errors (SE) with three replicates each. Data were analyzed by one-way analysis of variance (ANOVA) using SPSS 16.0 (SPSS Institute Inc., Cary, NC, USA), and the differences between the means were tested using Duncan's multiple range test at $P< 0.05$ level. The graphs were performed by Origin 8.5 (OriginLab Institute Inc., Northampton, MA, USA).

Results

Plant morphology and biomass accumulation

As shown in Figure 2, the morphology of sweet pepper seedlings at 30 DAT was found to be significantly affected by the monochromic and mixed RL and BL. Compared to WL, plant height grown under 1R3B was significantly reduced ($P< 0.05$), followed by plants grown under BL and 1R1B at 30 DAT, while RL produced the tallest plants (Figure 3A). The length for first internode, hypocotyl and leaf of seedlings under all light spectra exhibited a similar trajectory (Figures 4A–C). Relative to WL, the stem diameter was significantly greater for plants treated by 3R1B ($P< 0.05$), but thinner for plants under other treatments, although there were no statistically significant differences under WL and BL ($P > 0.05$) during the last experimental period and the smallest for plants under RL (Figure 3B). Moreover, seedlings under 3R1B had higher values for SLA, seedling index, leaf number, shoot and root DW (Figure 3C, D; Figure 4D; Figures 5A, B). The least values for these parameters were recorded in the RL-treated seedlings, respectively.

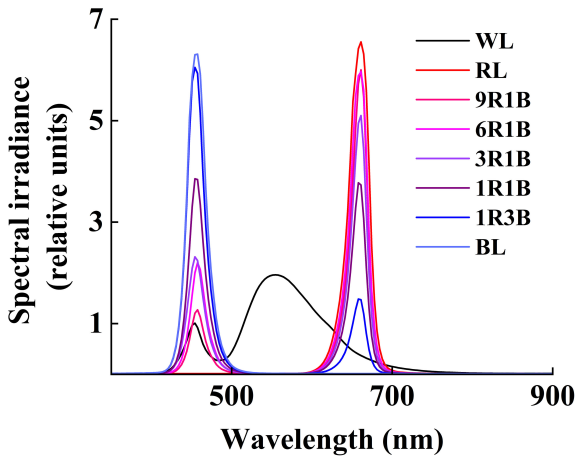

FIGURE 2
Effect of monochromatic and mixed red and blue light on plant morphology of sweet pepper seedlings at 30 day after treatment.

Plants under 3R1B had higher values for total root length, root surface area, root volume, average diameter and tips number comparing with WL and other treatments at 15 and 30 DAT (Table 1). The least values for all these parameters were recorded in the 1R3B-treated plants. Moreover, the total root length and root volume were not statistically different between 1R3B- and RL-illuminated plants at 30 DAT ($P > 0.05$), but these were significantly lower than WL ($P< 0.05$). Similarly, the total root length, root surface area, root volume and tips number of 6R1B- and 9R1B-treated seedlings were statistically the same.

Photosynthetic pigment content

To examine the effects of mixed RL and BL on the photosynthetic pigment content, sweet pepper seedlings were exposed to different light spectra for 30 d (Figure 6) and the findings showed that significantly lower levels of Chl *a*, Chl *b* and Car were observed under RL, 9R1B, 6R1B, 1R3B and BL compared to WL at 30 DAT ($P< 0.05$), and the least values were observed in plants with the treatment of RL at 15 and 30 DAT. Higher levels of Chl and Car were detected in other treatments at each treatment period, while no significant difference was present among WL and them. BL yielded the highest Chl *a*/*b* at 30 DAT, followed by 1R3B, and the lowest Chl *a*/*b* was found for RL.

Gas exchange and chlorophyll a fluorescence parameters

Generally, compared to WL, most leaf gas exchange parameters including *Pn*, *Gs* and *Tr* were significantly increased in seedlings under 3R1B ($P< 0.05$, Table 2), at 14%, 28% and 29% higher than in WL, respectively, while these parameters were largely decreased by RL and were not statistically different between the WL and BL treatments ($P > 0.05$). Furthermore, the levels of *Ci* and *Ls* were found to follow the opposite tendency.

The levels of F_v/F_m, Φ_{PSII}, ETR and *qP* showed the similar trajectory that they were evidently enhanced by 3R1B relative to WL, except the values of F_v/F_m and ETR was not statistically different among 6R1B, 1R1B, BL, and 1R1B, respectively (Figure 7). However, these parameters dropped drastically in

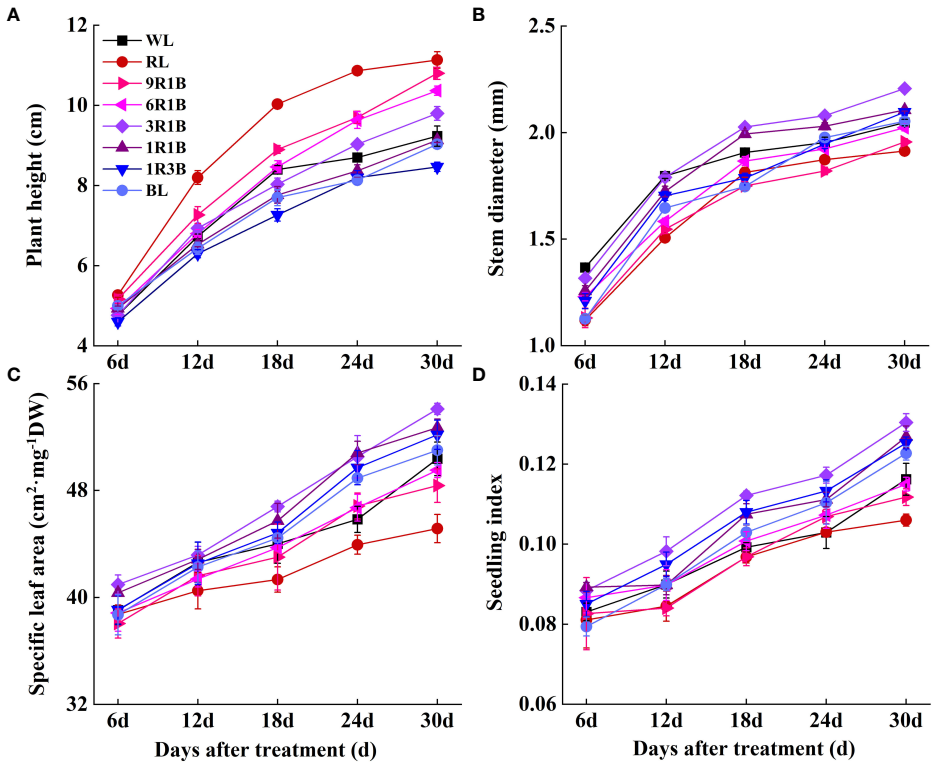

FIGURE 3
Effect of monochromatic and mixed red and blue light on growth of sweet pepper seedlings throughout 30 days after treatment. **(A)** plant height; **(B)** stem diameter; **(C)** specific leaf area; **(D)** seedling index.

RL-treated seedlings ($P< 0.05$). These results indicated that BL could raise the proportion of the reaction centers in PSII opening under light adaptation, enhance PSII reaction center activity, and improve the electron transfer rate.

Root vigor

The root vigor was significantly higher in 3R1B-treated seedlings than that in WL ($P< 0.05$) and at 13% and 15% higher than that under WL at 15 and 30 DAT, respectively (Figure 8). However, the root vigor did not differ significantly between WL and 6R1B ($P > 0.05$), and this parameter was evidently lower in seedlings under other light treatments than in WL and the lowest level was observed in plants under RL.

Discussion

For light-controlled development, it is generally assumed that the photoreceptors perceive and interpret incident light and transduce the signals to modulate light-responsive nuclear genes, amongst the spectral wavelengths, RL and BL are the primary spectral wavelengths and highly influence the plant photosynthesis, physiological metabolism and photomorphogenesis (Ooi et al., 2016). In the present research, the morphological and photosynthetic characteristics of sweet pepper seedlings were significantly influenced by light spectra. The results indicated that seedlings grown under mixed RL and BL, especially 3R1B, had improved plant growth parameters. This was consistent with sweet pepper seedlings in our previous study (Li et al., 2020).

In this study, we found that seedlings grown under RL revealed typical shade-avoidance syndrome, namely significantly enhanced plant height, internodal and hypocotyl length and this agreed with previous reports (Liu et al., 2011). It could be due to RL could stimulate hypocotyl and stem elongation (Izzo et al., 2020). Previous reports indicated that phyB is a major photoreceptor that mediates hypocotyl elongation inhibition under continuous RL (Shinomura et al., 1996). Therefore, RL may accelerate petiole and internode elongation by inactivating phyB, and then, inducing stem elongation by improved gibberellin (GA) levels, which affected by indole-3-acetic acid (IAA) (Li et al., 2021; Xiao et al., 2022). It has been reported that GA, brassinosteroid and auxin are involved in BL signaling through cry1 as the primary photoreceptor in the inhibition of hypocotyl elongation (He et al., 2019; Xu et al., 2021). However, unlike previous

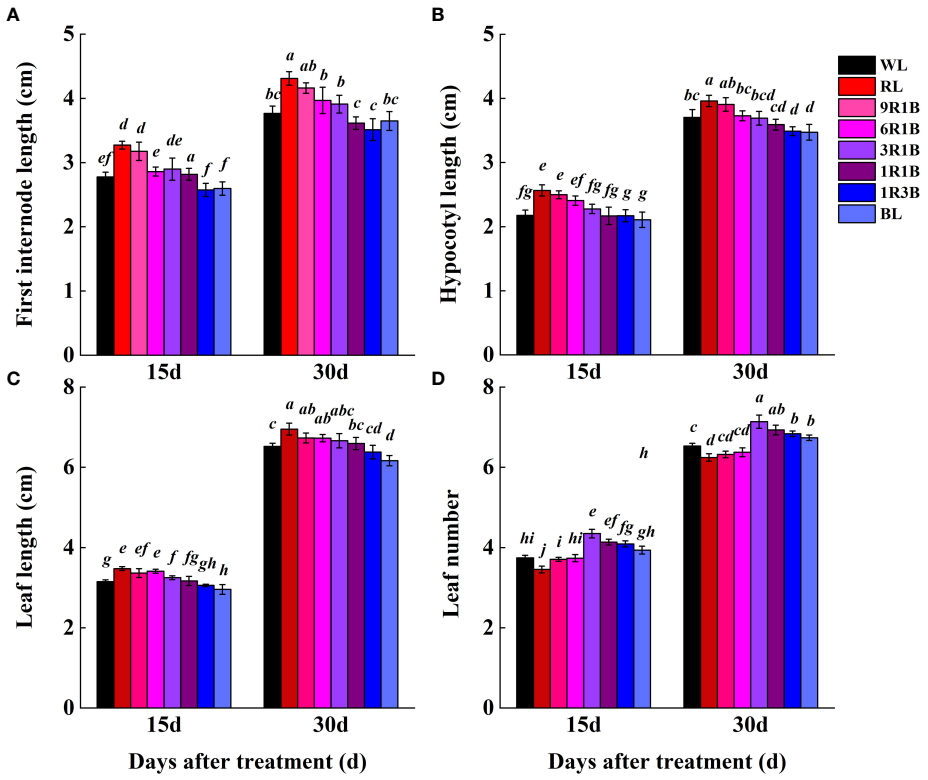

FIGURE 4
Effect of monochromatic and mixed red and blue light on plant morphology of sweet pepper seedlings at day 15 and 30 after treatment. **(A)** first internode length; **(B)** hypocotyl length; **(C)** leaf length; **(D)** leaf number. Difference in lower-case letters indicates significant difference at $P < 0.05$.

studies, the shortest seedlings were found under treatment of 1R3B in our present research. It is assumed that mixed RL and BL with higher ratio of BL were more inhibitive of hypocotyl and leaf elongation and inducing in the sweet pepper seedlings a more compact morphology with shorter stems and smaller leaf areas than monochromatic BL. These results indicated that increasing BL could inhibit cell division and expansion (Kang et al., 2021). Furthermore, lower levels of GA and IAA under a low RL/BL ratio of 1R3B may lead to reduced elongation of pepper seedlings' shoots (Islam et al., 2014; Matsuo et al., 2019).

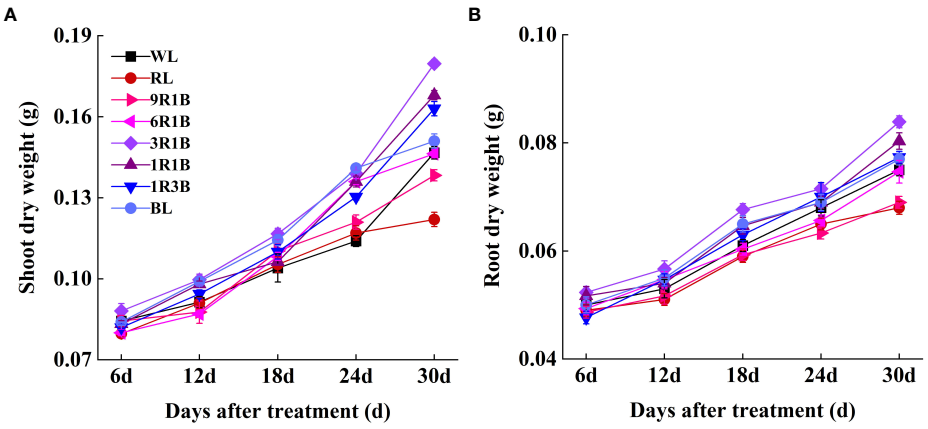

FIGURE 5
Effect of monochromatic and mixed red and blue light on **(A)** shoot dry weight and **(B)** root dry weight of sweet pepper seedlings throughout 30 days after treatment.

10.3389/fpls.2022.984051

TABLE 1 Effect of monochromatic and mixed red and blue light on root configuration indexes of sweet pepper seedlings at day 15 and 30 after treatment.

Treatment period (d)	Treatments	Total root length (cm)	Root surface area (cm^2)	Root volume (cm^3)	Average diameter (mm)	Tips number
15d	WL	118 ± 5.11 b	10.67 ± 0.52 bc	0.203 ± 0.02 b	0.234 ± 0.003 b	219 ± 5.22 b
	RL	72 ± 3.28 cd	5.57 ± 0.41 d	0.097 ± 0.01 d	0.195 ± 0.003 d	141 ± 4.31 d
	9R1B	115 ± 4.37 b	10.57 ± 0.27 bc	0.180 ± 0.01 bc	0.218 ± 0.002 c	210 ± 6.37 b
	6R1B	120 ± 6.12 b	10.90 ± 0.54 b	0.197 ± 0.01 bc	0.221 ± 0.003 c	217 ± 2.78 b
	3R1B	173 ± 5.45 a	13.67 ± 0.52 a	0.273 ± 0.02 a	0.250 ± 0.003 a	253 ± 4.29 a
	1R1B	111 ± 4.33 b	10.07 ± 0.38 c	0.173 ± 0.02 c	0.218 ± 0.004 c	212 ± 5.37 b
	1R3B	65 ± 4.21 d	5.50 ± 0.44 d	0.097 ± 0.02 d	0.184 ± 0.002 e	135 ± 4.03 d
	BL	77 ± 4.09 c	5.87 ± 0.43 d	0.110 ± 0.01 d	0.187 ± 0.002 e	153 ± 6.28 c
30d	WL	358 ± 4.12 b	36.07 ± 0.62 b	0.703 ± 0.01 b	0.408 ± 0.003 b	495 ± 9.16 b
	RL	176 ± 6.23 e	18.53 ± 0.63 e	0.357 ± 0.01 e	0.339 ± 0.003 e	260 ± 5.33 f
	9R1B	232 ± 6.34 d	30.37 ± 0.53 c	0.420 ± 0.01 d	0.362 ± 0.005 c	409 ± 6.32 c
	6R1B	241 ± 4.78 cd	29.67 ± 0.72 c	0.420 ± 0.01 d	0.348 ± 0.005 d	399 ± 4.24 c
	3R1B	457 ± 12.56 a	42.90 ± 0.67 a	0.900 ± 0.01 a	0.442 ± 0.004 a	672 ± 8.17 a
	1R1B	355 ± 6.33 b	30.83 ± 0.92 c	0.630 ± 0.02 c	0.347 ± 0.004 d	377 ± 3.45 d
	1R3B	168 ± 4.29 e	15.90 ± 0.44 f	0.350 ± 0.02 e	0.305 ± 0.001 f	248 ± 6.12 g
	BL	252 ± 6.18 c	25.57 ± 0.91 d	0.430 ± 0.04 d	0.299 ± 0.007 f	297 ± 5.21 e

Data are presented as means ± SE, n = 5. Different letters indicate significant differences between values ($P < 0.05$). WL, white light; RL, monochromatic red light; BL, monochromatic blue light; 9R1B, mixed RL and BL of 9:1; 6R1B, mixed RL and BL of 6:1; 3R1B, mixed RL and BL of 3:1; 1R1B, mixed RL and BL of 1:1; 1R3B, mixed RL and BL of 1:3.

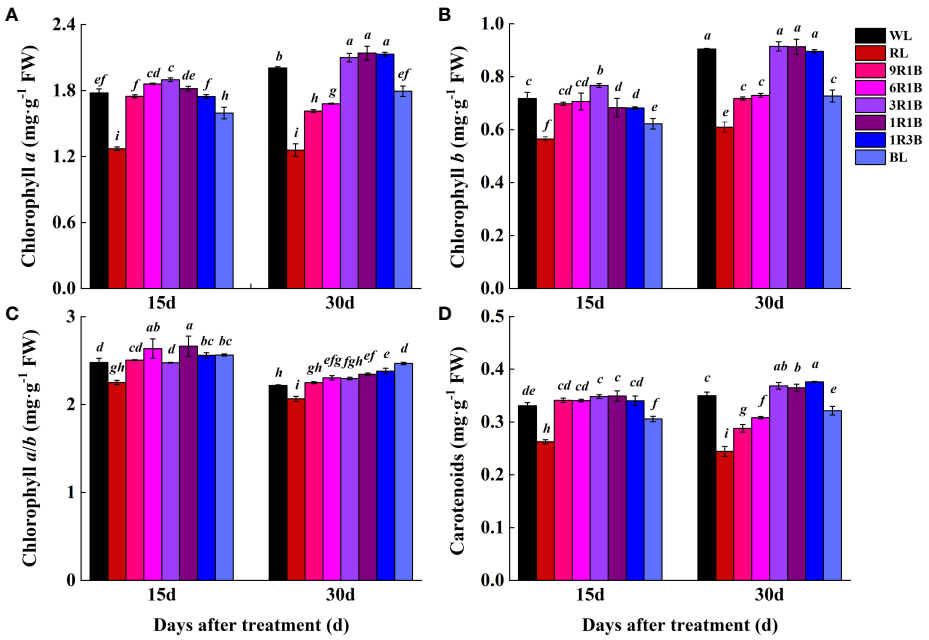

FIGURE 6
Effect of monochromatic and mixed red and blue light on photosynthetic pigment content in leaves of sweet pepper seedlings at day 15 and 30 after treatment. **(A)** chlorophyll *a*; **(B)** chlorophyll *b*; **(C)** chlorophyll *a*/*b*; **(D)** carotenoids. Difference in lower-case letters indicates significant difference at $P < 0.05$.

10.3389/fpls.2022.984051

TABLE 2 Effect of monochromatic and mixed red and blue light on gas exchange parameters in sweet pepper seedlings at day 30 after treatment.

Treatments	*Pn* (μmol·m^{-2}·s^{-1})	*Gs* (mmol·m^{-2}·s^{-1})	*Ci* (μmol·mol^{-1})	*Tr* (mmol·m^{-2}·s^{-1})	*Ls*
WL	9.37 ± 0.22 b	0.25 ± 0.03 b	330.33 ± 15.21 c	2.34 ± 0.11 e	0.16 ± 0.01 c
RL	5.95 ± 0.31 e	0.17 ± 0.01 d	375.67 ± 12.83 a	1.73 ± 0.13 g	0.19 ± 0.01 a
9R1B	6.96 ± 0.20 d	0.19 ± 0.04 cd	343.67 ± 13.05 b	2.69 ± 0.08 d	0.16 ± 0.01 c
6R1B	7.57 ± 0.35 c	0.20 ± 0.01 c	325.02 ± 7.64 cd	2.78 ± 0.14 c	0.17 ± 0.01 b
3R1B	10.70 ± 0.23 a	0.32 ± 0.03 a	316.67 ± 14.91 e	3.01 ± 0.21 a	0.16 ± 0.01 b
1R1B	7.71 ± 0.56 c	0.26 ± 0.04 b	321.00 ± 10.54 d	2.86 ± 0.12 b	0.16 ± 0.01 c
1R3B	6.20 ± 0.19 e	0.18 ± 0.02 cd	336.67 ± 11.24 c	2.06 ± 0.09 f	0.17 ± 0.02 bc
BL	9.77 ± 0.34 b	0.29 ± 0.02 ab	318.33 ± 17.62 de	2.37 ± 0.07 e	0.15 ± 0.02 c

Data are presented as means ± SE, n = 5. Different letters indicate significant differences between values ($P < 0.05$). WL, white light; RL, monochromatic red light; BL, monochromatic blue light; 9R1B, mixed RL and BL of 9:1; 6R1B, mixed RL and BL of 6:1; 3R1B, mixed RL and BL of 3:1; 1R1B, mixed RL and BL of 1:1; 1R3B, mixed RL and BL of 1:3.

Biomass is an important indicator in determining seedling qualities. In this present study, the DW and seedling index of seedlings under 3R1B was greater than that of WL and other treatments, which may implicate that this spectrum applied in the experiment is optimized effectively, since it promotes development and drives photosynthesis as a result of the increased contents of chl *a* and total chlorophyll in seedlings (Tang et al., 2019). It was also reported that the mixed RL and BL might promote fresh weight and DW in chrysanthemum and sweet pepper (Liu et al., 2011; Li et al., 2020). The biomass of pepper shoots was significantly increased under 3R1B compared with WL and other treatments probably due to the enlarged SLA in this study. The larger leaf is a good indicator of higher photosynthetic surface area per unit investment in leaf tissue, which may have led to the significant increment in biomass (Dieleman et al., 2019). This was in agreement with Bugbee (2016) who concluded that the fraction of light intercepted by a crop is more closely related to biomass than the short-term effects on quantum efficiency of photosynthesis. Besides, mixed RL and BL could also increase shoot regeneration and development by stimulating cell division (Kwon et al., 2015).

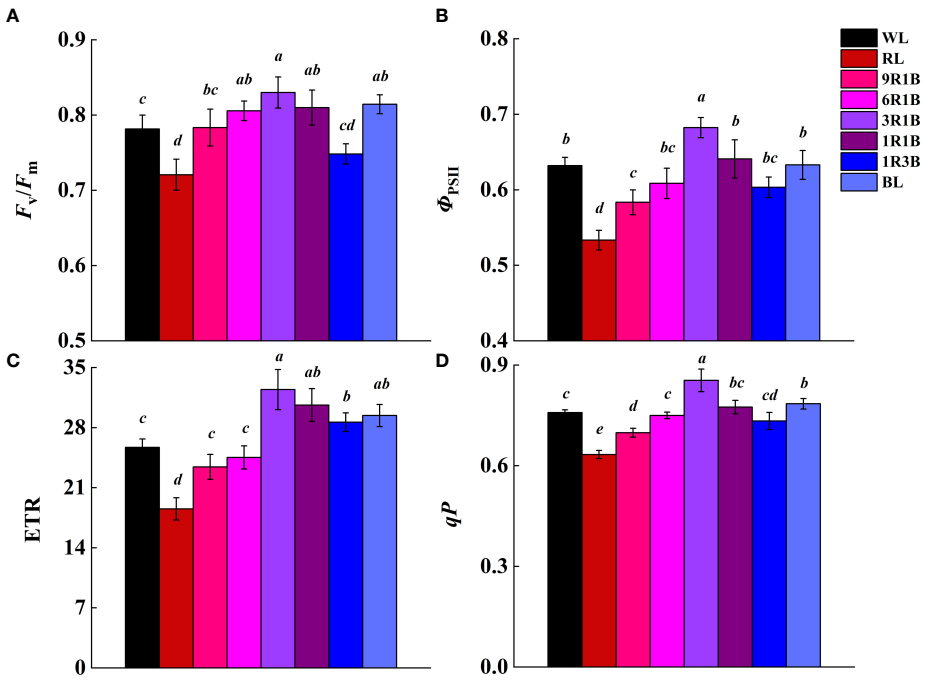

FIGURE 7
Effect of monochromatic and mixed red and blue light on chlorophyll *a* fluorescence parameters of leaves from sweet pepper seedlings at day 30 after treatment. **(A)** F_v/F_m; **(B)** Φ_{PSII}; **(C)** ETR; **(D)** *qP*. Difference in lower-case letters indicates significant difference at $P < 0.05$.

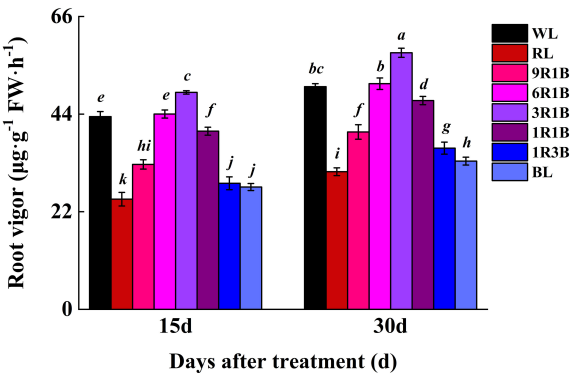

FIGURE 8
Effect of monochromatic and mixed red and blue light on root vigor of sweet pepper seedlings at day 15 and 30 after treatment. Difference in lower-case letters indicates significant difference at $P < 0.05$.

Chlorophyll content is an important determinant of photosynthesis and dry matter accumulation. In addition, carotenoids play a vital role in photosynthesis by absorbing light and protecting chlorophyll from photo-oxidation (Carvalho et al., 2013; Tuan et al., 2013). Our present results showed that BL plays an important role in the synthesis of plant chlorophyll, and plants grown under RL showed the lowest levels of chlorophyll and carotenoids. This was consistent with previous studies (Dutta-Gupta and Jatothu, 2013; Anuchai and Hsieh, 2017). It indicated that BL was more essential than RL for normal photosynthesis by mediating photosystems activity and photosynthetic electron transport capacity (Miao et al., 2016). However, these were unlike to the results of Bianchetti et al. (2018) and Tian et al. (2019). This suggested that plant responded to RL and BL are species-specific (Liu et al., 2011; Cope et al., 2014). Different plant species, or the same species at different growth stages, show diverse responses to the same light spectra and display complexity and instability of photobiological reactions. Moreover, stimulation of photosynthetic pigments under 3R1B was consistent with our previous results obtained in tomato seedlings (Li et al., 2017; Li et al., 2021). It might be due to the synergistic effect of RL and BL when the supplement of appropriate proportion for BL in RL has the property of promoting the biosynthesis of chlorophyll, and this property may be further reinforced when they work together (Mao and Guo, 2018).

Photosynthetic rate is a key factor affecting plant assimilation capacity and yield. A lower *P*n in plants under monochromatic RL has been shown in several crops (Hogewoning et al., 2010; Li et al., 2017; Li et al., 2021). Our data were consistent with previous results. This may be attributed to the excess ROS suppressed repair of photodamaged PSII and increased the degree of photodamage, which directly induced relatively low rate of CO_2 assimilation and redundant *C*i under RL (Takahashi and Murata, 2008). In addition, the beginning of the leaf senescence is accompanied by the lower *P*n and the degradation of related proteins (Hensel et al., 1993). Hence, RL significantly reduced *P*n and F_v/F_m, which might result in acceleration of leaf senescence (Su et al., 2014). The photodamaged PSII induced by RL could be alleviated by BL, which could benefit pepper seedling growth by improving light use efficiency and diminish photoinhibition (Miao et al., 2019; Kang et al., 2021). On the other hand, the *P*n and F_v/F_m, Φ_{PSII}, ETR and *qP* of seedlings exposed to 3R1B treatment was found to be significantly higher than those of other light spectra. These were consistent with our previous results (Li et al., 2017; Li et al., 2021), which indicated that the photosynthetic efficiency in pepper seedlings was promoted under this treatment, thereby more electrons were absorbed, captured and transported. Apparently, the increased concentration of light absorbing pigments in leaves has considerable consequences for leaf CO_2 uptake under this treatment. This may be also related to the well-developed stomata (Li et al., 2020; Kang et al., 2021), higher stomatal conductance (Hamedalla et al., 2022) and high nitrogen accumulation in leaves under this spectral wavelength (Fan et al., 2022). Consequently, the morphology of pepper seedlings under this light spectrum revealed higher SLA, FW and DW of shoots and roots, and thus better performance compared to other treatments.

Vigorous roots support shoot growth by fully supplying the plant with water and mineral nutrition. Moreover, root tip is an important site where root absorb water and nutrient in plants. The more root tips number, the longer root length, and the more root surface are, the more beneficial to capture nutrient effectively (Zhang et al., 1999). In this study, the growth and morphological features of 3R1B-treated pepper seedlings exhibited a tight appearance, but the shoot and root structure of RL- or 1R3B-treated seedlings were adversely affected plant performance, indicating poor root growth under RL and 1R3B. Therefore, growth and development are dependent on the spectral wavelength of light, and the addition of RL may have further increased plant growth and development since stronger RL might better penetrate the plant canopy than weaker RL. Perhaps 3R1B treatment achieved a balanced spectral environment by supplementing a favorable amount of RL to pepper seedlings at 300 $\mu mol \cdot m^{-2} \cdot s^{-1}$ PPFD (Lin et al., 2021). This agreed with our previous results obtained in tomato seedlings (Li et al., 2017). According to Manivannan et al. (2015), this growth may be related to the ability of 3R1B treatment to induce the formation of endogenous GA, which is an important growth regulator involved in cell elongation. Furthermore, the increase in root length and formation of adventitious roots for pepper seedlings under 3R1B may be due to IAA levels, as this treatment promoted polar IAA transport from apical shoot to downward portion, which regulated by genes involved in auxin formation and signal transduction as well as auxin transportation (Liu et al., 2011;

Shen et al., 2022), and thus longer root under 3R1B in this study might be related to higher IAA accumulation in root. Therefore, the better root development of pepper seedlings exposed to 3R1B leads to faster acclimatization.

Conclusion

This research provided a better understanding of the responses of growth and photosynthesis in sweet pepper seedlings exposed to mixed RL and BL. The mixed RL and BL had significant effects on the photosynthesis, morphogenesis and growth of sweet pepper seedlings. It was found that proper proportion for RL and BL of 3R1B promoted plant growth by controlling and optimizing photosynthetic performance. This was mainly manifested by an improvement in the *P*n, F_v/F_m, Φ_{PSII}, ETR, *qP*, increasing SLA and photosynthetic pigment content. Furthermore, this might ensure healthy chloroplast development under this treatment to achieve a higher photosynthetic capacity, thereby improving the growth and biomass accumulation of seedlings. These findings suggested that 3R1B was the most effective light treatment among spectral wavelength in this study for producing high quality of sweet pepper seedlings.

Data availability statement

The original contributions presented in the study are included in the article/supplementary material. Further inquiries can be directed to the corresponding authors.

Author contributions

YL and MW conceived the original research plan and designed the study. GX performed experiments and analyzed the data. YL analyzed data and drafted the manuscript. All authors read and agreed to the final draft.

Funding

This research was financially supported by the Natural Science Foundation of Shandong Province (ZR2020MC148) and China Agriculture Research System (CARS-23-C04).

Conflict of interest

The authors declare that the research was conducted in the absence of any commercial or financial relationships that could be construed as a potential conflict of interest.

Publisher's note

All claims expressed in this article are solely those of the authors and do not necessarily represent those of their affiliated organizations, or those of the publisher, the editors and the reviewers. Any product that may be evaluated in this article, or claim that may be made by its manufacturer, is not guaranteed or endorsed by the publisher.

References

Anuchai, J., and Hsieh, C. H. (2017). Effect of change in light quality on physiological transformation of *in vitro phalaenopsis* '*Fortune saltzman*' seedlings during the growth period. *Hortic. J.* 86, 395–402. doi: 10.2503/hortj.MI-151

Bianchetti, R. E., Lira, B. S., Monteiro, S. S., Demarco, D., Purgatto, E., Rothan, C., et al. (2018). Fruit-localized phytochromes regulate plastid biogenesis, starch synthesis, and carotenoid metabolism in tomato. *J. Exp. Bot.* 69, 3573–3586. doi: 10.1093/jxb/ery145

Bugbee, B. (2016). Toward an optimal spectral quality for plant growth and development: the importance of radiation capture. *Acta Hortic.* 1134, 1–12. doi: 10.17660/ActaHortic.2016.1134.1

Carvalho, E., Fraser, P. D., and Martens, S. (2013). Carotenoids and tocopherols in yellow and red rasberries. *Food Chem.* 139, 744–752. doi: 10.1016/j.foodchem.2012.12.047

Cope, K. R., Snowden, M. C., and Bugbee, B. (2014). Photobiological interactions of blue light and photosynthetic photon flux: Effects of monochromatic and broad-spectrum light sources. *Photochem. Photobiol.* 90, 574–584. doi: 10.1111/php.12233

Dieleman, J. A., De Visser, P. H. B., Meinen, E., Grit, J. G., and Dueck, T. A. (2019). Integrating morphological and physiological responses of tomato plants to light quality to the crop level by 3D modeling. *Front. Plant Sci.* 10. doi: 10.3389/fpls.2019.00839

Dutta-Gupta, S., and Jatothu, B. (2013). Fundamentals and applications of light-emitting diodes (LEDs) in *in vitro* plant growth and morphogenesis. *Plant Biotechnol. Rep.* 7, 211–220. doi: 10.1007/s11816-013-0277-0

Fan, X., Bian, Z., Song, B., and Xu, H. (2022). Transcriptome analysis reveals the differential regulatory effects of red and blue light on nitrate metabolism in pakchoi (*Brassica campestris* l.). *J. Integr. Agric.* 21, 1015–1027. doi: 10.1016/S2095-3119(21)63784-X

Hamedalla, A. M., Ali, M. M., Ali, W. M., Ahmed, M. A. A., Kaseb, M. O., Kalaji, H. M., et al. (2022). Increasing the performance of cucumber (*Cucumis sativus* l.) seedlings by LED illumination. *Sci. Rep.* 12, 852. doi: 10.1038/s41598-022-04859-y

Han, X., Tohge, T., Lalor, P., Dockery, P., Devaney, N., Esteves-Ferreira, A. A., et al. (2017). Phytochrome a and b regulate primary metabolism in *Arabidopsis* leaves in response to light. *Front. Plant Sci.* 8. doi: 10.3389/fpls.2017.01394

He, G., Liu, J., Dong, H., and Sun, J. (2019). The blue-light receptor CRY1 interacts with BZR1 and BIN2 to modulate the phosphorylation and nuclear function of BZR1 in repressing BR signaling in *Arabidopsis*. *Mol. Plant* 12, 689–703. doi: 10.1016/j.molp.2019.02.001

Hensel, L. L., Grbic, V., Baumgarten, D. A., and Bleecker, A. B. (1993). Developmental and age-related processes that influence the longevity and senescence of photosynthetic tissues in *Arabidopsis*. *Plant Cell* 5, 553–564. doi: 10.1105/tpc.5.5.553

Hogewoning, S. W., Trouwborst, G., Maljaars, H., Poorter, H., van Ieperen, W., and Harbinson, J. (2010). Blue light dose-responses of leaf photosynthesis, morphology, and chemical composition of *Cucumis sativus* grown under different combinations of red and blue light. *J. Exp. Bot.* 61, 3107–3117. doi: 10.1093/jxb/erq132

Islam, M. A., Tarkowská, D., Clarke, J. L., Blystad, D. R., Gislerød, H. R., Torre, S., et al. (2014). Impact of end-of-day red and far-red light on plant morphology and hormone physiology of poinsettia. *Sci. Hortic.* 174, 77–86. doi: 10.1016/j.scienta.2014.05.013

Izzo, L. G., Mele, B. H., Vitale, L., Vitale, E., and Arena, C. (2020). The role of monochromatic red and blue light in tomato early photomorphogenesis and photosynthetic traits. *Environ. Exp. Bot.* 179, 104195. doi: 10.1016/j.envexpbot.2020.104195

Kang, C., Zhang, Y., Cheng, R., Kaiser, E., Yang, Q., and Li, T. (2021). Acclimating cucumber plants to blue supplemental light promotes growth in full sunlight. *Front. Plant Sci.* 12. doi: 10.3389/fpls.2021.782465

Kwon, A. R., Cui, H. Y., Lee, H., Shin, H., Kang, K. S., and Park, S. Y. (2015). Light quality affects shoot regeneration, cell division, and wood formation in elite clones of *Populus euramericana*. *Acta Physiol. Plant* 37, 1–9. doi: 10.1007/s11738-015-1812-0

Li, Y., Liu, Z., Shi, Q., Yang, F., and Wei, M. (2021). Mixed red and blue light promotes tomato seedlings growth by influencing leaf anatomy, photosynthesis, CO_2 assimilation and endogenous hormones. *Sci. Hortic.* 290, 110500. doi: 10.1016/j.scienta.2021.110500

Lin, K. H., Huang, M. Y., and Hsu, M. H. (2021). Morphological and physiological response in green and purple basil plants (*Ocimum basilicum*) under different proportions of red, green, and blue LED lightings. *Sci. Hortic.* 275, 109677. doi: 10.1016/j.scienta.2020.109677

Liu, H., Fu, Y., Hu, D., Yu, J., and Liu, H. (2018). Effect of green, yellow and purple radiation on biomass, photosynthesis, morphology and soluble sugar content of leafy lettuce *via* spectral wavebands "knock out". *Sci. Hortic.* 236, 10–17. doi: 10.1016/j.scienta.2018.03.027

Liu, M., Xu, Z., Yang, Y., and Feng, Y. (2011). Effects of different spectral lights on oncidium PLBs induction, proliferation, and plant regeneration. *Plant Cell Tissue Organ Cult.* 106, 1–10. doi: 10.1007/s11240-010-9887-1

Li, Y., Xin, G., Liu, C., Shi, Q., Yang, F., and Wei, M. (2020). Effects of red and blue light on leaf anatomy, CO_2 assimilation and the photosynthetic electron transport capacity of sweet pepper (*Capsicum annuum* l.) seedlings. *BMC Plant Biol.* 20, 318. doi: 10.21203/rs.2.24179/v3

Li, Y., Xin, G., Wei, M., Shi, Q., Yang, F., and Wang, X. (2017). Carbohydrate accumulation and sucrose metabolism responses in tomato seedling leaves when subjected to different light qualities. *Sci. Hortic.* 225, 490–497. doi: 10.1016/j.scienta.2017.07.053

Manivannan, A., Soundararajan, P., Halimah, N., Ko, C. H., and Jeong, B. R. (2015). Blue LED light enhances growth, phytochemical contents, and antioxidant enzyme activities of *Rehmannia glutinosa* cultured *in vitro*. *Hortic. Environ. Biotechnol.* 56, 105–113. doi: 10.1007/s13580-015-0114-1

Mao, R., and Guo, S. (2018). Performance of the mixed LED light quality on the growth and energy efficiency of *Arthrospira platensis*. *Appl. Microbiol. Biotechnol.* 102, 5245–5254. doi: 10.1007/s00253-018-8923-7

Matsuda, R., Yamano, T., Murakami, K., and Fujiwara, K. (2016). Effects of spectral distribution and photosynthetic photon flux density for overnight LED light irradiation on tomato seedling growth and leaf injury. *Sci. Hortic.* 198, 363–369. doi: 10.1016/j.scienta.2015.11.045

Matsuo, S., Nanya, K., Imanishi, S., Honda, I., and Goto, E. (2019). Effects of blue and red lights on gibberellin metabolism in tomato seedlings. *Hortic. J.* 88, 76–82. doi: 10.2503/hortj.UTD-005

Miao, Y., Chen, Q., Qu, M., Gao, L., and Hou, L. (2019). Blue light alleviates 'red light syndrome' by regulating chloroplast ultrastructure, photosynthetic traits and nutrient accumulation in cucumber plants. *Sci. Hortic.* 257, 1–9. doi: 10.1016/j.scienta.2019.108680

Miao, Y., Wang, X., Gao, L., Chen, Q., and Qu, M. (2016). Blue light is more essential than red light for maintaining the activities of photosystem II and I and photosynthetic electron transport capacity in cucumber leaves. *J. Integr. Agr.* 15, 87–100. doi: 10.1016/S2095-3119(15)61202-3

Monostori, I., Heilmann, M., Kocsy, G., Rakszegi, M., Ahres, M., Altenbach, S. B., et al. (2018). LED lighting-modification of growth, metabolism, yield and flour composition in wheat by spectral quality and intensity. *Front. Plant Sci.* 9. doi: 10.3389/fpls.2018.00605

Ooi, A., Wong, A., Ng, T. K., Marondedze, C., Gehring, C., and Ooi, B. S. (2016). Growth and development of *Arabidopsis thaliana* under single-wavelength red and blue laser light. *Sci. Rep.* 6, 33885. doi: 10.1038/srep33885

Rehman, M., Ullah, S., Bao, Y., Wang, B., Peng, D., and Liu, L. (2017). Light-emitting diodes: Whether an efficient source of light for indoor plants? *Environ. Sci. Pollut. Res. Int.* 24, 1–10. doi: 10.1007/s11356-017-0333-3

Sartory, D. P., and Grobbelaar, J. U. (1984). Extraction of chlorophyll a from fresh water phytoplankton for spectrophotometric analysis. *Hydrobiologia* 114, 177–187. doi: 10.1007/BF00031869

Savvides, A., Fanourakis, D., and van Ieperen, W. (2012). Co-Ordination of hydraulic and stomatal conductances across light qualities in cucumber leaves. *J. Exp. Bot.* 63, 1135–1143. doi: 10.1093/jxb/err348

Shen, Y., Fan, K., Wang, Y., Wang, H., Ding, S., Song, D., et al. (2022). Red and blue light affect the formation of adventitious roots of tea cuttings (*Camellia sinensis*) by regulating hormone synthesis and signal transduction pathways of mature leaves. *Front. Plant Sci.* 13. doi: 10.3389/fpls.2022.943662

Shinomura, T., Nagatani, A., Hanzawa, H., Kubota, M., Watanabe, M., and Furuya, M. (1996). Action spectra for phytochrome a- and b-specific photoinduction of seed germination in *Arabidopsis thaliana*. *Proc. Natl. Acad. Sci. U.S.A.* 93, 8129–8133. doi: 10.1073/pnas.93.15.8129

Su, N., Wu, Q., Shen, Z., Xia, K., and Cui, J. (2014). Effects of light quality on the chloroplastic ultrastructure and photosynthetic characteristics of cucumber seedlings. *Plant Growth Regul.* 73, 227–235. doi: 10.1007/s10725-013-9883-7

Takahashi, S., and Murata, N. (2008). How do environmental stresses accelerate photoinhibition? *Trends Plant Sci.* 13, 178–182. doi: 10.1016/j.tplants.2008.01.005

Tang, Z., Yu, J., Xie, J., Lyu, J., Feng, Z., Dawuda, M. M., et al. (2019). Physiological and growth response of pepper (*Capsicum annum* l.) seedlings to supplementary red/blue light revealed through transcriptomic analysis. *Agronomy* 9, 139. doi: 10.3390/agronomy9030139

Tian, Y., Wang, H., Sun, P., Fan, Y., Qiao, M., Zhang, L., et al. (2019). Response of leaf color and the expression of photoreceptor genes of *Camellia sinensis* cv. huangjinya to different light quality conditions. *Sci. Hortic.* 251, 225–232. doi: 10.1016/j.scienta.2019.03.032

Tuan, P. A., Thwe, A. A., Kim, Y. B., Kim, J. K., Kim, S. J., Lee, S., et al. (2013). Effects of white, blue, and red light-emitting diodes on carotenoid biosynthetic gene expression levels and carotenoid accumulation in sprouts of tartary buckwheat (*Fagopyrum tataricum* gaertn.). *J. Agric. Food Chem.* 61, 12356–12361. doi: 10.1021/jf4039937

Wang, X., Zhang, W., Hao, Z., Li, X., Zhang, Y., and Wang, S. (2006). *Principles and techniques of plant physiological biochemical experiment* (Beijing: Higher Education Press), 118–119.

Xiao, L., Shibuya, T., Kato, K., Nishiyama, M., and Kanayama, Y. (2022). Effects of light quality on plant development and fruit metabolism and their regulation by plant growth regulators in tomato. *Sci. Hortic.* 300, 111076. doi: 10.1016/j.scienta.2022.111076

Xu, P., Chen, H., Li, T., Xu, F., Mao, Z., Cao, X., et al. (2021). Blue light-dependent interactions of CRY1 with GID1 and DELLA proteins regulate gibberellin signaling and photomorphogenesis in *Arabidopsis*. *Plant Cell* 33, 2375–2394. doi: 10.1093/plcell/koab124

Zhang, H. M., Jennings, A., Barlow, P. W., and Forde, B. G. (1999). Dual pathways for regulation of root branching by nitrate. *Proc. Natl. Acad. Sci. U.S.A.* 96, 6529–6534. doi: 10.1073/pnas.96.11.6529

frontiers | Frontiers in Plant Science

TYPE Original Research
PUBLISHED 10 February 2023
DOI 10.3389/fpls.2022.1057553

OPEN ACCESS

EDITED BY
Yuxin Tong,
Institute of Environment and Sustainable Development in Agriculture (CAAS), China

REVIEWED BY
Laura Cammarisano,
Leibniz Institute of Vegetable and Ornamental Crops, Germany
Tlili Imen,
Carthage University, Tunisia

*CORRESPONDENCE
Weibiao Zhou
weibiao@nus.edu.sg

SPECIALTY SECTION
This article was submitted to Technical Advances in Plant Science, a section of the journal Frontiers in Plant Science

RECEIVED 29 September 2022
ACCEPTED 28 December 2022
PUBLISHED 10 February 2023

CITATION
Huang JJ, Guan Z, Hong X and Zhou W (2023) Performance evaluation of a novel adjustable lampshade-type reflector (ALR) in indoor farming practice using choy sum (*Brassica rapa* var. *parachinensis*). *Front. Plant Sci.* 13:1057553. doi: 10.3389/fpls.2022.1057553

Performance evaluation of a novel adjustable lampshade-type reflector (ALR) in indoor farming practice using choy sum (*Brassica rapa* var. *parachinensis*)

Jim Junhui Huang[1], Zijie Guan[2], Xiaotang Hong[2] and Weibiao Zhou[1,2]*

[1]Environmental Research Institute, National University of Singapore, Singapore, Singapore, [2]Department of Food Science and Technology, National University of Singapore, Singapore, Singapore

The retrieval of lost light energy for promoting vegetable development could be a challenge in indoor farming practice, yet little is attempted so far. In this study, the performance of a novel adjustable lampshade-type reflector (ALR) was investigated to evaluate the feasibility of applying such a device in indoor farm racks (IFR). This application targeted at reflecting stray light back to the IFR for improving the growth and quality of leafy vegetable choy sum (*Brassica rapa* var. *parachinensis*). The optimal configuration of ALR was firstly confirmed *via* simulations using TracePro software. The combination of an included angle at 32° and a reflective board width of 10 cm, under 12 cm of distance between the light sources and the germination tray surface, was revealed to achieve a cost-optimal reflective effect. The simulation-based ALR was subsequently custom-built for actual performance validation. It was shown to effectively produce uniform distributions of temperature, relative humidity, and photosynthetic photon flux density as well as to accumulate more photosynthetic photon energy density along the cultivation shelf. Compared with the control where no ALR was used, the fresh weight and the dry weight of choy sum shoots cultivated using an ALR were increased by up to 14% and 18%, respectively. In addition, their morphological traits were found to be more uniform. Furthermore, their total carotenoid level was enhanced by up to 45%, while the chlorophyll *b* level was markedly decreased. However, no statistically significant difference was found in total phenolic content and antioxidant capacity across the shelf, indicating that the ALR application led to a more uniform antioxidant-related quality of choy sum shoot. ALR application in IFR can thus effectively boost vegetable production and result in quality improvements under an identical amount of electricity consumption in indoor farming compared with ALR-free control.

KEYWORDS

adjustable lampshade-type reflector, choy sum, biomass, morphology, pigments, antioxidant capacity

Highlights

- The optimal combination of ALR included angle and reflective board width was simulated.
- ALR significantly increased the fresh weight of choy sum shoot by up to 14%.
- ALR markedly enhanced the dry mass of choy sum shoot and total leaf by up to 24%.
- ALR remarkably elevated the total carotenoid level in choy sum shoot by up to 45%.

Introduction

Over decades, the over-development of urbanization in conjunction with a rapid increase in population has resulted in a significant reduction of arable land area per capita (hectares per person) in the world, which called for a bigger demand on common food such as grains and vegetables. This situation urged people to develop efficient methods to produce more food (Satterthwaite et al., 2010; Benke and Tomkins, 2017). Vegetables, especially leafy green vegetables, have been shown to present a variety of bioactive metabolites such as carotenoids, phenolic compounds, vitamins, and glucosinolates that could benefit human health and supplement daily nutritional needs (Li et al., 2018; Liang et al., 2018; Lee et al., 2020; Huang et al., 2021a; Du et al., 2022). Vegetables are traditionally cultivated by using outdoor farming methods such as the conventional flat planting approach. Nevertheless, the disadvantages of those traditional outdoor farming methods, such as unstable solar radiation and weather conditions, low land utilization rate due to flat planting, and pest invasion, make them inefficient (Buttar et al., 2006; Alvino and Barbieri, 2016; Ngosong et al., 2021). In recent years, indoor vertical farming has been gradually developed and become a more attractive approach to grow vegetables indoors by eliminating the above-mentioned limiting factors that hamper agricultural production. Among others, the most well-known lighting source currently applied in indoor farming is light-emitting diode (LED) due to its higher energy conversion efficiency and longer operating life span compared with other lighting sources (Despommier, 2013; Benke and Tomkins, 2017; Miao et al., 2019).

The setting of indoor farm racks (IFR) is among the basic devices for implementing vertical planting. It includes multiple shelves/storeys arranged in a vertical manner and/or equipped with lighting panels/groups as well as irrigation systems. This maximizes space utilization in all three dimensions, thereby dramatically increasing the productivity of an indoor farm (Benke and Tomkins, 2017; Kozai et al., 2019). It is noteworthy that the heterogeneous distribution of light on IFR cultivation shelves is always an ineluctable issue to be addressed (Asiabanpour et al., 2018). However, the common designs of IFR hardly consider the light distribution issue along a cultivation shelf. A significant amount of light ray originated from the lighting sources installed at the margins or even in the middle of a shelf is lost to the environment rather than being directed to the shelf (Kozai, 2019; Kim et al., 2021). In addition, IFR and its shelves also face issues of environmental variability, such as the uneven distribution of temperature and humidity (Akiyama and Kozai, 2016; Tsitsimpelis et al., 2016; Jiang et al., 2018; Sabudin et al., 2022), which may further lead to a jagged morphology of the seedlings grown on them. Thus, an efficient solution could be the application of a reflector or reflective device with a lampshade configuration in IFR.

The feature development of lampshade-type reflectors underwent several key stages such as those with un-adjustable planar reflective board (fixed shapes and angles) (Armstrong, 1978; Michaloski, 1991), those with adjustable planar reflective board but only applicable to a fixed configuration of lighting sources (Dumont, 2013), as well as those with adjustable curved/arched reflective boards (Chelf, 2002; Cronk, 2007; Keen, 2011). To the best of our knowledge, however, so far there has been no reflector that fully considers and combines all key features such as reflective boards that are adjustable in a wide range, structures applicable to multiple and different configurations of lighting sources, as well as maintenance of ventilation.

In this study, a novel adjustable lampshade-type reflector (ALR) was proposed, designed, built, and validated. This invention aims to redirect stray light rays towards desirable locations. The idea is to retrieve originally lost light energy for promoting vegetable development and consequently decrease vegetable production cost. In addition, it also tries to combine all the above-mentioned features of reflectors. To evaluate the efficiency of such a reflector, TracePro software was firstly applied to simulate and design ALR's optimal configuration to yield the desired performance outcome. The ALR-regulated distribution of environmental factors such as temperature, relative humidity (%RH), photosynthetic photon flux density (PPFD, 400–700 nm), and photosynthetic photon energy density (PPED) across the cultivation shelf was then tested under selected included angle of the reflective board. Choy sum (*Brassica rapa* var. *parachinensis*), a widely cultivated leafy green vegetable in Asia, was finally adopted as the target plant for comparison in terms of its growth and quality with and without ALR application. It was hypothesized that this ALR could efficiently improve the biomass and key quality attributes of choy sum seedlings when appropriately applied.

Materials and methods

Adjustable lampshade-type reflector

The conceptual model of ALR was designed and custom-built according to the schematic diagrams shown in Figure 1A. Its aluminum-alloy-made main frame (120 cm × 60 cm) was composed of the opposing first and second width sides followed by the opposing first and second length sides. The first and second reflective boards, made of bright anodized aluminum, were pivotably coupled to the main frame at the first and second width sides of the main frame, respectively. The third and fourth reflective boards, made of the same material mentioned above, were also pivotably coupled to the main frame at the first and second length sides of the main frame, respectively, wherein the distance between the respective pivot axes of the first and second reflective boards was adjustable in order to regulate a reflective region of ALR based on the specification of light source applied (Figure 1B). All the reflective boards could be adjusted

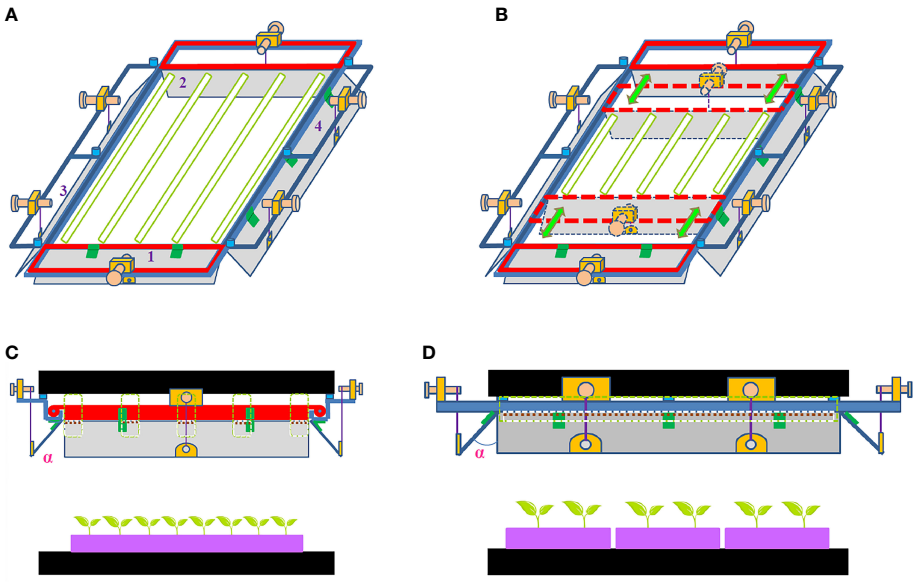

FIGURE 1
Adjustable lampshade-type reflector (ALR). **(A)** Three-dimensional schematic view of ALR with five LED tubes placed inside, illustrating its application in an indoor farm rack (IFR) lighting system. **(B)** Three-dimensional schematic view of ALR with five shorter LED tubes placed inside, illustrating its advantages for application in an IFR lighting system. **(C)** Front-width-side view of ALR installed at IFR. **(D)** Left-length-side view of ALR installed at IFR. α is the included angle of the reflective board. 1 and 2 in **(A)** stand for the first and second reflective boards coupled to the width sides of the main frame, while 3 and 4 in **(A)** represent the third and fourth reflective boards coupled to the length sides of the main frame.

with an included angle that ranges from 0° to 90°. This allowed achieving optimal light distribution on an IFR cultivation shelf. The included angle (α) of the reflective board is defined as the intersection angle between the direction perpendicular to the ground and the reflective board as shown in Figures 1C, D.

Simulation of the combined effects of included angle and reflective board width of ALR using TracePro software

In this novel reflector, the optimal combination of included angle and reflective board width under a certain distance between the light source and the germination tray surface is the key issue to be solved. However, it is a practically hard task to test all the included angles and various widths of the reflective boards because of the laborious works and exorbitant expenditures involved in order to seek an optimal combination for a well-performing reflector. Therefore, some optical software should be used for screening designs first.

In this study, TracePro software (TracePro® Expert—7.0.3 Release ACIS®, version 20.0.3, Lambda Research Corporation, USA), which includes a 3D CAD-based graphical user interface (Sun et al., 2014), was applied to simulate the light distribution maps across the IFR cultivation shelf with and without the adoption of an ALR under different combined conditions. This was to determine the optimal combination of the included angle and the reflective board width in a theoretical manner before a physical reflector was custom-built for performance validation. The parameter configurations in TracePro software required for the simulation are shown in Table 1, in which the specular reflectance of the simulated reflective boards was defined as 80%, the same as that of the bright anodized aluminum material employed in ALR as reflective boards (Powers and Dang, 1986). In this simulation, a five-LED-tube-constructed lighting group was designed and applied to the light source panel for the launching light rays to the cultivation shelf (Figures 2A, B).

Confirmation of the distance between the LED light source and the germination tray surface was also another key issue to be addressed, as a reduction of the distance could allow an IFR to accommodate more shelves, thus improving the IFR's productivity. However, the canopy of choy sum shoots has a potential to touch the LED light sources during growth. Thus, an essential criterion is to prevent the shoot canopy from eventually touching the LED tubes before transplantation. As a result, the distance in this study was set as 12 cm by considering that the shoot canopy height of choy sum was normally approximately 8 to 9 cm on day 16 when the transplantation happened (Huang et al., 2021b). To coordinate with the distance, the width of the reflective board was thus pre-set as 10 cm.

The simulation procedure using TracePro was divided into three steps. The first step was aimed to confirm an optimal range of the included angle of the reflective board by sketchy screening. The selected angles were at a wide range including 90° (set as ALR-free control), 75°, 60°, 45°, 30°, 23°, 15°, and 0° (Figure 3). Referring to the sketchily screened range confirmed by step 1, the second step further fine-tuned the angle from 24° to 35° at 1° interval. This step confirmed the optimal included angle among these tested angles based on a 10-cm-width reflective board (Figure 4). The third step finally verified the optimal combination of the reflective board width and the included angle (*i.e.*, the outcome of step 2) *via* testing boards of various widths ranging from 13 to 6 cm (Figure 5). In this testing, the available light distribution area (ALDA) was used as an index to describe the light distribution uniformity (LDU) of ALR, in which 10% and 15%

TABLE 1 Parameter configuration of TracePro software for the simulation of the novel adjustable lampshade-type reflector.

Parameters	Configuration
Size of the lambertian diffuser board acting as the upper shelf of indoor farm racks (IFR) for installation of the simulated LED light tubes [length (mm) × width (mm)]	1,200 × 450
Size of the absorber board acting as the lower shelf of IFR [length (mm) × width (mm)]	1,200 × 600
Distance between the lambertian diffuser board and the absorber board (mm)	120
Size of the long-side reflective board [length (mm) × width (mm)]	1,130 × 100
Size of the short-side reflective board [length (mm) × width (mm)]	444 × 100
Parameters for the reflective board and LED light source information	
Scatter	ABg
Absorptance	20%
Specular reflectance	80%
Number of simulated LED light tubes	5
Distance between two simulated LED light tubes (mm)	110
Number of simulated LED chips in per tube	96
Distance between two simulated LED chips in per tube (mm)	11.7
Type of simulated LED chip	5,730
Size of simulated LED chip [length (mm) × width (mm) × height (mm)]	5.7 × 3.0 × 0.9
Parameters for simulated LED chip	
Emission type	Flux
Units	Photometric
Angular distribution	Lambertian
Flux (lumens)	27
Average wavelength (nm)	555
Simulated rays for per LED chip	2,000

standard deviations (SD) of PPFD were set as the thresholds for different LDU standards.

Measurement of distribution maps of environmental factors under the selected included angles of ALR

Four 50-cavity [each 5 cm (length) × 5 cm (width) × 4 cm (depth)] germination trays (Arianetech Pte Ltd., Singapore) were placed in a parallel manner on a shelf of the custom-built IFR (Arianetech Pte Ltd., Singapore). Five 22-W white LED tubes and ALR were then mounted at the lower part of the upper shelf (Figures 1C, D, 2E–H). Various parameters related to the performance of the ALR, LED tubes, and trays were implemented in accordance with the simulated ones as shown in Table 1. **A** total of 200 cavities contained in the four trays were subsequently numbered and divided into five zones ($N_{zone\ 1}$ = 56, $N_{zone\ 2}$ = 48, $N_{zone\ 3}$ = 40, $N_{zone\ 4}$ = 32, $N_{zone\ 5}$ = 24, N_{total} = 200, where N stands for the cavity number) (Figures 2C, D). Such a partition in zones was reasonable because the PPFD distribution in the center of a cultivation shelf is always higher than those gradually distant from the center, until the four shelf brims, in an annular and gradually decreasing manner due to the parallel arrangement of the five LED tubes. This phenomenon could be observed from both the simulation results (Figure 3) and the actual experimental outcome (Figure 6C). Generally speaking, the PPFD values within the same zone were similar or close to each other. The temperature, %RH, PPFD and PPED values at each tray cavity were measured in triplicate by using a light meter (ASENSETEK® Lighting Passport, Taiwan). The experiments and measurements were conducted under three different conditions by adjusting the included angles of the four reflective boards to 15°, 32°, and 90° (control), respectively.

Leafy vegetable cultivation

Choy sum seeds provided by Ban Lee Huat Seed Pte Ltd. (Singapore) were planted for us to conduct performance validation. Before sowing, each cavity of the four 50-cavity germination trays was filled with a standardized potting mix purchased from Jiffy® (Jiffy Substrates, Toul, France). Each cavity was then sown with one seed. Subsequently, each tray was placed on the designated location of a cultivation shelf. To ensure that every cavity possessed a healthy seedling so as to make a fair comparison later, the fifth spare germination tray was sown simultaneously under the same light environment but was placed on

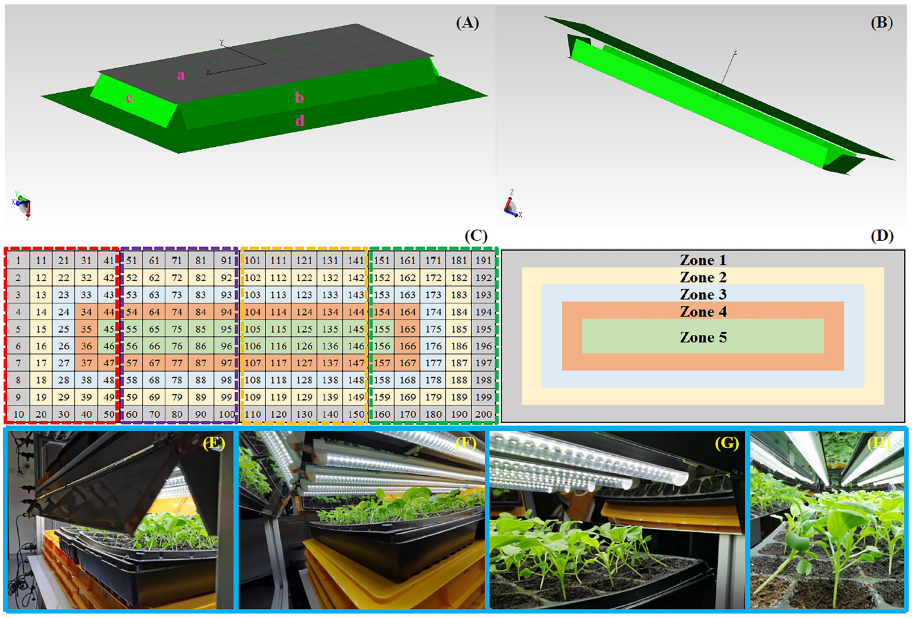

FIGURE 2
(A) Erected and **(B)** inverted schematic views of the three-dimensional simulative model of the adjustable lampshade-type reflector designed by the light simulative software TracePro. **(C)** Arrangement of four germination trays in the shelf of an indoor farm rack, marking the locations of a total of 200 cavities. **(D)** Definition of five zones on the four germination trays. Performance photos of the adjustable lampshade-type reflector observed from the viewing angles of **(E)** exterior, **(F)** short-side reflective board, **(G)** long-side reflective board, and **(H)** interior. The dashed rectangles with red, purple, earthy yellow, and green colors in **(C)** represent tray 1, 2, 3, and 4, respectively. In **(A)**, a is the lambertian diffuser board, b stands for the long-side simulative reflective board, c represents the short-side simulative reflective board, and d is the absorber board.

another shelf. At 2 days after the sowing day (day 0), the non-germinated seeds in the first four trays were removed, and the corresponding cavities were replaced with healthy seedlings from the fifth tray. The photoperiod was set as 12:12 h of light/dark cycle daily. The seedlings were cultivated until the 16th day, which was the day set for harvest (Huang et al., 2021b). The experiments were performed in triplicate, respectively, under two conditions: (1) ALR-free control group (*i.e.*, the included angle was set as 90°) and (2) ALR-implemented group where the included angle was 32°, which was confirmed by the simulation results as the optimal angle (Figure 5D). Each germination tray was irrigated with 3.0 L of water through sub-irrigation on the day of sowing (day 0) and subsequently watered with 1.0 L of tap water on days 4, 10, and 14, respectively.

Determination of biomass and morphological parameters

The biomass and morphological parameters were determined by following the methods of Huang et al. (2021b). On harvest day (day 16), all seedlings, together with the soil, were carefully removed from the cavities of the germination trays. The roots with a soil portion were gently dipped into a beaker of clear tap water by sketchily rinsing off the soil while keeping the roots intact. The choy sum roots were subsequently fully cleaned using another beaker of clear tap water while care was taken to make sure that the roots were not broken during washing. Afterwards, the stretching state of the whole seedling or the flattened laminas from each seedling, as well as a ruler, were placed together and photographed using a smartphone (MIUI 8, China). Image analysis was conducted for the measurement of morphological parameters, including total leaf area (TLA), hypocotyl length (HL), hypocotyl diameter (HD), and root length (RL), by using ImageJ 1.51j8 software (National Institute of Health, Bethesda, MD, USA). The actual scales of all the items in the photos were referred to the ruler, and the photo scale was set accordingly. The length or diameter values were then determined by drawing a straight line along the items and were automatically calculated by the software, while the leaf areas were automatically measured by the software after drawing irregular and enclosed lines along the margin of the leaf.

After photographs had been taken, the fresh weight (FW) of each seedling was measured using a three-decimal-point electronic balance (Mettler Toledo ML303 Precision Balance, Greifensee, Switzerland). Each seedling was then cut into shoot and root parts by using a pair of scissors. The shoot and root parts were weighed separately and placed into a 50-ml Falcon tube. The tubes containing the respective seedlings from each cavity were frozen (DW-86L959BP, Haier, China) overnight at -80°C and then freeze-dried (Lyovapor^{TM}L-300, BUCHI, Switzerland) for 4 days. After lyophilization, the dry weight (DW) of each part of the seedling sample was determined. The shoot parts of the selected seedling samples were kept and utilized for the subsequent metabolite analyses of photosynthetic pigments, total phenolic content (TPC) and antioxidant capacity.

With reference to Tan et al. (2020), the harvest index (HI) and shoot/root ratio were determined using the following formula, respectively:

$$HI = \frac{Choy\ \ sum\ \ shoot\ \ DW}{Whole\ \ choy\ \ sum\ \ seedling\ \ DW} \quad (1)$$

$$Shoot/root\ \ ratio = \frac{Choy\ \ sum\ \ shoot\ \ DW}{Choy\ \ sum\ \ root\ \ DW} \quad (2)$$

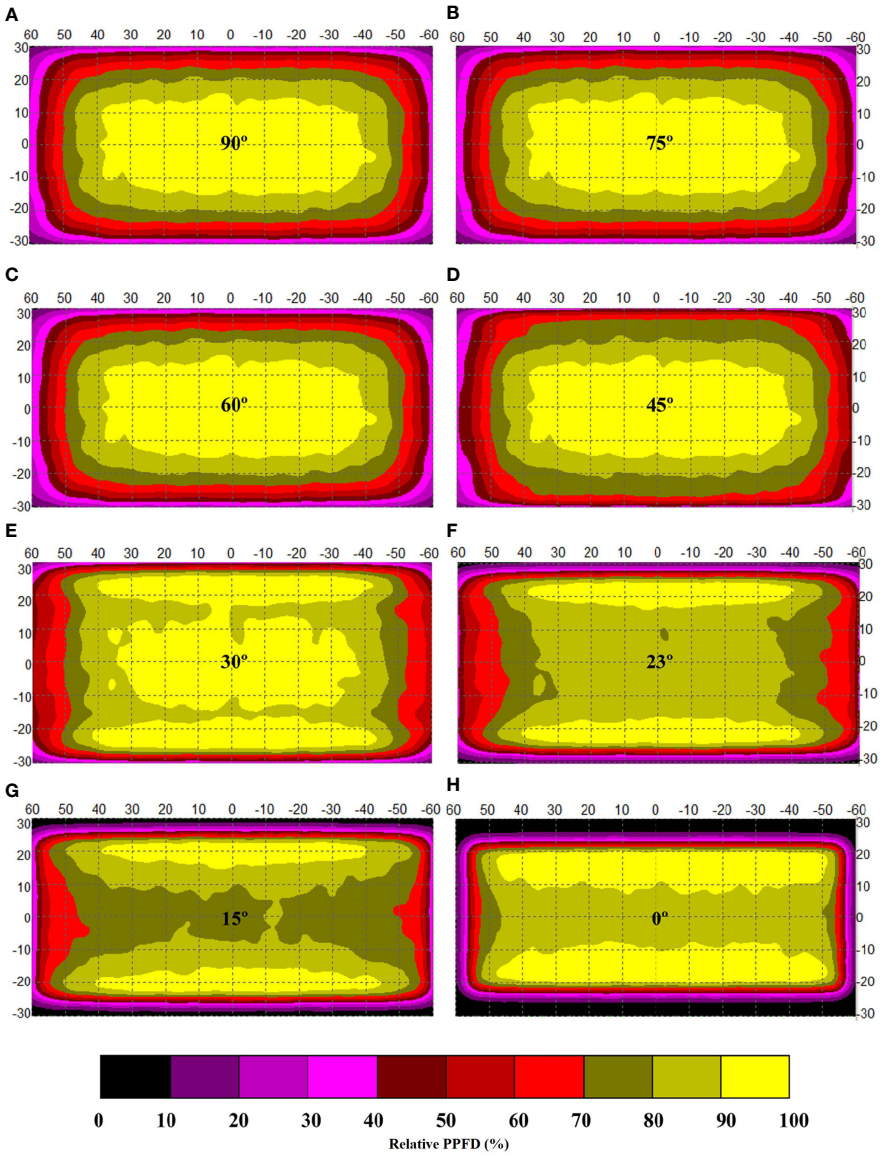

FIGURE 3
Sketchy screening of the appropriate included angles for the optimization of simulated light intensity distribution along an indoor farm rack shelf with the application of an adjustable lampshade-type reflector. Specifically, the screened included angles are **(A)** 90°, **(B)** 75°, **(C)** 60°, **(D)** 45°, **(E)** 30°, **(F)** 23°, **(G)** 15°, and **(H)** 0°, respectively. The width of the reflective board is set as 10 cm. The scale unit on the figures is centimeter. The numbers in the color bar indicate relative photosynthetic photon flux density values (%).

Determination of photosynthetic efficiency

With reference to Huang et al. (2016), the photosynthetic efficiency is defined as follows:

$$PE(\%) = \frac{E_B}{E_I} \times 100\,\% \quad (3)$$

where E_B represents the free energy contained in the dry biomass of choy sum shoot (*i.e.*, edible portion), and E_I stands for light energy in the spectrum of 380–780 nm containing the photosynthetically active radiation (PAR) range of 400–700 nm that was emitted by the white LED light tubes (Huang et al., 2021b). The light energy E_I [J/(m^2·s)] based on I [μmol/(m^2·s)] is expressed as follows:

$$E_I[J/(m^2 \cdot s)] = h \times c \times A \times 10^3 \times \sum_{\lambda=380}^{\lambda=780} \frac{I_\lambda}{\lambda} \quad (4)$$

where h is Planck constant (6.626×10^{-34} $J{\cdot}s$), c represents the light ray velocity (2.998×10^8 m/s), λ stands for photon wavelength (nm), I_λ is light intensity [μmol/(m^2·s)] under a certain wavelength from 380 to 780 nm, and A represents the Avogadro constant (6.022×10^{23}/mol). E_B was calculated according to the following assumption: under a normal growth condition without stress, 100 g choy sum edible portion (containing 5.8 g DW) had 49 kJ of energy (Wills et al., 1984).

Determination of pigments

For the measurement of pigments including chlorophyll *a* (chl*a*), chlorophyll *b* (chl*b*), total chlorophylls (Tchl), and total carotenoids (TC) in choy sum shoot, 30 shoot samples were selected from designated cavities to represent their respective zones, of which

10.3389/fpls.2022.1057553

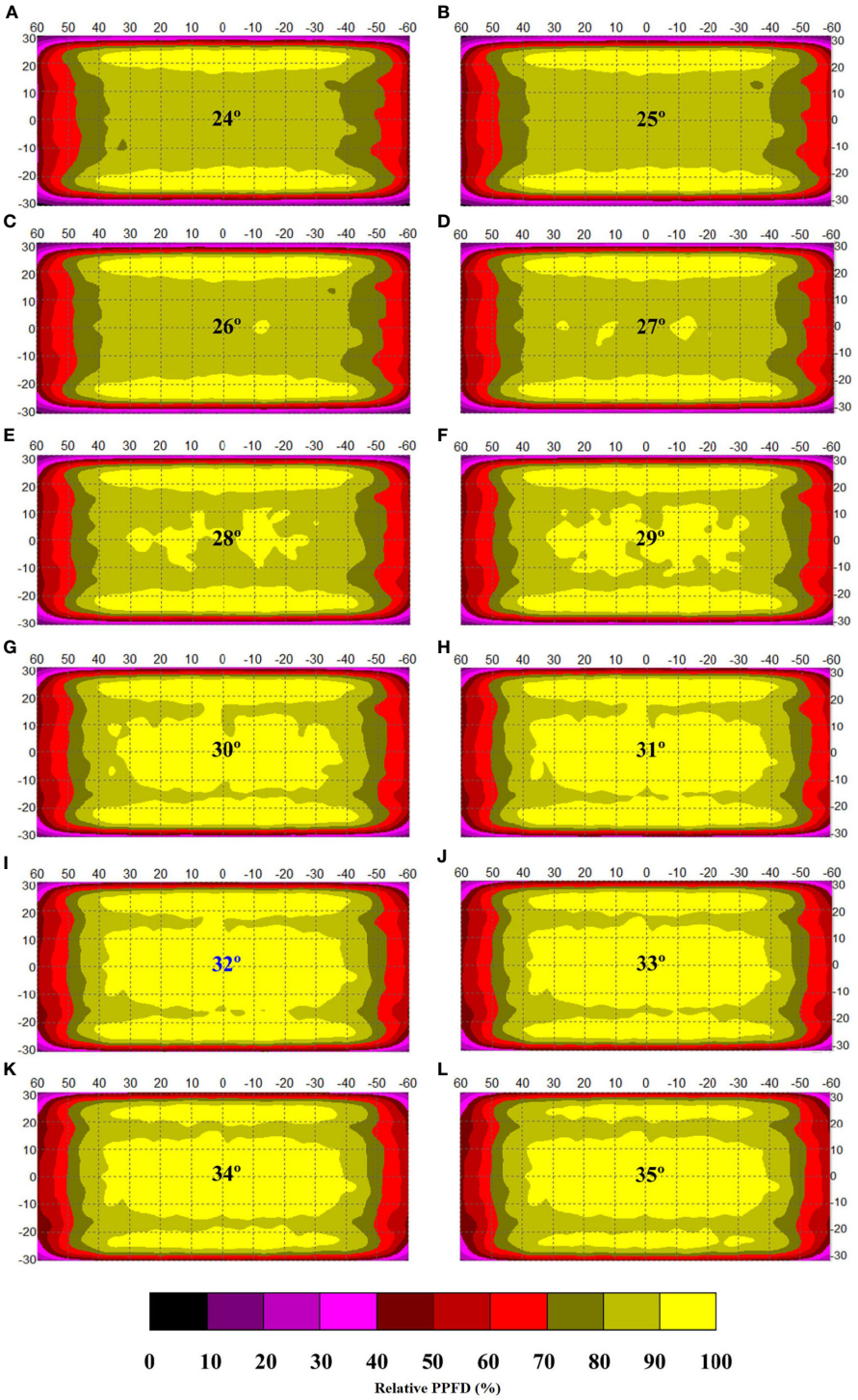

FIGURE 4
Fine-screening of the appropriate included angles for the optimization of simulated light intensity distribution along an indoor farm rack shelf with the application of an adjustable lampshade-type reflector. The screened included angles are **(A)** 24°, **(B)** 25°, **(C)** 26°, **(D)** 27°, **(E)** 28°, **(F)** 29°, **(G)** 30°, **(H)** 31°, **(I)** 32°, **(J)** 33°, **(K)** 34° and **(L)** 35°, respectively. The width of reflective board is set as 10 cm. The scale unit on the figure is centimeter. The numbers in the color bar indicate relative photosynthetic photon flux density values (%).

shoots from cavity numbers 5, 61, 70, 131, 140, and 195 were for zone 1, numbers 15, 62, 69, 132, 139, and 185 were for zone 2, numbers 25, 63, 68, 133, 138, and 175 were for zone 3, numbers 35, 64, 67, 134, 137, and 165 were for zone 4, and numbers 45, 65, 66, 135, 136, and 155 were for zone 5 (Figure 2C). As the cultivation experiments were conducted in triplicate, a total of 18 shoot samples were thus collected in each zone (n = 18). For pre-treatment, about 10 mg of weighed lyophilized choy sum shoots was quickly ground into powder in a pre-cooled mortar and pestle, which was covered with a black cloth to prevent the degradation of light-sensitive pigments. After that, 3, 3, and 4 ml of 80% acetone (HPLC grade, Sigma-Aldrich, St. Louis, MO, USA) in three consecutive steps, respectively, were added into the

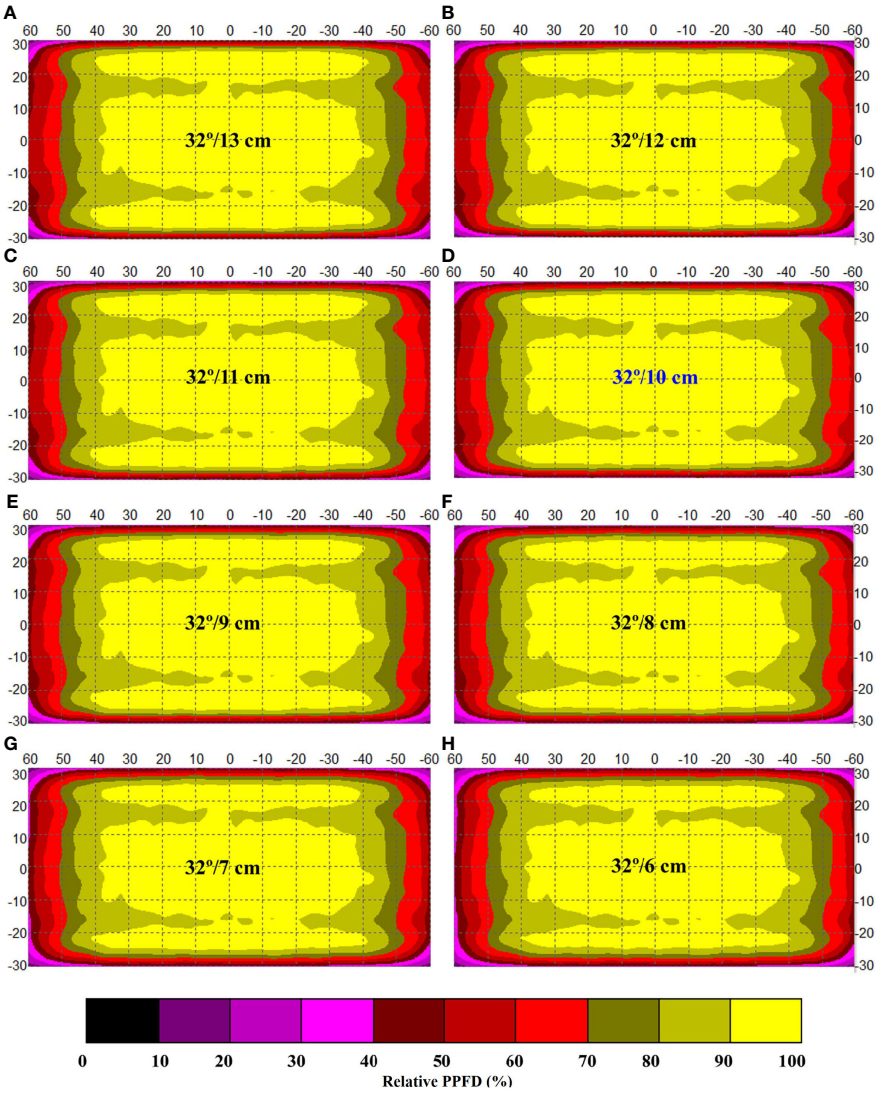

FIGURE 5
Screening of the appropriate width of the reflective board under the optimal included angle (32°) for the optimization of simulated light intensity distribution along an indoor farm rack shelf with the application of an adjustable lampshade-type reflector. The screened widths are **(A)** 13 cm, **(B)** 12 cm, **(C)** 11 cm, **(D)** 10 cm, **(E)** 9 cm, **(F)** 8 cm, **(G)** 7 cm, and **(H)** 6 cm, respectively. The scale unit on the figure is centimeter. The numbers in the color bar indicate relative photosynthetic photon flux density values (%).

mortar to fully extract the powder. The powder together with the solvent was then transferred into a 15-ml Falcon tube; the tube was vortexed for 30 s and left to stand at 4°C for 24 h to completely release the pigments from the powder into the solvent. The mixtures were sonicated using a sonicator (Elmasonic S 60H, Singen, Germany) for 15 min and subsequently centrifuged at 3,500 × *g* for 15 min in a pre-cooled 4°C centrifuge tube (Thermo Scientific™ 75004533, Thermo Fisher Scientific, USA). After centrifugation, the supernatant was collected, and its absorbance was scanned from 200 to 780 nm to obtain the values at 663.6, 646.6, and 440.5 nm, respectively, by using a UV–vis spectrophotometer (UV1800, Shimadzu, Japan). The chl*a*, chl*b*, and TC contents were finally calculated using the following equations (mg per gram DW) (Huang et al., 2021a):

$$Chla\quad content\quad (mg/gDW) = \frac{(12.25A_{663.6} - 2.55A_{646.6})(mg/L)}{Dry\quad weight\quad (g\quad DW/L)} \tag{5}$$

$$Chlb\quad content\quad (mg/gDW) = \frac{(20.31A_{646.6} - 4.91A_{663.6})(mg/L)}{Dry\quad weight\quad (gDW/L)} \tag{6}$$

$$TC\quad content\quad (mg/gDW) = \frac{(4.69A_{440.5} - 4.74A_{646.6} - 1.96A_{663.6})(mg/L)}{Dry\quad weight\quad (gDW/L)} \tag{7}$$

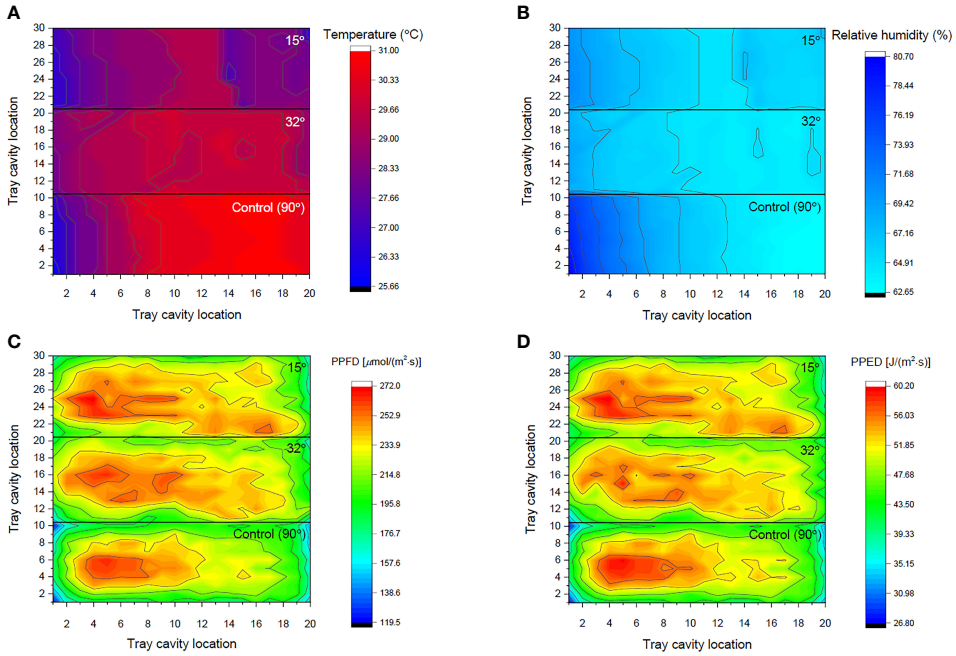

FIGURE 6
Heat maps of the measured **(A)** temperature, **(B)** relative humidity, **(C)** photosynthetic photon flux density on per cavity, and **(D)** photosynthetic photon energy density along the shelf of an indoor farm rack under different included angles of an adjustable lampshade-type reflector.

Sample preparation for antioxidant-related analyses

A total of 30 shoot samples were chosen to represent their respective zones. Shoots from cavity numbers 6, 71, 80, 121, 130, and 196 were for zone 1, numbers 16, 72, 79, 122, 129, and 186 were for zone 2, numbers 26, 73, 78, 123, 128, and 176 were for zone 3, numbers 36, 74, 77, 124, 127, and 166 were for zone 4, and numbers 46, 75, 76, 125, 126, and 156 were for zone 5, respectively (Figure 2C). With triplicate cultivation experiments, there were a total of 18 shoot samples for each zone (n = 18). For pre-treatment, 30 mg of freeze-dried choy sum shoot powder was added with 500 μl of acetone–water–acetic acid (70:29.5:0.5 v/v) and vortexed for 30 s to fully blend the mixture prior to sonication. The mixture was then sonicated in an ice bath for 15 min and centrifuged at 20,000 × g for 10 min at 4°C to collect the supernatants. The above-mentioned procedure was repeated twice, and the supernatants were pooled and then stored at -80°C prior to further analyses for TPC and antioxidant capacity (Huang et al., 2021a).

Determination of total phenolic content

The TPC of choy sum shoot samples was determined using the Folin–Ciocalteu method with minor modifications (Ainsworth and Gillespie, 2007). Briefly, an aliquot of 100 μl of the above-mentioned shoot sample extract was blended with 200 μl of 10% Folin–Ciocalteu's phenol reagent (Sigma-Aldrich, St. Louis, MO, USA), followed by 800 μl of 70 mM sodium carbonate solution, in a microtube and placed in the dark. After that, 200 μl of the sample, standard or blank, respectively, was transferred into microplate wells before the absorbance of each well at 765 nm was read using a microplate reader (Biotek SynergyMx, Vermont, USA). Different concentrations of gallic acid, ranging from 0.016 to 0.25 g/L, were used to establish a standard curve for calibration. The TPC of the choy sum shoots was determined, and the results were expressed as milligram gallic acid equivalents per gram dry weight of choy sum shoot (mg GAE/g DW).

Determination of 2,2-diphenyl-1-picrylhydrazyl radical scavenging activity

In this study, 2,2-diphenyl-1-picrylhydrazyl (DPPH) radical scavenging activity assay was performed based on the microplate method developed by Bobo-García et al. (2015) with some modifications. Briefly, a total of 20 μl of the above-mentioned diluted choy sum shoot sample extract was mixed with 180 μl of 0.2 mM DPPH solution (Sigma-Aldrich, St. Louis, MO, USA) in methanol and then pipetted into the wells of a 96-well microplate. After incubating the mixtures in the dark at room temperature for 2 h, the absorbance was read at the wavelength of 515 nm on a microplate reader (Biotek SynergyMx, Vermont, USA). A standard curve of % DPPH quenched was established with the concentration of Trolox (Acros Organics, NJ, USA) ranging from 50 to 500 μM for calibration. The DPPH assay was carried out, and the results were expressed as micromole Trolox equivalents per gram dry weight of choy sum shoot (μmol TE/g DW).

The DPPH quenched (%) was calculated from Equation 8, where A_{sample} is the absorbance at 515 nm of 20 μl of the extract or standard with 180 μl DPPH solution after 2 h, A_{blank} is the absorbance at 515 nm of 200 μl methanol after 2 h, and $A_{control}$ is the absorbance at 515

nm of 20 µl of water with 180 µl DPPH solution after 2 h.

$$DPPH \quad quenched(\%) = \left[1 - \left(\frac{A_{sample} - A_{blank}}{A_{control} - A_{blank}}\right)\right] \times 100(\%) \quad (8)$$

Statistical analysis

All the experiments, including cultivation, in this study were performed in triplicate (n = 3). The pigments, TPC, and DPPH of a total of 18 shoot samples for each zone (n = 18) were determined, respectively. Statistical analyses were performed using IBM Statistical Product and Service Solutions (SPSS version 17.0) software at a significant level of 0.05 (two-tailed). One-way analysis of variance (ANOVA) with Tukey's multiple-comparison was used to evaluate the differences among all the zones or among all the included angles tested. Student's t-test was employed to estimate the differences between two independent conditions (*e.g.*, included angle of 90° as control and that of 32° as treatment). In the growth comparison experiments, the top 80% of choy sum seedlings, which had healthy development, were used for data analysis. The unhealthy and poorly developed choy sum seedlings were removed to minimize the negative effect of seed quality on the reliability of the experiment results.

Results and discussion

Optimal combination of included angle and reflective board width of ALR by simulation approach

As mentioned earlier, laborious works and exorbitant expenditures could be greatly saved through the application of software to simulate real situations. This demands that the simulation conditions must strictly follow the actual settings. Among the consistencies was the configuration of LED tubes in IFR, including the type, size, and number of LED chips. In addition, the consistent distances between any two chips, as well as between LED tubes and tray surface, *etc.*, were also covered (Table 1). In this section, TracePro software was used to find the optimal combination of included angle and width of the ALR reflective board, based on which a physical reflector would be subsequently manufactured for *in situ* performance evaluation. As defined, the ALR included angles that ranged from 0° to 90°, among which an optimal angle existed to achieve the maximal reflection effect on retrieving stray LED light back to the IFR cultivation shelf. For a given LDU requirement (*e.g.*, 10% or 15%), the larger the uniform area generated by an included angle on the cultivation shelf, the better the performance achieved by the angle.

To achieve the goal, a sketchy screening to find the approximately optimal included angle was firstly carried out by presetting the reflective board width as 10 cm, which was chosen based on the distance between the LED tube and the tray surface being 12 cm after considering the final canopy height of choy sum shoot achieved on day 16 (Huang et al., 2021b). As shown in Figure 3 and Table 2, the included angles from 45° to 75° yielded minor variations in ALDA (within 10% SD of light intensity) which were almost the same as that of the control (3,406 cm^2). However, ALDA under 30° of included angle was significantly increased to 4,694 cm^2, which was remarkably higher than those under 23°, 15°, and 0°. The same tendency was also found under the LDU requirement of within 15% SD of light intensity, indicating that there should have been a peak value in a range approximately 30° that needed to be further investigated (Figure 3 and Table 2). From the simulation results, ALDA under 30° of included angle was bigger than that under 0°, which is in line with the conclusion of Akiyama and Kozai (2016) that an inclined (board) reflector with appropriate angle (approximately 20°) was better than a vertical (board) reflector to improve PPFD across a cultivation shelf.

To locate the exactly optimal included angle in this scenario, a fine screening was further carried out. In this second screening, the included angles ranging from 23° to 35°, at 1° interval, were simulated to investigate the varying tendency of ALDA thus affected and to confirm the optimal included angle. With reference to Figure 4 and Table 2, it was found that the peak ALDA value (67.1% of total shelf area), under the LDU requirement of within 10% SD of light intensity, fell on 32° of the included angle. Under the LDU requirement of within 15% SD of light intensity, the peak ALDA value (76.3% of total shelf area) was also found to be at 32°. Under both LDU requirements, an increasing trend was shown when the included angle increased from 23° to 32°, while a gradually decreasing trend was observed when the included angle further increased from 32° to 35° (Table 2). Compared with their respective reflector-free controls at 90°, the maximal ALDA values achieved by 32° under the LDU requirement of within 10% and 15% SD of light intensity were enhanced by 41.8% and 25.8%, respectively. Thus, 32° was finally selected as the optimal included angle to achieve the maximal ALDA value across a cultivation shelf, compared with all the other simulated angles with the same 10-cm width of the ALR reflective board (Figure 4 and Table 2).

The last and the most important step was to figure out the best combination of included angle and reflective board width that can provide a better cultivation environment for plants compared with the reflector-free control. After the above-mentioned confirmation of the optimal included angle (*i.e.*, 32°), the optimization of the ALR reflective board width under this angle was eventually carried out by testing the variation of ALDA under various widths of the reflective board, ranging from 6 to 13 cm at 1-cm interval. Based on Figure 5 and Table 2, it was obvious that ALDA (no matter within 10% or 15% SD of light intensity) was the largest, compared with all the other tested widths, when the board width was 13 cm. Furthermore, a decreasing tendency of area was found with the reduction of width, indicating that a larger width may help to reflect more of the stray light rays back to the IFR cultivation shelf under the same included angle. This is in agreement with the results from a previous reflector-related study showing that the average PPFD across the shelf under 15 cm of the side reflector width is 10% and 25% more than those under the 10- and 0-cm (no-reflector control) ones, respectively (Akiyama and Kozai, 2016).

Besides ALDA, two other issues should also be addressed when determining an optimal ALR reflective board width. Firstly, the ventilation issue has to be considered to match the preset distance between the LED tubes and the tray surface. In this study, the distance was 12 cm, which was to guarantee that the canopy height of choy sum shoot could grow up to approximately 8 to 9 cm on day 16

10.3389/fpls.2022.1057553

TABLE 2 Optimization of the included angles and widths of the four reflective boards of the novel adjustable lampshade-type reflector (based on a five-LED-tube panel).

Condition[a]	Included angle	Width (cm)	Highest light intensity [μmol/(m^2·s)]	Within 10% SD of light intensity distribution			Within 15% SD of light intensity distribution		
				Area (cm^2)	Percentage[b] (%)	Average light intensity [μmol/(m^2·s)]	Area (cm^2)	Percentage (%)	Average light intensity [μmol/(m^2·s)]
(1)	90°	10	253	3,406	47.3	228	4,369	60.7	215
(2)	75°	10	253	3,407	47.3	228	4,370	60.7	215
(3)	60°	10	253	3,409	47.4	228	4,371	60.7	215
(4)	45°	10	254	3,426	47.6	229	4,858	67.5	216
(5)	35°	10	253	4,763	66.2	228	5,476	76.1	215
(6)	34°	10	253	4,801	66.7	228	5,480	76.1	215
(7)	33°	10	253	4,817	66.9	228	5,481	76.1	215
(8)	**32°**	**10**	**253**	**4,830**	**67.1**	**228**	**5,496**	**76.3**	**215**
(9)	31°	10	256	4,808	66.8	230	5,481	76.1	218
(10)	30°	10	256	4,694	65.2	230	5,365	74.5	218
(11)	29°	10	263	4,598	63.9	237	5,349	74.3	224
(12)	28°	10	265	4,472	62.1	239	5,277	73.3	225
(13)	27°	10	269	4,347	60.4	242	5,210	72.4	229
(14)	26°	10	273	4,275	59.4	246	5,185	72.0	232
(15)	25°	10	276	4,173	58.0	248	5,142	71.4	235
(16)	24°	10	279	4,044	56.2	251	5,049	70.1	237
(17)	23°	10	280	3,938	54.7	252	4,997	69.4	238
(18)	15°	10	308	2,823	39.2	277	4,827	67.0	262
(19)	0°	10	320	4,108	57.1	288	4,439	61.7	272
(20)	32°	13	253	4,922	68.4	228	5,565	77.3	215
(21)	32°	12	253	4,895	68.0	228	5,533	76.9	215
(22)	32°	11	253	4,875	67.7	228	5,520	76.7	215
(23)	32°	9	253	4,785	66.5	228	5,440	75.6	215
(24)	32°	8	253	4,751	66.0	228	5,417	75.2	215
(25)	32°	7	253	4,697	65.2	228	5,385	74.8	215
(26)	32°	6	253	4,626	64.3	228	5,327	74.0	215

[a]Table background in yellow, green, and pink colors stands for the sketchy screening for the optimal range of the included angle, the fine screenings for the exact included angle, and the optimal combination of the included angle and the reflective board width, respectively.
[b]The available total shelf area for cultivation is 7,200 cm^2.
SD, standard deviation. Bold fonts in the table meant the selected included angle and reflective board width under within 10% SD and 15% SD of light intensity distribution, respectively.

(Huang et al., 2021b) and the canopy would receive as much light as possible without touching the LED tubes. Meanwhile, the IFR productivity could be significantly improved under such a distance. This is because the shorter shelf height achieved of 19 cm (noting the 5-cm height of the germination tray and the 2-cm height of the LED tubes) can accommodate more shelves in the IFR compared with 27 cm of the original IFR shelf height currently applied in our indoor plant factory. Therefore, the ALR reflective board width is suggested not to exceed 12 cm, considering that efficient ventilation should be maintained across the cultivation shelf for the entire seedling growth period. Another factor that needs to be considered is the material cost to manufacture the ALR reflective boards. The larger the width of an ALR reflective board that is applied, the higher the board would cost. Thus, 10 cm was chosen as the optimal width to save on the board material and its cost because ALDA under 10 cm was close to that under 11 cm (Table 2). From this simulation study, the combination of 32° of included angle and 10 cm of reflective board width was therefore selected as optimal, which acted as the basis for manufacturing a physical reflector to facilitate an *in situ* performance evaluation as described below.

Comparison between the distribution of environmental factors on the cultivation shelf with and without ALR application

After the optimal combination of included angle and reflector board width was determined, a custom-built ALR was manufactured (Figures 2E–H) to further investigate the actual performance and efficiency of this novel reflector. The first evaluation step was to compare the distribution of key environmental factors such as temperature, %RH, PPFD, and PPED on each cavity along a cultivation shelf between with and without the ALR. The acquired data could help us to check the distribution uniformity of these factors under selected included angles. A more uniform environment may facilitate the development of a more uniform morphology of seedlings and improve the total biomass accumulation. In this study, the included angles of 15°, 32° (the optimal simulated angle), and 90° (reflector-free control) were selected (Figures 6, 7).

As shown in Figure 6A, 32° of included angle could achieve the most uniform temperature distribution along a cultivation shelf, compared with those under 15° and 90° (the control). Under the control, the temperature range of the 200 cavities was 25.7–31.0°C, which indicates that the distribution was inhomogeneous. However, the temperature difference along the cultivation shelf was significantly smaller under the ALR. The temperature range became 28.0–30.0°C and 26.7–29.3°C when the included angle was 32° and 15°, respectively. Furthermore, from Figure 7A, the 90° control group displayed the biggest SD, resulting in an insignificant difference among their five zones, while the 32° and 15° groups demonstrated smaller SD values, leading to significant differences between zone 1 and the other zones under 32° as well as between zones 1 and 5 under 15°. This indicates that the ALR application could markedly minimize the temperature range/distribution difference along a cultivation shelf.

Among all the zones, the temperature values in zones 3, 4, and 5 of the control group were remarkably higher than those under the ALR of the 32° and 15° groups, respectively (Figure 7A). This could be due to the property of reflective boards made of bright anodized aluminum that absorbs part of the heat from the surroundings, as the spectral absorptivity of this material to far-red light (701–780 nm) may range from 35% to 60% (Moghadam et al., 2013). In addition, the temperature under the ALR of 32° included angle group was significantly higher than that under the 15° one across all the zones. This could be due to the fact that a smaller included angle (*i.e.*, 15°) generated more enclosed room for the board to efficiently absorb heat, resulting in a significant reduction of temperature across the cultivation shelf under the ALR of 15° included angle (Figure 7A).

Another interesting phenomenon observed was that 32° of included angle was superior to 15° in terms of uniform temperature distribution along the shelf (Figure 6A). One reason might be that an appropriate included angle like 32° could help to reflect not only visible light but also far-red light to a wider cultivation area owing to the reflectance property of the bright anodized aluminum (Li et al., 2021). However, an included angle like 15° mainly reflected far-red light onto the shelf center, thus lowering the average temperature values in all the zones and generating bigger SD (Figure 6A).

The experimental results showed that the %RH distribution across a shelf was inversely related with that of the temperature (Figures 6A, B). The absolute amount of water vapor or absolute humidity within the atmosphere of a shelf was relatively constant (Bencloski, 1982), regardless if an ALR was used. Similar to the

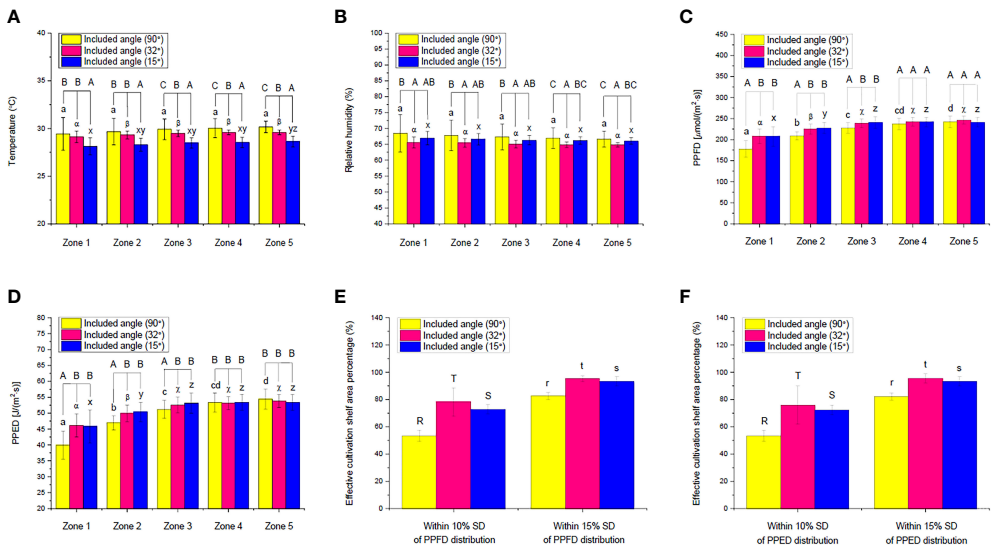

FIGURE 7
Comparisons of the measured **(A)** temperature, **(B)** relative humidity, **(C)** photosynthetic photon flux density (PPFD) and **(D)** photosynthetic photon energy density (PPED) in different shelf zones of an indoor farm rack under different included angles of an adjustable lampshade-type reflector as well as effective cultivation shelf area percentages within different SD of PPFD distribution under **(E)** PPFD-based and **(F)** PPED-based conditions. Different uppercase letters (A, B, and C) indicate significant differences among different included angles in the respective zones; different lowercase letters (a, b, c, d, x, y, and z) and Greek alphabets (α, β, and χ) indicate significant differences among all the zones under the respective included angles; different uppercase letters (R, S, and T) and lowercase letters (r, s, and t) indicate significant differences among the different included angles within 10% and 15% SD of the PPFD/PPED distribution along the whole shelf, respectively (N_{zone1} = 56, N_{zone2} = 48, N_{zone3} = 40, N_{zone4} = 32, N_{zone5} = 24, N_{total} = 200, one-way ANOVA; Tukey multiple-comparison; $p < 0.05$).

temperature distribution, the %RH values of the control group were in the range of 62.7%–80.7%, which was larger than those under the ALR of the 32° and 15° groups (63.7%–69.3% and 64.3%–71.0%, respectively). Thus, the ALR also minimized the %RH distribution difference along the cultivation shelf (Figure 7B). In the control group, the %RH SD was the highest in zone 1 and then gradually decreased until zone 5. In addition, the significant %RH differences among the control and the 32° and 15° groups in different zones were mainly caused by the bigger SD in the control group. Although there was no statistically significant difference among the five zones under the three respective groups, the %RH distribution under the 32° included angle group was the most even (Figure 6B). Therefore, the ALR of the 32° included angle was also confirmed to be able to improve the uniformity of %RH distribution along a cultivation shelf.

Equally important mentioning is that the PPFD and PPED on each cavity were the other two essential factors that are closely related to the growth and quality of a plant. PAR could be especially fully captured and utilized by the plant for photosynthesis (Huang et al., 2020). In this study, comparisons of the two factors and the effective cultivation shelf area percentages based on them (within 10% and 15% SD) were made (Figures 6C, D, 7C–F). The average PPFD and PPED under the control and ALR conditions were both progressively and significantly increased from zones 1 to 5. This is expected because light distributions around the center of a cultivation shelf are always higher than those outside it until the brim in a gradually decreasing manner. However, the values of these two factors under the ALR conditions from zones 1 to 3 were remarkably higher than those under the control. This indicates that implementing an ALR could dramatically improve the PPFD and PPED of those cavities that were located particularly at the brim and off-center areas of the shelf compared with the control. An improvement to enhance the brim PPFD was also observed in a plant lighting system equipped with a LED panel surrounded by four plates of 10 cm in width (Yano and Fujiwara, 2012). Actually, that plate-equipped LED panel system performed in a similar way to the condition of 0° included angle in our study, under which heat dissipation and ventilation would be non-negligible issues as explained earlier. In general, the above-mentioned results strongly support the objective of this invented ALR, *i.e.*, to retrieve stray light energy towards plant growth on the shelf. Furthermore, it was found that the statistical differences under the ALR application from zones 1 to 5 were markedly decreased compared with the control, substantiating the efficiency of ALR (Figures 7C,D).

Compared with the levels of PPFD and PPED on each cavity under the reflector-free control [which were 119.6 (min) to 265.8 (max) μmol/(m^2·s) and 26.9 (min) to 59.8 (max) J/(m^2·s), respectively], the ALR application under 32° produced 164.4 to 264.7 μmol/(m^2·s) and 29.2 to 56.9 J/(m^2·s), respectively, and that under 15° yielded 158.5 to 271.7 μmol/(m^2·s) and 35.0 to 60.2 J/(m^2·s), respectively. The ALR applications tremendously enhanced the PPFD and PPED on each cavity at the brim of a cultivation shelf and significantly decreased the difference within the shelf. Upon further examination of the heat maps (Figures 6C, D), the ALR of 32° and 15° included angles were found to retrieve back more PPFD and PPED onto the shelf and distribute them more evenly along the shelf compared with the control. Thus, the included angle of 32° was superior to 15° by aggregating less PPFD/PPED on the specific cavities of the trays, facilitating a more uniform development of the seedlings on the cultivation shelf (Figures 6C, D). The included angle of 32° was thus confirmed again as the best ALR included angle among all the angles tested.

Comparing the effective cultivation shelf area percentages (within 10% and 15% SD of PPFD/PPED) under all the included angles tested, the effective areas under 32° were significantly higher than those under 15° and the control, while those under 15° were also markedly higher than the control. Compared with the control, the included angle of 32° increased the effective area by up to 47% and 15% based on PPFD for 10% and 15% SD, respectively, as well as by 42% and 16% based on PPED for 10% and 15% SD, respectively (Figures 7E, F). An appropriate ALR application can thus effectively increase the effective cultivation shelf area.

Effect of ALR application on the growth and morphology of choy sum seedling

After the effectiveness of ALR on improving the key environmental conditions on a cultivation shelf was confirmed, validating the performance of ALR in real plant cultivation on the shelf would be essential to eventually prove that this reflector offers benefits to an indoor plant factory. As such, a popular leafy vegetable rich in bioactive metabolites and widely cultivated in Asia, choy sum, was chosen as the experimental plant (Liang et al., 2018; Huang et al., 2021a).

In this case, the influences of ALR on the FW of choy sum seedling, shoot, root, and total leaf, as well as the FW-based harvest index and shoot/root ratio, were firstly determined and compared between the control and ALR with the optimal included angle of 32° (Figure 8). Compared with the control, the seedling FW in zones 3 and 5 under the ALR of 32° included angle was significantly increased by up to 13% and 14%, respectively (Figure 8A). In addition, the shoot FW in zones 1, 2, 3, and 5 were also markedly enhanced by 12%, 11%, 17%, and 18%, respectively (Figure 8B). In addition, the total leaf FW (Figure 8D), FW-based harvest index (Figure 8E), and shoot/root ratio (Figure 8F) were remarkably increased across all the zones. In contrast, the root FW in zones 1, 2, 3, and 4 was significantly decreased (Figure 8C). It is worth to note that there was a significantly increasing trend from zone 1 to 5 in terms of FW of seedling, shoot, root, and total leaf under both the control and ALR conditions. This was concurrent with the gradual increases of PPFD distribution from zones 1 to 5 (Figure 7C), as the biomass accumulation of choy sum seedling was always positively related to light intensity below its light saturation point (Huang et al., 2021b). Nevertheless, the FW-based harvest index and shoot/root ratio under ALR did not show a significant difference among all the zones, although fluctuations across the zones were found under the control (Figures 8E, F). These results supported that implementing an ALR could increase the above-ground FW biomass of choy sum seedling along an IFR cultivation shelf as well as the uniformity of the biomass across the shelf.

The influences of ALR on the DW of choy sum seedling, shoot, root, and total leaf, as well as on the DW-based harvest index and shoot/root ratio, were likewise subsequently evaluated (Figure 9). Compared with the control, the DW of an average seedling and shoot in zone 5 was significantly increased by up to 14% and 18%,

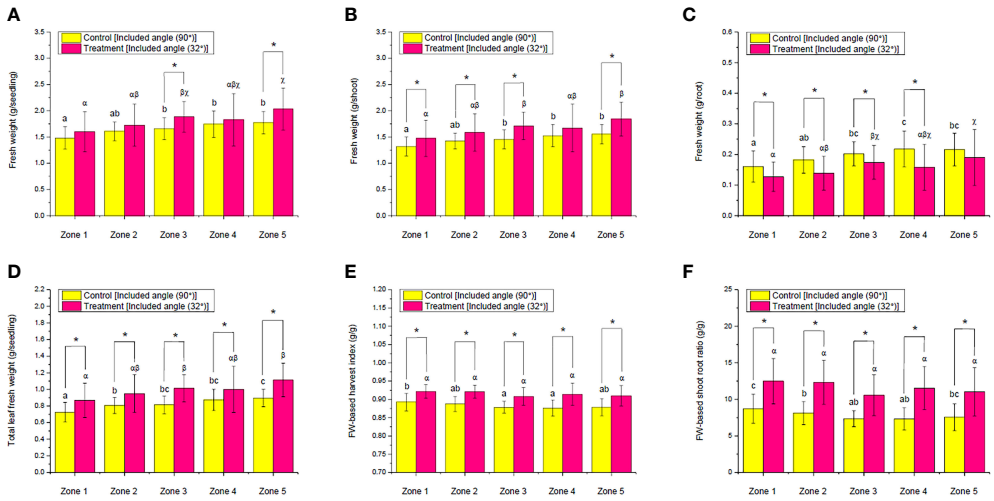

FIGURE 8
Comparison of the fresh weight (FW) of **(A)** seedling, **(B)** shoot, **(C)** root, and **(D)** total leaf as well as **(E)** FW-based harvest index and **(F)** FW-based shoot–root ratio of choy sum at seedling stage on day 16 grown in an indoor farm rack with and without the application of an adjustable lampshade-type reflector (ALR). The asterisk (*) indicates significant differences found between the control and treatment (Student's *t*-test; $p < 0.05$), while different Greek alphabets (α, β, and χ) and the lowercase letters (a, b, and c) indicate significant differences among all the zones with and without the application of ALR ($N_{zone1} = 45$, $N_{zone2} = 38$, $N_{zone3} = 32$, $N_{zone4} = 26$, $N_{zone5} = 19$, one-way ANOVA; Tukey multiple-comparison; $p < 0.05$).

respectively. However, only root DW in zone 2 was remarkably decreased instead. Except for that, there was no significant difference found in other zones between the control and the ALR of 32° included angle (Figures 9A–C). For total leaf DW, the implemented ALR resulted in a significant increase by up to 22% and 24% in zones 2 and 5, respectively, compared with the control (Figure 9D). Particularly, a significant increase in the DW-based harvest index among all the zones was observed due to the ALR implementation (Figure 9E). Moreover, similar outcomes among the zones were found in the DW-based shoot/root ratio, except for zone 4 (Figure 9F). When comparing the DW of seedling, shoot, root, and total leaf among all the zones within the same group, no significant difference in the DW of all parts of choy sum was observed in the ALR group. In the control group, however, the DW values of these parts in choy sum were fluctuating across the zones (Figures 9A–D). These findings again indicated that the ALR implementation could increase the developmental uniformity of choy sum seedlings among the different zones of an IFR shelf.

The morphological response of choy sum seedlings to the implemented ALR showed a similar outcome. The average TLA of

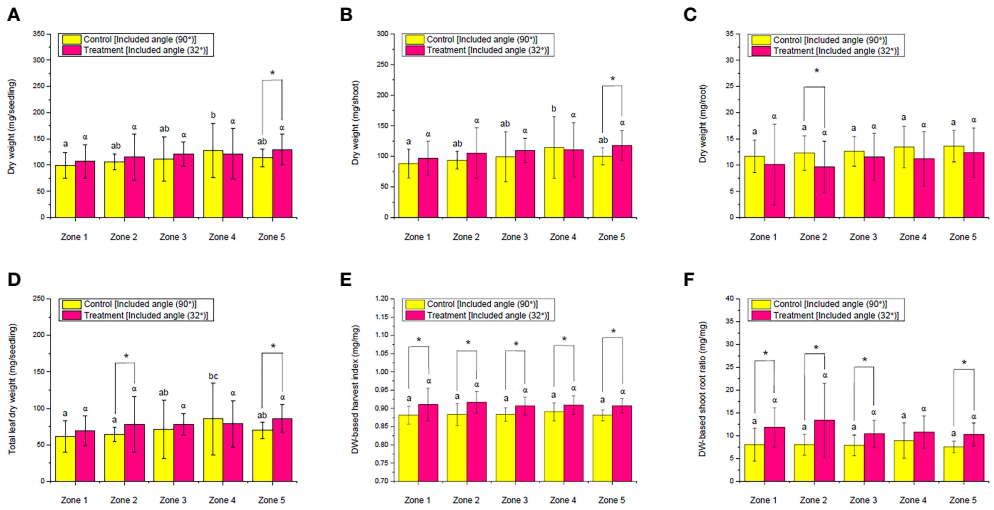

FIGURE 9
Comparison of the dry weight (DW) of **(A)** seedling, **(B)** shoot, **(C)** root, and **(D)** total leaf as well as **(E)** DW-based harvest index and **(F)** DW-based shoot–root ratio of choy sum at seedling stage on day 16 grown in an indoor farm rack with and without the application of an adjustable lampshade-type reflector (ALR). The asterisk (*) indicates significant differences found between the control and treatment (Student's *t*-test; $p < 0.05$), the lone Greek alphabet (α) indicates that there is no significant difference found among all the zones with the application of ALR, and the lowercase letters (a, b, and c) indicate significant differences among all the zones without the application of ALR ($N_{zone1} = 45$, $N_{zone2} = 38$, $N_{zone3} = 32$, $N_{zone4} = 26$, $N_{zone5} = 19$, one-way ANOVA; Tukey multiple-comparison; $p < 0.05$).

each seedling in all the zones increased by up to 34%, compared with the control (Figure 10A), which was primarily because the implemented ALR increased the PPFD and PPED on the cultivation shelf by reflecting stray light back (Figures 7C–F), provided that the light intensity was below choy sum's light saturation point (Huang et al., 2021b). The ALR group also did not have any significant difference among all the zones, while the control group showed a gradual and remarkable increase, indicating that the implemented ALR helped to achieve a more uniform leaf development across all the zones (Figure 10A). In addition, under both the control and ALR conditions, the shoot HL from zones 1 to 5 were gradually and significantly shortened, pointing towards the fact that the PPFD and PPED at the shelf center were significantly higher than those at the brim, as choy sum HL was found to be negatively related to light intensity in our earlier studies (Huang et al., 2021b). However, the shortening of HL in the control group was more significant than that of the ALR group, and the control group HL in some zones, such as zones 3 and 4, were markedly shorter than those in the ALR group. This revealed that the more uniform HL was achieved by the implemented ALR compared with the control (Figure 10B).

Looking into the shoot HD, the control group did not show any significant difference across all the zones, while the ALR group had a gradual increase from zones 1 to 5, which also led to significantly higher HD in some zones (*i.e.*, 2, 3, and 5) than the control group (Figure 10C). The positive correlation between light intensity and choy sum hypocotyl diameter could explain the current HD results (Huang et al., 2021b). Regarding RL, no significant difference was found either between the control and ALR conditions or across the zones under the same condition (Figure 10D). In short, the morphological responses of choy sum seedling to the implemented ALR indicated that ALR could help to facilitate a more uniform morphological development of choy sum seedling along a cultivation shelf.

Observing the moisture variations of seedling, shoot, and root between the control and ALR groups and across the zones within the same group, there was not any significant difference found (Figures 11A–C). Furthermore, except PE in zone 5 under the ALR condition, which was remarkably higher than that under the control, PE in other zones between the control and ALR groups as well as across zones 1 to 4 within the same group did not demonstrate any significant difference (Figure 11D). The PE as presented here is a vital index that represents a plant's capability to capture and convert light energy into its chemical potential energy (Huang et al., 2016; Huang et al., 2021b).

Effect of ALR application on the pigments of choy sum shoot

As for the pigment responses of choy sum shoots to ALR application, the levels of chl*a*, chl*b*, and Tchl, as well as TC, under the control and ALR conditions were investigated (Figure 12). There was no significant difference in the levels of chl*a* and Tchl between the control and ALR groups and also across the zones within the same group. The level of chl*b* in the control group was statistically the same across all the zones (Figures 12A–C). This revealed that the presence of ALR did not affect the biosynthesis of chlorophyll pigments significantly. However, the level of chl*b* in the ALR group remarkably decreased from zones 1 to 5 (Figure 12C). As chl*b* is normally negatively correlated to light intensity (Li et al., 2012; Huang et al., 2021a), the reduction of chl*b* level from zones 3 to 5 was consistent in such a way that the light intensities across these areas were significantly enhanced through the ALR application

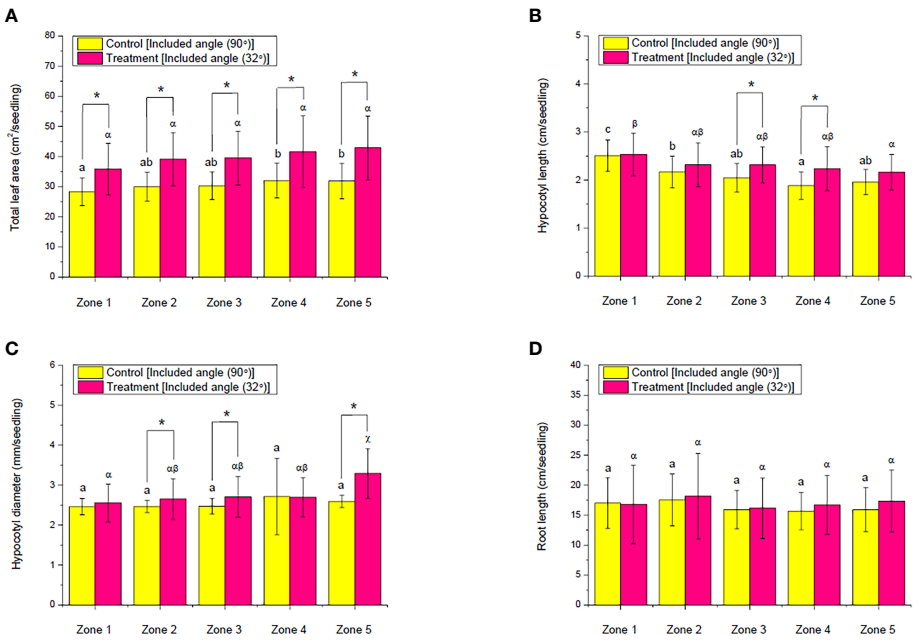

FIGURE 10
Comparison of the **(A)** total leaf area, **(B)** hypocotyl length, **(C)** hypocotyl diameter, and **(D)** root length of choy sum at seedling stage on day 16 grown in an indoor farm rack with and without the application of an adjustable lampshade-type reflector (ALR). The asterisks (*) indicate significant differences found between the control and treatment (Student's *t*-test; $p < 0.05$), while different Greek alphabets (α, β, and χ) and the lowercase letters (a, b, and c) indicate significant differences among all the zones with and without the application of ALR (N_{zone1} = 45, N_{zone2} = 38, N_{zone3} = 32, N_{zone4} = 26, N_{zone5} = 19, one-way ANOVA; Tukey multiple-comparison; $p < 0.05$).

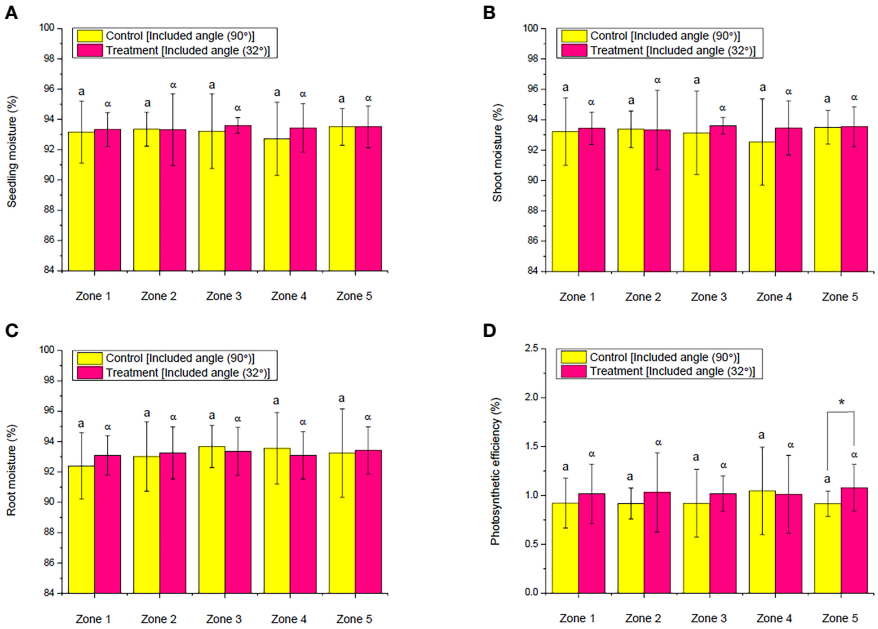

FIGURE 11
Comparison of the moisture of **(A)** seedling, **(B)** shoot, and **(C)** root as well as **(D)** photosynthetic efficiency of choy sum at seedling stage on day 16 grown in an indoor farm rack with and without the application of an adjustable lampshade-type reflector (ALR). The asterisks (*) indicate significant differences found between the control and treatment (Student's *t*-test; $p < 0.05$), while the lone Greek alphabet (α) and the lowercase letter **(a)** indicate that there are no significant differences found among all the zones with and without the application of ALR ($N_{zone1} = 45$, $N_{zone2} = 38$, $N_{zone3} = 32$, $N_{zone4} = 26$, $N_{zone5} = 19$, one-way ANOVA; Tukey multiple-comparison; $p < 0.05$).

(Figures 7C, 12C). On the contrary, the levels of TC in the control and ALR groups did not show any significant difference across the zones within the same group. Nevertheless, significant differences were found between the control and ALR groups. The levels of TC in all five zones of the ALR group were all markedly higher than their counterparts in the control group by up to 45% (Figure 12D). It was well documented in the literature that carotenoids might possess a light-harvesting property and function in the energy transfer process through capturing purple to blue light photons and delivering energy to chl*a* molecules for photosynthesis (Nurachman et al., 2015; Huang et al., 2017). Therefore, the enhanced TC level in the ALR group could be due to the improved light environment on the cultivation shelf, such as higher PPFD and PPED

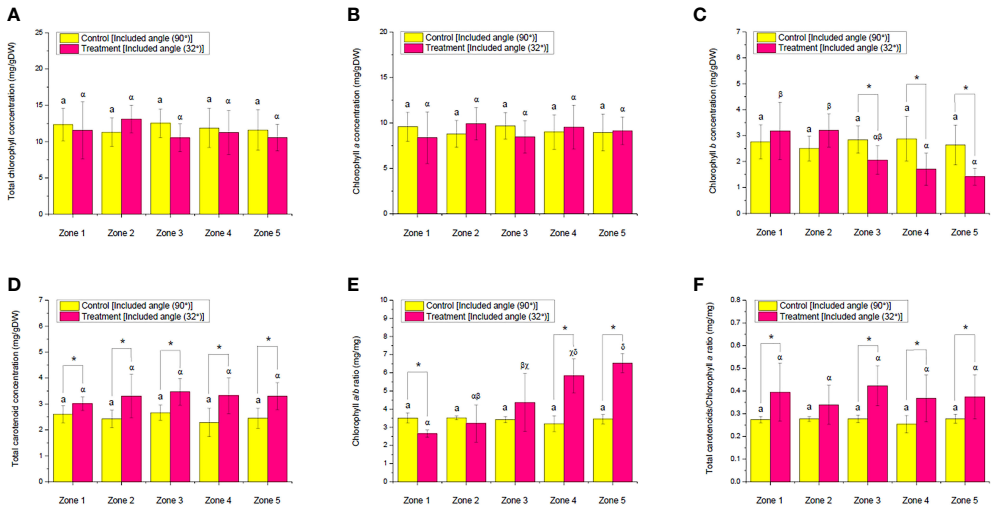

FIGURE 12
Comparison of the concentration of **(A)** total chlorophylls, **(B)** chlorophyll *a*, **(C)** chlorophyll *b* and, **(D)** total carotenoids as well as **(E)** chlorophyll *a*/*b* ratio and **(F)** total carotenoids/chlorophyll *a* ratio of choy sum shoots at seedling stage on day 16 grown in an indoor farm rack with and without the application of an adjustable lampshade-type reflector (ALR). The asterisks (*) indicate significant differences found between the control and treatment (Student's *t*-test; $p < 0.05$), the lone lowercase letter (a) indicates that there is no significant difference found among all the zones without the application of ALR, and different Greek alphabets (α, β, χ, and δ) indicate significant differences found among all the zones with the application of ALR ($N_{zone1} = 6$, $N_{zone2} = 6$, $N_{zone3} = 6$, $N_{zone4} = 6$, $N_{zone5} = 6$, one-way ANOVA; Tukey multiple-comparison; $p < 0.05$).

and more uniform light distribution, thus inducing carotenoid biosynthesis to seize more light energy to support plant growth (Figures 6C, D, 7C, D, 12D). As carotenoids have been shown to benefit human wellness by acting as antioxidants, anti-inflammatory agents, and anti-cancer compounds (Huang et al., 2017), the implementation of ALR could thus be proposed as an effective approach to improve the nutritional quality of choy sum shoot while using the same amount of electricity as the control.

To further observe two essential parameters—chl*a*/chl*b* and TC/chl*a* ratios—that are closely related to photosynthesis and light stress (Filella et al., 2009; Huang et al., 2020; Huang and Cheung, 2021), the chl*a*/chl*b* ratio in the ALR group was found to increase sharply from zones 1 (which had relatively low PPFD) to 5 (which had relatively high PPFD) compared with the control group that did not show any significant difference across the five zones. However, the chl*a*/chl*b* ratio at the shelf brim (*i.e.*, zone 1) in the ALR group was remarkably lower than that in the control group, while the ratio at the shelf center (zones 4 and 5) was markedly higher than that of the control (Figure 12E). It was clear that the significant increase of chl*a*/chl*b* ratio from zones 1 to 5 was corresponding to the reduction of the chl*b* level (Figure 12C). The upregulation of this parameter could help to minimize the size of auxiliary light-harvesting chlorophyll antenna for maximizing PE (Figure 11D) (Melis, 2009; Huang and Cheung, 2021).

On the other hand, the TC/chl*a* ratio of the ALR group was found to be significantly higher than its counterpart in the control group across all the zones except zone 2. Nevertheless, there was no significant difference across the zones within the same group (Figure 12F). Although the TC/chl*a* ratio is usually recognized as an indicator of light stress because one of carotenoid's role is to scavenge reactive oxygen species induced by light stress (Filella et al., 2009), the current results seemed to support the other role of carotenoid, as a light-harvesting tool, that was described earlier. Because the light-harvesting complexes of photosystem II (LHC II) in vegetables are usually more than one type and the carotenoid compositions in the respective LHC II are commonly different (Phillip and Young, 1995), the wane and wax of LHC II under different plant growth conditions have potential to upregulate the TC proportion of LHC II. Thus, it was possible that a stable chl*a* level was maintained, whereas a higher TC level in the vegetable was achieved when the environment was changed (Figures 12B, D, F). However, future studies should look into the profile of carotenoid in our choy sum case for clarification. It is worth noting that the implementation of ALR in this study was not intended to generate a light stress environment for plants, which could be further proved by the TPC and DPPH results (Figure 13) that are to be discussed in the following section. Overall, the TC/chl*a* ratio in the ALR group was significantly enhanced by up to 52.5% compared with that of the control group (Figure 12F).

Effect of ALR application on total phenolic contents and the antioxidant capacity of choy sum shoot

Phenolic compounds are the essential secondary metabolites found in plants, which function in the protection of plants against biotic and abiotic stresses (Wong et al., 2020). Thus, they could be utilized as indicators to check whether the plants are under a stressed light environment or not. In this work, the TPC and DPPH assays were conducted to compare the level of antioxidant-related metabolites and the antioxidant activities of choy sum shoots cultivated on an IFR shelf with and without the implementation of an ALR. As shown in Figures 13A, B, the implementation of ALR did not significantly influence the TPC and DPPH values of choy sum shoots across all the zones, indicating that the PPFD and PPED distribution along the cultivation shelf was more uniform by using an ALR compared with the reflector-free control. The TPC and DPPH values in the control group were fluctuating across the zones due to the fluctuating light distribution in the absence of ALR (Figures 6C, D). Owing to the uneven distribution of PPFD and PPED under the control, the levels of phenolics in some zones, such as zones 2 and 5, were markedly higher than those in the ALR group (Figure 13A). However, this led to the heterogeneity of choy sum seedling quality along the shelf in the absence of ALR.

Conclusion

The implementation of an ALR with optimized angle, distance, *etc.*, can minimize the distribution differences of temperature and relative humidity along an IFR cultivation shelf. It can also enhance the PPFD and PPED distribution along the cultivation shelf. Such improvements could significantly improve the growth and morphological traits,

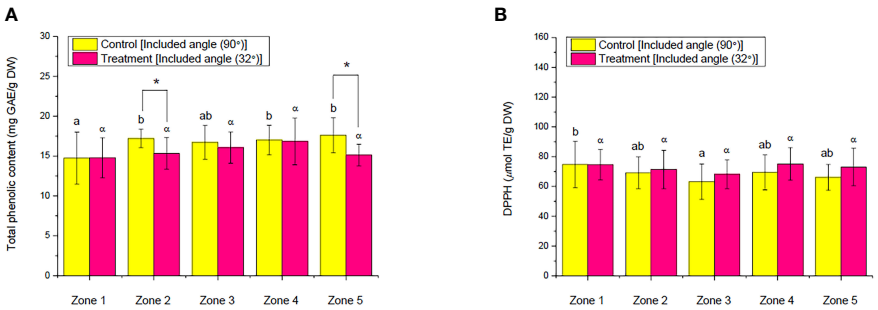

FIGURE 13
Comparison of the **(A)** total phenolic content and **(B)** 2,2-diphenyl-1-picrylhydrazyl of choy sum shoots at seedling stage on day 16 grown in an indoor farm rack with and without the application of an adjustable lampshade-type reflector (ALR). Different Greek alphabets (α and β) and the lowercase letters (a, b, and c) indicate significant differences among all the zones with and without the application of ALR (N_{zone1} = 6, N_{zone2} = 6, N_{zone3} = 6, N_{zone4} = 6, N_{zone5} = 6, one-way ANOVA; Tukey multiple-comparison; p< 0.05).

including the nutritional quality of choy sum seedlings in indoor farm practice. In short, the ALR designed in this study is suitable and efficient to be applied in indoor plant factories for leafy vegetable production. According to the relative scale between the reflective board and the shelf setting in IFR used in this study, the proportion of board width and distance between the light source and the tray surface is suggested to be 10:12 to achieve the optimal growth and quality improvement of plant. The ALR can be adapted further for diverse growth systems and plant species. Future studies should be focused on the effects of combined ALR and red/blue lights as the light source and photoperiod as well on the growth and quality of vegetable seedlings in order to further reduce power consumption and enhance the energy conversion efficiency in indoor farming.

Nomenclature

%RH, relative humidity; ALDA, available light distribution area; ALR, adjustable lampshade-type reflector; AWA, acetone–water–acetic acid; Chl*a*, chlorophyll *a*; Chl*b*, chlorophyll *b*; DPPH, 2,2-diphenyl-1-picrylhydrazyl; DW, dry weight; FCR, Folin–Ciocalteu's phenol reagent; FW, fresh weight; GAE, gallic acid equivalents; GUI, graphical user interface; HD, hypocotyl diameter; HI, harvest index; HL, hypocotyl length; IFR, indoor farm racks; LDU, light distribution uniformity; LED, light-emitting diode; PAR, photosynthetically active radiation; PE, photosynthetic efficiency; PPED, photosynthetic photon energy density; PPFD, photosynthetic photon flux density; RL, root length; ROS, reactive oxygen species; SD, standard deviation; TC, total carotenoids; Tchl, total chlorophylls; TE, Trolox equivalents; TLA, total leaf area; TPC, total phenolic content.

Data availability statement

The original contributions presented in the study are included in the article/supplementary materials, further inquiries can be directed to the corresponding author/s.

Author contributions

JH: conceptualization, methodology, investigation, data collection and processing, writing—original draft, and writing—review and editing. ZG: data collection and processing and writing—original draft. XH: data collection and processing and writing—original draft. WZ: conceptualization, methodology, writing—review and editing, supervision, and project administration. All authors contributed to the article and approved the submitted version.

Funding

This work was funded by the National Research Foundation, Prime Minister's Office, Republic of Singapore under its Competitive Research Programme (grant name: Novel integrated agrotechnologies, plant nutrients and microbials for improved production of green leafy vegetables in Singapore; CRP award no. NRF-CRP 16-2015-04).

Conflict of interest

The authors declare that the research was conducted in the absence of any commercial or financial relationships that could be construed as a potential conflict of interest.

Publisher's note

All claims expressed in this article are solely those of the authors and do not necessarily represent those of their affiliated organizations, or those of the publisher, the editors and the reviewers. Any product that may be evaluated in this article, or claim that may be made by its manufacturer, is not guaranteed or endorsed by the publisher.

References

Ainsworth, E. A., and Gillespie, K. M. (2007). Estimation of total phenolic content and other oxidation substrates in plant tissues using folin–ciocalteu reagent. *Nat. Protoc.* 2, 875–877. doi: 10.1038/nprot.2007.102

Akiyama, T., and Kozai, T. (2016). "Part II. plant growth and development as affected by light: chapter 7 – light environment in the cultivation space of plant factory," in *LED lighting for urban agriculture*. Eds. T. Kozai, K. Fujiwara and E. S. Runkle (Singapore: Springer Science+ Business Media Singapore Pte Ltd), 91–109.

Alvino, A., and Barbieri, G. (2016). "Vegetables of temperate climates: Leafy vegetables," in *Encyclopedia of food and health*. Eds. B. Caballero, P. Finglas and F. Toldrá (Waltham, MA: Oxford Academic Press), 393–400. doi: 10.1016/b978-0-12-384947-2.00712-1

Armstrong, J. D. (1978). Apparatus for promoting plant growth with artificial light. United States Patent. Patent No.: 4,078169, 1978. Date of Patent: Mar. 7.

Asiabanpour, B., Estrada, A., Ramirez, R., and Downey, M. S. (2018). Optimizing natural light distribution for indoor plant growth using PMMA optical fiber: Simulation and empirical study. *J. Renew. Energy* 9429867, 10. doi: 10.1155/2018/9429867

Bencloski, J. W. (1982). Air temperature and relative humidity: A simulation. *J. Geogr.* 81, 64–65. doi: 10.1080/00221348208980713

Benke, K., and Tomkins, B. (2017). Future food-production systems: Vertical farming and controlled-environment agriculture. *Sustainabil.: Sci. Pract. Policy* 13, 13–26. doi: 10.1080/15487733.2017.1394054

Bobo-García, G., Davidov-Pardo, G., Arroqui, C., Vírseda, P., Marín-Arroyo, M. R., and Navarro, M. (2015). Intra-laboratory validation of microplate methods for total phenolic content and antioxidant activity on polyphenolic extracts, and comparison with conventional spectrophotometric methods. *J. Sci. Food Agr.* 95, 204–209. doi: 10.1002/jsfa.6706

Buttar, G. S., Thind, H. S., and Aujla, M. S. (2006). Methods of planting and irrigation at various levels of nitrogen affect the seed yield and water use efficiency in transplanted oilseed rape (*Brassica napus* l.). *Agr. Water Manage.* 85, 253–260. doi: 10.1016/j.agwat.2006.05.008

Chelf, B. (2002). Convertible lighting fixture with adjustable reflectors and a method of installing a reflector to a lighting fixture. General Innovation, LLC, Mansfield, TX(US) United States Patent. Patent No.: US 6,382,817 B1. Date of Patent: May 7, 2002.

Cronk, P. A. (2007). Adjustable reflector device. United States Patent. Patent No.: US 7,156,539 B2. Date of Patent: Jan. 2, 2007.

Despommier, D. (2013). Farming up the city: the rise of urban vertical farms. *Trends Biotechnol.* 31, 388–389. doi: 10.1016/j.tibtech.2013.03.008

Dumont, G. (2013). Light reflector for a horticultural device. United States Patent. Patent No.: US 2013/0343048 A1. Date of Patent: Dec. 26, 2013.

Du, Y. Y., Tan, W. K., Zou, L., Lei, J. J., and Ong, C. N. (2022). New insights into the phenolic constituents and their relationships with antioxidant capacity during the growth of a commonly consumed Asian vegetable, *Brassica rapa* var. *parachinensis* (choy sum). *Food Chem. Adv.* 1, 100038. doi: 10.1016/j.focha.2022.100038

Filella, I., Porcar-Castell, A., Munné-Bosch, S., Bäck, J., Garbulsky, M. F., and Peñuelas, J. (2009). PRI assessment of long-term changes in carotenoids/chlorophyll ratio and short-term changes in de-epoxidation state of the xanthophyll cycle. *Int. J. Remote Sens.* 30, 4443–4455. doi: 10.1080/01431160802575661

Huang, J. J., Bunjamin, G., Teo, E. S., Ng, D. B., and Lee, Y. K. (2016). An enclosed rotating floating photobioreactor (RFP) powered by flowing water for mass cultivation of photosynthetic microalgae. *Biotechnol. Biofuels* 9, 1–18. doi: 10.1186/s13068-016-0633-8

Huang, J. J., and Cheung, P. C. K. (2021). Cold stress treatment enhances production of metabolites and biodiesel feedstock in porphyridium cruentum via adjustment of cell membrane fluidity. *Sci. Total. Environ.* 780, 146612. doi: 10.1016/j.scitotenv.2021.146612

Huang, J. J., D'Souza, C., Tan, M. Q., and Zhou, W. (2021a). Light intensity plays contrasting roles in regulating metabolite compositions in choy sum (*Brassica rapa* var. *parachinensis*). *J. Agr. Food Chem.* 69, 5318–5331. doi: 10.1021/acs.jafc.1c00155

Huang, J. J., D'Souza, C., and Zhou, W. (2021b). Light-time-biomass response model for predicting the growth of choy sum (*Brassica rapa* var. *parachinensis*) in soil-based LED-constructed indoor plant factory for efficient seedling production. *Front. Plant Sci.* 12. doi: 10.3389/fpls.2021.623682

Huang, J. J., Huang, W., Li, J., Li, P., and Cheung, P. C. K. (2020). Potential advancement of ultraviolet-free solar radiation technology in enriching the nutrient composition and biodiesel feedstock production in marine green microalga *Platymonas subcordiformis*. *Bioresour. Technol. Rep.* 11, 100534. doi: 10.1016/j.biteb.2020.100534

Huang, J. J., Lin, S., Xu, W., and Cheung, P. C. K. (2017). Occurrence and biosynthesis of carotenoids in phytoplankton. *Biotechnol. Adv.* 35, 597–618. doi: 10.1016/j.biotechadv.2017.05.001

Jiang, J. A., Liao, M. S., Lin, T. S., Huang, C. K., Chou, C. Y., Yeh, S. H., et al. (2018). Toward a higher yield: A wireless sensor network-based temperature monitoring and fan-circulating system for precision cultivation in plant factories. *Precis. Agric.* 19, 929–956. doi: 10.1007/s11119-018-9565-6

Keen, S. B. (2011). High intensity light reflector apparatus. United States Patent. Patent No.: US 7,954,982 B2. Date of Patent: Jun. 7, 2011.

Kim, K. Y., Huh, J. H., and Ko, H. J. (2021). Research on crop growing factory: Focusing on lighting and environmental control with technological proposal. *Energies* 14, 2624. doi: 10.3390/en14092624

Kozai, T. (2019). "Part 1. overview and concept of closed plant production system (CPPS): chapter 3 – PFAL business and R&D in Asia and north America: status and perspectives," in *Plant factory – an indoor vertical farming system for efficient quality food production*. Eds. T. Kozai, G. H. Niu and M. Takagaki (Waltham, MA: Oxford Academic Press), 35–39.

T. Kozai, G. Niu and M. Takagaki (Eds.) (2019). *Plant factory: An indoor vertical farming system for efficient quality food production* (London: Academic press).

Lee, H. W., Zhang, H., Liang, X., and Ong, C. N. (2020). Simultaneous determination of carotenoids, tocopherols and phylloquinone in 12 *Brassicaceae* vegetables. *LWT-Food. Sci. Technol.* 130, 109649. doi: 10.1016/j.lwt.2020.109649

Liang, X., Lee, H. W., Li, Z., Lu, Y., Zou, L., and Ong, C. N. (2018). Simultaneous quantification of 22 glucosinolates in 12 *Brassicaceae* vegetables by hydrophilic interaction chromatography–tandem mass spectrometry. *ACS Omega.* 3, 15546–15553. doi: 10.1021/acsomega.8b01668

Li, Z., Lee, H. W., Liang, X., Liang, D., Wang, Q., Huang, D., et al. (2018). Profiling of phenolic compounds and antioxidant activity of 12 cruciferous vegetables. *Molecules* 23, 1139. doi: 10.3390/molecules23051139

Li, H., Tang, C., Xu, Z., Liu, X., and Han, X. (2012). Effects of different light sources on the growth of non-heading Chinese cabbage (*Brassica campestris* l.). *J. Agr. Sci.* 4, 262. doi: 10.5539/jas.v4n4p262

Li, Z., Wei, H., Chen, D., Chang, M., Hu, H., Ye, X., et al. (2021). Optical properties of multicolor, hierarchical nanocomposite films based on anodized aluminum oxide. *Opt. Mater.* 111, 110557. doi: 10.1016/j.optmat.2020.110557

Melis, A. (2009). Solar energy conversion efficiencies in photosynthesis: Minimizing the chlorophyll antennae to maximize efficiency. *Plant Sci.* 177, 272–280. doi: 10.1016/j.plantsci.2009.06.005

Miao, Y., Ke, Y., Wang, N., Zou, W., Xu, M., Cao, Y., et al. (2019). Stable and bright formamidinium-based perovskite light-emitting diodes with high energy conversion efficiency. *Nat. Commun.* 10, 1–7. doi: 10.1038/s41467-019-11567-1

Michaloski, A. J. (1991). Method and apparatus for ultraviolet treatment of plants. United States Patent. Patent No.: 5,040,329. Date of Patent: Aug. 20, 1991.

Moghadam, H., Samimi, A., and Behzadmehr, A. (2013). Effect of nanoporous anodic aluminum oxide (AAO) characteristics on solar absorptivity. *Transp. Phenom. Nano. Micro. Scales.* 1, 110–116. doi: 10.7508/TPNMS.2013.02.004

Ngosong, N. T., Boamah, E. D., Fening, K. O., Kotey, D. A., and Afreh-Nuamah, K. (2021). The efficacy of two bio-rational pesticides on insect pests complex of two varieties of white cabbage (*Brassica oleracea* var. *capitata* l.) in the coastal savanna region of Ghana. *Phytoparasitica* 49, 397–406. doi: 10.1007/s12600-020-00859-8

Nurachman, Z., Hartini, H., Rahmaniyah, W. R., Kurnia, D., Hidayat, R., Prijamboedi, B., et al. (2015). Tropical marine *Chlorella* sp. PP1 as a source of photosynthetic pigments for dye-sensitized solar cells. *Algal. Res.* 10, 25–32. doi: 10.1016/j.algal.2015.04.009

Phillip, D., and Young, A. J. (1995). Occurrence of the carotenoid lactucaxanthin in higher plant LHC II. *Photosynth. Res.* 43, 273–282. doi: 10.1007/BF00029940

Powers, J. H., and Dang, H. T. (1986). High reflectance semi-specular anodized aluminum alloy product and method of forming same. Aluminum Company of America, Pittsburgh, PA, United States Patent. Patent No.: 4,601,796. Date of Patent: Jul. 22, 1986.

Sabudin, S., Zulkarnaen, M. E., Mohammed, A. N., and Batcha, M. F. B. M. (2022). Numerical investigation of temperature distribution in a container-type plant factory. *J. Adv. Res. Appl. Sci. Eng. Technol.* 28, 90–101. doi: 10.37934/araset.28.2.90101

Satterthwaite, D., McGranahan, G., and Tacoli, C. (2010). Urbanization and its implications for food and farming. *Philos. Trans. R. Soc Lond. B. Biol. Sci.* 365, 2809–2820. doi: 10.1098/rstb.2010.0136

Sun, C. M., Zhao, F., and Zhang, Z. (2014). "Stray light analysis of large aperture optical telescope using TracePro," in *International symposium on optoelectronic technology and application 2014: Imaging spectroscopy; and telescopes and Large optics*, vol. 9298. (Beijing, China: International Society for Optics and Photonics), 92981F. doi: 10.1117/12.2072244

Tan, W. K., Goenadie, V., Lee, H. W., Liang, X., Loh, C. S., Ong, C. N., et al. (2020). Growth and glucosinolate profiles of a common Asian green leafy vegetable, *Brassica rapa* subsp. *chinensis* var. *parachinensis* (choy sum), under LED lighting. *Sci. Hortic.-Amsterdam.* 261, 108922. doi: 10.1016/j.scienta.2019.108922

Tsitsimpelis, I., Wolfenden, I., and Taylor, C. J. (2016). Development of a grow-cell test facility for research into sustainable controlled-environment agriculture. *Biosyst. Eng.* 150, 40–53. doi: 10.1016/j.biosystemseng.2016.07.008

Wills, R. B. H., Wong, A. W. K., Scriven, F. M., and Greenfield, H. (1984). Nutrient composition of Chinese vegetables. *J. Agr. Food Chem.* 32, 413–416. doi: 10.1021/jf00122a059

Wong, C. E., Teo, Z. W. N., Shen, L., and Yu, H. (2020). Seeing the lights for leafy greens in indoor vertical farming. *Trends Food Sci. Tech.* 106, 48–63. doi: 10.1016/j.tifs.2020.09.031

Yano, A., and Fujiwara, K. (2012). Plant lighting system with five wavelength-band light-emitting diodes providing photon flux density and mixing ratio control. *Plant Methods* 8, 46. doi: 10.1186/1746-4811-8-46

Frontiers in
Plant Science

Cultivates the science of plant biology and its applications

The most cited plant science journal, which advances our understanding of plant biology for sustainable food security, functional ecosystems and human health.

Discover the latest Research Topics

See more →

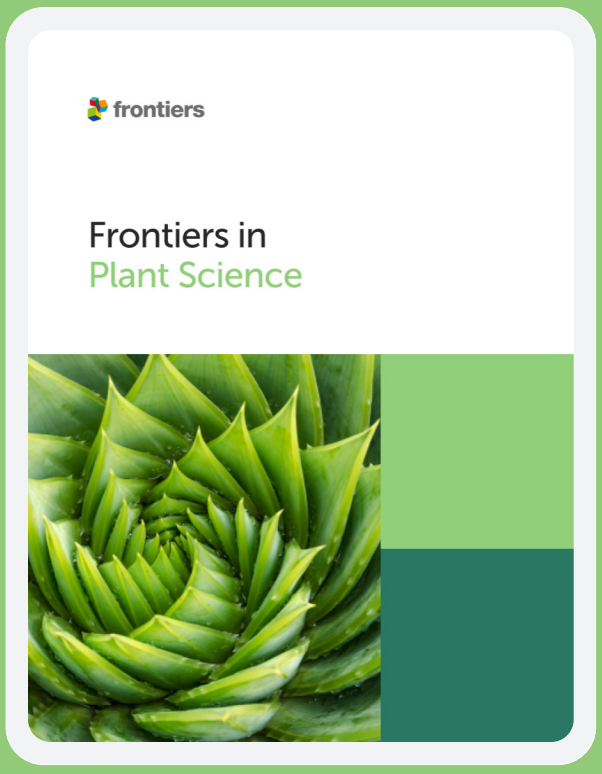

Frontiers

Avenue du Tribunal-Fédéral 34
1005 Lausanne, Switzerland
frontiersin.org

Contact us

+41 (0)21 510 17 00
frontiersin.org/about/contact